frontiers | Research Topics

Physiological, molecular and genetic perspectives of environmental stress response in plants

Edited by
Pasala Ratnakumar, Amaranatha Reddy Vennapusa, Mainassara Abdou Zaman-Allah and Padma Nimmakayala

Published in
Frontiers in Plant Science

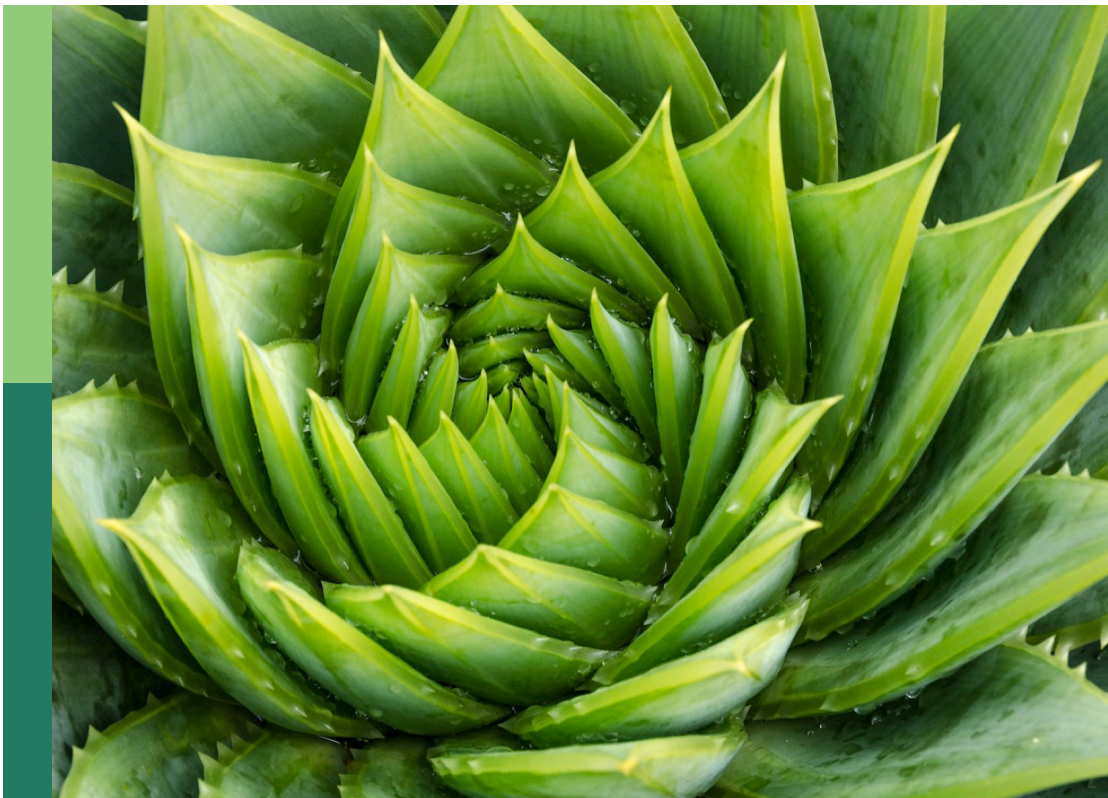

ISSN 1664-8714
ISBN 978-2-8325-2881-5
DOI 10.3389/978-2-8325-2881-5

About Frontiers

Frontiers is more than just an open access publisher of scholarly articles: it is a pioneering approach to the world of academia, radically improving the way scholarly research is managed. The grand vision of Frontiers is a world where all people have an equal opportunity to seek, share and generate knowledge. Frontiers provides immediate and permanent online open access to all its publications, but this alone is not enough to realize our grand goals.

Frontiers journal series

The Frontiers journal series is a multi-tier and interdisciplinary set of open-access, online journals, promising a paradigm shift from the current review, selection and dissemination processes in academic publishing. All Frontiers journals are driven by researchers for researchers; therefore, they constitute a service to the scholarly community. At the same time, the *Frontiers journal series* operates on a revolutionary invention, the tiered publishing system, initially addressing specific communities of scholars, and gradually climbing up to broader public understanding, thus serving the interests of the lay society, too.

Dedication to quality

Each Frontiers article is a landmark of the highest quality, thanks to genuinely collaborative interactions between authors and review editors, who include some of the world's best academicians. Research must be certified by peers before entering a stream of knowledge that may eventually reach the public - and shape society; therefore, Frontiers only applies the most rigorous and unbiased reviews. Frontiers revolutionizes research publishing by freely delivering the most outstanding research, evaluated with no bias from both the academic and social point of view. By applying the most advanced information technologies, Frontiers is catapulting scholarly publishing into a new generation.

What are Frontiers Research Topics?

Frontiers Research Topics are very popular trademarks of the *Frontiers journals series*: they are collections of at least ten articles, all centered on a particular subject. With their unique mix of varied contributions from Original Research to Review Articles, Frontiers Research Topics unify the most influential researchers, the latest key findings and historical advances in a hot research area.

Find out more on how to host your own Frontiers Research Topic or contribute to one as an author by contacting the Frontiers editorial office: frontiersin.org/about/contact

Physiological, molecular and genetic perspectives of environmental stress response in plants

Topic editors

Pasala Ratnakumar — Indian Institute of Oilseeds Research (ICAR), India

Amaranatha Reddy Vennapusa — Delaware State University, United States

Mainassara Abdou Zaman-Allah — International Maize and Wheat Improvement Center, Mexico

Padma Nimmakayala — West Virginia State University, United States

Citation

Ratnakumar, P., Vennapusa, A. R., Zaman-Allah, M. A., Nimmakayala, P., eds. (2023). *Physiological, molecular and genetic perspectives of environmental stress response in plants*. Lausanne: Frontiers Media SA. doi: 10.3389/978-2-8325-2881-5

Table of contents

frontiers | Frontiers in Plant Science

TYPE Editorial
PUBLISHED 16 June 2023
DOI 10.3389/fpls.2023.1213762

OPEN ACCESS

EDITED AND REVIEWED BY
Ravi Valluru,
University of Lincoln, United Kingdom

*CORRESPONDENCE
Amaranatha R. Vennapusa
avennapusa@desu.edu
Pasala Ratnakumar
pratnakumar@gmail.com

RECEIVED 28 April 2023
ACCEPTED 24 May 2023
PUBLISHED 16 June 2023

CITATION
Vennapusa AR, Nimmakayala P, Zaman-Allah MA and Ratnakumar P (2023) Editorial: Physiological, molecular and genetic perspectives of environmental stress response in plants.
Front. Plant Sci. 14:1213762.
doi: 10.3389/fpls.2023.1213762

Editorial: Physiological, molecular and genetic perspectives of environmental stress response in plants

Amaranatha R. Vennapusa[1]*, Padma Nimmakayala[2], Mainassara Abdou Zaman-Allah[3] and Pasala Ratnakumar[4]*

[1]Department of Agriculture and Natural Resources, Delaware State University, Dover, DE, United States, [2]Department of Biology and Gus R. Douglass Institute, West Virginia State University, Institute, Dunbar, WV, United States, [3]International Maize and Wheat Improvement Center (CIMMYT), Harare, Zimbabwe, [4]Indian Council of Agricultural Research (ICAR) Indian Institute of Oilseeds Research (IIOR), Hyderabad, India

KEYWORDS

environmental factors, abiotic stress, cutting-edge tools, scientific approaches, crop physiological response, genetics

Editorial on the Research Topic
Physiological, molecular and genetic perspectives of environmental stress response in plants

Rapid changes in environmental conditions due to climate change affect agricultural crop production worldwide and create unprecedented challenges. Despite new developments in plant science research and technology, achieving a decent yield under changing environmental conditions continues to be a great challenge (Ehrhardt and Frommer, 2012; Fuglie, 2021). Moreover, modern agriculture has to deal with future climate change and must meet the demands of a rapidly increasing population and food security. With the complexity of different environmental stresses caused by climate change, there is a need for the scientific community to deploy new approaches for understanding the ecological consequences, effect on physiological and agronomic traits, and to uncover the tolerant mechanisms, and identify the candidate targets for crop improvement programs (Yuan et al., 2019; Pascual et al., 2022; Zandalinas and Mittler, 2022; Garg et al., 2023). Understanding the physiological, molecular, and genetic perspectives of environmental stress responses in plants is crucial to cope with the hostile effects of climate change in the present and future scenarios in agriculture. This Research Topic aims to offer the opportunity to plant scientists worldwide to present past and emerging insights related to environmental stresses and crop improvement. Various contributions were received and those published are summarized as follows.

A total of 14 articles were published, of which four dealt with experiments related to moisture stress, three were related to temperature stress and two studies focused on the combined stresses. The remaining three articles were focused on salt stress and two articles were on cadmium stress.

These contributions addressed diverse topics, covering crop responses to experimental drought in combination or not with other stresses (Pinnamaneni et al.; Venkatesh et al.; Chilakala et al.; Tan et al.), drought and waterlogging (Singamsetti et al.), and dehydration

stress (Wang et al.). Pinnamaneni et al. focused on the photosynthetic responses of cotton and soybean to varying levels of irrigation regimes (moisture stress) and planting geometries in the USA. The gas exchange and chlorophyll fluorescence parameters provided a better understanding of the photosynthetic component's regulatory and adaptive mechanisms in response to different moisture levels. This study provided new information about how soybeans preferentially use non-photochemical energy dissipation. In contrast, cotton uses both photochemical and non-photochemical energy dissipation to protect photosystem centers (PSI and PSII) and the electron transport rate under moisture-limited environments. An article on tropical maize hybrids exposed to various moisture regimes (drought, waterlogging, and optimal moisture conditions) with multi-trait-based index selection (MGIDI) by Singamsetti et al. proposed an effective tool for the selection of superior lines based on multiple traits and helps breeders by determining the better strategic choice for climate resilient crop improvement programs. Venkatesh et al. reported a novel approach for multiple gene stacking to improve drought stress tolerance in groundnut. Pyramiding of transgenes belonging to three different transcription factor families, *MuMYB96*, *MuWRKY3*, and *MuNAC4*, from horsegram (*Macrotyloma uniflorum*) was shown to improve water conservation, water mining, and cellular level tolerance traits in groundnut, thus helping to sustain its plant morpho-physiological and biochemical functions under water-limited conditions and providing a viable option to maintain the yield penalty.

Chilakala et al. investigated the influence of drought and high temperature on the incidence and severity of dry root rot disease (caused by *Macrophomina phaseolina*) in chickpeas under extensive on- and off-season field trials and greenhouse conditions. Notably, the water relation studies in this Research Topic are unique, connecting plants' drought physiology and pathogen-induced physiological state with multiple pieces of evidence from field, greenhouse, and lab studies. The large-scale study by Tan et al. on perennial small tree grapevine species revealed that the combined effect of both heat and drought stresses is more severe compared to the individual stresses. Integrating physiological, transcriptome, and gene network analysis helped to identify candidate genes, complex pathways, and mechanisms involved in combined stresses. This article generated valuable transcriptomic datasets for grapevines and helpful resources for future research and breeding programs.

Persaud et al. evaluated carinata (*Brassica carinata* A. Braun) genotypes under low and high temperatures. The assessed physiological traits and the superior tolerant lines identified in this study are viable resources for plant breeders to develop cultivars that are adaptable to different climatic zones. In rice, Stephen et al. identified potential simple sequence repeat marker (SSR) candidates linked to heat tolerance using bulked segregant analysis (BSA) in the F_2 population of NERICA-L 44 × Uma. The study by Xu et al. reported the effect of heat stress on the early booting stage and assessed the reproductive, developmental, physiological, and yield parameters. The tolerant lines and the traits identified can be used to understand mechanisms involved in tolerance and for developing heat-tolerant wheat pre-breeding lines.

Ren et al. adopted a multi-omics approach to study molecular responses in sorghum under salt stress. The comparative analysis of transcriptomics, metabolomics, and proteomics aided in identifying the key mechanisms, pathways, genes, proteins, and metabolites responsible for stress tolerance. The novelty of this study is that integrating physiological data with multi-omics analysis provided a precise tool for identifying the molecular mechanisms and key traits to improve salt stress tolerance in sorghum. The study by Kumar et al. focused on deciphering trait-associated physiological alterations under salt stress conditions using pearl millet hybrids and inbred lines. The meticulous stress imposition methods and trait modeling approach helped to identify the crucial morpho-physiological characteristics governing the tolerance mechanisms and grain yield traits under irrigation-induced salinity stress. The identified pearl millet lines can be recommended for enhancing crop resilience to achieve stable production in saline agroecosystems. Ran et al. assessed the salt tolerance of *Salix matsudana* Koidz, which is a climate-resilient tree species. The study reveals the relationship between ion (Na, K, Ca) absorption and photosynthetic response under salt stress.

Yuan et al. reported the global metabolomic profiling of the edible and medicinal plant *Salvia miltiorrhiza* under cadmium (Cd) stress. The identified target metabolites in this study will be a potential source for improving heavy metal stress tolerance in medicinally important crop plants. The review article by Al-Khayri et al. discusses the Cd source, mobility, and toxicity in medicinal plant species and their effect on germination, plant growth, physiological and biochemical characteristics, and molecular aspects, with a focus on the biosynthesis of important secondary metabolites. Further, this review discusses multiple omics and biotechnological approaches, such as genetic engineering and genome editing to ameliorate Cd stress.

The broad range of articles published under this Research Topic offer the opportunity to extend our understanding of the physiological, molecular, and genetic responses of plants to multiple environmental stresses and their interactions. The reported recent advances in scientific approaches, research ideas, and cutting-edge tools will help to better understand how multiple environmental stresses affect crops and identify the best avenues for developing crops with improved climate resilience.

Author contributions

PR organized the Research Topic together with AV, PN, and MZ-A. AV and PN wrote the first draft of the editorial, and all coauthors edited the final version.

Acknowledgments

We would like to thank all authors for their excellent contributions, reviewers and other associate editors for their constructive comments and inputs to make this Research Topic successful.

Conflict of interest

The authors declare that the research was conducted in the absence of any commercial or financial relationships that could be construed as a potential conflict of interest.

Publisher's note

References

Ehrhardt, D. W., and Frommer, W. B. (2012). New technologies for 21st-century plant science. *Plant Cell.* 24, 374–394. doi: 10.1105/tpc.111.093302

Fuglie, K. (2021). Climate change upsets agriculture. *Nat. Clim. Change* 11, 294–295. doi: 10.1038/s41558-021-01017-6

Garg, R., Subudhi, P. K., Varshney, R. K., and Jain, M. (2023). Editorial: abiotic stress: molecular genetics and genomics, volume II. *Front. Plant Sci.* 13. doi: 10.3389/fpls.2022.1101139

Pascual, L. S., Segarra-Medina, C., Gómez-Cadenas, A., López-Climent, M. F., Vives-Peris, V., and Zandalinas, S. I. (2022). Climate change-associated multifactorial stress combination: a present challenge for our ecosystems. *J. Plant Physiol.*, 153764. doi: 10.1016/j.jplph.2022.153764

Yuan, Z., Chen, Y., Palta, J. A., and Prasad, P. V. (2019). Adaptation of dryland plants to a changing environment. *Front. Plant Sci.* 10, 1228. doi: 10.3389/fpls.2019.01228

Zandalinas, S. I., and Mittler, R. (2022). Plant responses to multifactorial stress combination. *New Phytol.* 234, 1161–1167. doi: 10.1111/nph.18087

frontiers | Frontiers in Plant Science

ORIGINAL RESEARCH
published: 03 May 2022
doi: 10.3389/fpls.2022.860111

Study on the Relationship of Ions (Na, K, Ca) Absorption and Distribution to Photosynthetic Response of *Salix matsudana* Koidz Under Salt Stress

*Xin Ran[1], Xiao Wang[1], Xiaoxi Huang[1], Changming Ma[1], Haiyong Liang[1] and Bingxiang Liu[1,2]**

[1] Department of Forest Cultivation, College of Forestry, Hebei Agricultural University, Baoding, China, [2] Hebei Urban Forest Health Technology Innovation Center, Baoding, China

OPEN ACCESS

Edited by:
Pasala Ratnakumar, Indian Institute of Oilseeds Research (ICAR), India

Reviewed by:
Salman Gulzar, University of Karachi, Pakistan
Abazar Ghorbani, University of Mohaghegh Ardabili, Iran
M. Iqbal R. Khan, Jamia Hamdard University, India

***Correspondence:**
Bingxiang Liu
proser211@126.com

Specialty section:
This article was submitted to Plant Abiotic Stress, a section of the journal Frontiers in Plant Science

Received: *22 January 2022*
Accepted: *28 March 2022*
Published: *03 May 2022*

Citation:
Ran X, Wang X, Huang X, Ma C, Liang H and Liu B (2022) Study on the Relationship of Ions (Na, K, Ca) Absorption and Distribution to Photosynthetic Response of Salix matsudana Koidz Under Salt Stress. Front. Plant Sci. 13:860111. doi: 10.3389/fpls.2022.860111

To identify the key indicators for salt tolerance evaluation of *Salix matsudana* Koidz, we explored the relationship of ion absorption and distribution with chlorophyll, fluorescence parameters (leaf performance index, maximum photochemical efficiency), and photosynthetic gas parameters (net photosynthetic rate, transpiration, stomatal conductance, intercellular carbon dioxide concentration) under salt stress. We established 4 treatment groups and one control group based on salinity levels of NaCl hydroponic solutions (171, 342, 513, and 684 mm). The Na^+/K^+, Na^+/Ca^{2+}, chlorophyll fluorescence, and photosynthetic parameters of leaves were measured on the 1st, 3rd, 5th, 8th, 11th, and 15th days to analyze the correlations of chlorophyll, chlorophyll fluorescence and photosynthetic parameters to the ion distribution ratio. The results showed that (1) The ratio of the dry weight of roots to leaves gradually increased with increasing salt concentration, whereas the water content of leaves and roots first increased and then decreased with increasing time. (2) The content of Na^+, Na^+/K^+, and Na^+/Ca^{2+} in roots and leaves increased with increasing salt stress concentration and treatment time, and the difference gradually narrowed. (3) Ca^{2+} was lost more than K^+ under salt stress, and Na^+/Ca^{2+} was more sensitive to the salt stress environment than Na^+/K^+. (4) Because the root system had a retention effect, both Na^+/K^+ and Na^+/Ca^{2+} in roots under different NaCl concentrations and different treatment times were higher than those in leaves, and Na^+/Ca^{2+} was much higher than Na^+/K^+ in roots. (5) Na^+/K^+ had a higher correlation with fluorescence parameters than Na^+/Ca^{2+}. Among them, Na^+/K^+ had a significantly negative correlation with the maximum photochemical efficiency, and the correlation coefficient R^2 was 0.8576. (6) Photosynthetic gas parameters had a higher correlation with Na^+/Ca^{2+} than with Na^+/K^+. Among them, significantly negative correlations were noted between Na^+/Ca^{2+} and Gs as well as between Na^+/Ca^{2+} and E under salt stress. The correlation between Na^+/Ca^{2+} and Gs was the highest with a correlation coefficient

of 0.9368. (7) Na^+/K^+ and Na^+/Ca^{2+} had no significant correlation with chlorophylls. Na^+/Ca^{2+} was selected as a key index to evaluate the salt tolerance of *S. matsudana* Koidz, and the results provided a reference for analyzing the relationship between ion transport and distribution for photosynthesis.

Keywords: chlorophyll content, fluorescence parameters, ion absorption and distribution, photosynthetic response, salt stress

INTRODUCTION

Soil salinization is one of the most severe environmental problems facing the world (Fang et al., 2021). It not only influences the normal growth and development of plants but also restricts the increase in yield and quality of agricultural products. There are approximately 2.6 million square kilometers of saline-alkali lands in China, which is equivalent to 1/4 of the country's total national territorial area (Guan et al., 2010). These lands are mainly extensively distributed in coastal and arid areas (Lu et al., 2021). The assessment of the salt tolerance of plants plays a crucial role in improving the application of plants in saline-alkali areas. At present, scholars' evaluation of plant salt tolerance mainly focuses on growth and development indicators, photosynthetic pigments, photosynthetic system characteristics, ion absorption, ion distribution and transportation indicators, and chlorophyll fluorescence parameters. Their research objects mainly cover some halophytes (Liu W. C. et al., 2013; Sun L. et al., 2021) and crops (Xu Y. et al., 2020; Dou et al., 2021), but few studies have focused on forest trees.

Most of the plants in the family Salicaceae resist salinization. *Salix matsudana* Koidz, an important economic and green tree species belonging to the family Salicaceae, features fast growth, waterlogging tolerance (Wang C. Y. et al., 2017) and easy propagation. It can grow well under saline-alkali, drought, waterlogging, and poor soil conditions. It also has the characteristics of wind prevention and sand fixation, so it is widely used for urban landscaping. *S. matsudana* Koidz has the strong ecological ability and mainly propagates through cottage with a very high survival rate (Liu et al., 2018), so it is difficult to be replaced by other tree species. For the above reasons, willows have received extensive attention from experts and scholars, and related research is being constantly deepened. At present, research on *S. matsudana* Koidz mainly focuses on germplasm resource screening (Yu et al., 2018), cultivation management (Ma et al., 2021), stress-resistant physiology, and genetic diversity (Zhang J. et al., 2021). Regarding stress resistance, studies have mainly focused on physiological characteristics under the conditions of plant diseases and insect pests (Zhang M. Y. et al., 2021), heavy metals (Yuan et al., 2019), moisture (Jiménez-Rodríguez et al., 2019), and salinity (Kumari et al., 2021). However, studies on the relationship of ion absorption and distribution to photosynthesis of roots and leaves under salt stress are rarely reported. It remains to be clarified whether the salt ion content and its ratio in *S. matsudana* leaves are the main factors affecting photosynthesis. What are the effects of sodium ions, sodium-potassium ratios, and sodium-to-calcium ratios, which are widely used in current research to evaluate plant salt tolerance, on the photosynthetic system? Which indicator has a greater impact on the photosynthetic system? Which index is more suitable for evaluating the effect of leaf ion distribution on the photosynthetic system? To clarify these problems, this study used *S. matsudana* as a representative plant to analyze the correlation between leaf salt ion content and its ratio and photosynthetic system to provide a theoretical reference for evaluating the salt tolerance of plants in saline-alkali areas.

MATERIALS AND METHODS

Plant Material and Salt Treatments

The test materials were collected from the germplasm resource nursery of Jinshatan Forest Farm in Huai'an County, Hebei Province. In 2020, annotinous branches of *S. matsudana* Koidz, which basically maintained the same strong growth vigor and were free of diseases and insect pests, were collected before germination in early spring and stored in the freezer at 0°C. On 26 June 2020, a water culture experiment was conducted in the artificial climate chamber of the west campus of Hebei Agricultural University (38°48′N, 115°25′E) of Baoding, Hebei Province. The temperature of the climate chamber was set to 28/25°C (light/dark), the LED cold light source maintained the light intensity at 1,000 $\mu mol \cdot m^{-2} \cdot {}^{-1}$, the photoperiod was 14/10 h (light/dark) and the relative humidity was 60%. Some studies have shown that PAR = 1,000 $\mu mol \cdot m^{-2} \cdot {}^{-1}$ is beneficial to determine the best photosynthetic system parameters (Liu T. et al., 2013; Zhu Y. X. et al., 2019). In addition, some scholars also set the PAR at 800–1,000 $\mu mol \cdot ; m^{-2} \cdot s^{-1}$ and the RH at 50–70% when setting up the experiment (Gerona et al., 2019; Zhu H. L. et al., 2019; Zhang et al., 2020; Liu et al., 2022; Ma et al., 2022). Therefore, we set the light intensity and relative humidity according to the previous research and the actual situation. The middle two-thirds of the selected branches were cut into 20 cm long cuttings. The uppermost bud was 0.5–1 cm from the top of the cuttings. The uppercut was a flat cut, and the lower cut was an oblique cut. The selection of branches refers to the method of Ran et al. (2021). On 15 July, when their growth reached the treatment requirement (the average root length was approximately 5 cm), seedlings with uniform growth potential and root systems were selected for stress treatment.

The test material was placed in a 55 cm × 38 cm × 15 cm (length × width × height) plastic box for hydroponic culture. When most scholars study the effects of salt stress on plants under hydroponic conditions, the salt concentration is mostly set between 100 and 700 mmol. We also converted the corresponding concentration into international units. For these

reasons, we decided to adopt such a salt concentration (Miranda-Apodaca et al., 2020; Roman et al., 2020; Gao et al., 2022; Gou et al., 2022; Ni et al., 2022). A 1/2 dilution of Hoagland's complete nutrient solution was used as the base to prepare hydroponic solutions with NaCl concentrations of 171, 342, 513, and 684 mmol, and 1/2 Hoagland's complete nutrient solution (pH = 7.2) was used as a control (CK). In brief, 1/2 Hoagland's complete nutrient solution includes: 30 mg $NaFeC1_0H_{12}N_2O_8{\cdot}3H_2O$, 472.5 mg $Ca(NO_3)_2{\cdot}_2O$, 15 mg $FeSO_4$, 303.5 mg K_2SO_4, 0.05 mg $CuSO_4$, 57.5 mg $NH_4H_2PO_4$, 2.13 mg $MnSO_4$, 246.5 mg $MgSO_4$, 2.86 mg H_3BO_3, 4.5 mg $Na_2B_4O_7{\cdot}10H_2O$, 0.22 mg $ZnSO_4$, and 0.02 mg $H_8MoN_2O_4$.

During the experiment, each treatment was repeated thrice, and 10 seedlings were directly placed in the solution with more than half of the height covered in the prepared solution. We changed the nutrient solution every 5 days during their growth. To prevent excessive accumulation of salt, we removed the seedlings and carefully rinsed off the residual salt from the roots with clean water before changing the nutrient solution. We randomly selected 3 seedlings with average growth vigor on the 1st, 3rd, 5th, 8th, 11th, and 15th days of the stress test for the determination of various growth physiological indices.

Growth Indicators

The ratio of the dry weight of roots and leaves and the water content of leaves and roots were determined by Li (2000). We took 3 weighing bottles (repeated thrice using the same procedure as described below), numbered them in turn and accurately weighed them. We selected the sample to be measured, immediately placed it into the above weighing bottle, closed the bottle cap tightly, and accurately weighed it. The weighing bottle was placed in an oven at 105°C for 15 min to kill the plant tissue cells and then baked at 80–90°C to a constant weight (it must be placed in a desiccator when weighing and weighed after cooling). Let the weight of the weighing bottle be W1, the weight of the weighing bottle and the sample be W2, and the weight of the weighing bottle and the dried sample be W3 (the above weight units are all g as described below). Then, the total water content of the plant tissue (%) can be calculated as follows. The value of the total water content of the plant tissue obtained by three repetitions was obtained, and the average value was further obtained.

$$W = [(W2-W3)/(W2-W1)]/3*100\% \quad (1)$$

$$\text{Root water content :Wroot} = [(W2root-W3root)/(W2root-W1)]/3*100\% \quad (2)$$

$$\text{Leave water content :Wleave} = [(W2leave-W3leave)/(W2leave-W1)]/3*100\% \quad (3)$$

$$\text{Root dry weirht : WDroot} = (W3root-W2root)/3 \quad (4)$$

$$\text{The leaf dry weight :WDleave} = (W3leave-W2leave)/3 \quad (5)$$

$$\text{The root dry weight/the leaf dry weight} = \text{WDroot/WDleave} \quad (6)$$

Ion Content, Absorption, and Transport in Roots and Leaves

The determination of ion content was performed according to the methods of Yang (2010) and Meng et al. (2020). The sample was first baked at 105°C for 30 min and then dried at 70–80°C to a constant weight. After it was ground into powder, the fixed mass was weighed. After 30 ml of deionized water was added, the sample was shaken well and placed in a boiling water bath for 2 h. After cooling, the sample was filtered and diluted to 50 ml. The Na^+, K^+, and Ca^{2+} contents were determined by the atomic absorption method. Zeenit 700P instrument of Analytik Jena Company in Germany was used for determination. The selective absorption and transport coefficients of X (K^+ and Ca^{2+}) ions in roots and leaves were calculated by referring to the methods of Yang et al. (2003) and Zhang et al. (2018). The following formula was used to calculate the selective absorption and transport coefficients of ions X (K^+ and Ca^{2+}) by roots and leaves, where ion absorption coefficient Eq. 7 and ion transport coefficient Eq. 8. In the formula, the K^+ content was 272 mg, and the Ca^{2+} content was 230 mg in the medium (culture broth).

$$SA_{X,Na} = \text{Root}([X]/[Na^+])/\text{Medium}([X]/[Na^+]) \quad (7)$$

$$ST_{X,Na} = \text{Leaf}([X]/[Na^+])/\text{Root}([X]/[Na^+]) \quad (8)$$

Measurements of Chlorophyll Content, Chlorophyll Fluorescence Parameters and Photosynthetic Parameters

Chlorophyll content was determined using the method proposed by Li (2000). The measurement of chlorophyll fluorescence parameters adopted the method of Ran et al. (2021). After the beginning of the stress test, three seedlings with average growth vigor were selected for each treatment to the determination of fluorescence parameters. Before the determination, leaves were subjected to dark adaptation for 15 min, and then the rapid chlorophyll fluorescence induction kinetic curve and related parameters were measured using a Pocket PEA plant efficiency analyzer (Hansatech, United Kingdom). The obtained OJIP curve was used to analyze the fast chlorophyll fluorescence induction curve data (Wang et al., 2004; Giorio and Sellami, 2021; Stefanov et al., 2021) (JIP-test), and related parameters were calculated. The initial fluorescence (Fo), maximum fluorescence (Fm), maximum photochemical efficiency (Fv/Fm) after dark adaptation, and performance index (PI_{ABS}) based on absorbed light energy were directly determined for leaves.

The photosynthetic parameters adopted the method of Ran et al. (2021). During the stress treatment, 3 seedlings with average growth vigor were selected for each treatment. After the 3 seedlings were subjected to normal lighting in the climate chamber for 3 h, the 3rd–5th fully expanded leaves of the

same position, size, and light receiving direction were selected from top to bottom to determine photosynthetic gas exchange parameters, such as stomatal conductance (Gs), intercellular CO_2 concentration (Ci), transpiration rate € and net photosynthetic rate (Pn), with the aid of a Li-6800 portable photosynthesizer (LI-COR of United States).

Experimental Design and Statistical Analysis

Microsoft Excel and Origin were used to fit the response curve data. The test data were calculated, processed, and plotted using Excel 2020 for the correlation evaluation and analysis of the ion absorption, distribution, and photosynthetic indices of *S. matsudana* Koidz seedlings. SPSS 18.0 data processing software was used for statistical analysis and the significance of the difference at the $p < 0.05$ level was tested based on the least significant difference (LSD).

RESULTS

Analysis of the Dry Weight Ratio and Water Content of Roots and Leaves Under Salt Stress

Under different concentrations of salt stress and different action times, the dry weight ratio of dry willow seedling roots to leaves and the degree of change in water content were different (**Figures 1A,B**). Intensified salt stress led to a gradual increase in the ratio of root to leaf dry weight. On the 1st day of stress, the water content of *S. matsudana* leaves was not significantly affected by salt stress; on the 3rd day, the water content of the leaves showed an increasing trend with increasing salt concentration. On the 5th day, the root water content showed an overall upward trend. Then, the root water content gradually decreased with increasing stress time and further aggravation of the stress.

Analysis of Selective Absorption and Transport Proportions of Na^+/K^+ and Na^+/Ca^{2+} in Roots and Leaves Under Salt Stress

Figures 1C,D shows that under stress by different concentrations of NaCl, the $SA_{k,\ Na}$ values of *S. matsudana* Koidz roots showed an overall downward trend as the treatment time increased. On the 1st day, the $SA_{k,\ Na}$ values of *S. matsudana* Koidz roots showed an overall upward trend with increasing NaCl concentration. After 3 days of stress, at each stress time, $SA_{k,\ Na}$ gradually decreased with increasing stress, and the difference between treatments was significant. In the first 3 days of stress, the $SA_{Ca,\ Na}$ values of roots showed a decreasing trend after increasing as the salt concentration increased. On the first day, the $SA_{Ca,\ Na}$ values under each treatment were always significantly higher than the $SA_{Ca,\ Na}$ values obtained under 171 mm NaCl treatment. Stresses at different concentrations of NaCl all caused the $SA_{Ca,\ Na}$ of *S. matsudana* Koidz roots to show an overall downward trend as the treatment time increased. In the first 5 days, the $ST_{k,\ Na}$ of leaves showed a decreasing trend after increasing as the degree of stress intensified, and the decrease was not significant. When the concentration of NaCl was greater than 342 mm, the $ST_{k,\ Na}$ of leaves gradually decreased as the treatment time increased. On the 1st day, as NaCl stress intensified, the $ST_{Ca,\ Na}$ values of leaves showed an increasing trend, and the difference was significant. In general, the $ST_{Ca,\ Na}$ values of leaves under different salt concentrations gradually decreased as the treatment time increased, and the difference was significant.

Correlation Analysis of Leaf Na^+/K^+ and Na^+/Ca^{2+} Under Salt Stress

With the increase in NaCl treatment days, the Na^+/K^+ of roots and leaves showed an increasing trend, and the increasing rate increased faster than that noted before the 5th day after treatment (**Figure 2A**). In particular, 684 mm NaCl increased with increasing treatment days. In addition, when the NaCl treatment time was the same, the Na^+/K^+ of roots and leaves increased with increasing NaCl stress, and the Na^+/K^+ of roots was greater than that of leaves. With the extension of NaCl treatment time, the Na^+/Ca^{2+} in roots and leaves also showed a gradual upward trend (**Figure 2B**). Under the same NaCl treatment time, Na^+/Ca^{2+} also increased with increasing NaCl stress concentration. Under the same concentration of NaCl, the Na^+/Ca^{2+} levels of the root system were greater than that of the leaves. When NaCl is greater than 342 mm, as the concentration of NaCl increases, Na^+/Ca^{2+} increases sharply. When NaCl is less than 342 mm, Na^+/Ca^{2+} rises slowly in roots and leaves. In the first 8 days, the Na^+ content in roots was higher than that in leaves at the same time (**Figure 2C**). **Figure 2D** shows that after NaCl stress treatment, Na^+/K^+ and Na^+/Ca^{2+} in leaves showed a linear correlation Eq. 9 ($R^2 = 0.9862$). **Figure 2E** shows that the correlation equation of Na^+ content in roots and leaves under salt stress is Eq. 10 ($R^2 = 0.9594$).

$$y = 0.1407x^{1.1314} \quad (9)$$

$$y = -0.0011x^3 + 0.1129x^2 - 2.1363x^1 + 14.867 \quad (10)$$

Analysis of the Correlation of Chlorophyll and Leaf Ions of *Salix matsudana* Koidz Under Salt Stress

With the increase in Na^+/Ca^{2+} caused by NaCl stress, the chlorophyll content decreased significantly. A negative linear correlation was noted between Na^+/Ca^{2+} and chlorophyll content under NaCl stress (**Figure 3A**). The fitted curve was Eq. 11 ($R^2 = 0.7615$). Na^+/K^+ increased and chlorophyll decreased under salt stress. The correlation between Na^+/K^+ and chlorophyll content under salt stress was a negative exponential, and the correlation equation was Eq. 12 ($R^2 = 0.7633$). In addition, Na^+/K^+ were negatively correlated with chlorophyll content. With the increase in salt stress, Na^+ continued to accumulate, and Ca^{2+} and K^+ were gradually displaced, resulting in a significant increase in Na^+, Na^+/Ca^{2+}, and Na^+/K^+ and a

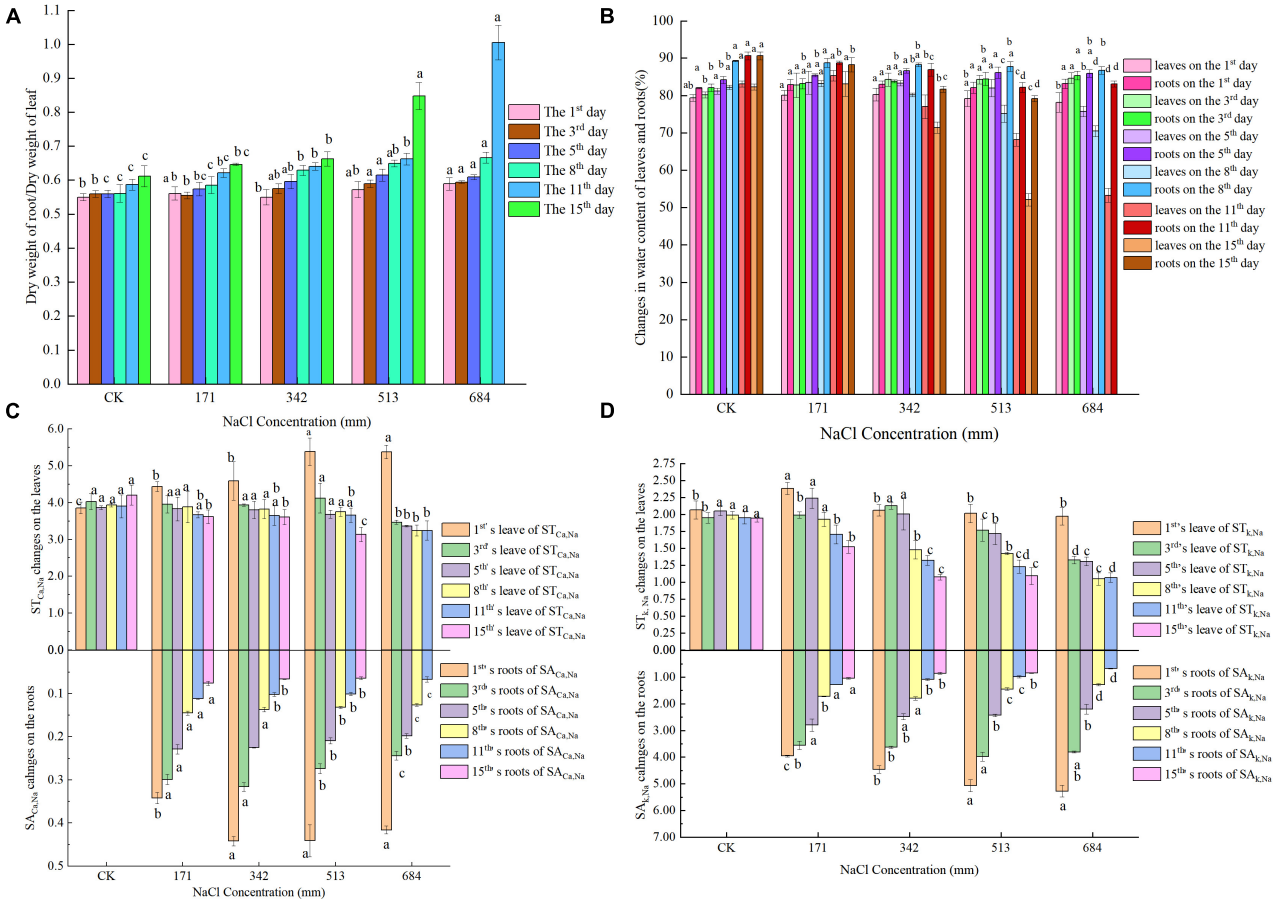

FIGURE 1 | Effects of salt stress on ratio of dry weight and water content of roots and leaves, ratio of selective absorption and transport of Na^+/K^+ and Na^+/Ca^{2+} in roots and leaves; **(A)** effects of salt stress on ratio of roots and leaves dry weight of *S. matsudana*; **(B)** effects of salt stress on water content of roots and leaves of *S. matsulosa* **(C)** effects of salt stress on selective uptake and transportation of Ca^{2+} in roots and leaves of *S. matsudana*; **(D)** effects of salt stress on selective uptake and transportation of K^+ in roots and leaves of *S. matsudana*. Data shown are means ± SEM. Different small letters indicate significant differences between treatments at 0.05 level among treatment.

decrease in chlorophyll content. **Figure 3D** shows the correlation equation between Na^+ content and chlorophyll content in leaves as Eq. 13 ($R^2 = 0.7209$).

$$y = -0.0018x^2 - 0.0963x^1 + 2.1742 \quad (11)$$

$$y = 0.0358x^2 - 0.4219x^1 + 2.10742 \quad (12)$$

$$y = 0.00004x^2 - 0.0284x^1 + 2.2157 \quad (13)$$

Analysis of the Correlation Between Leaf Fluorescence Parameters and Ions Under Salt Stress

Analysis of the Correlation Between the Leaf Performance Index PI_{ABS} and Ions Under Salt Stress

As shown in **Figure 3B**, Na^+/Ca^{2+} and PI_{ABS} are exponentially related (Eq. 14) ($R^2 = 0.8679$). Na^+/K^+ and PI_{ABS} are also exponentially related (Eq. 15) ($R^2 = 0.8464$). **Figure 3E** shows that the fitting curve of leaf Na^+ and PI_{ABS} is Eq. 16 ($R^2 = 0.8476$). As salt stress intensifies or time increases, Na^+/Ca^{2+} and Na^+/K^+ increase, and PI_{ABS} decreases significantly. Both Na^+/Ca^{2+} and Na^+/K^+ have a negative exponential relationship with PI_{ABS}. As the ion concentration ratio increases, PI_{ABS} continues to decrease. The degree of correlation between Na^+/Ca^{2+} and PI_{ABS} is greater than that between Na^+/K^+ and PI_{ABS}.

$$y = 5.3524e^{-0.087x} \quad (14)$$

$$y = 4.8635e^{-0.349x} \quad (15)$$

$$y = 0.0002x^2 - 0.116x^1 + 5.4883 \quad (16)$$

Analysis of the Correlation Between Leaf Maximum Photochemical Efficiency and Ions Under Salt Stress

Studies have confirmed that Fv/Fm can indicate the response of plants to stress environments (Zhang et al., 2009), so its decline is an important indicator of plants being inhibited by

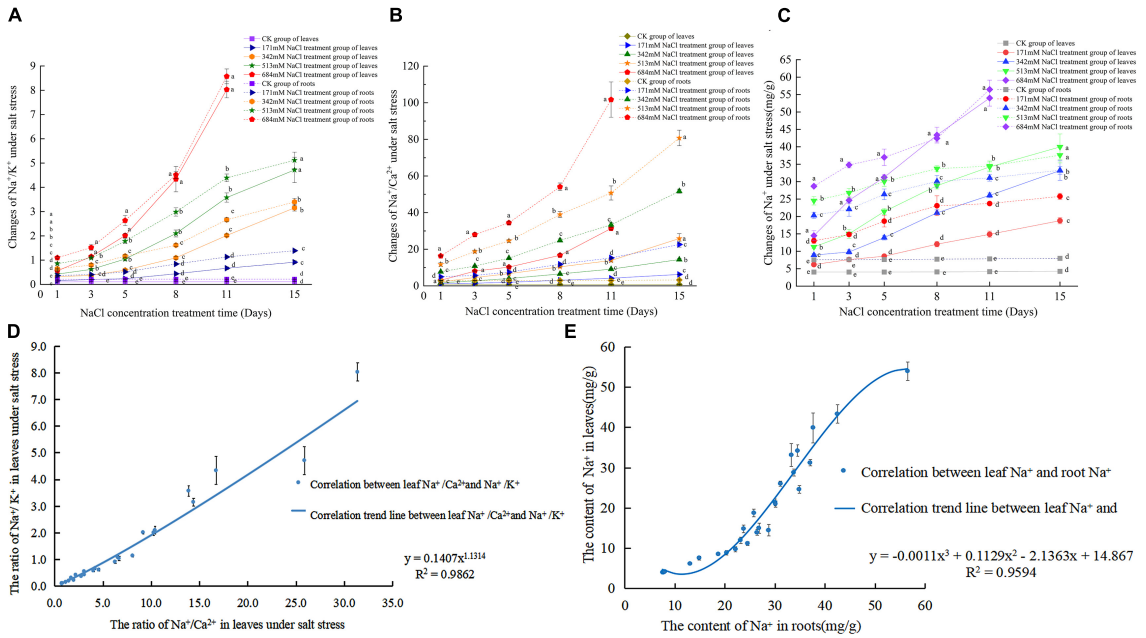

FIGURE 2 | Changes and correlation of Na^+,Na^+/ K^+ and Na^+/ Ca^{2+} in roots and leaves of *S. matsudana* under salt stress; **(A)** changes of Na^+/ K^+ in roots and leaves under salt stress; **(B)** changes of Na^+/ Ca^{2+} in roots and leaves under salt stress; **(C)** changes of Na^+ in roots and leaves under salt stress; **(D)** correlation between Na^+/ K^+ and Na^+/ Ca^{2+} in leaves under salt stress; **(E)** correlation between Na^+ in leaves and roots under salt stress.

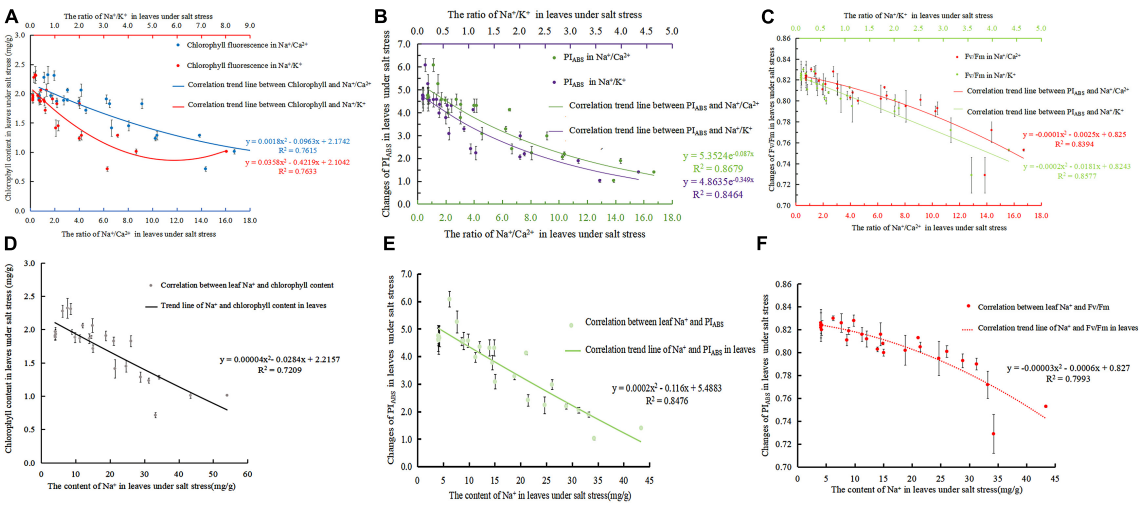

FIGURE 3 | The ion ratio of salt stress to leaves was correlated with chlorophyll and fluorescence parameters; **(A)** correlation of Na^+/ Ca^{2+} and Na^+/ K^+ to chlorophyll content in the leaves of *S. matsudana* under salt stress; **(B)** correlation between Na^+/Ca^{2+}, Na^+/ K^+, and PI_{ABS} in the leaves of *S. matsudana* under salt stress; **(C)** correlation of Na^+/Ca^{2+} and Na^+/K^+ in the leaves of *Salix matsudana* with Fv/Fm under salt stress; **(D)** correlation between Na^+ and chlorophyll content in *S. matsulosa* leaves under salt stress; **(E)** correlation between Na^+ and PI_{ABS} in *S. matsulosa* leaves under salt stress; **(F)** correlation between Na^+ and Fv/Fm in *S. matsulosa* leaves under salt stress.

light. As shown in **Figure 3C**, the fitting relationship curves of Na^+/Ca^{2+} and Na^+/K^+ with Fv/Fm under salt stress are Eq. 17 (R^2 = 0.8394) and Eq. 18 (R^2 = 0.8577). **Figure 3F** shows that the fitting equation of Na^+ content and Fv/Fm in leaves was Eq. 19 (R^2 = 0.7993). As the NaCl concentration intensifies or the time increases, both Na^+/Ca^{2+} and Na^+/K^+ are linearly negatively correlated with the maximum photochemical efficiency Fv/Fm. With the increase in salt stress, Fv/Fm will be irreversibly damaged.

$$y = -0.0001x^2 - 0.0025x^1 + 0.825 \quad (17)$$

$$y = -0.0002x^2 - 0.0181x^1 + 0.8243 \quad (18)$$

$$y = -0.00003x^2 - 0.0006x^1 + 0.827 \quad (19)$$

Analysis of the Correlation Between Photosynthetic Gas Parameters and Ions in Leaves Under Salt Stress

Analysis of the Correlation Between Leaf Net Photosynthetic Rate and Ions Under Salt Stress

Photosynthetic rate is an important parameter to measure the strength of plant photosynthesis that is a direct reflection of the function of the photosynthetic system and a key indicator of whether the plant's photosynthetic system is normal. Under salt stress, Na^+/Ca^{2+}, Na^+/K^+, and Pn showed exponential negative correlations (**Figure 4A**), and the correlations reached R^2 = 0.8369 (Eq. 20) and R^2 = 0.8722 (Eq. 21). **Figure 4E** shows that the fitting equation of Na^+ content and Pn in leaves was Eq. 22 (R^2 = 0.8308). As salt stress intensified, Na^+/Ca^{2+}, and Na^+/K^+ increased, whereas Pn decreased. Na^+/Ca^{2+} and Na^+/K^+ in leaves can reflect the changes in the photosynthetic capacity of leaves and reveal the reason for the reduction in the photosynthetic rate to a certain extent.

$$y = 13.85e^{-0.118x} \quad (20)$$

$$y = 12.351e^{-0.49x} \quad (21)$$

$$y = 0.0008x^2 - 0.335x^1 + 13.747 \quad (22)$$

Analysis of the Correlation Between Leaf Transpiration E and Ions Under Salt Stress

As shown in **Figures 4B,E** decreases significantly with increasing Na^+/Ca^{2+} concentration. Na^+/Ca^{2+} and E have a negative correlation, and the fitted relationship curve is Eq. 23 (R^2 = 0.9255). Na^+/K^+ increased with increasing NaCl stress, whereas E showed a downward trend. The correlation between Na^+/K^+ and E is exponential, and the correlation equation is Eq. 24 (R^2 = 0.9095). The correlation equation between Na^+ content and E in leaves from **Figure 4F** was Eq. 25 (R^2 = 0.9059).

$$y = 0.0189x^2 - 0.6017x^1 + 5.9583 \quad (23)$$

$$y = 0.4567x^2 - 2.9467x^1 + 5.6716 \quad (24)$$

$$y = 7.1024e^{-0.047x} \quad (25)$$

Analysis of the Correlation Between Leaf Stomatal Conductance and Ions Under Salt Stress

Figure 4C shows that Na^+/Ca^{2+} and Gs have a negative logarithmic correlation under salt stress with the correlation reaching R^2 = 0.9368 (Eq. 26). Under salt stress, Na^+/K^+ and Gs have a negative logarithmic correlation with the correlation reaching R^2 = 0.9066 (Eq. 27). **Figure 4G** shows the correlation equation between Na^+ content and Gs in leaves under salt stress : Eq. 28 (R^2 = 0.915).

$$y = -35.53\ln(x^1) + 157.14 \quad (26)$$

$$y = -30.62\ln(x^1) + 96.097 \quad (27)$$

$$y = 0.0869x^2 - 6.6813x^1 + 190.47 \quad (28)$$

Analysis of the Correlation Between Intercellular Carbon Dioxide Concentration and Ions in Leaves Under Salt Stress

As salt stress intensifies, the continuous loss of Ca^{2+} leads to an increase in the ratio of Na^+/Ca^{2+}. Photosynthesis is subsequently affected, and Ci decreases accordingly (**Figure 4D**). Under salt stress, Na^+/Ca^{2+} and Ci show a negative correlation relationship, and the fitted relationship curve is Eq. 29 (R^2 = 0.7454). As shown in **Figure 4D**, under NaCl stress, the ratio of Na^+/K^+ increased continuously, and Ci decreased accordingly. At the initial stage of salt stress, when the ratio of Na^+/K^+ is less than 1, Ci is at a higher level. Then, as the ratio of Na^+/K^+ increases, Ci gradually decreases. Under salt stress, Na^+/K^+ and Ci show a negative logarithmic relationship, and the fitted relationship curve is Eq. 30 (R^2 = 0.7661). **Figure 4H** shows that the correlation equation between Na^+ content and Ci in leaves under salt stress was Eq. 31 (R^2 = 0.7129).

$$y = 0.127x^2 - 4.5119x^1 + 300.5 \quad (29)$$

$$y = 4.0011x^2 - 25.094x^1 + 299.34 \quad (30)$$

$$y = 0.0194x^2 - 1.8653x^1 + 306.08 \quad (31)$$

DISCUSSION

Relationship Between Na^+ in Roots and Leaves and Na^+/K^+ and Na^+/Ca^{2+} in Leaves Under Salt Stress

The damage of salt stress to plants starts from the root system, and the cell membrane is the initial location of salt stress (Meng et al., 1996). The cell plasma membrane is first damaged by saline ions, leading to the continuous exosmosis of mineral ions, such as P^+, Mg^{2+}, K^+, and Ca^{2+}, in the cell; the entry of external saline ions, such as Na^+ and Cl^-, into the cell; disturbed physiological function of the cell membrane, affected transport of Na^+, K^+, and Ca^{2+} to the ground; changes in ion content in the leaves and irreversible damage to the corresponding functions of leaves (Zhou et al., 2021). Therefore, their water content suggests that the ability of roots and leaves to hold water is threatened. The ratio of root to leaf dry weight was also changed because growth was inhibited by salt stress. The change in the ion distribution law mirrors the damage extent of adverse environments to cells, and plants maintain the balance of nutrition by enhancing the absorption and transport of ions, which also reflects to a certain extent the ability of plants to resist stress. Therefore, the changes in Na^+/K^+ and Na^+/Ca^{2+} can represent the degree of plant damage and the change in nutrient balance in plants.

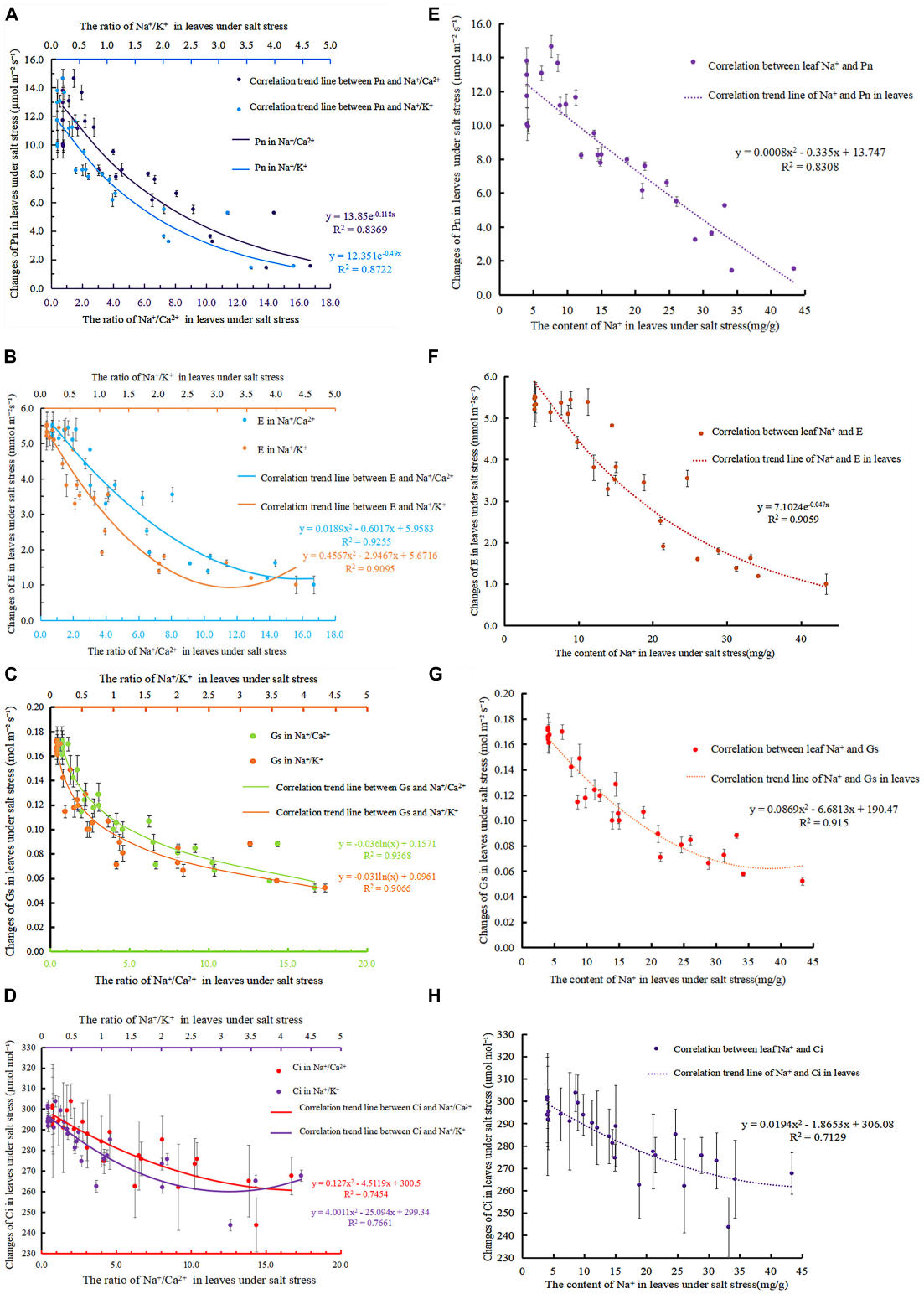

FIGURE 4 | Correlation between photosynthetic gas parameters and ions in leaves under salt stress; **(A)** correlation of Na^+/ Ca^{2+} and Na^+/ K^+ in the leaves of *S. matsudana* to Pn under salt stress; **(B)** correlation of Na^+/ Ca^{2+} and Na^+/ K^+ in the leaves of *S. matsudana* to E under salt stress; **(C)** analysis of the correlation of Na^+/Ca^{2+} and Na^+/K^+ in the leaves of *S. matsudana* with Gs under salt stress; **(D)** correlation of Na^+/Ca^{2+} and Na^+/ K^+ in the leaves of *S. matsudana* to Ci under salt stress; **(E)** correlation of Na^+ and Pn in the leaves of *S. matsudana* under salt stress; **(F)** correlation of Na^+ in the leaves of *S. matsudana* to E under salt stress; **(G)** correlation of Na^+ in the leaves of *S. matsudana* with Gs under salt stress; **(H)** correlation of Na^+ in the leaves of *S. matsudana* with Ci under salt stress.

K^+ and Na^+ may compete for absorption sites on the cell membrane (Tyerman and Skerrett, 1998; Frans and Anna, 1999; Mark and Romola, 2003). Therefore, salt stress not only induces K^+ efflux from cells but also reduces K^+ absorption by cells. When the K^+ efflux increases but the influx decreases, the K^+ content in the cell will be greatly reduced, the Na^+/K^+ ratio in the cell will be changed, and the plant will be injured. Calcium is an essential mineral element for plants and participates in various reactions, including stress and biological stimuli, such as salt and drought (Kudla et al., 2010). In this experiment, the selective absorption capacity of roots for K^+ and Ca^{2+} at the initial stage of stress increased as the stress intensified; the selective absorption capacity of roots for different salt stress levels increased as the treatment time increased. This finding indicates that large amounts of Na^+ in the roots of the plant in the early stage result in a violent stress response of root cells. Then, root cells increase the selective absorption capacity of K^+ and Ca^{2+} and control the transport of ions toward the ground to sustain low cell osmotic potential and cell membrane stability. This phenomenon is also the reason why the Na^+ content in roots is greater than that in leaves.

Under the same salt concentration and the same treatment time, the selective absorption of K^+ by roots was stronger than that of Ca^{2+}, and the selective transport of Ca^{2+} by leaves was stronger than that of K^+. Under different treatment times, Na^+/K^+ and Na^+/Ca^{2+} levels in roots were greater than those in leaves, indicating that roots have a certain role in retaining Na^+ ions under salt stress and increasing the selective absorption and transportation of K^+ and Ca^{2+}. However, after reaching a certain degree of salt stress, the limited ability cannot offset the harm caused by ions. Once this ability is disrupted, the Na^+/K^+ and Na^+/Ca^{2+} of plant roots and leaves will increase significantly. Studies have shown that the increase in Ca^{2+} content in cells under salt stress can restrain the efflux of K^+ (Guo et al., 2015), thereby relieving the damage caused by salt stress to plants. The correlation of Na^+/K^+ and Na^+/Ca^{2+} in leaves reached 0.9614, indicating that K^+ and Ca^{2+} are closely related under salt stress. *S. matsudana* Koidz will adjust the root system's selective absorption of K^+ and Ca^{2+} from the soil and transport it to the leaves to minimize the adverse effects caused by the blocked absorption function. However, this ability has a certain limit, as too high a concentration of salt stress will directly destroy the ability of selective absorption and cause irreparable damage to plants.

Relationship Between Na^+/K^+ and Na^+/Ca^{2+} With Chlorophyll and Fluorescence Under Salt Stress

The more chlorophyll on the thylakoid membrane on plant leaves, the stronger the photosynthesis power of plants. This is the basic ability of plants to maintain life activities and the basis for judging the ability of plants to resist stress (Zhang et al., 2013; Wang et al., 2021). In other respects, photosynthesis also affects the accumulation of plant dry matter and final yield (Thakur and Kumar, 2021). Yang's experiment showed that damage to chloroplast membrane structure could be observed under salt stress (Yang et al., 2020). Studies have shown that the chlorophyll content in the leaves of Jerusalem artichoke (Sun W. J. et al., 2021) and oats (Li et al., 2021) decreases significantly under salt stress. Therefore, many researchers regard the chlorophyll content under salt stress as an important index to measure the salt tolerance of plants. In this study, the correlations between Na^+/K^+ and chlorophyll and between Na^+/Ca^{2+} and chlorophyll were 0.7633 and 0.7615, respectively. This finding indicates that the correlation between the ion concentration ratio and chlorophyll is very high under salt stress, but no remarkable difference was noted between them. The correlation between Na^+/K^+ and chlorophyll was greater than that between Na^+/Ca^{2+} and chlorophyll. This may be because Na^+ is flushed into the cells of salt-stressed plants, causing the accumulation of Na^+ and affecting the absorption of K^+ by plants. This process induces ion toxicity and results in a higher correlation between Na^+/K^+ and chlorophyll (Zhang et al., 2022).

Fluorescence parameters are often used to examine the relationship between the photosynthesis of plants and the environment where they live (Zhao et al., 2021). Researchers generally observe the photosynthetic physiological status of plants under salt stress by means of the OJIP curve, Fv/Fm and PI_{ABS}. The Fv/Fm and PI_{ABS} of PS II are important indices to evaluate whether plants are stressed. The more intense the stress, the lower the values of both and the greater the damage to plant photosynthetic capacity. Studies have shown that the ratio of Fv/Fm is stable under non-stress conditions, and the ratio decreases obviously when stress conditions exist in the environment (Zhao et al., 2021), which was demonstrated by salt stress experiments with mangosteen seedlings (Li et al., 2005; Shu et al., 2021). In this study, the correlation between Na^+/Ca^{2+} and PI_{ABS} (R^2 = 0.8679) was greater than that between Na^+/K^+ and PI_{ABS} (R^2 = 0.8464). The correlation between Na^+/K^+ and Fv/Fm (R^2 = 0.8577) was greater than that between Na^+/Ca^{2+} and Fv/Fm (R^2 = 0.8394). The correlation between Na^+/K^+ and Fv/Fm (R^2 = 0.8577) was the highest among these indices, indicating that the chlorophyll fluorescence kinetic parameters can also reflect the photoenergy utilization status of photosystem II (Yu and Guy, 2004; Zhao et al., 2006). Under salt stress, *S. matsudana* Koidz leaves exhibited photoinhibition, which resulted in a notable decrease in Fv/Fm efficiency. However, the change in chlorophyll was relatively slow, which might be due to the gradual increase in chlorophyll content under low salt stress to increase light energy utilization. Under high salt stress, the synthesis and decomposition of chlorophyll were affected. The decomposition process of chlorophyll lagged somewhat, so the correlation with ions was lower than other indicators.

Relationship of Na^+/K^+ and Na^+/Ca^{2+} in Leaves to Gas Exchange Parameters Under Salt Stress

Salt stress can affect the normal growth of plants by reducing the photosynthesis of plants, so photosynthetic parameters can be used as crucial indicators to judge the salt–alkali

tolerance of plants (Zhou et al., 2021). Photosynthetic parameters mainly include the net photosynthetic rate (Pn), transpiration rate (E), stomatal conductance (Gs), and intercellular CO_2 concentration (Ci). Gs and E exhibit a high correlation with Na^+/Ca^{2+} and Na^+/K^+, respectively, and Gs has the highest correlation with Na^+/Ca^{2+} (R^2 = 0.9368). Stomatal limitation is tightly related to the photosynthetic rate of plants under adverse stress (Yang et al., 2019). Normally, under mild stress, stomatal limitation is the dominant reason for the reduction in the plant photosynthetic rate (Sarabi et al., 2019). Studies have indicated that salt stress causes changes in plant osmotic potential, thereby affecting the plant transpiration rate (Cambridge et al., 2017; Wang L. H. et al., 2017). With increasing salt concentration, the Gs of *S. matsudana* Koidz leaves is affected by osmotic stress and thus decreases. Then, the stomatal resistance of the leaves increases. By inhibiting E to increase the water potential, the influence of salt stress is reduced, and finally, the loss of water is reduced to ensure the stability of photosynthesis. Therefore, this notion may explain the higher correlation between Gs and E and the ion concentration ratio.

As the main factor affecting photosynthesis, transpiration, and respiration, stomatal conductance affects the circulation of oxygen, carbon dioxide, and water in plants (Xu P. Y. et al., 2020; Yan et al., 2020). Studies have shown that the Gs of plant leaves is significantly reduced due to intensified salt stress (Mafakheri et al., 2010; Zhao et al., 2019). The change direction of Ci is not only one of the main reasons for determining the photosynthetic rate change but also an indispensable basis for judging whether it is a stomatal factor. The correlation between it and Na^+/Ca^{2+}, Na^+/K^+ is relatively low (R^2 = 0.7183, R^2 = 0.7229). This finding may be attributed to the notion that the factors affecting Ci include not only Gs but also the photosynthetic activity of mesophyll cells, mesophyll conductance and the CO_2 concentration in the air around leaves, which cause the response of Ci to lag behind other photosynthetic gas parameters.

In this experiment, the correlation between Na^+/Ca^{2+}, Na^+/K^+, and Pn was lower than their correlation with E, which is different from the results of previous studies. Although many studies believe that the Pn of leaves under salt stress is a more accurate indicator that can directly reflect plant salt tolerance, its correlation with the transport concentration ratio of leaf ions is lower than that between other photosynthetic gas parameters and the leaf ion transport concentration ratio. This finding indicates that although Pn and the leaf ion concentration ratio are highly related, there are still differences in the sensitivity of net photosynthetic parameters as an indicator for different types of plants.

CONCLUSION

By increasing the ratio of dry weight and water content of roots and leaves, *S. matsudana* could lessen the damage caused by salt stress to a certain extent, which was of significance to the survival of plants under adverse situations. Different salt conditions have different effects on the ratio of ion absorption and transport, photosynthetic parameters, and fluorescence parameters of *S. matsudana* Koidz. The ratio of ion content in leaves had different correlations with photosynthetic and fluorescence parameters. Some scholars think that it is impossible to judge the salt tolerance level of plants by using a certain indicator or a certain type of indicator and ignore the correlation of each indicator in the process of development. Therefore, it is very important to select and evaluate the key indicator that has a high correlation coefficient with salt tolerance for the appraisal of salt tolerance of plants.

In this experiment, the loss of Ca^{2+} in roots was more serious than the loss of K^+ under salt stress, and the selective transport of Ca^{2+} in leaves was stronger than that of K^+, resulting in higher Na^+/Ca^{2+} than Na^+/K^+ in roots and leaves, indicating that Na^+/Ca^{2+} is more responsive to salt stress than Na^+/K^+. Under salt stress, the leaf Na^+, Na^+/Ca^{2+}, and Na^+/K^+ contents, which are commonly used to evaluate the salt tolerance of plants, were compared with the above parameters. The correlation between leaf Na^+ content and these indices was lower than that of Na^+/Ca^{2+} and Na^+/K^+. The correlations of the measured parameters with Na^+/Ca^{2+} and Na^+/K^+ were examined when evaluating the salt tolerance of *S. matsudana* Koidz. Among the photosynthetic gas parameters, Gs and E were highly correlated with Na^+/Ca^{2+} and Na^+/K^+, and the correlation with Na^+/Ca^{2+} was the highest, indicating that the influence of Na^+/Ca^{2+} on photosynthetic parameters is more obvious than that of Na^+/K^+. Among all the parameters, the correlation between Ci of photosynthetic gas parameters and the two was the lowest followed by the correlation between Pn and Na^+/Ca^{2+}. The correlation of the chlorophyll fluorescence parameters PI_{ABS} and Fv/Fm to Na^+/K^+ was generally higher than that with Na^+/Ca^{2+}. The correlations of Na^+/K^+ and Na^+/Ca^{2+} with chlorophyll content were basically the same.

Overall, with increasing time and salt concentration, Na^+/Ca^{2+} in leaves showed dynamic accumulation changes, which ultimately affected the performance of the photosynthetic system, and the Gs and E of leaves were greatly affected. In addition, the correlation between Na^+/Ca^{2+} and photosynthesis and fluorescence indicators is generally high, and it has a greater impact on the photosynthetic system. The research results provide a basis for understanding the relationship between ion absorption and distribution, fluorescence and photosynthetic parameters of *S. matsudana* in a saline environment.

We chose indicators of sodium, sodium potassium, sodium calcium, which are often used by scholars to evaluate salt tolerance. Because magnesium is an indispensable element in the molecular structure of chlorophyll, the synthesis of chlorophyll is hindered when magnesium is deficient, which also affects photosynthesis. This has been confirmed by Li et al. (2020): In chloroplasts, Mg^{2+} is dependent on transport genes, resulting in a phenomenon of diurnal fluctuation, which regulates plant photosynthesis by affecting enzyme activity. Therefore, increasing the input of Mg^{2+} ions may be a potential method to improve the photosynthetic efficiency of plants. Iron is not only a component of cytochrome and non-heme ferritin in photosynthesis but also an important raw material for the synthesis of chlorophyll–protein complex in chloroplasts.

Focusing on the effects of iron ions,magnesium ions,the sodium-iron ratio, and the sodium-magnesium ratio on photosynthesis in future research will be more helpful to clarify the overall impact of salt stress ion allocation on the photosynthetic system.

DATA AVAILABILITY STATEMENT

The original contributions presented in the study are included in the article/**Supplementary Material**, further inquiries can be directed to the corresponding author/s.

AUTHOR CONTRIBUTIONS

XR and XW conceptualized the manuscript. XR, XW, CM, HL, BL, and XH made the data curation. XW, XR, and BL made formal analysis. HL and BL made funding acquisition. CM and BL made the methodology. BL and XW provided the resources and wrote the original draft. CM, HL, and BL wrote the review. All authors contributed to the article and approved the submitted version.

FUNDING

This work was supported by the Natural Science Foundation of Hebei Province (Grant Number 17226320D-4).

SUPPLEMENTARY MATERIAL

The Supplementary Material for this article can be found online at: https://www.frontiersin.org/articles/10.3389/fpls.2022.860111/full#supplementary-material

REFERENCES

Cambridge, M. L., Zavala, P. A., Cawthray, G. R., Mondonet, J., and Kendrick, G. A. (2017). Effects of high salinity from desalination brine on growth, photosynthesis, water relations and osmolyte concentrations of seagrass *Posidonia australis*. *Mar. Pollut. Bull.* 115, 252–260. doi: 10.1016/j.marpolbul.2016.11.066

Dou, X. T., Wang, Y. J., Wang, H. Z., and Yu, J. Y. (2021). Physiological response and tolerance different of two wheat varieties to NaCl stress. *Acta Ecol. Sin.* 41, 1–17. doi: 10.5846/stxb202005251330

Fang, X., Li, W., Yuan, H. T., Chen, H. W., Bo, C., Ma, Q., et al. (2021). Mutation of ZmWRKY86 confers enhanced salt stress tolerance in maize. *Plant Physiol. Biochem.* 167, 840–850. doi: 10.1016/j.plaphy.2021.09.010

Frans, J. M., and Anna, A. (1999). K+ Nutrition and Na+ Toxicity: the basis of cellular K+ /Na+ Ratios. *Ann. Bot.* 84, 123–133. doi: 10.1006/anbo.1999.0912

Gao, Z. Q., Zhang, J. Y., Zhang, J., Zhang, W. X., Zheng, L. L., Tebuqin, B., et al. (2022). Nitric oxide alleviates salt-induced stress damage by regulating the ascorbate–glutathione cycle and Na+/K+ homeostasis in *Nitraria* tangutorum Bobr. *Plant Physiol. Biochem.* 173, 46–58. doi: 10.1016/j.plaphy.2022.01.017

Gerona, M. E. B., Deocampo, M. P., Egdane, J. A., Ismail, A. M., and Dionisio-Sese, M. L. (2019). Physiological responses of contrasting rice genotypes to salt stress at reproductive stage. *Rice Sci.* 26, 207–219. doi: 10.1016/j.rsci.2019.05.001

Giorio, P., and Sellami, M. H. (2021). Polyphasic OKJIP chlorophyll a fluorescence transient in a landrace and a commercial cultivar of sweet pepper (*Capsicum annuum* L.) under long-term salt stress. *Plants.* 10, 1–15. doi: 10.3390/plants10050887

Gou, T., Su, Y., Han, R., Jia, J. H., Zhu, Y. X., Huo, H. Q., et al. (2022). Silicon delays salt stress-induced senescence by increasing cytokinin synthesis in tomato. *Sci. Hortic.* 293:110750. doi: 10.1016/j.scienta.2021.110750

Guan, Z. Y., Chen, S. M., Wang, Y. Y., and Chen, F. D. (2010). Screening of salt-tolerance concentration and comparison of salt-tolerance for *chrysanthemum* and its related taxa. *Chin. J. Ecol.*. 29, 467–472. doi: 10.13292/j.1000-4890.2010.0089

Guo, R., Yang, Z., Li, F., Yan, C., Zhong, X., Liu, Q., et al. (2015). Comparative metabolic responses and adaptive strategies of wheat (*Triticum aestivum*) to salt and alkali stress. *BMC Plant Biol.* 15:170. doi: 10.1186/s12870-015-0546-x

Jiménez-Rodríguez, C. D., Coenders-Gerrits, M., Uhlenbrook, S., and Wenninger, J. (2019). What Do Plants Leave after Summer on the Ground?—The effect of afforested plants in arid environments. *Water* 11:2559. doi: 10.3390/w11122559

Kudla, J., Batistic, O., and Hashimoto, K. (2010). Calcium signals: the lead currency of plant information processing. *Plant Cell.* 22, 541–563. doi: 10.1105/tpc.109.072686

Kumari, P., Gupta, A., Chandra, H., Singh, P., and Yadav, S. (2021). "). effects of salt stress on the morphology, anatomy, and gene expression of crop plants," in *Physiology of Salt Stress in Plants*, eds P. Singh, M. Singh, R. K. Singh, and S. M. Prasad (Hobokin, NJ: John Wiley & Sons, Ltd), 87–105. doi: 10.1002/9781119700517.ch6

Li, H. S. (2000). *Principles and Techniques of Plant Physiological and Biochemical Experiments*. Beijing: Higher Education Press, 134–137.

Li, J., Yokosho, K., Liu, S., Cao, H. R., Yamaji, N. K., Zhu, X. G., et al. (2020). Diel magnesium fluctuations in chloroplasts contribute to photosynthesis in rice. *Nat. Plants.* 6, 848–859. doi: 10.1038/s41477-020-0686-3

Li, X. Z., Peng, F., Xu, Y. C., and Hao, R. M. (2005). Diurnal variation of leaf gas exchange in *Cyclobalanopsis* multinervis and *Michelia foveolata* seedlings under different shadings. *J. Zhejiang Univ.* 4, 380–384. doi: 10.3969/j.issn.2095-0756.2005.04.005

Li, Y., Zheng, D. F., Feng, N. J., Feng, S. J., Yu, M. L., Huang, L., et al. (2021). Effects of prohexadione-calcium on growth and resistance physiology of rice seedlings under salt stress. *Plant Physiol. J.* 57, 1897–1906. doi: 10.13592/j.cnki.ppj.2021.0276

Liu, J. X., Gu, L., Yu, Y. C., Ju, G. S., and Sun, Z. Y. (2018). Stem photosynthesis of twig and its contribution to new organ development in cutting seedlings of *Salix* Matsudana Koidz. *Forests.* 9:207. doi: 10.3390/f9040207

Liu, T., Cui, H. J., Wu, S. J., Zhu, J. Y., and Zhou, Z. Q. (2013). Response of photosynthetic and fluorescence characteristics of Japanese yew seedlings to different light conditions. *J. Beijing For. Univ.* 35, 65–70. doi: 10.13332/j.1000-1522.2013.03.018

Liu, W. C., Zheng, C. F., Chen, C., Peng, Y. Q., Zeng, G. Q., Ji, D. W., et al. (2013). Physiological responses of *Salicornia bigelovii* to salt stress during the flowering stage. *Acta Ecol. Sin.* 33, 5184–5193. doi: 10.5846/stxb201205250778

Liu, Y., Wang, L., Li, X., and Luo, M. (2022). Detailed sphingolipid profile responded to salt stress in cotton root and the GhIPCS1 is involved in the regulation of plant salt tolerance. *Plant Sci.* 316:111174. doi: 10.1016/j.plantsci.2021.111174

Lu, Q., Yang, L., Wang, H., Yuan, J. Q., and Fu, X. X. (2021). Calcium Ion Richness in *Cornus hongkongensis* subs elegans (WP Fang et YT Hsieh) QY Xiang Could Enhance Its salinity tolerance. *Forests.* 12:1522. doi: 10.3390/f12111522

Ma, S. G., Zhou, X. P., Jahan, M. S., Guo, S. R., Tian, M. M., Zhou, R. R., et al. (2022). Putrescine regulates stomatal opening of cucumber leaves under salt stress via the H2O2-mediated signaling pathway. *Plant Physiol. Biochem.* 170, 87–97. doi: 10.1016/j.plaphy.2021.11.028

Ma, X. D., Pang, Z., Wu, J. Y., Zhang, G. F., Dai, Y. C., Kan, H. M., et al. (2021). Seasonal pattern of stem radial growth of Salix matsudana and its response to climatic and soil factors in a semi-arid area of North China. *Glob. Ecol. Conserv.* 28:e01701. doi: 10.1016/j.gecco.2021.e01701

Mafakheri, A., Siosemardeh, A., Bahramnejad, B., Struik, P. C., and Sohrabi, Y. (2010). Effect of drought stress on yield, proline and chlorophyll contents in

three chickpea cultivars. *Aust. J. Crop Sci.* 4, 580–585. doi: 10.3316/informit.857341254680658

Mark, T., and Romola, D. (2003). Na+ Tolerance and Na+ Transport in higher plants. *Ann. Bot.* 91, 503–527. doi: 10.1093/aob/mcg058

Meng, N., Huang, J. H., Jia, R., Wei, M., and Wei, S. H. (2020). Effect of chloride channel blockerson lon absorption, transport and content of glycine max seedlings under NaCI induced stress. *Acta Agriculturae Boreali-occidentalis Sin.* 29, 1814–1821. doi: 10.7606/ji.ssn.1004-1389.2020.12.006

Meng, Q., Zhao, S. J., Xu, C. C., and Zou, Q. (1996). Photoinhibition of photosynthesis and protective effect of photorespiration in winter wheat leaves under field conditions. *Acta Agron. Sin.* 22, 470–475. doi: 10.3321/j.issn:0496-3490.1996.04.014

Miranda-Apodaca, J., Agirresarobe, A., Martínez-Goñi, X. S., Yoldi-Achalandabaso, A., and Pérez-López, U. (2020). N metabolism performance in *Chenopodium quinoa* subjected to drought or salt stress conditions. *Plant Physiol. Biochem.* 155, 725–734. doi: 10.1016/j.plaphy.2020.08.007

Ni, L. J., Wang, Z. Q., Liu, X. D., Wu, S. T., Hua, J. F., Liu, L. Q., et al. (2022). Genome-wide study of the GRAS gene family in *Hibiscus* hamabo Sieb. et Zucc and analysis of HhGRAS14-induced drought and salt stress tolerance in *Arabidopsis*. *Plant Sci.* 319:111260. doi: 10.1016/j.plantsci.2022.111260

Ran, X., Wang, X., Gao, X. K., Liang, H. Y., Liu, B. X., and Huang, X. X. (2021). Effects of salt stress on the photosynthetic physiology and mineral ion absorption and distribution in white willow (*Salix alba* L.). *PLoS One.* 16:e0260086. doi: 10.1371/journal.pone.0260086

Roman, V. J., den, T. L. A., Gamiz, C. C., Van der, P. N., Visser, R. G. F., Van, E. N. L., et al. (2020). Differential responses to salt stress in ion dynamics, growth and seed yield of European *quinoa* varieties. *Environ. Exp. Bot.* 177:104146. doi: 10.1016/j.envexpbot.2020.104146

Sarabi, B., Fresneau, C., Ghaderi, N., Bolandnazar, S., Streb, P., Badeck, F. W., et al. (2019). Stomatal and non-stomatal limitations are responsible in down-regulation of photosynthesis in melon plants grown under the saline condition: application of carbon isotope discrimination as a reliable proxy. *Plant Physiol. Biochem.* 141, 1–19. doi: 10.1016/j.plaphy.2019.05.010

Shu, J., Liu, S. H., Zhang, A. H., Wang, J. Q., and Lian, X. Y. (2021). Effects of NaCl stress on photosynthetic characteristicsosynthetic c fluorescence and osmotic adjustment substances of cherry seedlings in greenhouse. *J. Shanxi Agric. Sci.* 49, 834–838. doi: 10.3969/j.issn.1002-2481.2021.07.08

Stefanov, M. A., Rashkov, G. D., Yotsova, E. K., Borisova, P. B., Dobrikova, A. G., and Apostolova, E. L. (2021). Different Sensitivity Levels of the Photosynthetic Apparatus in *Zea mays* L.and *Sorghum bicolor* L. under Salt Stress. *Plants (Basel, Switzerland).* 10:1469. doi: 10.3390/plants10071469

Sun, L., Chen, C. L., Zhong, Z. H., Yang, J. C., Liu, K., Lan, X. Y., et al. (2021). Effects of brown algae oligosaccharides on seed germination and salt-resistance of *Suaeda* heteroptera. *Mol. Plant Breed.* 19, 1–11.

Sun, W. J., Jiang, X. H., Fu, Y. Y., Shen, X. J., Gao, Y., and Wang, X. P. (2021). The effects of salt stress on chlorophyll fluorescence of cotton seedling leaves. *J. Irrig. Drain.* 40, 23–28. doi: 10.13522/j.cnki.ggps.2020480

Thakur, M., and Kumar, R. (2021). Light conditions and mulch modulates the damask rose (*Rosa damascena* Mill.) yield, quality, and soil environment under mid hill conditions of the western himalaya. *Ind. Crops Prod.* 163:113317. doi: 10.1016/j.indcrop.2021.113317

Tyerman, S. D., and Skerrett, I. M. (1998). Root ion channels and salinity. *Sci. Hortic.* 78, 175–235. doi: 10.1016/S0304-4238(98)00194-0

Wang, B. L., Xu, M., Shi, Q. H., and Cao, J. S. (2004). Effects of high temperature stress on antioxidant systems, chlorophyll and chlorophyii fluorescence parameters in early caulflower leaves. *Sci. Agric. Sin.* 8, 1245–1250. doi: 10.3321/j.issn:0578-1752.2004.08.029

Wang, C. Y., Xie, Y. Z., He, Y. Y., Li, X. X., Yang, W. H., and Li, C. X. (2017). Growth and Physiological Adaptation of *Salix* matsudana koidz. to periodic submergence in the hydro-fluctuation zone of the three gorges dam reservoir of China. *Forests* 8:283. doi: 10.3390/f8080283

Wang, L. H., Li, G. L., Li, J., Zuo, S. Y., Cao, X. B., Tong, H. Y., et al. (2017). Effect of exogenous sugar on the sugar metabolism in triticale seedling under salt stress. *J. Triticeae Crops* 37, 548–553. doi: 10.7606/j.issn.1009-1041.2017.04.17

Wang, Y., Yu, L. H., Zhao, H. J., Liu, Y., and Geng, G. (2021). The effects of NaCl stress on growth and photosynthesis of sugarbeet at different growth stages. *Crop.* 4, 99–104. doi: 10.16035/j.issn.1001-7283.2021.04.015

Xu, P. Y., Wu, Y. X., and He, T. M. (2020). Research progress on adaptation mechanism of plants to salinech prog stress. *China wild plant Resour.* 39, 41–49. doi: 10.3969/j.issn.1006-9690.2020.10.007

Xu, Y., Zhang, G. C., Ding, H., Ci, D. W., Qin, F. F., Zhang, Z. M., et al. (2020). Effects of salt and drought stresses on rhizosphere soil bacterial community structure and peanut yield. *Chin. J. Appl. Ecol.* 31, 1305–1313. doi: 10.13287/j.1001-9332.202004.036

Yan, Y. Q., Ji, S. X., Wang, H., Zhao, Y., Fan, Q. W., and Wang, X. (2020). Effect of exogenous ALA on photosynthesis of *Nitraria sibirica* Pall. during salt stress. *J. Northeast Agric. Univ.* 51, 32–38. doi: 10.3969/j.issn.1005-9369.2020.08.005

Yang, H., Shukla, M. K., Mao, X. M., Kang, S. Z., and Du, T. (2019). Interactive regimes of reduced irrigation and salt stress depressed tomato water use efficiency at leaf and plant scales by affecting leaf physiology and stem sap flow. *Front. Plant Sci.* 10:160. doi: 10.3389/fpls.2019.00160

Yang, S. (2010). Study on selection and evaluation criteria of salinity-tolerance tree species in coastal region. [master's thesis]. [Beijing]. *Chin. Acad. For.* 5, 14–19.

Yang, W. J., Wang, F., Liu, L. N., and Sui, N. (2020). Responses of membranes and the photosynthetic apparatus to salt stress in cyanobacteria. *Front. Plant Sci.* 11:713. doi: 10.3389/fpls.2020.00713

Yang, X. Y., Zhang, W. H., Wang, Q. Y., and Liu, Y. L. (2003). Salt tolerance of wild soybeans in Jiangsu and its relation with ionic distribution and selective transportation. *Chin. J. Appl. Ecol.* 12, 2237–2240.

Yu, F. Y., and Guy, R. D. (2004). Variable chlorophyll fluorescence in response to water plus heat stress treatments in three coniferous tree seedlings. *J. For. Res.* 15, 24–28. doi: 10.1007/BF02858005

Yu, Z. X., Qin, G. H., Song, Y. M., Qia, Y. L., Jiang, Y. Z., and Wang, H. T. (2018). Collection and genetic diversity analysis of wild germplasm in *Salix* matsudana. *J. Beijing For. Univ.* 40, 67–76. doi: 10.13332/j.1000-1522.20170330

Yuan, L. H., Wan, P. W., Li, Q., Wang, Y., Guan, X., Wu, X. Q., et al. (2019). Accumulation characteristics of Zn and Cu in cuttings of *Salix* matsudana Koidz under hydroponic eutrophication condition. *Chin. J. Appl. Environ. Biol.* 25, 491–500. doi: 10.19675/j.cnki.1006-687x.2018.12047

Zhang, G. C., Dai, L. X., Ding, H., Ci, D. W., Ning, T. Y., Yang, J. S., et al. (2020). Response and adaptation to the accumulation and distribution of photosynthetic product in peanut under salt stress. *J. Integr. Agric.* 19, 690–699. doi: 10.1016/S2095-3119(19)62608-0

Zhang, J., Shi, S. Z., Jiang, Y. N., Zhong, F., Liu, G. Y., Yu, C. M., et al. (2021). Genome-wide investigation of the AP2/ERF superfamily and their expression under salt stress in Chinese willow (*Salix* matsudana). *PeerJ.* 9:e11076. doi: 10.7717/peerj.11076

Zhang, L. Y., Wen, X., Lin, Y. M., Li, J., Chen, C., and Wu, C. Z. (2013). Effect of salt stress on photosynthetic and chlorophyII fluorescent characteristics in *Alnus formosana* seedlings. *J. For. Environ.* 33, 193–199. doi: 10.3969/j.issn.1001-389X.2013.03.001

Zhang, M., Wang, H. J., and Yu, C. Q. (2009). The examination of high temperature stress of *Ammopiptanthus mongolicus* by chlorophyll fluorescence induction parameters. *Ecol. Environ. Sci.* 18, 2272–2277. doi: 10.3969/j.issn.1674-5906.2009.06.050

Zhang, M. X., Dong, Z., Li, H. L., Wang, Q., Liang, Y., and Han, X. F. (2018). Improvement Effects of Different *Ulmus pumila* strains on coastal saline alkali soil and distribution and absorption of salt ions. *J. Soil Water Conserv.* 32, 340–345. doi: 10.13870/j.cnki.stbcxb.2018.06.049

Zhang, M. Y., Si, Y. Z., Ju, Y., Li, D. W., and Zhu, L. H. (2021). First report of leaf spot caused by colletotrichum siamense on *Salix* matsudana in China. *Plant Dis.* 11:3744. doi: 10.1094/PDIS-04-21-0776-PDN

Zhang, X. H., Zhang, L., Ma, C., Su, M., Wang, J., Zheng, S., et al. (2022). Exogenous strigolactones alleviate the photosynthetic inhibition and oxidative damage of cucumber seedlings under salt stress. *Sci. Hortic.* 297:110962. doi: 10.1016/j.scienta.2022.110962

Zhao, L., Yang, J. X., Yu, S. H., He, L. F., Wang, J., Li, Y., et al. (2019). Effects of grafting on the photosynthetic physiological characteristic and chlorophyli fluorescence parameters of *Prumus mume* under salt Stress. *J. Northwest For. Univ.* 34, 43–48. doi: 10.3969/j.issn.1001-7461.2019.06.07

Zhao, Y., Wu, M., Deng, P., Zhou, X. W., and Huang, S. Y. (2021). Effects of salt stress on growth and chlorophyII fluorescence parameters of *Siraitia grosvenorii* seedlings. *South China Fruits.* 50, 103–107. doi: 10.13938/j.issn.1007-1431.20200431

Zhao, Z., Gao, Z. K., Xu, G. H., Wang, M., and Gao, R. F. (2006). Study on getting parameters of chlorophyll fluorescence dynamics by non-modulated fluorometer plant efficiency analyser. *Acta Biophysica Sin.* 22, 34–38. doi: 10.3321/j.issn:1000-6737.2006.01.006

Zhou, B. N., Mao, L., Hua, Z. Z., and Lu, J. G. (2021). Effects on photochemical fluorescence properties under salt-alkaline stresses about Sinocaly-*Canthus chinensis*. *Acta Agric. Zhejiangensis.* 33, 1416–1425. doi: 10.3969/j.issn.1004-1524.2021.08.09

Zhu, H. L., Li, D., He, Y. Y., and Feng, X. D. (2019). Effects of water stress on photosynthetic characteristics of Jujube jujube. *J. Yan"an Univ. (Nat. Sci Ed.)* 38, 72–75. doi: 10.13876/J.cnki.ydnse.2019.04.072

Zhu, Y. X., Yin, J. L., Liang, Y. F., Liu, J. Q., Jia, J. H., Huo, H. Q., et al. (2019). Transcriptomic dynamics provide an insight into the mechanism for silicon-mediated alleviation of salt stress in cucumber plants. *Ecotoxicol. Environ. Saf.* 174, 245–254. doi: 10.1016/j.ecoenv.2019.02.075

Conflict of Interest: The authors declare that the research was conducted in the absence of any commercial or financial relationships that could be construed as a potential conflict of interest.

Publisher's Note: All claims expressed in this article are solely those of the authors and do not necessarily represent those of their affiliated organizations, or those of the publisher, the editors and the reviewers. Any product that may be evaluated in this article, or claim that may be made by its manufacturer, is not guaranteed or endorsed by the publisher.

frontiers | Frontiers in Plant Science

ORIGINAL RESEARCH
published: 09 May 2022
doi: 10.3389/fpls.2022.890551

Combined Drought and Heat Stress Influences the Root Water Relation and Determine the Dry Root Rot Disease Development Under Field Conditions: A Study Using Contrasting Chickpea Genotypes

*Aswin Reddy Chilakala[1†], Komal Vitthalrao Mali[1†], Vadivelmurugan Irulappan[1], Basavanagouda S. Patil[2], Prachi Pandey[1], Krishnappa Rangappa[3], Venkategowda Ramegowda[4], M. Nagaraj Kumar[5], Chandra Obul Reddy Puli[6], Basavaiah Mohan-Raju[4] and Muthappa Senthil-Kumar[1]**

[1] National Institute of Plant Genome Research, Aruna Asaf Ali Marg, New Delhi, India, [2] ICAR-Indian Agricultural Research Institute (IARI), Regional Research Center, Dharwad, India, [3] Division of Crop Sciences, ICAR Research Complex for North Eastern Hill Region, Meghalaya, India, [4] Department of Crop Physiology, College of Agriculture, University of Agricultural Sciences, Bengaluru, India, [5] Division of Plant Physiology, ICAR-Indian Agricultural Research Institute, New Delhi, India, [6] Department of Botany, Yogi Vemana University, Kadapa, India

Abiotic stressors such as drought and heat predispose chickpea plants to pathogens of key importance leading to significant crop loss under field conditions. In this study, we have investigated the influence of drought and high temperature on the incidence and severity of dry root rot disease (caused by *Macrophomina phaseolina)* in chickpea, under extensive on- and off-season field trials and greenhouse conditions. We explored the association between drought tolerance and dry root rot resistance in two chickpea genotypes, ICC 4958 and JG 62, with contrasting resistance to dry root rot. In addition, we extensively analyzed various patho-morphological and root architecture traits altered by combined stresses under field and greenhouse conditions in these genotypes. We further observed the role of edaphic factors in dry root rot incidence under field conditions. Altogether, our results suggest a strong negative correlation between the plant water relations and dry root rot severity in chickpeas, indicating an association between drought tolerance and dry root rot resistance. Additionally, the significant role of heat stress in altering the dynamics of dry root rot and the importance of combinatorial screening of chickpea germplasm for dry root rot resistance, drought, and heat stress have been revealed.

Keywords: ***Macrophomina phaseolina*, *Cicer arietinum*, plant water status, drought, heat, combined stress, stress tolerance, disease resistance**

OPEN ACCESS

Edited by:
Amaranatha Reddy Vennapusa, Delaware State University, United States

Reviewed by:
Maria Isabel Balbi-Peña, State University of Londrina, Brazil
Rajneesh Singhal, Michigan State University, United States

****Correspondence:***
Muthappa Senthil-Kumar
skmuthappa@nipgr.ac.in

[†] These authors have contributed equally to this work

Specialty section:
This article was submitted to Plant Abiotic Stress, a section of the journal Frontiers in Plant Science

Received: *06 March 2022*
Accepted: *15 April 2022*
Published: *09 May 2022*

Citation:
Chilakala AR, Mali KV, Irulappan V, Patil BS, Pandey P, Rangappa K, Ramegowda V, Kumar MN, Puli COR, Mohan-Raju B and Senthil-Kumar M (2022) Combined Drought and Heat Stress Influences the Root Water Relation and Determine the Dry Root Rot Disease Development Under Field Conditions: A Study Using Contrasting Chickpea Genotypes. Front. Plant Sci. 13:890551. doi: 10.3389/fpls.2022.890551

INTRODUCTION

Dry root rot (DRR), caused by the necrotrophic fungal pathogen *Macrophomina phaseolina* (anamorph, formerly referred to as *Rhizoctonia bataticola*), is one of the devastating soil-borne diseases of chickpea whose severity and incidence has increased in the recent past due to climate change (Sharma and Pande, 2013; Sinha et al., 2019, 2021). Root tissue water status and water potential, gas exchange at the root zones, and the host's nutritional status are known to determine the incidence of DRR (Rai et al., 2022). Furthermore, at the physiological level, reduction in photosynthesis due to drought stress also predisposes the host plants to the disease (Cabral et al., 2020). However, the studies exploring drought-induced predisposition of chickpeas to dry root rot, highlighting the stress influence on plant physiology and metabolism are limited. Nevertheless, some evidence suggests a significant connection between leaf water potential and disease resistance. For instance, common bean cultivars with higher leaf water potential under drought stress showed resistance to root rot pathogens and vice versa (Mayek-Pérez et al., 2002). In addition, drought-stressed common bean plants exhibiting high stomatal resistance showed severe charcoal rot symptoms, which further indicated a high negative correlation between the disease severity, and the physiological and growth-related traits (Mayek-Pérez et al., 2002).

The role of temperature in influencing the severity of root diseases has been extensively investigated. For instance, melon accessions resistant at low temperatures were found to be susceptible to charcoal rot disease at high temperatures (de Sousa Linhares et al., 2020). Better adaptability of the pathogen to elevated temperature coupled with heat-mediated reduction of plant resistance could be the possible reasons for enhanced susceptibility to root pathogens under high temperatures. A study involving the growth of diverse isolates of *M. phaseolina* under different temperatures revealed that 35°C was the optimum temperature for its growth (Srinivas et al., 2017).

Here, we hypothesize the potential involvement of root water relations and morphological traits in affecting *M. phaseolina's* interactions with *Cicer arietinum* (chickpea). We studied dry root rot disease development in two chickpea genotypes, ICC 4958 and JG 62 under drought and high-temperature conditions to address this hypothesis. ICC 4958 was chosen as it is one of the 1,500 diverse germplasms that showed significant drought resistance under field screening (Deokar et al., 2011). Further, the capacity of ICC 4958 to withstand terminal drought was attributed to its root growth characteristics (Kashiwagi et al., 2006). On the other hand, JG 62 (aka. ICC 4951) has been reported as a highly susceptible genotype to dry root rot resistance, exhibiting more than 90% mortality under dry root rot infection (Jayalakshmi et al., 2008; Talekar et al., 2021). Overall, using thorough systematic observations of physiological and patho-morphological characteristics under field and laboratory conditions, our study reports an interesting link between the alterations in plant water relations due to drought and temperature stress and chickpea's response to *M. phaseolina*. In addition, edaphic factors were also studied for their influence on the DRR incidence under field conditions.

MATERIALS AND METHODS

Plant Material

Two chickpea genotypes *viz.,* ICC 4958 and JG 62 (aka. ICC 4951) were obtained from the Indian Agricultural Research Institute, New Delhi, and were used as plant materials in all the experiments conducted in this study. The morpho-phenological characteristics of the genotypes are given in **Supplementary Table 1**.

Field Trials

Field experiments, to understand the influence of root-water relations on dry root rot disease incidence were conducted as "on-season" and "off-season" field trials following randomized complete block design as described earlier (Sinha et al., 2019). Line sowing with a spacing of 10 cm × 30 cm (row-to-row × plant-to-plant) was practiced in both the field trials.

On-Seasonal Field Trial

A group of six diverse natural hotspot sites with low to high DRR pathogen inoculum load in the soil was selected during the year 2020–2021 (rabi season, October–March) (Irulappan and Senthil-Kumar, 2021; **Supplementary Figure 1**). The details of weather conditions for the experimental locations are given in **Supplementary Tables 2, 3** and **Supplementary Figure 2**. The experiment was performed during the chickpea cultivation period specific to the location. Details related to the maintenance of the field trial experiments at the six locations are given in **Supplementary Table 3**. The experiment included four different treatments *viz.,* mild pathogen, a mild pathogen with drought, severe pathogen, and combined severe pathogen with drought (**Supplementary Figure 3**). At location 1, control, drought, and heat treatments were maintained separately in isolated field conditions, and the remaining four treatments were maintained in the pathogen-infected plots. The details of the experimental design, field layout, and stress treatments are presented in **Supplementary Figure 4**. Drought stress was imposed on the field plots by regulating the irrigation interval across the treatments, and soil moisture of the field locations was measured using Lutron PMS-714 soil moisture meter (Lutron Electronic Enterprise Co., Ltd., Taipei, Taiwan) to ascertain the imposition of drought (**Supplementary Figure 5**).

Off-Season Field Trial

The off-season trial during summer 2021 was conducted at field plots of the National Institute of Plant Genome Research, New Delhi (location 1). The mean atmospheric and soil temperature was considered as heat stress (**Supplementary Figure 2G**). Thus, the four treatments included were, heat with a mild pathogen, heat with mild pathogen and drought, heat with a severe pathogen, and heat with severe pathogen stresses and drought. **Supplementary Figure 4** describes the experimental

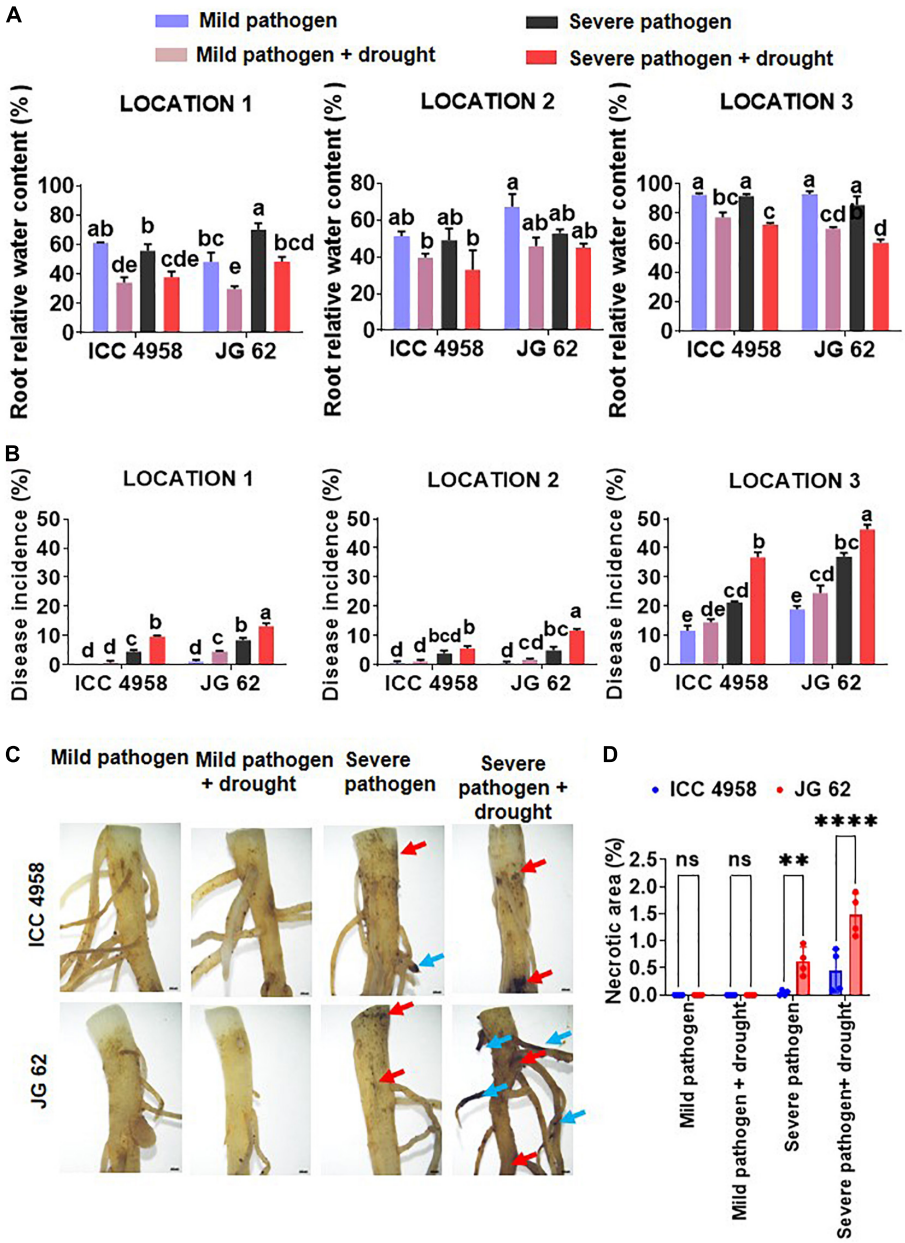

FIGURE 1 | On-season field trials exhibiting the influence of plant-water relations in dry root rot (DRR) disease aggravation. The four treatments considered were-mild pathogen (fields frequent irrigated to maintain 80% FC and treated with appropriate fungicide), mild pathogen + drought (less frequently irrigated fields to maintain 50% FC and treated with appropriate fungicide), severe pathogen (frequently irrigated fields to maintain 80% FC without any fungicide application), severe pathogen + drought (less frequently irrigated fields to maintain 50% FC without any fungicide application) for both the genotypes ICC 4958 and JG 62. **(A)** Root relative water content of the two contrasting chickpea genotypes under different stress and their combinations across different experimental locations. The bars in the following graphs are the averages of their respective block replicates with standard error as error bars. Under field conditions, we did not observe a non-symptomatic control plot as the minor infection was reported in the control (fungicide treated) plot as well. This treatment is mentioned as a "mild pathogen". **(B)** The disease incidence data, was collected at the late podding stage and additionally at the harvest stage from plants with symptomatic roots for confirmation from three locations under different stress treatments. The bars in the following graphs are the averages of their respective block replicates with standard error as error bars. **(C)** Root images showing the root branching zone 1 of 29 days old JG 62 and ICC 4958 plants exposed to a mild pathogen, severe pathogen, mild pathogen + drought, severe pathogen + drought, for 10 days under greenhouse conditions. The dark-colored lesions show the severity and higher infection in JG 62 over ICC 4958. Root images were captured under 0.63X objective lens of SMZ25 research stereomicroscope. Blue arrows show the necrotized lateral roots. Red arrows indicate the necrotic spots. The details of the locations are provided in **Supplementary Table 2**. Statistical significance between means was checked by two-way ANOVA and Tukey's Posthoc test. The different letters denote a significant difference between mean at $p < 0.05$. **(D)** Graph represents the root necrosis area (%) of two cultivars for different treatments mild pathogen, severe pathogen, mild pathogen + drought, severe pathogen + drought. The bars on the graph indicate the averages of different treatments for 4 replicates with standard error as an error bar. Statistical significance difference between means is checked by two-way ANOVA and sidak's mean multiple comparison test. The $^{**}p < 0.01$, $^{****}p < 0.0001$., ns, non-significant.

treatments and imposition of different stresses. **Supplementary Figure 6** shows the imposition of drought through dynamics in soil moisture during the trial.

Plant Growth Conditions for Pot Experiment

Growth Conditions

Chickpea seeds sterilized with 2% sodium hypochlorite were used for the experiments. Plants were grown under greenhouse conditions with a photoperiod of 16 h/8 h, light/ dark cycle, the light intensity of 150 mmol m^{-2} s^{-1}, and relative humidity of 52 ± 2% as described earlier in Sinha et al. (2019). For heat stress treatment, the temperature maintained was 37/25°C (day/night). The normal temperature maintained was 22/10°C (day/night).

Stress Treatments

Eight treatments viz., control, drought, pathogen, drought with pathogen, heat, heat with drought, heat with a pathogen, and heat and drought with pathogen were considered for the

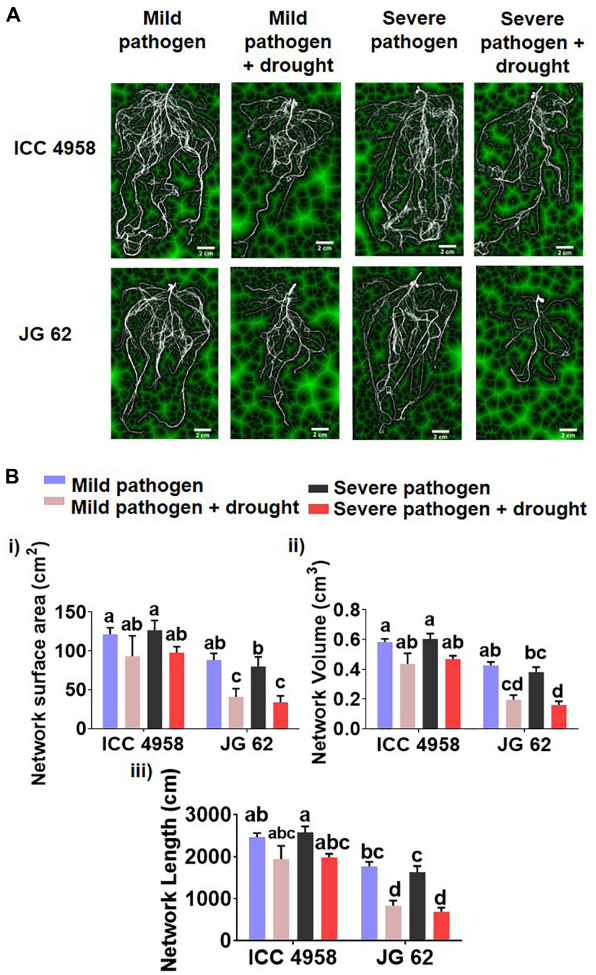

FIGURE 2 | Differences in root architectural traits in the two chickpea genotypes across the different stress treatments**. (A)** A representative segmentation figure panel from the root scanning image analysis of ICC 4958 and JG 62 plants subjected to the mild pathogen, severe pathogen, mild pathogen + drought, and severe pathogen + drought. The analysis was done using Scanjet G4050 Photo Scanner and the images were analyzed using GIA roots (Galkovskyi et al., 2012). **(B)** The root trait variations were observed in the genotypes across the treatments. The image analysis data was accrued from the images of washed roots of 43 days old plants grown in greenhouse conditions using field soil from location 1. The bars on the graph indicate the averages of different traits for 3 RCB replicates with standard error as an error bar. Statistical significance difference between means is checked by one-way ANOVA and Tukey's posthoc test. A significant difference between the mean at $p < 0.05$.

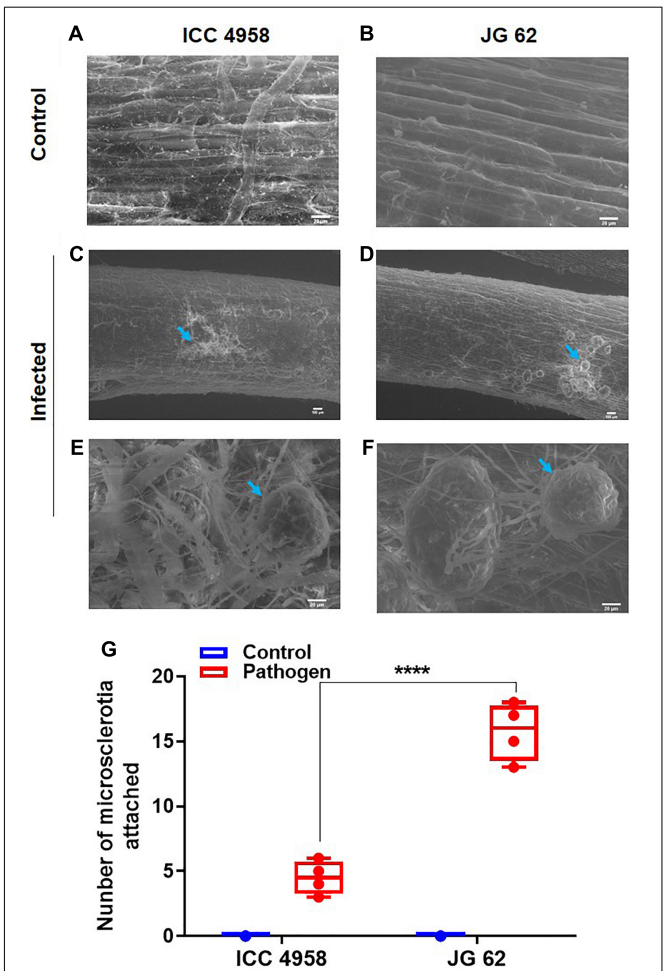

FIGURE 3 | Root images indicating the differential attachment of *M. phaseolina* microsclerotia on the ICC 4958 and JG 62. ICC 4958 showed resistance to DRR pathogen (MH509971.1) infection. ICC 4958 and JG 62 were subjected to infection by microsclerotia under well-watered conditions using the blotting paper method (Irulappan and Senthil-Kumar, 2021). Roots were collected and examined for the number of attached microsclerotia using the scanning electron microscope. **(A)** Uninfected root images of ICC 4958. **(B)** Uninfected root images of JG 62. **(C)** Infected ICC 4958 roots showing attached microsclerotia. **(D)** JG 62 roots show the attached microsclerotia. **(E)** Mycelial growth on ICC 4958 roots. **(F)** Extensive growth of mycelia from the attached microsclerotia in JG 62. **(G)** The graph shows the variation in attached microsclerotia. Two-way ANOVA was used. Asterisks show the significance at ****$p \leq 0.0001$. $N = 5$. The experiment was repeated three times at least.

pot experiments. The experimental design includes a complete factorial design. The drought was imposed by with-holding the irrigation during the vegetative stage of the plant as described earlier in Sinha et al. (2019). The sterile soil rite was added with an inoculum of *M. phaseolina* isolate- Dharwad (NCBI ID OM674331) for pathogen stress. The pathogen was isolated from a small part of surface-sterilized fungal-infected root tissue taken from plant samples from Location 3 (**Supplementary Figure 7**). The inoculum was prepared as described by Irulappan and Senthil-Kumar (2021). An inoculum of 5:100 (weight/weight) ratio of sick culture to dry soil rite was used. Relative water content, root water potential, and disease incidence parameters were measured.

Control Treatments

Under field conditions, the absolute control plots were maintained at a distant location and the data from these plots were not used in this manuscript. For all analysis the mild and severe pathogen infected plots were only used as indicated in the graphs. In green house conditions, plants growing under well-watered conditions in sterile pot mix served as a control.

Drought Stress Treatments

Drought stress in field and pot experiments was imposed by withholding irrigation. The soil moisture of the field locations was measured using Lutron PMS-714 soil moisture meter as described above. A field capacity of 40–60% was maintained as drought stress.

Pathogen Stress Treatments

Pathogen stress in the field plots was imposed by growing chickpea plants in plots enriched with DRR inoculum naturally. In greenhouse conditions, the plants were infected with the pathogen using the sick pot method (Irulappan and Senthil-Kumar, 2021). For SEM studies, plants were infected using the blotting paper technique (Irulappan and Senthil-Kumar, 2021).

Combined Stress Treatments

For the on season field trial experiments, for combined stress treatments plants were grown in plots with less frequent irrigation to maintain 50% FC. The soil was not treated with any fungicide. In the off season field trial experiments, similar treatment served as combined stress with additional component of heat stress imposed due to the high day temperature. Under greenhouse conditions, sick soil with less frequent irrigation under ambient temperature (combined drought and pathogen) and high temperature (combined drought, heat and pathogen stress) served as combined stress treatment. The details of all the treatments are summarized in **Supplementary Table 4**.

Measurement of Relative Water Content

Relative water content (RWC) from both roots and leaves was measured according to the protocol described earlier (González and González-Vilar, 2001; Sinha et al., 2019). Root and leaf samples from all the treatment plots were collected and their weights, recorded instantaneously, constituted the fresh weight. Then the samples were hydrated by placing them in de-ionized water and incubating on ice for 4 h. The tissues were weighed thereafter to measure the turgid weight. The samples were then oven-dried for 48 h at a temperature of 60° to measure the dry weight. Percentage RWC of the samples (roots and leaves) was calculated using the following formula:

$$\textit{Root relative water content}(\%) = \frac{\textit{Fresh tissue weight} - \textit{Dry tissue weight}}{\textit{Turgid tissue weight} - \textit{Dry tissue weight}} \times 100$$

Soil, Root, and Leaf Water Potential Quantification

Soil, root, and leaf samples were collected in 1.5 ml microcentrifuge tubes. The sample tubes were sealed with surgical tapes. The samples were then stored at −80°C till further processing. The uniformly kneaded soil samples or the cell sap from frozen leaf or root samples were used for water potential measurements. The cell sap was extracted from root and leaf samples by crushing followed by centrifugation at 12,000 rpm for 1 min. Then, the cell sap/soil samples were analyzed for water potential using a Psypro system with C52 sample chambers (Wescor PSYPRO Automated Soil and Leaf Water Potential System, United States) (Kumar et al., 2012).

Root System Architecture Measurement

The plants were grown in pots (24 cm × 15 cm length and diameter). Pathogen and drought stress was imposed in the same way as described above. Forty-five days old plants were uprooted and washed with RO water. The clean roots were then scanned using the Scanjet G4050 Photo Scanner (Hewlett-Packard, New Delhi). Image analysis was done using GiA Roots to acquire root architecture traits like network area, length, and volume (Galkovskyi et al., 2012).

Scanning Electron Microscope

Microsclerotia-infected plant root samples were sampled in intervals starting from 1 DAI to 5 DAI (Sinha et al., 2019; Irulappan and Senthil-Kumar, 2021). The samples were treated with 2.5% glutaraldehyde in 0.1 M sodium phosphate buffer (pH 7.2) later they are vacuum infiltrated. The roots were then dehydrated twice in acetone (30, 50, 70, 80, 90, 95, and 100%) for 10 mins each time in each percentage. The roots were maintained in 100% acetone. A critical point dryer (Leica EM CPD300, Leica Biosystems, Mumbai, India) was used to dry the critical points. Scanning electron microscopy (SEM, Carl Zeiss-Strasse, Oberkochen, Germany) was used to take pictures at 100×, 250×, and 500× magnifications.

Evaluation of Microsclerotial Attachment in Roots

Microsclerotia-infected and well-watered plant root samples from the two genotypes were subjected to SEM as described above. The plants were infected using the blotting paper method (Irulappan and Senthil-Kumar, 2021). The number of attached microsclerotia clearly visible in the images were manually

counted to estimate the extent of microslerotial attachment in the two genotypes (Irulappan et al., 2022).

Disease Identification and Assessment of Disease Incidence and Disease Index

Dry root rot disease was recognized based on its characteristic symptoms *viz.,* straw-colored dry leaves, taproot devoid of lateral roots, and presence of dark-colored microsclerotia in split open roots. Etiology was confirmed by the PCR method (Irulappan and Senthil-Kumar, 2021). Percent disease incidence (DI) was calculated in each treatment plot using the following formula:

$$\text{Disease incidence (\%)} = \frac{\text{Number of infected plants in a treatment plot}}{\text{Total number of plants present in that treatment plot}} \times 100$$

The disease index was calculated as described earlier (Sinha et al., 2019). The disease score for calculating the disease severity for both pot and field experiments was assigned using the representative symptom score panel given in **Supplementary Figure 8**.

Statistical Analysis

All field and greenhouse data were analyzed by calculating averages from replicates of each treatment for each parameter and were tested using two-way ANOVA analysis using Tukey's posthoc test. Associations among the disease incidence, weather data, and important edaphic factors were tested using the Pearson correlation using IBM® SPSS® Statistics 26.0 (or) 14[1]. The Pearson's correlation coefficient was used to test the relationship among the test treatments in the current study.

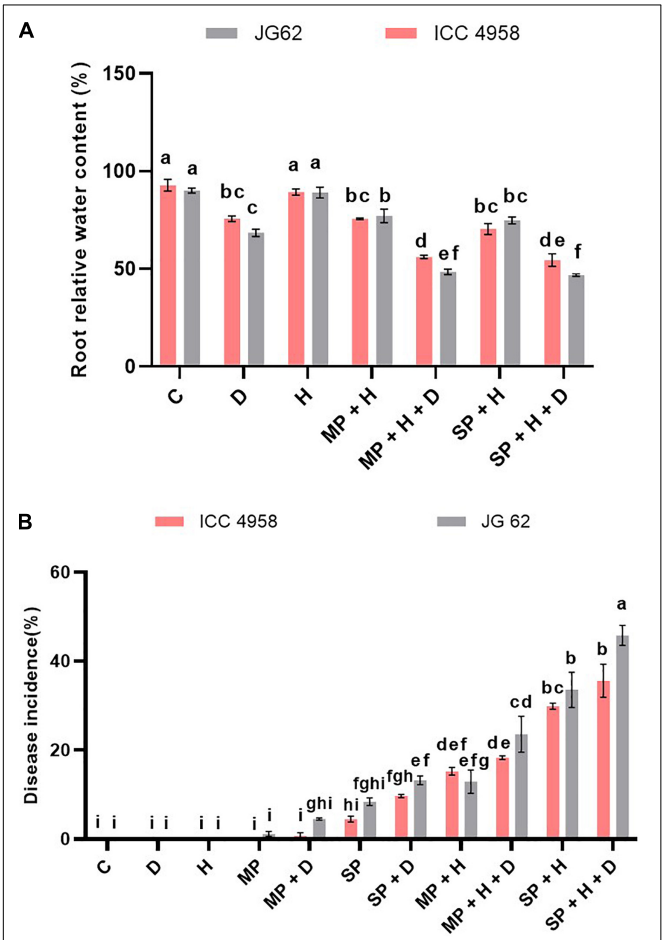

FIGURE 4 | Combined drought and heat stress significantly alter the DRR disease development in chickpeas. Chickpea plants were exposed to different treatments namely, control, drought, heat, mild pathogen, mild pathogen + drought, severe pathogen, severe pathogen + drought, mild pathogen + heat, mild pathogen + heat + drought, severe pathogen + heat, and severe pathogen + heat + drought under field conditions during the off-season field trials. The control, drought, heat treatments were maintained separately in the isolated field and greenhouse conditions (**Supplementary Figure 4**). **(A)** Root relative water content of the two contrasting chickpea genotypes under different individual and combined stresses from the off-season field trials. **(B)** The DRR disease incidence in chickpea plants exposed to DRR under individual and combined drought and heat stresses. The treatment combinations are from both the on-season and off-season trials at Location 1. The bars in the following graphs are the average of respective block replicates with standard deviation as an error bar. Statistical significance between means was checked by two-way ANOVA and Tukey's posthoc test.

RESULTS

Reduction in Plant Water Status Increases the Disease Incidence

Incoherence with our previous observations (**Supplementary Figure 9**; Sinha et al., 2019), we found that drought predisposes both the genotypes to DRR irrespective of their level of drought tolerance. The combined drought and DRR infection were also found to be more deleterious to the overall plant performance and caused a maximum reduction in the yield (**Supplementary Figure 10**). For instance, yield reductions of about 57.35 and 66.99% were observed under combined drought and severe pathogen stress in ICC 4958 and JG62 at location 1. Whereas, in severe pathogen stress-only treatments 30.35 and 24.09% yield reductions were observed in ICC 4958 and JG62, respectively. However, the trend was not statistically significant in some locations presumably due to environmental variations. Additionally, disease incidence (DI) observations across the different on-season field trial locations showed that the DRR incidence in ICC 4958 was less prominent than JG 62 under severe pathogen stress treatments with or without drought (**Supplementary Figures 11, 12**). Drought stress enhanced the susceptibility of JG 62 to DRR more significantly than ICC 4958, which was indicated by the notable difference between the DI of the two genotypes under drought conditions (**Figure 1B**). We compared the effect of individual and combined drought and DRR infection on plant water status at various stages of development in the two genotypes (**Supplementary Figure 13A**). Global transcriptome profile data

[1]https://www.ibm.com/support/pages/downloading-ibm-spss-statistics-26

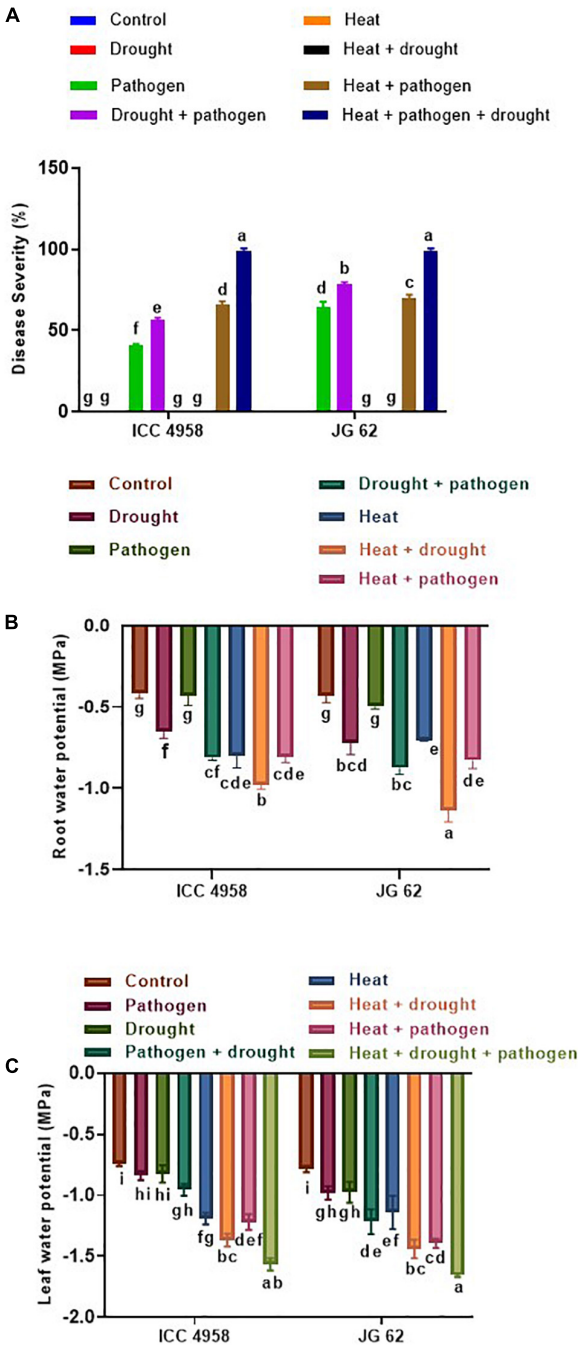

FIGURE 5 | Effect of drought and heat stress on DRR disease severity in ICC 4958 and JG 62 chickpea genotypes. **(A)** Disease severity in the two genotypes under different stress treatments, namely control, drought, pathogen, drought + pathogen, heat, heat + drought, heat + pathogen, heat + drought + pathogen. **(B)** Root water potential **(C)** Leaf water potential of the individual and combined stressed ICC 4958 and JG 62 as measured on the 30th day post-drought imposition (**Supplementary Figure 15**). Root and leaf water potential were measured using Wiscor Psyprometer in 3 biological replicates per treatment. One replicate constituted three pots per set with each pot having two plants. Error bar signifies the SEM. Statistical significance difference between means is checked by one-way ANOVA and Tukey's Posthoc test. The different letters denote a significant difference between mean at $p < 0.05$.

(Irulappan et al., 2022) was analyzed to study the molecular changes occurring under combined drought and DRR infection in chickpea. We observed differential regulation of genes related to water transport, root architecture, xylem modification (lignin deposition), and hormone response (auxin, ABA, and JA) under drought, pathogen, drought and pathogen stress treatments (**Supplementary Figure 13B**). On average, we observed that both drought and pathogen infection negatively affected the plant water status (**Figure 1A**), and the DI under combined stress was more in JG 62 as compared to ICC 4958 (**Figure 1B**). The observation was further corroborated by the microscopic observation of JG 62 roots that showed a greater number of *M. phaseolina* induced necrotic lesions and percent necrotic area than ICC 4958 (**Figures 1C,D**). Thus, our experiments suggest a tissue and/or stage-specific relation between the plant water status and DRR incidence in chickpea plants.

Drought Tolerant Genotype Displayed Reduced Severity to Dry Root Rot Disease

To further explore the relationship between the ability to maintain water status and disease resistance, we compared the root growth characteristics of the two genotypes under individual and combined drought and pathogen stresses (**Figure 2**). The two genotypes grown under greenhouse conditions displayed significant differences in root growth associated traits *viz.*, root network area, root length, and volume (**Figures 2A,B**). ICC 4958 exhibited widespread and 1.4 fold longer roots with 1.36-fold larger network area, at 43 days after sowing (DAS) as compared to JG 62 under unstressed conditions. Under drought conditions, both the genotypes exhibited a substantial reduction in the root growth traits. However, the reductions were more significant in JG 62. Likewise, combined drought and pathogen infection reduced the root network area, volume, and length in both the genotypes, the reductions being more significant in JG 62 (**Figure 2B**). Although not very significant, similar reductions were made when we compared the root architectural traits of the two genotypes under different treatments at the podding stage (**Supplementary Figure 14**). To further explore the response of the two genotypes toward DRR infection, we examined plant roots infected by *M. phaseolina* for the number of attached microsclerotia. We observed that the number of microsclerotia attached over the roots of two genotypes varied significantly. The percentage of microsclerotial attachment was 4-folds lesser in ICC 4958 than in JG 62 (**Figure 3**).

Heat Stress Alters Disease Dynamics in the Resistant Genotype Under Drought Stress

Plant water status is controlled by two major physiological processes, namely the absorption of water by roots and transpiration. The former is affected by the water level in soil, whereas the latter is influenced by the air temperature and relative humidity. Since we have found the possible relations between DRR incidence and root water status, we wanted to dissect

the role of heat stress on DRR incidence. To achieve this, we included the off-season field trials characterized by increased daily temperatures, thereby including heat stress as an additional abiotic stress component. On comparing the on- and off-season field trial observations, we found that heat perhaps acts as another important abiotic factor modulating chickpea susceptibility to DRR under field conditions (**Figure 4**). We observed that root water status of both genotypes was significantly reduced under combined heat, drought, and pathogen stress (**Figure 4A**). We further observed that heat stress further escalated the disease incidence in both the genotypes (**Figure 4B** and **Supplementary Figure 15**). To further validate the involvement of heat in enhancing the susceptibility of chickpea to DRR, we evaluated the performance of ICC 4958 and JG 62 under the individual and combined heat, drought, and pathogen stress treatments (**Supplementary Figure 16**). Our results showed increased disease severity under combined stress treatments as compared to individual stresses (**Figure 5A** and **Supplementary Figure 17**). Disease severity increased significantly when DRR infection was accompanied by combined drought and heat stress treatments. Interestingly, the disease severity was higher under the combined heat and pathogen treatment than under the combined drought and pathogen infection in ICC 4958 (**Figure 5A**). We further compared the plant water relations of both the genotypes under the different stress treatments (**Figures 5B,C**). The maximum reduction in leaf water potential occurred under combined heat, drought, and pathogen treatment as indicated by significantly low leaf water potential under this treatment (**Figure 5C**). Root water potential could not be calculated for this treatment as we were unable to extract enough root sap required for the measurement. However, the measurement of the relative water content of roots under the triple stress treatment corroborated the observations of shoot water potential (**Supplementary Figure 18**). Here again, we found that combined heat and pathogen stress caused more significant reductions in root and leaf water potentials as compared to the combined drought and pathogen stress. We found a significant negative correlation between leaf water potential and DRR disease incidence (**Table 1**), suggesting that high plant water status might be one of the key parameters that could ward off DRR infection.

Influence of Edaphic Factors on Dry Root Rot Disease Incidence

To explore the effect of environmental conditions other than drought and heat in determining DRR incidence, the soil-nutrient analysis was performed across the experimental locations. Soil physicochemical properties such as sand and silt content, clay, pH, electrical conductivity (EC), and water holding capacity (WHC), along with the nutrient parameters like organic carbon (OC), phosphorous (P), potassium (K), nitrogen (N), sulfur (S), and boron (B) were assessed (**Supplementary Table 5**). DRR disease incidence under severe pathogen treatments observed across the three locations in on-season field trials was used for correlation analysis with the observed soil properties. Results revealed a positive correlation of DRR incidence with clay content and soil nitrogen availability. However, no significant correlation between DRR incidence and other soil properties could be found (**Supplementary Table 6**).

Genetic Diversity Among Isolates of Macrophomina phaseolina

Pure isolates were obtained from culturing diseased root samples collected across different experimental and survey locations (**Supplementary Figure 19**). The fungus-specific regions were amplified using Internal transcribed space (ITS) based primers. The sequences were subjected to the phylogenetic analysis that grouped the isolates into three different major clades (I, II, and III) (**Supplementary Figure 20** and **Supplementary Table 7**). The clades I and II could have originated from a common ancestor isolate. No cluster of isolates from a particular geographical region was seen. Incidentally, we also observed a wide variety of weeds in the sick plots, which were uninfected. The observations suggest a possibility of exploring the weeds for non-host resistance against *M. phaseolina* (**Supplementary Figure 21** and **Supplementary Table 8**). However, further experiments in this regard are warranted.

DISCUSSION

Root Water Relations Impact Dry Root Rot Disease Development

Extensive evidence on DRR incidence and its increased severity under deficit soil moisture conditions has been reported (Sharma and Pande, 2013; Sinha et al., 2019, 2021; Sharath Chandran et al., 2021). Our results further confirm that drought-induced plant water reductions may aggravate DRR infection in chickpea. Indeed, a significant correlation between the relative leaf water content and severity of charcoal rot was reported in common bean and soybean under water stress conditions (Yasmin et al., 2020), indicating the pathogen's inclination for decreased plant-water content. In our study, a significant increment in DRR disease development was observed in chickpea plants exhibiting reduced root-relative water content in multiple field trial experiments. This indicates a high probability of DRR disease development under conditions that lead to reduced root water content. However, further experiments providing observations in a continuous-time interval could better establish the intricacies of the root-fungal interaction under drought stress. The positive association between soil moisture deficit and

TABLE 1 | Correlation analysis among disease susceptibility index, root, and leaf water potential.

	Root water potential	Leaf water potential	Disease susceptibility index
Root water potential	1		
Leaf water potential	0.881**	1	
Disease susceptibility index	0.034	−0.376	1

**Significance at p value of 0.05. **Significance at p value of 0.01. Difference between means was assessed by one way ANOVA and Tukey's Post-hoc test.*

DRR disease development may be attributed to the inability of fungus to maintain sclerotia viability under higher soil moisture conditions and on the plant, tissues maintained at higher water levels (Marquez et al., 2021). *Macrophomina phaseolina* also exhibits the ability to have sustained growth and better survival under osmotic stress conditions due to the *de novo* synthesis of osmolytes such as glycerol (Baird et al., 2003) and variations in the lipid contents of both mycelium and microsclerotia (Marquez et al., 2021). On the plant side, weakened endodermal barrier and suppression of overall host defenses can cause enhanced DRR severity under the water stress conditions (Irulappan et al., 2022).

Contrasting Genotypes Indicate the Role of Disrupted Root Water Relations in Enhancing Dry Root Rot

Macrophomina phaseolina is a root infecting pathogen and interferes with plant water relations. This fact supported by the observation that DRR infection is aggravated by drought compelled us to study the effect of DRR infection on two genotypes with contrasting drought tolerance. The ability of crops to absorb and transport nutrients and water is directly influenced by root system architecture (RSA), determined by the root length, root surface area, and root volume (Wang et al., 2019; Xiong et al., 2021), and root length density (Lynch et al., 2014; Zhan et al., 2015). ICC 4958 is known to have a robust root architecture with a dense root system (Kashiwagi et al., 2006). Earlier reports have shown that 35 days old ICC 4958 plants, sampled from two different seasons in the field and cylindrical experiments, had higher root length density than JG 62 (Kashiwagi et al., 2006). Since ICC 4958 also displayed enhanced DRR resistance, we were interested to see if the resistance could be related to the better root system architecture. As expected, we found that the root traits like root length, surface area, and volume varied significantly between the two genotypes across different treatments at the vegetative stage (**Figure 2**); ICC 4958 was found to possess a denser root system with a greater root area and volume as compared to JG 62. Since DRR symptoms are characteristically observed at later growth stages of chickpea, we observed the effect of pathogen infection on root architecture at podding stage under field conditions. Similar root trait differences between genotypes were found at podding stages but were found to be non-significant across the treatments (**Supplementary Figure 14**).

Root Water Relations Play a Role to Enhance the Dry Root Rot Disease Development Under High Temperatures

Substantial yield losses in major crops (soybean, sorghum, and groundnut) due to *M. phaseolina* occur under high temperatures (Marquez et al., 2021). Likewise, high temperature predisposes chickpea to DRR (Sharma and Pande, 2013; Sharma et al., 2015). High temperature leads to enhanced proliferation of *M. phaseolina* in chickpea roots, as indicated by increased fungal DNA in infected roots of plants grown at 35°C as compared to those growing at ambient temperature (Sharath Chandran et al., 2021). Furthermore, elevated temperatures improved microsclerotia production (Marquez et al., 2021). Moreover, it is suggested that the heat stress might cause more damage to the root membrane than drought causing the enhanced release of root exudates into the rhizospheric soil (Chai and Schachtman, 2022). In the present study, the disease incidence observed under on-and off-season field trials showed an increasing trend under drought stress, and the effect was more pronounced under elevated temperature (**Figures 4A,B**). Higher root-relative water content reduced disease incidence under ambient temperatures but there was no clear trend under elevated temperatures (**Figures 4A,B**). We observed a significant difference in the DI of the two genotypes under the combined heat, drought, and pathogen stress (**Figure 4B**) indicating that the genotype JG62 was more infected under triple combined stress as compared to ICC 4958. The difference in the disease severity was not found to be statistically significant (**Figure 5A**). DI is measure of whether a plant is diseased or not. However, the disease severity reflects is the degree of disease symptoms. Results showed that the heat differentially break the resistance barrier in the contrasting genotypes (ICC 4958 and JG 62) and hence the variation in pathogen aggressiveness in colonization of the genotypes. Our results indicate that the resistance of ICC 4958 to DRR, exhibited under ambient temperature, was compromised under high-temperature conditions. This is in agreement with the concept that *M. phaseolina* plant mortality is driven by elevated soil temperature rather than moisture stress (Marquez et al., 2021). More precise controlled pot experiments further substantiated the effect of heat stress in altering plant water status and increasing disease severity (**Figure 5**). We also found a significant negative correlation between the leaf water potential and disease severity (**Figure 5**). A similar negative correlation was found between lesion length and leaf water potential in different sorghum genotypes subjected to *M. phaseolina* infection and post-flowering drought stress (Mayek-Pérez et al., 2002).

Edaphic Factors Have a Mild Influence on Dry Root Rot Disease Incidence

The incidence of DRR disease is known to be impacted by several edaphic factors like soil pH, with the maximum DRR incidence being observed at pH 5.0 (Wagh, 2015). Our study indicated a positive correlation between clay content and DRR incidence (**Supplementary Table 5**). Clay content was reported to positively correlate with overall water retention through the increased specific surface area and occurrence of micropores (Reichert et al., 2009). Although the overall water retention increases under increased clay content, the amount of plant-available water is meager (O'Geen, 2012). Clay and sandy soil characteristics favor DRR occurrence (Wagh, 2015; Sinha et al., 2021). However, the amount of silt in the soil had a negative correlation (Sinha et al., 2021) with DRR incidence. We also show a positive correlation between soil nitrogen content and DRR incidence. Although the association between soil nitrogen content and DRR incidence has

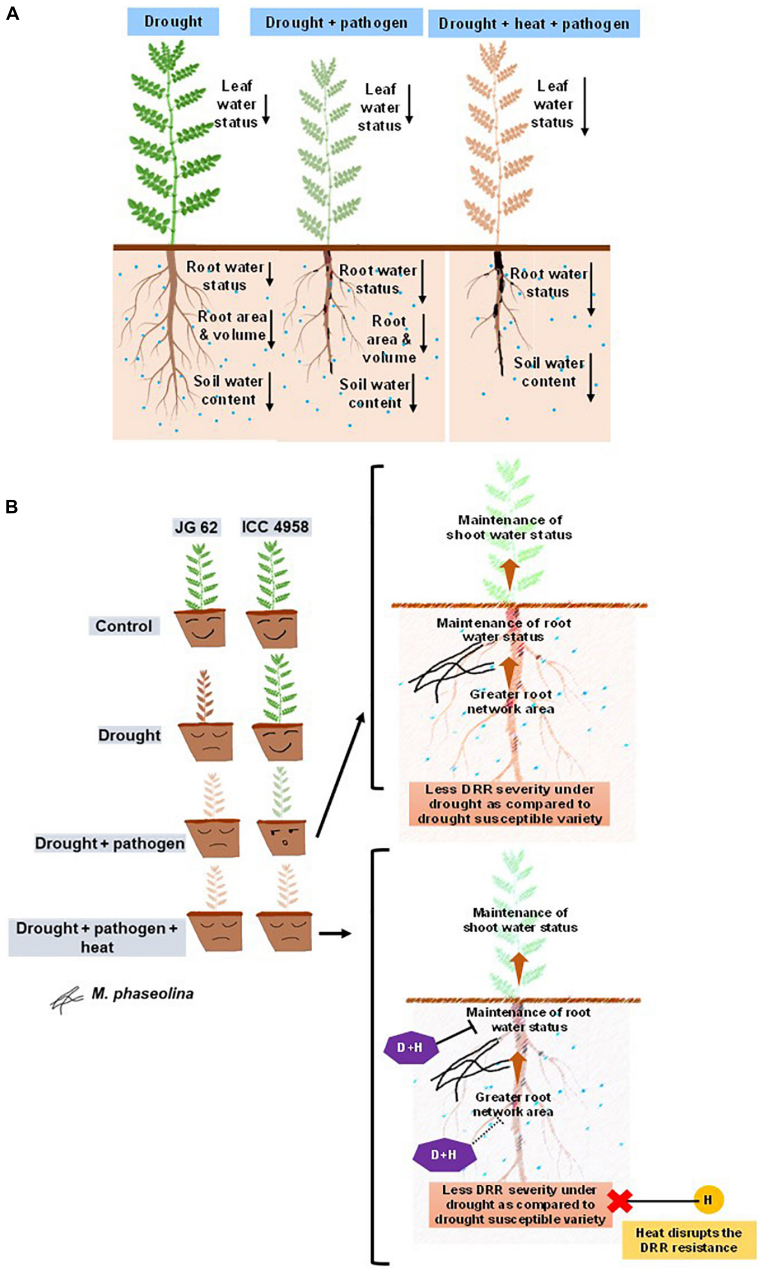

FIGURE 6 | Schematic summary showing the effect of drought and heat on chickpea water relations and response to DRR. **(A)** Illustration comparing the effect of individual drought, drought + pathogen, drought + pathogen + heat on water relations of chickpea. Both drought-only and combined drought and pathogen treatments reduce the root and leaf water content apparently due to reduction in the root-associated traits like network area, volume, and length. Enhanced transpiration under heat stress further reduces the root water status. The differences in the leaf and root water status, root architectural traits, and soil water content in the three treatments are indicated by black-colored arrows. The length of the arrows represents the extent of reduction (the longer the arrows, the more are the reductions). **(B)** Schematic representation of the possible mechanisms by which heat can reduce the resistance of a drought-tolerant variety to DRR. The left-hand side panel indicates the differential response of a drought-tolerant and susceptible variety to drought, pathogen, and combination of drought, heat, and pathogen. Whereas ICC 4958 can resist DRR infection better under drought conditions, heat makes it significantly susceptible to DRR. The right-hand panel represents the possible mechanism behind the same. A combination of pathogen and heat stress additively reduces the plant water content and disrupts the resistance to DRR shown by ICC 4958 under drought stress conditions. We hypothesize that drastic reduction in root water content mediated by heat may be one of the primary physiological processes behind the loss of resistance of ICC 4958 under heat stress. Broken arrows exhibit a predicted observation warranting future investigations. P, pathogen stress; H, heat stress, D + H, combined drought and heat stress. In panel **(A)**, the colors of the shoots represent the effect of soil water deficit and pathogen infection on plants. Since *M. phaseolina* is a root infecting pathogen, symptoms are not very visible in shoots. A combination of drought and DRR pathogen leads to enhanced disease and reduced shoot water status indicated by the faded color of the shoots. The combination of heat, drought, and pathogen causes further additive reductions in leaf water status and an increase in disease severity which is indicated by the brown coloration of the shoot showing the maximum deleterious effect of the triple stress combination.

not been reported before, an increase in DRR incidence upon nitrogen fertilization is shown (Hemissi et al., 2018).

CONCLUSION

Our study demonstrated the impact of drought and heat stress in elevating the incidence of DRR in chickpea and enhancing plant mortality under both greenhouse and field conditions (**Figure 6**). The disease susceptibility could be related to plant water relations suggesting that drought-tolerant varieties with better physiological traits (deep, widespread, and turgid roots), and plant water relations can resist the DRR infection better. Furthermore, we discovered that heat stress, often associated with drought under field conditions, disrupts the DRR resistance in the drought-tolerant variety, suggesting a heat-induced breach of plant defense against the pathogen. Overall, we indicate the significant association of plant water status with DRR resistance and highlight the prospects to extensively investigate the influence of DRR infection on physiological and molecular processes involved in the maintenance of plant water status through mechanisms including root hydraulic conductivity. Considering the significant influence of drought and heat on chickpea resistance to DRR, we insist on the pertinence of screening for DRR resistance in chickpea genotypes under heat and drought stress conditions for identifying better breeding resources.

DATA AVAILABILITY STATEMENT

The original contributions presented in the study are included in the article/**Supplementary Material**, further inquiries can be directed to the corresponding author.

AUTHOR CONTRIBUTIONS

MS-K conceived the idea, planned the study, designed the experiments, and edited and finalized the manuscript. AC, KM, and VI executed the field and laboratory experiments and analyzed the data. AC, VI, BP, CP, VR, BM-R, and KR have contributed to the execution of field experiments at various locations. MK contributed to leaf and root water measurements. PP contributed to data analysis and organization. AC, PP, and MS-K drafted the manuscript. All authors approved the manuscript.

FUNDING

Chickpea combined stress projects at the MS-K lab are supported by the National Institute of Plant Genome Research core funding.

ACKNOWLEDGMENTS

KM and AC acknowledged CSIR for fellowship [CSIR-JRF/09/803(0148)/2018-EMR-1 and CSIR- JRF09/803(0176)/2020-EMR-I, respectively]. VI acknowledged a fellowship from DBT (DBT-JRF/DBT/2015/NIPGR/430). Harvinder Kumar Singh was acknowledged for sending the soil samples from Raipur India and Akoijam Ratankumar Singh for technical help. We thank lab and field assistants Rahim Hussain Tarafdar, Shankar Badaik, Sundar Solanki, and Ashok Mandal for their help at the laboratory and field. We acknowledge DBT-eLibrary Consortium (DeLCON) and NIPGR Library for providing access to e-resources and NIPGR Plant Growth Facility for plant growth support/space. We also thank Mahesh Patil, Anupriya Singh, and Rishabh Mirchandani for scrutinizing the raw data and internally reviewing the manuscript.

SUPPLEMENTARY MATERIAL

The Supplementary Material for this article can be found online at: https://www.frontiersin.org/articles/10.3389/fpls.2022.890551/full#supplementary-material

Supplementary File 1 | Raw data of all the figures and table presented in the manuscript.

REFERENCES

Baird, R. E., Watson, C. E., and Scruggs, M. (2003). Relative longevity of *Macrophomina phaseolina* and associated mycobiota on residual soybean roots in the soil. *Plant Dis.* 87, 563–566. doi: 10.1094/PDIS.2003.87.5.563

Cabral, R. N., Marouelli, W. A., and Café-Filho, A. C. (2020). Irrigation management strategies for reducing verticillium wilt severity in eggplants. *Summa Phytopathol.* 46, 9–13. doi: 10.1590/0100-5405/190000

Chai, Y. N., and Schachtman, D. P. (2022). Root exudates impact plant performance under abiotic stress. *Trends Plant Sci.* 27, 80–91. doi: 10.1016/j.tplants.2021.08.003

de Sousa Linhares, C. M., Ambrósio, M. M. Q., Castro, G., Torres, S. B., Esteras, C., De Sousa Nunes, G. H., et al. (2020). Effect of temperature on disease severity of charcoal rot of melons caused by *Macrophomina phaseolina*: implications for selection of resistance sources. *Eur. J. Plant Pathol.* 158, 431–441. doi: 10.1007/s10658-020-02083-w

Deokar, A. A., Kondawar, V., Jain, P. K., Karuppayil, S. M., Raju, N., Vadez, V., et al. (2011). Comparative analysis of expressed sequence tags (ESTs) between drought-tolerant and-susceptible genotypes of chickpea under terminal drought stress. *BMC Plant Biol.* 11:70. doi: 10.1186/1471-2229-11-70

Galkovskyi, T., Mileyko, Y., Bucksch, A., Moore, B., Symonova, O., Price, C. A., et al. (2012). GiA Roots: software for the high throughput analysis of plant root system architecture. *BMC Plant Biol.* 12:116. doi: 10.1186/1471-2229-12-116

González, L., and González-Vilar, M. (2001). "Determination of relative water content," in *Handbook of Plant Ecophysiology Techniques*, ed. M. J. Reigosa Roger (Dordrecht: Springer), 207–212. doi: 10.1007/0-306-48057-3_14

Hemissi, I., Gargouri, S., Hlel, D., Hachana, A., Abdi, N., and Sifi, B. (2018). Impact of nitrogen fertilization on Fusarium foot and root rot and yield of durum wheat. *Tunis. J. Plant Prot.* 13, 31–38.

Irulappan, V., and Senthil-Kumar, M. (2021). Dry root rot disease assays in chickpea: a detailed methodology. *J. Vis. Exp.* 167:e61702. doi: 10.3791/61702

Irulappan, V., Kandpal, M., Saini, K., Rai, A., Ranjan, A., Sinharoy, S., et al. (2022). Drought stress exacerbates fungal colonization and endodermal invasion and dampens defense responses to increase dry root rot in chickpea. *Mol. Plant Microbe Interact.* doi: 10.1094/MPMI-07-21-0195-FI

Jayalakshmi, S., Usharani, S., Benagi, V., and Mannur, D. (2008). Sources of resistance to dry root rot of chickpea caused by *Rhizoctonia bataticola*. *Agric. Sci. Digest* 28, 147–148.

Kashiwagi, J., Krishnamurthy, L., Crouch, J. H., and Serraj, R. (2006). Variability of root length density and its contributions to seed yield in chickpea (*Cicer arietinum* L.) under terminal drought stress. *Field Crops Res.* 95, 171–181. doi: 10.1016/j.fcr.2005.02.012

Kumar, M. N., Jane, W.-N., and Verslues, P. E. (2012). Role of the putative osmosensor *Arabidopsis* histidine Kinase1 in dehydration avoidance and low-water-potential response. *Plant Physiol.* 161, 942–953. doi: 10.1104/pp.112.209791

Lynch, J. P., Chimungu, J. G., and Brown, K. M. (2014). Root anatomical phenes associated with water acquisition from drying soil: targets for crop improvement. *J. Exp.l Bot.* 65, 6155–6166. doi: 10.1093/jxb/eru162

Marquez, N., Giachero, M. L., Declerck, S., and Ducasse, D. A. (2021). *Macrophomina phaseolina*: general characteristics of pathogenicity and methods of control. *Front. Plant Sci.* 12:634397. doi: 10.3389/fpls.2021.634397

Mayek-Pérez, N., García-Espinosa, R., López-Castañeda, C., Acosta-Gallegos, J. A., and Simpson, J. (2002). Water relations, histopathology and growth of common bean (*Phaseolus vulgaris* L.) during pathogenesis of *Macrophomina phaseolina* under drought stress. *Physiol. Mol. Plant Pathol.* 60, 185–195. doi: 10.1006/pmpp.2001.0388

O'Geen, A. (2012). Soil water dynamics. *Nat. Educ. Knowl.* 3:12.

Rai, A., Irulappan, V., and Senthil-Kumar, M. (2022). Dry root rot of chickpea: a disease favored by drought. *Plant Dis.* 106, 346–356. doi: 10.1094/PDIS-07-21-1410-FE

Reichert, J. M., Albuquerque, J. A., Kaiser, D. R., Reinert, D. J., Urach, F. L., and Carlesso, R. (2009). Estimation of water retention and availability in soils of Rio Grande do Sul. *Rev. Bras. Cienc. Solo* 33, 1547–1560. doi: 10.1590/s0100-06832009000600004

Sharath Chandran, U. S., Tarafdar, A., Mahesha, H. S., and Sharma, M. (2021). Temperature and soil moisture stress modulate the host defense response in chickpea during dry root rot Incidence. *Front. Plant Sci.* 12:653265. doi: 10.3389/fpls.2021.653265

Sharma, M., Ghosh, R., and Pande, S. (2015). Dry root rot (*Rhizoctonia bataticola* (Taub.) Butler): an emerging disease of chickpea–where do we stand? *Arch. Phytopathol. Plant Prot.* 48, 797–812. doi: 10.1080/03235408.2016.1140564

Sharma, M., and Pande, S. (2013). Unravelling effects of temperature and soil moisture stress response on development of dry root rot [*Rhizoctonia bataticola* (Taub.)] butler in chickpea. *Am. J. Plant Sci.* 4, 584–589. doi: 10.4236/ajps.2013.43076

Sinha, R., Irulappan, V., Mohan-Raju, B., Suganthi, A., and Senthil-Kumar, M. (2019). Impact of drought stress on simultaneously occurring pathogen infection in field-grown chickpea. *Sci. Rep.* 9:5577. doi: 10.1038/s41598-019-41463-z

Sinha, R., Irulappan, V., Patil, B. S., Reddy, P. C. O., Ramegowda, V., Mohan-Raju, B., et al. (2021). Low soil moisture predisposes field-grown chickpea plants to dry root rot disease: evidence from simulation modeling and correlation analysis. *Sci. Rep.* 11:6568. doi: 10.1038/s41598-021-85928-6

Srinivas, P., Ramesh Babu, S., Sharma, M., Narayan Reddy, P., and Pushpavathi, B. (2017). Effect of temperature on *Rhizoctonia bataticola* and dry root rot in chickpea. *Int. J. Curr. Microbiol. Appl. Sci.* 6, 3349–3355.

Talekar, S., Viswanatha, K., and Lohithasawa, H. (2021). Screening chickpea genotypes for resistance to *rhizoctonia bataticola* in controlled conditions. *Legume Res.* 44, 101–108.

Wagh, P. (2015). *Studies on Dry Root Rot (Rhizoctonia bataticola Taub (Butler)) of Chickpea (Cicer arietinum)*. Raipur: Indira Gandhi Krishi Vishwavidyalaya.

Wang, W., Ding, G.-D., White, P. J., Wang, X.-H., Jin, K.-M., Xu, F.-S., et al. (2019). Mapping and cloning of quantitative trait loci for phosphorus efficiency in crops: opportunities and challenges. *Plant Soil* 439, 91–112. doi: 10.1007/s11104-018-3706-6

Xiong, R., Liu, S., Considine, M. J., Siddique, K. H. M., Lam, H.-M., and Chen, Y. (2021). Root system architecture, physiological and transcriptional traits of soybean (*Glycine max* L.) in response to water deficit: a review. *Physiol. Plant.* 172, 405–418. doi: 10.1111/ppl.13201

Yasmin, H., Naz, R., Nosheen, A., Hassan, M. N., Ilyas, N., Sajjad, M., et al. (2020). Identification of new biocontrol agent against charcoal rot disease caused by *Macrophomina phaseolina* in soybean (*Glycine max* L.). *Sustainability* 12:6856. doi: 10.3390/su12176856

Zhan, A., Schneider, H., and Lynch, J. P. (2015). Reduced lateral root branching density improves drought tolerance in maize. *Plant Physiol.* 168, 1603–1615. doi: 10.1104/pp.15.00187

Conflict of Interest: The authors declare that the research was conducted in the absence of any commercial or financial relationships that could be construed as a potential conflict of interest.

Publisher's Note: All claims expressed in this article are solely those of the authors and do not necessarily represent those of their affiliated organizations, or those of the publisher, the editors and the reviewers. Any product that may be evaluated in this article, or claim that may be made by its manufacturer, is not guaranteed or endorsed by the publisher.

frontiers | Frontiers in Plant Science

ORIGINAL RESEARCH
published: 16 May 2022
doi: 10.3389/fpls.2022.886541

The Effects of Brief Heat During Early Booting on Reproductive, Developmental, and Chlorophyll Physiological Performance in Common Wheat (*Triticum aestivum L.*)

*Jiemeng Xu[1], Claudia Lowe[1], Sergio G. Hernandez-Leon[2], Susanne Dreisigacker[3], Matthew P. Reynolds[3], Elisa M. Valenzuela-Soto[2], Matthew J. Paul[1] and Sigrid Heuer[1,4]**

[1] Plant Science Department, Rothamsted Research, Harpenden, United Kingdom, [2] Centro de Investigación en Alimentación y Desarrollo A.C., Carretera Gustavo Enrique Aztiazarán Rosas, Hermosillo, Mexico, [3] International Maize and Wheat Improvement Center (CIMMYT), Texcoco, Mexico, [4] Pre-Breeding Department, National Institute of Agricultual Botany (NIAB), Cambridge, United Kingdom

OPEN ACCESS

Edited by:
Pasala Ratnakumar,
Indian Institute of Oilseeds Research (ICAR), India

Reviewed by:
Renu Munjal,
Chaudhary Charan Singh Haryana Agricultural University, India
Ashok Singamsetti,
Banaras Hindu University, India

***Correspondence:**
Sigrid Heuer
sigrid.heuer@niab.com

Specialty section:
This article was submitted to Plant Abiotic Stress, a section of the journal Frontiers in Plant Science

Received: 28 February 2022
Accepted: 04 April 2022
Published: 16 May 2022

Citation:
Xu J, Lowe C, Hernandez-Leon SG, Dreisigacker S, Reynolds MP, Valenzuela-Soto EM, Paul MJ and Heuer S (2022) The Effects of Brief Heat During Early Booting on Reproductive, Developmental, and Chlorophyll Physiological Performance in Common Wheat (Triticum aestivum L.). Front. Plant Sci. 13:886541. doi: 10.3389/fpls.2022.886541

Rising temperatures due to climate change threaten agricultural crop productivity. As a cool-season crop, wheat is heat-sensitive, but often exposed to high temperatures during the cultivation period. In the current study, a bread wheat panel of spring wheat genotypes, including putatively heat-tolerant Australian and CIMMYT genotypes, was exposed to a 5-day mild (34°C/28°C, day/night) or extreme (37°C/27°C) heat stress during the sensitive pollen developmental stage. Worsening effects on anther morphology were observed, as heat stress increased from mild to extreme. Even under mild heat, a significant decrease in pollen viability and number of grains per spike from primary spike was observed compared with the control (21°C/15°C), with Sunstar and two CIMMYT breeding lines performing well. A heat-specific positive correlation between the two traits indicates the important role of pollen fertility for grain setting. Interestingly, both mild and extreme heat induced development of new tillers after the heat stress, providing an alternative sink for accumulated photosynthates and significantly contributing to the final yield. Measurements of flag leaf maximum potential quantum efficiency of photosystem II (Fv/Fm) showed an initial inhibition after the heat treatment, followed by a full recovery within a few days. Despite this, model fitting using chlorophyll soil plant analysis development (SPAD) measurements showed an earlier onset or faster senescence rate under heat stress. The data presented here provide interesting entry points for further research into pollen fertility, tillering dynamics, and leaf senescence under heat. The identified heat-tolerant wheat genotypes can be used to dissect the underlying mechanisms and breed climate-resilient wheat.

Keywords: heat stress, booting, pollen viability, tillering, SPAD and Fv/Fm, wheat

INTRODUCTION

Wheat is one of the most important crops for human consumption, grown on 220 million hectares with a total production of 760 million tons in 2020 (FAOSTAT). In scenarios of climate change, wheat plants are prone to be exposed to warmer and more variable temperatures (Trnka et al., 2014). Beyond a physiological threshold, high temperatures cause stress and impair plant growth and development. Both historical data and future predictions have revealed the negative effects of heat on wheat productivity at the global and regional scale (Liu et al., 2016; Zampieri et al., 2017; Pequeno et al., 2021). Therefore, it is crucial to identify and breed heat-adapted varieties to sustain wheat production and ensure food security.

In nature, the adverse effects of heat stress on plants can be variable depending on the intensity, duration, and developmental stage (Stone and Nicolas, 1995; Yeh et al., 2012). Most of the heat-related studies in wheat have been field-based and used late sowing to expose plants to high temperatures during the flowering and grain filling stages; however, short episodes of heat during earlier reproductive stages can also cause significant damage (Zampieri et al., 2017). Indeed, anther and pollen development are considered to be the stages most vulnerable to heat stress (Zinn et al., 2010; Rieu et al., 2017). Stage-specific treatments have found that wheat is particularly sensitive to heat around 8 days before anthesis, which coincides with the early meiosis to tetrad stage of pollen development (Saini and Aspinall, 1982; Prasad and Djanaguiraman, 2014). Because pollen development occurs during the booting stage, while spikes are still inside the developing pseudostem in wheat, the length of the auricles between the flag leaf and the penultimate leaf (referred as auricle interval length, AIL) has been used as a proxy for pollen development. AIL between 3 and 6 cm has been associated with this sensitive stage (Bokshi et al., 2021; Erena et al., 2021). Brief heat exposure during this sensitive period resulted in abnormal meiosis behavior (Omidi et al., 2014; Draeger and Moore, 2017) and a significant reduction in pollen fertility (Prasad and Djanaguiraman, 2014; Begcy et al., 2018; Browne et al., 2021). A few studies have examined the natural variation in pollen viability under heat stress and its association with yield, as booting usually occurs during the cooler time of the cropping season and it is difficult to apply precise stage-specific heat stress (Bheemanahalli et al., 2019; Bokshi et al., 2021). However, considering a warmer and increasingly erratic climate, this area warrants further investigation.

Spike number is one of the main components in determining wheat yield; it is highly variable and responsive to the environmental factors (Slafer et al., 2014). Interestingly, contrasting responses of spike number under heat stress have been reported. When exposed to continuous high temperatures during the terminal flowering and grain filling stages, spike formation and tillering were always reduced (Cai et al., 2016; Sharma et al., 2016; Dwivedi et al., 2017; Kumar et al., 2021). In contrast, after a short episode of heat stress during earlier developmental stages, spike numbers increased (Bányai et al., 2014; Chavan et al., 2019; Hütsch et al., 2019). Enhanced spike formation after early heat stress is surprising, but the underlying tillering dynamics and impact on final yield have not been discussed.

In addition to the effects on pollen fertility and spike number, heat-induced yield loss has also been ascribed to accelerated leaf senescence, shortening the duration of grain filling (Cossani and Reynolds, 2012; Pinto et al., 2016; Shirdelmoghanloo et al., 2016; Bergkamp et al., 2018; Sade et al., 2018). As indicators of senescence, chlorophyll soil plant analysis development (SPAD) (chlorophyll content index) (Richardson et al., 2002) and Fv/Fm (the maximum potential quantum yield of photosystem II) (Murchie and Lawson, 2013) have been widely used to evaluate this trait. Under terminal heat, SPAD and Fv/Fm were often reduced in leaf tissue during senescence and were closely related to yield-contributing traits, such as thousand grain weight (Talukder et al., 2014; Hassan et al., 2018; Mirosavljević et al., 2021; Touzy et al., 2022). Studies for the genetic analysis of these leaf senescence related traits are also available (Azam et al., 2015; Bhusal et al., 2018; Touzy et al., 2022). Nevertheless, time course measurements of SPAD and Fv/Fm, which enable model fitting and senescence parameter prediction, have rarely been captured in wheat under heat stress (Pinto et al., 2016; Šebela et al., 2020; Touzy et al., 2022), especially after brief heat during the early reproductive stage. In the present study, a wheat heat panel, including putatively heat-tolerant Australian and CIMMYT-nominated spring wheat genotypes, was exposed to a 5-day extreme (37°C/27°C) (Erena, 2018) or mild (34°C/28°C) heat stress during the early pollen developmental stage and analyzed for the effects on (i) pollen viability and seed set; (ii) spike formation and underlying tillering dynamics; (iii) leaf senescence measured with SPAD and Fv/Fm; and (iv) relationships among the reproductive, developmental, physiological, and yield-related traits.

MATERIALS AND METHODS

Plant Material

In this study, three greenhouse experiments (i.e., Exp1, Exp2, and Exp3) were conducted during 2020–2021 at the controlled environment and glasshouse facilities at Rothamsted Research, Harpenden, United Kingdom (51.8094°N, 0.3561°W). For Exp1 and Exp2, the same set of 14 wheat genotypes was used, and 22 lines (seven overlapping with Exp1 and Exp2) were grown in Exp3 (refer to **Supplementary Table 1** for genotype details). These lines are putatively heat-tolerant elite spring varieties (Sunstar, Sokoll, and Waagaan), parental lines and their pre-breeding materials (Cossani and Reynolds, 2015; Erena, 2018), as well as two lines from the United Kingdom included as controls.

Experimental Design and Heat Stress Treatment

Exp1

This experiment was conducted between June and September of 2020 and followed a split randomized complete block design (split RCBD) with four blocks/biological replicates. Fourteen genotypes (**Supplementary Table 1**) were randomly assigned to the whole plot within each block, and temperature treatments

(control/CT and heat/HT) were assigned to the subplots within each whole plot. Two seeds were sown in separate pots filled with Rothamsted Standard compost (75% medium grade peat; 12% screened sterilized loam; 3% medium grade vermiculite; 10% 5 mm screened lime-free grit) and fertilized with Osmocote Exact for 3–4 months at the rate of 3.5 kg/m^3. One week after sowing, seedlings were thinned down to one per pot and grown under natural light glasshouse conditions with a 16-h light period; they were supplemented with artificial light (230W LED; Kroptek Ltd., London, United Kingdom) if natural light intensity fell below 175 μmol/m^2/s^1. The temperature in the glasshouse was set at 21°C/15°C (day/night, actual value: 21.5 ± 0.4/16.3 ± 0.5°C) and the relative humidity (RH) was around 60/75% (day/night) (**Supplementary Figure 1A**). At the booting stage, plants with the primary tiller reached the targeted AIL (**Supplementary Figure 2A**) of 6 cm (actual value for each genotype in **Supplementary Figure 2B**) and were sequentially moved into Fitotron Modular Plant Growth Chambers (HGC1514; Weiss Technik UK Ltd., Loughborough, United Kingdom) for HT treatment (36.97 ± 0.03/26.95 ± 0.17°C, day/night). The light period was 16 h and the intensity was maintained around 600 μmol/m^2/s^1 at the plant level. The RH was maintained between 70 and 75% (**Supplementary Figure 1D**). Plants for CT treatment were kept in the glasshouse. After 5 days of HT treatment, heat-stressed plants were moved back to the glasshouse until final harvest.

Exp2

This experiment was conducted between August and December of 2020 and with the same set of 14 genotypes (**Supplementary Table 1**). The experiment design and plant cultivation conditions were similar as in Exp1. The temperature in the glasshouse was also set at 21°C/15°C (day/night, actual value: 20.6 ± 0.8/15.4 ± 0.7°C) and the RH was around 57/69% (day/night) (**Supplementary Figure 1B**). When the AIL of the primary tiller reached 2–3 cm (actual value for each genotype in **Supplementary Figure 2C**), plants for HT treatment were sequentially moved into the same growth chamber as Exp1 with the temperature of 37.02 ± 0.01/27.00 ± 0.01°C (day/night) (**Supplementary Figure 1E**). Plants for CT treatment were also moved into a similar growth chamber with the temperature of 21.01 ± 0.01/15.01 ± 0.01°C (**Supplementary Figure 1E**). The light period, intensity, and RH were similar between CT and HT treatments with settings of 16 h, 600 μmol/m^2/s^1, and 70–75% respectively. After 5 days in the growth chambers, plants were moved back to the glasshouse until final harvest.

Exp3

This experiment was conducted between January and May of 2021 and with 22 genotypes (**Supplementary Table 1**). The experiment design and plant cultivation conditions were the same as the previous two experiments. The temperature in the glasshouse was also set at 21°C/15°C (day/night, actual value: 21.7 ± 0.4/15.4 ± 0.3°C) and the RH was around 42/49% (day/night) (**Supplementary Figure 1C**). When the AIL of the primary tiller reached 2–3 cm (actual value in **Supplementary Figure 2D**), plants for HT treatment were sequentially moved into the growth chamber with a mild temperature of 34.00 ± 0.02/28.00 ± 0.01°C (day/night) (**Supplementary Figure 1F**). Plants for CT treatment were also moved into a similar growth chamber with the temperature of 21.01 ± 0.02/15.01 ± 0.01°C (**Supplementary Figure 1F**). The light period, intensity, and RH were similar between CT and HT treatments with settings of 16 h, 600 μmol/m/s, and 70–75% respectively. After 5 days in the growth chambers, plants were moved back to the glasshouse until final harvest.

Morphological, Phenological, and Physiological Measurements

On the day before (day 0) and after (day 6) HT treatment, the primary tiller of each plant was tagged and measured for AIL. Plant height (PH) was also recorded at these two time points in Exp2 and Exp3 (**Supplementary Figure 1G**). Chlorophyll SPAD and Fv/Fm (maximum potential quantum efficiency of Photosystem II) were measured at the same time as AIL and weekly thereafter (**Supplementary Figure 1G**). The SPAD measurement was performed with an MC-100 Chlorophyll Concentration Meter (Apogee Instruments, Inc., Logan, UT, United States). Fv/Fm was measured with a Pocket PEA (Hansatech Instruments Ltd., Norfolk, United Kingdom) after 15–20 min dark adaptation. For each plant, the mean SPAD value of measurements at the tip, middle, and bottom of flag leaf was obtained and one measurement of Fv/Fm was made in the middle of flag leaf. After the HT treatment, the heading date of each plant was recorded to calculate days to heading in Exp2 and Exp3. Physiological maturity of the spike on the tagged tiller was recorded as days to maturation. These measurements were conducted with four biological replicates of each genotype and treatment combination.

Measurement With Tagged Tillers/Spikes for Pollen Fertility and the Number of Grains Per Spike

During anthesis in Exp2 and Exp3, the fourth or fifth spikelet (counted from the bottom) was sampled from the tagged tiller. One anther from two florets at the bottom was photographed for a representative image and length of the anther was measured. In Exp3, the remaining five anthers from two florets at the bottom were pooled together for pollen viability analysis using staining with Lugol's solution. Fully stained pollen was scored as viable, whereas partially stained or aberrant shaped pollen was scored as non-viable. At maturity, the number of filled grains of the tagged spike was counted and recorded as the number of grains per spike, and also, spike length (cm) and number of spikelets were measured. Four biological replicates were used for these measurements.

Measurement of Tillering Dynamics

In Exp1, development of extra young spikes after heat stress was observed. In Exp2 and Exp3, tiller number was therefore continuously counted for four biological replicates of CT and HT-treated plants of each genotype on the day (day 0) before and

after (day 6) the 5-day HT treatment, and on weekly intervals thereafter until maximum tillering (**Supplementary Figure 1G**).

Yield-Related Measurements at Maturation

At maturity, the spikes per plant were distinguished into "old" spikes (labeled just before starting the HT treatment in Exp2 and Exp3) and "new" spikes, harvested separately, and then dried in oven at 40°C for 7 days prior to mechanical threshing and cleaning. The weight, number, length, and width were then determined for grain samples from old and new spikes separately with a scale and a MARViN digital seed analyzer (MARViTECH GmbH., Wittenburg, Germany). Grain yield per plant was calculated as the sum of grains from old and new spikes. The aboveground biomass for each plant was determined as the weight of all straw materials dried in an oven at 80°C for 48 h. The yield-related measurements were analyzed with four biological replicates.

Statistical Analysis

The data from the time course SPAD measurements were fitted using a generalized additive model (GAM) for each of the three experiments to estimate maximum SPAD (SPADmax), senescence onset (SenOnset), and senescence rate (SenRate) (**Supplementary Figure 3**). SPAD was predicted by a smooth function of time (days counted from stress initiation), with a separate smooth function fitted for each combination of genotype and treatment. The Exp1 model used eight basis functions, whereas Exp2 and Exp3 used seven basis functions. SPADmax was estimated from the fitted predicted model. SenOnset was calculated as the day that SPAD fell to 95% of the maximum SPAD. Senescence period was defined over 14 days from the onset or until the end of the measurement, whichever was shorter. SenRate was then calculated as the daily reduction of SPAD over the senescence period. GAMs were fitted in R package (version 3.6.1) using the "mgcv" package (version 1.8-35) (Wood, 2011).

All trait measurements and calculated parameters (**Supplementary Table 2**) were used for statistical analysis in R 4.0.3.[1]. First, descriptive statistics were summarized with the "describeBy" from the "psych" package (Revelle, 2020). The effects of genotype treatment and the interaction were obtained from ANOVA with the model fitted with "lmer" from the R package "lmerTest" (Kuznetsova et al., 2017); genotype, treatment, and their interaction were treated as fixed factors, while block and genotype nested in block were treated as random effects. Later, Tukey's *post hoc* test was carried out for multiple test comparisons to identify genotypic variation. Estimated marginal means were calculated for each combination of genotype and treatment. Subsequently, for either CT or HT treatment, Pearson correlation coefficient table was calculated by using "tab_corr" from "sjPlot" package (Lüdecke, 2021) among measurements and pairwise-deletion method was used to account for missing data. For each experiment and temperature treatment, correlations among different traits were visualized as networks with the "qgraph" package (Epskamp et al., 2012).

[1]https://www.R-project.org/

RESULTS

Heat-Impaired Pollen Fertility and Number of Grains Per Spike

To understand the effects of heat on pollen development and grain setting, the primary tiller of each plant was tagged and measured. In Exp1 and Exp2, the imposed severe heat treatment of 37°C/27°C caused nearly complete loss of grain setting for all genotypes, except for Paragon and Cadenza (**Supplementary Figure 4**). The anther morphology was also severely changed by the HT treatments indicating complete absence of viable pollen (**Figures 1A,B**). In Exp3, relatively mild heat stress (34°C/28°C) also significantly reduced anther length; however, this was less severe compared with Exp2 (**Figures 1A,B**) and pollen viability was therefore analyzed by staining with Lugol's solution. The results showed considerable variation among genotypes, ranging from 0 to 60%. One line (SWBL1.1, a progeny between the cross of Sokoll and Weebill1) had the highest pollen viability (relative to control value), followed by SWES, SUN (Sunstar), and WBL1.2 (Weebill1) (**Figure 1C**). The number of grains of the tagged primary spike was also variable among the genotypes, with SUN showing the highest value relative to control value (**Figure 1D**). Further analysis found a positive correlation between pollen viability and the number of grains per spike under HT (**Figure 1F**), but not under CT treatment (**Figure 1E**).

Heat-Stimulated Tillering/Spike Formation and Its Association With Yield

During the ripening stage of Exp1, the senescence status of tillers/spikes was clearly separated into two groups (**Figure 2A**) and tillers were therefore distinguished into old (pre-heat) and new (post-heat) spikes for each plant. About 1 week after heat treatment, new tiller outgrowth was noticed from the bottom of HT-stressed plants (**Figures 2B,C**). A final count of spikes found significantly more new spikes in the HT-treated plants compared with the CT plants in Exp1 ($p < 0.001$), Exp2 ($p < 0.001$), and Exp3 ($p < 0.001$) (**Figures 2D–F**), while the number of old spikes was similar between HT and CT conditions (**Supplementary Figure 5**). In addition, there was no significant interaction between treatment and genotype (**Figures 2D–F**), indicating that all genotypes responded similarly to the HT treatment in terms of new spike formation. The analysis of tillering dynamics in Exp2 and Exp3 showed that onset of new tiller development commenced at 2–3 weeks after the HT treatment, with a stronger effect observed in Exp2 (**Figures 2G,H**). Moreover, the more severe heat stress in Exp2 (37°C/27°C) also caused tiller retardation on day 6, 1 day after the end of the HT treatment (**Figure 2G**), but this was not observed under the milder heat stress condition in Exp3 (34°C/28°C) (**Figure 2H**).

As new tillers developed after the HT treatment and extended the days to maturity of the plants, the aboveground biomass per plant (including both old and new tillers) was very similar between HT and CT treatments (**Figures 3A–C**). Nevertheless, the overall grain yield per plant was significantly reduced after the HT treatment in all three experiments ($p < 0.001$ for all) (**Figures 3D–F**). This was primarily due

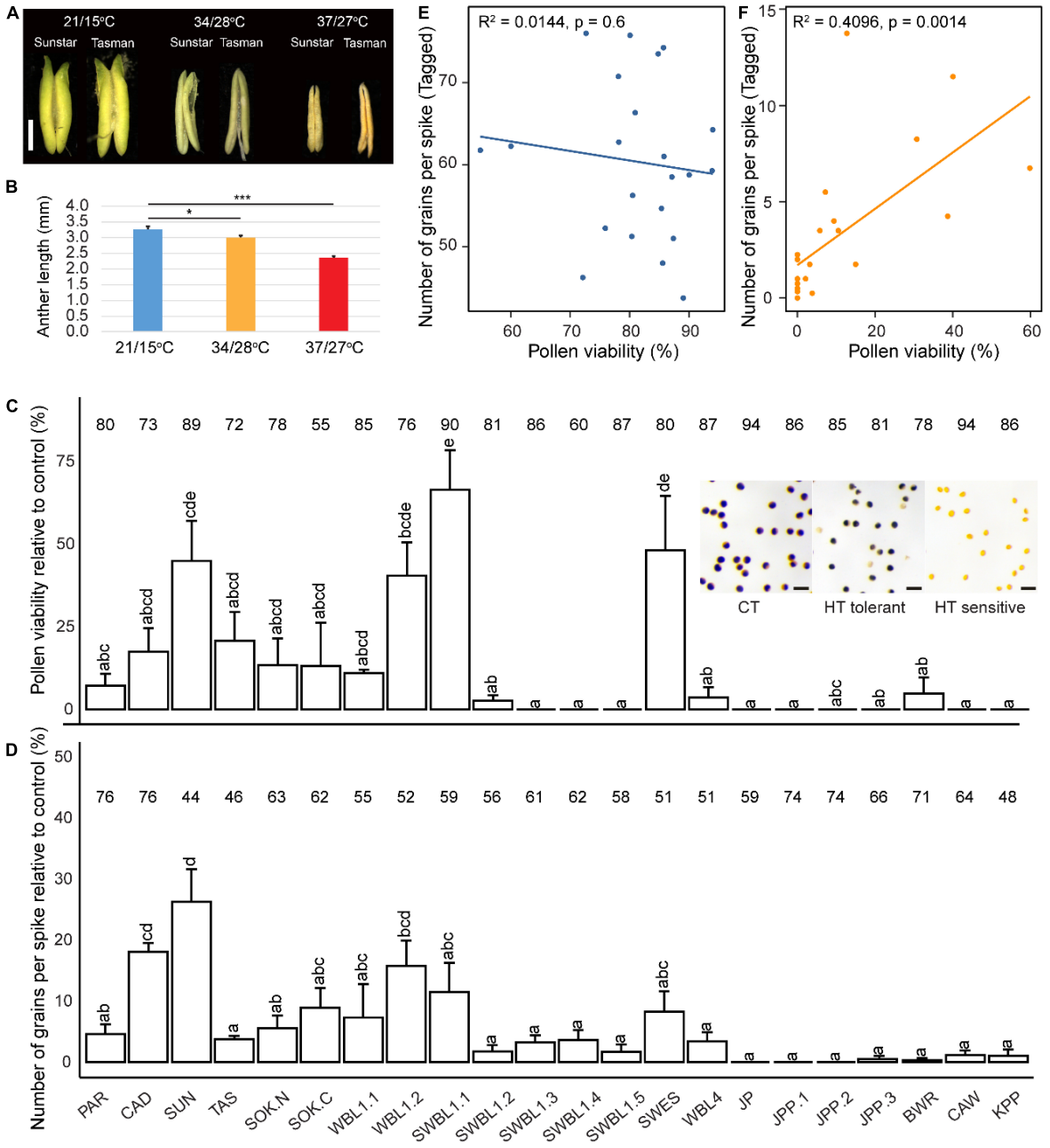

FIGURE 1 | The heat effects on wheat reproductive traits. Anther morphology after heat treatments in two representative genotypes is shown in (**A**, bar = 1 mm). Average anther length across all analyzed genotypes in Exp2 (37/27°C) and Exp3 (34/28°C) is shown in **(B)**. Genotypic variation of pollen viability **(C)** and the number of grains per spike **(D)** under heat in Exp3. Representative pollen images for CT, HT-tolerant, and HT-sensitive were inserted (**C**, bar = 100 μm). The data were obtained from the primary tiller and calculated as relative to control values, which are shown on the top of each bar. Pearson correlation between pollen viability and number of grains per spike under control **(E)** and heat **(F)**. Significance level: ***$p < 0.001$; **$p < 0.01$; *$p < 0.05$; *$p < 0.05$.

to heat-induced sterility in the old spikes (**Figures 3G–I**). However, heat-induced formation of new spikes gave rise to similar (Exp2, **Figure 3K**) or even significantly higher grain yield from new spikes in Exp1 and Exp3 (**Figures 3J,L**). The proportion of yield from new spikes after the HT treatment was therefore significantly higher than under CT conditions (**Supplementary Figure 6**). As sink size was reduced by limited seed setting of old spikes under HT condition, source supply became more than sufficient for the survived developing grains, and their width and length were significantly higher than grains of old spikes from control plants (**Supplementary Table 2**). By contrast, the grains from new spikes showed variable responses in terms of width and length (**Supplementary Table 2**).

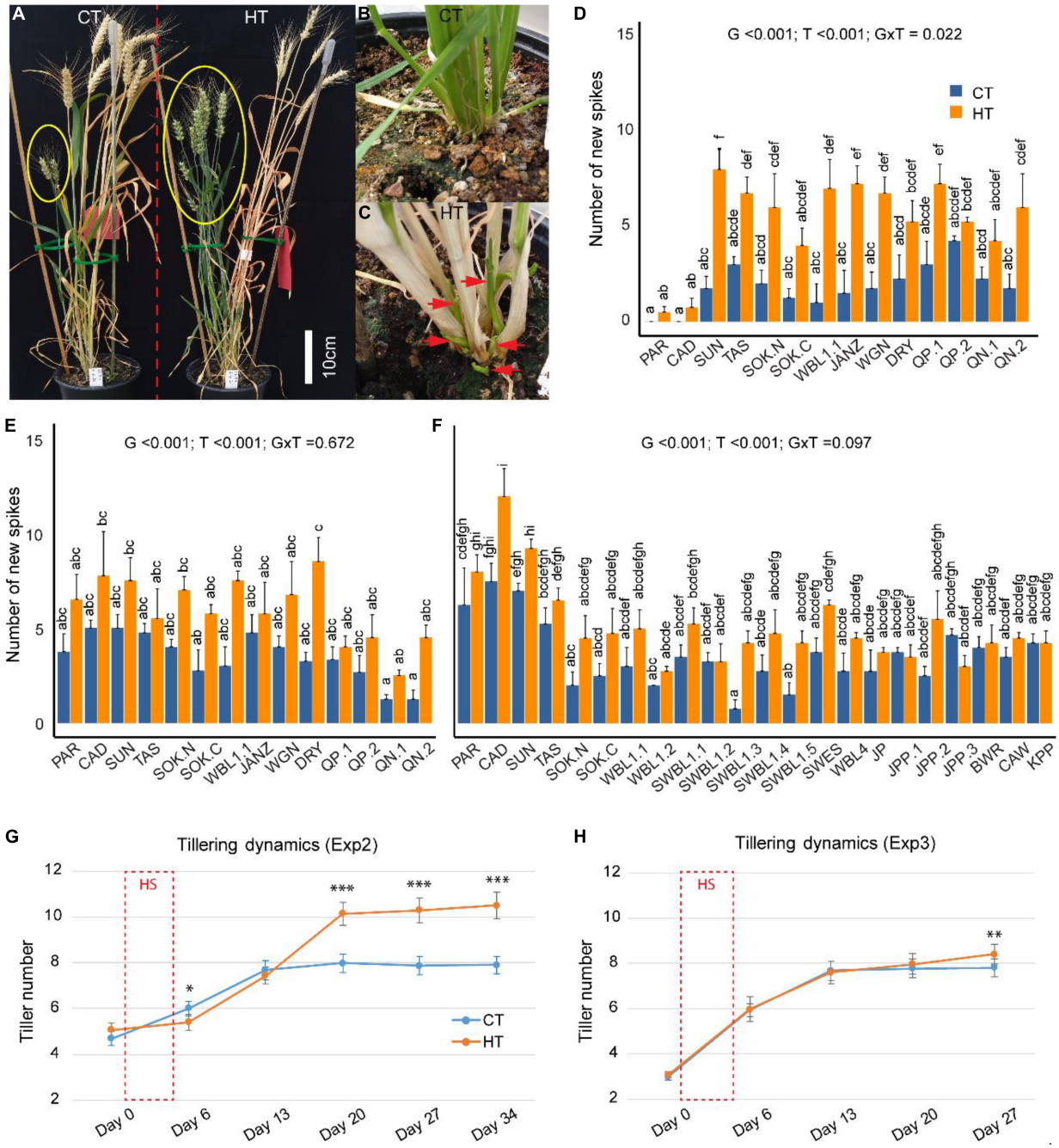

FIGURE 2 | The effects of heat treatments on tillering/spike formation. After heat (HT) treatment, new tillers/spikes (in yellow ellipse) were vigorously stimulated, while controls were not (CT, **A**). Tiller outgrowth from CT **(B)** and HT **(C)** around 1 week after stress treatment. A comparison of the number of new spikes between CT and HT in Exp1 **(D)**, Exp2 **(E)**, and Exp3 **(F)**. The effects of genotype/G, treatment/T, interaction/G × T were indicated for each panel. Dynamic change of tillering before (day 0), after (day 6) the 5-day HT treatment (days 1–5), and weekly intervals in Exp2 **(G)** and Exp3 **(H)**. Significance level: ***$p < 0.001$; **$p < 0.01$.

Heat Effects on Plant Morphology, Phenology, and Chlorophyll Dynamics

When wheat plants were exposed to heat stress during the early booting stage, the increase in AIL ($p < 0.001$ for Exp1 and Exp2) and PH ($p < 0.001$ Exp2) during the 5-day treatments was significantly reduced by the HT of 37°C/27°C compared with the CT of 21°C/15°C (**Figures 4A,B,D**). In contrast, the AIL ($p = 0.065$) and PH ($p = 0.279$) were marginally affected under the milder HT of 34°C/28°C in Exp3 (**Figures 4C,E**). HT treatments also changed plant phenology as indicated by the significantly reduced number of days to heading (DTH) ($p < 0.001$ for Exp2 and Exp3) (**Figures 4F,G**)

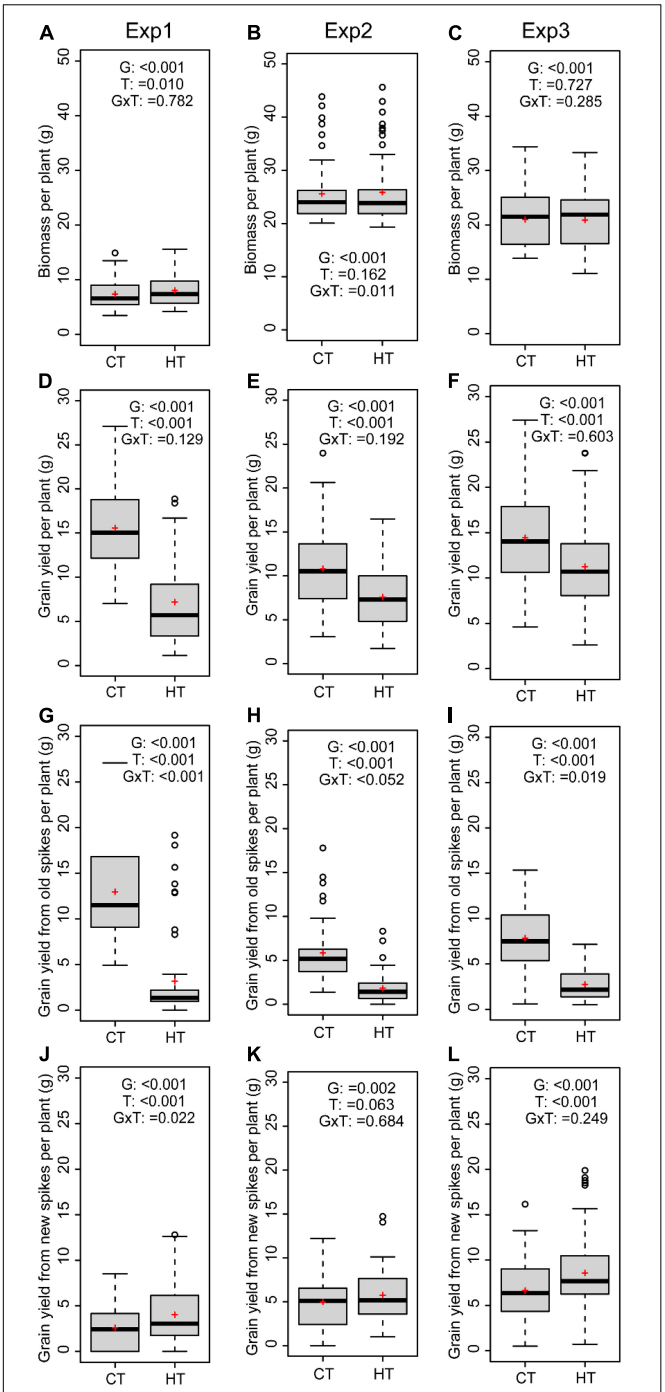

FIGURE 3 | Average values of wheat genotypes grown under high temperature (HT) or control (CT) across the three experiments are shown for biomass **(A–C)**, grain yield per plant **(D–F)**, grain yield from old spikes **(G–I)**, and grain yield from new spikes **(J–L)**. The effects of genotype (G), treatment (T), and interaction (G × T) are indicated for each panel.

and days to maturation (DTM) ($p < 0.001$ for Exp1, Exp2, and Exp3) (**Figure 4H**).

To understand the physiological basis of changes in phenology, dynamic changes in SPAD and Fv/Fm were compared between CT and HT treatments. On day 6 (1 day after treatment), in comparison to the corresponding CT conditions, SPAD value was significantly reduced by the severe heat (37°C/27°C) in Exp1 (**Figure 5A**) and Exp2 (**Figure 5B**), but surprisingly increased slightly after the mild heat (34°C/28°C) in Exp3 and maintained a higher maximum SPAD value (**Figures 5E,F**). At later stages, however, an accelerated decrease in SPAD was observed under HT conditions in all three experiments, irrespective of heat stress intensity (**Figures 5A,B,E**). Based on the time course of SPAD measurements, GAMs were fitted to estimate maximum SPAD (SPADmax), senescence onset (SenOnset), and senescence rate (SenRate) for each combination of genotype and treatment. In Exp1 and Exp3, SenOnset from HT treatment was reproducibly and significantly advanced in comparison with CT conditions, whereas SenRate was similar between treatments (**Figures 5C,F**). By contrast, Exp2 showed an opposite response with similar SenOnset between treatments, but an increased SenRate under HT (**Figure 5D**). This variation between the three experiments may be due to variable intensities of natural sunlight. Even within the same experiment, some genotypes showed earlier SenOnset, while others showed faster SenRate under HT treatment (**Supplementary Figures 7–9**). In addition, the Fv/Fm value at day 6 was always significantly reduced by HT treatment in all three experiments indicating a negative effect of the HT on PSII (**Supplementary Figure 10**).

Analysis of Trait Correlations From Different Experiments and Temperature Conditions

To understand the relationships among different traits across genotypes, correlations were calculated (**Supplementary Table 3**) and visualized as networks (**Figure 6**). Number of grain per spike (GpS) showed different correlations under control and HT conditions; In Exp1 and Exp2, there was no correlation between GpS and any other trait under HT, but under CT, it was strongly and positively correlated with the number of spikelets (SpikeletN) ($r = 0.98^{***}$ for Exp1 and 0.81^{**} for Exp2) and length (SpikeL) ($r = 0.94^{***}$ for Exp1 and 0.79^{**} for Exp2) of the tagged spike, as well as with biomass ($r = 0.88^{***}$) and yield ($r = 0.88^{***}$) in Exp1. In Exp3, GpS was also associated with different traits between CT and HT. The importance of induced new tillers and spikes after heat stress was corroborated by the reproducible strong positive correlations ($r = 0.98^{***}$, 0.92^{***}, 0.80^{***} for Exp1, Exp2, and Exp3, respectively) between grain yield of new tillers (GY.NT) and total grain yield (GY), observed in all three experiments (**Figure 6** and **Supplementary Table 3**). This suggests a critical role of new spikes in mitigating heat-induced yield reduction. In addition, the morphological traits, increase in AIL and PH, were generally positively correlated with yield or biomass-related traits, regardless of temperature treatments. Ultimately, SPAD and Fv/Fm parameters were not consistently correlated with other traits from different experiments and treatments. In Exp1, SenOnset showed HT-specific weak positive correlations with a grain yield of old tillers (GY.OT) ($r = 0.62^{*}$) and a spike number of new tillers (SpikeN.NT) ($r = 0.69^{*}$); SenRate was closely related

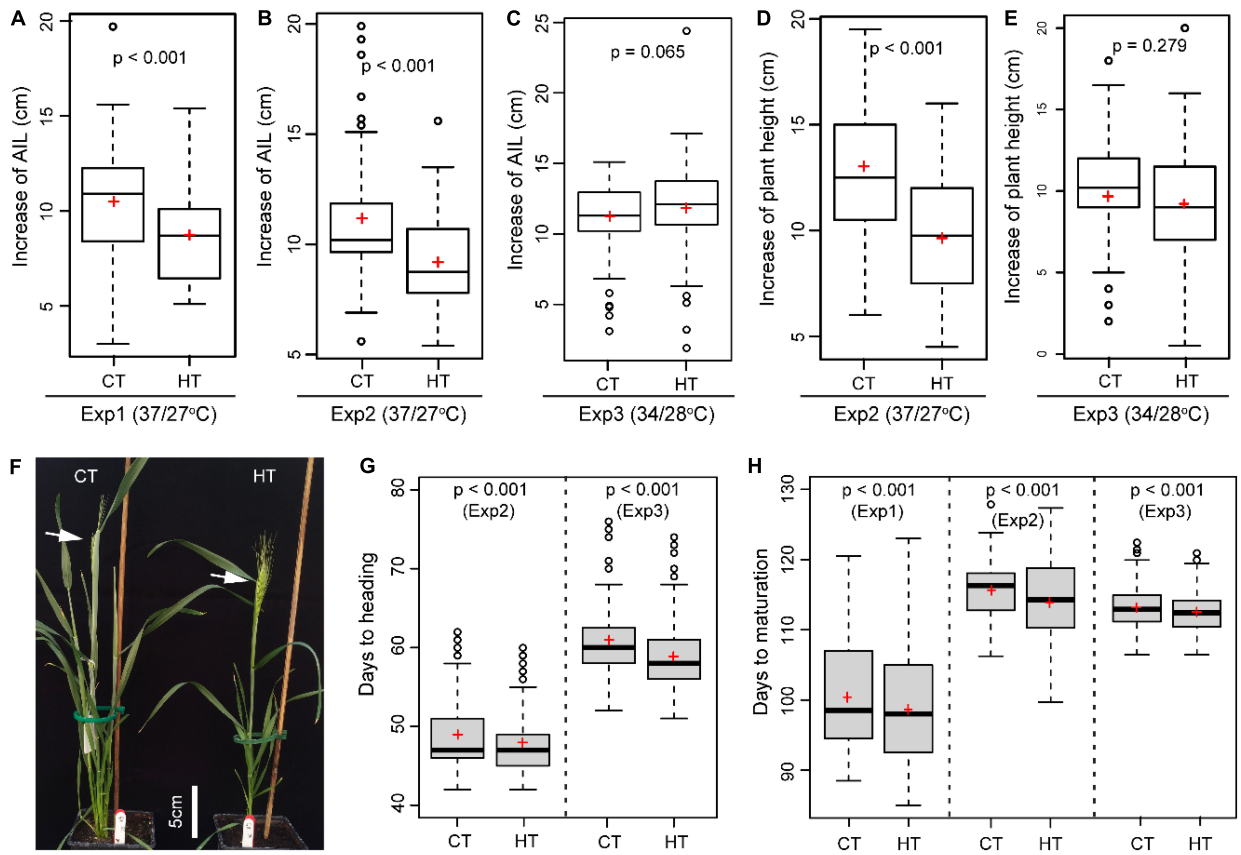

FIGURE 4 | The heat effects on plant morphology and phenology. Comparison of the effect of heat (HT) and control (CT) treatments on the increase of auricle interval length (AIL, **A–C**), the increase in plant height **(D,E)**, days to heading **(F,G)**, and days to maturation **(H)**.

to yield traits in both Exp2 (r = 0.62* with GY.NT under CT; r = 0.79** with GY.NT and 0.69* with GY under HT) and Exp3 (r = 0.47* with GY and 0.53* with SpikeL under CT; r = 0.45* with GpS and 0.49* with SpikeL under HT), but not heat-specific; in Exp2, SPADmax was important, as it was strongly correlated with Spikelet (r = 0.66* under CT, 0.75** under HT) and SpikeL (r = 0.70* under CT, 0.74** under HT) of tagged spike (**Figure 6** and **Supplementary Table 3**).

DISCUSSION

Importance and Limitation of Pollen Viability as a Target Trait for Wheat Heat Research

In the present study, anther morphology was gradually affected under two levels of heat stress, 34°C/28°C (day/night) and 37°C/27°C, applied for 5 days during early booting stage coinciding with pollen development. The more severe heat stress condition in this study led to a complete loss of pollen viability, while results from a parallel study, in which the same 37°C/27°C heat treatment was applied that lasted for only 3 days (Erena, 2018), were similar to the 5-day, milder temperature (34°C/28°C) treatment, suggesting that both stress intensity and duration are critical to screening reproductive heat tolerance. Under the 34°C/28°C condition, pollen viability was considerably variable among genotypes. Two of the lines (SWB1.1 and SWES) with high pollen viability share one common parent, Sokoll, in their pedigree. Sokoll is an advanced wheat line derived from synthetic hexaploid wheat and has shown a yield advantage under terminal heat stress in other reports (Cossani and Reynolds, 2015; Thistlethwaite et al., 2020), although it did not show particularly high pollen viability after early booting-stage heat stress in this study. These results suggest stage-specific heat tolerance; therefore, it is necessary to pyramid tolerant traits across different developmental stages. Another parental line included in this study, Weebill1 (WBL1.1 and WBL1.2), has previously been reported to be tolerant to a wide range of variable environmental conditions (Singh et al., 2007). One of the most tolerant genotypes identified in this study was Sunstar, in agreement with data reported by Erena (2018) who also demonstrated the reproductive heat tolerance of Sunstar. These identified genotypes with heat tolerance during pollen development may be suitable donors for breeding and warrant further studies to understand the underlying genetic and molecular-physiological mechanisms. The importance of pollen viability is supported by its positive

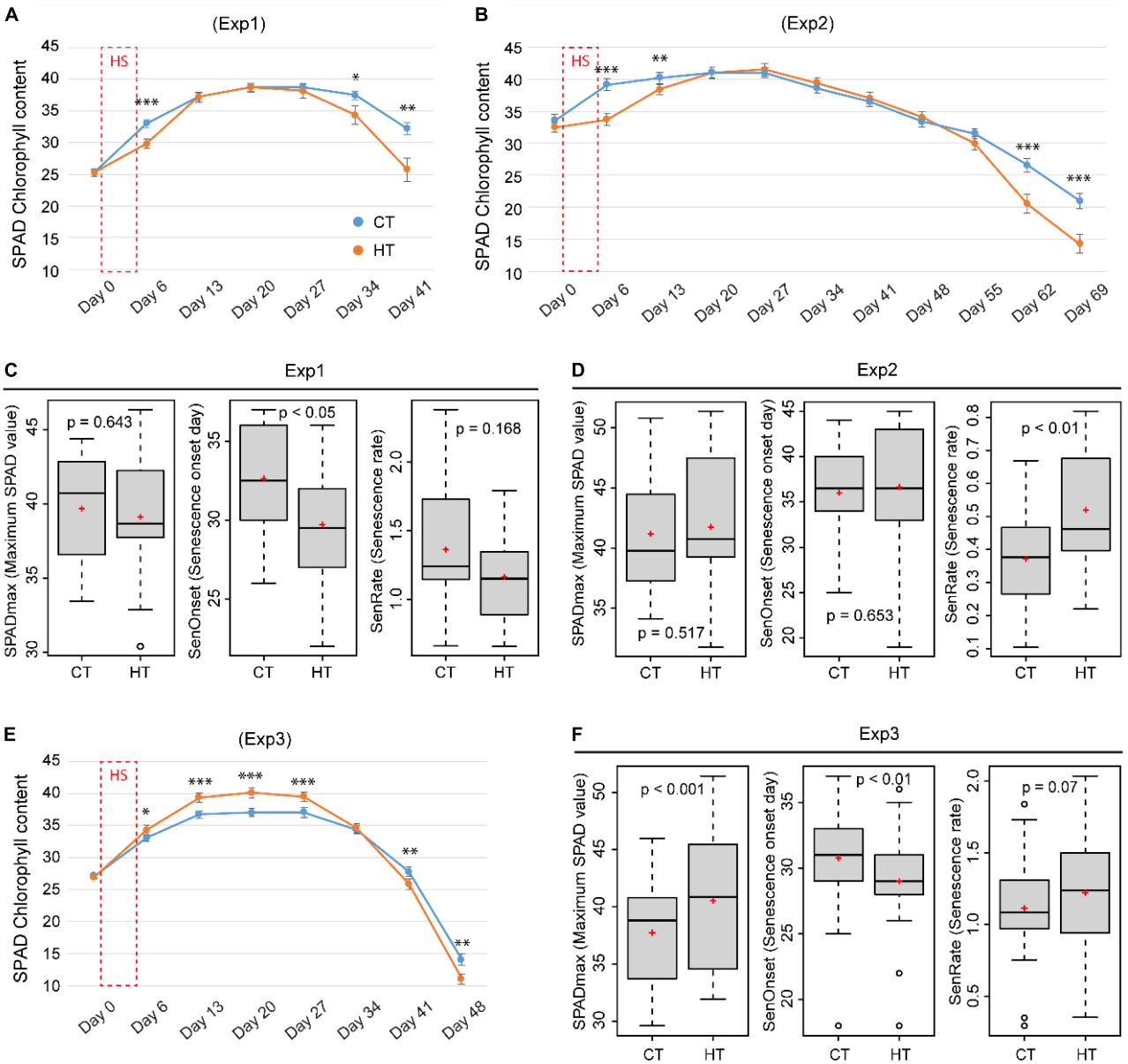

FIGURE 5 | The effects of heat on SPAD (chlorophyll content index) and leaf senescence parameters. Comparison of the effect of heat (HT) and control (CT) treatments on the dynamic change of SPAD measured before (day 0) and 1 day after (day 6) a 5-day HT treatment, and in weekly intervals thereafter in Exp1 **(A)**, Exp2 **(B)**, and Exp3 **(E)**. Senescence-related parameters, SPADmax (maximum SPAD value), SenOnset (Senescence onset day), and SenRate (Senescence rate), were compared between CT and HT for Exp 1 **(C)**, Exp2 **(D)**, and Exp3 **(F)**. Significance level: ***$p < 0.001$; **$p < 0.01$; *$p < 0.05$.

correlation with the number of grains per spike under heat stress. Interestingly, similar relationships have been reported in other crops (Xu et al., 2017; Shi et al., 2018) and abiotic stresses (Ji et al., 2010), indicating that pollen fertility is a general limiting factor for final grain number under suboptimal growth conditions. Therefore, it should be an important target trait for heat-related research and breeding. Nevertheless, the response of pollen viability to heat stress is highly dependent on the developmental stage when stress is applied (Saini and Aspinall, 1982; Prasad and Djanaguiraman, 2014) and it is thus important to consider genotypic differences and carefully target meiosis to microspore stage when applying heat stress to exclude confounding effects. Currently, the most widely used morphological marker for pollen developmental stage is AIL, which is also known as auricle distance (Ji et al., 2010; Erena, 2018; Bokshi et al., 2021). However, AIL corresponding to a specific pollen developmental stage varies among different genotypes (Erena, 2018) and must be determined for each genotype, which is laborious. Fortunately, progress has been made by non-destructive X-ray micro-computed tomography

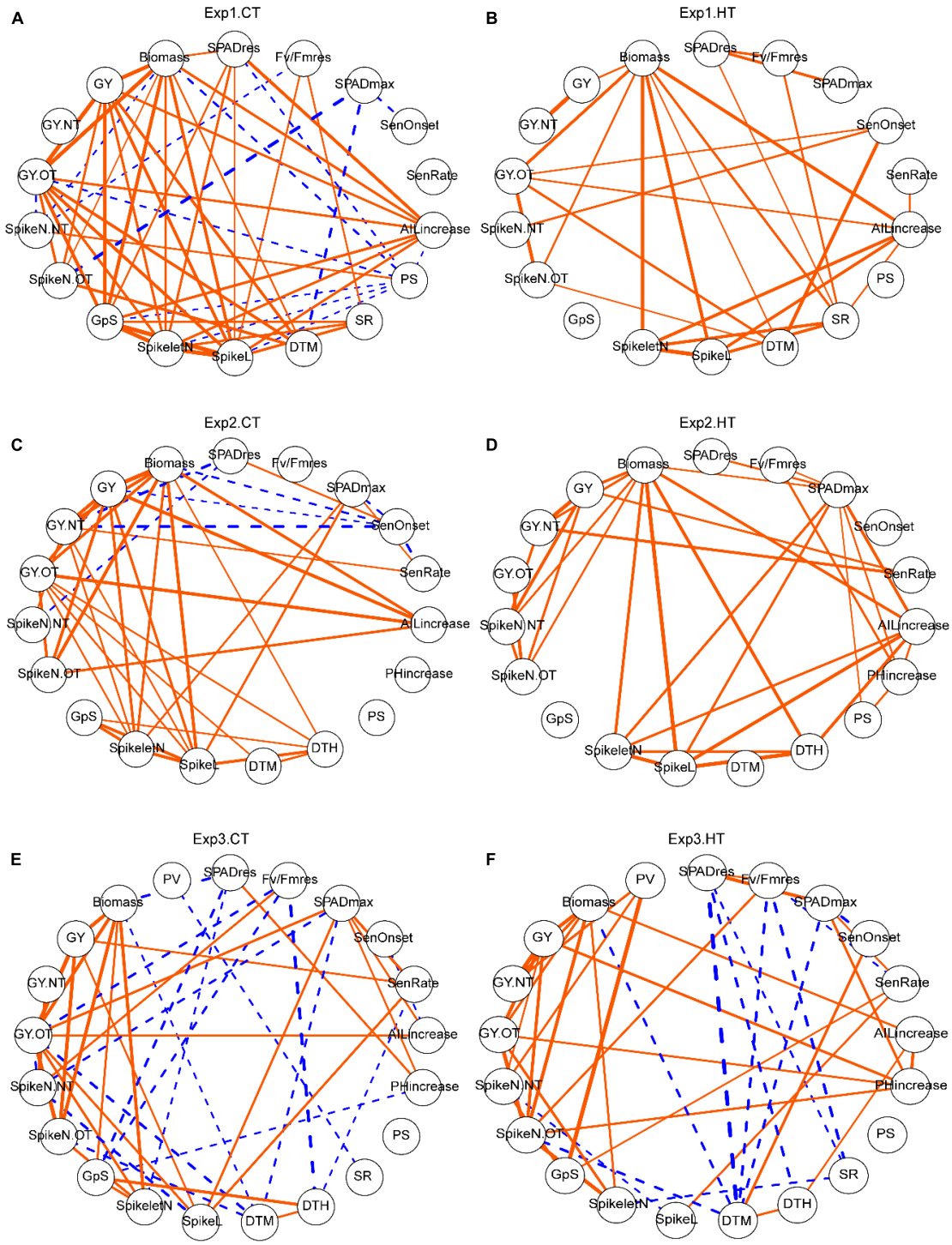

FIGURE 6 | The effects of heat on trait relationships across different experiments. Correlation networks for Exp1 **(A,B)**, Exp2 **(C,D)**, and Exp3 **(E,F)**. Only significant correlations are shown and the width of the edges indicated correlation *r*-value. Orange solid edges represent positive correlations, while blue dashed edges represent negative correlations. Trait abbreviations: *SPADres*: (SPAD at day 6—SPAD at day 0)/SPAD at day 0; *Fv/Fmres*: (Fv/Fm at day 6 -Fv/Fm at day 0)/(Fv/Fm at day 0); *SPADmax*, maximum value of SPAD; *SenOnset*, senescence onset time; *SenRate*, senescence rate; *AILincrease*, auricle interval length increase during the 5-day treatment; *PHincrease*, plant height increase during the 5-day treatment; *PS*, observed frequency of paired spikelet from all spikes; *SR*, observed frequency of sham ramification from all spikes; *DTH*, days to heading; *DTM*, days to maturation; *SpikeL*, spike length (tagged primary spike); *SpikeletN*, number of spikelets (tagged primary spike); *GpS*, number of grains per spike (tagged primary spike); *SpikeN.OT*, number of spikes from old tillers; *SpikeN.NT*, number of spikes from new tillers; *GY.OT*, grain yield of old tillers; *GY.NT*, grain yield of new tillers; *GY*, grain yield per plant (sum of old and new tillers); *Biomass*, the dry weight of all straw per plant; *PV*, pollen viability from the middle spikelet of tagged spike.

scanning (Fernández-Gómez et al., 2020), and integrating this with modeling could be a promising way to overcome difficulties with accurate identification of developmental stages of wheat pollen.

Utilizing Developmental Plasticity to Mitigate Heat Effects on Yield

The number of spikes per plant, interacting with spikelet number and floret fertility, determines grain number and thereby final yield. Our data show that a short episode of heat stress during early booting stage induced the development of new tillers and spikes, which is in agreement with other studies (Bányai et al., 2014; Chavan et al., 2019; Hütsch et al., 2019). Although tillering was initially inhibited under severe heat stress, new tillers started emerging at 2 weeks after recovery, corresponding to about 1 week after anthesis. This timing suggests that available photosynthates stored in vegetative tissue that cannot be translocated into grain due to spikelet sterility can be reallocated into the development of new tillers and spikes. Additional photo-assimilates for new tillers and spikes would be produced during recovery and this is reflected by its positive correlation with delayed onset of senescence (**Figure 6C**). The observed formation of new spikes after heat stress compensating for heat-induced biomass and yield losses under controlled environment conditions now needs to be corroborated under field conditions to ensure that it is a valid target trait for breeding. In addition, a higher frequency of paired spikelets (Boden et al., 2015) and sham ramification (Amagai et al., 2017) was observed in heat-treated plants and this may also be related to excessive source supply. Although these traits were not correlated with yield, they could contribute to understand mechanisms underlying such developmental abnormalities.

Accelerated Leaf Senescence After Brief Heat Stress During Early Booting Stage

Screening wheat for heat tolerance in the field is generally implemented by late-sowing to impose continuous terminal heat stress during grain filling, often resulting in accelerated leaf senescence (Bergkamp et al., 2018). In the present study, a similar stimulation of flag leaf senescence was observed after a brief episode of heat stress was applied during early booting. It is possible that plants are able to measure and memorize phenology or leaf age to program the senescence process (Woo et al., 2019). In our study, model fitting using SPAD time course data proved to be successful in identifying senescence parameters. Both earlier onset and faster senescence rate were identified and were closely related to accelerated leaf senescence, in agreement with similar results reported by Šebela et al. (2020). Heat-specific positive correlations between senescence onset (SenOnset), new spike formation (SpikeN.NT), and yield of old tillers (GY.OT) in Exp1 support the important role of late senescence. The observed positive associations between senescence rate (SenRate) and yield traits (grain yield/GY, number of grains per spike/GpS, spike length/SpikeL) in Exp2 and Exp3 suggest fast nutrient remobilization in high-yielding lines. Finally, both SPAD and Fv/Fm were reduced by heat immediately after the treatment (day6) in Exp1 and Exp2, but the mild temperature of 34°C/28°C only decreased Fv/Fm, not SPAD. These results indicate that Fv/Fm may be more sensitive and therefore a better parameter for heat tolerance evaluation (Cao et al., 2019). Therefore, these senescence-related parameters are useful for crop phenotyping, and integrating modeling with high-throughput imaging measurements will enable large-scale analysis.

CONCLUSION

In this study, a spring wheat panel, including heat-tolerant elite varieties and their pre-breeding lines, was dissected for reproductive, developmental, physiological, and yield responses along with their inter-relationships after a 5-day heat stress application during the early booting stage. In comparison with the control treatment, pollen viability from the tagged primary spike was significantly decreased by heat and subsequently reduced number of grains per spike. The heat stress, however, resulted in late tillering after the disruption of sink strength. Consequently, more new spikes were formed contributing to final yield and biomass, though an additional week was needed for the maturation of the late tillers. Flag leaf SPAD (Chlorophyll content index) and Fv/Fm (maximum potential quantum efficiency of Photosystem II) were reduced by heat stress. Model fitting with time course SPAD measurements showed accelerated leaf senescence by either earlier onset or faster senescence rate, and these parameters were associated with yield traits. Ongoing genomic and genetic studies will subsequently be used to dissect the mechanism of identified heat-tolerant genotypes (Sunstar, SWBL1.1). Taken together, these reproductive, developmental, and physiological traits could be further used as targets for understanding basic mechanisms and breeding heat-tolerant wheat.

DATA AVAILABILITY STATEMENT

The original contributions presented in the study are included in the article/**Supplementary Material**, further inquiries can be directed to the corresponding author/s.

AUTHOR CONTRIBUTIONS

SH conceived and supervised the project, together with EV-S and MP. JX designed and implemented the experiments and analyzed the data, with support from CL. MR and SD advised on the selection of genotypes included in this study and provided the seeds. SH, EV-S, SH-L, and MP held regular project planning discussions. JX wrote the manuscript, which was reviewed and edited by SH, CL, MR, SD, EV-S, SH-L, and MP. All authors contributed to the article and approved the submitted version.

FUNDING

This project was funded by the BBSRC UK-Mexico Newton Fund (BB/S012885/1 "Safeguarding Sonora's Wheat from Climate Change"). SH and MP were supported by the Designing Future Wheat (DFW) Institute Strategic Programme (BB/P016855/1) and SH by NIAB.

ACKNOWLEDGMENTS

We would like to thank Tess Rose and Maria Oszvald for their support and suggestions on the manuscript, as well as Matthew Dale for advice on the experimental setup. We would also like to thank Fiona Gilzean, Jill Maple, and Jack Turner for taking excellent care of the plants and for their technical support, as well as Chris Hall for helping with the sample processing. Seeds were kindly provided by the CIMMYT and Nick Collins, University of Adelaide.

SUPPLEMENTARY MATERIAL

The Supplementary Material for this article can be found online at: https://www.frontiersin.org/articles/10.3389/fpls.2022.886541/full#supplementary-material

REFERENCES

Amagai, Y., Gowayed, S., Martinek, P., and Watanabe, N. (2017). The third glume phenotype is associated with rachilla branching in the spikes of tetraploid wheat (*Triticum* L.). *Genet. Resour. Crop Evol.* 64, 835–842. doi: 10.1007/s10722-017-0503-7

Azam, F. I, Chang, X., and Jing, R. (2015). Mapping QTL for chlorophyll fluorescence kinetics parameters at seedling stage as indicators of heat tolerance in wheat. *Euphytica* 202, 245–258. doi: 10.1007/s10681-014-1283-1

Bányai, J., Karsai, I., Balla, K., Kiss, T., Bedö, Z., and Láng, L. (2014). Heat stress response of wheat cultivars with different ecological adaptation. *Cereal Res. Commun.* 42, 413–425. doi: 10.1556/CRC.42.2014.3.5

Begcy, K., Weigert, A., Egesa, A. O., and Dresselhaus, T. (2018). Compared to australian cultivars, european summer wheat (*Triticum aestivum*) overreacts when moderate heat stress is applied at the pollen development stage. *Agronomy* 8:99. doi: 10.3390/agronomy8070099

Bergkamp, B., Impa, S. M., Asebedo, A. R., Fritz, A. K., and Jagadish, S. V. K. (2018). Prominent winter wheat varieties response to post-flowering heat stress under controlled chambers and field based heat tents. *Field Crop Res.* 222, 143–152. doi: 10.1016/j.fcr.2018.03.009

Bheemanahalli, R., Sunoj, V. S. J., Saripalli, G., Prasad, P. V. Vara, Balyan, H. S., Gupta, P. K., et al. (2019). Quantifying the impact of heat stress on pollen germination, seed set, and grain filling in spring wheat. *Crop Sci.* 59, 684–696. doi: 10.2135/CROPSCI2018.05.0292

Bhusal, N., Sharma, P., Sareen, S., and Sarial, A. K. (2018). Mapping QTLs for chlorophyll content and chlorophyll fluorescence in wheat under heat stress. *Biol. Plant* 62, 721–731. doi: 10.1007/s10535-018-0811-6

Boden, S. A., Cavanagh, C., Cullis, B. R., Ramm, K., Greenwood, J., Jean Finnegan, E., et al. (2015). Ppd-1 is a key regulator of inflorescence architecture and paired spikelet development in wheat. *Nat. Plants* 1, 1–6. doi: 10.1038/nplants.2014.16

Bokshi, A. I., Tan, D. K. Y., Thistlethwaite, R. J., Trethowan, R., and Kunz, K. (2021). Impact of elevated CO2and heat stress on wheat pollen viability and grain production. *Funct. Plant Biol.* 48, 503–514. doi: 10.1071/FP20187

Browne, R. G., Li, S. F., Iacuone, S., Dolferus, R., and Parish, R. W. (2021). Differential responses of anthers of stress tolerant and sensitive wheat cultivars to high temperature stress. *Planta* 254:4. doi: 10.1007/s00425-021-03656-7

Cai, C., Yin, X., He, S., Jiang, W., Si, C., Struik, P. C., et al. (2016). Responses of wheat and rice to factorial combinations of ambient and elevated CO2 and temperature in FACE experiments. *Glob. Change Biol.* 22, 856–874. doi: 10.1111/gcb.13065

Cao, Z., Yao, X., Liu, H., Liu, B., Cheng, T., Tian, Y., et al. (2019). Comparison of the abilities of vegetation indices and photosynthetic parameters to detect heat stress in wheat. *Agric. For. Meteorol.* 265, 121–136. doi: 10.1016/J.AGRFORMET.2018.11.009

Chavan, S. G., Duursma, R. A., Tausz, M., and Ghannoum, O. (2019). Elevated CO2 alleviates the negative impact of heat stress on wheat physiology but not on grain yield. *J. Exp. Bot.* 70, 6447–6459. doi: 10.1093/JXB/ERZ386

Cossani, C. M., and Reynolds, M. P. (2012). Physiological traits for improving heat tolerance in wheat. *Plant Physiol.* 160, 1710–1718. doi: 10.1104/pp.112.207753

Cossani, C. M., and Reynolds, M. P. (2015). Heat stress adaptation in elite lines derived from synthetic hexaploid wheat. *Crop Sci.* 55, 2719–2735. doi: 10.2135/cropsci2015.02.0092

Draeger, T., and Moore, G. (2017). Short periods of high temperature during meiosis prevent normal meiotic progression and reduce grain number in hexaploid wheat (*Triticum aestivum* L.). *Theor. Appl. Genet.* 130, 1785–1800. doi: 10.1007/s00122-017-2925-1

Dwivedi, S. K., Basu, S., Kumar, S., Kumari, S., Kumar, A., Jha, S., et al. (2017). Heat stress induced impairment of starch mobilisation regulates pollen viability and grain yield in wheat: study in Eastern Indo-Gangetic Plains. *Field Crop Res.* 206, 106–114. doi: 10.1016/J.FCR.2017.03.006

Epskamp, S., Cramer, A. O. J., Waldorp, L. J., Schmittmann, V. D., and Borboom, D. (2012). {qgraph}: network visualizations of relationships in psychometric data. *J. Stat. Softw.* 48, 1–18.

Erena, M. F. (2018). *Genetic and Physiological Bases of Heat-Induced Floret Sterility in Wheat*. Adelaide: University of Adelaide.

Erena, M. F., Lohraseb, I., Munoz-Santa, I., Taylor, J. D., Emebiri, L. C., and Collins, N. C. (2021). The WtmsDW locus on wheat chromosome 2B controls major natural variation for floret sterility responses to heat stress at booting stage. *Front. Plant Sci.* 12:376. doi: 10.3389/FPLS.2021.635397/BIBTEX

Fernández-Gómez, J., Talle, B., Tidy, A. C., and Wilson, Z. A. (2020). Accurate staging of reproduction development in Cadenza wheat by non-destructive spike analysis. *J. Exp. Bot.* 71, 3475–3484. doi: 10.1093/jxb/eraa156

Hassan, F. S. C., Solouki, M., Fakheri, B. A., Nezhad, N. M., and Masoudi, B. (2018). Mapping QTLs for physiological and biochemical traits related to grain yield under control and terminal heat stress conditions in bread wheat (*Triticum aestivum* L.). *Physiol. Mol. Biol. Plants* 24:1231. doi: 10.1007/S12298-018-0590-8

Hütsch, B. W., Jahn, D., and Schubert, S. (2019). Grain yield of wheat (*Triticum aestivum* L.) under long-term heat stress is sink-limited with stronger inhibition of kernel setting than grain filling. *J. Agron. Crop Sci.* 205, 22–32. doi: 10.1111/JAC.12298

Ji, X., Shiran, B., Wan, J., Lewis, D. C., Jenkins, C. L., Condon, A. G., et al. (2010). Importance of pre-anthesis anther sink strength for maintenance of grain number during reproductive stage water stress in wheat. *Plant Cell Environ.* 33, 926–942. doi: 10.1111/j.1365-3040.2010.02130.x

Kumar, P., Gupta, V., Singh, G., Dhakar, R., and Ramakrishnan, R. S. (2021). Assessment of terminal heat tolerance based on agro-morphological and stress selection indices in wheat. *Cereal Res. Commun.* 49, 217–226. doi: 10.1007/s42976-020-00112-2

Kuznetsova, A., Brockhoff, P. B., and Christensen, R. H. B. (2017). {lmerTest} package: tests in linear mixed effects models. *J. Stat. Softw.* 82, 1–26. doi: 10.18637/jss.v082.i13

Liu, B., Asseng, S., Müller, C., Ewert, F., Elliott, J., Lobell, D. B., et al. (2016). Similar estimates of temperature impacts on global wheat yield by three independent methods. *Nat. Clim. Change* 6, 1130–1136. doi: 10.1038/nclimate3115

Lüdecke, D. (2021). *sjPlot: Data Visualization for Statistics in Social Science Version 2.8.10*.

Mirosavljević, M., Mikić, S., Župunski, V., Špika, A. K., Trkulja, D., Ottosen, C. O., et al. (2021). Effects of high temperature during anthesis and grain filling on physiological characteristics of winter wheat cultivars. *J. Agron. Crop Sci.* 207, 823–832. doi: 10.1111/jac.12546

Murchie, E. H., and Lawson, T. (2013). Chlorophyll fluorescence analysis: a guide to good practice and understanding some new applications. *J. Exp. Bot.* 64, 3983–3998. doi: 10.1093/jxb/ert208

Omidi, M., Siahpoosh, M. R., Mamghani, R., and Modarresi, M. (2014). The influence of terminal heat stress on meiosis abnormalities in pollen mother cells of wheat. *Cytologia* 79, 49–58. doi: 10.1508/cytologia.79.49

Pequeno, D. N. L., Hernández-Ochoa, I. M., Reynolds, M., Sonder, K., Molero-Milan, A., and Robertson, R. (2021). Climate impact and adaptation to heat and drought stress of regional and global wheat production. *Environ. Res. Lett.* 16:54070. doi: 10.1088/1748-9326/abd970

Pinto, R. S., Lopes, M. S., Collins, N. C., and Reynolds, M. P. (2016). Modelling and genetic dissection of staygreen under heat stress. *Theor. Appl. Genet.* 129, 2055–2074. doi: 10.1007/s00122-016-2757-4

Prasad, P. V. V., and Djanaguiraman, M. (2014). Response of floret fertility and individual grain weight of wheat to high temperature stress: sensitive stages and thresholds for temperature and duration. *Funct. Plant Biol.* 41, 1261–1269. doi: 10.1071/FP14061

Revelle, W. (2020). *psych: Procedures for Psychological, Psychometric, and Personality Research Version 2.2.3.*

Richardson, A. D., Duigan, S. P., and Berlyn, G. P. (2002). An evaluation of noninvasive methods to estimate foliar chlorophyll content. *New Phytol.* 153, 185–194. doi: 10.1046/j.0028-646X.2001.00289.x

Rieu, I., Twell, D., and Firon, N. (2017). Pollen development at high temperature: from acclimation to collapse. *Plant Physiol.* 173, 1967–1976. doi: 10.1104/pp.16.01644

Sade, N., Del Mar Rubio-Wilhelmi, M., Umnajkitikorn, K., and Blumwald, E. (2018). Stress-induced senescence and plant tolerance to abiotic stress. *J. Exp. Bot.* 69, 845–853. doi: 10.1093/jxb/erx235

Saini, H. S., and Aspinall, D. (1982). Abnormal sporogenesis in wheat (*Triticum aestivum* L.) induced by short periods of high temperature. *Ann. Bot.* 49, 835–846. doi: 10.1093/OXFORDJOURNALS.AOB.A086310

Šebela, D., Bergkamp, B., Somayanda, I. M., Fritz, A. K., and Krishna Jagadish, S. V. (2020). Impact of post-flowering heat stress in winter wheat tracked through optical signals. *Agron. J.* 112, 3993–4006. doi: 10.1002/AGJ2.20360

Sharma, D., Singh, R., Rane, J., Gupta, V. K., Mamrutha, H. M., and Tiwari, R. (2016). Mapping quantitative trait loci associated with grain filling duration and grain number under terminal heat stress in bread wheat (*Triticum aestivum* L.). *Plant Breed.* 135, 538–545. doi: 10.1111/pbr.12405

Shi, W., Li, X., Schmidt, R. C., Struik, P. C., Yin, X., and Jagadish, S. V. K. (2018). Pollen germination and in vivo fertilization in response to high-temperature during flowering in hybrid and inbred rice. *Plant Cell Environ.* 41, 1287–1297. doi: 10.1111/pce.13146

Shirdelmoghanloo, H., Cozzolino, D., Lohraseb, I., and Collins, N. C. (2016). Truncation of grain filling in wheat (*Triticum aestivum*) triggered by brief heat stress during early grain filling: association with senescence responses and reductions in stem reserves. *Funct. Plant Biol.* 43, 919–930. doi: 10.1071/FP15384

Singh, R. P., Huerta-Espino, J., Sharma, R., Joshi, A. K., and Trethowan, R. (2007). High yielding spring bread wheat germplasm for global irrigated and rainfed production systems. *Euphytica* 157, 351–363. doi: 10.1007/s10681-006-9346-6

Slafer, G. A., Savin, R., and Sadras, V. O. (2014). Coarse and fine regulation of wheat yield components in response to genotype and environment. *Field Crop Res.* 157, 71–83. doi: 10.1016/j.fcr.2013.12.004

Stone, P. J., and Nicolas, M. E. (1995). Effect of timing of heat stress during grain filling on two wheat varieties differing in heat tolerance. I. Grain growth. *Aust. J. Plant Physiol.* 22, 927–934. doi: 10.1071/PP9950927

Talukder, A. S. M. H. M., McDonald, G. K., and Gill, G. S. (2014). Effect of short-term heat stress prior to flowering and early grain set on the grain yield of wheat. *Field Crop Res.* 160, 54–63. doi: 10.1016/J.FCR.2014.01.013

Thistlethwaite, R. J., Tan, D. K. Y., Bokshi, A. I., Ullah, S., and Trethowan, R. M. (2020). A phenotyping strategy for evaluating the high-temperature tolerance of wheat. *Field Crop Res* 255:107905. doi: 10.1016/j.fcr.2020.107905

Touzy, G., Lafarge, S., Redondo, E., Lievin, V., Decoopman, X., Le Gouis, J., et al. (2022). Identification of QTLs affecting post-anthesis heat stress responses in European bread wheat. *Theor. Appl. Genet.* 135, 947–964. doi: 10.1007/S00122-021-04008-5

Trnka, M., Rötter, R. P., Ruiz-Ramos, M., Kersebaum, K. C., Olesen, J. E., Žalud, Z., et al. (2014). Adverse weather conditions for European wheat production will become more frequent with climate change. *Nat. Clim. Change* 4, 637–643. doi: 10.1038/nclimate2242

Woo, H. R., Kim, H. J., Lim, P. O., and Nam, H. G. (2019). Leaf senescence: systems and dynamics aspects. *Annu. Rev. Plant Biol.* 70, 347–376. doi: 10.1146/annurev-arplant-050718-095859

Wood, S. N. (2011). Fast stable restricted maximum likelihood and marginal likelihood estimation of semiparametric generalized linear models. *J. R. Stat. Soc. Series B* 73, 3–36. doi: 10.1111/j.1467-9868.2010.00749.x

Xu, J., Wolters-Arts, M., Mariani, C., Huber, H., and Rieu, I. (2017). Heat stress affects vegetative and reproductive performance and trait correlations in tomato (*Solanum lycopersicum*). *Euphytica* 213:156. doi: 10.1007/s10681-017-1949-6

Yeh, C. H., Kaplinsky, N. J., Hu, C., and Charng, Y. Y. (2012). Some like it hot, some like it warm: phenotyping to explore thermotolerance diversity. *Plant Sci.* 195, 10–23. doi: 10.1016/j.plantsci.2012.06.004

Zampieri, M., Ceglar, A., Dentener, F., and Toreti, A. (2017). Wheat yield loss attributable to heat waves, drought and water excess at the global, national and subnational scales. *Environ. Res. Lett.* 12:064008. doi: 10.1088/1748-9326/aa723b

Zinn, K. E., Tunc-Ozdemir, M., and Harper, J. F. (2010). Temperature stress and plant sexual reproduction: uncovering the weakest links. *J. Exp. Bot.* 61, 1959–1968. doi: 10.1093/jxb/erq053

Conflict of Interest: The authors declare that the research was conducted in the absence of any commercial or financial relationships that could be construed as a potential conflict of interest.

Publisher's Note: All claims expressed in this article are solely those of the authors and do not necessarily represent those of their affiliated organizations, or those of the publisher, the editors and the reviewers. Any product that may be evaluated in this article, or claim that may be made by its manufacturer, is not guaranteed or endorsed by the publisher.

frontiers | Frontiers in Plant Science

ORIGINAL RESEARCH
published: 23 May 2022
doi: 10.3389/fpls.2022.886805

Multiomics Analyses of Two Sorghum Cultivars Reveal the Molecular Mechanism of Salt Tolerance

*Genzeng Ren[1,2†], Puyuan Yang[1,2†], Jianghui Cui[1,2†], Yukun Gao[1,2], Congpei Yin[1,2], Yuzhe Bai[1,2], Dongting Zhao[1,2] and Jinhua Chang[1,2]**

[1]College of Agronomy, Hebei Agricultural University, Baoding, China, [2]North China Key Laboratory for Germplasm Resources of Education Ministry, Hebei Agricultural University, Baoding, China

OPEN ACCESS

Edited by:
Amaranatha Reddy Vennapusa, Delaware State University, United States

Reviewed by:
Tushar Suhas Khare, Savitribai Phule Pune University, India
Aarthy Thiagaraya Selvam, Kansas State University, United States
Prasad Parchuri, Washington State University, United States

***Correspondence:**
Jinhua Chang
jhchang2006@126.com

[†]These authors have contributed equally to this work

Specialty section:
This article was submitted to Plant Abiotic Stress, a section of the journal Frontiers in Plant Science

Received: 01 March 2022
Accepted: 29 April 2022
Published: 23 May 2022

Citation:
Ren G, Yang P, Cui J, Gao Y, Yin C, Bai Y, Zhao D and Chang J (2022) Multiomics Analyses of Two Sorghum Cultivars Reveal the Molecular Mechanism of Salt Tolerance. Front. Plant Sci. 13:886805. doi: 10.3389/fpls.2022.886805

Sorghum [*Sorghum bicolor* (L.) Moench] is one of the most important cereal crops and contains many health-promoting substances. Sorghum has high tolerance to abiotic stress and contains a variety of flavonoids compounds. Flavonoids are produced by the phenylpropanoid pathway and performed a wide range of functions in plants resistance to biotic and abiotic stress. A multiomics analysis of two sorghum cultivars (HN and GZ) under different salt treatments time (0, 24, 48, and 72) was performed. A total of 45 genes, 58 secondary metabolites, and 246 proteins were recognized with significant differential abundances in different comparison models. The common differentially expressed genes (DEGs) were allocated to the "flavonoid biosynthesis" and "phenylpropanoid biosynthesis" pathways. The most enriched pathways of the common differentially accumulating metabolites (DAMs) were "flavonoid biosynthesis," followed by "phenylpropanoid biosynthesis" and "arginine and proline metabolism." The common differentially expressed proteins (DEPs) were mainly distributed in "phenylpropanoid biosynthesis," "biosynthesis of cofactors," and "RNA transport." Furthermore, considerable differences were observed in the accumulation of low molecular weight nonenzymatic antioxidants and the activity of antioxidant enzymes. Collectively, the results of our study support the idea that flavonoid biological pathways may play an important physiological role in the ability of sorghum to withstand salt stress.

Keywords: sorghum, transcriptome, metabolome, proteome, flavonoids, salt stress

INTRODUCTION

Salinity is one of abiotic stresses and it limits crop production (Xie et al., 2015). According to estimated statistics from UNESCO[1] and FAO,[2] in recent years, due to seawater indwelling and inadequate irrigation, over 7% of the world's lands and 20% of irrigated lands are currently salt affected (Wang et al., 2003; Singh, 2021). Approximately half of cultivated fields will

[1]https://www.unesco.org/
[2]https://www.fao.org/

be affected by salinization by the middle of this century (Wang et al., 2004; Singh, 2021). Sodium salt, especially sodium chloride (NaCl), is the main substance that causes salt stress in the natural environment. Thus, one of the most important topics in crop stress resistance is to understand the resistance mechanism to salt stress, especially NaCl salt stress.

Excessive levels of Na^+ and Cl^- ions affect the root system of plants firstly, impairing development in the short term due to osmotic stress (Munns and Tester, 2008). Long term and high levels of salt stress can disrupt the ability of plants to regulate ion homeostasis and also induce oxidative stress mediated by reactive oxygen species (ROS). Plant produced various peroxides, e.g., singlet oxygen ($^1O_2$), hydroxyl radical (HO•), hydrogen peroxide (H_2O_2), and superoxide radical (O_2•$^-$) under salt stress. To escape the damage of stress, plants evolved variable adaptation mechanisms, such as the enhancement of metabolic adjustment, osmotic adjustment to compensate for osmotic stress. Non-enzymatic compatible solutes and antioxidants, such as proteins, phenolic compounds and flavonoids, and enzymatic antioxidants, such as peroxidase (POD), superoxide dismutase (SOD), catalase (CAT), ascorbate peroxidase (APX), played important roles in the ROS detoxification (Gupta and Huang, 2014; Ismail and Horie, 2017). As important secondary metabolites, flavonoids has been investigated extensively and were proofed having great role in response to abiotic stresses (Petrussa et al., 2013). The scavenging of free radicals by flavonoid molecules improves salt stress tolerance of plants (Yan et al., 2014; Chandran et al., 2019). For example, it has been reported that the accumulation of flavonoid could be induced by salt stress, and exogenous application of flavonoid could enhance salt tolerance in *Arabidopsis thaliana* (Chan and Lam, 2014). Similar results were obtained in *Ligustrum vulgare* (Agati et al., 2011). Bian et al. (2020) found that the HSFB2b, a class B heat shock factor, improves salt tolerance of *Glycine max* through the promotion of flavonoid accumulation (Bian et al., 2020). Kusano et al. (2011) compared the metabolic responses of wild-type *Arabidopsis* with that of mutants impaired in flavonoid and found that the accumulation of anthocyanin and tocopherol could improve the resistance to UV stress in *Arabidopsis* (Kusano et al., 2011).

Sorghum [*Sorghum bicolor* (L.) Moench] is the world's fifth major cereal in terms of production and area harvested (FAOSTAT, 2019)[3] and has been widely cultivated in more than 100 countries. Sorghum is not only an important staple food crop in the semi-arid tropics of Asia and Africa, but also an important source of forage and biofuel (Xie and Xu, 2019). Sorghum is widely grown in harsh environments because of its strong ability to resist drought and salt-alkali stress (Xie and Xu, 2019). Therefore, studying the salt tolerance mechanism of sorghum is essential for ensuring food security and promoting human health.

In recent years, multiomics analysis technology has been extensively utilized to examine abiotic stress. Transcriptomics, proteomics, and metabolomics technologies can enable more detailed monitoring of metabolic regulation and molecular processes to be implemented in plants grown in hostile environments (Masike et al., 2020; Li et al., 2020a; Hou et al., 2021). To examine how high salt content influences sorghum seedling development, we developed a research strategy whereby two conventional sorghum cultivars with contrasting salt sensitivity, the highly salt-tolerant landrace cultivar Gaoliangzhe (GZ) and hypersensitive improved cultivar Henong16 (HN), were initially cropped with a normal nutrient solution for 14 days and then the seedlings were placed under salt conditions for varying time periods. We performed a comprehensive omics analysis to reveal the striking changes in gene, metabolite, and protein pools. By comparing the transcriptome, metabolome, and proteome profiles of root tissues grown under salt stress, we identified specific genes, secondary metabolites, and protein complexes that are targeted for flavonoids and phenylalanine. Through omics technology analyses, we have obtained valuable information for understanding the salt tolerance mechanisms of sorghum and provided a better utilization for salt land.

MATERIALS AND METHODS

Plant Materials and Growth Conditions

The seeds of two sorghum cultivars (HN and GZ) were chosen according to standard GB/T3543-1995 (Rules for agricultural seed testing-general directives)[4] and disinfected with 75% ethanol, rinsed clean with deionized water, and cultivated in vermiculite for 5 days. Then, the uniform seedlings were transferred to hydroponic boxes and grown in an artificial climate chamber (ZRY-YY1000, Saifu, Ningbo, China). The growth conditions as follows: light/dark cycles: 14 h/10 h; light photosynthetic photon flux density: 1,000–1,200 μmol m^{-2} s^{-1}; temperature: 28°C (light)/23°C (dark); relative humidity: 60 ± 5%. Every hydroponic box containing 2 L Hoagland's solution [5 mM $Ca(NO_3)_2.4H_2O$, 5 mM KNO_3, 2 mM $MgSO_4.7H_2O$, 1 mM KH_2PO_4, 4.5 mM NH_4HPO_4, 100 μM EDTA-2Na, 100 μM $FeSO_4.7H_2O$, 4.5 μM H_3BO_3, 0.5 μM MnSO4, 0.1 μM CuSO4,$ZnSO_4.7H_2O$, 0.1 μM $(NH_4)_6Mo_7O_{24}.4H_2O$] and the nutrient solution was changed once a day (Van Delden et al., 2020). When the sorghum seedlings grew to the three-leaf stage (~14 days), seedlings with even growth were carefully selected and divided into quarters, one for exposure to salt conditions (120 mM NaCl) and one for controlled conditions. Root tissue samples were harvested after 0 h (controlled conditions, referred to as C hereafter), 24 h (short-term treatment, referred to as S hereafter), 48 h (middle-time treatment, referred to as M hereafter), and 72 h (long-term treatment, referred to as L hereafter), immediately fixed with liquid nitrogen, and stored at −80°C for further analysis. The four treatments were harvested at same time. We selected two treatments (C and M) for transcriptome sequencing and RT-qPCR verification and chose four treatments (C, S, M, and L) for physiological parameters, proteome profiling, and metabolite detection. At least three independent biological replicates were used for each analysis (i.e., three for multiomics

[3]https://www.fao.org/faostat/

[4]http://openstd.samr.gov.cn/bzgk/gb/index

studies, and four for phenotypic and physiological characterizations studies; transcriptome sequencing uses three biological samples in RNA mixed sequencing). Five technical replicates of each treatment were conducted. Root lengths were measured after harvest.

Phenotypic and Physiological Characterizations

Determination of antioxidant enzyme activities, including superoxide dismutase (SOD), peroxidase (POD), and malondialdehyde (MDA), were determined using the Superoxide Dismutase Activity Assay Kit, Peroxidase Activity Assay Kit, and Micro Malondialdehyde Assay Kit (Solarbio, Beijing, China), respectively. The tannin, total flavonoid (TF), and total phenol (TP) contents were detected with a Tannic Acid Content Assay Kit, Micro Plant Total Flavonoids Assay Kit, and Micro Plant Total Phenol Assay Kit (Solarbio, Beijing, China), respectively. The POD and SOD activities were determined by measuring the oxidation of 3,3′-dimethoxybenzidine and percentage of inhibition of pyrogallol autoxidation at 470 and 560 nm, respectively (Johansson and Håkan Borg, 1988; Doerge et al., 1997). The contents of tannins, TF, and TP were measured based on the tannic acid standard solution, the rutin acid standard solution, and gallic acid standard solution at 275, 470, and 760 nm, respectively (Wang et al., 2020; Palacios et al., 2021). The contents of MDA were measured at 450, 532, and 600 nm and calculated according to the manufacturer's instructions (Spitz and Oberley, 1989). Statistical analysis was performed using IBM SPSS statistics for Windows, version 19.0 (SPSS, Chicago, IL, United States). Statistical significance tests were calculated using general Student's *t*-test, and one-way analysis of variance (ANOVA) with Duncan's multiple comparison test.

Total RNA Isolation and Quantification

Total RNA was extracted using the Omini Plant RNA Kit (CWBIO, Beijing, China). The digestion of DNA was performed using DNase I. RNA purity and concentration were measured using a Nanodrop and Qubit 2.0 (Thermo Scientific, United States). RNA integrity was monitored on 1.2% agarose gels.

RNA Library Construction and Data Analysis

The mRNA library was generated using the NEBNext Ultra™ RNA Library Prep Kit for Illumina (NEB, CA, United States). Briefly, the mRNA was purified using poly-T oligo-attached magnetic beads and fragmented using NEBNext First Strand Synthesis Reaction Buffer (NEB United States). First strand cDNA was synthesized using random hexamer primer and second strand cDNA was synthesized using RNase H and DNA Polymerase I. The double-stranded cDNA was purified by AMPure XP system (Beckman Coulter, Beverly, United States) after remaining overhangs converted into blunt ends and 3′ ends adenylation. Adapter ligation was carried out after adding "A" tail, and templates with the desired size range (200–250 bp) were subjected to PCR. Then the mRNA libraries were enriched by PCR and tested with Agilent 2100 and Qubit 2.0, and finally sequenced using Illumina HiSeq 2500 method. Raw data quality was controlled with criteria of less than 10% low-quality bases (Phred score < 20), followed by removing adapter sequences and of primers. Then, the clean reads were mapped to the sorghum reference genome (Sorghum_bicolor_NCBIv3)[5] using TopHat2 software. Gene expression was quantified using the fragments per kilobase of transcript per million base pairs (FPKM) method. The differentially expressed genes (DEGs) were evaluated using DESeq R package (version 1.18.0; Ross Ihaka, University of Auckland, New Zealand) and screened with a fold change ≥ 2 and FDR ≤ 0.01.

Reverse Transcription Quantitative PCR (RT-qPCR)

To validate the result of RNA-Sequencing, we selected eight up-regulated genes we are interested in after transcriptome analysis to further assess their expression patterns using RT-qPCR. The qualified RNA extraction was described in section the total RNA isolation and quantification. First-strand cDNA synthesis was conducted using a SuperRT cDNA Synthesis Kit (CWBIO, Beijing, China). RT-qPCR analysis was performed using a AugeGreen™ qPCR Master Mix (US EVERBRIGHT, Suzhou, China). The primers were designed by the NCBI primer-blast tool (**Supplementary Table S2**). The reaction was performed on a LightCycler 96 System (Roche, CA, United States) using the following protocol: predenaturation at 95°C for 5 min; 35 cycles of denaturation at 95°C for 15 s and renaturation at 60°C for 30 s; and extension at 72°C for 30 s. The β-actin gene (X79378) was used as an internal reference gene. The relative expression levels were calculated using the $2^{-\Delta\Delta Ct}$ method (Vastarelli et al., 2013). Each sample was performed in three replicates.

Metabolite Extraction and Quantification

Secondary metabolite extraction and quantification were performed with the help of Wuhan MetWare Biotechnology Co., Ltd.[6] following their standard procedures (Yuan et al., 2018; Zhang et al., 2019). Briefly, the freeze-dried roots were crushed using a grinder (MM 400, Retsch) at 30 Hz for 1.5 min. The powder (100 mg) was placed in 1.2 ml of 70% aqueous methanol at 4°C overnight and vortexed six times. The extracts were filtrated through a microporous membrane (0.22-μm pore size) after centrifuged at 12,000 *g* for 10 min. The sample extracts were analyzed using ultra-performance liquid chromatography–tandem mass spectrometry (UPLC-MS/MS) system. UPLC analysis was conducted with the SHIMADZU Nexera X2 instrument (Shimadzu, Kyoto, Japan) equipped with an Agilent SB-C18 column (1.8 μm, 2.1 mm × 100 mm). The mobile phase was consisted of pure water and acetonitrile (0.1% formic acid). The column temperature was 40°C. Gradient elution was performed at a flow rate of 0.35 ml min^{-1}, with an injection volume of 4 μl for each sample. MS/MS analysis was completed

[5]https://plants.ensembl.org/Sorghum_bicolor
[6]www.metware.cn

with an Applied Biosystems 4500 Q TRAP system (Thermo, MA, United States). Quality control (QC) samples were inserted in every 10 test samples. Principal component analysis (PCA) and orthogonal partial least squares discriminant analyses (OPLS-DA) were performed. The differentially accumulating metabolites (DAPs) screened by combining the fold change and the variable importance in project (VIP) value. The metabolites with a fold change $\geq$1.5 or a fold change $\leq$0.67 and VIP $\geq$ 1 considered to the DAPs.

Protein Extraction and Proteomics Analysis

Protein extraction and TMT-based proteomics analysis were conducted by Applied Protein Technology Co., Ltd.[7] Briefly, sample (approximately 200 mg) lysis and protein extraction were performed using a sodium dodecyl sulfate (SDS)-DL-dithiothreitol (DTT) buffer (4% SDS, 100 mM Tris-HCl, 1 mM DTT, pH 7.6; Li et al., 2020b). 200 μg of protein was taken from each sample and digested using the filter-aided proteome preparation (FASP) method for trypsin digestion. Twenty microgram of protein for each sample were mixed with 5× loading buffer, respectively, and boiled for 5 min. The proteins were separated on 12.5% SDS-PAGE gel (constant current 14 mA, 90 min). Protein bands were visualized by Coomassie Blue R-250 staining. Next, 100 μg of peptide mixture was labeled with a tandem mass tag (TMT) reagent. TMT-labeled sample fractionation was conducted through strong cation exchange (SCX) resin chromatography using an AKTA purifier system. Liquid chromatography–tandem mass spectrometry (LC-MS/MS) analysis was performed using a Q Exactive hybrid quadrupole orbitrap mass spectrometer (Thermo Fisher, CA, United States). The raw data for each sample were searched using the MASCOT engine (Matrix Science, London, United Kingdom) embedded in Proteome Discoverer 1.4 software for identification and quantitation analysis.

Bioinformatics Analysis

Gene Ontology (GO) annotation of the genes and proteins was implemented using Blast2GO software. The enrichment analysis of the DEGs, DEPs, and DAMs was determined by the GOseq R packages. The Kyoto Encyclopedia of Genes and Genomes (KEGG) annotation of the genes, proteins, and metabolites using a database[8] mapped the pathways in the KEGG. KEGG pathway enrichment analysis was performed by KOBAS software. Subcellular localization of proteins was predicted by CELLO,[9] which is a multi-class SVM classification system. Domain annotation of proteins was using the InterProScan software and identify protein domain signatures from the InterPro member database Pfam. Omics correlation analysis was performed using Metware cloud tools.[10]

[7]http://www.aptbiotech.com/
[8]http://geneontology.org/
[9]http://cello.life.nctu.edu.tw/
[10]https://119.3.166.241/

RESULTS

Phenotypic and Physiological Differences Between GZ and HN Under Salt Treatments

We analyzed the physiological and phenotypic characteristics of sorghum under salt stress. Under salt stress, the growth of the two sorghum varieties was inhibited to varying degrees (**Figure 1A**). The hypersensitive cultivar HN showed strong growth inhibition, but the highly tolerant cultivar GZ only displayed significantly accelerated root growth inhibition after 48 h (**Figure 1B, Supplementary Table S1**).

TP, TF, and tannin content in root of sorghum were significantly affected by salt stress. The tannin contents in GZ were significantly higher than HN. TP contents in GZ were significantly higher than HN excepted for M and L treatment. TF contents in GZ were significantly higher than HN excepted for C treatment (**Figures 1C–E, Supplementary Table S1**).

Peroxidase and SOD activity significantly increased with the increasing stress time and reach to the summit at M and S treatment, respectively, then decreased. MDA content significantly increased with the increasing stress time. POD and SOD activity of the highly tolerant cultivar GZ was significantly higher than that in the hypersensitive cultivar HN at four treatments (**Figures 1F,G, Supplementary Table S1**). MDA content in the highly salt-tolerant cultivar GZ was significantly lower than that in the salt hypersensitive cultivar HN under L treatment (**Figure 1H, Supplementary Table S1**).

Transcriptome Differences Between GZ and HN Under Salt Treatments

We performed RNA-Sequencing, in order to investigate if the differential expression of genes affects the physiological and phenotypic differences under salt stress. Based on phenotypic and physiological trait analysis, 48 h (M) was the turning point at which the stress effect was significant in the two varieties (**Figure 1B**). Therefore, the samples of the two sorghum cultivars at 0 h (C) and 48 h (M) of salt stress treatment were selected for transcriptomic analysis.

After quality control, we obtained a total of 25.07 Gb clean data with 84.98–85.07% of bases scoring Q30 and 53.02–53.93% of GC among the roots from the two cultivars grown with or without salt stress. The overwhelming majority of reads (75.37–77.42%) could be mapped to the sorghum reference genome, among which 72.12–74.49% were uniquely mapped (**Supplementary Table S3**). A total of 26,553 genes were functionally annotated in the databases and 841 new genes were found and enriched in the genomic information available in sorghum (**Supplementary Table S4**). Moreover, cross-comparisons (HN-C vs. GZ-C, HN-M vs. GZ-M, GZ-M vs. GZ-C, and HN-M vs. HN-C) identified 3,032, 3,411, 1,236, and 878 DEGs, respectively (**Figure 2A**). The top enriched KEGG terms contributed by these DEGs were ko00940 (phenylpropanoid biosynthesis), ko00360 (phenylalanine metabolism), ko00500 (starch and sucrose metabolism), and ko04075 (plant hormone signal transduction; **Supplementary Figure S1**).

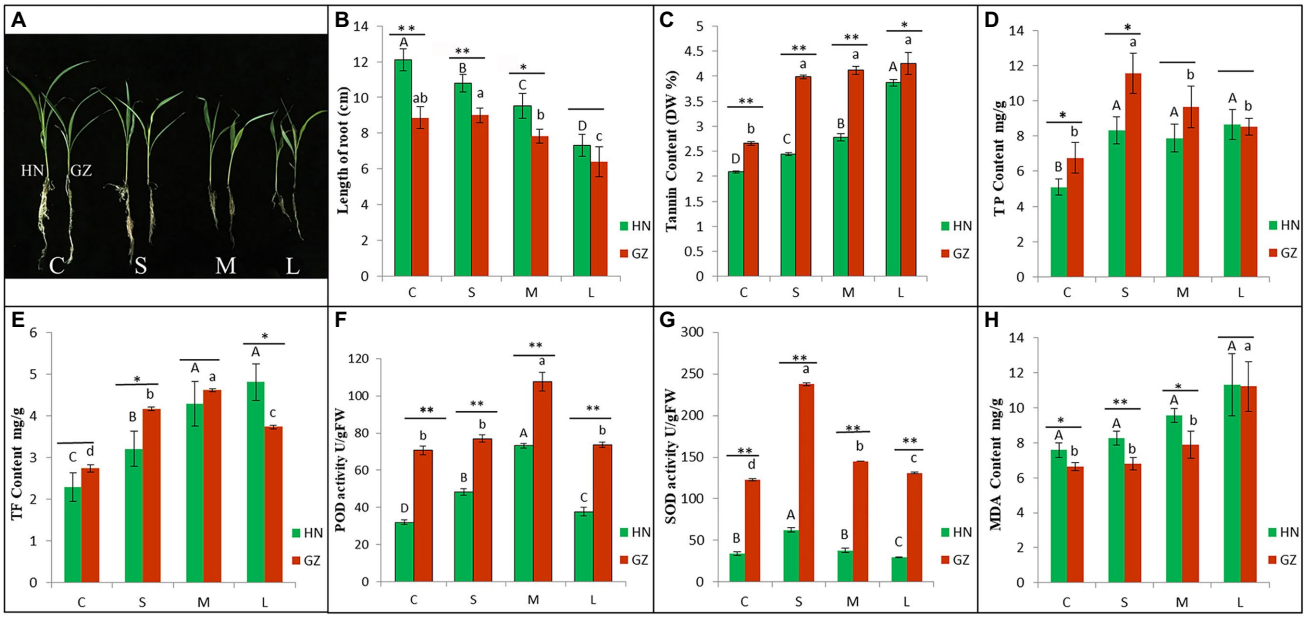

FIGURE 1 | The differences of phenotypic and physiological between HN and GZ under salt treatments. **(A)** Phenotypes of Sorghum "GZ" and "HN" under salt stress. **(B)** Length of root. **(C)** Tannin content. **(D)** The total phenol (TP) content. **(E)** The total flavonoid (TF) content. **(F)** POD activity. **(G)** SOD activity. **(H)** MDA content. Error bars represent standard errors of three biological replicates. The statistical significance between varieties was determined by the Student's *t* test (**$p < 0.01$,*$p < 0.05$). The statistical significance between treatments was evaluated by one-way analysis of variance (ANOVA) with Duncan's multiple comparison test ($p < 0.05$). Capital letters indicate HN. Lowercase letters indicate GZ.

Common DEGs were identified in the four comparisons to reduce the impact of time and/or circadian clock on salt stress. According to the Venn analysis, in total, 45 common DEGs were sustained, of which eight were upregulated and 37 were downregulated (**Figure 2B**). Based on the KEGG database, out of the eight upregulated common DEGs, four genes were allocated to the flavonoid biosynthesis pathway (ko00941; **Figure 3A**), encoding dihydroflavonol 4-reductase (DFR), leucoanthocyanidin dioxygenase (LDOX), anthocyanidin synthase (ANR), and flavonoid 3-hydroxylase (F3H).

To illustrate the correlation between gene expression and RNA-seq data with the salt stress response, the eight upregulated genes we interested in were selected to conduct RT-qPCR analysis. Detailed information on these genes is listed in **Supplementary Table S2**, and the RT-qPCR results are presented in **Figure 2C**. The results of RT-qPCR were in general agreement with those from the RNA-seq, with a Spearman correlation coefficient of 0.884, indicating that the transcriptome data were able to reflect transcript abundance in our study (**Figure 2D**). The elevated expression of the genes based on RNA-sequencing was higher in the highly salt-tolerant sorghum cultivar GZ than that in HN under salt stress by RT-qPCR, especially for the genes involved in flavonoid biosynthesis.

Secondary Metabolites Differences Between GZ and HN Under Salt Treatments

Based on the transcriptome and physiological differences between the two sorghum cultivars, we expected that secondary metabolites, especially flavonoid compounds, may make an important contribution to sorghum salt resistance. To assess how secondary metabolites impact sorghum salt resistance, we conducted the metabolites analyses. We generated quantitative profiles of 315 secondary metabolites, of which 157 were identified in positive-ionization mode and 158 in negative-ionization mode in roots of salt tolerant (GZ) and sensitive (HN) cultivar under control and salt-treated environment. Among the 315 secondary metabolites identified, 150 metabolites were annotated from the Kyoto Encyclopedia of Genes and Genomes (KEGG).[11] Total ion current (TIC) plots and multipeak detection plots of one QC sample are shown in **Supplementary Figure S2**. Overlay analysis for three QC samples and hierarchical heatmap clustering and correlation analysis for all samples were performed to evaluate the technical repeatability and reliability, respectively (**Supplementary Figures S3**, **S4**). We observed that the TIC plots had a perfect overlap, and all the biological replicates were grouped together, indicating good instrumental stability and repeatability. These metabolites were clustered into seven classes in terms of their contents. The most abundant class was flavonoids (126), followed by phenolic acids (103; **Figure 4A**). Detailed information on the 315 secondary metabolites is presented in **Supplementary Table S5**.

Combined analysis of three biological replicates, each containing root tissues, revealed substantial changes in the levels of numerous metabolites in HN and GZ seedlings. As expected, in the PCA score plot, two principal components

[11]https://www.kegg.jp

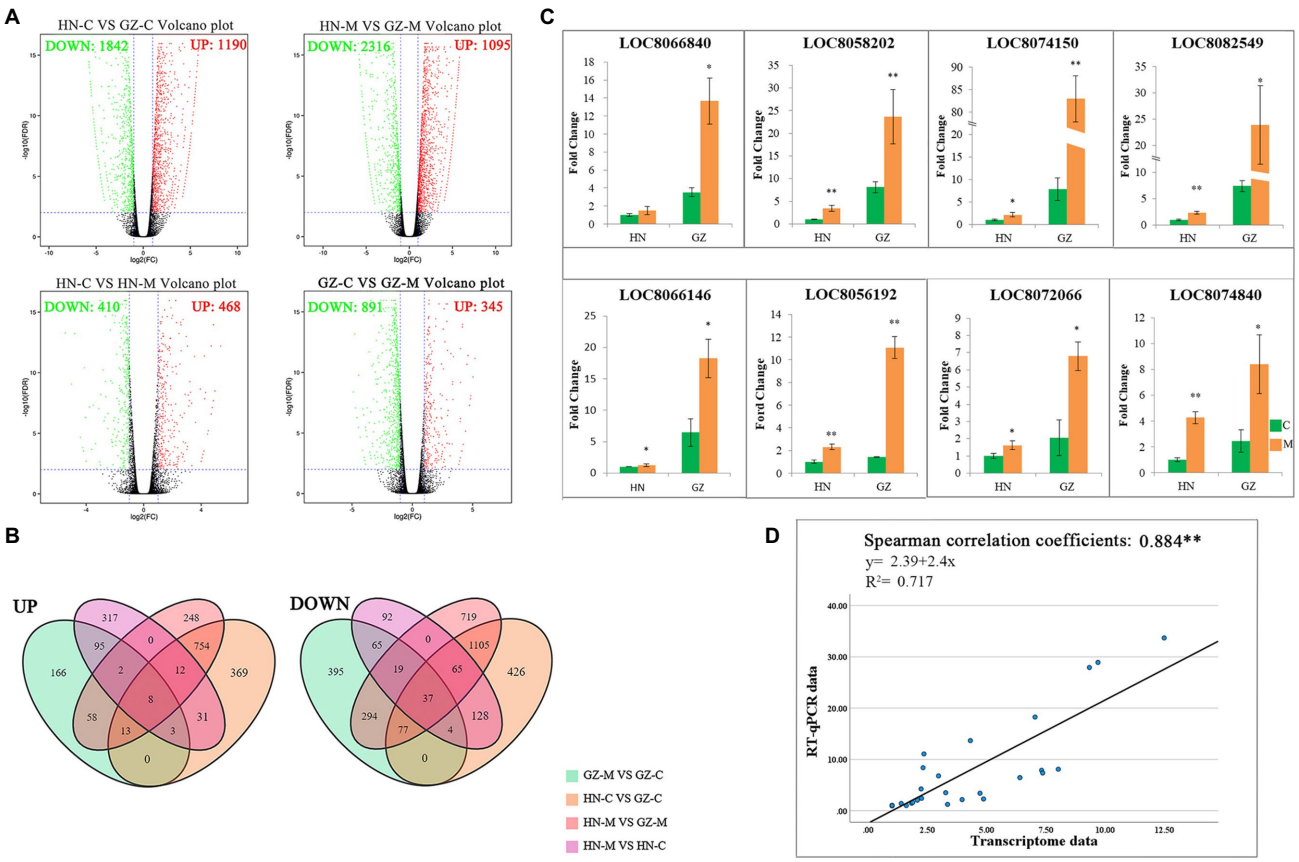

FIGURE 2 | Transcriptome Differences between GZ and HN under salt treatments. **(A)** Volcano plot analysis on DEGs under control conditions and 48 h (M) salt treatments. The expressions of genes are showed by red spots (up-regulated), green spots (down-regulated). **(B)** Venn diagram of the DEGs under different salt treatments. UP: up-regulated, DOWN, down-regulated. **(C)** RT-qPCR of up-regulated expression genes. Error bars represent standard errors of three biological replicates. The statistical significance was determined by the Student's *t* test (**$p < 0.01$; *$p < 0.05$). **(D)** Linear regression between the levels of RT-qPCR data and transcript expression.

(PC1 and PC2) were extracted to be 32.54 and 13.26%, respectively (**Figure 4C**). The PCA results showed that all samples presented as two groups, which revealed a clear separation between the two sorghum cultivars and a high similarity among the three biological replicates within each salt treatment, indicating that the experiment was reproducible and reliable. Interestingly, a clear separation of the stress treatments from the highly tolerant cultivar GZ was observed, in contrast to the sensitive cultivar HN, revealing that the two sorghum varieties responded to salt stress significantly differently at the metabolic level (**Figure 4C**). OPLS-DA was used to further discriminate the samples, and the metabolites of the GZ samples were obviously separated from those of the HN samples ($R^2X = 0.339$, $R^2Y = 0.974$, $Q^2 = 0.958$; **Figure 4B**). The PCA and OPLS-DA results suggested that genetic variation strongly influenced the metabolite profiles of different sorghum varieties.

Pairwise analysis of metabolic differences under salt treatments was also performed. Hundreds of metabolites were shown to be significantly different between the two cultivars under the same treatment, in which there were 161 (44 upregulated and 117 downregulated), 143 (57 upregulated and 86 downregulated), 133 (75 upregulated and 58 downregulated), and 129 (74 upregulated and 55 downregulated) DAMs in HN-C vs. GZ-C, HN-S vs. GZ-S, HN-M vs. GZ-M, and HN-L vs. GZ-L, respectively (**Figure 4F**). The results of KEGG enrichment statistics showed that under same salt stress times were similar and a large number of the DAMs between the two cultivars enrichment in the five pathways: metabolic pathways, biosynthesis of secondary metabolites, flavonoid biosynthesis, phenylpropanoid biosynthesis, and flavone and flavonol biosynthesis (**Supplementary Figure S5**).

The Venn diagram depicted 59 common DAMs in the two cultivars under all stress conditions (**Figure 4E**). To further analyze the abundance profiles of metabolites under the different stress conditions, we performed hierarchical clustering of the common metabolites. This analysis resulted in two distinguishable groupings that revealed different metabolic patterns of the two cultivars under salt stress. Metabolites in Group I comprised 31 compounds (14 flavanols, seven phenolic acids, five dihydroflavones, two phenolamines, one lignan, one coumarin, and one alkaloid), which preferentially accumulated in the

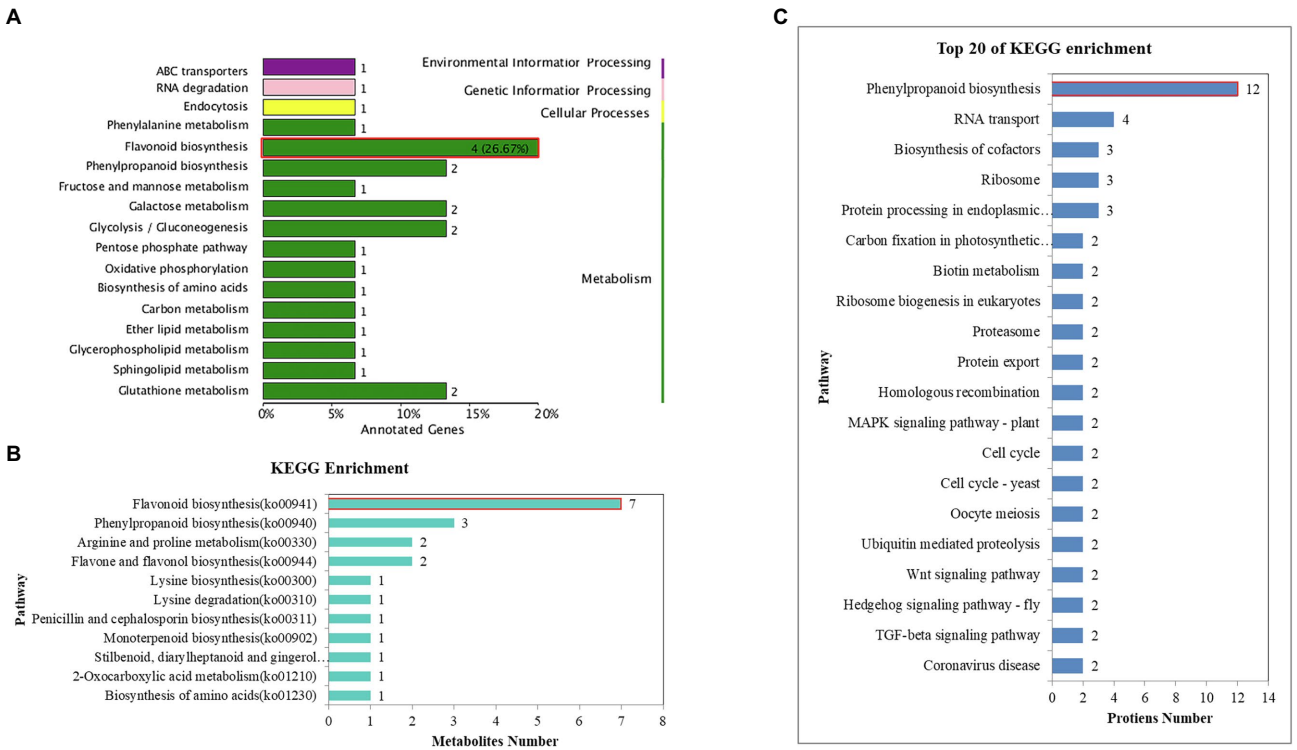

FIGURE 3 | KEGG annotation and enrichment of the common DEGs, DAMs, and DEPs. **(A)** KEGG enrichment of the common DEGs. **(B)** KEGG annotation and enrichment of the common DAMs. **(C)** KEGG annotation and enrichment of the common DAPs.

tolerant cultivar GZ. In contrast, Group II comprised 27 compounds (nine phenolic acids, six alkaloids, three flavonoids, two flavonoid carbonosides, two lignans, one coumarin, one chalcone, one monoterpenoid, one stilbene, and one tannin) accumulated mainly in the sensitive cultivar HN (**Figure 4D**). Further bioinformatic KEGG pathway analysis of the common DAMs revealed that the most prominent pathways included flavonoid biosynthesis, phenylpropanoid biosynthesis, and arginine and proline metabolism (**Figure 3B**). Seven metabolites (trihydroxyflavanone-rhamnosylglucoside, tetrahydroxyflavone, pentahydroxyflavanone, tetrahydroxyflavanol, caffeoylquinic acid, pentahydroxyflavan, and tetrahydroxyflavanone) were involved in the flavonoid biosynthesis process.

Protein Differences Between GZ and HN Under Salt Treatments

To correlate the difference in transcriptome levels to secondary metabolite data, we analyzed the proteomic differences of the two sorghum cultivars at different salt treatment times. A total of 2,351,747 spectra (262,000 were the matched peptide spectrums), 60,119 peptides (50,635 were unique peptides), and 9,002 proteins (8,024 were quantified) were identified through LC-MS/MS identification and a search against the UniProt database employing MASCOT integrated with Proteome Discoverer 1.4 software, with 1% FDR by TMT quantification (**Supplementary Table S6**). The analysis results based on the peptide ion score distribution of the proteomic showed that ion score for 69.14% peptides surpassed 20 with 29.25 median score. Most of the peptides (>95%) were 5–23 amino acid residues long. In addition, almost 70% of the identified proteins corresponded to ≥2 peptides, suggesting that the MS data can be further analyzed. The smallest protein mass was just 3.61 kDa, while the largest reached 614.68 kDa. Most of the protein masses ranged from 10 to 60 kDa, accounting for 70.11% of all the identified proteins (**Supplementary Figure S6**). We performed subcellular localization analysis of these proteins. Out of the total proteins, 39, 28, and 22% proteins were located in the nuclear, cytoplasmic, and chloroplast, respectively. Other proteins were either localized at mitochondrial, plasma membrane or were extracellular (**Supplementary Figure S7**). A total of 7,527 proteins were annotated to the GO database and grouped into 52 functional groups, of which 22 functional groups were associated with biological processes, 15 with molecular functions, and 15 with cellular components. Among the GO classifications, "cellular process," "metabolic process," "binding," "catalytic activity," "cell," "cell part," and "organelle" were highly represented, with more than 3,000 proteins in each classification (**Supplementary Figure S8**).

Similar to the metabolomic analysis, the proteomic PCA showed that genotype and salt stress had discernible effects, with HN being more severely impacted than GZ (**Figure 5A**). Furthermore, to identify the proteins most affected by salt stress, we selected those that were significantly impacted (fold change ≥1.5 or fold change ≤0.67 and FDR < 0.05). By pairwise

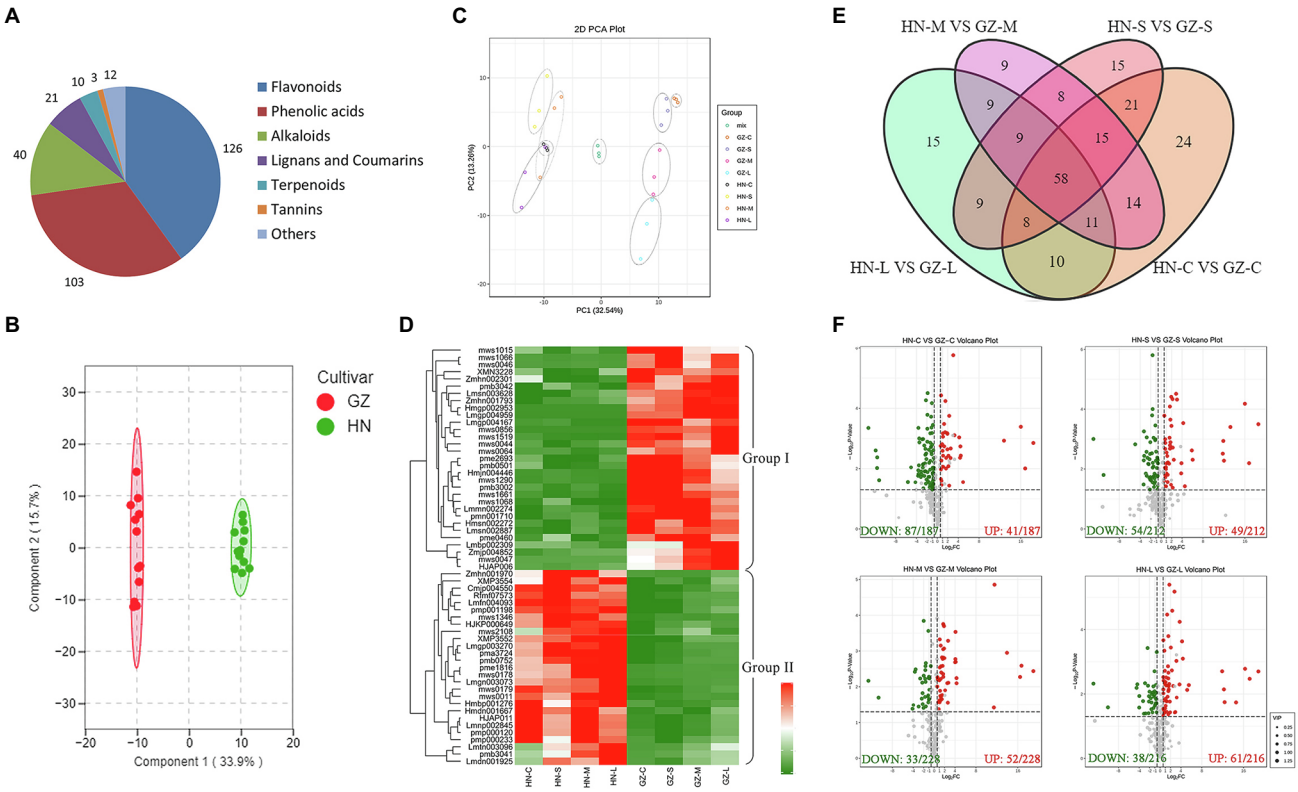

FIGURE 4 | Metabolome differences between GZ and HN under salt treatments. **(A)** The classification of 315 secondary metabolites. **(B)** Principal component analysis (PCA) scores plot. **(C)** OPLS-DA score plot. **(D)** The heatmap of the common DAMs. **(E)** Venn diagram of the DAMs. **(F)** Volcano plot analysis on the DAMs under normal conditions and salt stress. Metabolite accumulation are represented by red spots (up-regulated), green spots (down-regulated).

comparisons at the same treatment time, C, S, M, L, in HN and GZ, we identified 1,261 (743 upregulated and 788 downregulated), 3,270 (1,507 upregulated and 1,763 downregulated), 3,591 (1,640 upregulated and 1,951 downregulated), and 1,093 (376 upregulated and 717 downregulated) DEPs, respectively (**Figure 5D**). Obviously, these results indicated that the proteomic effects of S and M treatment times were significantly greater than those of L treatment time. In the GO enrichment analysis. The DEPs were significantly enriched into 285, 352, 398, and 247 functional GO terms, respectively, of which 142,202,223,132 belonged to biological processes (BPs), 68, 80, 84, and 56 belonged to molecular functions (MFs), and 75, 70, 91, and 59 to cellular components (CCs), respectively (**Supplementary Table S7**). By using the Fisher's Exact Test, we obtained the top 20 DEPs enriched GOs. We observed that the most significant GOs terms enriched in the BP, MF, and CC category were different (**Supplementary Figure S9**). KEGG enrichment analysis of DEPs from the same treatment time group showed enrichment of 86, 115, 114, and 74 pathways, respectively (**Supplementary Table S8**). It is worth noting that most of the significantly enriched KEGG pathways at different stress were similar and related to phenylpropanoid biosynthesis, ribosome, oxidative phosphorylation, protein processing in endoplasmic reticulum, and spliceosome (**Supplementary Figure S10**).

In total, according to the Venn analysis, a core set of 246 common DEPs that were significantly more or less abundant under the same treatments between the two varieties was obtained (**Figure 5C**). When the significantly common DEPs were illustrated by heatmaps, strong differences in GZ and HN tendencies were evident. Trend analysis shows that the accumulation of these common proteins in the two varieties is different (**Figures 5E,F**). The first cluster (including 82 proteins) showed downregulated stable-upregulated expression in HN but downregulated stable-regulated expression in GZ, and the second cluster (including 46 proteins) showed downregulated expression in HN and upregulated expression in GZ. We observed diverse subcellular localization of the common DEPs. Out of total 224 common DEPs, 136, 58, and 46 proteins were located in the nuclear, extracellular, and cytoplasmic, respectively. Other proteins were either localized at chloroplast, mitochondrial or were plasma membrane (**Figure 5B**). The result of the common DEPs domain annotation show that the most domain is peroxidase (**Supplementary Figure S11**). Protein functional analyses of the common DEPs were carried out using the GO and UniProt databases. The 246 common DEPs were classified into biological process (BP), cellular component (CC), and molecular function (MF) categories based on their functional features (**Supplementary Figure S12**). The major functional categories

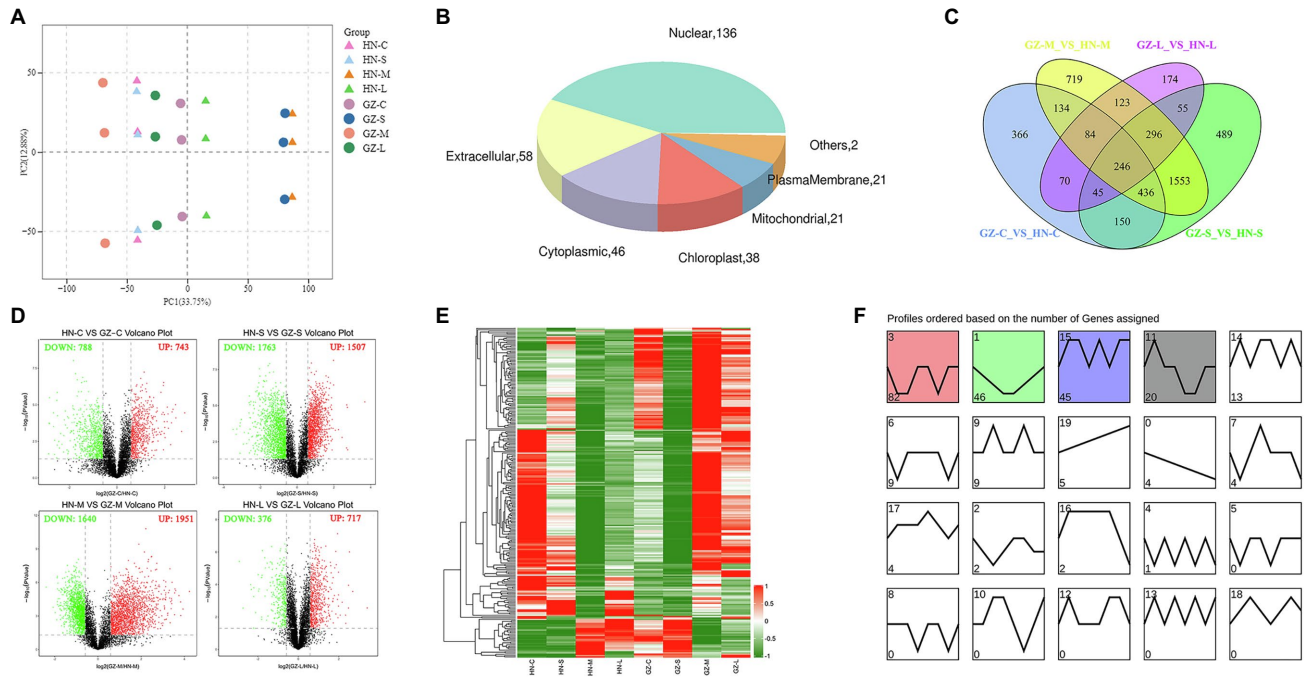

FIGURE 5 | Proteome differences between GZ and HN under salt treatments. **(A)** Principal component analysis (PCA) analysis. **(B)** Subcellular localization analysis of the common DEPs. **(C)** Venn diagram of the DEPs. **(D)** Volcano plot analysis on the DEPs. Protein accumulation are represented by red spots (up-regulated), green spots (down-regulated). **(E)** The heatmap of the common DEPs. **(F)** Trend analysis shows of the common DEPs.

in the BP category were cellular process, metabolic process, single-organism process, and response to stimulus. For MF, binding and transporter activity were the most abundant groups. The cell, cell part, and organelle categories were the most abundant groups under CC. Most notably, by KEGG annotation, a total of 246 common DEPs were assigned to 40 pathways. These proteins were mainly distributed in phenylpropanoid biosynthesis, RNA transport, and biosynthesis of cofactors. The largest significantly enriched group was in phenylpropanoid biosynthesis, including 12 proteins (**Figure 3C**).

Comprehensive Analysis of Transcriptome, Metabolome, and Proteome

The results of transcriptome, proteomics, and metabolome analysis showed the differentiation of genes, proteins, and secondary metabolites in the phenylpropanoid pathway and flavonoid biosynthesis pathway between the different sorghum cultivars. In the transcriptome analysis, the genes regulating the biosynthesis of flavonoids were upregulated. Similar to the proteomics and metabolome analyses, an obvious separation between the two different samples was observed, of which the largest group was related to phenylpropanoids and flavonoids. As shown in **Figure 6A**, the common DEPs showed a positive correlation for the common DEGs of HN-C vs. GZ-C, HN-C vs. HN-M, GZ-C vs. GZ-M, and a negative correlation with HN-M vs. GZ-M, implying that salt stress may have different effects on proteins and genes. This result is similar to the results obtained above.

The metabolism and protein regulation network in plants is very complex. One of the important ways for proteins/metabolites to function is to interact with other proteins/metabolites. Highly correlated proteins/metabolites may have similar functions and may be the key factor affecting metabolism or signal transduction. Therefore, the study of protein–metabolite correlations is of great significance. Pearson correlation coefficients for common DEPs and common DAMs were calculated to reveal the synergistic interaction between the proteome and metabolome and identify more important factors. The results show that there are complex correlations between the common DEPs and the common DAMs. Sixty-five common DEPs were strongly correlated ($R^2 > 0.7$ and $p < 0.05$), with 39 common DAMs under salt stress (**Figure 6B**). The correlation between metabolites and proteins does not have a one-to-one correspondence. For example, the protein A0A1Z5R3Q3 (LOC8061086) was significantly correlated with the relative content of 31 common DAMs. The top five highly correlated metabolites were chrysoeriol-glucoside, dihydroquercetin, demethyl coniferin, caffeoyl xylose, and p-Coumaric acid-4-O-glucoside. There was also a significant correlation between naringenin (Lmgp004959) and 41 common DEPs. The top five proteins were C5X3B3, C5Z176, C5Z4C0, C5Y6E8, C5YUB1, encoded by LOC8073079, LOC8072721, LOC8069161, LOC8068289, and LOC8065892, respectively.

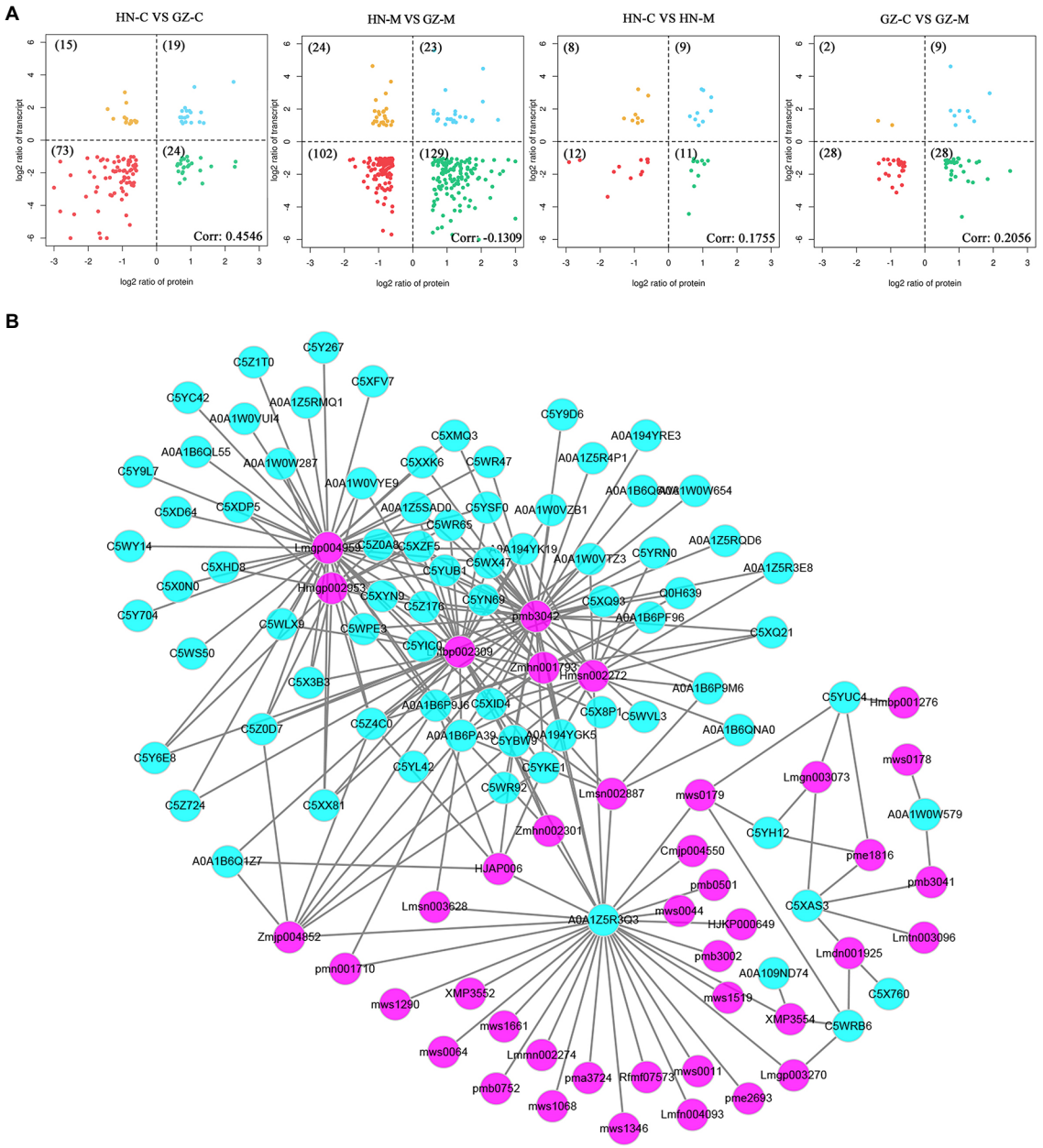

FIGURE 6 | Multi-omics analyses of GZ and HN under salt treatments. **(A)** Four-quadrant diagram analysis between the common DEGs and the common DEPs in sorghum in response to salt. **(B)** Correlation network constructed with the common DEPs (green) and the common DAMs (purple) under salt stress ($R^2 > 0.7$).

DISCUSSION

The Different Effect of Salt Stress on Phenotypic and Physiological at Seedling Stage in Two Sorghum Cultivars

In general, the germination and seedling stage is the weakest period of plant to abiotic stress. Therefore, the germination and seedling stage is crucial for the establishment of plants (Song et al., 2008; Vennapusa et al., 2021). Salt stress has serious influence on root length, especially for hypersensitive improved cultivars (Ukwatta et al., 2021). It is similar to the results of our current study (**Figure 1B**). ROS are generated by plants under high exogenous salt concentration. As key secondary messengers, ROS can trigger subsequent defensive measures. To overcome salt-mediated oxidative stress, plants have developed a comprehensive and intricate system for scavenging high levels of ROS by using antioxidant enzymes (Dietz et al., 2016). The correlation between salt tolerance and antioxidant capacity has been found in wheat (Meneguzzo et al., 1999). In the present study, the antioxidant enzyme activities under salt conditions were significantly higher than those under the control treatment, and the antioxidant enzyme

activities in GZ increased faster than that in HN (**Figures 1F,G**). Similar results have been also observed in spring wheat previously (Raza et al., 2007). On the other hand, abiotic stress leads to the upregulated expression of polyphenol compounds, which promotes the antioxidant capacities of plants (Hodaei et al., 2018). In maize, the accumulation of tannin, TP, and TF in salt-tolerant varieties were higher than that in salt-sensitive varieties under salt stress (Hichem et al., 2009). The same phenomenon was observed in the present study (**Figures 1C–E**). A more rapid and elevated accumulation of flavones was observed in the resistant cultivar GZ than in the susceptible cultivar HN.

Comparison of Different Omics Studies on Sorghum Under Salt Stress Condition

In recent years, omics technologies have been widely utilized by researchers in the field of sorghum abiotic stress especially salt stress (Surender Reddy et al., 2015; Punia et al., 2020). The experimental designs and outcomes of our study showed differences as well as similarities from previous studies. In the previous studies (Ma et al., 2020; Sun et al., 2020), integrated transcriptomic and metabolomic and transcriptomics techniques were used, respectively. In our work, three omics techniques were performed, to detect the differences in two different salt tolerance sorghum cultivars under salt stress, which help us improve the understanding of the biosynthetic networks more comprehensively (Zhou et al., 2019).

Transcriptomic analysis provides a fast way to find different expression genes in the plant response to abiotic stress. Some genes, as key components, were the primary factors affecting the signal transduction pathways in response to stress (Fujita et al., 2006). Hundreds of genes inducible by drought, cold, and high salinity have been identified in *Arabidopsis* using transcriptomic analysis (Seki et al., 2002). Our previous studies also explored dozens of DEGs related to salt tolerance in other sorghum genotypes planted in salt environments based on transcriptomic technology (Cui et al., 2018). Although the salt stress condition is different, the outcomes of our study showed similarities from previous studies by Ma et al. (2020). Ma et al. (2020) found that anthocyanin biosynthesis-related genes such as LOC8074150 which editing anthocyanidin synthase were up-regulated under moderate salt−alkali stress. In our work, the comparative analysis using RNA-Sequence revealed that a lot of the DEGs were located in the flavonoid biosynthesis pathway, indicating flavonoid may potentially confer protection against salt stress (**Figure 3A**).

The biosynthesis of flavonoids starts with phenylalanine and involves a series of enzymatic reactions. CHS, CHI, F3H, F3'H or F3'5'H, DFR and ANR are the key enzymes in this pathway. Our results of transcriptome analyses showed that the majority of the common DEGs were distributed to flavonoids biosynthesis and conducted the synthesis of key enzymes including ANR, DFR, and F3H. *F3H* genes have been cloned and characterized from a variety of plant species (Arnone et al., 1992; Charrier et al., 1995; Si et al., 2022). Overexpression of *F3H* from *Pohlia nutans* increased the tolerance of *A. thaliana* to salt stresses (Li et al., 2017). Liu et al. (2013) also previously reported that *F3H* gene is the key regulator of flavonoid biosynthesis that participates in the responses to UV stress and salinity (Liu et al., 2013). Kim et al. (2017) previously reported that *DFR* gene can be effectively manipulated to modulate salt and drought stress tolerance in *Brassica napus* L.

Metabolism makes an important contribution to the regulation mechanisms under abiotic stress because plants have extremely rich and variable metabolic profiles (Li et al., 2021). Some metabolites are vital for signaling and adaptation to environmental stress (Yang et al., 2020). As one of the most important secondary metabolites, flavonoids are widely distributed in plants (Tanaka et al., 2010). Studies on several plant species have demonstrated that the accumulation of flavonoids is critical for survival under difficult growth conditions (Liu et al., 2012; Petrussa et al., 2013; Chen et al., 2017). Increasing the levels of flavonoids by transgenes UDP-sugar glycosyltransferases (UGTs) into *Arabidopsis* can increase salt and drought stress tolerance (Zhang et al., 2021). It has been reported that the sorghum variety with high pathogen resistance showed a more rapid and elevated accumulation of flavonoids than the susceptible cultivar after inoculation with the anthracnose pathogen (Du et al., 2010). In our study, the sorghum-resistant cultivar showed a more rapid and elevated accumulation of flavonoids than the susceptible cultivar after salt stress. Out of the seven common DAMs involved in the flavonoid biosynthesis process, the levels of five metabolite accumulations were higher in the highly tolerant cultivar GZ, including trihydroxyflavanone-rhamnosylglucoside, tetrahydroxyflavone, dihydroquercetin, pentahydroflavan, and tetrahydroxyflavanone (**Figures 3B**, **7**). Previous studies show that pentahydroxyflavan on the outer surface of the chloroplast envelope might additionally quench ROS formed outside the chloroplast (Mullineaux and Karpinski, 2002). The C-glycosyl flavone maysin in silk tissues is responsible for *maize* insecticidal activity toward corn earworms (Rector et al., 2002). Flavones also serve as antioxidants to protect *Arabidopsis* from UV irradiation (Bieza and Lois, 2001). In our work, the TF and TP contents in the two cultivars were affected by salt. These results indicated that there were links between sorghum salt resistance and the flavonoid pathways.

Plant resist to environment stress is a complex pathway, including transcriptome, metabolome, and proteomic. Proteomics is a powerful tool and can provide more qualitative and quantitative information about responses to abiotic stress. A study in sorghum leaves using comparative proteomics identified protein groups responding to salt stress (Swami et al., 2011). In our research, in contrast to the transcriptome sequencing and metabolome results, the proteomic sequencing results showed that most of the differential proteins were allocated to the phenylalanine pathway (**Figure 3C**). The result is partial consistency with the transcriptome and metabolism. Interestingly, most of the DEPs participated in the phenylalanine pathway are the enzymes of flavonoid or flavone biosynthesis in our result. Peroxidase (A0A109ND74, E1.11.1.7) catalyzes the oxidation of phenylpropanoids to their

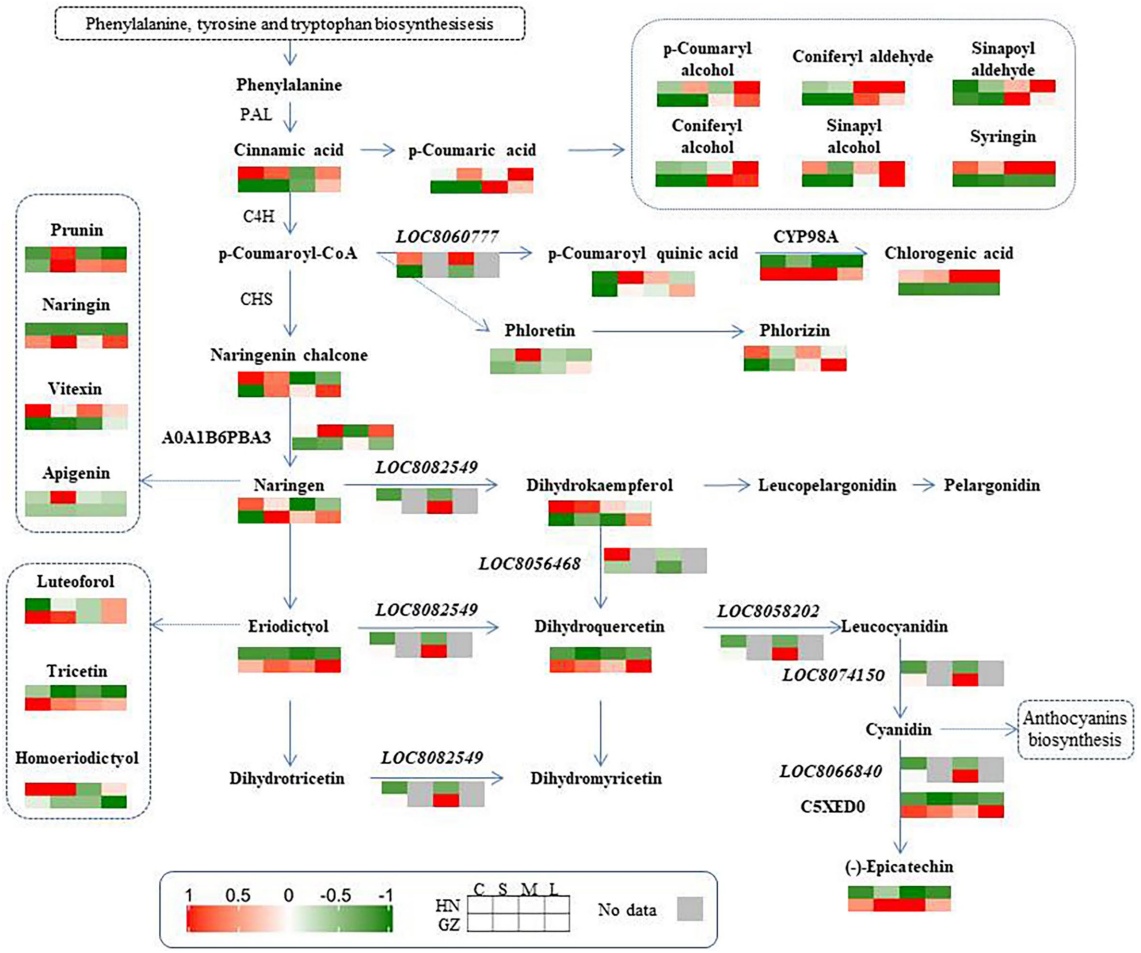

FIGURE 7 | Phenylpropanoid and Flavonoid biosynthesis pathway. Genes, proteins, and metabolites with differential abundance involved in phenylpropanoid and flavonoid biosynthesis metabolism were mapped to the corresponding metabolic pathways in KEGG.

phenoxyl radicals. In this study, peroxidase induced by salt stress and the expression of peroxidase in GZ is higher than that in HN. In addition, glutathione S-transferase (C5WY74 EC:2.5.1.18) is one of the "core" enzymes acting in the flavone and flavonol biosynthesis. Glutathione S-transferase were induced in GZ and degraded in HN in our study. Previous research indicated that overexpression of the glutathione S-transferase could enhanced salt resistance of mulberry (Gan et al., 2021).

In plants, the amino acid phenylalanine is a substrate of both primary and secondary metabolic pathways (Peng et al., 2018). Phenylalanine is the precursor of flavonoid, phenol, and anthocyanin synthesis, which plays a crucial role in the plant response to biotic and abiotic stress (Agati et al., 2013). Previous research indicated that the pathways associated with phenylalanine have important functions in the plant response to environmental stress (Savoi et al., 2016). The proteomics analysis in our experiment linked the DEGs and DAMs and enhanced the understanding of flavonoid function in sorghum resistance to salt.

In-depth Multiomics Analysis to Identify Possible Salt Tolerance Pathway of Sorghum

Our in-depth omics analysis also provides a feasibility to map how sorghum seedlings are impacted by salt stress at the transcriptional and posttranscriptional levels. Based on the flavonoid pathway and the phenylalanine pathway downloaded by the KEGG, three proteins, six genes, and 25 secondary metabolites were mapped (**Figure 7**). Four genes (LOC8058202, LOC8074150, LOC8066840, and LOC8082549) were upregulated at the two cultivars under salt stress. In contrast, two genes (LOC8060777 and LOC8056468) were upregulated only at HN. The contents of seven metabolites (trihydroxyflavanone-rhamnosylglucoside, dihydroquercetin, eriodictyol, tricetin, naringenin-glucoside, epicatechin, and pentahydroxyflavan) in the salt-tolerant cultivar were higher than those in the hypersensitive cultivar. For proteins, two proteins (CYP98A and C5XED0) were upregulated in GZ under salt stress.

In sorghum, the abundance of some flavonoid metabolites is significantly related to the expression of flavonoid biosynthesis

genes (Ma et al., 2020). Similar to the current study, flavonoids varied with the degree of stress and genotype, and the dynamic changes in flavonoid content at different genotypes were of great significance, particularly in the highly tolerant cultivar. The genes, proteins, and metabolites involved in this pathway were obviously different between highly tolerant and sensitive cultivars, and coordinated variations were detected. For example, it is noteworthy that the abundance of epicatechin was significantly correlated with the expression of the anthocyanidin reductase (EC 1.3.1.77) gene and its coding protein (C5XED0; **Figure 7**).

These results provide us with references for further studying the deep mechanisms of the molecular network in response to salinity stress. Combining phenotype and multiomics analysis considerably improves our knowledge of the molecular mechanisms and pathways underlying the response of sorghum to salt stress and provides important clues on how to relieve salt stress during the seeding stage.

CONCLUSION

The results of the current study showed that salt stress led to differentially regulated expression of genes as well as significant variations in proteins and secondary metabolites. We identified four key genes and seven key secondary metabolites enriched in the flavonoid biosynthesis pathway. We also identified 12 key proteins enriched in the phenylpropanoid biosynthesis pathway. By the multiomics analyses, we found that flavonoid biosynthesis pathway plays important role in sorghum resistance to salt stress and the gene LOC8066840 which is responsible for protein C5XED0 and epicatechin biosynthesis may be the key gene in regulating the ability of sorghum to withstand salt stress. The results of our study provide insights for further understanding the molecular mechanism of salt tolerance in sorghum, and lay the foundation for exploring and cloning salt-resistant gene and genetic improvement of sorghum. Meanwhile, this work can also provide reference to other crops in salt resistance improving.

DATA AVAILABILITY STATEMENT

The datasets presented in this study can be found in online repositories. The names of the repository/repositories and accession number(s) can be found at: The raw data files for this RNA-seq during our experiment are deposited in NCBI (BioProject: PRJNA395348 and PRJNA816817). The mass spectrometry proteomics data have been deposited to the ProteomeXchange Consortium (http://proteomecentral.proteomexchange.org) *via* the iProX partner repository with the dataset identifier PXD032125.

AUTHOR CONTRIBUTIONS

GR and PY: roles/writing—original draft and investigation. CY and YG: supervision. YB and DZ: software. JCu and JCh: methodology, project administration, and writing—review and editing. All authors contributed to the article and approved the submitted version.

FUNDING

This work was supported by the National Key R&D Program of China (2019YFD1000700 and 2019YFD1000703) and the Hebei Key Research & Development Program (20326347D and 21326305D).

SUPPLEMENTARY MATERIAL

The Supplementary Material for this article can be found online at: https://www.frontiersin.org/articles/10.3389/fpls.2022.886805/full#supplementary-material

SUPPLEMENTARY FIGURE S1 | KEGG annotation and enrichment of DEGs.

SUPPLEMENTARY FIGURE S2 | Total ions current overlaps of the three quality control samples by mass spectrometry detection. **(A)** TIC overlay plot in positive ionization mode. **(B)** TIC overlay plot in negative ionization mode.

SUPPLEMENTARY FIGURE S3 | Correlation analysis for all samples and metabolites.

SUPPLEMENTARY FIGURE S4 | Heatmap clustering all samples and metabolites.

SUPPLEMENTARY FIGURE S5 | KEGG annotation and enrichment of DAMs. **(A)** HN-C vs. GZ-C. **(B)** HN-S vs. GZ-S. **(C)** HN-M vs. GZ-M. **(D)** HN-L vs. GZ-L.

SUPPLEMENTARY FIGURE S6 | The quality control (QC) of Proteomics.

SUPPLEMENTARY FIGURE S7 | Subcellular localization analysis of all proteins.

SUPPLEMENTARY FIGURE S8 | GO analysis of all proteins.

SUPPLEMENTARY FIGURE S9 | GO analysis of the DEPs. **(A)** HN-C vs. GZ-C. **(B)** HN-S vs. GZ-S. **(C)** HN-M vs. GZ-M. **(D)** HN-L vs. GZ-L.

SUPPLEMENTARY FIGURE S10 | KEGG analysis of the DEPs. **(A)** HN-C vs. GZ-C. **(B)** HN-S vs. GZ-S. **(C)** HN-M vs. GZ-M. **(D)** HN-L vs. GZ-L.

SUPPLEMENTARY FIGURE S11 | Domain analysis of the common DEPs.

SUPPLEMENTARY FIGURE S12 | GO analysis of the common DEPs.

SUPPLEMENTARY TABLE S1 | Phenotypic and physiological characterizations.

SUPPLEMENTARY TABLE S2 | The primers of RT-qPCR.

SUPPLEMENTARY TABLE S3 | Statistics of transcriptome sequencing results.

SUPPLEMENTARY TABLE S4 | Numbers of transcripts, unigenes and new genes from transcriptome sequencing results.

SUPPLEMENTARY TABLE S5 | 315 secondary metabolite information.

SUPPLEMENTARY TABLE S6 | Spectra, peptides, and proteins information.

SUPPLEMENTARY TABLE S7 | GO analysis of the DEPs.

SUPPLEMENTARY TABLE S8 | KEGG analysis of the DEPs.

REFERENCES

Agati, G., Biricolti, S., Guidi, L., Ferrini, F., Fini, A., and Tattini, M. (2011). The biosynthesis of flavonoids is enhanced similarly by UV radiation and root zone salinity in *L. vulgare* leaves. *J. Plant Physiol.* 168, 204–212. doi: 10.1016/j.jplph.2010.07.016

Agati, G., Brunetti, C., Di Ferdinando, M., Ferrini, F., Pollastri, S., and Tattini, M. (2013). Functional roles of flavonoids in photoprotection: new evidence, lessons from the past. *Plant Physiol. Biochem.* 72, 35–45. doi: 10.1016/j.plaphy.2013.03.014

Arnone, M. I., Birolo, L., Giamberini, M., Cubellis, M. V., Nitti, G., Sannia, G., et al. (1992). Limited proteolysis as a probe of conformational changes in aspartate aminotransferase from *Sulfolobus solfataricus*. *Eur. J. Biochem.* 204, 1183–1189. doi: 10.1111/j.1432-1033.1992.tb16745.x

Bian, X. H., Li, W., Niu, C. F., Wei, W., Hu, Y., Han, J. Q., et al. (2020). A class B heat shock factor selected for during soybean domestication contributes to salt tolerance by promoting flavonoid biosynthesis. *New Phytol.* 225, 268–283. doi: 10.1111/nph.16104

Bieza, K., and Lois, R. (2001). An Arabidopsis mutant tolerant to lethal ultraviolet-B levels shows constitutively elevated accumulation of flavonoids and other phenolics. *Plant Physiol.* 126, 1105–1115. doi: 10.1104/pp.126.3.1105

Chan, C., and Lam, H. M. (2014). A putative lambda class glutathione S-Transferase enhances plant survival under salinity stress. *Plant Cell Physiol.* 55, 570–579. doi: 10.1093/pcp/pct201

Chandran, A. K. N., Kim, J. W., Yoo, Y. H., Park, H. L., Kim, Y. J., Cho, M. H., et al. (2019). Transcriptome analysis of rice-seedling roots under soil-salt stress using RNA-Seq method. *Plant Biotechnol. Rep.* 13, 567–578. doi: 10.1007/s11816-019-00550-3

Charrier, B. N. D., Coronado, C., Kondorosi, A., and Ratet, P. (1995). Molecular characterization and expression of alfalfa (*Medicago sativa* L.) flavanone-3-hydroxylase and dihydroflavonol-4-reductase encoding genes. *Plant Mol. Biol.* 29, 773–786. doi: 10.1007/BF00041167

Chen, Y., Ma, X., Fu, X., and Yan, R. (2017). Phytochemical content, cellular antioxidant activity and antiproliferative activity of *Adinandra nitida* tea (Shiyacha) infusion subjected to in vitro gastrointestinal digestion. *RSC Adv.* 7, 50430–50440. doi: 10.1039/C7RA07429H

Cui, J. H., Ren, G. Z., Qiao, H. Y., Xiang, X. D., Huang, L. S., and Chang, J. H. (2018). Comparative transcriptome analysis of seedling stage of two sorghum cultivars under salt stress. *J. Plant Growth Regul.* 37, 986–998. doi: 10.1007/s00344-018-9796-9

Dietz, K. J., Mittler, R., and Noctor, G. (2016). Recent Progress in understanding the role of reactive oxygen species in plant cell signaling. *Plant Physiol.* 171, 1535–1539. doi: 10.1104/pp.16.00938

Doerge, D. R., Divi, R. L., and Churchwell, M. I. (1997). Identification of the colored Guaiacol oxidation product produced by peroxidases. *Anal. Biochem.* 250, 10–17. doi: 10.1006/abio.1997.2191

Du, Y. G., Chu, H., Wang, M. F., Chu, I. K., and Lo, C. (2010). Identification of flavone phytoalexins and a pathogen-inducible flavone synthase II gene (SbFNSII) in sorghum. *J. Exp. Bot.* 61, 983–994. doi: 10.1093/jxb/erp364

FAOSTAT (2019). Food and agriculture data [Online]. Available at: https://www.fao.org/faostat/en/#home

Fujita, M., Fujita, Y., Noutoshi, Y., Takahashi, F., Narusaka, Y., Yamaguchi-Shinozaki, K., et al. (2006). Crosstalk between abiotic and biotic stress responses: a current view from the points of convergence in the stress signaling networks. *Curr. Opin. Plant Biol.* 9, 436–442. doi: 10.1016/j.pbi.2006.05.014

Gan, T., Lin, Z., Bao, L., Hui, T., Cui, X., Huang, Y., et al. (2021). Comparative proteomic analysis of tolerant and sensitive varieties reveals That Phenylpropanoid biosynthesis contributes to salt tolerance in mulberry. *Int. J. Mol. Sci.* 22:9402. doi: 10.3390/ijms22179402

Gupta, B., and Huang, B. (2014). Mechanism of salinity tolerance in plants: physiological, biochemical, and molecular characterization. *Int. J. Genomics* 2014:701596. doi: 10.1155/2014/701596

Hichem, H., Mounir, D., and Naceur, E. A. (2009). Differential responses of two maize (*Zea mays* L.) varieties to salt stress: changes on polyphenols composition of foliage and oxidative damages. *Ind. Crop. Prod.* 30, 144–151. doi: 10.1016/j.indcrop.2009.03.003

Hodaei, M., Rahimmalek, M., Arzani, A., and Talebi, M. (2018). The effect of water stress on phytochemical accumulation, bioactive compounds and expression of key genes involved in flavonoid biosynthesis in *Chrysanthemum morifolium* L. *Ind. Crop. Prod.* 120, 295–304. doi: 10.1016/j.indcrop.2018.04.073

Hou, S. Y., Du, W., Hao, Y. R., Han, Y. H., Li, H. Y., Liu, L. L., et al. (2021). Elucidation of the regulatory network of flavonoid biosynthesis by profiling the metabolome and transcriptome in tartary buckwheat. *J. Agric. Food Chem.* 69, 7218–7229. doi: 10.1021/acs.jafc.1c00190

Ismail, A. M., and Horie, T. (2017). Genomics, physiology, and molecular breeding approaches for improving salt tolerance. *Annu. Rev. Plant Biol.* 68, 405–434. doi: 10.1146/annurev-arplant-042916-040936

Johansson, L. H., and Håkan Borg, L. A. (1988). A spectrophotometric method for determination of catalase activity in small tissue samples. *Anal. Biochem.* 174, 331–336. doi: 10.1016/0003-2697(88)90554-4

Kim, J., Lee, W. J., Vu, T. T., Jeong, C. Y., Hong, S.-W., and Lee, H. (2017). High accumulation of anthocyanins via the ectopic expression of AtDFR confers significant salt stress tolerance in Brassica napus L. *Plant Cell Rep.* 36, 1215–1224. doi: 10.1007/s00299-017-2147-7

Kusano, M., Tohge, T., Fukushima, A., Kobayashi, M., Hayashi, N., Otsuki, H., et al. (2011). Metabolomics reveals comprehensive reprogramming involving two independent metabolic responses of Arabidopsis to UV-B light. *Plant J.* 67, 354–369. doi: 10.1111/j.1365-313X.2011.04599.x

Li, H., Li, Y., Ke, Q., Kwak, S. S., Zhang, S., and Deng, X. (2020a). Physiological and differential proteomic analyses of imitation drought stress response in Sorghum bicolor root at the seedling stage. *Int. J. Mol. Sci.* 21:9174. doi: 10.3390/ijms21239174

Li, C., Liu, S., Yao, X., Wang, J., Wang, T., Zhang, Z., et al. (2017). PnF3H, a flavanone 3-hydroxylase from the Antarctic moss *Pohlia nutans*, confers tolerance to salt stress and ABA treatment in transgenic Arabidopsis. *Plant Growth Regul.* 83, 489–500. doi: 10.1007/s10725-017-0314-z

Li, J., Van Vranken, J. G., Pontano Vaites, L., Schweppe, D. K., Huttlin, E. L., Etienne, C., et al. (2020b). TMTpro reagents: a set of isobaric labeling mass tags enables simultaneous proteome-wide measurements across 16 samples. *Nat. Methods* 17, 399–404. doi: 10.1038/s41592-020-0781-4

Li, W., Wen, L., Chen, Z., Zhang, Z., Pang, X., Deng, Z., et al. (2021). Study on metabolic variation in whole grains of four proso millet varieties reveals metabolites important for antioxidant properties and quality traits. *Food Chem.* 357:129791. doi: 10.1016/j.foodchem.2021.129791

Liu, M. L., Li, X. R., Liu, Y. B., and Cao, B. (2013). Regulation of flavanone 3-hydroxylase gene involved in the flavonoid biosynthesis pathway in response to UV-B radiation and drought stress in the desert plant, Reaumuria soongorica. *Plant Physiol. Biochem.* 73, 161–167. doi: 10.1016/j.plaphy.2013.09.016

Liu, C., Li, S., Wang, M. C., and Xia, G. M. (2012). A transcriptomic analysis reveals the nature of salinity tolerance of a wheat introgression line. *Plant Mol. Biol.* 78, 159–169. doi: 10.1007/s11103-011-9854-1

Ma, S., Lv, L., Meng, C., Zhang, C., and Li, Y. (2020). Integrative analysis of the metabolome and transcriptome of sorghum bicolor reveals dynamic changes in flavonoids accumulation under saline-alkali stress. *J. Agric. Food Chem.* 68, 14781–14789. doi: 10.1021/acs.jafc.0c06249

Masike, K., De Villiers, A., Hoffman, E. W., and Stander, M. A. (2020). Application of metabolomics tools to determine possible biomarker metabolites linked to leaf blackening in protea. *J. Agric. Food Chem.* 68, 12595–12605. doi: 10.1021/acs.jafc.0c03607

Meneguzzo, S., Navari-Izzo, F., and Izzo, R. (1999). Antioxidative responses of shoots and roots of wheat to increasing NaCl concentrations. *J. Plant Physiol.* 155, 274–280. doi: 10.1016/S0176-1617(99)80019-4

Mullineaux, P., and Karpinski, S. (2002). Signal transduction in response to excess light: getting out of the chloroplast. *Curr. Opin. Plant Biol.* 5, 43–48. doi: 10.1016/S1369-5266(01)00226-6

Munns, R., and Tester, M. (2008). Mechanisms of salinity tolerance. *Annu. Rev. Plant Biol.* 59, 651–681. doi: 10.1146/annurev.arplant.59.032607.092911

Palacios, C. E., Nagai, A., Torres, P., Rodrigues, J. A., and Salatino, A. (2021). Contents of tannins of cultivars of sorghum cultivated in Brazil, as determined by four quantification methods. *Food Chem.* 337:127970. doi: 10.1016/j.foodchem.2020.127970

Peng, Z., He, S. P., Gong, W. F., Xu, F. F., Pan, Z. E., Jia, Y. H., et al. (2018). Integration of proteomic and transcriptomic profiles reveals multiple levels of genetic regulation of salt tolerance in cotton. *BMC Plant Biol.* 18:128. doi: 10.1186/s12870-018-1350-1

Petrussa, E., Braidot, E., Zancani, M., Peresson, C., Bertolini, A., Patui, S., et al. (2013). Plant flavonoids—biosynthesis, transport and involvement in stress responses. *Int. J. Mol. Sci.* 14, 14950–14973. doi: 10.3390/ijms140714950

Punia, H., Tokas, J., Bhadu, S., Mohanty, A. K., Rawat, P., Malik, A., et al. (2020). Proteome dynamics and transcriptome profiling in sorghum [*Sorghum bicolor* (L.) Moench] under salt stress. *3 Biotech.* 10:412. doi: 10.1007/s13205-020-02392-1

Raza, S. H., Athar, H. R., Ashraf, M., and Hameed, A. (2007). Glycinebetaine-induced modulation of antioxidant enzymes activities and ion accumulation in two wheat cultivars differing in salt tolerance. *Environ. Exp. Bot.* 60, 368–376. doi: 10.1016/j.envexpbot.2006.12.009

Rector, B. G., Snook, M. E., and Widstrom, N. W. (2002). Effect of husk characters on resistance to corn earworm (Lepidoptera: Noctuidae) in high-maysin maize populations. *J. Econ. Entomol.* 95, 1303–1307. doi: 10.1603/0022-0493-95.6.1303

Savoi, S., Wong, D. C., Arapitsas, P., Miculan, M., Bucchetti, B., Peterlunger, E., et al. (2016). Transcriptome and metabolite profiling reveals that prolonged drought modulates the phenylpropanoid and terpenoid pathway in white grapes (*Vitis vinifera* L.). *BMC Plant Biol.* 16:67. doi: 10.1186/s12870-016-0760-1

Seki, M., Narusaka, M., Ishida, J., Nanjo, T., Fujita, M., Oono, Y., et al. (2002). Monitoring the expression profiles of 7000 Arabidopsis genes under drought, cold and high-salinity stresses using a full-length cDNA microarray. *Plant J.* 31, 279–292. doi: 10.1046/j.1365-313X.2002.01359.x

Si, C., Dong, W., Da Silva, J. A. T., He, C., Yu, Z., Zhang, M., et al. (2022). Functional analysis of Flavanone 3-hydroxylase (F3H) from *Dendrobium officinale*, which confers abiotic stress tolerance. *Hortic. Plant J.* 8, 143–152. doi: 10.1016/j.hpj.2022.03.006

Singh, A. (2021). Soil salinization management for sustainable development: a review. *J. Environ. Manag.* 277:111383. doi: 10.1016/j.jenvman.2020.111383

Song, J., Fan, H., Zhao, Y. Y., Jia, Y. H., Du, X. H., and Wang, B. S. (2008). Effect of salinity on germination, seedling emergence, seedling growth and ion accumulation of a euhalophyte *Suaeda salsa* in an intertidal zone and on saline inland. *Aquat. Bot.* 88, 331–337. doi: 10.1016/j.aquabot.2007.11.004

Spitz, D. R., and Oberley, L. W. (1989). An assay for superoxide dismutase activity in mammalian tissue homogenates. *Anal. Biochem.* 179, 8–18. doi: 10.1016/0003-2697(89)90192-9

Sun, X., Zheng, H. X., Li, J. L., Liu, L. N., Zhang, X. S., and Sui, N. (2020). Comparative transcriptome analysis reveals new lncRNAs responding to salt stress in sweet sorghum. *Front. Bioeng. Biotechnol.* 8:331. doi: 10.3389/fbioe.2020.00331

Surender Reddy, P., Jogeswar, G., Rasineni, G. K., Maheswari, M., Reddy, A. R., Varshney, R. K., et al. (2015). Proline over-accumulation alleviates salt stress and protects photosynthetic and antioxidant enzyme activities in transgenic sorghum [*Sorghum bicolor* (L.) Moench]. *Plant Physiol. Biochem.* 94, 104–113. doi: 10.1016/j.plaphy.2015.05.014

Swami, A. K., Alam, S. I., Sengupta, N., and Sarin, R. (2011). Differential proteomic analysis of salt stress response in Sorghum bicolor leaves. *Environ. Exp. Bot.* 71, 321–328. doi: 10.1016/j.envexpbot.2010.12.017

Tanaka, Y., Brugliera, F., Kalc, G., Senior, M., Dyson, B., Nakamura, N., et al. (2010). Flower color modification by engineering of the flavonoid biosynthetic pathway: practical perspectives. *Biosci. Biotechnol. Biochem.* 74, 1760–1769. doi: 10.1271/bbb.100358

Ukwatta, J., Pabuayon, I. C. M., Park, J., Chen, J. P., Chai, X. Q., Zhang, H., et al. (2021). Comparative physiological and transcriptomic analysis reveals salinity tolerance mechanisms in *Sorghum bicolor* (L.) Moench. *Planta* 254:98. doi: 10.1007/s00425-021-03750-w

Van Delden, S. H., Nazarideljou, M. J., and Marcelis, L. F. M. (2020). Nutrient solutions for *Arabidopsis thaliana*: a study on nutrient solution composition in hydroponics systems. *Plant Methods* 16:72. doi: 10.1186/s13007-020-00606-4

Vastarelli, P., Moschella, A., Pacifico, D., and Mandolino, G. (2013). Water stress in *Beta vulgaris*: osmotic adjustment response and gene expression analysis in ssp. *vulgaris* and *maritima*. *Am. J. Plant Sci.* 4, 11–16. doi: 10.4236/ajps.2013.41003

Vennapusa, A. R., Assefa, Y., Sebela, D., Somayanda, I., Perumal, R., Riechers, D. E., et al. (2021). Safeners improve early-stage chilling-stress tolerance in sorghum. *J. Agron. Crop Sci.* 207, 705–716. doi: 10.1111/jac.12503

Wang, Y., Gao, S., He, X., Li, Y., Zhang, Y., and Chen, W. (2020). Response of total phenols, flavonoids, minerals, and amino acids of four edible fern species to four shading treatments. *PeerJ* 8:e8354. doi: 10.7717/peerj.8354

Wang, W. X., Vinocur, B., and Altman, A. (2003). Plant responses to drought, salinity and extreme temperatures: towards genetic engineering for stress tolerance. *Planta* 218, 1–14. doi: 10.1007/s00425-003-1105-5

Wang, W. X., Vinocur, B., Shoseyov, O., and Altman, A. (2004). Role of plant heat-shock proteins and molecular chaperones in the abiotic stress response. *Trends Plant Sci.* 9, 244–252. doi: 10.1016/j.tplants.2004.03.006

Xie, F. L., Wang, Q. L., Sun, R. R., and Zhang, B. H. (2015). Deep sequencing reveals important roles of microRNAs in response to drought and salinity stress in cotton. *J. Exp. Bot.* 66, 789–804. doi: 10.1093/jxb/eru437

Xie, Q., and Xu, Z. H. (2019). Sustainable agriculture: From sweet sorghum planting and ensiling to ruminant feeding. *Mol. Plant* 12, 603–606. doi: 10.1016/j.molp.2019.04.001

Yan, J. H., Wang, B. A., Jiang, Y. N., Cheng, L. J., and Wu, T. L. (2014). GmFNSII-controlled soybean flavone metabolism responds to abiotic stresses and regulates plant salt tolerance. *Plant Cell Physiol.* 55, 74–86. doi: 10.1093/pcp/pct159

Yang, B., He, S., Liu, Y., Liu, B., Ju, Y., Kang, D., et al. (2020). Transcriptomics integrated with metabolomics reveals the effect of regulated deficit irrigation on anthocyanin biosynthesis in cabernet sauvignon grape berries. *Food Chem.* 314:126170. doi: 10.1016/j.foodchem.2020.126170

Yuan, H. J., Zeng, X. Q., Shi, J., Xu, Q. J., Wang, Y. L., Jabu, D. Z., et al. (2018). Time-course comparative metabolite profiling under osmotic stress in tolerant and sensitive Tibetan Hulless barley. *Biomed. Res. Int.* 2018, 1–12. doi: 10.1155/2018/9415409

Zhang, K., Sun, Y., Li, M., and Long, R. (2021). CrUGT87A1, a UDP-sugar glycosyltransferases (UGTs) gene from *Carex rigescens*, increases salt tolerance by accumulating flavonoids for antioxidation in *Arabidopsis thaliana*. *Plant Physiol. Biochem.* 159, 28–36. doi: 10.1016/j.plaphy.2020.12.006

Zhang, S. S., Ying, H., Pingcuo, G. S., Wang, S., Zhao, F., Cui, Y. N., et al. (2019). Identification of potential metabolites mediating bird's selective feeding on *Prunus mira* flowers. *Biomed. Res. Int.* 2019:1395480. doi: 10.1155/2019/1395480

Zhou, X., Shi, F., Zhou, L., Zhou, Y., Liu, Z., Ji, R., et al. (2019). iTRAQ-based proteomic analysis of fertile and sterile flower buds from a genetic male sterile line 'AB01' in Chinese cabbage (*Brassica campestris* L. ssp. pekinensis). *J. Proteome* 204:103395. doi: 10.1016/j.jprot.2019.103395

Conflict of Interest: The authors declare that the research was conducted in the absence of any commercial or financial relationships that could be construed as a potential conflict of interest.

Publisher's Note: All claims expressed in this article are solely those of the authors and do not necessarily represent those of their affiliated organizations, or those of the publisher, the editors and the reviewers. Any product that may be evaluated in this article, or claim that may be made by its manufacturer, is not guaranteed or endorsed by the publisher.

frontiers | Frontiers in Plant Science

ORIGINAL RESEARCH
published: 14 June 2022
doi: 10.3389/fpls.2022.900011

Low- and High-Temperature Phenotypic Diversity of *Brassica carinata* Genotypes for Early-Season Growth and Development

Leelawattie Persaud[1], Raju Bheemanahalli[1], Ramdeo Seepaul[2], K. Raja Reddy[1] and Bisoondat Macoon[3]*

[1] Department of Plant and Soil Sciences, Mississippi State University, Starkville, MS, United States, [2] North Florida Research and Education Center, University of Florida, Quincy, FL, United States, [3] United States Department of Agriculture-National Institute of Food and Agriculture, Clinton, MS, United States

OPEN ACCESS

Edited by:
Pasala Ratnakumar, Indian Institute of Oilseeds Research (ICAR), India

Reviewed by:
Federica Zanetti, Alma Mater Studiorum – Università di Bologna, Italy
Deborah Paola Rondanini, Consejo Nacional de Investigaciones Científicas y Técnicas (CONICET), Argentina

***Correspondence:**
K. Raja Reddy
krreddy@pss.msstate.edu

Specialty section:
This article was submitted to Plant Abiotic Stress, a section of the journal Frontiers in Plant Science

Received: *19 March 2022*
Accepted: *19 May 2022*
Published: *14 June 2022*

Citation:
Persaud L, Bheemanahalli R, Seepaul R, Reddy KR and Macoon B (2022) Low- and High-Temperature Phenotypic Diversity of Brassica carinata Genotypes for Early-Season Growth and Development. Front. Plant Sci. 13:900011. doi: 10.3389/fpls.2022.900011

Temperature is a major abiotic stress factor limiting plant growth and development during the early developmental stage. Information on carinata (*Brassica carinata* A. Braun) traits response to low and high temperatures is necessary for breeding or selecting genotypes suited for specific ecoregions, which is limited. In the present study, 12 carinata genotypes were evaluated under low (17/09°C), optimum (22/14°C), and high (27/19°C) day/night temperatures at the early developmental stage. This study quantified temperature effects on several physiological and morphological characteristics of 12-advanced carinata lines. High-temperature plants decreased (15%) the accumulation of flavonoids and increased the nitrogen balance index by 25%. Low-temperature treatment significantly inhibited the aboveground (plant height, leaf area, number, and shoot weight) and root (length, surface area, and weight) traits. Across all genotypes, the shoot weight decreased by 55% and the root weight by 49% under low temperature. On the other hand, the maximum proportion of biomass was partitioned to roots under low temperature than at the high temperature. A poor relationship (r^2 = 0.09) was found between low- and high-temperature indices, indicating differences in trait responses and tolerance mechanisms. AX17004 and AX17009 with higher root to shoot ratios might be suitable for late planting windows or regions with low-temperature spells. The two genotypes (AX17015 and AX17005) accumulated higher biomass under low- and high-temperature treatments can be used for planting in later summer or early winter. The identified low- and high-temperature stress-tolerant carinata genotypes could be a valuable resource for increasing stress tolerance during the early developmental stage.

Keywords: biomass partitioning, cold stress, heat stress, plant vigor, thermal tolerance

INTRODUCTION

Globally, carinata (*Brassica carinata* A. Braun) is an important oilseed crop in several countries, including the United States (Seepaul et al., 2021). The origin of the oilseed crop makes it well adapted to its native habitat, the highlands of Ethiopia, in cold temperatures of 14–18°C at elevations of 2200–2800 m above sea level. Along with other oilseed species, such as oilseed rape and canola, the use of carinata for biofuel production has picked up interest in recent years due to its high concentration of erucic acid (Escobar et al., 2009). It also has other industrial uses such as manufacturing plastics, lubricants, paints, leather tanning, soaps, and cosmetics (Taylor et al., 2010). Carinata has the potential to reduce weed pressure during the growing season, and it can be used as a feed crop due to its combination of low-fiber and high-protein (Seepaul et al., 2021). This crop has a long growing season of 180 days (Alvarado and Bradford, 2002). The yields of *Brassica* species are highly dependent on environmental conditions during their growth and developmental stages (Nóia Júnior et al., 2022). Carinata can be double-cropped as a winter cover crop in subtropical regions (Kumar et al., 2020). Field tests across Canada and various areas of the United States (Marillia et al., 2014; Mulvaney et al., 2019) established management practices for carinata cultivation (Magarey et al., 2008).

Carinata is a relatively new winter oilseed crop in the southeastern United States (Christ et al., 2020), where studies are currently ongoing to identify lines best suited for commercial production (Kumar et al., 2020) and understand how this crop would fit the local cropping systems in the United States (Mulvaney et al., 2019; Seepaul et al., 2021; Nóia Júnior et al., 2022). To support the adoption and commercialization of carinata production in the southeastern United States, a consortium known as the Southeastern Partnership for Advanced Renewables from Carinata (SPARC), led by the University of Florida (UF), is focused on removing physical, environmental, economic, and social constraints to its adoption and production, and reduce risks along the supply chain (George et al., 2021). Carinata has been cultivated commercially as a summer crop in the Canadian prairie and the northern plains of the United States and as a winter crop in the Southeastern United States (Seepaul et al., 2021). Currently, there is an opportunity for row crop growers in the Southeastern United States to invest in the cultivation of carinata to diversify their existing systems and profitability (Christ et al., 2020; Nóia Júnior et al., 2022). Since the carinata crop is planted in late fall in the United States, variations in late fall (low temperature) or late summer and early spring (high temperature) temperatures can affect growth and developmental events. Variations in temperatures affect the carinata crop establishment and growth when trying to plant it as a rotation crop or cover crop during fall in the United States. For example, carinata planting dates vary by region (North Carolina growers plant their carinata between late September/early October; while Florida growers plant in mid or late November). These stressful events could affect early seedling vigor, canopy growth (leaf area), and root development. It was reported that earlier/late planting is most likely to result in weaker plants (reduced vigor) at the seedling stage due to reduced leaf and root growth and biomass production. To take the fullest advantage of management practices, there is a need to identify carinata genotypes that maintain superior vigor (high biomass) at the early growth stage under low- and high-temperature conditions.

Temperature is an important abiotic stress factor that plays a dominant role in controlling plant growth and developmental processes. Plant species, and genotypes within species, vary in their sensitivity to temperature (Munyon et al., 2021; Reddy et al., 2021). Several studies used variations in morpho-physiological and yield responses to evaluate stress tolerance in oilseed crops: canola (Elferjani and Soolanayakanahally, 2018), peanut (*Arachis hypogaea* L.) (Kakani et al., 2002), and cotton (*Gossypium hirsutum*) (Reddy et al., 2020). In addition, to shoot traits, root traits have been used to investigate crop responses to a range of stresses, including drought (Raju et al., 2014), low temperature (Reddy et al., 2021), high temperature (Alsajri et al., 2019), nutrient (Jia et al., 2022), salinity (Kakar et al., 2019), waterlogging (Walne and Reddy, 2021), and UV-B (Ramamoorthy et al., 2022). These studies identified morpho-physiological traits enabling the selection of superior stress-tolerant genotypes at the early growth stage in rice (Kakar et al., 2019; Reddy et al., 2021), corn (*Zea mays*) (Wijewardana et al., 2015), sweet potato (*Ipomoea batatas*) (Ramamoorthy et al., 2022), and cotton (Brand et al., 2016). Likewise, variations in stress tolerance among carinata genotypes have been reported (Angadi et al., 2000; Gesch et al., 2019; Zoong Lwe et al., 2021). There is limited information on carinata response to different temperature ranges during the early season.

In this study, we hypothesized that introducing early-stage chilling (low)/heat stress (high temperature) tolerance can help reduce the impact of temperature stress on carinata production. One of the ways to minimize the stress (low- and high temperature) effect is by identifying stress-tolerant genotypes at the early vegetative stage. To address the above knowledge gaps, we screened 12 carinata genotypes to identify low and high-temperature stress-tolerant genotypes, one of the prerequisites for breeding for tolerance or expanding the genetic base. The present study was conducted with the following objectives (a) to determine how low and high temperatures affect the early vegetative growth of carinata, (b) to determine which carinata parameters (physiology, shoot, and root growth) are sensitive to low- and high-temperature stress at the early vegetative stage, and (c) to classify carinata genotypes based on a stress response for low and high temperatures stress.

MATERIALS AND METHODS

Experimental Conditions

This study was conducted at the Rodney Foil Plant Science Research facility of Mississippi State University, Mississippi State, MS (33°20′N, 88°47′W), from November to December

2018. Carinata genotypes were planted in three sunlit, controlled environment units called Soil-Plant-Atmosphere-Research (SPAR) chambers. Each of these chambers consists of a built-in soil bin made from steel (1-m depth × 2-m length × 0.5-m width) to accommodate belowground plant parts and a transparent chamber made of 1.27-cm thick Plexiglas (2.5-m height × 2-m length × 1.5-m width) as room for aboveground plant growth. The Plexiglas on each unit allows 97% of visible incoming solar radiation to pass without spectral variation in absorption, with a wavelength of 400–700 nm (Zhao et al., 2003). These SPAR chambers are equipped to monitor and control air temperature accurately and maintain the atmospheric CO_2 concentration at a fixed calibrated point. The SPAR chambers are also equipped with a cooling and heating system connected to air ducts that carry conditioned air through the crop canopy to cause leaf flutter. Further details on this SPAR unit control and operations were described by Reddy et al. (2001).

Additionally, chilled ethylene glycol was provided *via* parallel solenoid valves to the cooling system, which opened or closed based on the cooling requirement. Two electrical resistance heaters, which give off short heat pulses to regulate the air temperature, provide the required heat. Humidity and temperature sensors (HMV 70Y, Vaisala Inc., San Jose, CA, United States) installed in the returning path of the airline ducts helped to monitor the relative humidity. Different density of shade cloths placed around the perimeter of the plant canopy designed to simulate canopy spectral properties was readjusted to match the canopy height daily, which also eliminated the need for border plants. The CO_2 concentration, the air temperature inside the chamber, an irrigation system in each SPAR unit, and the continuous monitoring of plant and environmental gas exchange variables were automatically controlled and monitored every 10 s by a dedicated network system, also equipped to record and store data automatically. Soil moisture was monitored in all SPAR units using soil moisture probes (5TM Soil Moisture and Temperature Sensor, Decagon Devices, Inc., Pullman, WA, United States). These probes were inserted at a depth of 15 cm from the surface of five pots in each temperature treatment and set to measure soil moisture content every 60 s and recorded it at 15-min intervals. The CO_2 concentration inside the chamber was measured and maintained at 420 μmol mol^{-1} daily. Irrigation was done with installed fertigation systems with a full-strength Hoagland plant nutrient solution. This process was carried out three times daily using an automatic drip system.

Seed Materials and Temperature Treatments

For this study, seed material of 11 advanced carinata genotypes of 3 breeding types (inbred, double haploid, and hybrid) close to commercial deployment and 1 commercial check genotype were evaluated (**Table 1**). Seeds sourced from Agrisoma Biosciences Inc., Canada (now Nuseed) were treated with Helix Vibrance, which contains four fungicides (difenoconazole, metalaxyl-M, fludioxonil, and sedaxane) and one insecticide (thiamethoxam), to control insects and diseases. The treated seeds were sown in 180 polyvinyl-chloride (PVC) pots (5.24-cm diameter, 30.5-cm height, and 5.5-L volume) filled with 3:1 sand and soil. The pots were initially sown with four seeds and thinned to one seedling per pot 11 days after planting (DAP). Pots were set up in a completely randomized design inside the SPAR chambers, in 15 rows with 4 pots per row. Each carinata genotype was replicated five times within each temperature treatment. A total of 180 pots (12 genotypes × 3 treatments × 5 replications) were used in the study. Three temperature treatments (17/09°C – low, 22/14°C – optimum, and 29/19°C – high; day/night temperatures, respectively) were imposed 11 DAP, and plants were harvested 24 days after treatment (DAT) application.

TABLE 1 | Details of *Brassica carinata* genotypes used in the study.

Genotype	Type†	Source/justification
AX17001	I	Selection from SE16-17 AYT (Avanza family selection) Florida
AX17002	I	Selection from SE16-17 AYT (Avanza family selection) Florida
AX17004	I	High shatter tolerance family, good potential in a winter environment
AX17005	I	High shatter tolerance family, good potential in a winter environment
AX17006	I	High shatter tolerance family, good potential in a winter environment
AX17007	DH	Among the highest Sclerotinia incidence, Jay and Quincy, FL
AX17008	DH	Selection from SE16-17 PYTB Florida
AX17009	DH	Selection from SE16-17 PYTA Florida
AX17010	DH	Selection from SE16-17 PYTB Florida
AX17014	H	Top 2016–2017 Quincy test hybrid Florida
AX17015	H	Promising test hybrid from 2017, frost tolerant female
Avanza 641	I	Commercial check

†*Genotypes are classified into three types (I, inbred; DH, double haploid; and H, hybrid). Seed trials (SE, Southeast; AYT, advanced yield trial; PYT, preliminary yield trial).*

Measurements

Physiology Parameters

At 23 DAT, 1 day before final harvesting, physiological parameters, including chlorophyll (Chl), flavonoids (Flav), anthocyanin (Anth), and nitrogen balance index (NBI), were measured using a Dualex® Scientific Polyphenols and Chlorophyll Meter (FORCE-A, Orsay, France). Additionally, a FluorPen FP 100 (Photon Systems Instruments, Drasov, Czech Republic) was used to collect the chlorophyll fluorescence (Fv′/Fm′). All measurements were collected from the second fully expanded leaf from the top of each plant.

Biomass Parameters

The shoot growth and developmental components for all 12 carinata genotypes evaluated included plant height, the total number of leaves, leaf area, leaf dry weight, stem dry weight, shoot weight, root dry weight, total dry weight, and root/shoot

ratio (RS). The PH and LN were measured and counted 1 day before harvesting, and LA was recorded using an LI-3100 leaf-area meter (LI-COR, Inc., Lincoln, NE, United States). Leaves and stems were separated and dried in a forced-air oven at 75°C for 72 h, after which final dry biomass was recorded.

Root Parameters

At 24 DAT, all plants were harvested by separating the stem of each plant at ground level from its root system. Roots were then removed from the pots, placed on a wire screen, and washed thoroughly to remove the soil medium, using a moderate hydro flow speed and exercising maximum caution to avoid damage to the root structures. The longest root length was recorded using a meter ruler for each plant root. The individually cleaned root system was scanned using a Epson Expression 11000XL scanner, attached to a computer system. The individually cleaned root structures were placed onto a waterproof Plexiglas tray (40-cm length × 30-cm width) filled with approximately 5 mm of water and fitted onto the scanner. The roots were submerged, and the crossings and tips were spread using a small paintbrush to avoid overlapping. The acquired gray-scale root images were obtained through a high accuracy setting (resolution of 800 by 800 dpi) for the parameters measured by the WinRHIZO Pro 2009C software (Regent Instruments, Québec, Canada). The software calculated the following components: total root length, root surface area, average root diameter, root volume, number of root tips, forks, root crossings, root length density (ratio of total root length to root volume), and root to shoot percentage (ratio of root weight to shoot weight).

Cumulative Low- and High-Temperature Response Index

Cumulative low-temperature response index (CLTRI) and cumulative high-temperature response index (CHTRI) values were calculated using the standardized vigor index (Wijewardana et al., 2015; Ramamoorthy et al., 2022). Initially, the individual stress response index (ISRI) for low temperature was calculated as the value of a parameter (P_l) for a given genotype at the low temperature divided by the value of the same parameter at the optimum temperature (P_o; Equation 1). Likewise, the ISRI for high temperature was calculated for each genotype as the parameter's value at high temperature (P_h) divided by the constant recorded for the same parameter at the optimum temperature (P_o; Equation 2). The CLTRI (Equation 3) and CHTRI (Equation 4) were determined for each genotype by summing all the ISRI calculated for all the shoot and growth developmental, physiological, and root parameters measured across all genotypes. Trait acronyms and units are given in **Table 2**.

$$\mathrm{ISRI}\ (\mathrm{low}) = \mathrm{P_l}/\ \mathrm{P_o} \quad (1)$$

$$\mathrm{ISRI}\ (\mathrm{high}) = \mathrm{P_h}/\ \mathrm{P_o} \quad (2)$$

$$\begin{aligned}\mathrm{CLTRI} = {} & \left(\frac{\mathrm{Chl_l}}{\mathrm{Chl_o}}\right) + \left(\frac{\mathrm{Flav_l}}{\mathrm{Flav_o}}\right) + \left(\frac{\mathrm{Anth_l}}{\mathrm{Anth_o}}\right) + \left(\frac{\mathrm{NBI_l}}{\mathrm{NBI_o}}\right) \\ & + \left(\frac{\mathrm{Fv'/Fm'_l}}{\mathrm{Fv'/Fm'_o}}\right) + \left(\frac{\mathrm{PH_l}}{\mathrm{PH_o}}\right) + \left(\frac{\mathrm{LA_l}}{\mathrm{LA_o}}\right) + \left(\frac{\mathrm{LN_l}}{\mathrm{LN_o}}\right) \\ & + \left(\frac{\mathrm{LWT_l}}{\mathrm{LWT_o}}\right) + \left(\frac{\mathrm{SteWT_l}}{\mathrm{SteWT_o}}\right) + \left(\frac{\mathrm{SWT_l}}{\mathrm{SWT_o}}\right) + \left(\frac{\mathrm{TDM_l}}{\mathrm{TDM_o}}\right) \\ & + \left(\frac{\mathrm{LRL_l}}{\mathrm{LRL_o}}\right) + \left(\frac{\mathrm{TRL_l}}{\mathrm{TRL_o}}\right) + \left(\frac{\mathrm{RSA_l}}{\mathrm{RSA_o}}\right) + \left(\frac{\mathrm{RD_l}}{\mathrm{RD_o}}\right) \\ & + \left(\frac{\mathrm{RV_l}}{\mathrm{RV_o}}\right) + \left(\frac{\mathrm{RT_l}}{\mathrm{RT_o}}\right) + \left(\frac{\mathrm{RF_l}}{\mathrm{RF_o}}\right) + \left(\frac{\mathrm{RC_l}}{\mathrm{RC_o}}\right) \\ & + \left(\frac{\mathrm{RWT_l}}{\mathrm{RWT_o}}\right) + \left(\frac{\mathrm{RLD_l}}{\mathrm{RLD_o}}\right) + \left(\frac{\mathrm{RS_l}}{\mathrm{RS_o}}\right) \end{aligned} \quad (3)$$

$$\begin{aligned}\mathrm{CHTRI} = {} & \left(\frac{\mathrm{Chl_h}}{\mathrm{Chl_o}}\right) + \left(\frac{\mathrm{Flav_h}}{\mathrm{Flav_o}}\right) + \left(\frac{\mathrm{Anth_h}}{\mathrm{Anth_o}}\right) + \left(\frac{\mathrm{NBI_h}}{\mathrm{NBI_o}}\right) \\ & + \left(\frac{\mathrm{Fv'/Fm'_h}}{\mathrm{Fv'/Fm'_o}}\right) + \left(\frac{\mathrm{PH_h}}{\mathrm{PH_o}}\right) + \left(\frac{\mathrm{LA_h}}{\mathrm{LA_o}}\right) + \left(\frac{\mathrm{LN_h}}{\mathrm{LN_o}}\right) \\ & + \left(\frac{\mathrm{LWT_h}}{\mathrm{LWT_o}}\right) + \left(\frac{\mathrm{SteWT_h}}{\mathrm{SteWT_o}}\right) + \left(\frac{\mathrm{SWT_h}}{\mathrm{SWT_o}}\right) + \left(\frac{\mathrm{TDM_h}}{\mathrm{TDM_o}}\right) \\ & + \left(\frac{\mathrm{LRL_h}}{\mathrm{LRL_o}}\right) + \left(\frac{\mathrm{TRL_h}}{\mathrm{TRL_o}}\right) + \left(\frac{\mathrm{RSA_h}}{\mathrm{RSA_o}}\right) + \left(\frac{\mathrm{RD_h}}{\mathrm{RD_o}}\right) \\ & + \left(\frac{\mathrm{RV_h}}{\mathrm{RV_o}}\right) + \left(\frac{\mathrm{RT_h}}{\mathrm{RT_o}}\right) + \left(\frac{\mathrm{RF_h}}{\mathrm{RF_o}}\right) + \left(\frac{\mathrm{RC_h}}{\mathrm{RC_o}}\right) \\ & + \left(\frac{\mathrm{RWT_h}}{\mathrm{RWT_o}}\right) + \left(\frac{\mathrm{RLD_h}}{\mathrm{RLD_o}}\right) + \left(\frac{\mathrm{RS_h}}{\mathrm{RS_o}}\right) \end{aligned} \quad (4)$$

Data Analysis

Phenotypic data were subjected to statistical analysis to determine the effect of temperature, genotype, and their interactions on the shoot, root, and physiological parameters using the library ("doebioresearch") in RStudio 4.0.2.[1] Least square difference (LSD) was used to compare the difference in the mean value between treatments or genotypes. Additionally, regression analysis was used to determine the relationship between temperature response indices and growth parameters among these response indices. Based on r^2 values, best-fit regression functions were selected. Graphical analysis was done using Sigma Plot® 14.5.

RESULTS AND DISCUSSION

Limited studies have phenotyped carinata genotypes for thermotolerance (low and high temperature) using different breed types (inbred, double haploid, and hybrid) at the early vegetative stage. Based on our knowledge, this is the first study to report variability in physiology, shoot and root morphological traits of advanced carinata genotypes to low-

[1]https://www.rstudio.com/

TABLE 2 | Summary of ANOVA across the genotype (G), temperature treatments (T), and their interaction (G × T) on a different shoot, root, and physiological traits measured 35 days after planting (24 days after temperature treatments imposition).

Trait	Unit	LT			HT			LT	OT	HT	Change (%)	
		G	T_a	G × T_a	G	T_b	G × T_b				LT	HT
Physiology												
Chlorophyll (Chl)	μg cm^{-2}	*	ns	ns	**	ns	ns	20.5a	20.2a	20.6a	1.9	2.0
Flavonoids (Flav)	Unitless	ns	***	ns	**	***	ns	0.93a	0.68b	0.55c	36.9	−19.0
Anthocyanin (Anth)	Unitless	ns	**	ns	*	ns	ns	0.15a	0.14b	0.13b	7.9	−1.5
Nitrogen balance index (NBI)	Unitless	**	***	ns	***	***	ns	23.3c	31.1b	39.1a	−25.1	25.4
Chlorophyll fluorescence (Fv′/Fm′)	Unitless	ns	***	ns	ns	ns	ns	0.57b	0.66a	0.64a	−13.7	−3.3
Shoot												
Plant height (PH)	cm	***	***	*	***	**	ns	3.2c	9.8b	11.2a	−67.1	14.1
Leaf number (LN)	Number $plant^{-1}$	**	***	ns	**	**	ns	3.3c	5.0b	5.5a	−34.8	9.3
Leaf area (LA)	cm^2 $plant^{-1}$	**	***	ns	***	ns	ns	265.3b	584.3a	595.4a	−54.6	1.9
Leaf weight (LWT)	g $plant^{-1}$	**	***	ns	**	ns	ns	0.97b	1.89a	1.97a	−50.6	−3.7
Stem weight (SteWT)	g $plant^{-1}$	**	***	ns	*	ns	ns	0.33b	0.91a	0.87a	−64.3	−4.7
Shoot weight (SWT)	g $plant^{-1}$	**	***	ns	**	ns	ns	1.3b	2.9a	2.8a	−54.9	−4.0
Total dry matter (TDM)	g $plant^{-1}$	*	***	ns	*	ns	ns	1.4b	3.1a	3.0a	−54.5	−4.3
Root												
Longest root length (LRL)	cm $plant^{-1}$	ns	*	ns	ns	ns	ns	39.7b	44.7a	43.8ab	−11.1	−2.0
Total root length (TRL)	cm $plant^{-1}$	ns	*	ns	ns	*	ns	1757.2b	2633.7a	1873.5b	−33.3	−28.9
Root surface area (RSA)	cm^2 $plant^{-1}$	ns	*	ns	ns	ns	ns	214.4b	314.2a	264.8ab	−31.8	−15.7
Root diameter (RD)	mm	ns	ns	ns	**	ns	ns	0.41a	0.40a	0.43a	2.1	9.1
Root volume (RV)	cm^3	ns	*	ns	ns	ns	ns	2.1a	3.2a	3.1a	−32.9	−2.2
Root tips (RT)	Number $plant^{-1}$	ns	***	ns	ns	ns	ns	4578b	9402.9a	9364.5a	−51.3	−0.4
Root forks (RF)	Number $plant^{-1}$	ns	***	ns	ns	ns	ns	10195.3b	20264.8a	16458.5ab	−49.7	−18.8
Root crossings (RC)	Number $plant^{-1}$	ns	***	ns	ns	**	ns	1205.2b	2333.4a	1426.1b	−48.4	−38.9
Root weight (RWT)	g $plant^{-1}$	ns	***	ns	ns	ns	ns	0.13b	0.25a	0.23a	−48.7	−8.0
Root length density (RLD)	Ratio	*	*	ns	**	**	ns	819.8ab	909.3a	744.6b	−9.8	−18.1
Root to shoot ratio (RS)	Ratio	ns	**	ns	ns	ns	ns	0.09a	0.08b	0.07b	18.9	−6.3

*Significance level: *$p < 0.05$, **$p < 0.01$, ***$p < 0.001$; ns, non-significant. LT, low temperature; OT, optimum temperature; and HT, high temperature. T_a, control and low temperature; T_b, control and high temperature treatment. Different letters indicate statistically significant least square difference (LSD) for treatments at the level of $p < 0.05$.*

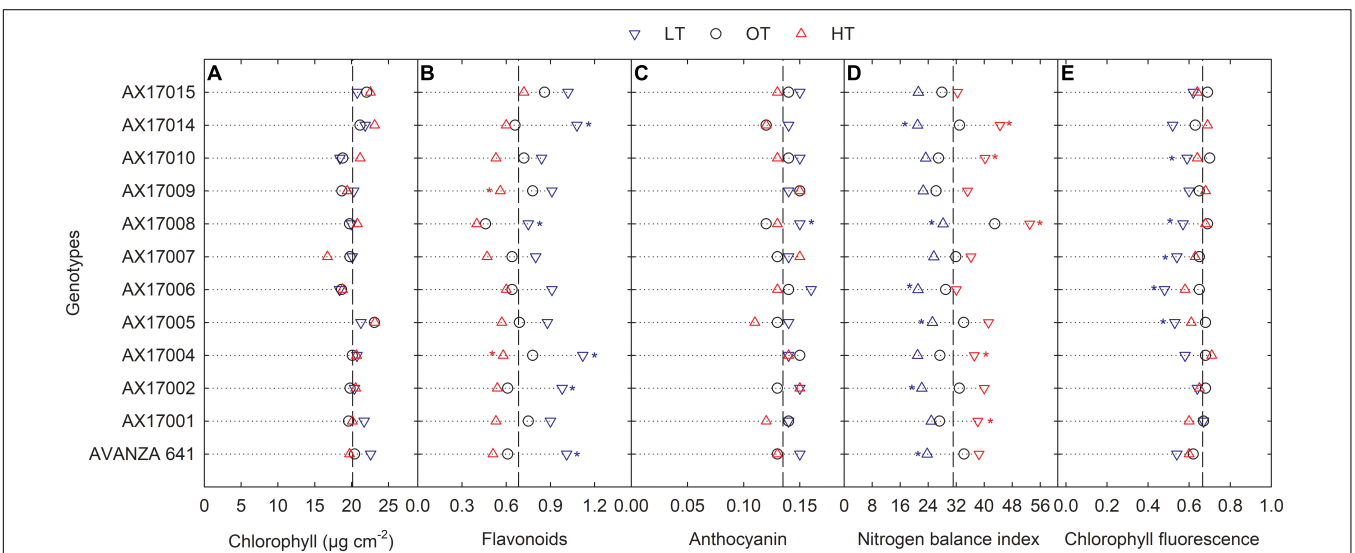

FIGURE 1 | Line plots showing the phenotypic variations in physiological traits such as chlorophyll content **(A)**, flavonoids **(B)**, anthocyanin **(C)**, nitrogen balance index **(D)**, and chlorophyll fluorescence **(E)** of 12 advanced *Brassica carinata* genotypes measured 35 days after planting or 24 days after temperature treatments imposition. The dotted middle line indicates the average trait of 12 genotypes under optimum temperature. LT, low temperature; OT, optimum temperature; and HT, high temperature. Asterisk indicates a significant difference between the temperature treatments (blue – between LT and OT; red – between HT and OT) in a genotype at 5% LSD.

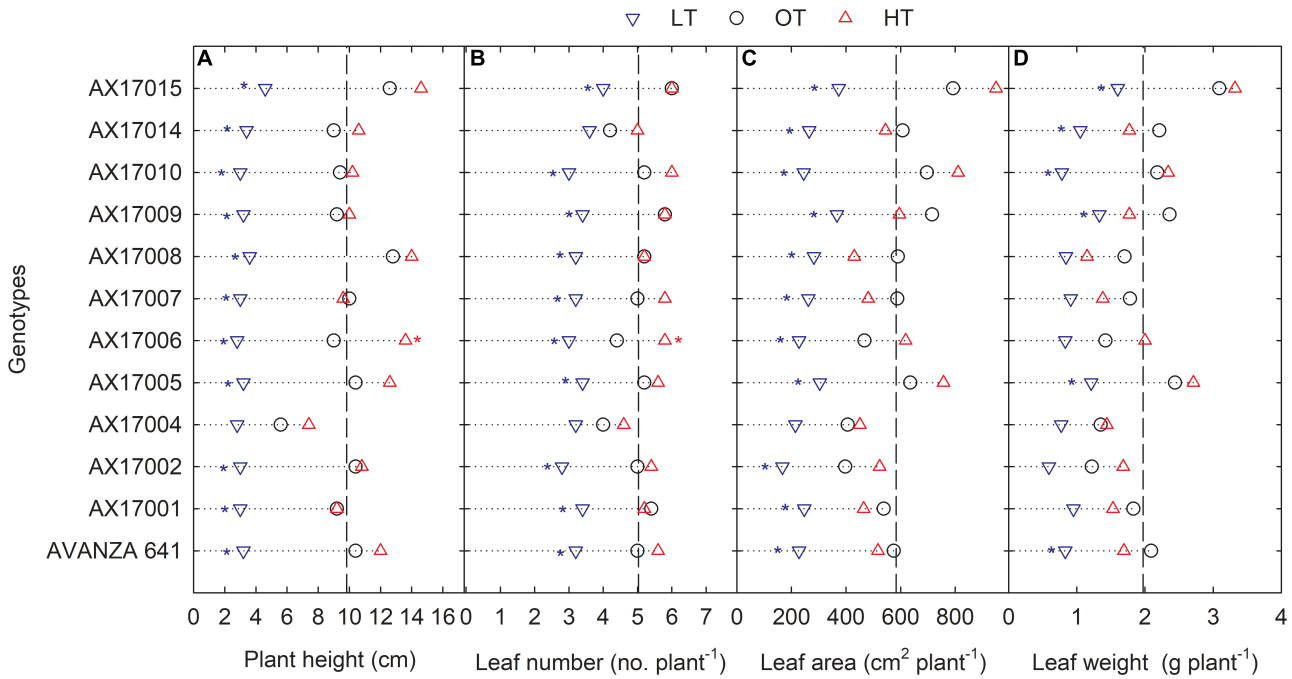

FIGURE 2 | Line plots showing the phenotypic variations of shoot-related traits such as plant height **(A)**, number of leaves **(B)**, leaf area **(C)**, and leaf weight **(D)** of 12 advanced *Brassica carinata* genotypes measured 35 days after planting or 24 days after temperature treatments imposition. The dotted middle line indicates the average trait of 12 genotypes under optimum temperature. LT, low temperature; OT, optimum temperature; and HT, high temperature. Asterisk indicates a significant difference between the temperature treatments (blue – between LT and OT; red – between HT and OT) in a genotype at 5% LSD.

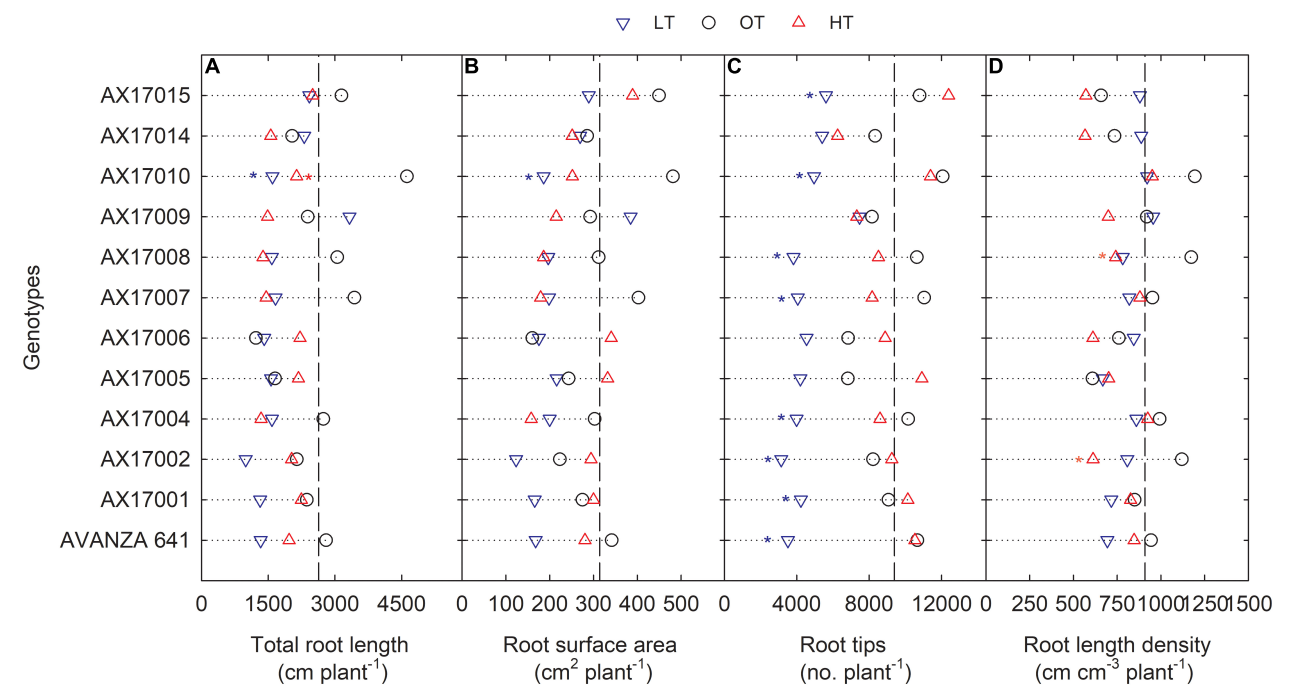

FIGURE 3 | Line plots showing the phenotypic variations of root-related traits such as total root length **(A)**, root surface area **(B)**, root tips **(C)**, and root length density **(D)** of 12 advanced *Brassica carinata* genotypes measured 35 days after planting or 24 days after temperature treatments imposition. The dotted middle line indicates the average trait of 12 genotypes under optimum temperature. LT, low temperature; OT, optimum temperature; and HT, high temperature. Asterisk indicates a significant difference between the temperature treatments (blue – between LT and OT; red – between HT and OT) in a genotype at 5% LSD.

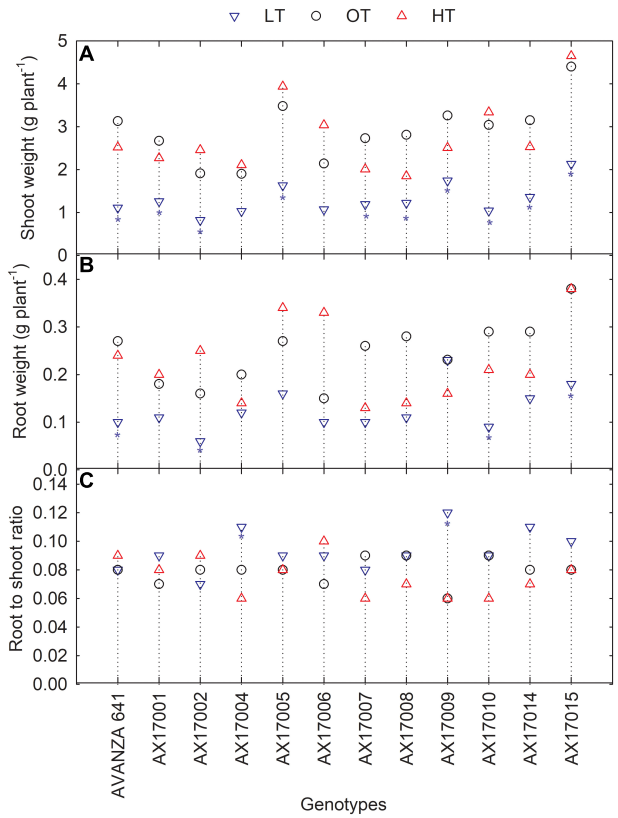

FIGURE 4 | Line plots showing the phenotypic variations in shoot weight **(A)**, root weight **(B)**, and root to shoot ratio **(C)** of 12 carinata genotypes measured 35 days after planting or 24 days after temperature treatments imposition. The dotted middle line indicates the average trait of 12 genotypes under optimum temperature. LT, low temperature; OT, optimum temperature; and HT, high temperature. Asterisk indicates a significant difference between the temperature treatments (blue – between LT and OT; red – between HT and OT) in a genotype at 5% LSD.

and high-temperature stresses during the early growth stage (**Table 2**). The information generated on carinata response to different temperatures will be beneficial for selecting genotypes for trait-based breeding programs.

Physiological Parameters

Low temperature affected the flavonoids, anthocyanin, NBI, and chlorophyll fluorescence (Fv′/Fm′) ($p < 0.01$, **Table 2**). The effect of treatment (low or high) was not significant for chlorophyll content (**Table 2**), which indicates the differential spread in response to treatment (**Figure 1A**). Low temperatures resulted in greater anthocyanin accumulation than at the optimum and high temperatures, but there was no difference between high and optimum temperatures (**Table 2**). The low temperature increased the accumulation of flavonoids (**Figure 1B** and **Table 2**) and anthocyanin (**Figure 1C** and **Table 2**). Five genotypes (AX17004, AX17014, AVANZA 641, AX17002, and AX17008) recorded significantly higher flavonoid values under low temperatures than the control (**Figure 1B**). At low temperature treatment, AX17008 recorded 25% ($p < 0.05$) higher anthocyanin than the optimum temperature (**Figure 1C**). The mean NBI decreased with decreasing temperature regimes by 25% ($p < 0.05$) from the optimum to the low temperature (**Table 2**). Across all treatments, genotype AX17008 had the greatest NBI (**Figure 1D**). Mean Fv′/Fm′ was not different between high temperature and optimum temperature treatments but decreased by 16% at the low temperature (**Figure 1E**). The Fv′/Fm′ was the least at low temperatures, and there was no difference between the optimum and high temperatures (**Table 2**). An increase in growing temperatures decreased leaves' flavonoids and increased the NBI, indicating a negative relationship with flavonoids and a positive relationship with increased growing temperature (**Figure 1**). The effect of temperature on pigments indicates a strong thermal impact on the nitrogen status of carinata genotypes. Increased leaf flavonoid production can make plants resilient to environmental stresses by reducing oxidative stress damages (Kuk et al., 2003).

Shoot Traits

The genotypes significantly differed for plant height, leaf number, leaf weight, stem weight, and shoot weight (**Table 2**). Low temperature significantly decreased the plant height, leaf number, leaf weight, stem weight, and shoot weight for all genotypes by 67, 35, 55, 50, 64, and 60% at 24 days after stress (**Table 2**). In contrast, plant height, leaf number, and leaf weight were increased under high-temperature stress (**Table 2**). Two traits, PH and LN, had apparent differences among treatments ranking greatest to least from the high to low temperatures regimes (**Figures 2A,B**). The mean PH at the high temperature was 14% taller than the optimum temperature. The height reduction from optimum to low temperature was 67% (**Figure 2A**), showing the strong negative impact of low-temperature cell elongation and leaf expansion (Ben-Haj-Salah and Tardieu, 1995). Under the low temperature, a significantly lower number of leaves was observed in AX17002, while AX17006 grown under high temperature recorded a 51% greater number of leaves than at optimum temperature (**Figure 2B**). Under high temperatures, AX17015 had the tallest plants and the greatest LN, and AX17004 had the shortest plants (**Figures 2A,B**). Carinata stem elongation and leaf area expansion determine crop development and biomass accumulation in the early season. Across all the genotypes, shorter plants observed under low temperatures may be attributed to a reduction in cell division and elongation activities caused by low thermal conditions, affecting cellular functions and photosynthetic processes (Miedema, 1982; Ben-Haj-Salah and Tardieu, 1995). Under low temperature, the leaf area varied from 167 (AX17002) to 374 (AX17015), which is significantly lower than the other 2 treatments (**Figure 2C**). Under low temperature, all genotypes recorded a significant reduction in leaf area compared to optimum temperature treatment (**Figure 2C**). Leaf weight of 12 genotypes at the low temperature was lesser (55%) than at optimum temperature, but the response at high temperature was not different from the optimum (**Figure 2D**). The high temperature had no significant influence on the shoot biomass (leaf and stem weight, **Table 2**), but low-temperature treatment reduced the shoot weight by 55%. Likewise, studies of the same phenomena were noted in response to high temperatures in different crops (Wijewardana et al., 2015; Munyon et al., 2021; Reddy et al., 2021). The percentage of total

dry matter reduction under high temperature was less than 5%, which was 50% lesser than the percentage reduction under low temperature (**Table 2**).

Root Growth and Developmental Parameters

The effect of low temperature was significant ($p < 0.05$ to <0.001) on all the root parameters except root diameter. There were no temperature × genotype interactions (**Table 2**). The effect of high temperature was significant for total root length, root crossing, and root length density (**Table 2**). For all parameters except RD, trait values were highest at the optimum temperature (**Table 2**). Mean longest and total root length at the low temperature were 11% ($p < 0.05$) and 33% ($p < 0.05$) less than the optimum temperature, while at high temperature the same traits differed by 2 ($p > 0.05$) and 29% ($p < 0.05$) (**Table 2**). At low and high temperatures, AX17010 recorded a significantly lower total root length, 65 and 54% less than the total compared to the optimum temperature (**Figure 3A**). A reduction in plant root development under low temperatures may be due to its limited ability to access or uptake moisture and nutrient (Miedema, 1982). Suboptimal temperatures had similar damaging effects on root development in rice (Reddy et al., 2021) and cover crops (Munyon et al., 2021).

The root surface area of the 12 genotypes was 32% less at the low (214.4 cm^2) than at the optimum temperature (314.2 cm^2) (**Table 2** and **Figure 3B**). The mean root volume of AX17010 was 57% less at the low temperature (2.1 cm^3) compared to the optimum level (3.1 cm^3), and the response at the high temperature was the same as the optimum (**Figure 3C**). This response suggests a more profound effect of low temperature on this root trait than the high temperature during the early growth stage. AX17009 showed no differences in root surface area, root tips, and root length density across treatments (**Figure 3B**). The mean number of root tips was reduced by 51% under low temperature than at the optimum, but the reduction was not significant between optimum and high temperature (**Table 2** and **Figure 3C**). The average root fork of the 12 carinata genotypes decreased by 50% under low temperatures compared to the optimum temperature (**Table 2**). Mean root crossing among carinata genotypes was similar at low and high temperatures and was 48% less (low temperature) and 39% less (high temperature) compared to the optimum temperature (**Table 2**). The root length density (expressed as a total root length to volume) varied with treatment and genotypes (**Table 2**). In response to low and high temperatures, root length density decreased from 10% under low temperatures to 18% under high temperatures (**Figure 3D**). This study shows that low temperature inhibits most of the root traits' development compared to optimum and high temperatures (**Figure 3**). This indicates that low thermal levels can restrict root growth and developmental processes due to a reduction in activities of enzymes related to membrane lipids of roots and decreased transport of photosynthetic products from shoots to the root system (Kaspar and Bland, 1992; Du and Tachibana, 1994; Arai-Sanoh et al., 2010).

Biomass Production and Partitioning

Low temperature significantly affected the biomass (root and shoot) and root to shoot ratio (**Table 2**). While there was significant variation among genotypes for shoot weight, the high-temperature treatment had non-significant effects on the shoot and root weights (**Table 2**). Shoot weight decreased by 55% under low temperatures compared to the control (**Figure 4A**). Likewise, mean root weight across genotypes was also reduced by 49% (**Figure 4B**), indicating a thinner or shallow root system. Low temperature inhibited root component traits such as root tips, root crossing, root forks, and root surface (**Table 2**). Changes to the root to shoot ratio were significant, with a mean increase of 19% under low temperature compared to optimum temperature (**Figure 4C**). Conversely, root to shoot was substantially lower (6%) under high temperatures than the optimum temperature (**Figure 4C**). At the same time, all genotypes had no difference between high and optimum temperatures for root to shoot ratio. At low temperatures, AX17004 and AX17009 recorded significantly ($p < 0.05$) higher root to shoot ratios compared to the control (**Figure 4C**). The roots developed under low air or soil temperature were found to influence shoot biomass

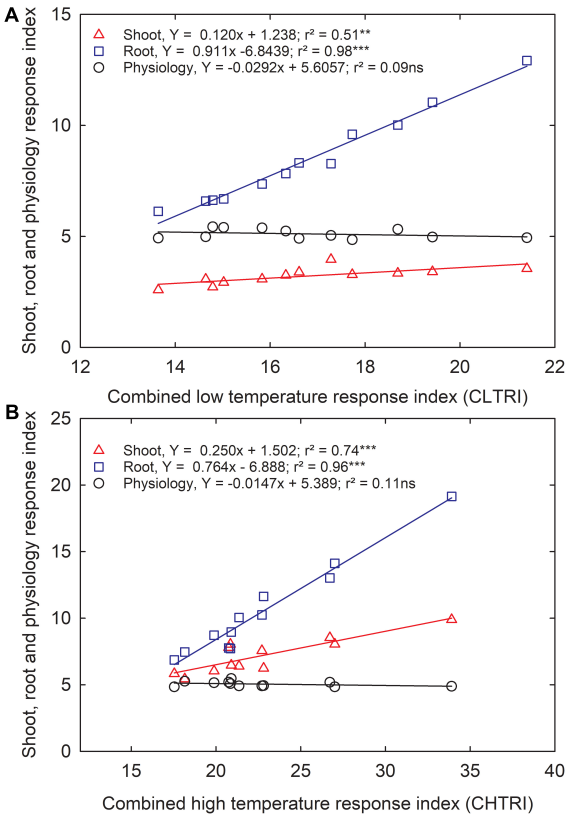

FIGURE 5 | The relationship between shoot, root, and physiological response index and cumulative low-temperature response index (CLTRI, **A**) or cumulative high-temperature response index (CHTRI, **B**) of 12 advanced *Brassica carinata* genotypes was measured 35 days after planting or 24 days after temperature treatments. Significance level: $^{**}p < 0.01$, $^{***}p < 0.001$; ns, non-significant.

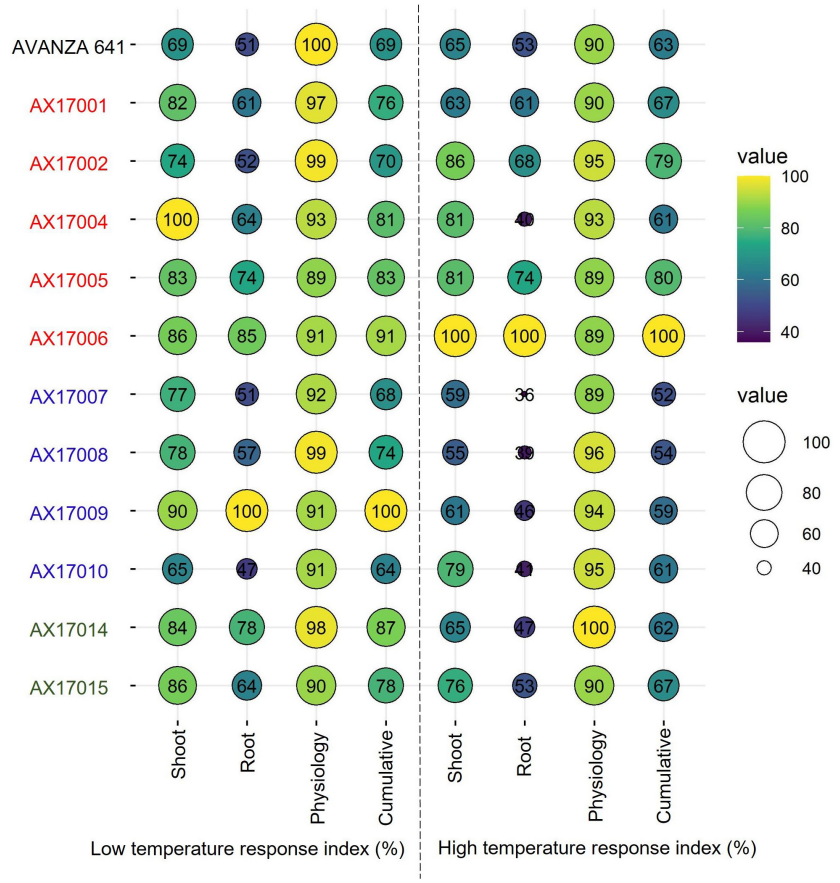

FIGURE 6 | Bubble plot showing cumulative shoot, root, physiological, and cumulative low-temperature response index or high-temperature response index of 12 advanced *Brassica carinata* genotypes measured 35 days after planting or 24 days after temperature treatments. The colors of the genotypes represent four *Brassica carinata* breed types (*black* – cultivar or commercial check, *red* – inbred, *blue* – double haploid, and *green* – hybrid) used in the study.

accumulation and resource allocation (**Figure 4**). These results show a stronger dependence on the physiology or metabolism of the shoot and root traits under stress conditions (Viana et al., 2022). Poor or weaker root growth and development during early crop establishment limit canopy growth and resource use efficiency at later crop stages (Moghimi et al., 2019; Nóia Júnior et al., 2022). In general, greater biomass allocation was recorded toward leaf (68, 63, and 63%) and stem (23, 29, and 29%) then to root (9, 8, and 7%) across (low, optimum, and high temperatures, respectively) treatments. Carinata shoot and root traits were more sensitive to low temperature than high-temperature stress (**Table 1** and **Figure 4**).

Additionally, changes in traits' response to low or high temperatures indicate that each trait or developmental event has its specific optimal temperature, which will decline above or below plant growth processes (Munyon et al., 2021). Our findings indicate that the short duration of high temperatures may not show a more significant impact on shoot traits. However, 24 days of high temperature was enough to induce changes in root formation, such as total root length and root length to density values. On the other hand, this study suggests the importance of future studies of carinata genotypes at different growth stages under gradient temperature conditions. As observed in our research, most growth traits had the most substantial growth and the developmental rate at the optimum temperature treatment. Although this was not tested under field conditions, carinata genotypes (AX17004 and AX17009) with higher tolerance to low temperature or chilling may be suitable for the southeastern United States climate.

Selection of Promising Low Temperature and High-Temperature Stress-Tolerant Carinata Genotypes

Since information about carinata low- and high-temperature tolerance characteristics is unavailable, this study facilitates a better understanding of how the genotypes respond to low and high-temperature treatments at the early growth stage. The CLTRI and CHTRI were calculated to determine the relationship between shoot, root, and physiological components for the 12 advanced carinata genotypes grown under 3 temperature treatments during seedling growth and development. Under the low temperature, a strong relationship was observed between CLTRI and shoot (r^2 = 0.51, $p < 0.01$) and root (r^2 = 0.98, $p < 0.001$) components, indicating the importance of these

two traits when selecting carinata genotypes for cold tolerance during the early vegetative growth stage (**Figure 5A**). A weak relationship (r^2 = 0.07, $p > 0.05$) between physiological characteristics and CLTRI indicates greater sensitivity to low temperatures. Likewise, positive associations were observed between CHTRI and shoot (r^2 = 0.74, $p < 0.001$) and root (r^2 = 0.97, $p < 0.001$) components, which emphasized the dependence on the shoot and root development to improve stress tolerance of carinata genotypes during the early growth stage (**Figure 5B**). Also, a weak relationship was observed between CHTRI and the physiological traits (r^2 = 0.10, $p > 0.05$; **Figure 5B**), indicating the sensitivity of physiological characteristics among the carinata genotypes. A weak linear relationship (r^2 = 0.09, $p > 0.05$) between CLTRI and CHTRI suggests that genotype responses to low and high temperature are the same, indicating the presence of different stress tolerance mechanisms in carinata. Therefore, trait-based selection must be considered to improve low and high-temperature stress tolerance.

Furthermore, individual genotype stress response index of the shoot, root, and physiological parameters or cumulative temperature response index was used to identify potential low- and high-temperature tolerant carinata genotypes (**Figure 6**), similar to other recent studies (Bheemanahalli et al., 2021; Reddy et al., 2021; Ramamoorthy et al., 2022). Among the genotypes studied, genotype AX17009 recorded a superior root system (no change in roots between low and optimum temperatures) coupled with shoot and physiology responses than the sensitive genotype (AX17010) at the early vegetative stage. The CHTRI percentage score varied between 52% (high temperature sensitive) and 100% (high temperature tolerant) among the genotypes (**Figure 6**). The genotype AX17006 was the highest temperature tolerant, while the genotypes such as AX17007 were highly heat-sensitive with CHTRI values less than 52% (**Figure 6**). The carinata genotype (AX17006) showed higher tolerance to low and high-temperature stresses based on the cumulative temperature response index. On the contrary, genotype AX17009 that top performed (high biomass) under low temperature became a weak performer under high temperature (**Figure 6**), indicating differential tolerance or adaptive to low and temperature stress at the early growth stage. When genotypes were grouped breed types (see color legend in **Figure 6**), a double haploid (AX17009) and an inbred (AX17006) had the maximum CLTRI than the commercial check (AVANZA 641). On average (relative scale), inbred genotypes (AX17001, AX17002, AX17005, and AX17006) exhibited substantially greater high-temperature tolerance to four double haploids (AX17007, AX17008, AX17009, and AX17010) at the early growth stage (**Figure 6**). Furthermore, given that this study was conducted under enclosed sunlit environmental conditions that mimic open field settings, these results could be transferred to natural field conditions (Allen et al., 2020), as was suggested in a similar study with cotton (Reddy et al., 1997). The data collected from this study will benefit future screening of carinata for low and high-temperature stress tolerance since it gives a more unambiguous indication of which traits are most relevant and should be considered when selecting for tolerance levels.

CONCLUSION

Under low-temperature treatment, the 12 advanced carinata genotypes evaluated had substantial variability for the shoot, root, and physiological traits. Carinata genotypes are susceptible to low-temperature stress. The low temperature significantly limits various shoot traits, causing a 67, 34, 55, and 55% reduction in plant height, leaf number, leaf area, and total biomass. The suboptimal temperature had a higher impact on root formation traits such as root tips, root forks, and root crossings. Accordingly, total biomass was substantially reduced under low temperature, followed by high temperature compared to plants grown under optimum conditions. The maximum proportion of biomass partitioned to roots under low temperature than at the high-temperature stress, indicating the balance between the source and sink like growth and development. On a relative scale, the breed types used in the study showed differential tolerance to low and high temperatures at the early growth stage. Although we have not tested under field conditions, carinata genotypes (AX17004 and AX17009) with higher root to shoot ratios may be suitable for late-planting windows or regions with low-temperature spells. Further research is required to assess how carinata genotypes respond to low and high temperatures at later growth stages and in open field conditions. The heat- and cold-tolerant genotypes identified in this study would benefit plant breeders in developing genotypes adaptable to different climatic zones.

DATA AVAILABILITY STATEMENT

The original contributions presented in the study are included in the article/**Supplementary Material**, further inquiries can be directed to the corresponding author.

AUTHOR CONTRIBUTIONS

KR contributed to the conception and design of the work. LP and KR collected the data. RB edited the original draft and performed most of the writing, data analysis, and data visualization. LP, RS, KR, and BM review and editing. All authors contributed to the article's critical revision.

FUNDING

This research was funded by the USDA NIFA 201934263 30552 and MIS 043050 and USDA-NIFA Bioenergy-Coordinated Agricultural Projects grant no. 2016-11231.

ACKNOWLEDGMENTS

We thank David Brand for his technical assistance and the graduate students of the Environmental Plant

Physiology Lab at Mississippi State University for their support during data collection. This manuscript is from the Department of Plant and Soil Sciences, Mississippi State University, Mississippi Agricultural and Forestry Experiment Station.

SUPPLEMENTARY MATERIAL

The Supplementary Material for this article can be found online at: https://www.frontiersin.org/articles/10.3389/fpls.2022.900011/full#supplementary-material

REFERENCES

Allen, L. H., Boote, k. J, Jones, J. W., Jones, P. H., Pickering, N. B., Baker, J. T., et al. (2020). Sunlit, controlled-environment chambers are essential for comparing plant responses to various climates. *Agron. J.* 112, 4531–4549. doi: 10.1002/agj2.20428

Alsajri, F. A., Singh, B., Wijewardana, C., Irby, J. T., Gao, W., and Reddy, K. R. (2019). Evaluating soybean cultivars for low- and high-temperature tolerance during the seedling growth stage. *Agronomy* 9:13. doi: 10.3390/agronomy9010013

Alvarado, V., and Bradford, K. J. (2002). A hydrothermal time model explains the cardinal temperatures for seed germination: hydrothermal time model of seed germination. *Plant Cell Environ.* 25, 1061–1069. doi: 10.1046/j.1365-3040.2002.00894.x

Angadi, S. V., Cutforth, H. W., Miller, P. R., McConkey, B. G., Entz, M. H., Brandt, S. A., et al. (2000). Response of three *Brassica* species to high temperature stress during reproductive growth. *Can. J. Plant Sci.* 80, 693–701. doi: 10.4141/P99-152

Arai-Sanoh, Y., Ishimaru, T., Ohsumi, A., and Kondo, M. (2010). Effects of soil temperature on growth and root function in rice. *Plant Prod. Sci.* 13, 235–242. doi: 10.1626/pps.13.235

Ben-Haj-Salah, H., and Tardieu, F. (1995). Temperature affects expansion rate of maize leaves without change in spatial distribution of cell length (Analysis of the coordination between cell division and cell expansion). *Plant Physiol.* 109, 861–870. doi: 10.1104/pp.109.3.861

Bheemanahalli, R., Gajanayake, B., Lokhande, S., Singh, K., Seepaul, R., Collins, P., et al. (2021). Physiological and pollen-based screening of shrub roses for hot and drought environments. *Sci. Hortic.* 282:110062. doi: 10.1016/j.scienta.2021.110062

Brand, D., Wijewardana, C., Gao, W., and Reddy, K. R. (2016). Interactive effects of carbon dioxide, low temperature, and ultraviolet-B radiation on cotton seedling root and shoot morphology and growth. *Front. Earth Sci.* 10:607–620. doi: 10.1007/s11707-016-0605-0

Christ, B., Bartels, W.-L., Broughton, D., Seepaul, R., and Geller, D. (2020). In pursuit of a homegrown biofuel: navigating systems of partnership, stakeholder knowledge, and adoption of *Brassica* carinatain the Southeast United States. *Energy Res. Soc. Sci.* 70:101665. doi: 10.1016/j.erss.2020.101665

Du, Y. C., and Tachibana, S. (1994). Effect of supraoptimal root temperature on the growth, root respiration and sugar content of cucumber plants. *Sci. Hortic.* 58, 289–301. doi: 10.1016/0304-4238(94)90099-X

Elferjani, R., and Soolanayakanahally, R. (2018). Canola responses to drought, heat, and combined stress: shared and specific effects on carbon assimilation, seed yield, and oil composition. *Front. Plant Sci.* 9:1224. doi: 10.3389/fpls.2018.01224

Escobar, J. C., Lora, E. S., Venturini, O. J., Yáñez, E. E., Castillo, E. F., and Almazan, O. (2009). Biofuels: environment, technology and food security. *Rene. Sustain. Energy Rev.* 13, 1275–1287. doi: 10.1016/j.rser.2008.08.014

George, S., Seepaul, R., Geller, D., Dwivedi, P., DiLorenzo, N., Altman, R., et al. (2021). A regional inter- disciplinary partnership focusing on the development of a *carinata*- centered bioeconomy. *GCB Bioenergy* 13, 1018–1029. doi: 10.1111/gcbb.12828

Gesch, R. W., Long, D. S., Palmquist, D., Allen, B. L., Archer, D. W., Brown, J., et al. (2019). Agronomic performance of brassicaceae oilseeds in multiple environments across the western USA. *Bioenergy Res.* 12, 509–523. doi: 10.1007/s12155-019-09998-1

Jia, X., Wu, G., Strock, C., Li, L., Dong, S., Zhang, J., et al. (2022). Root anatomical phenotypes related to growth under low nitrogen availability in maize (*Zea mays* L.) hybrids. *Plant Soil* doi: 10.1007/s11104-022-05331-6

Kakani, V., Prasad, P., Craufurd, P., and Wheeler, T. (2002). Response of *in vitro* pollen germination and pollen tube growth of groundnut (*Arachis hypogaea* L.) genotypes to temperature. *Plant Cell Environ* 25, 1651–1661.

Kakar, N., Jumaa, S. H., Redoña, E. D., Warburton, M. L., and Reddy, K. R. (2019). Evaluating rice for salinity using pot-culture provides a systematic tolerance assessment at the seedling stage. *Rice* 12:57. doi: 10.1186/s12284-019-0317-7

Kaspar, T. C., and Bland, W. L. (1992). Soil temperature and root growth. *Soil Sci.* 154, 290–299. doi: 10.1097/00010694-199210000-00005

Kuk, Y. I., Shin, J. S., Burgos, N. R., Hwang, T. E., Han, O., Cho, B. H., et al. (2003). Antioxidative enzymes offer protection from chilling damage in rice plants. *Crop Sci.* 43, 2109–2117. doi: 10.2135/cropsci2003.2109

Kumar, S., Seepaul, R., Mulvaney, M. J., Colvin, B., George, S., Marois, J. J., et al. (2020). *Brassica carinata* genotypes demonstrate potential as a winter biofuel crop in South East United States. *Ind. Crops Prod.* 150:112353. doi: 10.1016/j.indcrop.2020.112353

Magarey, R. D., Borchert, D. M., and Schlegel, J. W. (2008). Global plant hardiness zones for phytosanitary risk analysis. *Sci. Agric.* 65, 54–59. doi: 10.1590/S0103-90162008000700009

Marillia, E.-F., Francis, T., Falk, K. C., Smith, M., and Taylor, D. C. (2014). Palliser's promise: *Brassica carinata*, An emerging western Canadian crop for delivery of new bio-industrial oil feedstocks. *Biocatal. Agric. Biotechnol.* 3, 65–74. doi: 10.1016/j.bcab.2013.09.012

Miedema, P. (1982). The effects of low temperature on *Zea mays*. *Adv. Agron.* 35, 93–128. doi: 10.1016/S0065-2113(08)60322-3

Moghimi, N., Desai, J. S., Bheemanahalli, R., Impa, S. M., Vennapusa, A. R., Sebela, D., et al. (2019). New candidate loci and marker genes on chromosome 7 for improved chilling tolerance in sorghum. *J. Exp. Bot.* 70, 3357–3371. doi: 10.1093/jxb/erz143

Mulvaney, M. J., Leon, R. G., Seepaul, R., Wright, D. L., and Hoffman, T. L. (2019). *Brassica carinata* seeding rate and row spacing effects on morphology, yield, and oil. *Agron. J.* 111, 528–535. doi: 10.2134/agronj2018.05.0316

Munyon, J. W., Bheemanahalli, R., Walne, C. H., and Reddy, K. R. (2021). Developing functional relationships between temperature and cover crop species vegetative growth and development. *Agron. J.* 113, 1333–1348. doi: 10.1002/agj2.20537

Nóia Júnior, R., de, S., Fraisse, C. W., Bashyal, M., Mulvaney, M. J., Seepaul, R., et al. (2022). *Brassica carinata* as an off-season crop in the southeastern USA: determining optimum sowing dates based on climate risks and potential effects on summer crop yield. *Agric. Syst.* 196:103344. doi: 10.1016/j.agsy.2021.103344

Raju, B. R., Narayanaswamy, B. R., Mohankumar, M. V., Sumanth, K. K., Rajanna, M. P., Mohanraju, B., et al. (2014). Root traits and cellular level tolerance hold the key in maintaining higher spikelet fertility of rice under water limited conditions. *Funct. Plant Biol.* 41:930. doi: 10.1071/FP13291

Ramamoorthy, P., Bheemanahalli, R., Meyers, S. L., Shankle, M. W., and Reddy, K. R. (2022). Drought, low nitrogen stress, and ultraviolet-B radiation effects on growth, development, and physiology of sweetpotato cultivars during early season. *Genes* 13:156. doi: 10.3390/genes13010156

Reddy, K., Hodges, H. F., and McKinion, J. M. (1997). Crop modeling and applications: a cotton example. *Adv. Agron.* 59, 225–290. doi: 10.1016/S0065-2113(08)60056-5

Reddy, K. R., Bheemanahalli, R., Saha, S., Singh, K., Lokhande, S. B., Gajanayake, B., et al. (2020). High-temperature and drought-resilience traits among interspecific chromosome substitution lines for genetic improvement of Upland Cotton. *Plants* 9:1747. doi: 10.3390/plants9121747

Reddy, K. R., Hodges, H., Read, J., Mckinion, J., Baker, J. T., Tarpley, L., et al. (2001). Soil-plant-atmosphere-research (SPAR) facility: a tool for plant research and modeling. *Biotronics* 30, 27–50.

Reddy, K. R., Seghal, A., Jumaa, S., Bheemanahalli, R., Kakar, N., Redoña, E. D., et al. (2021). Morpho-physiological characterization of diverse rice genotypes for seedling stage high- and low-temperature tolerance. *Agronomy* 11:112. doi: 10.3390/agronomy11010112

Seepaul, R., Kumar, S., Iboyi, J. E., Bashyal, M., Stansly, T. L., Bennett, R., et al. (2021). *Brassica carinata*: biology and agronomy as a biofuel crop. *GCB Bioenergy* 13, 582–599. doi: 10.1111/gcbb.12804

Taylor, D. C., Falk, K. C., Palmer, C. D., Hammerlindl, J., Babic, V., Mietkiewska, E., et al. (2010). *Brassica carinata* – a new molecular farming platform for delivering bio-industrial oil feedstocks: case studies of genetic modifications to improve very long-chain fatty acid and oil content in seeds. *Biofuels Bioprod. Biorefin.* 4, 538–561. doi: 10.1002/bbb.231

Viana, V. E., Aranha, B. C., Busanello, C., Maltzahn, L. E., Panozzo, L. E., de Oliveira, A. C., et al. (2022). Metabolic profile of canola (*Brassica napus* L.) seedlings under hydric, osmotic and temperature stresses. *Plant Stress* 3:100059. doi: 10.1016/j.stress.2022.100059

Walne, C. H., and Reddy, K. R. (2021). Developing functional relationships between soil waterlogging and corn shoot and root growth and development. *Plants* 10:2095. doi: 10.3390/plants10102095

Wijewardana, C., Hock, M., Henry, B., and Reddy, K. R. (2015). Screening corn hybrids for cold tolerance using morphological traits for early-season seeding. *Crop Sci.* 55, 851–867. doi: 10.2135/cropsci2014.07.0487

Zhao, D., Reddy, K. R., Kakani, V. G., Read, J. J., and Sullivan, J. H. (2003). Growth and physiological responses of cotton (Gossypium hirsutum L.) to elevated carbon dioxide and ultraviolet-B radiation under controlled-environmental conditions. *Plant Cell Environ.* 26, 771–782. doi: 10.1046/j.1365-3040.2003.01019.x

Zoong Lwe, Z., Sah, S., Persaud, L., Li, J., Gao, W., Reddy, K. R., et al. (2021). Alterations in the leaf lipidome of *Brassica carinata* under high-temperature stress. *BMC Plant Biol.* 21:404. doi: 10.1186/s12870-021-03189-x

Conflict of Interest: The authors declare that the research was conducted in the absence of any commercial or financial relationships that could be construed as a potential conflict of interest.

Publisher's Note: All claims expressed in this article are solely those of the authors and do not necessarily represent those of their affiliated organizations, or those of the publisher, the editors and the reviewers. Any product that may be evaluated in this article, or claim that may be made by its manufacturer, is not guaranteed or endorsed by the publisher.

frontiers | Frontiers in Plant Science

ORIGINAL RESEARCH
published: 28 July 2022
doi: 10.3389/fpls.2022.889370

Untargeted LC–MS/MS-Based Metabolomic Profiling for the Edible and Medicinal Plant *Salvia miltiorrhiza* Under Different Levels of Cadmium Stress

Jun Yuan[1], *Rongpeng Liu*[2], *Shasha Sheng*[2], *Haihui Fu*[3]* *and Xiaoyun Wang*[2]*

[1] School of Nursing, Jiangxi University of Chinese Medicine, Nanchang, China, [2] Research Center for Traditional Chinese Medicine Resources and Ethnic Minority Medicine, Jiangxi University of Chinese Medicine, Nanchang, China, [3] Key Laboratory of Crop Physiology, Ecology and Genetic Breeding, Ministry of Education, Jiangxi Agricultural University, Nanchang, China

OPEN ACCESS

Edited by:
Mainassara Abdou Zaman-Allah, International Maize and Wheat Improvement Center, Mexico

Reviewed by:
Ling Xu, Zhejiang Sci-Tech University, China
Kamel Msaada, Center of Biotechnology of Borj Cedria (CBBC), Tunisia

***Correspondence:**
Xiaoyun Wang
wxy20052002@aliyun.com
Haihui Fu
fhh819@163.com

Specialty section:
This article was submitted to Plant Abiotic Stress, a section of the journal Frontiers in Plant Science

Received: *04 March 2022*
Accepted: *23 June 2022*
Published: *28 July 2022*

Citation:
Yuan J, Liu R, Sheng S, Fu H and Wang X (2022) Untargeted LC–MS/MS-Based Metabolomic Profiling for the Edible and Medicinal Plant Salvia miltiorrhiza Under Different Levels of Cadmium Stress. Front. Plant Sci. 13:889370. doi: 10.3389/fpls.2022.889370

Salvia miltiorrhiza, a medicinal and edible plant, has been extensively applied to treat cardiovascular diseases and chronic hepatitis. Cadmium (Cd) affects the quality of *S. miltiorrhiza,* posing serious threats to human health. To reveal the metabolic mechanisms of *S. miltiorrhiza*'s resistance to Cd stress, metabolite changes in *S. miltiorrhiza* roots treated with 0 (CK), 25 (T1), 50 (T2) and 100 (T3) mg kg^{-1} Cd by liquid chromatography coupled to mass spectrometry (LC–MS/MS) were investigated. A total of 305 metabolites were identified, and most of them were amino acids, organic acids and fatty acids, which contributed to the discrimination of CK from the Cd-treated groups. Among them, *S. miltiorrhiza* mainly upregulated o-tyrosine, chorismate and eudesmic acid in resistance to 25 mg kg^{-1} Cd; DL-tryptophan, L-aspartic acid, L-proline and chorismite in resistance to 50 mg kg^{-1} Cd; and L-proline, L-serine, L-histidine, eudesmic acid, and rosmarinic acid in resistance to 100 mg kg^{-1} Cd. It mainly downregulated unsaturated fatty acids (e.g., oleic acid, linoleic acid) in resistance to 25, 50, and 100 mg kg^{-1} Cd and upregulated saturated fatty acids (especially stearic acid) in resistance to 100 mg kg^{-1} Cd. Biosynthesis of unsaturated fatty acids, isoquinoline alkaloid, betalain, aminoacyl-tRNA, and tyrosine metabolism were the significantly enriched metabolic pathways and the most important pathways involved in the Cd resistance of *S. miltiorrhiza*. These data elucidated the crucial metabolic mechanisms involved in *S. miltiorrhiza* Cd resistance and the crucial metabolites that could be used to improve resistance to Cd stress in medicinal plant breeding.

Keywords: ***Salvia miltiorrhiza*, Cd treatment, LC-MS/MS, discriminating metabolites, metabolic pathways**

INTRODUCTION

Salvia miltiorrhiza Bge., a well-known plant used as a medicinal and food product, belongs to the Salvia species (Labiatae) and has a wide range of ecological adaptations (Wu, 1977). Its roots contain many metabolites (e.g., phenolic acids, tanshinones, flavonoids, lipids, carbohydrates, carboxylic acids and terpenoids), chiefly phenolic acids, carbohydrates and tanshinones (Tong et al., 2022). Phenolic acids and tanshinones, which are water-soluble active substances and fat-soluble active substances, respectively, are two groups of pharmaceutical components (Commission, 2020). They can promote blood circulation to remove blood stasis, cool blood to remove carbuncles, and clear heart heat to relieve restlessness (Su et al., 2015). Due to their pharmacological actions, they have been widely used in the treatment of various diseases, including coronary heart disease, angina pectoris, tachycardia, and chronic hepatitis (Li et al., 2009; Shi et al., 2019). In addition to tablets, dripping pills, capsules, granules, injections, oral liquids, and sprays, they can be prepared as a vinum, tea or medicined diet (Su et al., 2015; Tan, 2017). Currently, many studies have been conducted on *S. miltiorrhiza*, such as exploring and optimizing its cultivation modes, improving the contents of its active components, and uncovering its pharmacological effects (Shi et al., 2019; Fu et al., 2020; Yan et al., 2020; Lv, 2021). These findings lay a theoretical foundation for the study of ensuring *S. miltiorrhiza* safety based on metabonomics.

Cd, along with arsenic (As), lead (Pb), mercury (Hg) and chromium (Cr), is a toxic nonessential metal and it accumulates in organisms with a long half-life of approximately 25-30 years (Kabata and Pendias, 1992; Genchi et al., 2020b). Over the past century, various human activities have resulted in environmental Cd pollution (Rahimzadeh et al., 2017; Genchi et al., 2020a,b). Characterized by strong bioaccumulation, high bioavailability, and strong biotoxicity, Cd can cause the wilting of leaves, the browning of roots, and even the death of plant cells, leading to a decline in plant yield and quality (Sarangthem et al., 2011; Wang et al., 2019; Grajek et al., 2020). Cd accumulates in the human body through the food chain and causes irreversible damage (Valverde et al., 2001; Satarug et al., 2003; Filipič, 2012). Therefore, plant Cd contamination has attracted much attention from researchers.

With the aggravation of heavy metal pollution in soil, heavy metals (e.g., Cd, As, Pb, Hg) have become important pollutants in traditional Chinese medicine (TCM), which would restrain the sustainable development of the TCM industry (Meng et al., 2009; Yan et al., 2012). According to previous studies, Cd stress could inhibit growth, accumulate Cd residue and affect secondary metabolites of *S. miltiorrhiza* roots (Zhang et al., 2013; Wei et al., 2020). However, little has been published on the Cd-resistance mechanisms of *S. miltiorrhiza* based on metabolomics.

In the present study, taking *S. miltiorrhiza* seedlings under different levels of Cd treatment as the research object, metabolites of *S. miltiorrhiza* roots were determined by LC–MS/MS in a pot experiment. The objective of this study was to investigate the main metabolites of *S. miltiorrhiza* in resistance to Cd under different levels of Cd stress and how *S. miltiorrhiza* resists Cd stress based on the metabolome. This study provides deep knowledge of the response to Cd stress in *S. miltiorrhiza* and lays a foundation for further revealing the Cd resistance mechanisms of *S. miltiorrhiza*, which can be used as a reference by plant breeders and forest managers.

MATERIALS AND METHODS

Plant Materials

The *S. miltiorrhiza* seedlings used in the study were purchased from the plantation of *S. miltiorrhiza* in Pingyi County, Shandong Province (35°30' N, 117°35' E). The area has a temperate seasonal climate with an average elevation of 87.9 m. The annual mean precipitation, air temperature, and average relative humidity are 836.0 mm, 14.3 °C and 67.1%, respectively (Lu, 2020; Tian et al., 2021). Healthy seedlings with approximately 4 basal leaves were cultivated from the upper and middle parts of the annual root. They were identified as *S. miltiorrhiza* Bge. By Associate professor Xiaoyun Wang from the Research Center for Traditional Chinese Medicine Resources and Ethnic Minority Medicine of Jiangxi University of Chinese Medicine (JXUCM).

Healthy and disease-free seedlings were selected and planted in Shennong garden of JXUCM. The physical and chemical properties of the topsoil (0–20 cm) in the planting area of *S. miltiorrhiza* in Shennong garden were as follows: total nitrogen 0.30 g kg^{-1}, total phosphorus 0.28 g kg^{-1}, total potassium 27.15 g kg^{-1}, available nitrogen 0.01 g kg^{-1}, available phosphorus 0.01 g kg^{-1}, available potassium 0.08 g kg^{-1}, organic matter 1.97 g kg^{-1}, pH 4.6, and total Cd 0.92 mg kg^{-1}. The total Cd content was lower than the critical value of Cd (1.0 mg kg^{-1}) in soils, which could ensure the normal growth of plants.

The indicated amounts of cadmium chloride hemi (pentahydrate) ($CdCl_2 \cdot 2.5H_2O$) were mixed well with sieved topsoils from Shennong garden. Based on the study of Zhang et al. (2013) and Wei et al. (2020), four Cd treatment levels were set in the present study as follows: 0 (CK), 25 mg kg^{-1} (T1), 50 mg kg^{-1} (T2), and 100 mg kg^{-1} (T3). Subsequently, 2 kg of the soils were placed a flower pot (16 × 17 cm) and incubated for 30 d. Then, the *S. miltiorrhiza* seedlings, which had grown in Shennong garden for 30 d, were transplanted into the pots, and each pot included one seedling. There were three repetitions at each level and three seedlings in each repetition. After 15 d of treatment, root samples were collected, washed with ultrapure water, quickly frozen with liquid nitrogen, and transferred to −80°C until further metabolomic analysis. Voucher specimens (No. DS-001) were deposited in a public herbarium in the Research Center for Traditional Chinese Medicine Resources and Ethnic Minority Medicine of JXUCM.

Metabolite Extraction

A 25 mg fresh sample in a 500 μL mixture of methanol and water (3:1, v/v) (including an isotope-labeled internal standard mixture) was ground at 35 Hz for 4 min and lysed in an ultrasonic water bath for 5 min. After sitting at −40°C for 1 h, the samples were centrifuged at 12000 rpm for 15 min at 4°C. The supernatant was stored at −80°C until liquid chromatography-tandem mass spectrometry (LC–MS/MS) analysis. Quality

control (QC) samples were prepared with a mix of the supernatants from all samples.

LC–MS/MS Analysis

Ultrahigh-performance liquid chromatography and quadrupole orbital well hybrid TM mass spectrometry coupled with an Acquity UPLC HSS T3 liquid chromatographic column were conducted to separate the target compounds.

The chromatographic conditions were as follows: an Acquity UPLC HSS T3 liquid chromatographic column (2.1 mm × 100 mm, 1.8 μm) was used; the column temperature was 35°C; mobile phase A and phase B were the aqueous phase (containing 5 mmol L^{-1} ammonium acetate and 5 mmol L^{-1} acetic acid) and acetonitrile, respectively; gradient elution was carried out (0–0.7 min, 1% B; 0.7–9.5 min, 1–99% B; 9.5–11.8 min, 99% B; 11.8–12.0 min, 99–1% B; 12–14.8 min, 1% B); the flow rate was 0.5 mL min^{-1} and the injection volume was 3 μL.

A Thermo Q Exactive HFX mass spectrometer was used to collect the primary and secondary mass spectrometry data of the samples under the control of Xcalibur 4.0.27 (Thermo Scientific). The detailed parameters are presented in **Supplementary Table S1**.

Metabolite Data Acquisition

The raw data were converted into mzXML format with the software ProteoWizard (https://proteowizard.sourceforge.io/), and the recognition, extraction, alignment and integration of the peaks was conducted with the R package (XCMS as the core). Then, the MS2 database was applied for metabolite annotation. The cutoff for annotation was set at 0.3. Data with no definite substance name and no spectral ratio or substances with a missing quantity greater than 50% in the comparison group samples were filtered and removed. For substances with a missing quantity less than 50%, the K-nearest neighbor (KNN) algorithm was used to simulate the missing value. Finally, the total ion current (TIC) or internal standard (IS) of each sample was used to normalize the data, and 305 metabolites were identified for further analysis.

Data Analysis

Unsupervised principal component analysis (PCA) was performed to analyze the distribution of root samples in CK, T1, T2 and T3. Supervised orthogonal partial least squares-discriminant analysis (OPLS-DA) was used to distinguish the metabolic profiles of the roots between the CK and each Cd-added group (T1, T2 and T3). To test the OPLS-DA model, a cross-validation residual variance test (CV-ANOVA test) and 200 permutation tests were carried out. The model with $p < 0.05$ in the CV-ANOVA test or $R2 > 0.7$ and $Q2 > 0.4$ in the permutation test was reliable (Yuan et al., 2020). The variable importance in projection (VIP) was vital for explaining the data of the OPLS-DA model. The discriminating metabolites were defined based on a VIP value above 1 and a p value below 0.05 (Yuan et al., 2020). Metabolic pathway analysis of these discriminating metabolites was conducted. Meanwhile, one-way ANOVA was performed to calculate the variability in the relative contents of the metabolites.

Multivariate statistical analysis (PCA and OPLS-DA) and validation of the OPLS-DA model were carried out with SIMCA-P 14.1 (Umetrics, Sweden). Univariate statistical analysis and one-way ANOVA were conducted with IBM SPSS Statistics 20.0 (SPSS, Inc., IBM Corp, New York, USA). The metabolic pathway analysis was carried out with the online software MetaboAnalyst 4.0 (http://www. Metaboanalyst.ca/faces/ModuleView.xhtml). The heatmap was drawn by online software (https://matrix2png.msl.ubc.ca/bin/matrix2png.cgi). The Venn diagrams were drawn by Venny 2.1 (https://bioinfogp.cnb.csic.es/tools/venny/index.html).

RESULTS

Metabolites Responding to Different Levels of Cd Stress

By observing the differences in the peak height of the internal standard between the QC samples and the peak conditions of the internal standard in the blank samples, this study determined whether the instrument was stable and whether there were residues in the detection process. **Supplementary Figure S1** shows that both the retention time and the response strength of the internal standard in the QC samples were stable, and the data acquisition stability of the instrument was excellent. **Supplementary Figure S2** shows that no obvious peaks other than the internal standards were detected in the blank samples.

The metabolite profiles of the roots were investigated using an untargeted global metabolomic platform with LC–MS/MS. A total of 305 metabolites were annotated and quantified in *S. miltiorrhiza* roots with different levels of Cd treatment (**Supplementary Table S2**), which could be categorized into seven major groups based on their molecular structure: amino acids, organic acids, fatty acids, ketones, sugars, amides, and others (**Figure 1C**; **Supplementary Table S3**).

There were 136 upregulated metabolites and 169 downregulated metabolites in T1 and 141 upregulated metabolites and 164 downregulated metabolites in both T2 and T3 (**Figures 1A,B**). Proportions of the metabolites in the roots changed in response to Cd addition (**Figure 1C**; **Supplementary Table S3**). Compared to CK, the total content of amino acids increased by 0.2-fold in T1, approximately 0.9-fold in T2 and T3 ($p < 0.05$), and the total content of fatty acids decreased by 87% in T1, 59% in T2 and 75% in T3 ($p < 0.05$). There were no significant differences in the total content of organic acids between CK and each Cd-added group (**Figure 1**; **Supplementary Table S3**).

Discriminating Metabolites in Roots Between CK and Each Cd-Added Group

According to the results of the PCA, root samples from CK could be separated from the Cd-treated groups (**Figure 2**). Based on the reliable OPLS-DA model with a p value below 0.05 (**Figure 3**; **Supplementary Figure S3A**), *S. miltiorrhiza* roots in T1 and CK could be distinguished by metabolites with major contributions from amino acids, organic acids, and fatty acids (**Figure 4**): 174 discriminating metabolites were selected, 56 of which were

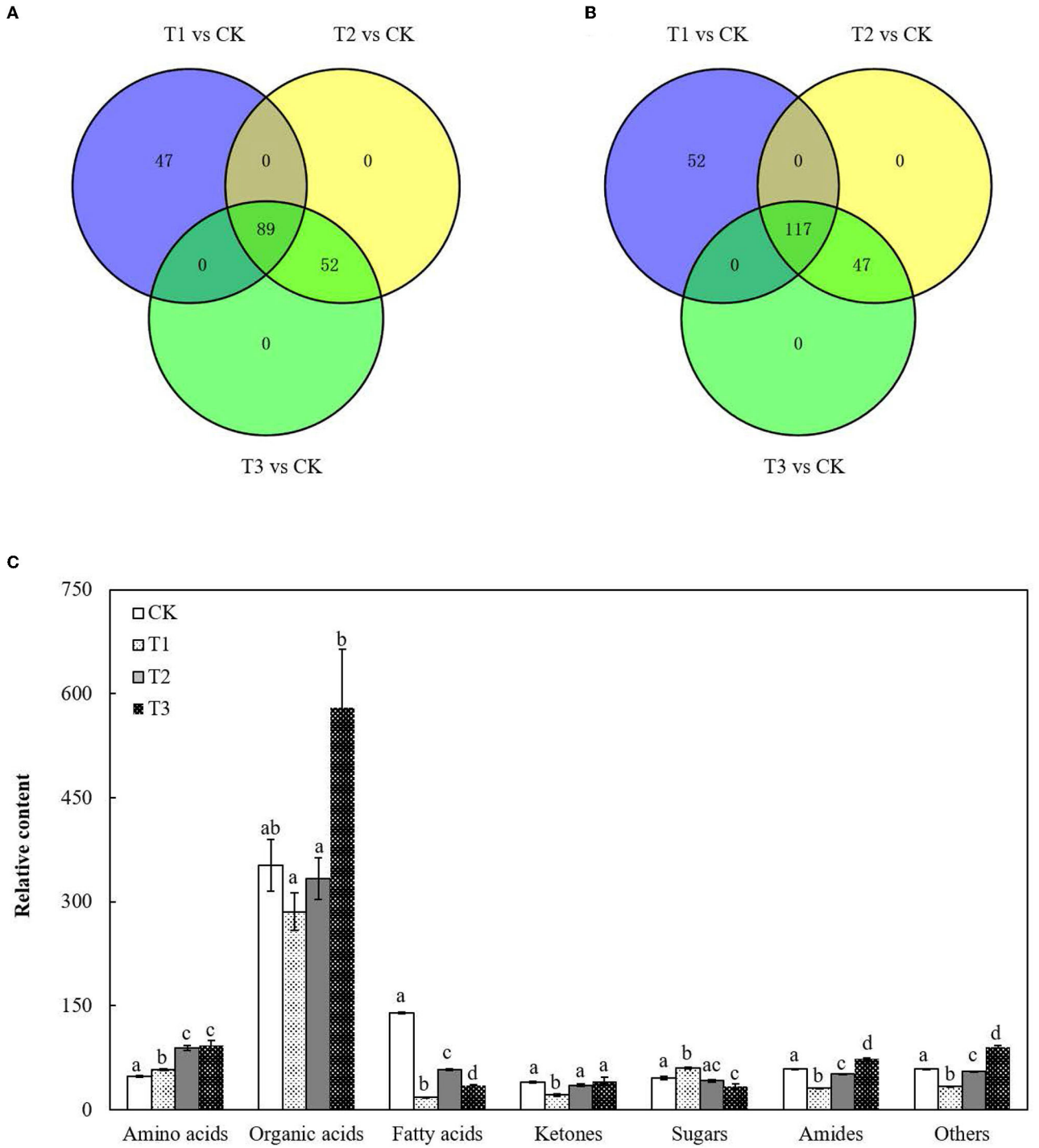

FIGURE 1 | Variation in the total metabolites in *S. miltiorrhiza* roots under different levels of Cd stress. **(A,B)** represent changes in the total number of upregulated and downregulated metabolites in *S. miltiorrhiza* roots with different levels of Cd treatment, respectively; different colors in **(A,B)** represent different sources of upregulated metabolites and downregulated metabolites, respectively; **(C)**, Total relative amino acid, organic acid, fatty acid, ketones, sugar, amide and others content in *S. miltiorrhiza* roots; Different lowercase letters on the columns of the same metabolite indicate significant differences within each treatment in the roots ($p < 0.05$); vertical bars above the columns indicate the standard error of each mean (mean ± SE).

upregulated and 118 of which were downregulated. Among them, most fatty acids (especially α-linolenic acid, linoleic acid (C18:2), and oleic acid (C18:1)) and organic acids were downregulated, with chorismate and o-tyrosine contributing the most to the

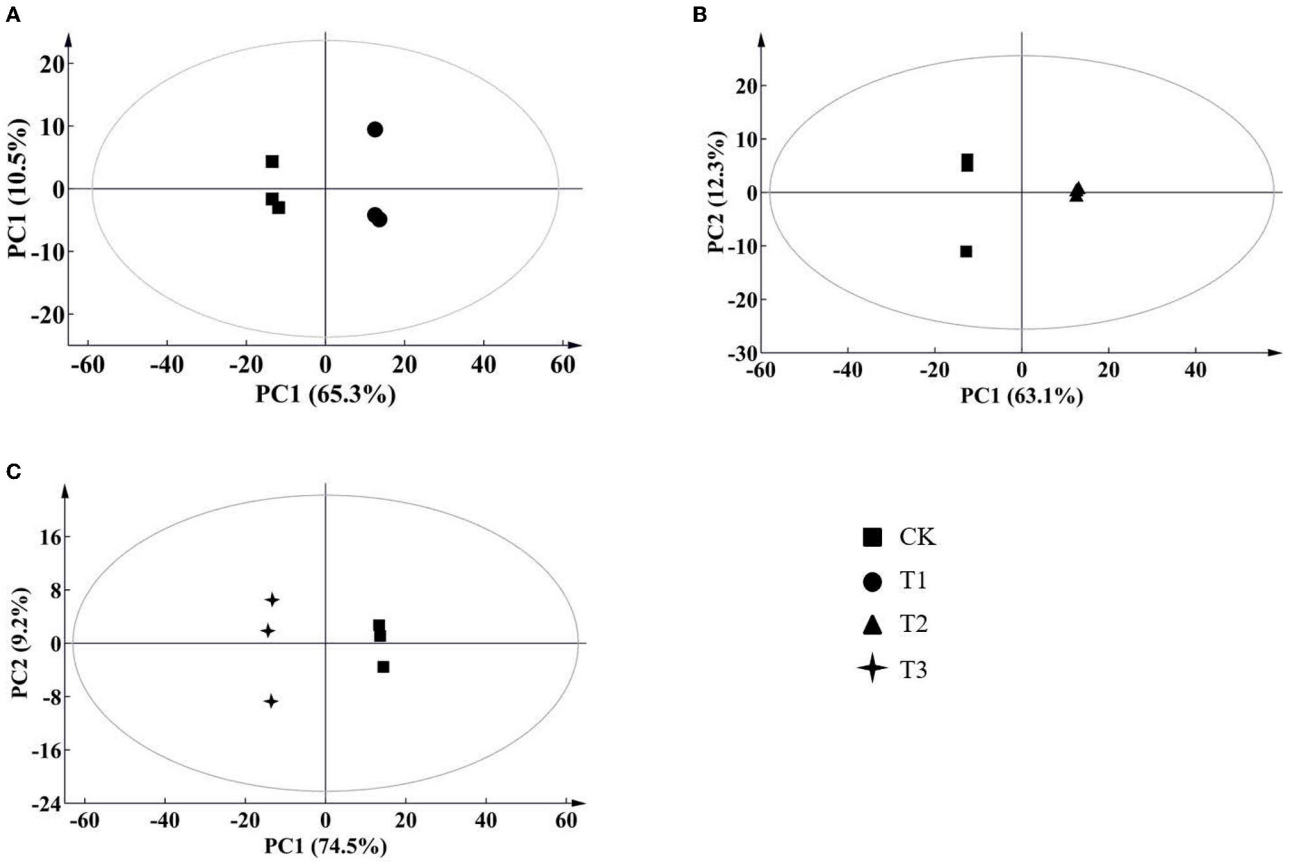

FIGURE 2 | Score plots of principal component analysis (PCA) for metabolomic data from *S. miltiorrhiza* roots under different levels of Cd stress. PC1, the first principal component; PC2, the second principal component. The ellipse indicates Hotelling's T2 (95%); **(A–C)** stand for score plots PCA of metabolite data obtained from LC–MS/MS in *S. miltiorrhiza* roots of T1 (25 mg/kg Cd group) and CK (control group), of T2 (50 mg/kg Cd group) and CK, and of T3 (100 mg/kg Cd group) and CK, respectively.

upregulation of organic acids and amino acids in *S. miltiorrhiza* roots, respectively.

Similarly, based on the significant OPLS-DA model (**Supplementary Figures S3B,C**), the root samples could be significantly distinguished by metabolites with the major contributions from 161 metabolites (81 of them were upregulated and 80 were downregulated) in T2 and CK and from 191 metabolites (120 of them were upregulated and 71 were downregulated) in T3 and CK. Major contributors to the differences were amino acids, organic acids, and fatty acids (**Figure 4**): compared to CK, in T2, all of these amino acids (especially DL-tryptophan, L-aspartic acid, and L-proline) were upregulated, and most fatty acids (e.g., linoleic acid, oleic acid) were downregulated, with chorismate contributing the most to the upregulation of the organic acids (**Figure 4**); in T3, most of the amino acids (especially L-proline, L-serine and L-histidine), organic acids (especially eudesmic acid and rosmarinic acid) and all of the saturated fatty acids (e.g., stearic acid (C18:0)) were upregulated, and oleic acid was downregulated (**Figure 4**).

Metabolic Pathways Involving All Discriminating Metabolites

The discriminating metabolites were annotated into the Kyoto Encyclopedia of Genes and Genomes (KEGG) database, and 65 metabolic pathways were obtained (**Figure 5A**; **Supplementary Table S4**). Among them, biosynthesis of unsaturated fatty acids, isoquinoline alkaloid biosynthesis, betalain biosynthesis, aminoacyl-tRNA biosynthesis, and tyrosine metabolism were the significantly enriched metabolic pathways ($p < 0.05$) (**Figure 5B**; **Supplementary Table S4**). In addition, a metabolic map of the resistance process was developed based on these results (**Figure 6**).

DISCUSSION

To the best of our knowledge, this study is the first to illustrate how the medicinal and food plant *S. miltiorrhiza* resists abiotic stress in terms of the metabolome. The discussions focused on changes in the metabolic profiles of roots and the identification

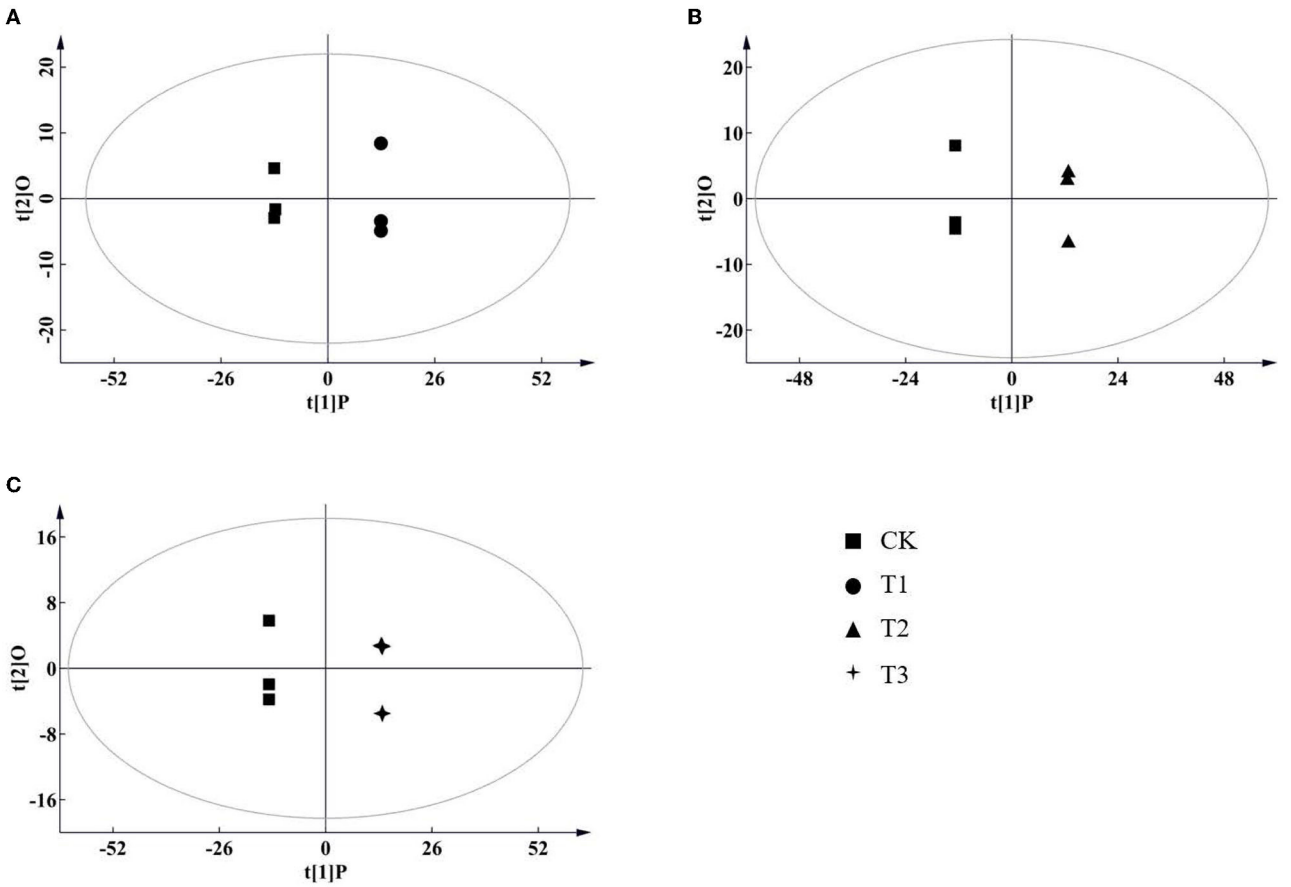

FIGURE 3 | Score plots of orthogonal projections to latent structures discriminant analysis (OPLS-DA) of metabolite data in *S. miltiorrhiza* roots. **(A–C)** stand for score plots OPLS-DA of metabolite data obtained from LC–MS/MS in *S. miltiorrhiza* roots of T1 (25 mg/kg Cd group) and CK (control group), of T2 (50 mg/kg Cd group) and CK, and of T3 (100 mg/kg Cd group) and CK, respectively.

of metabolites that played key roles in metabolic regulation under different levels of Cd stress.

Global Responses of the Metabolome Under Cd Stress

Our results clearly revealed that amino acids, organic acids and fatty acids in *S. miltiorrhiza* roots played essential roles in resisting Cd stress. As the basic components of proteins, amino acids can participate in the regulation of ion transport and nitrogen metabolism and play vital roles in resisting abiotic stress in plants (Sharma and Dietz, 2006; Xu et al., 2012; Tian, 2021). Organic acids are a class of compounds containing carboxyl groups (excluding amino acids), most of which can combine with metal ions or alkaloids (Kuang, 2017). Fatty acids and their derivatives are essential energy stores and the main components of membrane lipids (Chaffai et al., 2009; Liu et al., 2014; Li-Beisson et al., 2016). Due to the important roles of these three classes of metabolites in plant survival and stress resistance (Liu et al., 2014; Panchal et al., 2021; Trovato et al., 2021), in this study, the changes in the proportions of amino acids, organic acids, and fatty acids were larger than those of the other metabolites in *S. miltiorrhiza* roots under Cd treatment (**Figure 1**).

In comparison with CK, in T1, T2 and T3, the total relative contents of the amino acids significantly increased ($p < 0.05$), the total relative contents of the fatty acids significantly decreased ($p < 0.05$), and the total relative contents of the organic acids presented no significant differences (**Figure 1**; **Supplementary Table S3**). In disagreement with these results, in *Oryza sativa* L. roots, Cd at a low content could promote the production of amino acids and organic acids, and Cd at a high content could inhibit the production of amino acids and organic acids (Tang et al., 2016), while in agreement with our results, there was a significant decline in the production of fatty acids in *Sedum plumbizincicola* L. roots under Cd stress (Sun et al., 2020). This might result from the fact that the plant metabolic response to abiotic stress is affected by the stress modes, stress intensity, and plant species (Hu and Xu, 2014; Zhang and Chen, 2021).

Amino Acids Play Vital Roles in Resisting Cd Stress

As reported above, amino acids were the main contributors to the differences in *S. miltiorrhiza* roots under different levels of Cd stress (**Figure 4**). Well known as an abiotic and biotic stress indicator, proline can function as a hydroxyl radical

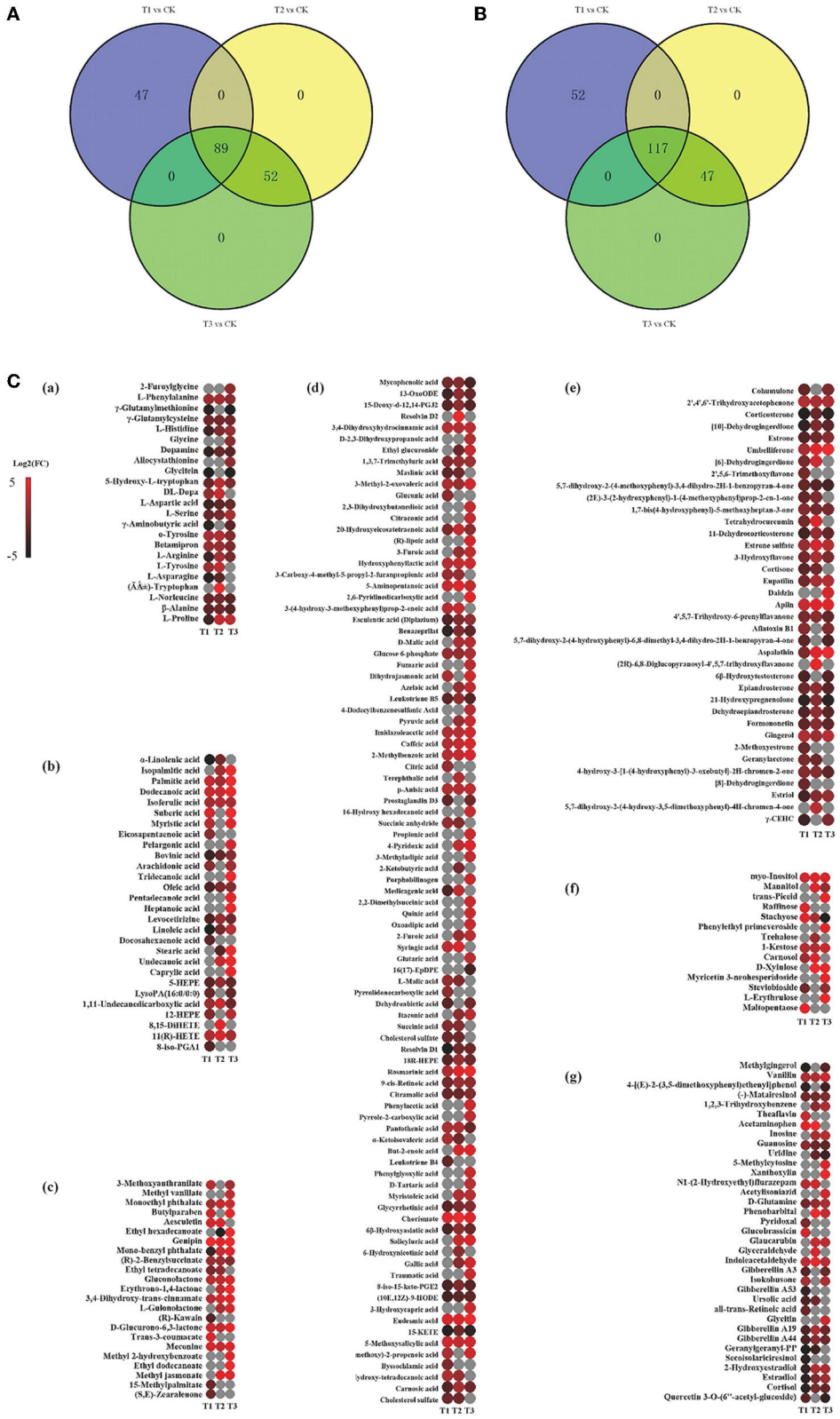

FIGURE 4 | Variation in the discriminating metabolites in *S. miltiorrhiza* roots under different levels of Cd stress. **(A,B)** stand for overlap of the upregulated and downregulated discriminating metabolites of *S. miltiorrhiza* roots in response to different Cd treatments, respectively; different colors in **(A,B)** represent different sources of upregulated discriminating metabolites, and downregulated discriminating metabolites, respectively; **(C)**, Heatmap analysis of amino acids ((Li et al.), fatty

(Continued)

FIGURE 4 | acids (b), esters (c), organic acids (d), ketones (e), sugars (f) and others (g) of the discriminating metabolites in *S. miltiorrhiza* roots between the control and Cd stressed groups; T1, T2 and T3 stand for discriminating metabolites in roots between the control and 25 mg kg^{-1} Cd group (T1), 50 mg kg^{-1} group (T2), and 100 mg kg^{-1} Cd group (T3), respectively; Log2(FC), an estimate of the log2-transformed ratio of the relative content of metabolites in *S. miltiorrhiza* roots of the Cd treated group to that of the control group. The colors indicate the log2 transform of the ratios for the relative content of metabolites between the control and Cd treated groups in *S. miltiorrhiza* roots, ranging from black (low level) to red (high level). The gray ellipses stand for not discriminating metabolites.

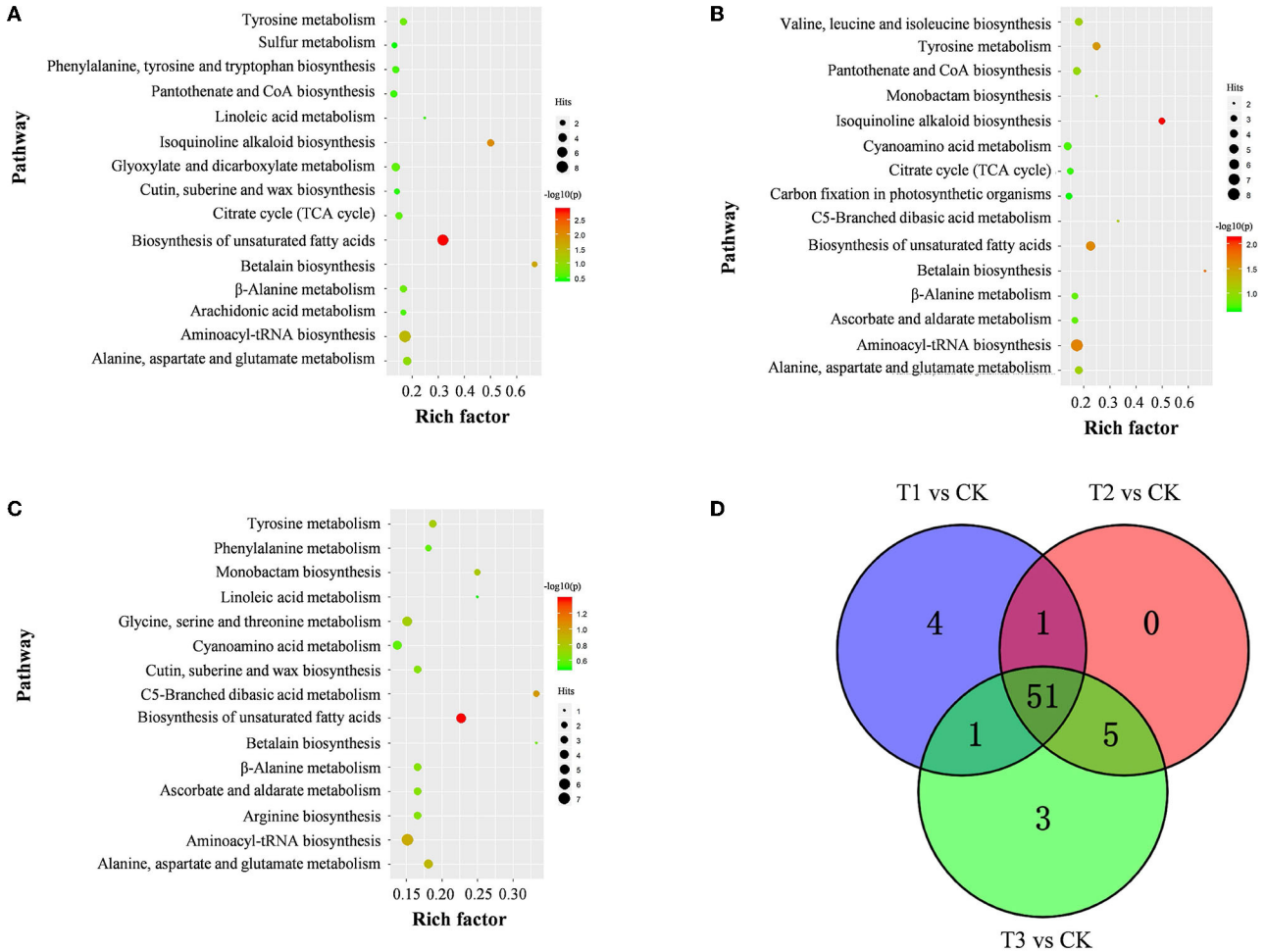

FIGURE 5 | Pathway of discriminating metabolites in *S. miltiorrhiza* roots between the control and Cd-stressed groups. **(A–C)** represent pathways of discriminating metabolites between CK and T1 **(A)**, T2 **(B)**, and T3 **(C)**, respectively; the size and color of the bubble represent the number hits and -log10(p) values for each pathway from pathway analysis; **(D)**, overlap of metabolic pathways discriminating metabolites of *S. miltiorrhiza* roots based on KEGG in response to different levels of Cd stress; different colors represent different sources of metabolic pathways for discriminating metabolites.

scavenger and it plays a vital role in the adjustment to osmotic stresses in plants (Sharma and Dietz, 2006; Zemanov et al., 2017). Tyrosine is the precursor of many metabolites (including tocopherol, plastoquinone and ubiquinone) that are essential to the survival and stress resistance of plants (Kilgore and Kutchan, 2016; Cassels and Sáez-Briones, 2018; Xu et al., 2020). Tryptophan, an aromatic amino acid, plays important roles in the regulation of plant development and it acts as a precursor for the biosynthesis of the hormone auxin (Sanjaya et al., 2008; Liu et al., 2011a). Histidine plays important roles in the regulation of the biosynthesis of other amino acids and in the chelation and transport of metal ions (Stepansky and Leustek, 2006). Aspartic acid can be fed into the synthesis of other amino acids (e.g., lysine, methionine and threonine) (Angelovici et al., 2009). Serine is essential for the synthesis of proteins and other biomolecules, including nucleotides and serine-derived lipids (e.g., phosphatidylserine and sphingolipids), and is involved in the resistance to various stresses (Ho and Saito, 2001; Waditee et al., 2007; Ros et al., 2013). Due to the different roles of these amino acids in the stress resistance of plants, with different levels

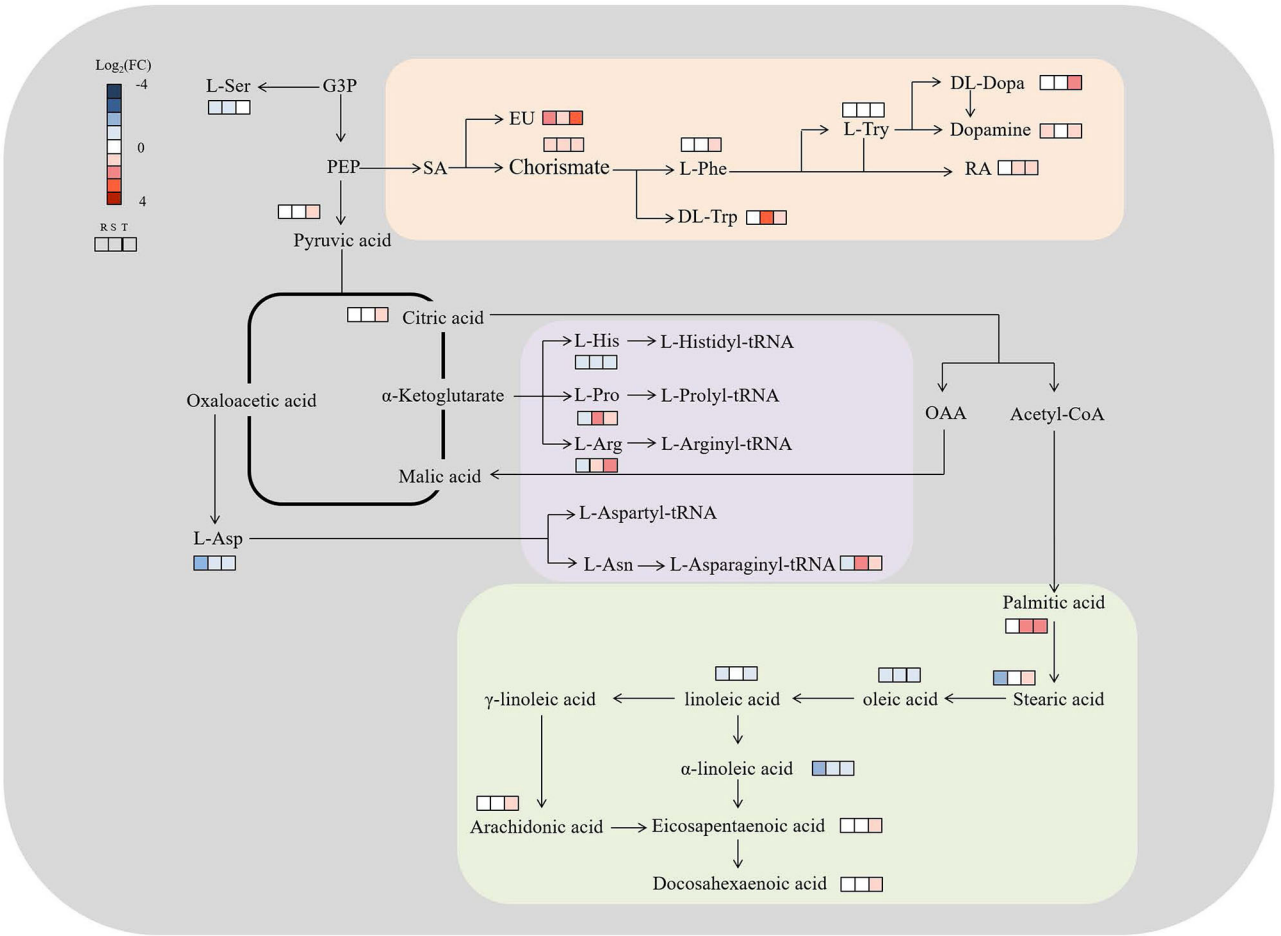

FIGURE 6 | Metabolic map of *S. miltiorrhiza* roots based on LC–MS/MS with different levels of Cd stress. Metabolisms in orange were involved in isoquinoline alkaloid biosynthesis, betalain biosynthesis, and tyrosine metabolism, and purple and green were involved in aminoacyl-tRNA biosynthesis and unsaturated fatty acids biosynthesis, respectively; G3P, PEP, L-Ser, SA, EU, L-Phe, L-Try, RA, L-Asp, L-His, L-Pro, L-Arg and L-Asn represent glucose-3-phosphate, phosphoenolpyruvic acid, L-serine, shikimic acid, eudesmic acid, L-phenylalanine, L-tyrosine, rosmarinic acid, L-aspartic acid, L-histidine, L-proline, L-arginine, and L-asparagine, respectively; Log2(FC), an estimate of the log2-transformed ratio of the relative content of metabolites in *S. miltiorrhiza* roots of the Cd treated group to that of the control group.

of Cd treatment, the levels of amino acids playing vital roles in resisting Cd stress were different (Benral and McGrath, 1994; Wang et al., 2015; Cosio and Renault, 2020) (**Figures 5**, **6**).

In the present study, o-tyrosine contributed more to the upregulation of the discriminating amino acids between T1 and CK; DL-tryptophan, L-aspartic acid, and L-proline contributed more to the upregulation of the discriminating amino acids between T2 and CK, and L-proline, L-serine and L-histidine contributed more to the upregulation of the discriminating amino acids between T3 and CK (**Figure 4**; **Supplementary Table S2**). This illustrated that there were different Cd stress resistance patterns of amino acids in *S. miltiorrhiza* roots under different levels of Cd stress. Under moderate Cd (T2) stress, *S. miltiorrhiza* roots might mainly increase the relative contents of DL-tryptophan, L-aspartic acid, and L-proline to resist Cd, but under high-level Cd (T3) stress, the roots might mainly increase the relative contents of L-proline, L-serine and L-histidine to resist Cd. Inconsistent with this, compared to CK, the proline content declined significantly and the aspartic acid content increased significantly with moderate Cd treatment; and the histidine content increased significantly and the serine content declined significantly with high Cd treatment ($p < 0.05$) of *Crassocephalum crepidioides* (Zhu et al., 2018). As the level of Cd increased, the contents of tryptophan and proline increased significantly, and the L-aspartic acid content declined significantly in *Solanum nigrum* (Xu et al., 2012). These differences might be caused by the differences in the Cd sensitivity of different plants or by the different methods of applying Cd stress (Zhang and Chen, 2021).

Organic Acids Play Vital Roles in Resisting Cd Stress

Our study revealed that based on the changes in the relative contents of organic acids in *S. miltiorrhiza* roots with different

levels of Cd treatment, chorismate and eudesmic acid in T1, chorismate in T2, and eudesmic acid and rosmarinic acid in T3 were upregulated. In the present study, organic acids were among the main contributors in distinguishing CK samples from Cd treated samples (T1, T2 and T3) (**Figure 4**; **Supplementary Table S2**): most organic acids showed a decreasing accumulation, with chorismate and eudesmic acid contributing the most to the upregulation of organic acids in T1; most organic acids showed an increasing accumulation, with chorismate contributing most to the upregulation of organic acids in T2; and most organic acids presented an increasing accumulation (especially eudesmic acid and rosmarinic acid) in T3.

Chorismate could function as a key branching point between primary and secondary metabolisms, as well as being a precursor of aromatic amino acids (e.g., tryptophan, phenylalanine, tyrosine) and hormonal substances (e.g., indoleacetic acid and salicylic acid) that play essential roles in plant metabolism (Kristin and Michael, 2010). Eudesmic acid and rosmarinic acid are polyphenol derivatives and phenol compounds, respectively, and both have strong antioxidation activity and strong hydroxyl radical scavenging activity (Lv et al., 2005; Wang et al., 2014; Korkmaz et al., 2018). Under Cd stress, the elevation of intracellular chorismite would result in some pathways, including the biosynthesis of aromatic amino acids (e.g., phenylalanine and tryptophan) and secondary metabolites (e.g., polyphenols and flavonoids) (**Figure 6**; **Supplementary Table S2**) (Malik, 1979), and the activity of the enzymes involved in phenolic compound metabolism might increase (Michalak, 2006). This might lead to an increase in phenolic compounds and polyphenol derivatives, which could bind heavy metals, enhance the activity of antioxidant enzymes, and reduce the harmful effects of heavy metals on plants (Güez et al., 2017; Manquián-Cerdaa et al., 2018) (**Figure 6**). Therefore, in response to low-level (T1) and high-level (T3) Cd treatment, *S. miltiorrhiza* roots upregulate their secondary metabolism, mainly by upregulating eudesmic acid and rosmarinic acid to resist Cd stress (**Figure 6**) (Zoufan et al., 2020).

Fatty Acids Play Vital Roles in Resisting Cd Stress

Our study proved that fatty acids played vital roles in resisting Cd stress. Compared to CK, most discriminating fatty acids (e.g., oleic acid and linoleic acid) decreased significantly both in T1 and T2, and unsaturated fatty acids (e.g., oleic acid and linoleic acid) decreased significantly, with all of the discriminating saturated fatty acids (e.g., stearic acid) being upregulated (**Figure 5**; **Supplementary Table S2**) in T3. As discussed above, in plants, fatty acids and their derivatives play vital roles in improving stress tolerance by participating in various defense pathways, including basal, systemic, and effector-triggered immunity (Chaffai et al., 2009; Liu et al., 2014; Li-Beisson et al., 2016). Unsaturated fatty acids (e.g., oleic acid and linoleic acid) are produced by the catalysis of fatty acid desaturases (FADs), which can catalyze the formation of double bonds at specific positions in the chain of saturated fatty acids (e.g., stearic acid) to regulate the response to various stresses (Liu et al., 2011b; Park et al., 2015). It is important to regulate the lipid composition and adjust the unsaturation level of membrane fatty acids to cope with metal stress (Thompson, 1992) (**Figures 4**, **6**; **Supplementary Table S2**).

Therefore, oleic acid and linoleic acid, which could induce the production of plant reactive oxygen species, showed a decreased accumulation in T1, T2 and T3 to maintain the normal growth of *S. miltiorrhiza* under Cd stress (Cury-Boaventura and Curi, 2005) (**Figure 5**), and high-level Cd stress might inhibit the expression of FADs, leading to the enrichment of saturated fatty acids (especially stearic acid) (**Figure 5**) (Liu et al., 2013). In contrast to our study, other researchers found that Cd stress increased the contents of oleic acid, linoleic acid, and stearic acid in *Asterioneilu glacialis* (Jones et al., 1987) and decreased the linoleic acid content in *Sedum plumbizincicola* (Sun et al., 2020) and the oleic acid content in *Sedum alfredii* (Luo et al., 2014). As mentioned above, these differences might be caused by the differences in the Cd sensitivities of different plants (Zhang and Chen, 2021).

CONCLUSION

Metabolic regulation is one of the vital mechanisms by which plants respond to various stresses. In this study, we characterized the roles of metabolic regulation in *S. miltiorrhiza* roots under different levels of Cd stress in a pot experiment. First, amino acids, organic acids, and fatty acids played essential roles in resisting Cd stress in *S. miltiorrhiza* roots due to their larger proportions than the other metabolites and their major contributions in distinguishing roots between the CK and each Cd treatment group (T1, T2, and T3). Moreover, biosynthesis of unsaturated fatty acids, isoquinoline alkaloid biosynthesis, betalain biosynthesis, aminoacyl-tRNA biosynthesis, and tyrosine metabolism played vital roles in Cd resistance due to their involvement in the synthesis of these metabolites. Second, amino acids, organic acids, and fatty acids, which play vital roles in resisting Cd stress, were different in *S. miltiorrhiza* roots under different levels of Cd stress. Because of the important roles of these metabolites in stress resistance, *S. miltiorrhiza* roots might mainly upregulate o-tyrosine, chorismite and eudesmic acid under low Cd (25 mg kg^{-1}) stress; DL-tryptophan, L-aspartic acid, L-proline and chorismite under moderate Cd (50 mg kg^{-1}) stress; and L-proline, L-serine, L-histidine, eudesmic acid, and rosmarinic acid under high Cd (100 mg kg^{-1}) stress. *S. miltiorrhiza* mainly downregulated unsaturated fatty acids (e.g., oleic acid and linoleic acid) under all levels of Cd stress and upregulated saturated fatty acids (especially stearic acid) under high Cd stress.

DATA AVAILABILITY STATEMENT

The original contributions presented in the study are included in the article/**Supplementary Material**, further inquiries can be directed to the corresponding author/s.

AUTHOR CONTRIBUTIONS

JY, HF, and XW: conceptualization, writing-original draft preparation, writing-review and editing, and supervision. JY and HF: validation. RL and SS: investigation and project administration. JY, RL, and SS: resources. JY and XW: funding acquisition. All authors contributed to the article and approved the submitted version.

FUNDING

This work was supported by the Scientific Research Foundation for Doctor of the Jiangxi University of Chinese Medicine (2020BSZR011); and the National Key R&D Program of China (2019YFC1712302).

ACKNOWLEDGMENTS

In addition, we thank Assoc Prof. Yuye Zhu (School of Pharmacy of Jiangxi University of Traditional Chinese Medicine) and Nanjing Genepioneer Biotechnologies Co. Ltd.

SUPPLEMENTARY MATERIAL

The Supplementary Material for this article can be found online at: https://www.frontiersin.org/articles/10.3389/fpls.2022.889370/full#supplementary-material

Supplementary Figure S1 | Total ion chromatograms (TICs) with positive **(A)** and negative **(B)** ion modes of CK and (quality control) QC samples.

Supplementary Figure S2 | Total ion chromatograms (TICs) with positive **(A)** and negative **(B)** ion modes of (quality control) QC samples.

Supplementary Figure S3 | Permutation test results of OPLS-DA models for metabolomic data from *S. miltiorrhiza* roots with different levels of Cd stress. **(A–C)** represent the permutation test results of OPLS-DA models for *S. miltiorrhiza* roots of the control and 25 mg kg^{-1} Cd stress groups (R2Y [1] = 0.74, Q2 [1] = 0.99, CV-ANOVA $p = 0.02$), the control and 50 mg kg^{-1} Cd stress groups (R2Y [1] = 0.74, Q2 [1] = 0.99, CV-ANOVA $p = 0.03$) and the control and 100 mg kg^{-1} Cd stress groups (R2Y [1] = 0.81, Q2 [1] = 0.99, CV-ANOVA $p = 0.01$), respectively.

Supplementary Table S1 | Primary and secondary mass spectrometry analysis conditions.

Supplementary Table S2 | All metabolites identified by LC–MS/MS in *S. miltiorrhiza* roots with different levels of Cd stress. CK, T1, T2 and T3 represent roots in the control, 25 mg kg^{-1} Cd, 50 mg kg^{-1} Cd, and 100 mg kg^{-1} Cd treated groups ($n = 3$), respectively (the same below). All data are presented as the mean ± SE.

Supplementary Table S3 | Relative contents of metabolites of different types in *S. miltiorrhiza* roots with different levels of Cd stress. CK, T1, T2 and T3 represent roots in the control, 25 mg kg^{-1} Cd, 50 mg kg^{-1} Cd, and 100 mg kg^{-1} Cd treated groups, respectively (the same below). Different lowercase letters indicate significant differences within each treatment in the roots ($p < 0.05$). All data are presented as the mean ± SE ($n = 3$).

Supplementary Table S4 | Results of pathway analysis involving all of the discriminating metabolites in *S. miltiorrhiza* roots with different levels of Cd stress. All pathways shown in the table are potential target metabolic pathways with pathway impacts above 0.1; Total Cmpd, total number of compounds in the pathway; Hits, the number of actually matched compounds in the pathway; Holm adjust, *p* value adjusted by the Holm–Bonferroni method; FDR, *p* value adjusted using the False Discovery Rate; Impact, pathway impact value.

REFERENCES

Angelovici, R., Fait, A., Zhu, X., Szymanski, J., Feldmesser, E., Fernie, A. R., et al. (2009). Deciphering transcriptional and metabolic networks associated with lysine metabolism during Arabidopsis seed development. *Plant Physiol.* 151, 2058–2072. doi: 10.1104/pp.109.145631

Benral, M. P., and McGrath, S. P. (1994). Effects of pH and heavy metal concentrations in solution culture on the proton release, growth and elemental composition of *Alyssum murale* and *Raphanus sativus* L. *Plant and Soil.* 166, 83–92. doi: 10.1007/BF02185484

Cassels, B., and Sáez-Briones, P. (2018). Dark classics in chemical neuroscience: mescaline. *ACS Chem. Neurosci.* 9, 2448–2458. doi: 10.1021/acschemneuro.8b00215

Chaffai, R., Seybou, T. N., Marzouk, B., and El Ferjani, E. (2009). A comparative analysis of fatty acid composition of root and shoot lipids in *Zea mays* under copper and cadmium stress. *Acta Biol. Hungarica.* 60, 109–125. doi: 10.1556/ABiol.60.2009.1.10

Commission, C. P. (2020). *Pharmacopoeia of the People's Republic of China*. China: China Medical Science and Technology Press.

Cosio, C., and Renault, D. (2020). Effects of cadmium, inorganic mercury and methyl-mercury on the physiology and metabolomic profiles of shoots of the macrophyte *Elodea nuttallii*. *Environ. Pollut.* 257, 113557. doi: 10.1016/j.envpol.2019.113557

Cury-Boaventura, M. F., and Curi, R. (2005). Regulation of reactive oxygen species (ROS) production by C18 fatty acids in Jurkat and Raji cells. *Clin. Sci.* 108, 245–253. doi: 10.1042/CS20040281

Filipič, M. (2012). Mechanisms of cadmium induced genomic instability. *Mutat. Res. Fundam. Molec. Mechan. Mutagen.* 733, 69–77. doi: 10.1016/j.mrfmmm.2011.09.002

Fu, R., Shi, M., Deng, C., Zhang, Y., Zhang, X., Wang, Y., et al. (2020). Improved phenolic acid content and bioactivities of *Salvia miltiorrhiza* hairy roots by genetic manipulation of RAS and CYP98A14. *Food Chem.* 331, 127365. doi: 10.1016/j.foodchem.2020.127365

Genchi, G., Carocci, A., Lauria, G., Sinicropi, M. S., and Catalano, A. (2020a). Nickel: Human health and environmental toxicology. *Int. J. Environ. Res. Public Health* 17, 679. doi: 10.3390/ijerph17030679

Genchi, G., Sinicropi, M. S., Lauria, G., Carocci, A., and Catalano, A. (2020b). The effects of cadmium toxicity. *Int. J. Environ. Res. Public Health* 17, 3782. doi: 10.3390/ijerph17113782

Grajek, H., Rydzyński, D., and Piotrowicz-Cieslak, A. (2020). Cadmium ion-chlorophyll interaction-examination of spectral properties and structure of the cadmium-chlorophyll complex and their relevance to photosynthesis inhibition. *Chemosphere* 261, 127434. doi: 10.1016/j.chemosphere.2020.127434

Güez, C. M., de Souza, R. O., Fischer, P., Leão, M. F. M., Duarte, J. A., Boligon, A. A., et al. (2017). Evaluation of basil extract (*Ocimum basilicum* L.) on oxidative, anti-genotoxic and anti-inflammatory effects in human leukocytes cell cultures exposed to challenging agents. *Brazilian J. Pharmaceut. Sci.* 53, 1–12. doi: 10.1590/s2175-97902017000115098

Ho, C. L., and Saito, K. (2001). Molecular biology of the plastidic phosphorylated serine biosynthetic pathway in *Arabidopsis thaliana*. *Amino Acids* 20, 243–259. doi: 10.1007/s007260170042

Hu, L., and Xu, Q. (2014). Review of current progress in the metabolomics for plant response to abiotic stress. *Crop Res.* 28, 428–434.

Jones, G. J., Nichols, P. D., Johns, R. B., and Smith, J. D. (1987). The effect of mercury and cadmium on the fatty acid and sterol composition of the marine diatom *Asterionella glacialis*. *Phytochemistry* 26, 1343–1348. doi: 10.1016/S0031-9422(00)81809-9

Kabata, P. A., and Pendias, H. (1992). *Trace Elements in Soils and Plants.* Baton Rouge: CRC Press.

Kilgore, M. B., and Kutchan, T. M. (2016). The Amaryllidaceae alkaloids: biosynthesis and methods for enzyme discovery. *Phytochem. Rev.* 15, 317–337. doi: 10.1007/s11101-015-9451-z

Korkmaz, K., Ertürk, O., Ayvaz, M. C., Özcan, M. M., Akgün, M., Kirli, A., et al. (2018). Effect of cadmium application on antimicrobial, antioxidant and total phenolic content of basil genotypes. *Indian J. Pharmac. Educ. Res.* 52, S108–S114. doi: 10.5530/ijper.52.4s.84

Kristin, T. Z., and Michael, D. T. (2010). Nucleophile specificity in anthranilate synthase, aminodeoxychorismate synthase, isochorismate synthase, and salicylate synthase. *Biochemistry* 49, 2851–2859. doi: 10.1021/bi100021x

Kuang, H. X. (2017). *Chemistry of Traditional Chinese Medicine.* Beijing, China: China Press of Traditional Chinese Medicine.

Li, Y. G., Song, L., Liu, M., Hu, Z. B., and Wang, Z. T. (2009). Advancement in analysis of *Salviae miltiorrhizae* Radix et Rhizoma (Danshen). *J. Chromatogr. A* 1216, 1941–1953. doi: 10.1016/j.chroma.2008.12.032

Li-Beisson, Y., Nakamura, Y., and Harwood, J. (2016). "Lipids: from chemical structures, biosynthesis, and analyses to industrial applications" in *Lipids in Plant and Algae Development.* eds. Nakamura, Y., Libeisson, Y. (Switzerland: Springer International Publishing). 1–20. doi: 10.1007/978-3-319-25979-6_1

Liu, H., Zhang, J., Chen, H., Yi, Y., Liu, J., and Zhang, H. (2013). Fatty acid desaturation and plant responses to biotic and abiotic stresses. *J. Bnortheast Agric. Univ.* 44, 154–160. doi: 10.19720/j.cnki.issn.1005-9369.2013.01.032

Liu, W., Liu, Z., Xie, W., and Wang, Y. (2014). Responses of fatty acid and its derivatives to stress in plants. *Pratac. Sci.* 31, 1556–1565. Available online at: https://kns.cnki.net/kcms/detail/detail.aspx?dbcode=CJFD&dbname=CJFD2014&filename=CYKX201408024&uniplatform=NZKPT&v=lajV5-Hu9wMllTgwSfeuIUdcLocTze3dCkQYIH42GMNXct_TU0AQrkz57k4SMyPB

Liu, X. L., Yang, C. Y., Zhang, L. B., Li, L. Z., Liu, S. J., Yu, J. B., et al. (2011a). Metabolic profiling of cadmium-induced effects in one pioneer intertidal halophyte *Suaeda salsa* by NMR-based metabolomics. *Ecotoxicology* 20, 1422–1431. doi: 10.1007/s10646-011-0699-9

Liu, Y., Zhang, L., Zhang, H., and Fu, H. (2011b). Progress of research on Δ12 fatty acid desaturases and theircodinggenes. *Acta Prataculturae Sinica* 20, 256–267. Available online at: https://kns.cnki.net/kcms/detail/detail.aspx?dbcode=CJFD&dbname=CJFD2011&filename=CYXB201103034&uniplatform=NZKPT&v=QiitSHplj4mqCn1E_J2ZewDZyqRtglqsi7JGBJ3rVI_y0aU8L2YQD0rr1fhiJTXj

Lu, S. (2020). Analysis and evaluation of climate comfort characteristics in Linyi. *South China Agriculture* 14, 191–192. doi: 10.19415/j.cnki.1673-890x.2020.26.086

Luo, Q., Sun, L., Hu, X., and Zhou, R. (2014). The variation of root exudates from the hyperaccumulator *Sedum alfredii* under cadmium stress: metabonomics analysis. *PLoS ONE* 9, e115581. doi: 10.1371/journal.pone.0115581

Lv, C. (2021). *Effect of "Swelling Agent" Application on the Quality of Root and Rhizome Medicinal Materials*. China: Academy of Chinese Medical Sciences.

Lv, X., Zhu, H., Jiang, P., and Zhang, L. (2005). In vitro scavenging activity on reactive oxygen radicals of perillae leaves extract. *Chin. Food Addit.* 67–70. Available online at: https://kns.cnki.net/kcms/detail/detail.aspx?dbcode=IPFD&dbname=IPFD9914&filename=OGSK200503001011&uniplatform=NZKPT&v=1u8ZBtGNaNuQLOHy5A4uvn6IRqGHhOv05oD5CwDZdP6G6x30HohhGfzWzkYTKveHIgcnNhvOdkw%3d

Malik, V. S. (1979). Regulation of chorismate-derived antibiotic production. *Adv. Appl. Microbiol.* 25, 75–93. doi: 10.1016/S0065-2164(08)70147-3

Manquián-Cerdaa, K., Cruces, E., Escudey, M., Zúñigaa, G., and Calderónd, R. (2018). Interactive effects of aluminum and cadmium on phenolic compounds, antioxidant enzyme activity and oxidative stress in blueberry (*Vaccinium corymbosum* L.) plantlets cultivated in vitro. *Ecotoxicol. Environ. Safety* 150, 320–326. doi: 10.1016/j.ecoenv.2017.12.050

Meng, M., Tao, C., Li, J., Ma, Z., Jia, W., and Jia, M. (2009). Determination of Pb, Cd, As, Hg, Cu in radix *Salviae miltiorrhizae*. *Tianjin J. Tradit. Chin. Med.* 26, 248–249.

Michalak, A. (2006). Phenolic compounds and their antioxidant activity in plants growing under heavy metal stress. *Polish J. Environ. Stud.* 15, 523–530.

Panchal, P., Miller, A. J., and Giri, J. (2021). Organic acids: versatile stress-response roles in plants. *J. Experim. Botany.* 72, 4038–4052. doi: 10.1093/jxb/erab019

Park, W., Feng, Y., Kim, H., Suh, M. C., and Ahn, S. (2015). Changes in fatty acid content and composition between wild type and CsHMA3 overexpressing *Camelina sativa* under heavy-metal stress. *Plant Cell Rep.* 34, 1489–1498. doi: 10.1007/s00299-015-1801-1

Rahimzadeh, M. R., Rahimzadeh, M. R., and Kazemi, S. (2017). Cadmium toxicity and treatment: an update. *Caspian J. Internal Med.* 8, 135–145.

Ros, R., Cascales-Miñana, B., Segura, J., Anoman, A. D., Toujani, W., Flores-Tornero, M., et al. (2013). Serine biosynthesis by photorespiratory and nonphotorespiratory pathways: an interesting interplay with unknown regulatory networks. *Plant Biol.* 15, 707–712. doi: 10.1111/j.1438-8677.2012.00682.x

Sanjaya, H. P. Y., Su, R. C., Ko, S. S., Tong, C. G., Yang, R. Y., and Chan, M.T. (2008). Overexpression of *Arabidopsis thaliana tryptophan synthase beta* 1 (AtTSB1) in *Arabidopsis* and tomato confers tolerance to cadmium stress. *Plant Cell Environ.* 31, 1074–1085. doi: 10.1111/j.1365-3040.2008.01819.x

Sarangthem, J., Jain, M., and Gadre, R. (2011). Inhibition of δ-amino levulinic acid dehydratase activity by cadmium in excised etiolated maize leaf segments during greening. *Plant Soil Environ.* 57, 332–337. doi: 10.17221/45/2011-PSE

Satarug, S., Baker, J. R., Urbenjapol, S., Haswell-Elkins, M., Reilly, P. E. B., Williams, D. J., et al. (2003). A global perspective on cadmium pollution and toxicity in non-occupationally exposed population. *Toxicol. Lett.* 137, 65–83. doi: 10.1016/S0378-4274(02)00381-8

Sharma, S. S., and Dietz, K. J. (2006). The significance of amino acids and amino acid-derived molecules in plant responses and adaptation to heavy metal stress. *J. Experim. Botany* 57, 711–736. doi: 10.1093/jxb/erj073

Shi, M., Huang, F., Deng, C., Wang, Y., and Kai, G. (2019). Bioactivities, biosynthesis and biotechnological production of phenolic acids in *Salvia miltiorrhiza*. *Crit. Rev. Food Sci. Nutr.* 59, 953–964. doi: 10.1080/10408398.2018.1474170

Stepansky, A., and Leustek, T. (2006). Histidine biosynthesis in plants. *Amino Acids* 30, 127–142. doi: 10.1007/s00726-005-0247-0

Su, C. Y., Ming, Q. L., Rahman, K., Han, T., and Qin, L. P. (2015). *Salvia miltiorrhiza*: Traditional medicinal uses, chemistry, and pharmacology. *Chin. J. Nat. Med.* 13, 163–182. doi: 10.1016/S1875-5364(15)30002-9

Sun, L., Cao, X., Tan, C., Deng, Y., Cai, R., Peng, X., et al. (2020). Analysis of the effect of cadmium stress on root exudates of *Sedum plumbizincicola* based on metabolomics. *Ecotoxicol. Environ. Safety* 205, 111152. doi: 10.1016/j.ecoenv.2020.111152

Tan, F. (2017). *Study on Present Situation of Medicinal Diets and Composition and Application of Medicinal Diets for Phlegm-Dampness Constitution*. China: Peking Union Medical College.

Tang, J., Xu, H., Wang, C., Wang, Y., Li, B., and Cao, L. (2016). Effect of cadmium stress on root growth and organic acids and amino acid secretion of three rice varieties. *J. Hunan Agric. Univ.* 42, 118–124. doi: 10.13331/j.cnki.jhau.2016.02.002

Thompson, G. A. (1992). *The Regulation of Membrane Lipid Metabolism.* Boca Raton: CRC Press.

Tian, P. (2021). *Physiological Metabolic Response of Brassica Juncea to Cadmium Stress and Regulation of Exogenous Proline*. China: Central South University of Forestry and Technology.

Tian, Y., Zhang, R., and Zhang, L. (2021). Analysis of climatic conditions and study on measures for good-quality and high-yield of wheat planting in Linyi. *Agric. Technol.* 41, 67–69.

Tong, Q., Zhang, C., Tu, Y., Chen, J., Li, Q., Zeng, Z., et al. (2022). Biosynthesis-based spatial metabolome of *Salvia miltiorrhiza* Bunge by combining metabolomics approaches with mass spectrometry-imaging. *Talanta* 238, 123045. doi: 10.1016/j.talanta.2021.3045

Trovato, M., Funck, D., Forlani, G., Okumoto, S., and Amir, R. (2021). Amino acids in plants: regulation and functions in development and stress defense. *Front. Plant Sci.* 12, 772810. doi: 10.3389/fpls.2021.772810

Valverde, M., Trejo, C., and Rojas, E. (2001). Is the capacity of lead acetate and cadmium chloride to induce genotoxic damage due to direct DNA-metal interaction? *Mutagenesis* 16, 265–270. doi: 10.1093/mutage/16.3.265

Waditee, R., Bhuiyan, N. H., Hirata, E., Hibino, T., Tanaka, Y., Shikata, M., et al. (2007). Metabolic engineering for betaine accumulation in microbes and plants. *J. Biol. Chem.* 282, 34185–34193. doi: 10.1074/jbc.M704939200

Wang, M., Duan, S., Zhou, Z., Chen, S., and Wang, D. (2019). Foliar spraying of melatonin confers cadmium tolerance in *Nicotiana tabacum* L. *Ecotoxicol. Environ. Safety* 170, 68–76. doi: 10.1016/j.ecoenv.2018.11.127

Wang, T., Xing, Y., Tan, Z., Tang, W., Su, M., Ye, F., et al. (2014). Study on the radical scavenging activities by several natural aromatic compounds. *Food Res. Develop.* 35, 5–7.

Wang, Y., Xu, L., Shen, H., Wang, J., Liu, W., Zhu, X., et al. (2015). Metabolomic analysis with GC-MS to reveal potential metabolites and biological pathways involved in Pb and Cd stress response of radish roots. *Sci. Rep.* 5, 18296. doi: 10.1038/srep18296

Wei, X., Cao, P., Wang, G., and Han, J. (2020). Microbial inoculant and garbage enzyme reduced cadmium (Cd) uptake in *Salvia miltiorrhiza* (Bge.) under Cd stress. *Ecotoxicol. Environ. Safety* 192, 110311. doi: 10.1016/j.ecoenv.2020.110311

Wu, Z. Y. (1977). *Flora of China.* China: Science Press.

Xu, J., Fang, X., Li, C., Yang, L., and Chen, X. (2020). General and specialized tyrosine metabolism pathways in plants. *aBIOTECH* 1, 95–105. doi: 10.1007/s42994-019-00006-w

Xu, J., Zhu, Y., Ge, Q., Li, Y., Sun, J., Zhang, Y., et al. (2012). Comparative physiological responses of *Solanum nigrum* and *Solanum torvum* to cadmium stress. *New Phycol.* 196, 125–138. doi: 10.1111/j.1469-8137.2012.04236.x

Yan, H., Feng, H., Huang, W., Li, H., and Feng, C. (2012). Evaluation for heavy metal pollution of soil and herb from the main production area of *Salvia miltiorrhiza* Bge. in China. *Chin. Agric. Sci. Bull.* 28, 288–293.

Yan, J., Jing, X., Yue, W., and Jian, W. (2020). Stimulation of tanshinone production in *Salvia miltiorrhiza* hairy roots by β-cyclodextrin-coated silver nanoparticles. *Sustainable Chem. Pharm.* 18, 100271. doi: 10.1016/j.scp.2020.100271

Yuan, J., Sun, N., Du, H., Yin, S., Kang, H., Umair, M., et al. (2020). Roles of metabolic regulation in developing *Quercus variabilis* acorns at contrasting geologically-derived phosphorus sites in subtropical China. *BMC Plant Biol.* 20, 389. doi: 10.1186/s12870-020-02605-y

Zemanov,á, V., Pavlík, M., and Pavlíkov,á, D. (2017). Cadmium toxicity induced contrasting patterns of concentrations of free sarcosine, specific amino acids and selected microelements in two Noccaea species. *PLoS ONE* 12, e0177963. doi: 10.1371/journal.pone.0177963

Zhang, F., and Chen, W. (2021). Research progress of metabolomics in plant stress biology. *Biotechnol. Bull.* 37, 1–11. doi: 10.13560/j.cnki.biotech.bull.1985.2021-0861

Zhang, X., Li, K., Chen, K., Liang, J., and Cui, L. (2013). Effects of cadmium stress on seedlings growth and active ingredients in *Salvia miltiorrhiza*. *Plant Sci. J.* 31, 583–589. doi: 10.3724/SP.J.1142.2013.60583

Zhu, G., Xiao, H., Guo, Q., Zhang, Z., Zhao, J., and Yang, D. (2018). Effects of cadmium stress on growth and amino acid metabolism in two Compositae plants. *Ecotoxicol. Environ. Safety* 158, 300–308. doi: 10.1016/j.ecoenv.2018.04.045

Zoufan, P., Azad, Z., Ghahfarokhie, A. R., and Kolahi, M. (2020). Modification of oxidative stress through changes in some indicators related to phenolic metabolism in *Malva parviflora* exposed to cadmium. *Ecotoxicol. Environ. Safety* 187, 109811. doi: 10.1016/j.ecoenv.2019.109811

Conflict of Interest: The authors declare that the research was conducted in the absence of any commercial or financial relationships that could be construed as a potential conflict of interest.

Publisher's Note: All claims expressed in this article are solely those of the authors and do not necessarily represent those of their affiliated organizations, or those of the publisher, the editors and the reviewers. Any product that may be evaluated in this article, or claim that may be made by its manufacturer, is not guaranteed or endorsed by the publisher.

frontiers | Frontiers in Plant Science

ORIGINAL RESEARCH
published: 08 August 2022
doi: 10.3389/fpls.2022.894706

Photosynthetic Response of Soybean and Cotton to Different Irrigation Regimes and Planting Geometries

Srinivasa R. Pinnamaneni[1,2]*, *Saseendran S. Anapalli*[3] and *Krishna N. Reddy*[1]

[1] Crop Production Systems Research Unit, USDA-ARS, Stoneville, MS, United States, [2] Oak Ridge Institute for Science and Education, Oak Ridge, TN, United States, [3] Sustainable Water Management Research Unit, USDA-ARS, Stoneville, MS, United States

Soybean [*Glycine max* (L.) Merr.] and cotton (*Gossypium hirsutum* L.) are the major row crops in the USA, and growers are tending toward the twin-row system and irrigation to increase productivity. In a 2-year study (2018 and 2019), we examined the gas exchange and chlorophyll fluorescence parameters to better understand the regulatory and adaptive mechanisms of the photosynthetic components of cotton and soybean grown under varying levels of irrigations and planting geometries in a split-plot experiment. The main plots were three irrigation regimes: (i) all furrows irrigation (AFI), (ii) alternate or skipped furrow irrigation (SFI), and iii) no irrigation or rainfed (RF), and the subplots were two planting patterns, single-row (SR) and twin-row (TR). The light response curves at vegetative and reproductive phases revealed lower photosynthesis rates in the RF crops than in AFI and SFI. A higher decrease was noticed in RF soybean for light compensation point (LCP) and light saturation point (LSP) than that of RF cotton. The decrease in the maximum assimilation rate (Amax) was higher in soybean than cotton. A decrease of 12 and 17% in Amax was observed in RF soybean while the decrease is limited to 9 and 6% in RF cotton during the 2018 and 2019 seasons, respectively. Both stomatal conductance (gs) and transpiration (E) declined under RF. The moisture deficit stress resulted in enhanced operating quantum efficiency of PSII photochemistry (ΦPSII), which is probably due to increased photorespiration. The non-photochemical quenching (NPQ), a measure of thermal dissipation of absorbed light energy, and quantum efficiency of dissipation by down-regulation (ΦNPQ) increased significantly in both crops up to 50% under RF conditions. The photochemical quenching declined by 28% in soybean and 26% in cotton. It appears soybean preferentially uses non-photochemical energy dissipation while cotton uses elevated electron transport rate (ETR) under RF conditions for light energy utilization. No significant differences among SR and TR systems were observed for LCP, LSP, AQE, Amax, gs, E, ETR, and various chlorophyll fluorescence parameters. This study reveals preferential use of non-photochemical energy dissipation in soybean while cotton uses both photochemical and non-photochemical energy dissipation to protect PSI and PSII centers and ETR, although they fall under C3 species when exposed to moisture limited environments.

Keywords: photosynthesis, irrigation levels, planting geometry (PG), chlorophyll fluorescence (CF), electron transport, non-photochemical quenching, light compensation point

OPEN ACCESS

Edited by:
Amaranatha Reddy Vennapusa, Delaware State University, United States

Reviewed by:
Prathibha M. Dharmappa, University of Agricultural Sciences, Bangalore, India
Sivasakthi Kaliamoorthy, International Crops Research Institute for the Semi-Arid Tropics (ICRISAT), India

***Correspondence:**
Srinivasa R. Pinnamaneni
sri.pinnamaneni@usda.gov

Specialty section:
This article was submitted to Plant Abiotic Stress, a section of the journal Frontiers in Plant Science

Received: *12 March 2022*
Accepted: *24 June 2022*
Published: *08 August 2022*

Citation:
Pinnamaneni SR, Anapalli SS and Reddy KN (2022) Photosynthetic Response of Soybean and Cotton to Different Irrigation Regimes and Planting Geometries. Front. Plant Sci. 13:894706. doi: 10.3389/fpls.2022.894706

INTRODUCTION

The United States accounts for about 35.45 million ha of soybean cultivated with a production of about 240 million Mg and a productivity of 3.4 Mg ha^{-1} (Plumblee et al., 2019). Cotton is the most important natural fiber crop worldwide, with about 34 M ha cultivated in 85 countries, and the United States accounts for 4.65 million ha with a production of 19.9 million bales (Plumblee et al., 2019). In Mississippi (MS), cotton is grown on over 0.25 M ha with an estimated production of 1.46 million bales, and soybean occupied 0.79 M ha with an estimated production of 2.8 million Mg (USDA-NASS, 2020).

In the MS Delta, many soybean and cotton growers are moving away from the traditional single-row (SR) planting geometry to twin-row (TR) geometry owing to a significant gain in productivity in most of the seasons and also to reduce machinery-associated costs as TR planters and combines can be used on multiple row crops with minor adjustments keeping the cultivation costs same for SR and TR patterns (Bruns, 2011; Bellaloui et al., 2020; Pinnamaneni et al., 2020a,b, 2021). In cotton, TR pattern adoption resulted in 35 to 106 kg ha^{-1} higher lint (Reddy et al., 2009; Stephenson et al., 2011). A range of 0–23% seed yield enhancement was reported in the TR soybean compared to the SR system (Grichar, 2007; Bruns, 2011; Pinnamaneni et al., 2020b). In the lower MS Delta, the precipitation pattern was shown to have wide fluctuations within the crop season and among the seasons resulting in drought, leading to crop yield losses (Anapalli et al., 2016).

Photosynthesis is a complex biochemical and biophysical process comprising three unique components: synthesis of photosynthetic pigments, absorption of light energy and electron transport, and the Calvin cycle of carbon fixation. It is widely believed that the photosynthetic performance appears to be a very useful indicator, owing to its strong negative correlation with different environmental stresses (Massacci et al., 2008; Zhang et al., 2011; Yao et al., 2017a; Singh and Reddy, 2018; Ye et al., 2020; Poorter et al., 2022). The capacity to utilize incident light energy by the photosynthetic system for carbon assimilation generally declines under moisture deficit conditions (Gilbert et al., 2011; Yao et al., 2017a; Poorter et al., 2022). This often leads to excessive light energy absorption than required for the efficient functioning of photosynthetic reactions, resulting in photoinhibition and cell damage (Gilbert et al., 2011; Jumrani and Bhatia, 2019). However, plants have evolved innate photoprotective mechanisms such as photorespiration and thermal emission to dissipate excess light energy to protect their machinery. Besides gas exchange assessment, often, chlorophyll fluorescence parameters are measured to understand clearly the functioning of photosynthetic components as it gives additional information on PSI and PSII reaction centers' efficiencies, energy trapping and dissipation efficiencies, and photorespiration (Massacci et al., 2008; Poorter et al., 2022). Chlorophyll fluorescence analyses reveal that the quantum efficiency of PSII (ΦPSII) is closely related to the quantum efficiency of CO_2 assimilation when photorespiration is negligible. It was reported that soybean and cotton have distinct strategies to protect photosynthetic machinery and perform photosynthesis under moisture deficit conditions, and the reproductive stage is more critical (Zhang et al., 2011). This study further showed that soybean uses non-photochemical dissipation while cotton uses electron transport flux for light energy dissipation as their mechanism of photoprotection of photosynthetic apparatus under drought. A greenhouse study on cotton and soybean subjected to water stress revealed that the photosynthesis rate declined by 46% and 73% in cotton and soybean, respectively, while non-photochemical quenching (NPQ), an indicator of the thermal dissipation of excess excitation energy increased by 197% in soybean but only 25% in cotton under severe water stress (Inamullah and Isoda, 2005). It has been demonstrated that paraheliotropic movement in soybean (Hirata et al., 1983) and diaheliotropic movement in cotton helps to avoid photoinhibition while trying to keep leaf temperature lower under water stress (Ehleringer and Forseth, 1989). Peanut showed a greater increase than cotton in leaf temperature and NPQ and a greater decrease in chlorophyll content and ΦPSII in the water stress condition. On the other hand, the water stress lowered the transpiration rate and leaf area (LA) more in cotton than in peanut (Isoda, 2010). Furthermore, planting-row spacing impacted the photosynthetic capacity of cotton due to differences in light interception, canopy architecture, and leaf area index. A wider spacing of 76 cm in cotton recorded higher photosynthesis and boll production, while soybean did not respond to alteration in-row spacing (Slattery et al., 2017; Yao et al., 2017a). Also, differences in photosynthesis rate in soybean monocropping and intercropping with corn were reported (Yao et al., 2017b). There are no studies on the effects of SR and TR on photosynthetic and chlorophyll fluorescence parameters in the literature.

The specific objective of this research was to characterize cotton and soybean photosynthetic parameters estimated from light response curves and chlorophyll fluorescence measurements in two planting patterns (PP) i.e., SR and TR planting systems that were furrow-irrigated at the following rates (i) all furrows irrigation (AFI) (ii) skipped furrow irrigation (SFI), and (iii) rainfed (RF) at Stoneville, MS. Assessing these measurements will enhance our understanding on the regulation of photosynthesis under moisture deficit environments.

MATERIALS AND METHODS

Two-year (2018–2019) field experiments were conducted at the USDA-ARS, Crop Production Systems Research Unit's research farm, in Stoneville, MS, USA (33° 42′ N, 90° 55′ W, elevation: 32 m above mean sea level). The experimental area soil type was a Dundee silt loam (fine silty, mixed, active, thermic Typic Endoaqualfs) with 0.92% organic matter, 0.46% carbon, 0.07% nitrogen, and 1.26 g cm^{-3} bulk density averaged across 60 cm soil depth. As measured in this study, the field saturated hydraulic conductivity (Kfs) of the soil ranged from 0.39 to 1.26 cm hr^{-1}. Field preparation consists of deep tillage in the fall, disking in winter, and harrowing in early spring to make ridges and furrows at 102 cm spacing as described earlier (Pinnamaneni et al., 2020a). A 7300-vacuum planter (John Deere, East Moline, IL) was used to plant in the SR planting geometry while a

Monosem NG+3 TR vacuum planter (A.T.I., Inc. Monosem, Lenexa, KS) was used to plant the TR planting geometry in cotton. Both planters were set to achieve a similar population density of approximately 120,000 plants $ha^{-1.}$ Soybean SR plantings were made using an Almaco cone plot planter (Allen Machine Company, Nevada, IA), and TR plots were planted with a four-unit Monosem NG-3 (Monosem, Edwardsville, KS) twin-row vacuum planter. Both planters were set to achieve a similar overall plant population density of approximately 336,000 plants ha^{-1}. Plots were maintained weed-free using both pre-emergence and postemergence herbicide programs (Pinnamaneni et al., 2020b).

The cotton cultivar "FiberMax1944GLB2," a medium-maturing Bt-transgenic (Cry1Ac and Cry2Ab genes) variety with broad adaptation, possessing in-plant tolerance to glyphosate, and glufosinate reaches 50% flowering by 75 days, and soybean maturity group IV cultivar "31RY45 Dyna-Gro" with roundup ready trait reaching 50% flowering by 43 days were planted in two separate studies. Both cultivars are popular in MS Delta. The former is known for its fiber yield while the latter is tolerant to drought. The treatments were arranged as a split-plot design with six replications. The main plots were three irrigation regimes (a) AFI, (b) SFI, and (c) RF. Subplots consisted of two planting geometries: (a) SR, single rows evenly spaced at 102 cm centered seedbeds, and (b) TR, two rows spaced 25 cm apart on 102 cm centered seedbeds. Cotton seeds were planted on 8 May 2018 and 16 May 2019. Soybean was planted on 8 May 2018 and 2 May 2019. Each plot consisted of four SR or eight TR rows and was 40 m long. Sensors for measuring soil–matrix water potential (Irrometer Company, Inc, Riverside, CA, USA) were installed in the selected representative plots, and irrigations were scheduled based on a soil matrix potential of about −90 kPa at 45 cm soil depths, as Plumblee et al. (2019) recommended. Soybean was grown without any fertilizer while cotton received nitrogen in the form of 32% urea–ammonium nitrate, which was injected 7.5 cm deep in a split application of 112 kg N ha^{-1} 50% at planting and 50% at 35 days after planting. Average crop evapotranspiration of soybean and cotton was 546 and 552 mm, respectively, in the lower MS Delta, and annual average effective rainwater deficits for soybean and cotton were estimated to be 340 mm and 395 mm, respectively (Tang et al., 2018). In 2018, a total of 220 mm of irrigation was applied to the AFI treatments in four irrigation events while 152 mm was applied in three irrigations in 2019 for soybean, and cotton received 175 mm in five irrigation events and 152 mm in three irrigation events in 2018 and 2019, respectively. The SFI plots received 50% of AFI treatment (Pinnamaneni et al., 2020b, 2021). Irrigation was stopped at the R6 stage of growth of pod development in both years for soybean, while for cotton it was at the boll cracking stage (C5). Weather data was collected from the Stoneville AWS station (latitude:33.43122, longitude: −90.91077), Delta Research and Extension Center, Stoneville, MS. The grain yield in soybean and lint yield in cotton were estimated as reported earlier (Pinnamaneni et al., 2020a,b).

Data on light response curves and gas exchange rates were measured at vegetative (V6 in both the crops) and reproductive phases (R5 in soybean and C5, 5th boll cracking in cotton) using a portable infrared (IR) gas analyzer (LI-6800, LI-COR, Lincoln, NE) equipped with a standard 2 × 3 cm leaf chamber. The dates of measurement in soybean were between 21 June and 16 July 2018 and between 11 June and 17 July 2019, while the data on cotton were collected on 30 June and 3 August 2018 and 3 July 3 and 12 August 2019 between 9 am and 3 pm. The leaf temperature was between 28 and 31 °C, while the RH was maintained at 60% and the CO_2 concentration in the chamber was 400 mg L^{-1}. Ten photosynthetic photon flux density (PPFD) levels (−2,000, 1,500, 1,000, 500, 250, 120, 60, 30,15, and 0 μmol $m^{-2}s^{-1}$) were used. Fully expanded top leaves on 3 randomly selected plants per plot were used for measurements. The leaves were allowed to adapt to each light level for 10 min before measurement. Then, after linear fitting, light compensation point (LCP), light saturation point (LSP), light-saturated net photosynthetic rate (Amax), apparent quantum efficiency (AQE), and dark respiration rate (Rd) were estimated by the method of Ye (2007).

Pre-dawn measurements of minimal fluorescence (F_o) and maximal fluorescence (F_m) were measured on dark adapted fully expanded top leaves according to Baker (2008). The maximum fluorescence value in the light (F'_m) was estimated after applying a 0.8-s saturation flash (10,000 μmol m^{-2} s^{-1}). The minimal fluorescence in the light-adapted leaves (F'_o) was calculated according to Oxborough and Baker (Oxborough and Baker, 1997). Electron transport rate (ETR) was calculated by assuming a leaf absorption of 0.85 and a PSII:PSI ratio of 1:1.

The chlorophyll fluorescence parameters were calculated according to Rosenqvist and van Kooten (Genty et al., 1989; Rosenqvist and van Kooten, 2003; Kramer et al., 2004).

$$Fo' = Fo/(\frac{\mathrm{Fv}}{Fm} + \frac{\mathrm{Fo}}{Fm'})$$

Operating quantum efficiency of PSII photochemistry,

$$\Phi\mathrm{PSII} = \frac{\mathrm{Fm}' - \mathrm{F}'}{\mathrm{Fm}'}$$

$$\text{Photochemical quenching (QP) as QP} = \frac{\mathrm{Fm}' - \mathrm{F}'}{\mathrm{Fm}' - \mathrm{Fo}'}$$

$$\text{Non} - \text{photochemical quenching (NPQ) was expressed as NPQ} = \frac{\mathrm{Fm}}{\mathrm{Fm}'} - 1$$

$$\text{Quantum efficiency of dissipation by down} - \text{regulation as } \Phi NPQ = \left(\frac{F'}{Fm'}\right) - 1/(\frac{Fm}{Fm'} + \frac{Fq'*Fo'*Fv}{Fv'*F'*Fo})$$

An analysis of variance (ANOVA) was conducted using PROC MIXED (JMP Pro v. 14.1.0 software, SAS Institute, Cary, NC). Year, PP, irrigation levels, and interactions were considered fixed effects. Replicates within a year were considered random effects. Mean comparisons were conducted by Fishers Protected LSD test, and the level of significance of $P \leq 0.05$ was used. The graphs were made using Sigmaplot (Version 14.0, Systat software).

RESULTS AND DISCUSSION

Seasonal Weather

The two cropping seasons in 2018 and 2019 were vividly different in weather conditions (**Figure 1**). Warmer weather prevailed during reproductive growth and boll filling (July–September) in 2019 (92 GDD more than in 2018). The 2019 crop season was dry (348 mm less rainfall) and had more monthly total solar radiation of 500 MJ m^{-2} than in 2018. However, vegetative growth (May–July) in 2018 coincided with periods of lower rainfall (375 mm <2019) and higher mean minimum and maximum temperatures. Due to the impacts of contrasting weather across the two growing seasons, the analysis of variance (ANOVA) revealed that year has significant interaction with different photosynthetic parameters (**Table 1**).

Light Response Curves in Soybean

Figure 2 shows light response curves (assimilation rate vs. the photosynthetic photon quanta flux density, PPFD) in soybean at the vegetative stage (V6) and reproductive stage (R5) for all the irrigation and planting geometry combinations for the 2018 and 2019 seasons. The CO_2 assimilation rate is relatively lower at the reproductive stage in both the years than in the vegetative stage. Further, the figure reveals that the assimilation rates were higher in 2018 than in 2019, although comparatively less. The assimilation rates under different treatments initially increased with a rise in PPFD ranging from 0 to 2,000 μmol $m^{-2}s^{-1}$. The increasing trend subsequently plateaued and eventually reached a saturation point at 1,500 μmol $m^{-2}s^{-1}$. As the PPFD continued to increase, the light response curves of the net assimilation rate under AFI and SFI became higher than those of RF treatments. There appears to be no significant difference caused by PP on photosynthesis in both years. The TR planting system recorded a 13% higher grain yield on an average than the SR system primarily due to a 9% higher plant stand per unit area (Pinnamaneni et al., 2020b). These results suggest that both AFI and SFI positively impacted the CO_2 assimilation rate. The RF soybean in both seasons recorded a significantly lower photosynthesis rate under saturated light conditions. These results conform to the earlier reports of reduced photosynthesis under water-stressed conditions (Zhang et al., 2011; Yao et al., 2017a; Du et al., 2020).

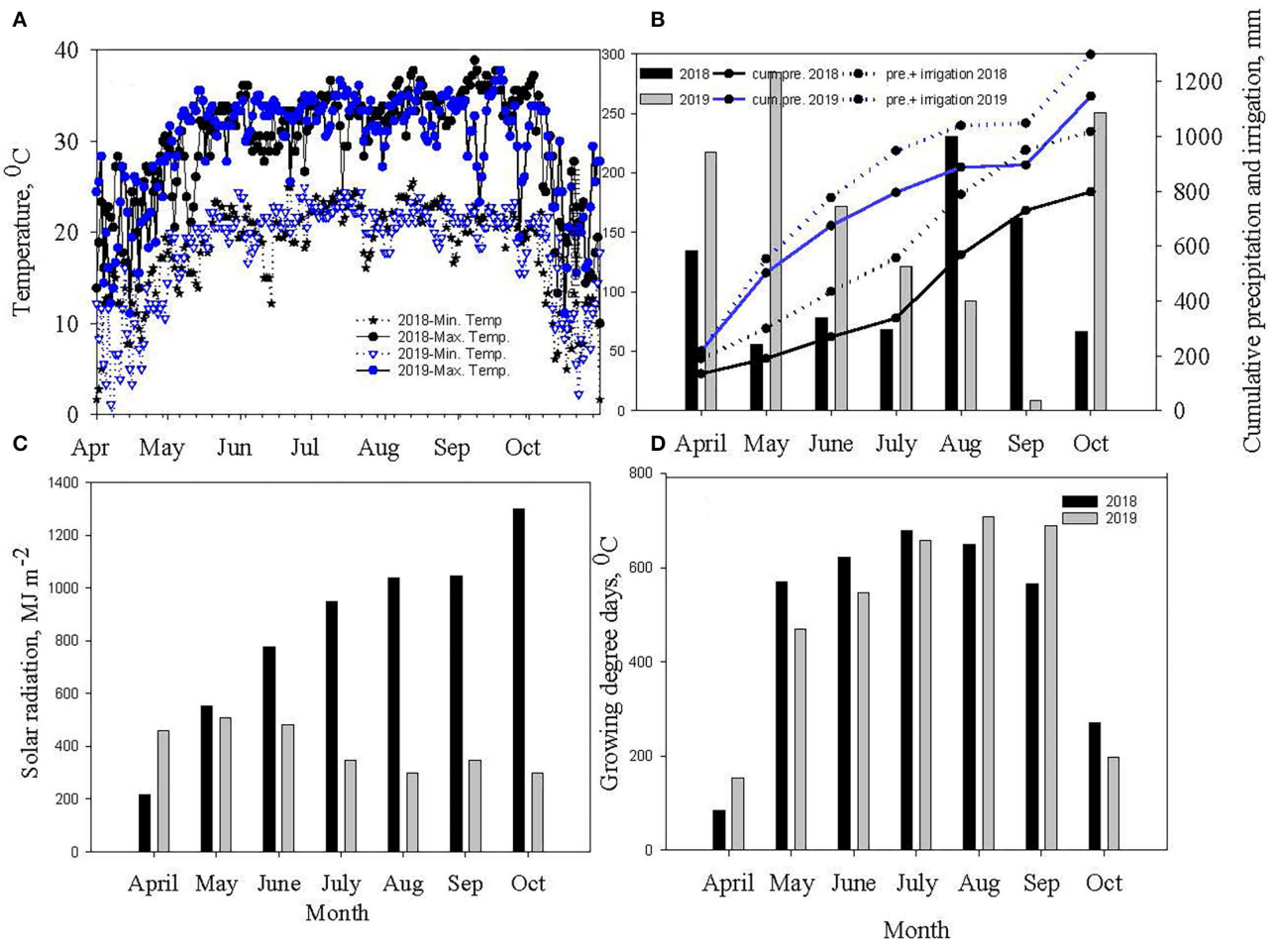

FIGURE 1 | Measured **(A)** daily air temperature and **(B)** monthly precipitation, and cumulative precipitation and irrigation **(C)** monthly solar radiation, and **(D)** monthly growing degree days (GDD) for 2018 and 2019 soybean and cotton growing seasons at Stoneville, MS.

TABLE 1 | Analysis of variance (*F* and *P* values[a]) for the effect of year (Y), planting pattern (PP), and irrigation levels (I) and their interaction on soybean photosynthesis chlorophyll fluorescence parameters.

Effect	DF	LCP		LSP		AQE		A		gs		E		ETR		ΦPSII		QP		NPQ		ΦNPQ		Rd	
		F	P	F	P	F	P	F	P	F	P	F	P	F	P	F	P	F	P	F	P	F	P	F	P
Year (Y)	1	8.65	ns	44.63	ns	2.31	*	18.44	*	9.12	*	5.08	**	43.82	**	2.41	*	1.2	*	1.25	*	1.03	ns	5.62	ns
PP	1	4.68	ns	15.67	ns	1.28	ns	2.21	ns	1.32	ns	1.66	ns	10.55	ns	1.43	*	9.82	ns	4.11	ns	0.82	ns	1.56	ns
Y*PP	1	3.58	ns	11.52	ns	2.52	ns	1.73	ns	1.49	ns	0.56	ns	1.22	ns	0.45	ns	1.09	ns	1.09	ns	1.09	ns	1.14	ns
Irrigation (I)	2	18.74	*	86.94	*	11.24	*	1.77	**	12.76	**	2.56	**	185	ns	7.93	**	0.25	**	0.47	**	1.02	**	10.25	**
Y*I	2	9.65	ns	18.57	*	4.68	ns	21.81	**	7.59	**	1.36	**	3.59	*	8.02	**	0.98	ns	0.98	ns	0.98	ns	1.42	ns
PP*I	2	2.82	ns	15.69	ns	2.44	ns	0.43	ns	0.15	ns	0.66	ns	0.71	ns	0.19	ns	0.32	ns	0.24	ns	0.61	ns	1.24	ns
PP*I*Y	2	1.44	ns	6.57	ns	2.05	ns	1.22	ns	1.01	ns	0.18	ns	0.16	ns	0.59	ns	0.11	ns	0.18	ns	0.19	ns	0.47	ns
Residuals		0.35	ns	3.68	ns	0.189	ns	501		1.662		0.252		11.14		0.033		1.992		0.032		0.014		0.029	

[a] **Significance at P ≤ 0.05; **Significance at P ≤ 0.001; ns, not significant.*

LCP, light compensation point (μmol m^{-2} s^{-1}); LSP, light saturation point (μmol m^{-2} s^{-1}); AQE, apparent quantum efficiency; Amax, Light saturated net photosynthesis (μmol CO$_2$ m^{-2} s^{-1}); gs, stomatal conductance (mmol H$_2$O m^{-2} s^{-1}); E, transpiration (mmol H$_2$O m^{-2} s^{-1}); ETR, electron transport rate (μmol m^{-2} s^{-1}); ΦPSII, quantum efficiency of primary PSII photochemistry; QP, photochemical quenching; NPQ, non-photochemical quenching; ΦNPQ, quantum efficiency of non-photochemical quenching; R$_d$, dark respiration (μmol m^{-2} s^{-1}).

The experiment was conducted in Stoneville, MS, USA, in 2018 and 2019.

Light Response Curves in Cotton

Figure 3 shows light response curves (assimilation rate vs. the photosynthetic photon flux density, PPFD) for cotton in the vegetative stage (V6) and reproductive stage (C5) for all the irrigation and planting geometry combinations for both seasons. Cotton plants exhibited a significantly higher CO_2 assimilation rate under irrigated conditions (AFI and SFI) than in a rainfed situation in both the vegetative and reproductive stages (**Figure 3**). No differences were observed among SR and TR plantings for CO_2 assimilation rate. The TR pattern recorded a 23% increased plant population per unit area over the SR system, which probably has contributed to a 15% lint yield advantage in spite of similar assimilate rates (Pinnamaneni et al., 2020a). Like soybean, the CO_2 assimilation rate plateaued under light saturation conditions at 1500 μmol $m^{-2}s^{-1}$in cotton. The results of this study echo the observations of Massacci et al. (Massacci et al., 2008) while contradicting the findings of Yao et al. (2017a). In a study from China, Yao et al. (2017a) demonstrated that photosynthesis rate is influenced by plant spacing in the following order: wide row spacing > medium row spacing > narrow row spacing. This is probably due to differences in canopy characteristics as cotton was demonstrated to change canopy architecture *vis a vis* row spacing, cultivar differences, and plant stand establishment. It has been demonstrated that narrow-row and twin-row cotton have a higher leaf area index, which contributes to higher CO_2 assimilation (Heitholt et al., 1992; Pettigrew, 2015; Pinnamaneni et al., 2020a).

Photosynthesis and Chlorophyll Fluorescence Parameters at the Reproductive Stage

Soybean

The ANOVA revealed significant differences in photosynthetic and chlorophyll fluorescence traits such as A, gs, E, LSP, LCP, AQE, ETR, ΦPSII, NPQ, QP, ΦNPQ, and R_d among the treatments (**Table 1**). The irrigation level had significant effects on A, gs, E, LSP, LCP, ETR, ΦPSII, NPQ, QP, ΦNPQ, and R_d, while year affected all the traits except $Ø_{NPQ}$ and R_d probably due to differences in weather parameters, such as solar radiation (**Figure 1C**), temperature (**Figure 1A**), and humidity (data not shown), in spite of collecting data on non-cloudy days. None of the interactions were significant except for irrigation X year. The mean values for all the traits year-wise are presented in **Table 2** as ANOVA revealed significant differences for most of the traits among the two seasons. The LCP ranged from 58 to 95 μmol m^{-2} s^{-1} in 2018 while it was between 43 and 77 μmol m^{-2} s^{-1}, and RF crops recorded 42 and 59% decreases in 2018 and 2019, respectively. Similar results were earlier reported on water-stressed soybean by Zhang et al. (2011). The LSP decreased significantly in both years by 37%. The AQE in RF crops increased by 10 and 7% in 2018 and 2019, respectively. The Amax ranged between 28.84 and 29.15 μmol CO_2 m^{-2} s^{-1} in the irrigated crop, while the range for the rainfed crop is between 25.71 and 26.01 μmol CO_2 m^{-2} s^{-1} in 2018. It ranged between 19.77 and 22.94 μmol CO_2 m^{-2} s^{-1} in the irrigated crop of the 2019 season, while it was

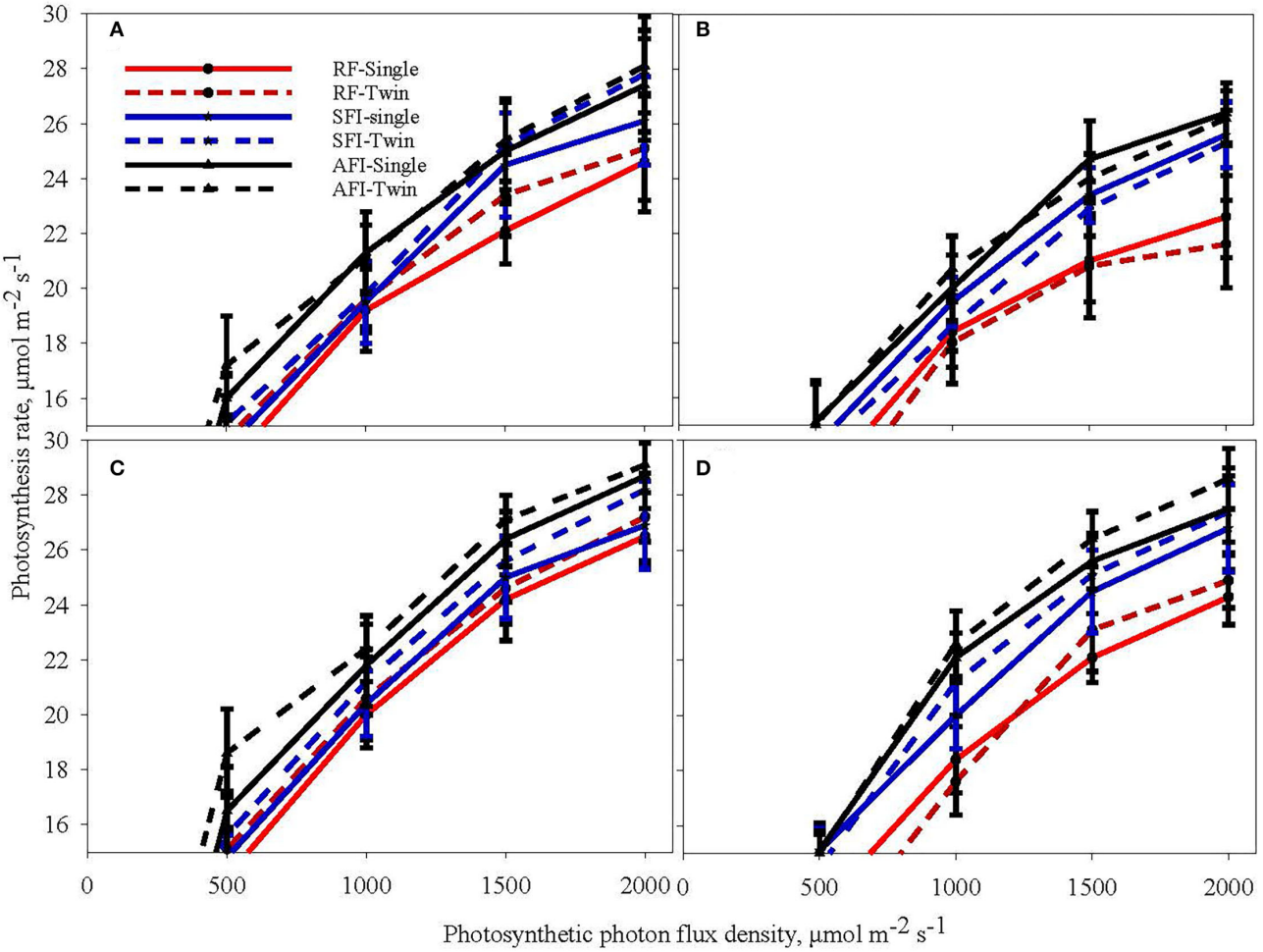

FIGURE 2 | Light response curves of soybean at the sixth leaf (V6) stage **(A,B)** and beginning seed set (R5) stage **(C,D)** during the crop growing seasons in 2018 **(A,C)** and 2019 **(B,D)** at different levels of irrigation (AFI- all furrow irrigation SFI- skipped furrow irrigation and RF-rainfed) and planting geometries (SR-single row and TR-twin row).

between 18.31 and 19.00 µmol CO_2 m^{-2} s^{-1} for the rainfed crop. On average, irrigated crops recorded about 12 and 17% higher photosynthesis in 2018 and 2019, respectively, compared to the rainfed crop. A similar decrease in photosynthesis under water-deficit conditions was reported earlier (Gilbert et al., 2011; Zhang et al., 2011; Cotrim et al., 2021). It is believed that decrease in LSP, LCP, and Amax, and increased AQE in soybeans under shading stress an acclimation strategy (Hussain et al., 2020). The stomatal conductance varied between 0.44 and 0.55 mmol H_2O m^{-2} s^{-1} in 2018, while the range was from 0.45 to 0.62 mmol H_2O m^{-2} s^{-1} in 2019. The PP did not affect this parameter in the three irrigation regimes. The gs reduced by 17% in 2018 and 24% in 2019, under RF, as stomata closure under moisture deficit conditions is widely believed to be a major physiological response to resist leaf wilting, desiccation, and plant death (Gilbert et al., 2011; Cao et al., 2017). The E levels also negatively impacted 32% and 19% in 2018 and 2019, respectively. However, the ETR was significantly higher in the rainfed crop by 6 and 9% in 2018 and 2019, respectively. These findings echo the earlier observations (Jumrani and Bhatia, 2019). Significant differences were observed in most of the chlorophyll fluorescence parameters studied among the irrigation treatments. The water deficit in RF soybean resulted in a sharp increase in ΦPSII. The rise in ΦPSII (17% in 2018 and 8% in 2019) could be attributed to the fact that moisture deficit activates the mitochondrial alternative oxidase leading to less heat dissipation, which probably delays the ΦPSII decrease (Bartoli et al., 2005). The data among AFI, SFI, and RF treatments reveals that an increase of NPQ by 34% in 2018 and 44% in 2019 under water-deficit conditions is probably a consequence of a concomitant decrease in the excitation energy trapping efficiency of PSII and the non-photochemical energy dissipation. Similarly, a significant increase of ΦNPQ in RF (30% in 2018 and 29% in 2019) was observed, revealing its role in protecting the photosynthetic apparatus from heat damage. These observations support the earlier findings where water-limited environments

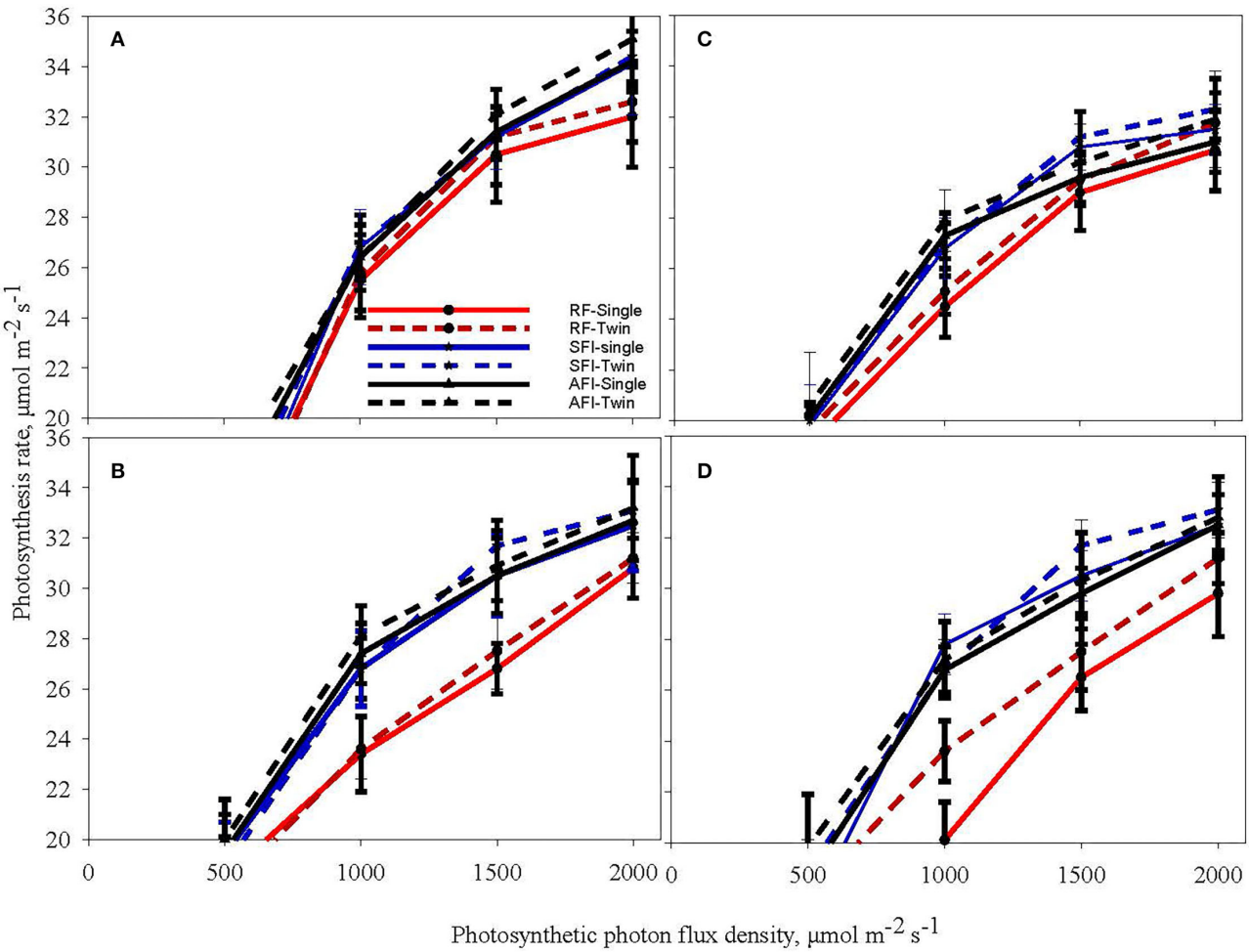

FIGURE 3 | Light response curves of cotton at the sixth leaf (V6) stage **(A,B)** and boll cracking stage-C5 **(C,D)** during the crop growing seasons in 2018 **(A,C)** and 2019 **(B,D)** at different levels of irrigation (AFI- all furrow irrigation SFI- skipped furrow irrigation and RF-rainfed) and planting geometries (SR-single row and TR-twin row).

triggered a significant increase in NPQ and ΦNPQ than that of well-irrigated crops (Zhang et al., 2011, 2016; Cao et al., 2017). In contrast, QP levels, an indicator of the fraction of open PS II reaction centers, declined to the extent of 21% and 35% in the 2018 and 2019 seasons, respectively, in the RF crop, which is believed to affect the balance between the excitation rate and the ETR. This change may have led to a reduced state of the PSII reaction centers as ETR levels increased marginally in the RF crop (6% in 2018 and 9% in 2019). These findings confirm the previously published reports (Gilbert et al., 2011; Zhang et al., 2011, 2016; Yao et al., 2017a). The Rd is another key parameter estimating CO_2 loss and mitochondrial respiration increased by 34 and 22% in 2018 and 2019, respectively, indicating its role in sustaining the photosynthesis rates under low gs. These results corroborates with the observations of Yao (Slattery et al., 2017; Yao et al., 2017a). Photosynthesis is a good indicator of plant growth and metabolism owing to its significant association with biomass production and grain yield (Gilbert et al., 2011). The current results of photosynthesis and chlorophyll fluorescence parameters corroborate well with previously published results, and the grain yield in different irrigation- planting geometry combinations were 4.8 Mg ha^{-1} in AFI under TR, 4.7 in Mg ha^{-1} in SFI under TR, 4.2 Mg ha^{-1} in AFI under SR, 4.1 Mg ha^{-1} each in RF under TR and SFI under SR, and 3.6 Mg ha^{-1} in RF under SR (Pinnamaneni et al., 2020b).

Cotton

The ANOVA revealed significant differences in photosynthetic and chlorophyll fluorescence traits such as A, gs, E, LSP, LCP, AQE, ETR, NPQ, QP, ΦNPQ, ΦPSII, and R_d among the treatments (**Table 3**). The irrigation level had significant effects on A, gs, E, LSP, LCP, AQE, ETR, NPQ, QP, ΦNPQ, and R_d, while year affected all the traits except QP, NPQ, ΦNPQ, and R_d. None of the interactions were significant except for irrigation X year. The mean values for all the traits year-wise are presented

TABLE 2 | Effect of irrigation and planting geometry on soybean and cotton photosynthetic parameters in 2018 and 2019.

2018	Soybean							Cotton						
	AFI		SFI		RF			AFI		SFI		RF		
	SR	TR	SR	TR	SR	TR	LSD	SR	TR	SR	TR	SR	TR	LSD
LCP	95a	82b	88b	78b	63c	58c	11	122a	108b	125a	112b	99c	95c	13
LSP	1879a	1842a	1865a	1784	1270c	1238c	65	2245a	2146b	2257a	2180b	1738c	1643d	62
AQE	0.057c	0.052e	0.055d	0.053e	0.061a	0.059b	0.004	0.059a	0.057b	0.057b	0.053c	0.051d	0.048e	0.004
Amax	29.15a	28.94a	28.84a	28.92a	25.71b	26.01b	1.01	33.22a	32.77a	33.26a	32.5a	29.12b	30.54b	1.45
R_d	−2.98b	−2.83b	−3.42a	−3.22a	−2.4oc	−2.25c	0.24	−3.44a	−3.25a	−3.46a	−3.22ab	−3.33a	−2.48c	0.22
gs	0.51a	0.55a	0.52a	0.5a	0.45b	0.44b	0.06	0.67a	0.68a	0.64a	0.59b	0.61a	0.55b	0.06
E	2.95a	2.86a	2.87a	2.75a	2.12b	2.2b	0.17	3.91a	3.85a	3.77a	3.45b	3.35b	2.84c	0.17
ETR	224.8b	201.4b	228.1a	234.3a	238.6a	235.4a	13.22	288.6b	291.5b	284.7b	294.3b	322.1a	324.7a	19.9
ΦPSII	0.48bc	0.46c	0.5b	0.49b	0.58a	0.59a	0.04	0.56b	0.58b	0.56b	0.57b	0.65a	0.68a	0.06
qp	0.65a	0.68a	0.65a	0.66a	0.54b	0.55b	0.04	0.78a	0.77a	0.75a	0.73a	0.62b	0.59b	0.12
NPQ	0.87b	0.85b	0.9b	0.92b	1.34a	1.34a	0.1	2.1c	1.98c	2.22c	2.34b	3.19a	3.45a	0.31
ΦNPQ	0.23b	0.20b	0.19b	0.21b	0.31a	0.30a	0.07	0.15b	0.16b	0.16b	0.18b	0.29a	0.27a	0.04
2019	**SR**	**TR**	**SR**	**TR**	**SR**	**TR**	**LSD**	**SR**	**TR**	**SR**	**TR**	**SR**	**TR**	**LSD**
LCP	77	67	72	64	45	43	5	125	112	136	118	106	98	11
LSP	1789a	1721b	1634c	1687bc	1338d	1352d	52	2324b	2411a	2287b	2316b	1946c	1958c	54
AQE	0.059a	0.057a	0.053a	0.051b	0.06a	0.058a	0.008	0.054a	0.051a	0.053a	0.055a	0.049a	0.05a	0.009
Amax	21.67	22.94	19.77	22.71	19	18.31	1.3	34.32a	35.01a	34.15a	34.49a	32.13b	32.55b	1.85
R_d	−3.11a	−3.34a	−2.72b	−3.26a	−2.45b	−2.65b	0.29	−3.48a	−3.4a	−3.36a	−3.34a	−2.74b	−2.85b	0.28
gs	0.56b	0.59a	0.49c	0.62a	0.46c	0.45c	0.03	0.74a	0.76a	0.71a	0.64b	0.6b	0.58b	0.05
E	3.78a	3.75a	3.04b	3.85a	3.01b	3.06b	0.13	4.25a	4.32a	4.35a	4.45a	3.54b	3.58b	0.34
ETR	196.8bc	186.9c	218.6a	202.3ab	214.6a	225.6a	19.21	254.6bc	260.5b	280.5b	276.5b	302.1a	297.6a	24.5
ΦPSII	0.43a	0.42a	0.43a	0.44a	0.49a	0.48a	0.09	0.52b	0.53b	0.55ab	0.52b	0.61a	0.63a	0.1
QP	0.74a	0.76a	0.69b	0.72a	0.56c	0.52c	0.07	0.82a	0.81a	0.83a	0.80a	0.65b	0.62b	0.11
NPQ	0.74b	0.77b	0.81b	0.72b	1.28a	1.42a	0.13	2.40b	2.26b	2.34b	2.48b	2.97a	3.07a	0.24
ΦNPQ	0.22b	0.25b	0.21b	0.24b	0.33a	0.32a	0.08	0.12b	0.12b	0.13b	0.14b	0.24b	0.27b	0.05

LSD, Least Significant Difference test; significant at $P \leq 0.05$. Means followed by the same letter within each row and crop are not significantly different. AFI, All furrow irrigation; SFI, Skip furrow irrigation; RF, rainfed; LCP, light compensation point (μmol m^{-2} s^{-1}); LSP, light saturation point (μmol m^{-2} s^{-1}); AQE, apparent quantum efficiency; Amax, maximum assimilation (μmol CO_2 m^{-2} s^{-1}); gs, stomatal conductance (mmol H_2O m^{-2} s^{-1}); E, transpiration (mmol H_2O m^{-2} s^{-1}); ETR, electron transport rate (μmol m^{-2} s^{-1}); ΦPSII, quantum efficiency of primary PSII photochemistry; QP, photochemical quenching; NPQ, non-photochemical quenching; ΦNPQ, quantum efficiency of non-photochemical quenching; R_d, dark respiration (μmol m^{-2} s^{-1}).
The experiment was conducted in Stoneville, MS.

TABLE 3 | Analysis of variance (*F* and *P* values[a]) for the effect of year (Y), planting pattern (PP), and irrigation levels (I) and their interaction on cotton photosynthesis and chlorophyll fluorescence parameters.

Effect	DF	LCP		LSP		AQE		A		gs		E		ETR		ΦPSII		QP		NPQ		ΦNPQ		R_d	
		F	*P*	*F*	*P*	*F*	*P*	*F*	*P*	*F*	*P*	*F*	*P*	*F*	*P*	*F*	*P*	*F*	*P*	*F*	*P*	*F*	*P*	*F*	*P*
Year (Y)	1	13.56	ns	31.45	ns	1.25	*	236	**	22.82	**	15.08	**	65.25	**	8.46	**	5.32	*	2.62	*	1.68	*	2.54	*
PP	1	7.65	ns	12.65	ns	0.96	ns	8.69	ns	20.12	ns	5.63	*	14.54	ns	6.48	ns	3.42	ns	1.64	ns	1.44	ns	9.82	ns
Y*PP	1	4.21	ns	14.22	ns	1.22	ns	2.82	ns	2.49	ns	2.67	ns	6.36	ns	1.49	ns	1.33	ns	1.09	ns	1.09	ns	1.09	ns
Irrigation (I)	2	22.65	*	76.49	*	8.87	*	168	**	105.64	**	185	**	256	**	11.93	**	12.21	**	9.67	**	11.25	**	21.44	*
Y*I	2	11.57	ns	14.35	*	3.54	ns	32.68	ns	11.57	ns	18.36	ns	44.56	*	9.32	*	1.98	ns	0.67	ns	1.02	ns	0.74	ns
PP*I	2	3.42	ns	13.48	ns	1.86	ns	2.46	ns	2.74	*	14.66	**	12.57	ns	8.19	ns	0.62	ns	0.24	ns	0.31	ns	0.27	ns
PP*I*Y	2	1.68	ns	5.98	ns	1.55	ns	1.69	ns	1.65	ns	4.52	ns	8.53	ns	0.55	ns	0.18	ns	0.26	ns	0.14	ns	0.13	ns
Residuals		1.24	ns	4.96	ns	0.28	ns	368		1.245		0.324		0.214		0.033		1.223		0.042		0.073		0.013	

[a]**Significance at $P \leq 0.05$; **Significance at $P \leq 0.001$; ns, not significant.*

LCP, light compensation point (μmol m^{-2} s^{-1}); LSP, light saturation point (μmol m^{-2} s^{-1}); AQE, apparent quantum efficiency; Amax, Light saturated net photosynthesis (μmol CO_2 m^{-2} s^{-1}); gs, stomatal conductance (mmol H_2O m^{-2} s^{-1}); E, transpiration (mmol H_2O m^{-2} s^{-1}); ETR, electron transport rate (μmol m^{-2} s^{-1}); ΦPSII, quantum efficiency of primary PSII photochemistry; QP, photochemical quenching; NPQ, non-photochemical quenching; ΦNPQ, quantum efficiency of non-photochemical quenching; R_d, dark respiration (μmol m^{-2} s^{-1}).

The experiment was conducted in Stoneville, MS, USA, in 2018 and 2019.

in **Table 2** as ANOVA revealed significant differences for most of the traits among the two seasons. The LCP ranged from 95 to 125 μmol m^{-2} s^{-1} in 2018 and between 98 and 136 μmol m^{-2} s^{-1} in 2019. The RF crop recorded a 20% decrease in both seasons for LCP. A decrease of 38% in water-stressed soybean (Zhang et al., 2011) and between 41% and 72% decrease in sorghum under drought (Zhang et al., 2019) was earlier reported. However, the decrease in RF crop for LSP was 31% and 25% in 2018 and 2019, respectively. The AQE ranged from 0.048 to 0.059 in 2018 while it varied between 0.049 and 0.055 in 2019. The RF crop recorded a 14% and 11% decrease compared to irrigated crops for AQE in the 2018 and 2019 seasons, respectively. Similar levels of decrease in AQE in drought-stressed cotton were observed in a drip-irrigated study in China (Zhang et al., 2011). The Amax ranged between 32.77 and 33.26 μmol CO_2 m^{-2} s^{-1} in the irrigated crop while the range for the RF crop is between 29.12 and 30.54 μmol CO_2 m^{-2} s^{-1} in 2018. The Amax ranged between 34.15 and 35.01 μmol CO_2 m^{-2} s^{-1} in the irrigated crop of the 2019 season, while the RF crop ranged between 32.13 and 32.55 μmol CO_2 m^{-2} s^{-1}. On average, irrigated crops recorded about 9% and 6% higher photosynthesis in 2018 and 2019, respectively, compared to the RF crop. A similar decrease in photosynthesis under RF conditions was reported earlier (Heitholt et al., 1992; Massacci et al., 2008; Zhang et al., 2011). The stomatal conductance varied between 0.55 and 0.68 mmol H_2O m^{-2} s^{-1} in 2018, while the range was 0.58–0.76 mmol H_2O m^{-2} s^{-1} in 2019. The PP did not affect this parameter in the three irrigation regimes. The gs reduced by 12% in 2018 and 21% in 2019, a key parameter restricting photosynthesis under RF conditions (Massacci et al., 2008; Zhang et al., 2011; Araújo et al., 2019). Similarly, the water losses through E were reduced by 17% in 2018 and 22% in the 2019 seasons, respectively. However, the ETR under RF conditions was higher by 10% and 11% in 2018 and 2019, respectively. Higher ETR is believed to be due to the enhanced operating efficiency of PSII rather than a decrease in the photosynthesis rate in RF crops. This corroborates that ΦPSII increased by 16 and 14% in the 2018 and 2019 seasons, respectively. A similar study conducted in MS reported that leaves of dryland cotton have higher ΦPSII than that of the well-irrigated crop (Pettigrew, 2004). However, other chlorophyll fluorescence parameters, such as NPQ and ΦNPQ, have been recorded significantly higher in RF crops *vis a vis* an irrigated crop. For example, NPQ was higher by 35 and 21% in 2018 and 2019, respectively, while ØNPQ recorded 42 and 50% enhanced levels in 2018 and 2019, respectively. The greater non-photochemical quenching in RF crops is expected to limit energy dissipation, thereby reducing heat damage to the photosynthetic apparatus (Massacci et al., 2008; Gilbert et al., 2011; Slattery et al., 2017). However, the QP reduced in RF crops by 25% in 2018 and 28% in 2019 is probably believed to be a mechanism for reducing electron pressure and increasing open PSII reaction center efficiency by altering redox potential (Massacci et al., 2008; Araújo et al., 2019; Poorter et al., 2022). In contrast, the carbon losses increased by enhanced dark respiration in rainfed crops to the extent of 13% in 2018 and 22% in 2019, thus affecting the cotton lint yields. It was reported earlier by Pinnamaneni et al. (2020a) that the average lint yields in the irrigation and planting

geometry combinations were 1,779 kg ha^{-1} in AFI under SR; 2,029 kg ha^{-1} in AFI under TR; 1,803 kg ha^{-1} in SFI under SR; 2,082 in kg ha^{-1} in SFI under TR; 1,573 kg ha^{-1} in RF under SR; and 1,788 kg ha^{-1} in RF under TR.

Comparison Between Soybean and Cotton Photosynthetic Parameters

Although both soybean and cotton are C3 crops, similar trends for different photosynthetic and chlorophyll fluorescence parameters were observed. Still, the extent of differences in regulatory photosynthetic traits and their impact on crop productivity appears to be different. The LCP reduction in soybean was 50% while it was only 20% in cotton under RF conditions. This is probably attributed to paraheliotropic leaf movement in soybean and diaheliotropic movement in cotton under abiotic stress, corroborating with previous reports (Zhang et al., 2011; Hussain et al., 2020). About, 12 and 17% decrease in the photosynthetic rate was observed in RF soybean while the decrease is limited to 9% and 6% in RF cotton during the 2018 and 2019 seasons, respectively. The decrease in photosynthetic rate in soybean is significantly higher than that of cotton under RF compared to irrigated (AFI and SFI) crops. However, a similar decrease in gs and E was observed in the RF condition in both crops. At the same time, the increase in ETR was sharp in RF cotton compared to that of RF soybean (average increase of 10.5% in cotton while 7% in soybean).

Similarly, the NPQ and ΦNPQ, which play a critical role in protecting PSI and PSII reaction centers by dissipating excess energy, recorded an average increase of 39% and 46%, respectively, in RF soybean. In comparison, a 28 and 30% rise was observed in RF cotton for NPQ and ΦNPQ, respectively. These findings are in confirmation with that of earlier reports (Kitao and Lei, 2007; Massacci et al., 2008) but differ from the observations on RF cotton response wherein the quantum yield of PSII was increased, and the regulated non-photochemical energy dissipation was decreased under a water-limited environment (Zhang et al., 2011). This discrepancy could probably be due to the differences in the degree of soil moisture stress and cultivar response. Further, it can be noted that plants dissipate excess solar radiation by triggering NPQ to maintain optimal rates of photosynthesis and provide the plant against oxidative damage (Mishanin et al., 2016). Another study on pot-grown cotton revealed that the PSII quantum yield of photochemistry may or may not be affected by drought in the vegetative stage, subject to drought intensity (Ennahli and Earl, 2005). However, in the case of QP and ΦPSII, there appears to be a similar impact on both RF crops compared to the irrigated crop. The above observations in regulating photosynthetic and chlorophyll fluorescence parameters under The average decrease in soybean grain yield was 16%, while the cotton lint was reduced by 14% (Pinnamaneni et al., 2020a,b).

CONCLUSION

It appears that the photosynthetic and chlorophyll fluorescence parameters under diverse irrigation regimes in both soybean and cotton were not affected by alterations in planting geometry, despite the reported higher yields in the TR system. The decrease in LSP, LCP, and Amax in RF crops appears to be relatively lower in cotton than that of soybean, indicating either lower water requirement or better tolerance to moisture deficit. However, soybean recorded decreased AQE while cotton exhibited higher AQE under RF conditions. The results of this study indicated preferential use of non-photochemical energy dissipation in soybean while cotton uses both photochemical and non-photochemical energy dissipation to protect PSI and PSII centers and ETR, although they fall under the C3 species. Detailed studies with diverse moisture stress intensities coupled with physiological and anatomical parameters during multiple crop growth stages will help further delineate the mechanistic role of photosynthetic and chlorophyll fluorescence pathways in determining soybean and cotton productivities.

DATA AVAILABILITY STATEMENT

The raw data supporting the conclusions of this article will be made available by the authors, without undue reservation.

AUTHOR CONTRIBUTIONS

SP: conceptualization, experiment design, data collection, project administration, analysis, writing the manuscript, and visualization. SA: conceptualization, project administration, manuscript review and editing, resources, and visualization. KR: conceptualization, project administration, manuscript review, editing, and resources. All authors contributed to the article and approved the submitted version.

FUNDING

This work was supported by the U. S. Department of Agriculture, Agriculture Research Service through project number 6066-22000-089-000D.

ACKNOWLEDGMENTS

The authors appreciate the technical assistance provided by Mr. Russell Coleman, Biological Science Research Technician. CPSRU, Stoneville, MS.

REFERENCES

Anapalli, S., Fisher, D., Reddy, K., Pettigrew, W., Sui, R., et al. (2016). Vulnerabilities and adapting irrigated and rainfed cotton to climate change in the lower Mississippi delta region. *Climate* 4, 55. doi: 10.3390/cli4040055

Araújo, W. P., Pereira, J. R., Zonta, J. H., Guerra, HOC., Cordão, M. A., et al. (2019). Gas exchange in upland cotton cultivars under water deficit strategies. *Afr. J. Agric. Res.* 14, 986–998. doi: 10.5897/AJAR2019.13904

Baker, N. R. (2008). Chlorophyll fluorescence: a probe of photosynthesis *in vivo*. *Annu. Rev. Plant Biol.* 59, 89–113. doi: 10.1146/annurev.arplant.59.032607.092759

Bartoli, C. G., Gomez, F., Gergoff, G., Guiamét, J. J., and Puntarulo, S. (2005). Up-regulation of the mitochondrial alternative oxidase pathway enhances photosynthetic electron transport under drought conditions. *J. Exp. Bot.* 56, 1269–1276. doi: 10.1093/jxb/eri111

Bellaloui, N., McClure, A. M., Mengistu, A., and Abbas, H. K. (2020). The influence of agricultural practices, the environment, and cultivar differences on soybean seed protein, oil, sugars, amino acids. *Plants* 9, 378. doi: 10.3390/plants9030378

Bruns, H. A. (2011). Comparisons of single-row and twin-row soybean production in the Mid-South. *Agron. J* 103, 702–708. doi: 10.2134/agronj2010.0475

Cao, Z., Stowers, C., Rossi, L., Zhang, W., Lombardini, L., and Ma, X. (2017). Physiological effects of cerium oxide nanoparticles on the photosynthesis and water use efficiency of soybean (Glycine max (L.) Merr.). *Environ. Sci. Nanosci. Nano* 4, 1086–1094. doi: 10.1039/C7EN00015D

Cotrim, M. F., Gava, R, Campos, C. N. S., de David, C. H. O., de Reis, I. A., Teodoro, L. P. R., et al. (2021). Physiological performance of soybean genotypes grown under irrigated and rainfed conditions. *J. Agron. Crop Sci.* 207, 34–43. doi: 10.1111/jac.12448

Du, Y., Zhao, Q., Chen, L., Yao, X., Zhang, H., Wu, J., et al. (2020). Effect of drought stress during soybean R2–R6 growth stages on sucrose metabolism in leaf and seed. *Int. J. Mol. Sci.* 21, 618. doi: 10.3390/ijms21020618

Ehleringer, J. R., and Forseth, I. N. (1989). Diurnal leaf movements and productivity in canopies. *Plant Canopies* 31, 129–142. doi: 10.1017/CBO9780511752308.008

Ennahli, S., and Earl, H. J. (2005). Physiological limitations to photosynthetic carbon assimilation in cotton under water stress. *Crop Sci.* 45, 2374–2382. doi: 10.2135/cropsci2005.0147

Genty, B., Briantais, J. M., and Baker, N. R. (1989). The relationship between the quantum yield of photosynthetic electron transport and quenching of chlorophyll fluorescence. *Biochim. Biophys. Acta* 990, 87–92. doi: 10.1016/S0304-4165(89)80016-9

Gilbert, M. E., Zwieniecki, M. A., and Holbrook, N. M. (2011). Independent variation in photosynthetic capacity and stomatal conductance leads to differences in intrinsic water use efficiency in 11 soybean genotypes before and during mild drought. *J. Exp. Bot.* 62, 2875–2887. doi: 10.1093/jxb/erq461

Grichar, W. J. (2007). Row spacing, plant populations, and cultivar effects on soybean production along the texas gulf coast. *Crop Manag.* 6, 1–6. doi: 10.1094/CM-2007-0615-01-RS

Heitholt, J. J., Pettigrew, W. T., and Meredith, W. R. (1992). Light interception and lint yield of narrow-row cotton. *Crop Sci.* 32, 728–733. doi: 10.2135/cropsci1992.0011183X003200030030x

Hirata, M., Ishii, R., Kumura, A., and Murata, Y. (1983). Photoinhibition of Photosynthesis in Soybean Leaves: II. Leaf orientation-adjusting movement as a possible avoiding mechanism of photoinhibition. *Jpn. J. Crop Sci.* 52, 319–322. doi: 10.1626/jcs.52.319

Hussain, S., Pang, T., Iqbal, N., Shafiq, I., Skalicky, M., et al. (2020). Acclimation strategy and plasticity of different soybean genotypes in intercropping. *Funct. Plant Biol.* 47, 592–610. doi: 10.1071/FP19161

Inamullah and Isoda, A. (2005). Adaptive responses of soybean and cotton to water stress II. Changes in CO2 assimilation rate, chlorophyll fluorescence and photochemical reflectance index in relation to leaf temperature. *Plant Prod. Sci.* 8, 131–138. doi: 10.1626/pps.8.131

Isoda, A. (2010). Effects of water stress on leaf temperature and chlorophyll fluorescence parameters in cotton and peanut. *Plant Prod. Sci.* 13, 269–278. doi: 10.1626/pps.13.269

Jumrani, K., and Bhatia, V. S. (2019). Identification of drought tolerant genotypes using physiological traits in soybean. *Physiol. Mol. Biol. Plants* 25, 697–711. doi: 10.1007/s12298-019-00665-5

Kitao, M., and Lei, T. T. (2007). Circumvention of over-excitation of PSII by maintaining electron transport rate in leaves of four cotton genotypes developed under long-term drought. *Plant Biol.* 9, 69–76. doi: 10.1055/s-2006-924280

Kramer, D. M., Johnson, G., Kiirats, O., and Edwards, G. E. (2004). New fluorescence parameters for the determination of QA redox state and excitation energy fluxes. *Photosynth. Res.* 79, 209–218. doi: 10.1023/B:PRES.0000015391.99477.0d

Massacci, A., Nabiev, S. M., Pietrosanti, L., Nematov, S. K., Chernikova, T. N., et al. (2008). Response of the photosynthetic apparatus of cotton (Gossypium hirsutum) to the onset of drought stress under field conditions studied by gas-exchange analysis and chlorophyll fluorescence imaging. *Plant Physiol. Biochem.* 46, 189–195. doi: 10.1016/j.plaphy.2007.10.006

Mishanin, V., Trubitsin, B., Benkov, M. A, Minin, A. A, and Tikhonov, A. N. (2016). Light acclimation of shade-tolerant and light-resistant Tradescantia species: induction of chlorophyll a fluorescence and P700 photooxidation, expression of PsbS and Lhcb1 proteins. *Photosynth. Res.* 130, 275–291. doi: 10.1007/s11120-016-0252-z

Oxborough, K., and Baker, N. R. (1997). Resolving chlorophyll a fluorescence images of photosynthetic efficiency into photochemical and non-photochemical components–calculation of qP and Fv-/Fm-; without measuring Fo. *Photosynth. Res.* 54, 135–142. doi: 10.1023/A:1005936823310

Pettigrew, W. T. (2004). Physiological consequences of moisture deficit stress in cotton. *Crop Sci.* 44, 1265–1272. doi: 10.2135/cropsci2004.1265

Pettigrew, W. T. (2015). Twin-row production of cotton genotypes varying in leaf shape. *J. Cotton Sci.* 19, 319–327.

Pinnamaneni, S., Anapalli, S. S., Fisher, D. K., and Reddy, K. N. (2020a). Irrigation and planting geometry effects on cotton (Gossypium hirsutum L.) Yield and water use. *J. Cotton Sci.* 24, 87–96.

Pinnamaneni, S. R., Anapalli, S. S., Reddy, K. N., Fisher, D. K., and Quintana-Ashwell, N. E. (2020b). Assessing irrigation water use efficiency and economy of twin-row soybean in the Mississippi Delta. *Agron. J.* 112, 4219–4231. doi: 10.1002/agj2.20321

Pinnamaneni, S. R., Anapalli, S. S., Sui, R., Bellaloui, N., and Reddy, K. N. (2021). Effects of irrigation and planting geometry on cotton (Gossypium hirsutum L.) fiber quality and seed composition. *J. Cotton Res.* 4, 2. doi: 10.1186/s42397-020-00078-w

Plumblee, M. T., Dodds, D. M., Krutz, L. J., Catchot, A. L., Irby, J., and Jenkins, J. N. (2019). Determining the optimum irrigation schedule in furrow irrigated cotton using soil moisture sensors. *Crop Forage Turfgrass Manag.* 5, 1–6. doi: 10.2134/cftm2018.06.0047

Poorter, H., Knopf, O., Wright, I. J., Temme, A. A., Hogewoning, S. W., et al. (2022). A meta-analysis of responses of C3 plants to atmospheric CO2: dose–response curves for 85 traits ranging from the molecular to the whole-plant level. *New Phytol.* 233, 1560–1596. doi: 10.1111/nph.17802

Reddy, K. N., Burke, I. C., Boykin, J. C., and Ray Williford, J. (2009). Narrow-row cotton production under irrigated and non-irrigated environment: Plant population and lint yield. *J. Cotton Sci.* 13, 48–55.

Rosenqvist, E., and van Kooten, O. (2003). *Chlorophyll fluorescence: A General Description and Nomenclature*. Practical applications of chlorophyll fluorescence in plant biology. Springer. *p.* 31–77. doi: 10.1007/978-1-4615-0415-3_2

Singh, S. K., and Reddy, V. R. (2018). Co-regulation of photosynthetic processes under potassium deficiency across CO 2 levels in soybean: mechanisms of limitations and adaptations. *Photosynth. Res.* 137, 183–200. doi: 10.1007/s11120-018-0490-3

Slattery, R. A., Vanloocke, A., Bernacchi, C. J., Zhu, X. G., and Ort, D. R. (2017). Photosynthesis, light use efficiency, and yield of reduced-chlorophyll soybean mutants in field conditions. *Front. Plant Sci.* 8, 549. doi: 10.3389/fpls.2017.00549

Stephenson, D. O., Barber, L. T., and Bourland, F. M. (2011). Agronomy and soils: Effect of twin-row planting pattern and plant density on cotton growth, yield, fiber quality. *J. Cotton Sci.* 15, 243–250.

Tang, Q., Feng, G., Fisher, D., Zhang, H., Ouyang, Y., et al. (2018). Rain water deficit and irrigation demand of major row crops in the Mississippi Delta. *Trans ASABE* 61, 927–935. doi: 10.13031/trans.12397

USDA-NASS. (2020). *Mississippi Cotton County Estimates*. Available online at: https://www.nass.usda.gov/Statistics_by_State/Mississippi/Publications/County_Estimates/2018/18_MS_cotton_all.pdf (accessed January 20, 2022).

Yao, H., Zhang, Y., Yi, X., Zuo, W., Lei, Z., Sui, L., et al. (2017a). Characters in light-response curves of canopy photosynthetic use efficiency of light and N in responses to plant density in field-grown cotton. *Field Crops Res.* 203, 192–200. doi: 10.1016/j.fcr.2016.12.018

Yao, X., Zhou, H., Zhu, Q., Li, C., Zhang, H., Wu, J. J., et al. (2017b). Photosynthetic response of soybean leaf to wide light-fluctuation in maize-soybean intercropping system. *Front. Plant Sci.* 8, 1695. doi: 10.3389/fpls.2017.01695

Ye, Z. P. (2007). A new model for relationship between irradiance and the rate of photosynthesis in Oryza sativa. *Photosynthetica* 45, 637–640. doi: 10.1007/s11099-007-0110-5

Ye, Z. P., Ling, Y., Yu, Q., Duan, H. L., Kang, H. J., et al. (2020). Quantifying light response of leaf-scale water-use efficiency and its interrelationships with photosynthesis and stomatal conductance in C3 and C4 species. *Front. Plant Sci.* 11, 374. doi: 10.3389/fpls.2020.00374

Zhang, F., Zhu, K., Wang, Y. Q., Zhang, Z. P, Lu, F., et al. (2019). Changes in photosynthetic and chlorophyll fluorescence characteristics of sorghum under drought and waterlogging stress. *Photosynthetica* 57, 1156–1164. doi: 10.32615/ps.2019.136

Zhang, J., Liu, J., Yang, C., Du, S., and Yang, W. (2016). Photosynthetic performance of soybean plants to water deficit under high and low light intensity. *South Afr. J. Bot.* 105, 279–287. doi: 10.1016/j.sajb.2016.04.011

Zhang, Y. L., Hu, Y. Y., Luo, H. H., Chow, W. S., and Zhang, W. F. (2011). Two distinct strategies of cotton and soybean differing in leaf movement to perform photosynthesis under drought in the field. *Funct. Plant Biol.* 38, 567–575. doi: 10.1071/FP11065

Author Disclaimer: Trade names are necessary to report factually on available data; however, the USDA neither guarantees nor warrants the standard of the product or service. The use of the name by USDA implies no approval of the product or service to exclude others that may also be suitable.

Conflict of Interest: The authors declare that the research was conducted in the absence of any commercial or financial relationships that could be construed as a potential conflict of interest.

Publisher's Note: All claims expressed in this article are solely those of the authors and do not necessarily represent those of their affiliated organizations, or those of the publisher, the editors and the reviewers. Any product that may be evaluated in this article, or claim that may be made by its manufacturer, is not guaranteed or endorsed by the publisher.

frontiers | Frontiers in Plant Science

TYPE Original Research
PUBLISHED 20 September 2022
DOI 10.3389/fpls.2022.987606

OPEN ACCESS

EDITED BY
Pasala Ratnakumar,
Indian Institute of Oilseeds Research (ICAR), India

REVIEWED BY
Prachi Pandey,
National Institute of Plant Genome Research (NIPGR), India
Cun Wang,
Northwest A&F University, China

*CORRESPONDENCE
Guoning Qi
gnqi@zafu.edu.cn
Jamshaid Hussain
jamshaidhussain@cuiatd.edu.pk

†These authors have contributed equally to this work and share first authorship

SPECIALTY SECTION
This article was submitted to Plant Abiotic Stress, a section of the journal Frontiers in Plant Science

RECEIVED 06 July 2022
ACCEPTED 29 August 2022
PUBLISHED 20 September 2022

CITATION
Wang Z, Ouyang Y, Ren H, Wang S, Xu D, Xin Y, Hussain J and Qi G (2022) Transcriptome profiling of Arabidopsis *slac1-3* mutant reveals compensatory alterations in gene expression underlying defective stomatal closure. *Front. Plant Sci.* 13:987606. doi: 10.3389/fpls.2022.987606

Transcriptome profiling of Arabidopsis *slac1-3* mutant reveals compensatory alterations in gene expression underlying defective stomatal closure

Zheng Wang[1†], Yinghui Ouyang[1†], Huimin Ren[1†], Shuo Wang[1], Dandan Xu[1], Yirui Xin[1], Jamshaid Hussain[2*] and Guoning Qi[1*]

[1]State Key Laboratory of Subtropical Silviculture, School of Forestry and Biotechnology, Zhejiang A&F University, Hangzhou, Zhejiang, China, [2]Department of Biotechnology, COMSATS University Islamabad, Abbottabad, Pakistan

Plants adjust their stomatal aperture for regulating CO_2 uptake and transpiration. S-type anion channel SLAC1 (slow anion channel-associated 1) is required for stomatal closure in response to various stimuli such as abscisic acid, CO_2, and light/dark transitions etc. Arabidopsis *slac1* mutants exhibited defects in stimulus-induced stomatal closure, reduced sensitivity to darkness, and faster water loss from detached leaves. The global transcriptomic response of a plant with defective stimuli-induced stomatal closure (particularly because of defects in SLAC1) remains to be explored. In the current research we attempted to address the same biological question by comparing the global transcriptomic changes in Arabidopsis *slac1-3* mutant and wild-type (WT) under dark, and dehydration stress, using RNA-sequencing. Abscisic acid (ABA)- and dark-induced stomatal closure was defective in Arabidopsis *slac1-3* mutants, consequently the mutants had cooler leaf temperature than WT. Next, we determined the transcriptomic response of the *slac1-3* mutant and WT under dark and dehydration stress. Under dehydration stress, the molecular response of *slac1-3* mutant was clearly distinct from WT; the number of differentially expressed genes (DEGs) was significantly higher in mutant than WT. Dehydration induced DEGs in mutant were related to hormone signaling pathways, and biotic and abiotic stress response. Although, overall number of DEGs in both genotypes was not different under dark, however, the expression pattern was very much distinct; whereas majority of DEGs in WT were found to be downregulated, in *slac1-3* majority were upregulated under dark. Further, a set 262 DEGs was identified with opposite expression pattern between WT and mutant under light–darkness transition. Amongst these, DEGs belonging to stress hormone pathways, and biotic and abiotic stress response were over-represented. To sum up, we have reported gene expression reprogramming underlying *slac1-3* mutation and resultantly defective stomatal closure in Arabidopsis. Moreover, the induction of biotic and abiotic response in mutant under dehydration and darkness

could be suggestive of the role of stomata as a switch in triggering these responses. To summarize, the data presented here provides useful insights into the gene expression reprogramming underlying *slac1-3* mutation and resultant defects in stomatal closure.

KEYWORDS

drought stress, abscisic acid, stomata, anion channel, transcriptome

Introduction

Stomatal pores are surrounded by a pair of guard cells. The emergence of latter is considered as a major landmark in the land plants' evolution and adaptation to harsh environmental conditions (Umezawa et al., 2010). Stomata open and close in response to diverse stimuli and are involved in efficiently taking up CO_2 for photosynthesis and regulating water loss through transpiration (Jezek and Blatt, 2017).

The opening and closing of the stomatal aperture are brought about by changes in turgor pressure through ion and water channel proteins present in the guard cell plasma membrane (Schroeder et al., 2001; Kim et al., 2010; Engineer et al., 2016). Stomatal movements are tightly regulated under the influence of environmental stimuli and endogenous factors, such as light, water status, carbon dioxide (CO_2), ABA, calcium (Ca^{2+}), and reactive oxygen species (ROS; Schroeder et al., 2001; Young et al., 2006).

It is now well established that light-induced stomatal opening is regulated by plasma membrane inward-rectifying K^+ channels while stomatal closure involves outward K^+ channels and anion channels. When plants are challenged with stressful conditions, the activation of guard cell anion channels becomes a key step in inducing stomatal closure. Different signaling components including second messengers, phospholipases, protein kinases, and phosphatases are involved in regulation of stomatal movements. Moreover, stomatal opening and closure are also governed by changes in gene expression.

Abscisic acid- and drought stress induce anion efflux through anion channels, causing membrane depolarization in guard cells. One of the main guard cell anion channels SLAC1 (slow anion channel-associated 1) was identified as an S-type anion channel during the screenings for ozone-sensitive and CO_2 insensitive mutants (Negi et al., 2008; Vahisalu et al., 2008). SLAC1 is required for stomatal closure in response to various stimuli such as abscisic acid, CO_2, light/dark transitions, ozone, Ca^{2+} ions, humidity change, nitric oxide, and hydrogen peroxide. Localized in plasma membrane of guard cells, SLAC1 constitutes a trimer in which each subunit forms a channel pore independently (Chen et al., 2010). SLAC1 is a highly conserved S-type anion channel in diverse plant species. SLAC1 homologues have been identified in various species ranging from green algae to higher plants (Hedrich and Geiger, 2017; Ren et al., 2021). Rice *slac1* mutants showed higher stomatal conductance and photosynthetic rate under well-watered conditions (Kusumi et al., 2012). In maize, ZmSLAC1 is involved in stomatal closure mainly by mediating the nitrate efflux (Qi et al., 2018).GhSLAC1 is an essential element for stomatal closure in response to drought in cotton (Ren et al., 2021).In Arabidopsis, five members of SLAC/SLAH family have been reported. Among those, AtSLAC1 and AtSLAH3 are responsible for chloride and nitrate efflux across guard cell plasma membrane (Negi et al., 2008; Vahisalu et al., 2008; Meyer et al., 2010; Qi et al., 2018).

Drought stress triggers increase in ABA which is an important stimulus for SLAC1 activation. After being bound by ABA, PYR/PYL/RCAR receptors interact with PP2C phosphatases and, thereby, previously inhibited Open stomata 1 (OST1) kinase is released which, through phosphorylation, activates SLAC1 channel (Murata et al., 2001; Mustilli et al., 2002; Yoshida et al., 2006; Geiger et al., 2009; Lee et al., 2009; Nishimura et al., 2010; Brandt et al., 2012). This leads to anion efflux from guard cells and subsequent stomatal closure. Besides OST1, other kinases like Leucine-rich repeat kinase (LRR-RLK), Calcium-dependent protein kinases (CPK/CDPK), Mitogen-activated protein kinase (MPK), and Calcineurin-B like protein (CBL)-CBL-interacting protein kinase (CIPK) are also involved in SLAC1 regulation (Mori et al., 2006; Cheong et al., 2007; Jammes et al., 2009; Geiger et al., 2010; Brandt et al., 2012; Scherzer et al., 2012; Maierhofer et al., 2014; Khokon et al., 2015; Prodhan et al., 2018). Moreover, few other stimuli like salicylic acid (SA), methy1 jasmonate (MeJA), and bacterial invasion also trigger stomatal closure *via* SLAC1 (Melotto et al., 2008; Khokon et al., 2011; Yan et al., 2015). In the light of above-cited literature, SLAC1 seems to be a converging point for different stomata closure pathways.

In Arabidopsis, loss-of-function mutations in SLAC1 result in strong impairment of S-type anion channel activity and inhibition of stimulus-induced stomatal closure (Negi et al., 2008; Vahisalu et al., 2008). The *slac1* mutant exhibited reduced sensitivity to darkness. Moreover, higher CO_2-induced increase in leaf temperature was also inhibited in *slac1-2* mutant. The detached leaves of *slac1* mutants lost water significantly faster than WT, pointing to defects in transpiration regulation under drought stress (Negi et al.,

2008; Vahisalu et al., 2008). Mutations in *slac1* also unexpectedly affected the stomatal opening induced by light, low CO_2, and higher air humidity. This phenotype was found to be associated with higher concentration of resting cytosolic Ca^{2+} and drastically low activity of inward K^+ channels in *slac1* guard cells (Laanemets et al., 2013).

Although handful literature is available on SLAC1 regulation mechanism, however, the effects of *slac1* mutation, and resultant defects in stomatal closure, on global gene expression need to be explored yet. In current study, we have attempted to answer this question by determining global transcriptomic changes in Arabidopsis *slac1-3* mutant under dark and dehydration stress, by using RNA-sequencing.

Materials and methods

Plant materials and growth conditions

The wild-type (WT) Arabidopsis Columbia ecotype was used for the experiments unless otherwise indicated. In all the experiments Arabidopsis *slac1-3* mutant was used. Seeds were surface sterilized with Plant Preservative Mixture (PPM) by keeping at 4°C for 2 days. The seeds were then placed on 1/2 strength Murashige and Skoog (MS) medium (pH 5.7–5.8), containing 1% sucrose and 0.8% agar, and the plates were kept in incubator at 22°C with 12:12 h, light:dark cycle settings for 2 weeks. The seedlings were then transplanted into the soil. Plants were grown at 12:12 h, light:dark, 23:18°C, and 60:70% humidity cycle.

Plant treatments for RNA sequencing experiment

The aboveground part of WT and mutant plants was cut out at 2 pm (Beijing time) for control. For dark treatment, the material was collected after 2 h of darkness in the greenhouse. For dehydration stress, the aboveground part of the plant was cut off and harvested after 25 min of water loss under natural conditions, as previously reported (Zotova et al., 2018). Samples were immediately frozen in liquid nitrogen and stored at −80°C and then subjected to Illumina sequencing. The experiment was performed in three biological replicates with each replicate consisting of three seedlings.

Identification of differentially expressed genes and functional enrichment analysis

Bioinformatic analysis was performed using the OmicStudio tools at https://www.omicstudio.cn/tool. The DEGs were identified based on |log2 fold-change| ≥ 1 and value of $p < 0.05$. The genes with expression level greater than 5 were retained. Venn and GO enrichment analysis were also performed using OmicShare Tools.[1] The heatmaps were drawn by TBtools (Chen et al., 2020).

Stomatal movement experiment

Fresh plant leaves from 3 weeks old plants were collected at about 2 pm (Beijing time) and placed in stomatal opening buffer (50 μM $CaCl_2$, 5 mM KCl, 10 mM MES-Tris, and pH 6.15). The leaves were soaked in buffer with the back side up and exposed to light (200–250 μmol m^{-2} s^{-1}) for 2 h to fully open their stomata. Then, the lower epidermis of the leaves was peeled off to make temporary pieces. These were then observed under Zeiss microscope and pictures were taken (as control). For dark treatment, the samples were collected after shading the plants for 2 h. For ABA treatment, 200 μM ABA was sprayed on the plant leaves and the samples of lower epidermis were collected after 25 min. Three replicates were included for each treatment, and at least 30 stomata were measured in each group. The width of stomatal aperture was measured from the images with the help of ImageJ.

Thermal imaging experiment

The plants (Col-0 and *slac1-3* mutants) were grown for 6 weeks under normal conditions. For dark treatment, the plants were grown without light for 30 min. Plants grown under normal light conditions were used as controls. The aboveground part of the plants was cut and placed on white paper for taking pictures immediately. Three seedlings were observed under each condition. The images were captured with HIKVISION H10 thermal Imager.

Results

The dark- and ABA-induced stomatal closure was defective in Arabidopsis *slac1-3* mutants

We determined the response of stomata to ABA and dark in epidermal peels of the WT and *slac1-3* mutants of *Arabidopsis thaliana*. Under normal conditions, the stomatal aperture of *slac1-3* mutant was slightly larger than that of WT (Figures 1A,B). When treated with ABA or dark, the stomatal aperture in WT significantly decreased; being about 50% of that of untreated plants. In contrast to this, under ABA treatment, stomatal aperture in *slac1-3* mutant was not significantly different than its untreated control, showing a nearly complete insensitivity to ABA. When shifted from light to dark, although the stomatal aperture in *slac1-3* mutants decreased compared with its non-treated

1 www.omicshare.com/tools

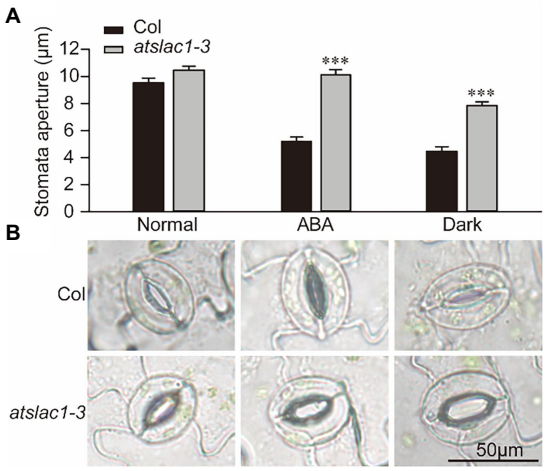

FIGURE 1
Arabidopsis *slac1-3* mutants are insensitive to abscisic acid (ABA) and darkness. **(A)** Graphical presentation of stomatal aperture under ABA, dark treatment, or light. **(B)** Representative images of stomatal aperture in WT and *slac1-3* mutants under ABA, dark, or light. Three replicates were included for each treatment, and at least 30 stomata were measured in each group. Bars represent mean±S.E. *** Denotes statistically significant difference (*t*-test $p<0.01$).

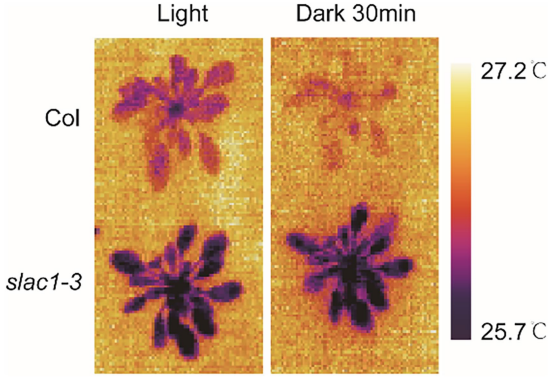

FIGURE 2
Determination of plant leaf temperature in Arabidopsis WT and *slac1-3* mutants in light and dark conditions. Multiple images of both genotypes under light/dark conditions were captured with thermal Imager. The representative images are shown here.

counterpart, however, the extent of stomatal closure was still significantly less than dark-treated WT. These data demonstrate that ABA- and dark-induced stomatal closure is defective in *slac1-3* mutant.

Arabidopsis *slac1-3* mutation resulted in lower leaf temperature

After establishing the defects in stimuli-induced stomatal closure, next, we aimed to confirm if this phenotype had any effect on leaf temperature, by using thermal imaging technique. Under light, *slac1-3* mutants showed lower leaf temperature compared with WT (Figure 2). After the dark treatment for 30 min, whereas the temperature of WT leaves clearly increased, the same was only slightly increased in mutants compared with its untreated counterpart (Figure 2). These data confirmed the defective dark-induced stomatal closure in *slac1-3* mutants.

Transcriptome profiling identified 891 genes upregulated only in Arabidopsis *slac1-3* mutant under dehydration stress

Next, we determined the molecular response of *slac1-3* mutant and WT in dehydration stress condition by carrying out global gene expression using RNA-sequencing. When exposed to dehydration for 25 min, *slac1-3* mutant showed highly variable response, compared to WT, with respect to changes in gene expression. Overall, the number of differentially expressed genes (DEGs; $|\log2 \text{ fold-change}| \geq 1$ and value of $p < 0.05$) was much higher in *slac1-3* mutants than WT (1,956 vs. 1,156; Figure 3A). Interestingly, though the number of downregulated genes was not much different between mutant and WT (389 and 353), however, that of upregulated genes was much greater in *slac1-3* mutants than in WT (1,567 vs. 803). Of these, 891 genes were only upregulated in *slac1-3* mutants but not in WT in dehydration stress (Figure 3A).

A heat map, representing the above mentioned 891 genes, was created based on FPKM of RNA-sequencing data to visualize the quantitative differences in the expression of these genes in *slac1-3* mutants under control and dehydration stress (Figure 4A). The level of expression of DEGs was divided into various classifications in the bar. The red and green regions are indicative of high and low expression, respectively. A color change from red to green, showing that the values of log10 (FPKM+1) change from high to low. Based on GO enrichment analysis the genes were classified into 30 functional categories (Figure 4B). The highest number of DEGs was related to plasma membrane function, followed by the genes related to plant hypersensitive response, response of chitin, defense response to fungus, protein targeting to membrane, response to water deficiency, and systemic acquired resistance (SAR). Based on enrichment factor, the major pathways significantly enriched in DEGs were cell communication pathway, innate immune response pathway, and salicylic acid biosynthesis and signaling pathways. To sum up, these data reveal the specific transcriptomic changes undertaken by the *slac1-3* mutant under dehydration stress to cope up with defective stomatal closure.

Transcriptomic response of *slac1-3* mutant was variable than WT under light as well as dark

To determine the molecular response of two genotypes under day-night transition, we set to compare the pattern of gene

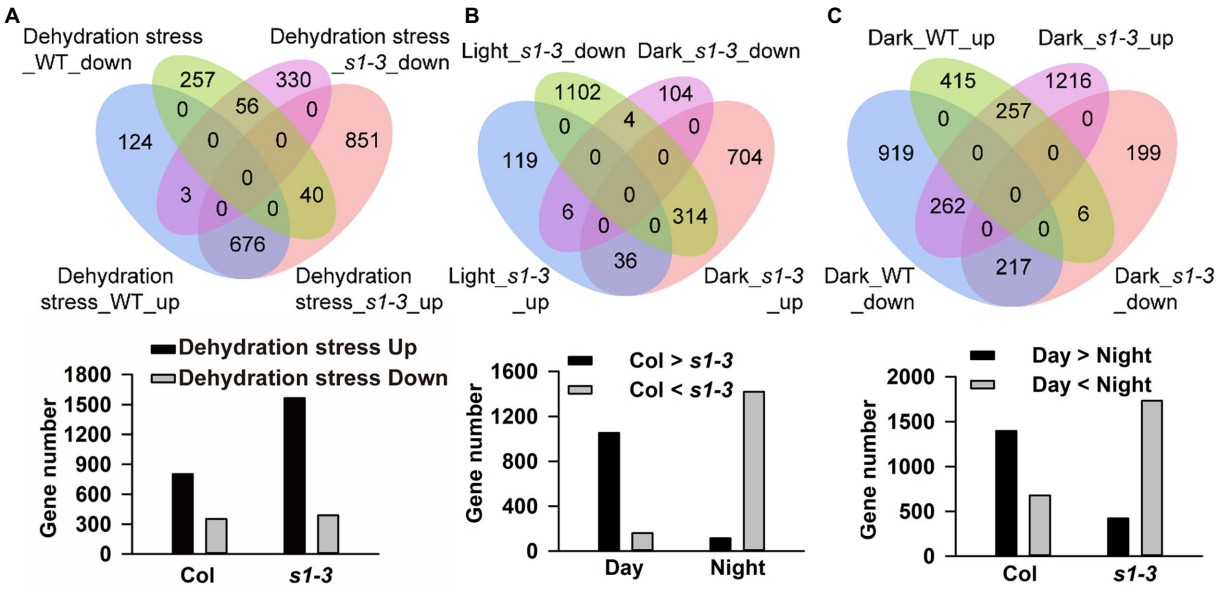

FIGURE 3
Differentially expressed gene (DEG) integration of each data set. DEGs of each data set are overlapped and presented as a Venn plot, including total, upregulated, and downregulated genes. DEGs, differently expressed genes. **(A)** Venn diagram of gene expression and gene number of up- or downregulated in dehydration stress; **(B)** up- or downregulated in dark conditions; and **(C)** up- or downregulated between WT and *slac1-3* mutant.

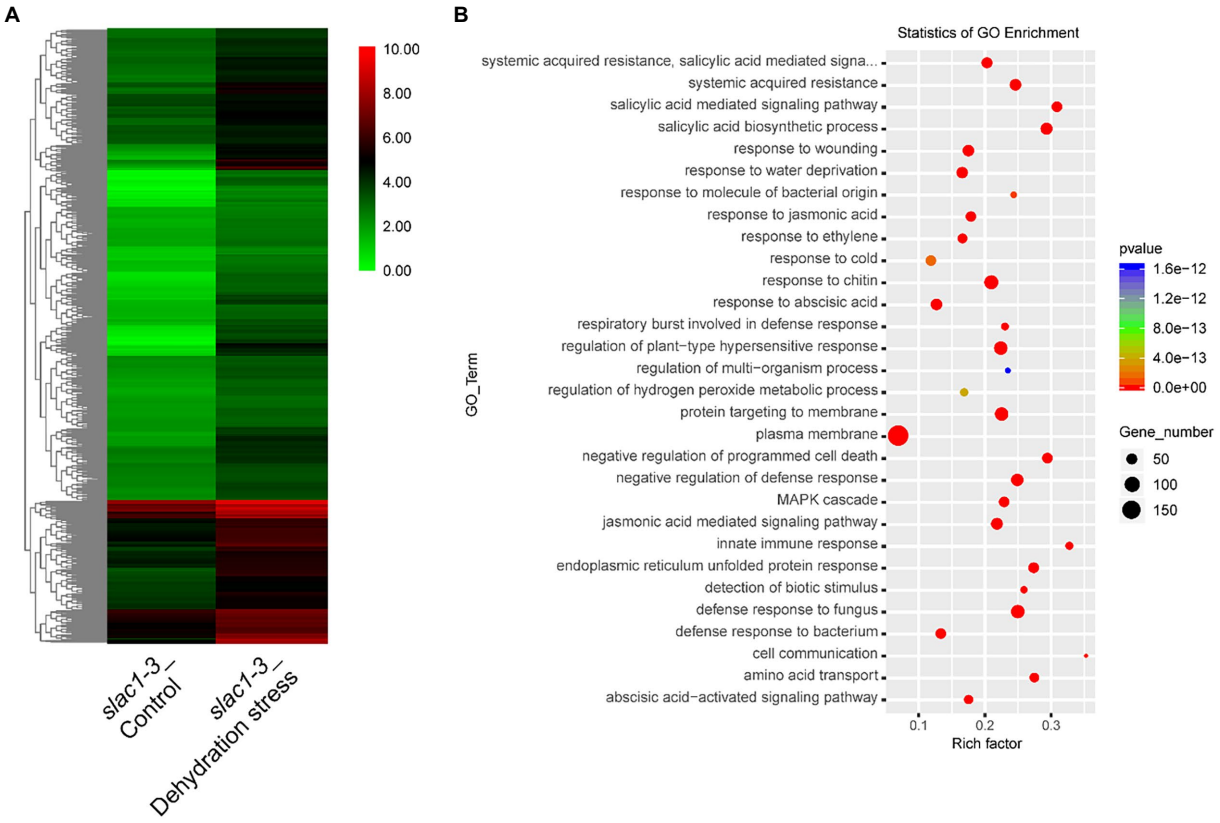

FIGURE 4
RNA-seq analysis of dehydration stress induced upregulated genes in *slac1-3* mutant. **(A)** Heat map of DEGs (891 in Figure 3A) in *slac1-3* mutants between control and dehydration stress **(B)** GO enrichment analysis of DEGs in *slac1-3* mutants in control and dehydration stress.

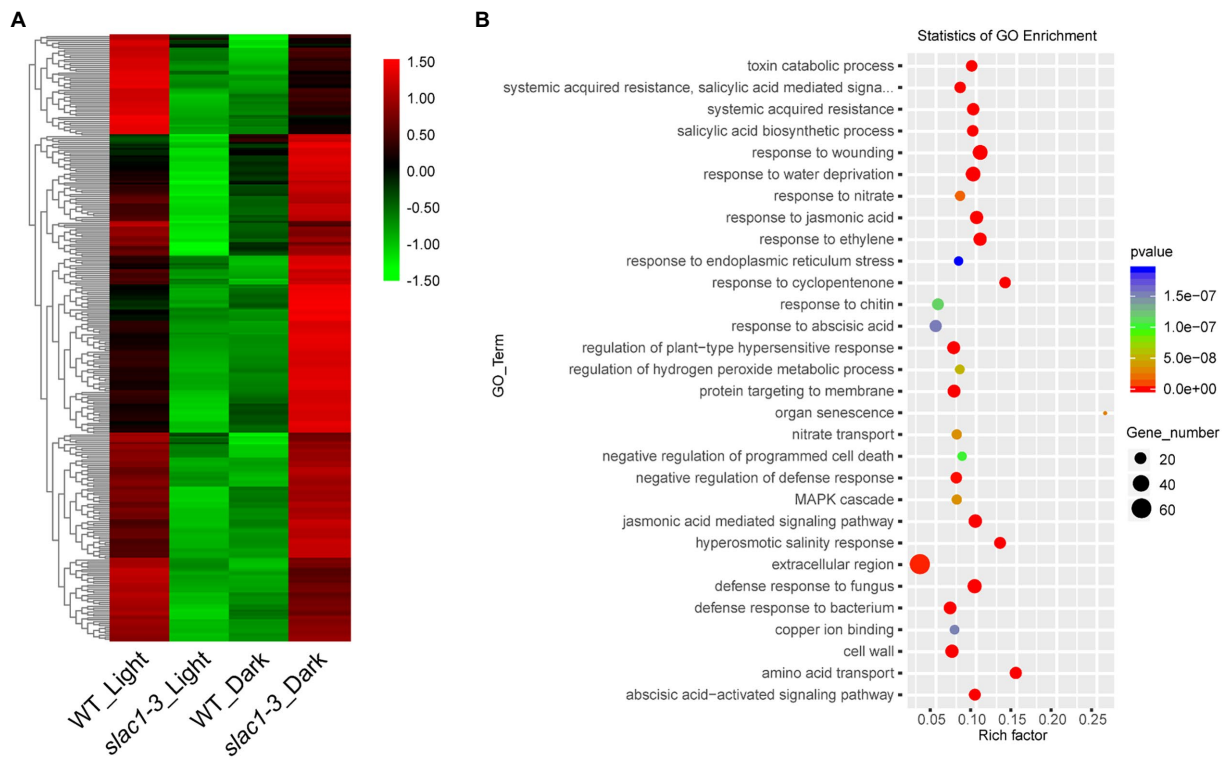

FIGURE 5
RNA-seq analysis of DEGs (314 in Figure 3B) at daytime or night. **(A)** Heat map of DEGs in *slac1-3* mutants in dark and light conditions **(B)** GO enrichment analysis of DEGs in *slac1-3* mutants in dark and light conditions.

expression in WT and mutants under light and dark. Under light conditions, 1,581 DEGs (161 upregulated and 1,420 downregulated) were identified between *slac1-3* mutant and WT (Figure 3B). On the other hand, 1,168 DEGs (1,054 upregulated and 114 downregulated) were identified between mutant and WT under dark conditions (Figure 3B). These findings point to a highly variable response of *slac1-3* mutant as compared with WT, under light as well as dark.

Further, we identified 314 DEGs which, compared with WT, had higher expression in mutant under dark but lower expression under light (Figure 3B).

Next, we set to get further insight into the transcriptome profiling of both genotypes under dark. The number of upregulated and downregulated genes was 678 and 1,398, respectively, in WT while it was 1,735 and 422, respectively, in *slac1-3* mutant under dark (Figure 3C). These data highlight the contrasting pattern of gene expression in the genotypes; under dark, whereas majority of DEGs in WT were found to be downregulated, in *slac1-3* majority were upregulated. Further, 262 DEGs were identified which were downregulated in WT but upregulated in mutant under dark. Since the dark-induced stomatal closure was defective in *slac1-3* mutants, the higher number of upregulated DEGs could represent a compensatory response of the mutant.

We created a heat map of 314 DEGs shown in Figure 3B, to show the quantitative differences in the DEGs (Figure 5A). At daytime, these DEGs were downregulated in *slac1-3* mutant while, under dark, these were upregulated in the mutant, compared with WT (Figure 5A).

GO enrichment analysis was performed, and the genes were assorted into 30 functional categories (Figure 5B). The highest number of DEGs was related to extracellular region, wounding response, dehydration stress response, jasmonic acid and ethylene signaling pathways, and defense response to fungus. The major pathways significantly enriched with DEGs included the one associated with organ senescence, amino acid transport, hyperosmotic salinity response, and response to cyclopentenone.

Next, we focused on the 262 DEGs (shown in Figure 3C) with opposite expression pattern in day/night between WT/mutant and developed a heatmap to represent quantitative differences in expression pattern (Figure 6A). These DEGs exhibited downregulation in WT but upregulation in *slac1-3* mutant under dark while in light these DEGs were up-regulated in WT but down-regulated in *slac1-3*. The DEGs were further subjected to GO enrichment analysis, and the genes were assigned a particular functional category (Figure 6B). Among these, DEGs belonging to hormonal response (jasmonic acid, ethylene, and abscisic acid), wounding response, defense to fungal disease, salt stress response, and jasmonic acid signaling pathway were over-represented. The major pathways significantly enriched with DEGs were related to

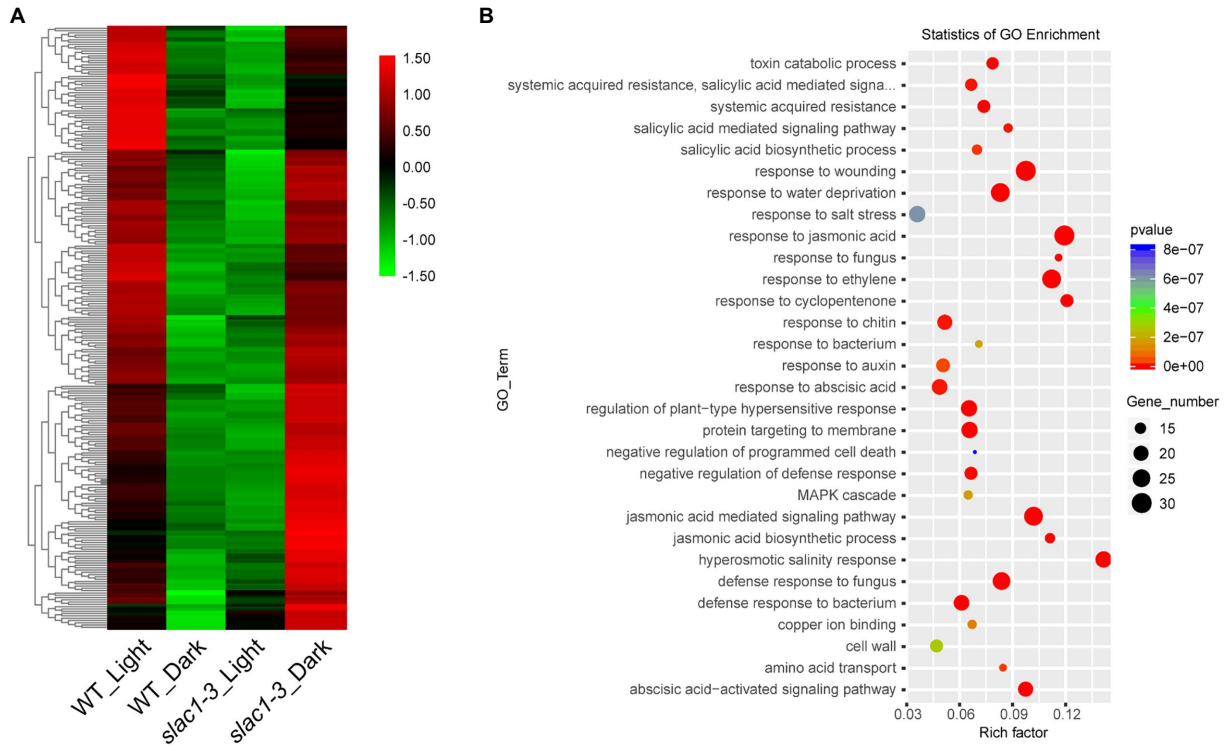

FIGURE 6
RNA-seq analysis of DEGs (262 in Figure 3C) between day and night. **(A)** Heat map of DEGs from day to night between *slac1-3* mutant and WT. **(B)** GO enrichment analysis of DEGs from day to night between *slac1-3* mutant and WT.

hyperosmotic salinity response, and responses to cyclopentenone, jasmonic acid, ethylene, and fungus infection.

Analysis of DEGs under light, dark, and dehydration stress

We further analyzed the DEGs shown in Figures 3A–C. The focus was on 40 DEGs upregulated in *slac1-3* mutant under dehydration stress but downregulated in WT (Figure 3A), 314 DEGs downregulated in *slac1-3* mutant under light, but upregulated in the mutant under dark, and 262 DEGs (shown in Figure 3C) with opposite expression pattern in day/night between WT/mutant. Table 1 shows a list of 18 unique DEGs with opposite expression pattern in *slac1-3* mutant and WT, under the above-mentioned conditions. These DEGs include drought-induced 21 (DI21), senescence related gene (SRG1), nitrilase 2 (NIT2), Kunitz trypsin inhibitor 1, plant invertase/pectin methyl esterase inhibitor superfamily, and lactoylglutathione lyase/glyoxalase I family protein.

Furthermore, in *slac1-3* mutants, six DEGs were identified showing higher expression in WT (and lower expression in *slac1-3* mutant) under light but lower expression in WT (and higher expression in *slac1-3* mutant) under dark (Table 2). These included RING/FYVE/PHD zinc finger superfamily protein, three hypothetical proteins, and a transmembrane protein.

As shown in Table 3, six DEGs were identified with opposite pattern of expression in WT and mutant under light–dark transition. These include an ovate family protein 16, a HXXXD-type acyl-transferase family protein, and a myo-inositol oxygenase 1 protein. We also identified three DEGs which, under dehydration stress, were upregulated in *slac1-3* mutant but downregulated in WT. One of these proteins was phloem protein 2-A13 while the other was nine-cis-epoxycarotenoid dioxygenase 4 (NCED4; Table 4).

Discussion

Owing to their central role in regulating CO_2 uptake and transpiration in plants, changes in stomatal opening and development exhibit adaptive relationships to the environmental conditions in which the plant is growing (Richardson et al., 2017). Being sessile in nature, plants adjust their physiological processes like stomatal movements in response to external factors. The guard cells perceive and respond to various environmental cues to optimize the gas exchange, and at the same time avoiding drought stress (Pillitteri and Torii, 2012). Being a central player in mediating stimuli-induced stomatal closure, SLAC1 seems to be a converging point for different stomata closure pathways.

TABLE 1 List of 18 DEGs common between dehydration stress (40, Figure 3A), *slac1-3* mutant (314, Figure 3B), and day and night (262, Figure 3C) showing opposite expression pattern in WT and mutant under different conditions.

Gene ID	Light_Col *VS s1-3*	Dark_Col *VS s1-3*	Col_ Light *VS* Dark	*s1-3*_light *VS* Dark	Col_control *vs* Dehydration Stress	*s1-3*_ control *VS* Dehydration Stress	Description
AT1G62480	−4.74	1.32	−4.21	1.86	−3.52	1.55	Vacuolar calcium-binding protein-like protein
AT4G15910	−3.54	1.36	−3.19	1.71	−2.56	1.24	Drought-induced 21 (DI21)
AT4G37520	−4.01	1.39	−1.76	3.63	−3.72	1.26	Peroxidase superfamily protein
AT5G40730	−2.18	1.90	−2.77	1.31	−2.10	1.20	Arabinogalactan protein 24 (AGP24)
AT2G05540	−4.93	2.01	−3.75	3.19	−2.27	3.28	Glycine-rich protein family
AT5G07440	−2.28	2.35	−1.94	2.69	−1.53	1.66	Glutamate dehydrogenase 2 (GDH2)
AT4G15610	−4.93	2.53	−3.04	4.41	−3.10	3.23	Uncharacterized protein family (UPF0497)
AT1G76930	−3.20	2.94	−3.57	2.57	−2.87	2.47	Extensin 4 (EXT4)
AT1G17020	−4.33	3.12	−2.50	4.95	−2.95	4.09	Senescence-related gene 1 (SRG1)
AT1G23800	−2.40	3.21	−1.91	3.69	−2.57	3.14	Aldehyde dehydrogenase 2B7 (ALDH2B7)
AT1G74010	−3.59	3.29	−2.17	4.71	−2.53	3.69	Calcium-dependent phosphotriesterase superfamily protein
AT2G29350	−4.64	3.53	−2.62	5.56	−2.00	4.07	Senescence-associated gene 13 (SAG13)
AT5G54510	−5.44	3.58	−2.99	6.03	−3.98	4.41	Auxin-responsive GH3 family protein (DFL1)
AT4G33150	−3.45	3.63	−2.48	4.61	−1.90	2.15	lysine-ketoglutarate reductase/saccharopine dehydrogenase bifunctional enzyme
AT3G44300	−5.14	3.94	−3.65	5.43	−4.48	3.93	Nitrilase 2 (NIT2)
AT1G73260	−10.62	4.40	−3.99	11.03	−4.00	7.66	Kunitz trypsin inhibitor 1 (KTI1)
AT2G45220	−5.37	5.05	−4.61	5.80	−2.90	3.81	Plant invertase/pectin methylesterase inhibitor superfamily (GLYI7)
AT1G80160	−6.18	5.25	−3.03	8.40	−3.44	6.19	Lactoylglutathione lyase / glyoxalase I family protein

The positive values represent upregulation while negative values represent downregulation.

TABLE 2 List of six DEGs (Figure 3B) showing higher expression in WT (and lower expression in *slac1-3* mutant) under light but lower expression in WT (and higher expression in *slac1-3* mutant) under dark.

Gene ID	Light_Col *VS s1-3*	Dark_Col *VS s1-3*	Description
AT5G63780	1.05	−1.16	RING/FYVE/PHD zinc finger superfamily protein (SHA1)
AT4G04293	1.14	−1.33	Hypothetical protein
AT5G03120	1.16	−1.87	Transmembrane protein
AT3G11110	1.19	−1.48	RING/U-box superfamily protein
AT5G19190	1.22	−1.27	Hypothetical protein
AT3G06070	1.47	−1.62	Hypothetical protein

The positive values represent upregulation while negative values represent downregulation.

TABLE 3 List of six DEGs (Figure 3C) with opposite expression pattern in mutant and WT in light–dark transition (in light upregulation in WT but in dark upregulation in *slac1-3* mutant).

Gene ID	Col_Light *VS* Dark	s1-3_Light *VS* Dark	Description
AT4G04293	1.07	−1.40	Hypothetical protein
AT5G19190	1.46	−1.03	Hypothetical protein
AT3G06070	1.39	−1.71	Hypothetical protein
AT2G32100	1.05	−2.01	Ovate family protein 16 (OFP16)
AT5G39080	1.01	−1.17	HXXXD-type acyl-transferase family protein
AT1G14520	1.18	−1.02	Myo-inositol oxygenase 1 (MIOX1)

The positive values represent upregulation while negative values represent downregulation.

TABLE 4 List of three DEGs (Figure 3A) with opposite expression pattern in mutant and WT (downregulated in WT but upregulated in *slac1-3* mutant under dehydration stress).

Gene ID	Col_Control vs. Dehydration Stress	*s1-3*_Control vs. Dehydration Stress	Description
AT5G11070	1.46	−1.27	Hypothetical protein
AT3G61060	1.28	−1.03	Phloem protein 2-A13 (PP2-A13)
AT4G19170	1.19	−2.46	Nine-cis-epoxycarotenoid dioxygenase 4 (NCED4)

The positive values represent upregulation while negative values represent downregulation.

The regulation of stomatal movements could also be governed through transcriptional changes (Sirichandra et al., 2009) as demonstrated by the fact that the transcriptional inhibitors negatively affected stomatal opening, and that two RNA-binding proteins were involved in ABA-induced stomatal closure (Hugouvieux et al., 2001; Li et al., 2002). Furthermore, studies focusing on ABA-induced transcriptomic changes in the guard cell have led to the identification of transcription factors (TFs) involved in regulating the stomatal movements. The TFs involved in stomatal closure include AtMYB15, AtMYB44, AtMYB61, and SNAC1 etc. (Cominelli et al., 2010). Hence it seems that gene expression also plays important role in stomatal movements.

It is evident that failure in proper stomatal closure and/or opening could lead to changes in gene expression. We identified many differentially modulated genes between *slac1-3* mutant and WT under different stimuli like light, dark, and dehydration stress (Figures 3A–C), showing that mutation in SLAC1 results in larger rearrangements at transcriptome level. So, what could be the link between SLAC1 disruption and alterations in gene expression? The failure of stomata to close normally results in water loss, changes in leaf temperature, osmotic changes, and pathogen invasion etc. All these factors can affect the expression of many genes. Moreover, the altered gene expression could be plant's compensatory response due the failure in properly opening and closing the stomatal pore. It is already known that aberrations in stomatal movements lead to compensatory alterations in gene expression, or reorganization of the signaling pathways to compensate for the WT function of the gene (Webb and Baker, 2002).

It is well established that stomatal movements affect the transpiration rate which results in changes in osmotic potential and leaf temperature (Kaňa and Vass, 2008). Similarly, stomatal movements induced by day-night transition also result in changes in osmotic potential and temperature. As shown in Figure 2, the leaves of *slac1-3* mutants were cooler than WT in dark, which could have led to differences in the expression pattern of genes between WT and the mutant. These data showed that stomatal switch could be linked to changes in gene expression. Moreover, it has been demonstrated that guard cells of *slac1-3* mutants exhibit higher resting Ca^{2+} level (Laanemets et al., 2013). As Ca^{2+} is a ubiquitous signaling molecule, therefore, perturbations in Ca^{2+} level could also be associated with differential gene expression in *slac1-3* mutants.

When challenged with drought stress, plants adopt few urgent measures alongside few long-term responses. The former, known as drought avoidance response, includes immediate stomatal closure to conserve water (Dobra et al., 2010) while the long-term response includes induction of drought stress responsive genes. As demonstrated in our study, dehydration stress-induced stomatal closure was defective in *slac1-3* mutants (Figure 1) and therefore, these mutants lost more water than WT from detached leaves. As the extent of dehydration stress was more pronounced in mutants, therefore, a significantly higher number of genes were upregulated in dehydration stress only in the mutant but not in WT, possibly to initiate compensatory responses.

We identified few DEGs in mutant which could represent such compensatory mechanisms. For example, a gene encoding for nine-cis-epoxycarotenoid dioxygenase 4 (NCED4) was about 2.5-fold upregulated in *slac1-3* mutant under dehydration stress (Table 4). NCED is involved in *de novo* ABA synthesis and catalyzes the first committed step in synthesizing ABA by converting 9-cis-neoxanthin to xanthoxin (Tan et al., 1997; Huang et al., 2018). It was observed that detached leaves of *slac1* mutants lost water significantly faster than WT, showing defects in transpiration regulation under drought stress (Negi et al., 2008; Vahisalu et al., 2008). Since the mutant is unable to properly close stomata under dark and dehydration stress, the upregulation of NCED could reflect a strategy by *slac1-3* mutant to promote ABA biosynthesis and thus induce stomatal closure to avoid water loss. Similarly, another gene encoding a member of ovate family had two-fold higher expression in *slac1-3* mutants than WT (Table 3). Ovate family proteins (OFPs) are plant-specific transcription factors, which regulate the content of epicuticular wax, a coating of wax covering the outer surface of the plant cuticle in land plants to reduce the water loss *via* surfaces (Tang et al., 2018). It is possible that lack of normal stomatal closure, could be linked with deploying other strategies like increasing epicuticular waxes for reducing water loss from plant surface. However, further investigations will be needed to experimentally prove if mutant deposit more wax over their surfaces.

In current study, we found that a lactoylglutathione lyase family protein (also known as Glyoxalase I) had lower expression in *slac1-3* mutants in dark and dehydration stress (Table 1). Under abiotic stress, methylglyoxal (MG), a toxic molecule, accumulates in plants. It has been reported that at a certain optimum concentration MG induces stomatal closure, involving oxidative burst and $[Ca^{2+}]$cyt oscillations but in ABA-independent manner (Hoque et al., 2012a,b). MG also inhibits Kin channel currents in Arabidopsis guard cells and interferes with light-induced stomatal opening (Hoque et al., 2012a,b, 2016). Glyoxalase I (also known as

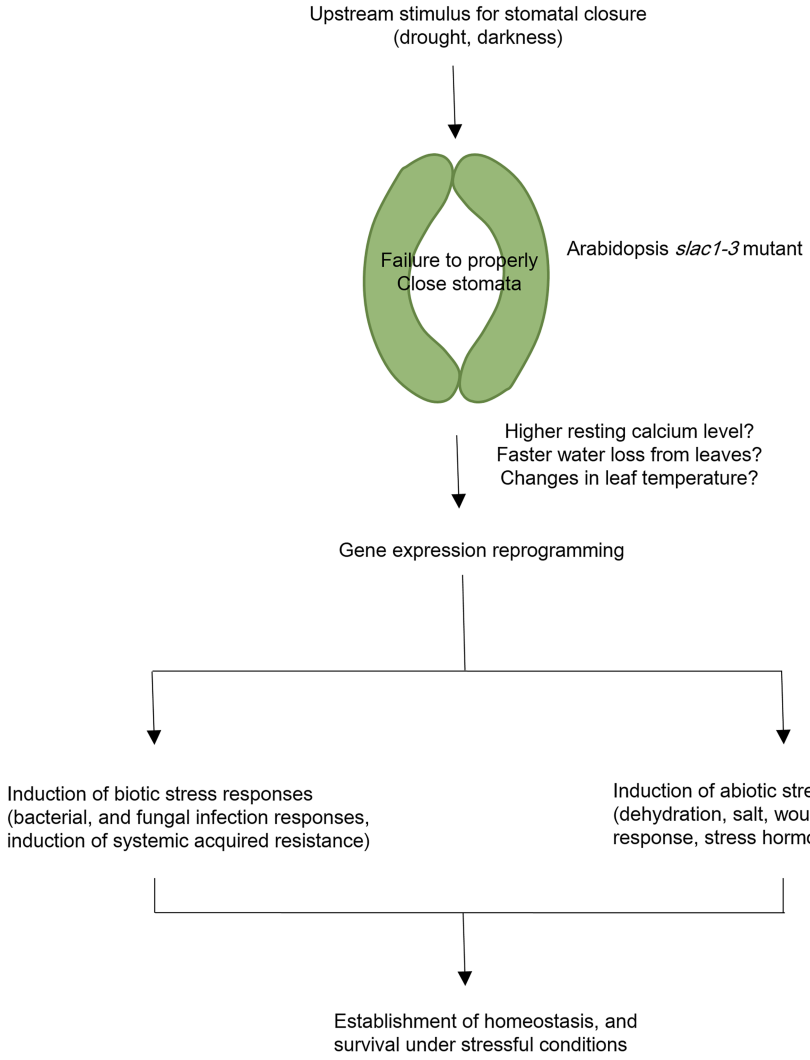

FIGURE 7
A model representing transcriptomic changes undertaken by Arabidopsis *slac1-3* mutant in response to dehydration stress and dark treatment. Under these stimuli, *slac1-3* mutant shows defective stomatal closure. Resultantly, plants lose more water and exhibit cooler leaf temperature. Mutation in Arabidopsis SLAC1 is also linked with higher resting calcium level in mutant. These factors could be among the possible links between *slac1-3* mutation and differential transcriptomic response in mutant. To compensate for defective stomatal closure and its consequences, mutant undergo biotic and abiotic stress responses. The former involves induction of bacterial and fungal infection pathways, and systemic acquired resistance while the latter involves dehydration, salt, wounding, and cold stress responses, and induction of stress hormone pathways. However, it should be noted that few of these hormones may also be simultaneously associated with biotic stress response.

lactoylglutathione lyase) is involved in MG detoxification (Norton et al., 1990; Maiti et al., 1997). It seems that by keeping glyoxalase I expression at low level, mutant could be attempting to increase MG level and thereby promote stomatal closure under dehydration stress and darkness. However, further experimentation is needed to prove whether differential expression of Glyoxalase I had any impact on MG level by directly determining the latter's level in both genotypes.

Interestingly, under both stimuli for stomatal closure (i.e., dark and dehydration stress), a major chunk of DEGs was found to be associated with abiotic and biotic stress responses (e.g., response to bacterial and fungal infections, wounding, chilling, salinity, dehydration stress etc.) and stress related-hormonal pathways (e.g., abscisic acid, salicylic acid, jasmonic acid, and ethylene pathways). This shows that defects in stimulus-induced stomatal closure may result in the induction of stress response pathways.

To conclude, in current study, we have identified specific changes in gene expression underlying *slac1-3* mutation and resultant defects in stomatal closure in Arabidopsis. The large-scale changes in gene expression in *slac1-3* mutants could be attributed to changes in osmotic potential, leaf temperature, and/or higher resting Ca^{2+} level in mutant. Furthermore, the induction of stress responsive pathways in mutant could be suggestive of the role of stomata as a switch in triggering abiotic and biotic stress responsive genes, which could help the plant to survive under stressful conditions. The conclusions of current research are presented as a model in Figure 7.

Data availability statement

The original contributions presented in the study are included in the article/Supplementary material, further inquiries can be directed to the corresponding authors.

Author contributions

ZW, SW, DX, and YX: methodology, formal analysis, investigation, and writing–review and editing. YO: methodology, formal analysis, investigation, and writing–original draft. HR: conceptualization, methodology, formal analysis, investigation, writing–original draft, writing–review and editing, and funding acquisition. JH: conceptualization and manuscript writing, review, and editing. GQ: conceptualization. All authors contributed to the article and approved the submitted version.

Funding

This study was supported by the Natural Science Foundation of Zhejiang Province (Grant No: LY20C020001), the Open Project Program of State Key Laboratory of Crop Stress Biology for Arid Areas, NWFU, Yangling, Shanxi, China (Grant No: CSBAAKF2021008), and the State Key Laboratory of Subtropical Silviculture (Grant No: ZY20190201).

Conflict of interest

The authors declare that the research was conducted in the absence of any commercial or financial relationships that could be construed as a potential conflict of interest.

Publisher's note

All claims expressed in this article are solely those of the authors and do not necessarily represent those of their affiliated organizations, or those of the publisher, the editors and the reviewers. Any product that may be evaluated in this article, or claim that may be made by its manufacturer, is not guaranteed or endorsed by the publisher.

Supplementary material

The Supplementary material for this article can be found online at: https://www.frontiersin.org/articles/10.3389/fpls.2022.987606/full#supplementary-material

SUPPLEMENTARY FIGURE S1
Venn diagram of DEGs between dehydration stressdrought (40, **Figure 3A**), slac1-3 mutant 698 (314, **Figure 3B**), and day and night (262, **Figure 3C**).

References

Brandt, B., Brodsky, D. E., Xue, S., Negi, J., Iba, K., Kangasjärvi, J., et al. (2012). Reconstitution of abscisic acid activation of SLAC1 anion channel by CPK6 and OST1 kinases and branched ABI1 PP2C phosphatase action. *Proc. Natl. Acad. Sci. U. S. A.* 109, 10593–10598. doi: 10.1073/pnas.1116590109

Chen, C., Chen, H., Zhang, Y., Thomas, H. R., Frank, M. H., He, Y., et al. (2020). TBtools: an integrative toolkit developed for interactive analyses of big biological data. *Mol. Plant* 13, 1194–1202. doi: 10.1016/j.molp.2020.06.009

Chen, Y. H., Hu, L., Punta, M., Bruni, R., Hillerich, B., Kloss, B., et al. (2010). Homologue structure of the SLAC1 anion channel for closing stomata in leaves. *Nature* 467, 1074–1080. doi: 10.1038/nature09487

Cheong, Y. H., Pandey, G. K., Grant, J. J., Batistic, O., Li, L., Kim, B. G., et al. (2007). Two calcineurin B-like calcium sensors, interacting with protein kinase CIPK23, regulate leaf transpiration and root potassium uptake in Arabidopsis. *Plant J.* 52, 223–239. doi: 10.1111/j.1365-313X.2007.03236.x

Cominelli, E., Galbiati, M., and Tonelli, C. (2010). Transcription factors controlling stomatal movements and drought tolerance. *Transcription* 1, 41–45. doi: 10.4161/trns.1.1.12064

Dobra, J., Motyka, V., Dobrev, P., Malbeck, J., Prasil, I. T., Haisel, D., et al. (2010). Comparison of hormonal responses to heat, drought and combined stress in tobacco plants with elevated proline content. *J. Plant Physiol.* 167, 1360–1370. doi: 10.1016/j.jplph.2010.05.013

Engineer, C. B., Hashimoto-Sugimoto, M., Negi, J., Israelsson-Nordström, M., Azoulay-Shemer, T., Rappel, W. J., et al. (2016). CO2 sensing and CO2 regulation of stomatal conductance: advances and open questions. *Trends Plant Sci.* 21, 16–30. doi: 10.1016/j.tplants.2015.08.014

Geiger, D., Scherzer, S., Mumm, P., Marten, I., Ache, P., Matschi, S., et al. (2010). Guard cell anion channel SLAC1 is regulated by CDPK protein kinases with distinct Ca2+ affinities. *Proc. Natl. Acad. Sci. U. S. A.* 107, 8023–8028. doi: 10.1073/pnas.0912030107

Geiger, D., Scherzer, S., Mumm, P., Stange, A., Marten, I., Bauer, H., et al. (2009). Activity of guard cell anion channel SLAC1 is controlled by drought-stress signaling kinase-phosphatase pair. *Proc. Natl. Acad. Sci. U. S. A.* 106, 21425–21430. doi: 10.1073/pnas.0912021106

Hedrich, R., and Geiger, D. (2017). Biology of SLAC1-type anion channels - from nutrient uptake to stomatal closure. *New Phytol.* 216, 46–61. doi: 10.1111/nph.14685

Hoque, T. S., Hossain, M. A., Mostofa, M. G., Burritt, D. J., Fujita, M., and Tran, L. S. (2016). Methylglyoxal: an emerging signaling molecule in plant abiotic stress responses and tolerance. *Front. Plant Sci.* 7:1341. doi: 10.3389/fpls.2016.01341

Hoque, T. S., Okuma, E., Uraji, M., Furuichi, T., Sasaki, T., Hoque, M. A., et al. (2012a). Inhibitory effects of methylglyoxal on light-induced stomatal opening and inward K+ channel activity in Arabidopsis. *Biosci. Biotechnol. Biochem.* 76, 617–619. doi: 10.1271/bbb.110885

Hoque, T. S., Uraji, M., Ye, W., Hossain, M. A., Nakamura, Y., and Murata, Y. (2012b). Methylglyoxal-induced stomatal closure accompanied by peroxidase-mediated ROS production in Arabidopsis. *J. Plant Physiol.* 169, 979–986. doi: 10.1016/j.jplph.2012.02.007

Huang, Y., Guo, Y., Liu, Y., Zhang, F., Wang, Z., Wang, H., et al. (2018). 9-cis-epoxycarotenoid dioxygenase 3 regulates plant growth and enhances multi-abiotic stress tolerance in rice. *Front. Plant Sci.* 9:162. doi: 10.3389/fpls.2018.00162

Hugouvieux, V., Kwak, J. M., and Schroeder, J. I. (2001). An mRNA cap binding protein, ABH1, modulates early abscisic acid signal transduction in Arabidopsis. *Cell J.* 106, 477–487. doi: 10.1016/S0092-8674(01)00460-3

Jammes, F., Song, C., Shin, D., Munemasa, S., Takeda, K., Gu, D., et al. (2009). MAP kinases MPK9 and MPK12 are preferentially expressed in guard cells and positively regulate ROS-mediated ABA signaling. *Proc. Natl. Acad. Sci. U. S. A.* 106, 20520–20525. doi: 10.1073/pnas.0907205106

Jezek, M., and Blatt, M. R. (2017). The membrane transport system of the guard cell and its integration for stomatal dynamics. *Plant Physiol.* 174, 487–519. doi: 10.1104/pp.16.01949

Kaňa, R., and Vass, I. (2008). Thermoimaging as a tool for studying light-induced heating of leaves. *Environ. Exp. Bot.* 64, 90–96. doi: 10.1016/j.envexpbot.2008.02.006

Khokon, A. R., Okuma, E., Hossain, M. A., Munemasa, S., Uraji, M., Nakamura, Y., et al. (2011). Involvement of extracellular oxidative burst in salicylic acid-induced

stomatal closure in Arabidopsis. *Plant Cell Environ.* 34, 434–443. doi: 10.1111/j.1365-3040.2010.02253.x

Khokon, M. A., Salam, M. A., Jammes, F., Ye, W., Hossain, M. A., Uraji, M., et al. (2015). Two guard cell mitogen-activated protein kinases, MPK9 and MPK12, function in methyl jasmonate-induced stomatal closure in Arabidopsis thaliana. *Plant Biol.* 17, 946–952. doi: 10.1111/plb.12321

Kim, T. H., Bohmer, M., Hu, H., Nishimura, N., and Schroeder, J. I. (2010). Guard cell signal transduction network: advances in understanding abscisic acid, CO2, and Ca2+ signaling. *Annu. Rev. Plant Biol.* 61, 561–591. doi: 10.1146/annurev-arplant-042809-112226

Kusumi, K., Hirotsuka, S., Kumamaru, T., and Iba, K. (2012). Increased leaf photosynthesis caused by elevated stomatal conductance in a rice mutant deficient in SLAC1, a guard cell anion channel protein. *J. Exp. Bot.* 63, 5635–5644. doi: 10.1093/jxb/ers216

Laanemets, K., Wang, Y. F., Lindgren, O., Wu, J., Nishimura, N., Lee, S., et al. (2013). Mutations in the SLAC1 anion channel slow stomatal opening and severely reduce K+ uptake channel activity via enhanced cytosolic [Ca2+] and increased Ca2+ sensitivity of K+ uptake channels. *New Phytol.* 197, 88–98. doi: 10.1111/nph.12008

Lee, S. C., Lan, W., Buchanan, B. B., and Luan, S. (2009). A protein kinase-phosphatase pair interacts with an ion channel to regulate ABA signaling in plant guard cells. *Proc. Natl. Acad. Sci. U. S. A.* 106, 21419–21424. doi: 10.1073/pnas.0910601106

Li, J., Kinoshita, T., Pandey, S., Ng, C. K. Y., Gygi, S. P., Shimazaki, K. I., et al. (2002). Modulation of an RNA-binding protein by abscisic-acid-activated protein kinase. *Nature* 418, 793–797. doi: 10.1038/nature00936

Maierhofer, T., Diekmann, M., Offenborn, J. N., Lind, C., Bauer, H., Hashimoto, K., et al. (2014). Site- and kinase-specific phosphorylation-mediated activation of SLAC1, a guard cell anion channel stimulated by abscisic acid. *Sci. Signal.* 7:ra86. doi: 10.1126/scisignal.2005703

Maiti, M. K., Krishnasamy, S., Owen, H. A., and Makaroff*, C. A. (1997). Molecular characterization of glyoxalase II from *Arabidopsis thaliana*. *Plant Mol. Biol.* 35, 471–481. doi: 10.1023/A:1005891123344

Melotto, M., Underwood, W., and He, S. Y. (2008). Role of stomata in plant innate immunity and foliar bacterial diseases. *Annu. Rev. Phytopathol.* 46, 101–122. doi: 10.1146/annurev.phyto.121107.104959

Meyer, S., Mumm, P., Imes, D., Endler, A., Weder, B., al-Rasheid, K. A. S., et al. (2010). AtALMT12 represents an R-type anion channel required for stomatal movement in Arabidopsis guard cells. *Plant J.* 63, 1054–1062. doi: 10.1111/j.1365-313X.2010.04302.x

Mori, I. C., Murata, Y., Yang, Y., Munemasa, S., Wang, Y. F., Andreoli, S., et al. (2006). CDPKs CPK6 and CPK3 function in ABA regulation of guard cell S-type anion- and ca(2+)-permeable channels and stomatal closure. *PLoS Biol.* 4:e327. doi: 10.1371/journal.pbio.0040327

Murata, Y., Pei, Z. M., Mori, I. C., and Schroeder, J. (2001). Abscisic acid activation of plasma membrane ca(2+) channels in guard cells requires cytosolic NAD(P)H and is differentially disrupted upstream and downstream of reactive oxygen species production in abi1-1 and abi2-1 protein phosphatase 2C mutants. *Plant Cell* 13, 2513–2523. doi: 10.1105/tpc.010210

Mustilli, A. C., Merlot, S., Vavasseur, A., Fenzi, F., and Giraudat, J. (2002). Arabidopsis OST1 protein kinase mediates the regulation of stomatal aperture by abscisic acid and acts upstream of reactive oxygen species production. *Plant Cell* 14, 3089–3099. doi: 10.1105/tpc.007906

Negi, J., Matsuda, O., Nagasawa, T., Oba, Y., Takahashi, H., Kawai-Yamada, M., et al. (2008). CO2 regulator SLAC1 and its homologues are essential for anion homeostasis in plant cells. *Nature* 452, 483–486. doi: 10.1038/nature06720

Nishimura, N., Sarkeshik, A., Nito, K., Park, S. Y., Wang, A., Carvalho, P. C., et al. (2010). PYR/PYL/RCAR family members are major in-vivo ABI1 protein phosphatase 2C-interacting proteins in Arabidopsis. *Plant J.* 61, 290–299. doi: 10.1111/j.1365-313X.2009.04054.x

Norton, S. J., Talesa, V., Yuan, W. J., and Principato, G. B. (1990). Glyoxalase I and glyoxalase II from Aloe vera: purification, characterization and comparison with animal glyoxalases. *Biochem. Int.* 22, 411–418.

Pillitteri, L. J., and Torii, K. U. (2012). Mechanisms of stomatal development. *Annu. Rev. Plant Biol.* 63, 591–614. doi: 10.1146/annurev-arplant-042811-105451

Prodhan, M. Y., Munemasa, S., Nahar, M. N., Nakamura, Y., and Murata, Y. (2018). Guard cell salicylic acid signaling is integrated into Abscisic acid signaling via the ca(2+)/CPK-dependent pathway. *Plant Physiol.* 178, 441–450. doi: 10.1104/pp.18.00321

Qi, G. N., Yao, F. Y., Ren, H. M., Sun, S. J., Tan, Y. Q., Zhang, Z. C., et al. (2018). The S-type Anion Channel ZmSLAC1 plays essential roles in stomatal closure by mediating nitrate efflux in maize. *Plant Cell Physiol.* 59, 614–623. doi: 10.1093/pcp/pcy015

Ren, H., Su, Q., Hussain, J., Tang, S., Song, W., Sun, Y., et al. (2021). Slow anion channel GhSLAC1 is essential for stomatal closure in response to drought stress in cotton. *J. Plant Physiol.* 258-259:153360. doi: 10.1016/j.jplph.2020.153360

Richardson, F., Brodribb, T. J., and Jordan, G. J. (2017). Amphistomatic leaf surfaces independently regulate gas exchange in response to variations in evaporative demand. *Tree Physiol.* 37, 869–878. doi: 10.1093/treephys/tpx073

Scherzer, S., Maierhofer, T., Al-Rasheid, K. A., Geiger, D., and Hedrich, R. (2012). Multiple calcium-dependent kinases modulate ABA-activated guard cell anion channels. *Mol. Plant* 5, 1409–1412. doi: 10.1093/mp/sss084

Schroeder, J. I., Allen, G. J., Hugouvieux, V., Kwak, J. M., and Waner, D. (2001). Guard cell signal transduction. *Annu. Rev. Plant Physiol. Plant Mol. Biol.* 52, 627–658. doi: 10.1146/annurev.arplant.52.1.627

Sirichandra, C., Wasilewska, A., Vlad, F., Valon, C., and Leung, J. (2009). The guard cell as a single-cell model towards understanding drought tolerance and abscisic acid action. *J. Exp. Bot. [J].* 60, 1439–1463. doi: 10.1093/jxb/ern340

Tan, B. C., Schwartz, S. H., Zeevaart, J. A., and McCarty, D. R. (1997). Genetic control of abscisic acid biosynthesis in maize. *Proc. Natl. Acad. Sci. U. S. A.* 94, 12235–12240. doi: 10.1073/pnas.94.22.12235

Tang, Y., Zhang, W., Yin, Y. L., Feng, P., Li, H. L., and Chang, Y. (2018). Expression of ovate family protein 8 affects epicuticular waxes accumulation in *Arabidopsis thaliana*. *Bot. Stud.* 59:12. doi: 10.1186/s40529-018-0228-8

Umezawa, T., Nakashima, K., Miyakawa, T., Kuromori, T., Tanokura, M., Shinozaki, K., et al. (2010). Molecular basis of the core regulatory network in ABA responses: sensing, signaling and transport. *Plant Cell Physiol.* 51, 1821–1839. doi: 10.1093/pcp/pcq156

Vahisalu, T., Kollist, H., Wang, Y. F., Nishimura, N., Chan, W. Y., Valerio, G., et al. (2008). SLAC1 is required for plant guard cell S-type anion channel function in stomatal signalling. *Nature* 452, 487–491. doi: 10.1038/nature06608

Webb, A. A. R., and Baker, A. J. (2002). Stomatal biology: new techniques, new challenges. *New Phytol.* 153, 365–369. doi: 10.1046/j.0028-646X.2001.00347.x

Yan, S., Mclamore, E. S., Dong, S., Gao, H., Taguchi, M., Wang, N., et al. (2015). The role of plasma membrane H(+) -ATPase in jasmonate-induced ion fluxes and stomatal closure in Arabidopsis thaliana. *Plant J.* 83, 638–649. doi: 10.1111/tpj.12915

Yoshida, R., Umezawa, T., MizoguchI, T., Takahashi, S., Takahashi, F., and Shinozaki, K. (2006). The regulatory domain of SRK2E/OST1/SnRK2.6 interacts with ABI1 and integrates abscisic acid (ABA) and osmotic stress signals controlling stomatal closure in Arabidopsis. *J. Biol. Chem.* 281, 5310–5318. doi: 10.1074/jbc.M509820200

Young, J. J., Mehta, S., Israelsson, M., Godoski, J., Grill, E., and Schroeder, J. I. (2006). CO(2) signaling in guard cells: calcium sensitivity response modulation, a ca(2+)-independent phase, and CO(2) insensitivity of the gca2 mutant. *Proc. Natl. Acad. Sci. U. S. A.* 103, 7506–7511. doi: 10.1073/pnas.0602225103

Zotova, L., Kurishbayev, A., Jatayev, S., Khassanova, G., Zhubatkanov, A., Serikbay, D., et al. (2018). Genes encoding transcription factors TaDREB5 and TaNFYC-A7 are differentially expressed in leaves of bread wheat in response to drought, dehydration and ABA. *Front. Plant Sci.* 9:1441. doi: 10.3389/fpls.2018.01441

frontiers | Frontiers in Plant Science

TYPE Original Research
PUBLISHED 16 November 2022
DOI 10.3389/fpls.2022.1055851

OPEN ACCESS

EDITED BY
Arun K. Shanker,
Central Research Institute for Dryland Agriculture (ICAR), India

REVIEWED BY
Suvendu Mondal,
Bhabha Atomic Research Centre (BARC), India
Hafiz Muhammad Ahmad,
Government College University, Pakistan
Abdulwahab Saliu Shaibu,
Bayero University Kano, Nigeria
Anil Kumar Singh,
Academy of Scientific and Innovative Research (AcSIR), India

*CORRESPONDENCE
Chinta Sudhakar
chintasudhakar@yahoo.com

SPECIALTY SECTION
This article was submitted to Plant Abiotic Stress, a section of the journal Frontiers in Plant Science

RECEIVED 28 September 2022
ACCEPTED 28 October 2022
PUBLISHED 16 November 2022

CITATION
Venkatesh B, Vennapusa AR, Kumar NJ, Jayamma N, Reddy BM, Johnson AMA, Madhusudan KV, Pandurangaiah M, Kiranmai K and Sudhakar C (2022) Co-expression of stress-responsive regulatory genes, *MuNAC4, MuWRKY3* and *MuMYB96* associated with resistant-traits improves drought adaptation in transgenic groundnut (*Arachis hypogaea* l.) plants. *Front. Plant Sci.* 13:1055851. doi: 10.3389/fpls.2022.1055851

Co-expression of stress-responsive regulatory genes, *MuNAC4, MuWRKY3* and *MuMYB96* associated with resistant-traits improves drought adaptation in transgenic groundnut (*Arachis hypogaea* l.) plants

Boya Venkatesh[1], Amaranatha R. Vennapusa[2], Nulu Jagadeesh Kumar[1], N. Jayamma[1], B. Manohara Reddy[3], A. M. Anthony Johnson[4], K. V. Madhusudan[5], Merum Pandurangaiah[1], K. Kiranmai[1] and Chinta Sudhakar[1]*

[1]Plant Molecular Biology Laboratory, Department of Botany, Sri Krishnadevaraya University, Anantapuram, India, [2]Department of Agriculture and Natural Resources, Delaware State University, Dover, DE, United States, [3]Department of Botany, Government College (Autonomous), Anantapuram, India, [4]Department of Biotechnology, St. Josephs University, Bengaluru, India, [5]Department of Botany, Government College, Cluster University, Kurnool, India

Groundnut, cultivated under rain-fed conditions is prone to yield losses due to intermittent drought stress. Drought tolerance is a complex phenomenon and multiple gene expression required to maintain the cellular tolerance. Transcription factors (TFs) regulate many functional genes involved in tolerance mechanisms. In this study, three stress-responsive regulatory TFs cloned from horse gram, (*Macrotyloma uniflorum* (Lam) Verdc.), *MuMYB96*, involved in cuticular wax biosynthesis; *MuWRKY3*, associated with anti-oxidant defense mechanism and *MuNAC4*, tangled with lateral root development were simultaneously expressed to enhance drought stress resistance in groundnut (*Arachis hypogaea* L.). The multigene transgenic groundnut lines showed reduced ROS production, membrane damage, and increased superoxide dismutase (SOD) and ascorbate peroxidase (APX) enzyme activity, evidencing improved antioxidative defense mechanisms under drought stress. Multigene transgenic plants showed lower proline content, increased soluble sugars, epicuticular wax content and higher relative water content suggesting higher maintenance of tissue water status compared to wildype and mock plants. The scanning electron microscopy (SEM) analysis showed a substantial increase in deposition of cuticular waxes and variation in stomatal number in multigene transgenic lines compared to wild type and mock plants. The multigene transgenic plants showed increased growth of lateral roots, chlorophyll

content, and stay-green nature in drought stress compared to wild type and mock plants. Expression analysis of transgenes, *MuMYB96*, *MuWRKY3*, and *MuNAC4* and their downstream target genes, *KCS6*, *KCR1*, *APX3*, *CSD1*, *LBD16* and *DBP* using qRT-PCR showed a two- to four-fold increase in transcript levels in multigene transgenic groundnut plants over wild type and mock plants under drought stress. Our study demonstrate that introducing multiple genes with simultaneous expression of genes is a viable option to improve stress tolerance and productivity under drought stress.

KEYWORDS

groundnut, drought stress, transcription factor, roots, multigene transgenics, water use efficiency

Introduction

Drought, the detrimental abiotic stress, majorly affects the productivity of rain-fed crops and results in yield losses. Groundnut (*Arachis hypogaea* L.) is one of the major oil seed crops with a worldwide production of ~48.75 million metric tons cultivated under ~34.10 million hectares. Nearly 2/3rd of its production was used for oil production (FAOSTAT, 2019). As a rain-fed crop, groundnut is more prone to periodic drought stress, and significant effects on plant physiological processes were reported both in vegetative and reproductive phases (Kambiranda et al., 2011; Farooq et al., 2012; Jongrungklang et al., 2013). Drought tolerance is a complex phenomenon accomplished by the multiple traits at morphological, cellular, and molecular levels. To substantiate the adverse effects of drought stress, plants have adopted multiple drought tolerance traits such as cellular level tolerance, reduced transpirational water loss, improved water mining, and conservation traits, which are controlled either directly or indirectly by regulatory and/or functional genes (Mickelbart et al., 2015; Xiao et al., 2017). Transcription factors (TFs) act as molecular switches by regulating the expression of downstream genes by binding to the cis-acting elements at the promoter region of the genes (Franco-Zorrilla et al., 2014). MYB (Myeloblastosis), WRKY, and NAC (NAM, ATAF, and CUC) are the three large TF families in the plant kingdom and are involved in diverse developmental and stress tolerance mechanisms (Guo et al., 2013; Hrmova and Hussain, 2021; Manna et al., 2021). Overexpression of TF genes through genetic engineering was reported as a viable option to integrate stress adaptive/stress tolerance traits and confer tolerance against various abiotic stresses, including drought in crop plants (Yamaguchi-Shinozaki and Shinozaki, 2006; Buscaill and Rivas, 2014; Shao et al., 2015; Erpen et al., 2018).

The architecture and distribution of the root system is the key feature of water mining traits (de Dorlodot et al., 2007; Coudert et al., 2010) and determines plants' ability to acquire water and nutrients from the soil to maintain plant growth under drought conditions (Lynch, 1995). Root perceives water scarcity and allows plants to adapt to drought stress by increasing their length, density, and volume (Hammer et al., 2009; Bengough et al., 2011; Anjum et al., 2017). Improving root traits through the genetic engineering approach conferred enhanced drought tolerance in most agricultural crops (Hodge et al., 2009). Overexpression of TFs like NAC1, ERF48, Alfin1, DREB2A, etc. has been involved in root growth and development under moisture stress (Janiak et al., 2016; Ramu et al., 2016; Jung et al., 2017). NAC4, TF with a characteristic NAC domain, was reported to induce lateral root growth under water-limited conditions through auxin signaling in an ABA-dependent manner. Overexpression of the *NAC4* gene shows increased root length and lateral roots and enhanced drought tolerance in transgenic groundnut plants (Pandurangaiah et al., 2014). Root growth was stimulated under osmotic stress in transgenic Arabidopsis lines upon overexpression of the *TaNAC4-3A* gene and showed an improved drought tolerance (Mei et al., 2021).

Conservation of tissue water status was a great challenge for the plants during limited water conditions. Plants maintain relatively high tissue water content by minimizing water loss through increased cellular level tolerance (CLT), reduced cellular damage, and evapotranspiration. Osmolytes like proline, soluble sugars, and quaternary ammonium compounds like betaines. etc., will be produced in higher concentration inside the cell and maintains cell turgor and water potential during drought stress (Varshney et al., 2011; Fang and Xiong, 2015; Nahar et al., 2017; Yao et al., 2021). Overexpression of TF genes, *DREB*, *NAC*,

MYB, *WRKY*, and *bZIPs*, etc., in groundnut and other plants showed enhanced osmolyte accumulation and antioxidative defense systems along with other physio-biochemical traits conferring tolerance to different abiotic stresses, including drought through cellular level tolerance (Bhatnagar-Mathur et al., 2007; Pruthvi et al., 2014; Joshi et al., 2016; Kiranmai et al., 2016; Sarkar et al., 2016; Kishor et al., 2018; Manna et al., 2021). A WRKY transcription factor, WRKY3, belonging to group-I WRKY TFs, has been reported to induce resistance against several biotic stressors such as pathogens bacteria and fungi, etc. (Lai et al., 2008; Şahin-Çevik et al., 2014; Guo et al., 2018) and herbivory (Skibbe et al., 2008). In addition to biotic stresses, WRKY3 TF is also reported to be involved in cellular level tolerance mechanisms against different abiotic stresses, including salt, cold, and drought (Liu et al., 2013; Kiranmai et al., 2016; Hichri et al., 2017).

Along with CLT, anatomical traits such as stomata, cuticular wax content, etc., help plants to conserve tissue water under moisture stress (Gomes and Prado, 2007). Cuticle serves as an indispensable barrier and protects the plants from harmful radiations (UV-B), evapotranspiration water loss and also has a positive effect on water use efficiency during water-limited conditions (Jenks et al., 2001; Lee and Suh, 2015; Fich et al., 2016; Iqbal et al., 2020). Biosynthesis and deposition of cuticular waxes in response to drought stress were genetically controlled (Riederer and Schreiber, 2001; Nawrath, 2006) by several TF genes such as *WAX1, MYB96, MYB94, WIN1/SHN1, WXP1, WR1, AP2/EREBP, DWA1*, and functional genes, *KCS1, CER1*, and *FAR1*, etc., were reported to be conferring resistance in several crop plants (Seo and Park, 2011; Xue et al., 2017; Lewandowska et al., 2020). MYB96, an R2R3-MYB TF characterized by two MYB domain repeats, is reported to positively regulate biosynthesis and deposition of cuticular waxes on aerial plant organs and increased drought resistance upon overexpression (Seo et al., 2009; Seo et al., 2011; Lee et al., 2014; Lee et al., 2016).

Introducing multiple genes contributing to different traits with simultaneous expression in a single construct is a reliable and time-saving approach (Goel and Singh, 2018; Vennapusa et al., 2022). Furthermore, co-expression of multiple genes in plants has been shown to improve the tolerance against different abiotic stresses compared to single gene transgenics (Singla-Pareek et al., 2003; Babitha et al., 2013; Nguyen et al., 2013; Augustine et al., 2015; Parvathi et al., 2015) including groundnut (Pruthvi et al., 2014; Ramu et al., 2016).

Horsegram is a potential dryland legume crop for future and is source of mining genes for abiotic stress tolerance, as this crop is well suited for cultivation in very poor soils under receding moisture level in drought prone areas, saline soils and high temperature regions (Reddy et al., 2008; Pandurangaiah et al., 2014; Kiranmai et al., 2018) In the present study, three transcription factor genes, *MuMYB96, MuWRKY3*, and *MuNAC4*, involved in improving the water conservation, cellular level tolerance, and root traits cloned in a single cassette through modified gateway cloning technology, and transferred to groundnut for developing the multigene transgenic plants for improved drought stress tolerance.

Materials and methods

Plant material, growth conditions and stress treatments

Seeds of horsegram (*Macrotyloma uniflorum* (Lam) Verdc.) cultivar VZM1 and groundnut (*Arachis hypogaea* L.) cultivar K-6 were procured from Regional Agricultural Station, Rekulakunta and Kadiri, Anantapuram, respectively. Seeds were sown in earthen pots containing soil and farmyard manure in a 3:1 proportion maintained in the departmental botanical garden under natural photoperiod (10–12 h; 27 ± 4 °C). After 30 days post-sowing, drought stress was induced by withholding water to one set of pots, and respective fully watered controls were maintained in another set of pots. Ten days after stress imposition, fully opened fresh leaf samples were collected, pooled, flash frozen in liquid nitrogen, for futher analysis.

Isolation of genes

Total RNA was isolated from stress-adapted horse gram leaves subjected to drought stress using the Trizol reagent (Invitrogen). The leaf material (100mg) from drought stressed horsegram plants was ground to amorphous powder using liquid nitrogen and added with 1ml of Trizol reagent containing guanidium thiocyanate (Simms et al., 1993). The supernatant was separated after centrifugation and nucleic acids portion was aspired using chloroform. The RNA was precipitated with isopropanol and sodium citrate/NaCl (1:1) solution. The RNA precipitate washed with ethanol, dried and dissolved in sterile diethylpyrocarbonate (DEPC) water and the same was used as a template for cDNA synthesis using the RevertAid reverse transcriptase enzyme (Thermo Scientific, USA).

Individual gene-specific primers were used to isolate individual genes. The PCR setup and annealing temperatures were optimized for all three genes *MuMYB96, MuWRKY3*, and *MuNAC4*, individually to get the specific gene amplification in the gradient thermal cycler (Eppendorf, Hamburg). PCR was initiated by a hot start at 94 °C for 5 min followed by 30 cycles of 94 °C for 1 min, 59.1 °C (*MuMYB96*), 58.2 °C (*MuWRKY3*) and 53.1 °C (*MuNAC4*) for 45 s and 72 °C for 1 min with a final extension of 10 min. and the list of primer sets were given in Supplementary Table 1. The amplification was checked on 0.8% agarose gel. The authenticity of the PCR product was checked by restriction enzyme digestion, confirmed and cloned into a T/A vector (Thermo Scientific, USA) and sequenced.

Development of gene cassettes and gateway entry vectors

Each gene was cloned under the specific promoter by conventional restriction digestion and ligation strategy to develop gene expression cassettes. *MuMYB96* gene was cloned under *rbcs* promoter and terminator in the Impact vector (IM1.1) (P_{rbcs}: *MuMYB96*:T_{rbcs}), *MuWRKY3* gene was cloned into the pRT100 vector under CaMV2x35S promoter and a polyA tail terminator ($P_{CaMV2x35S}$: *MuWRKY3*:T_{polyA}) and *MuNAC4* gene expression cassette were developed using a pB4NU plasmid vector carrying ubiquitin promoter and *nos* terminator (P_{Ubi}: *MuNAC4*: T_{nos}) using specific restriction enzymes. Then, these three gene cassettes were sub-cloned into modified gateway entry vectors. The *MuMYB96* gene cassette was released by digesting with *HindIII* and *PacI* and was ligated to the linearized pGATE L1-L4 entry vector, and the *MuWRKY3* gene construct was sub-cloned into pGATE R4-R3 using *SphI* enzyme. Finally, the *MuNAC4* expression cassette was excised from the pB4NU vector and introduced into the pGATE L3-L2 vector between *EcoRI* and *HindIII* restriction sites to prepare the entry clones.

Construction of multigene cassette

The three genes were stacked together in a plant expression binary vector by recombination reaction. Three gateway entry vectors, *pGATEL1L4-*P_{rbcs} *: MuMYB96:*T_{rbcs}, *pGATE R4R3-*$P_{CaMV2x35S}$*:MuWRKY3:*$T_{polyA,}$and *pGATEL3L2-*P_{Ubi} *: MuNAC4:*T_{nos}were allowed to a recombination reaction with destination vector, pKM12GW containing a neomycin phosphotransferase (*nptII*) gene as plant selectable marker in 1:1:1:3 ratio respectively. The reaction was carried out at 25°C overnight in the presence of LR clonase enzyme, and proteinase K was used to terminate the reaction (Vemanna et al., 2013). The resulting recombinant vector was used to transform *Agrobacterium tumefaceins*.

Transformation of multigene construct into groundnut

The binary vector expressing *pKM12GW-MuMYB96*: *MuWRKY3:MuNAC4* was transferred into *Agrobacterium tumefaciens* EHA105 strain by Freeze-thaw method, and colony PCR was carried out to identify positive transformants (Weigel and Glazabrook, 2006). A tissue culture-independent agrobacterium mediated *in planta* transformation protocol (Rohini and Rao, 2001) was adopted to develop the groundnut transgenics. Two-day-old germinating groundnut (cultivar variety K6) sprouts were pricked at the embryonic site and co-cultivated with agrobacterium culture for 16 hours at 28°C with gentle agitation, followed by rinsing with cefotaxime (500µg/ml) for 2 minutes and later with sterile distilled water. The seedlings were acclimatized in a plant growth chamber on a sterilized soilrite at controlled conditions (28 ± 2°C; 16 hours of light/day; light intensity-400-550 µE/m^2/s) RH-60%). Another set of seeds were transformed with *Agrobacterium* cells carrying *pKM12GW* vector without transgenes and were treated as mock plants. After acclimatization, plantlets were transferred to a greenhouse, maintained at 28°C, and allowed to grow under natural photoperiodic conditions till harvest. Putative transgenic groundnut plants were identified by kanamycin screening and PCR analysis using npt-II primers. The seeds from the T_0 generation were germinated on MS agar medium (Himedia, Mumbai, India) supplemented with 200mg/L of kanamycin under controlled environment chambers (Conviron A1000, Canada). The seedlings showing normal shoot and root growth were transferred to sterile soilrite for acclimatization, then transferred to the earthen pots and maintained in the greenhouse. Integration of all three genes in genomic DNA was confirmed by PCR using gene-specific primers. Transgenic plants showing the integration of three genes were considered positive transgenic plants and advanced to the subsequent generations.

Expression analysis of transgenes by qRT-PCR

The expression of transgenes, *MuMYB96, MuWRKY3*, and *MuNAC4* was analyzed in putative T_3 transgenic groundnut plants and wild type, subjected to drought stress for 10 days. Fully opened leaf samples were used for analysis. Total RNA isolated from leaf samples was treated with a Turbo DNase treatment kit (Thermo Fisher Scientific, USA) as per the manufacturer's protocol to remove any DNA traces. cDNA was synthesized using Revert Aid M-MuLV Reverse Transcriptase (Thermo Fisher Scientific) as per the manufacturer's instructions. qRT-PCR mix was comprised of 1× using Power SYBR Green Master Mix (Ambion, USA), 20 ng of cDNA, and 0.2 µM of forward and reverse primers. The housekeeping gene, *actin*, was used as an internal control in the reaction. The RT-PCR analysis was done on Applied Biosystems Step One Real-Time PCR machine with standard cycling comprising 95°C for 30 s, 40 cycles of 95°C for 1 s, 60°C for 20 s, and a melt curve analysis. Relative quantification was studied using $2^{-\Delta\Delta}$ CT method (Livak and Schmittgen, 2001).

In addition to transgenes, a few downstream genes such as *KCS6*, *KCR1, APX3, CSD, LBD16* and *DBP* were also analyzed using qRT-PCR. The gene sequences of the selected down-stream genes were obtained from genome of *Arachis hypogaea* (http://peanutbase.org/home) and the same sequences were used to design primers using Primer Express™ Software v3.0.1. Each gene was analyzed in three biological samples, and three reaction replicates were performed for each biological sample. The primers used for PCR analysis were given in Supplementary Table 2.

Scanning electron microscopy

Scanning Electron Microscopy (SEM) was employed to investigate the cuticular wax depositions and stomatal structure on the leaf surface of transgenic, mock, and wild type groundnut plants subjected to drought stress. First, the freshly harvested leaf bits of $1cm^2$ were vacuum dried and mounted onto aluminum stubs, followed by gold nanoparticle coating with a fully automated vacuum sputter smart coater (DII-29030SCTR, JOEL, USA). Then, leaf-mounted stubs were transferred to the scanning electron microscope (JOEL JSM-IT500, Japan) to visualize the extent of epicuticular wax depositions on the leaf surface (Lokesh et al., 2019).

Evaluation of transgenic groundnut plants for drought stress tolerance

Physiological and biochemical parameters related to cellular level tolerance and WUE were carried out under drought stress in putative transgenic groundnut lines along with mock and wild type plants. The drought stress was imposed on thirty-day-old plants by withholding irrigation for ten days and fully opened leaf samples were collected uniformly from each set of plants. Three biological samples, and three reaction replicates were performed for each physiological and biochemical assay.

Relative water content

Relative water content (RWC) was measured in multigene transgenic plants along with wild type plants under drought stress conditions. First, leaf discs were prepared from matured leaves, and fresh weight was measured. Then the leaf discs were immersed in sterile water for four hours, and the weight was recorded as turgid weight; then, the leaf discs were dried in a hot air oven for 48 h, and the dry weight was determined. Finally, RWC was calculated using the formula (Vemanna et al., 2017).

Total chlorophyll content

Chlorophyll pigments were extracted from drought-stressed leaves of multigene transgenics and wild type plants by boiling them in dimethyl sulfoxide (DMSO) at 65°C for 10 min. The extracted chlorophylls were read at 645nm and 663nm using a spectrophotometer (Shimadzu UV 1800, Japan). The total chlorophyll content was estimated according to Hiscox and Israelstam (1979) and expressed as mg/g F.W (Vennapusa et al., 2022).

Epicuticular wax content

Epicuticular waxes on the leaf surface were separated and quantified according to the method given by Mamrutha et al. (2010). The waxes were extracted with chloroform from the leaf surface and treated with acidic-potassium dichromate ($K_2Cr_2O_7$) to give a coloured compound. The ECW content was calculated using a colorimetric method and expressed as µg/g F.W.

Total soluble sugars (TSS) and proline content

Total soluble sugar content was determined following Kiranmai et al. (2018). Water extract of leaf was treated with 5% phenol and 98% sulphuric acid and incubated at room temperature for 1 hr, and the absorbance was measured at 485nm. The TSS content was expressed as µg/g F.W.

Accumulation of proline content in the leaf samples was determined as described by Bates et al. (1973). Leaf extract was prepared in 3% sulphosalicylic acid, heated, treated with acid ninhydrin and acetic acid, and incubated at 100°C for 1hr. The reaction was terminated on ice, and the chromophore was extracted with 4 mL toluene and mixed thoroughly. The toluene phase was separated and measured with a spectrophotometer 540nm using toluene as blank, and the proline content was calculated from the standard curve and expressed as µmol/g F.W (Vemanna et al., 2017).

Lipid peroxidation

The extent of cell membrane damage was calculated indirectly by measuring the malondialdehyde content, a product of lipid peroxidation of membrane lipids. The leaf material from drought stressed transgenic, mock and wild type plants was used to estimate thiobarbituric acid, a reactive compound of malondialdehyde, and calculated against a standard MDA graph (Nisarga et al., 2017).

ROS and scavenging system

Superoxide ion and hydrogen peroxide contents were quantified in the transgenic groundnut plants, wild type and mock plants exposed to drought stress. Superoxide ions were estimated by a colorimetric method according to Kiranmai et al. (2018) by treating with nitroblue tetrazolium (NBT) solution, and hydrogen peroxide content was measured as described by Junglee et al. (2014) and Nareshkumar et al. (2015).

The efficacy of the anti-oxidant defense system was analyzed by measuring the activity of superoxide dismutase (SOD) (Kiranmai et al., 2018) and ascorbate peroxidase (APX) (Vemanna et al., 2017) in the leaves of multigene transgenic and wild type plants using a colorimetric method.

Growth and yield attributes

After harvesting, morphological and yield traits such as shoot length, root length, shoot dry weight, root dry weight, number of pegs, number of pods, and dry weight of pods were measured for transgenic plants along with the wild type and mock plants (Vemanna et al., 2017).

Briefly, multigene transgenic groundnut lines, wild type and mock plants were gently uprooted from the pots. Roots were cleaned using tap water to remove debris and soil particles properly and maximum care was taken to avoid the loss of roots. Number of pegs and pods were recorded. Shoot and root parts were separated and their length was recorded using an ordinary ruler. Then the shoot, root parts and pods were dried at 50°C for 48 hours in a hot air oven and dry weight was recorded using digital scale. Data was recoded in three biological sets with triplicates and the results were shown mean-values per plant.

Statistical analysis

All the physiological and biochemical experiments were conducted in three biologically independent experiments, statistical analyses were performed using R version 4.2.0, and ANOVA was performed using the R package agricolae with Fisher's LSD test to separate means and significance at $P \leq 0.05$ (de Mendiburu, 2014; Pandian et al., 2020). Data presented are mean values and standard error (± SE).

Results

Development of multigene expressing transgenics groundnut plants

The three TF genes, *MuMYB96, MuWRKY3*, and *MuNAC4* were amplified from cDNA synthesized from horse gram leaf RNA samples (Supplementary Figure 1) and sequence (Supplementary Table 3). All the three genes, were sub cloned to pRT100 vectors under CaMV35S promoter and polyA terminator at Apa1 and Nco1, Kpn1 and Nco1, and Kpn1 and BamH1 sites, respectively (Supplementary Figure 1A). The individual gene cassettes, P_{rbcs}: *MuMYB96*:T_{rbcs} $P_{CaMV2x35S}$: *MuWRKY3*:T_{polyA} and P_{Ubi} : *MuNAC4*:T_{nos} were stacked into a single multigene construct in a plant binary vector, *pKM12GW* through the LR clonase reaction using a modified multisite gateway cloning technology (Vemanna et al., 2013). The plant destination vector carrying all the three genes, *pKM-MuMYB96: MuWRKY3:MuNAC4* in *Agrobacterium* (Figures 1A, B), was transferred to groundnut seedlings. Putative transgenic groundnut lines were selected on a kanamycin medium. The putative multigene transgenic groundnut plants showed growth on the kanamycin selection medium, whereas the wild type plants failed to germinate or showed stunted growth. Transgenic plants that showed normal growth were acclimatized in the greenhouse, maintained till harvest, and/or advanced to the next generation (Figure 2). Integration of all three transgenes was confirmed in putative transgenic plants by PCR analysis using genomic DNA as a template (Supplementary Figure 2). The multigene transgenic groundnut plants showing kanamycin resistance and gene integration were advanced to the next generation and the transgenic events were shown in Supplementary Figure 3.

Expression of transgenes and stress responsive genes in multigene transgenic groundnut plants under drought stress

Quantitative real-time expression analysis (qRT-PCR) of transgenes was carried out in transgenic groundnut lines along with wild type plants in the T_3 generation. The transgenic groundnut plants showed enhanced transcript levels compared to wild type under drought stress conditions. For example, *MuMYB96* showed a 2.88 to 4.38-fold increase in transcript abundance in multigene transgenic plants over wild type plants, whereas *MuWRKY3* transcript levels showed a 3.50 to 3.618-fold increase and 3.15 to 3.46-fold increase in transcript levels of *MuNAC4* gene. The overexpression of transcription factors resulted a significant increase in transcript level of downstream genes such as *KCS6*, and *KCR1, APX3* and *CSD1 LBD16* and *DBP* in transgenic plants over wild type plants under drought stress conditions (Figure 3).

Morpho-physiological, growth and yield-related traits in multigene transgenic groundnut plants under drought stress

In T_3 generation, 30-days-old multigene transgenic groundnut plants, wild type and mock plants were subjected to drought stress by withholding the water for 10-days. Drought stress resulted visible leaf wilting in both multigene transgenic plants, wild type and mock plants under drought stress, however, the symptoms appeared much earlier in wild type and mock plants, with significant phenotypic difference under drought stress. The transgenic plants showed mild wilting symptoms and remained green after ten days of drought stress imposition

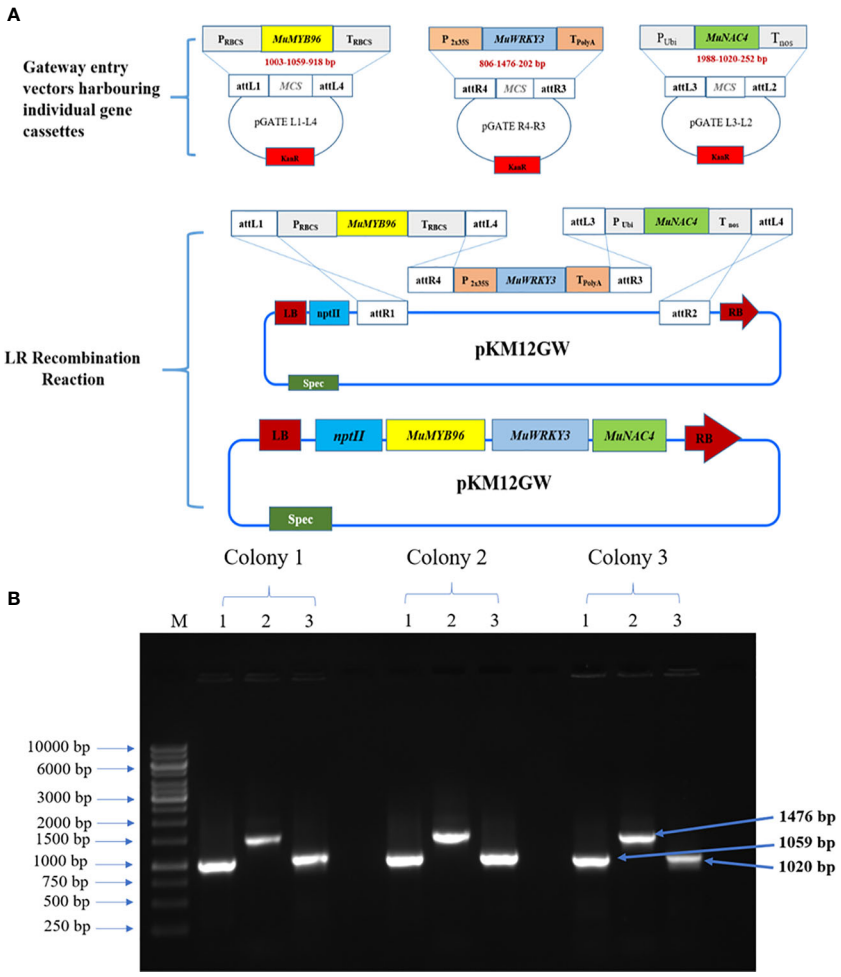

FIGURE 1
Development of multigene cassette harboring *MuMYB96, MuWRKY3* and *MuNAC4* genes: **(A)**. Over view of steps involved in the development of multigene construct through modified gateway cloning technology. **(B)** PCR confirmation of *MuMYB96* (1059 bp), *MuWRKY3* (1476 bp) and *MuNAC4* (1020 bp) in *Agrobacterium tumefaciens*. Lane M: DNA ladder, Lane 1,2,3: positive colony.

whereas wild type and mock plants showed severe visible wilting symptoms (Figure 4A).

Further, morphological parameters and yield related data was recorded for transgenic lines, wild type and mock plants after harvest and the multigene transgenic groundnut plants showed better growth and increased root length, more number of pegs and pods compared to wild type and mock plants (Figure 4B). In general, multigene transgenic lines, wild and mock plants showed significant difference in their growth. Multigene transgenic plants exhibited superior growth than the wild type and mock plants. Growth of lateral roots and overall root length of multigene transgenic groundnut lines significantly increased compared to wild type and mock plants. Consequently, pronounced increase in the root dry weights observed. Total number of pods was more in multigene transgenic lines compared to wild type and mock plants (Table 1).

Variation in the epicuticular wax accumulation was observed between the multigene transgenic lines and wild type and mock plants. The transgenic plants showed a significant increase in the deposition of cuticular wax crystals over the wild type and mock samples. Leaf sample of TL2-2-2 transgenic line showed condensed cuticular crystals resulting in plaque-like deposits (Figure 5). The surface of the transgenic leaves (TL19-1-3, TL 40-2-4 and TL 41-1-3) exhibited dense wax crystals accumulation, whereas the mock and wild type plants have sparse wax accumulation In addition to the wax deposition, we observed variations in the stomatal number between multigene transgenic lines and wild type and mock plants. Wild type plants showed more number of stomata, whereas the transgenic plants showed less number of stomata (Figure 6).

The relative water content was significantly less in wild type compared to multigene transgenic lines under drought stress.

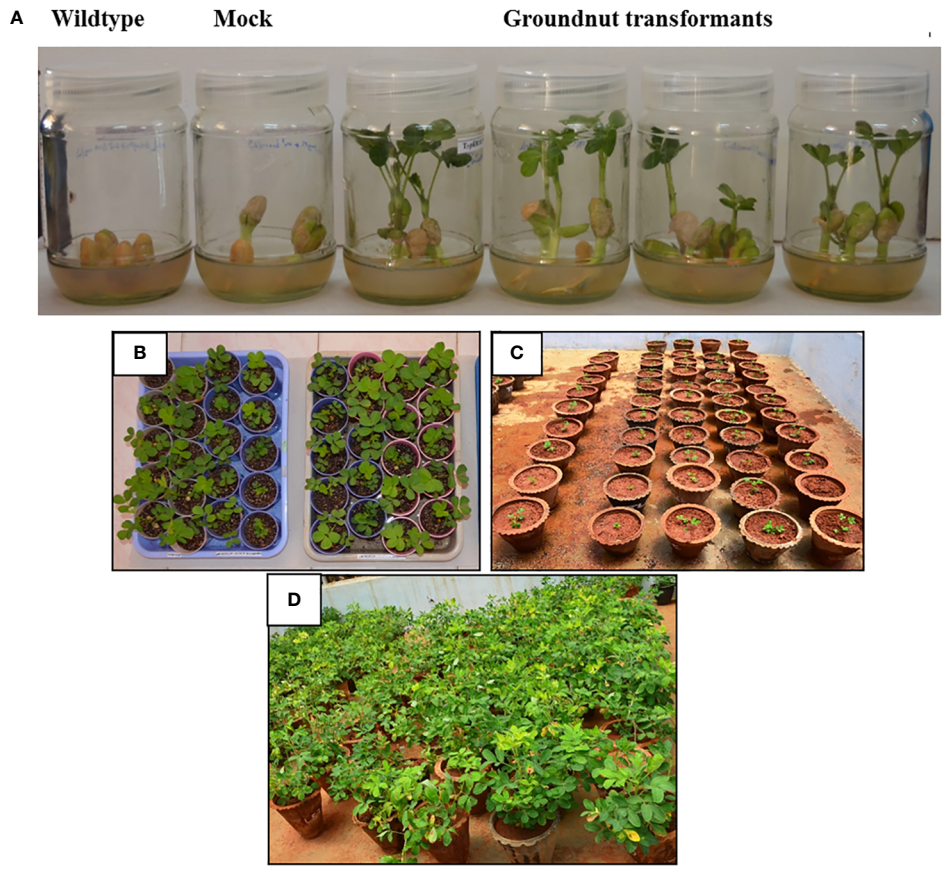

FIGURE 2
Screening of putative transformants on selection media and advancement: **(A)**. Selection of groundnut transformants on Kanamycin screening. Wild type seeds showing inhibited germination on kanamycin containing MS half strength medium. Mock plant (groundnut plants transformed with empty vector) seeds showing the delayed germination on kanamycin containing MS half strength medium. Multigene (*pKM-MuMYB96: MuWRKY3:MuNAC4*) transgenic groundnut plants showing normal growth on the kanamycin medium. Different stages of growth and development of T_3 transgenic groundnut plants. **(B)**. Plants growing on soil-rite in a plant-growth chamber after kanamycin screening. **(C)** Acclimatization of plants on pot culture containing soil manure mixture (3:1) in green house. **(D)** 90-day-old plants in the green house under natural photoperiodic condition.

The transgenic groundnut plants showed a range of 40.27 to 66.89% of relative water content. In contrast, wild type and mock plants showed 32.39% and 34.88%, respectively, demonstrating superior water retention capacity of transgenic plants than wild type plants under water stress conditions (Figure 7A). Stress effect was more pronounced in wild type as evidenced by reduction in total chlorophyll content. The transgenic groundnut plants showed significantly higher chlorophyll content (0.26 to 0.42mg/g. FW) compared to wild-type (0.18mg/g. FW) and mock plants (0.218 mg/g. FW) (Figure 7B).

The multigene transgenic groundnut plants showed significantly higher epicuticular wax content ranging from 12.42 to 16.51µg/g F.W under drought stress conditions compared to wild type and mock plants (6.54 and 7.08µg/g F.W respectively), which is 2 to 2.5 folds lower than that of the transgenic groundnut plants (Figure 7C).

Total soluble sugars, proline and malondialdehyde content in multigene transgenic groundnut plants under drought stress

The transgenic groundnut plants showed significantly higher levels of total soluble sugars ranging from 760-997µg/g F.W under stress conditions. In comparison with transgenic plants, wild type and mock plants showed relatively lower levels of TSS, ranging 321.71 and 409.49µg/g F.W respectively (Figure 8A). The transgenic lines showed lower proline content ranging from 72-131µg/g F.W than wild type and mock plants which showed 184 and 179µg/g F.W, respectively (Figure 8B). There was significant decrease in proline content in multigene transgenic lines compared to wild type and mock plants under drought stress. The lower proline content could be due to better RWC

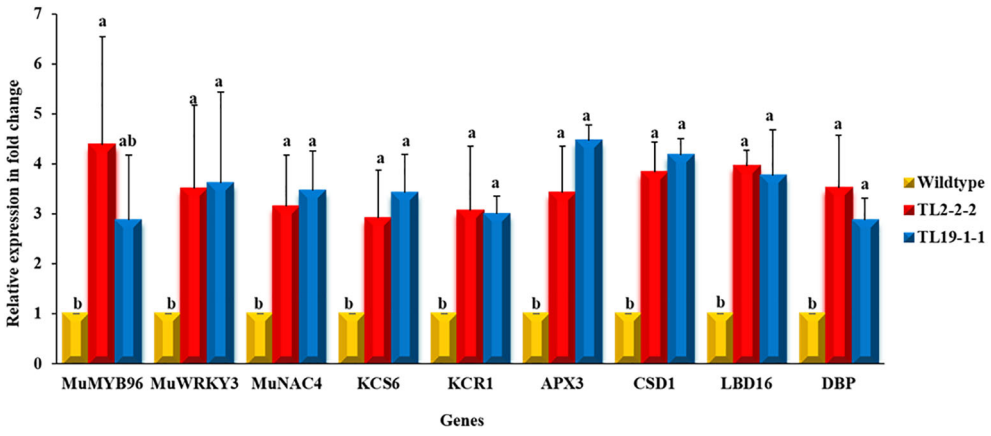

FIGURE 3
Expression profiling of transgenes and downstream genes using qRT-PCR: The leaf samples of multigene groundnut transgenic plants and wild type subjected to drought stress were used for gene expression analysis. Bars represents mean of three biological samples and error bars depicts the standard error and different alphabets represent statistically significant difference with $P \leq 0.05$.

and maintenance of high turgor potential which perhaps not sufficient enough to induce high proline content in multigene transgenic groundnut plants than the wild type and mock plants. Malondialdehyde, the end product of membrane lipid peroxidation, was quantified to assess the extent of oxidative damage caused by imposed drought stress. The multigene transgenic groundnut plants showed significantly lower levels of MDA (310.68-432.28nmol/g F.W) content than the wild type (627.85nmol/g F.W) and mock plants (491.57nmol/g F.W) (Figure 8C).

Antioxidative efficacy in multigene transgenic groundnut plants under drought stress

The wild type and mock plants showed a significant increase in superoxide production under drought stress conditions compared to transgenic plants. A two to four fold decrease in superoxide production was observed in multigene transgenic groundnut plants compared to wild type and mock plants (Figure 9A). Similarly, H_2O_2 production significantly increased in wild type and mock plants with 4.14µmol/g. F.W and 3.41µmol/g F.W of H_2O_2, respectively. The multigene transgenic plants showed a 2-3 fold lower levels of H_2O_2 production (Figure 9B).

The ROS was counter-attacked by antioxidative defense enzymes, such as SOD, and APX were measured in multigene transgenic groundnut plants, wild type, and mock plants under drought stress conditions. Results indicated significantly higher levels of SOD activity with a 2 to 2.2-fold increase in transgenic groundnut plants compared to wild type and mock plants (Figure 9C). In addition, the multigene transgenic plants exhibited APX activity with a range of 0.63-1.04µmol/mg protein/min, which is 3-5 folds higher than that of the wild type (0.18µmol/mg protein/min) and mock plants (0.24µmol/mg protein/min) (Figure 9D).

Discussion

Drought stress affects several morpho-physiological, biochemical, and molecular changes in plants and often triggers the activation of signaling molecules and cascades involved in cellular responses (Sampaio et al., 2022). Several TFs as master regulators of gene expression were identified and reported to be controlling the mechanisms involved in drought stress tolerance (Erpen et al., 2018; Manna et al., 2021; Yoon et al., 2022). Several studies evidenced that overexpression of TF genes in crop plants resulted in enhanced drought stress tolerance (Yuan et al., 2020; Li et al., 2020). Drought stress resulted leaf wilting in multigene transgenic groundnut plants, wild type and transgenic lines. The visible wilting symptoms appeared much earlier in wild type and mock plants with reduced growth than transgenic plants under drought stress (Figure 3).

Multigene transgenic groundnut plants were developed by pyramiding *MuMYB96, MuWRKY3*, and *MuNAC4* genes through gateway cloning technology and evaluated for drought tolerance in comparison with wild type and mock plants. The multigene transgenic plants showed increased expression of the *MuMYB96* gene under drought conditions similar to that of the reports in *Camelina sativa* conferring enhanced drought tolerance (Lee et al., 2014). Cuticular wax forms the outer layer of areal parts and considered an early adaptive trait against water stress and protect the plants from harmful UV

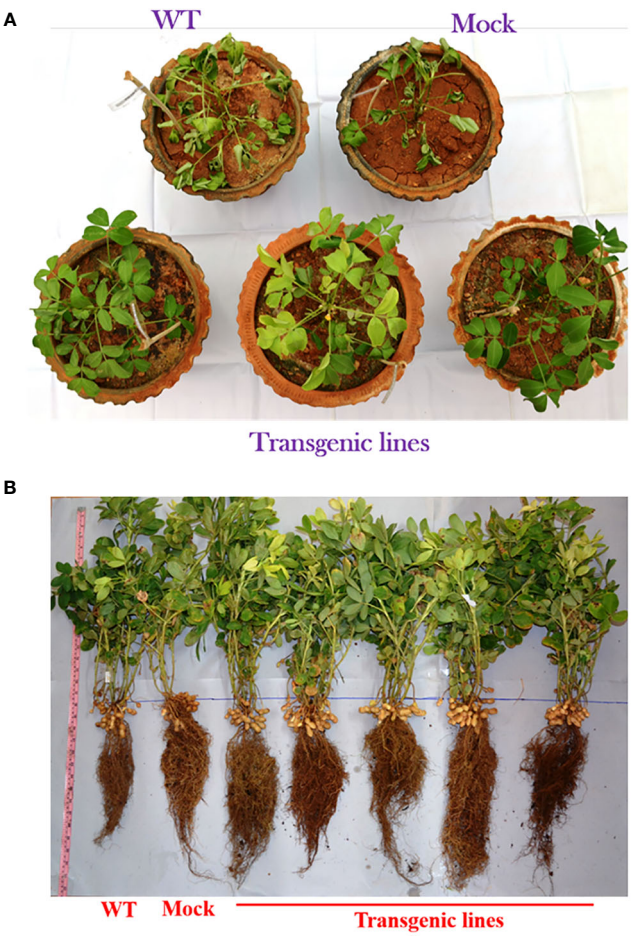

FIGURE 4
Response of groundnut transgenic plants to drought stress. **(A)**. Drought stress assay - Image showing the stay-green nature of multigene transgenic groundnut plants after 10 days of drought stress. Wild type (WT) and mock plants showed severe visible wilting symptoms whereas transgenic plants showed stay green nature under drought stress. **(B)** Phenotypic-trait analysis of multigene transgenic groundnut plants at harvest stage. Image showing profuse growth of lateral root density, shoot biomass and more pods in multigene transgenic plants compared to wild type and mock plants.

TABLE 1 Growth and yield related parameters in multigene transgenic groundnut plants, wild type and mock plants subjected to drought stress.

Genotype	Shoot length (cm/plant)	Root length (cm/plant)	Shoot dry weight (g/plant)	Root dry weight (g/plant)	No. of Pegs/ plant	No. of Pods/ plant	Pod dry weight/ plant(g)
Wild type	34.33 ± 3.18^{c}	26.40 ± 2.77^{e}	19.50 ± 1.40^{f}	1.47 ± 0.37^{g}	21.33 ± 1.52^{d}	16.00 ± 3.60^{c}	13.32 ± 2.19^{d}
Mock	35.00 ± 1.41^{c}	24.93 ± 3.95^{e}	18.60 ± 3.40^{f}	2.32 ± 0.93^{fg}	22.33 ± 4.72^{d}	14.33 ± 1.52^{c}	14.62 ± 3.74^{d}
TL2-2-2	54.33 ± 4.58^{a}	39.73 ± 3.05^{abcd}	36.60 ± 1.03^{ab}	3.81 ± 0.59^{bcd}	40.33 ± 5.13^{ab}	26.33 ± 4.16^{ab}	26.04 ± 5.39^{abc}
TL6-2-1	47.00 ± 1.81^{b}	40.93 ± 2.87^{abc}	25.89 ± 3.36^{e}	4.58 ± 1.21^{bc}	34.33 ± 4.16^{bc}	27.00 ± 2.64^{ab}	27.81 ± 2.19^{ab}
TL11-1-3	53.33 ± 4.42^{a}	39.70 ± 7.80^{abcd}	31.01 ± 2.00^{cd}	3.72 ± 0.44^{cd}	42.00 ± 3.60^{a}	28.33 ± 3.51^{a}	25.05 ± 3.57^{abc}
TL19-1-3	48.30 ± 2.12^{b}	42.33 ± 6.20^{ab}	41.43 ± 2.08^{a}	5.07 ± 0.32^{b}	40.66 ± 3.05^{ab}	26.66 ± 4.72^{ab}	29.06 ± 1.18^{a}
TL23-1-3	48.00 ± 2.47^{b}	41.00 ± 4.52^{abc}	33.59 ± 4.34^{bcd}	3.93 ± 0.90^{bcd}	33.66 ± 0.57^{c}	24.33 ± 1.52^{ab}	25.84 ± 1.74^{abc}
TL29-1-1	48.50 ± 2.48^{b}	43.50 ± 4.17^{ab}	35.10 ± 5.25^{bc}	3.14 ± 0.32^{def}	37.66 ± 1.52^{abc}	23.66 ± 1.52^{ab}	23.25 ± 2.52^{bc}
TL36-1-4	45.76 ± 3.02^{b}	46.33 ± 1.29^{a}	28.583 ± 2.78^{de}	6.44 ± 0.24^{a}	34.33 ± 4.04^{bc}	24.33 ± 3.05^{ab}	24.98 ± 2.86^{abc}
TL40-2-4	43.76 ± 1.91^{b}	34.86 ± 1.05^{cd}	32.34 ± 2.53^{bcd}	2.42 ± 0.23^{efg}	35.00 ± 4.00^{bc}	23.33 ± 3.21^{ab}	23.93 ± 3.38^{abc}
TL41-1-3	48.33 ± 2.15^{b}	33.60 ± 1.75^{d}	34.38 ± 2.62^{bc}	3.18 ± 1.55^{def}	38.66 ± 6.50^{abc}	24.66 ± 3.05^{ab}	21.19 ± 4.92^{c}
TL42-2-3	45.26 ± 2.75^{b}	39.26 ± 1.49^{bcd}	28.90 ± 0.98^{de}	3.62 ± 0.44^{cde}	36.00 ± 2.00^{abc}	22.66 ± 2.08^{b}	26.16 ± 1.49^{abc}

The values are the mean of three biological experiments with triplicates ± SE. ($P \leq 0.05$).

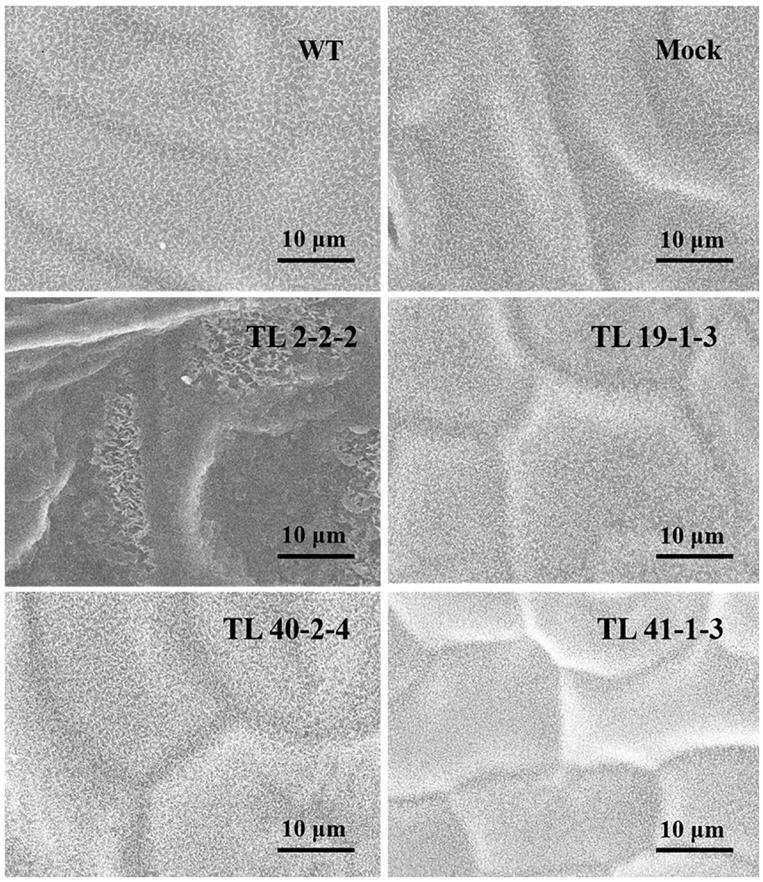

FIGURE 5
Scanning electron microscope (SEM) analysis of wax deposition on leaf surface in groundnut transgenics under drought stress: The image depicting the variation in deposition of cuticular waxes on the leaf surface (adaxial surface) of wild type (WT), mock and multigene transgenic groundnut lines (TL 2-2-2, TL 19-1-3, TL 40-2-4 and TL 41-1-3) under drought stress. The SEM images were taken at 10µm focal length.

radiation and herbivory (Yeats and Rose, 2013; Tafolla-Arellano et al., 2018). Many researchers employed cuticular wax-related genes at the molecular level in conferring stress tolerance in crop plants (Lewandowska et al., 2020). The SEM analysis displayed dense deposition of wax crystals on the leaf surface of transgenic plants, whereas sparingly distributed wax crystals were observed in wild type plants (Figure 4). SEM results were supported by the wax content in transgenic plants under drought stress. The transgenic plants showed more than two-fold increase in cuticular wax content in the leaves of multigene transgenic plants than the wild type. *MuMYB96* transcript levels were significantly increased in multigene transgenic plants and also resulted in the overexpression of its downstream target genes *KCS6* and *KCR1*, supporting their role increased cuticular wax accumulation. Earlier drought induced expression of *MYB96* and its downstream genes *KCS6* and *KCR1* were reported in response to drought stress (Lee et al., 2016; Zhang et al., 2019; Lewandowska et al., 2020; Ahmad et al., 2021; Huang et al., 2022) (Figure 8).

Drought stress adversely affects plant-water relations, resulting in reduced cell turgor, stomata closure, restricted gas exchange, and photosynthetic machinery (Kheradmand et al., 2014; Kosar et al., 2015). Therefore, the stability of chlorophylls under water deficit conditions is considered a good criterion for drought tolerance (Arunyanark et al., 2008; Ahmed et al., 2020). In the present study, maximum retention of relative water content and chlorophylls was observed in the leaf tissues of transgenic groundnut plants compared to wild type and mock plants (Figures 5A, B). Furthermore, several previous investigations on overexpressing different regulatory and functional genes reported relatively higher chlorophyll content and RWC in transgenic groundnut plants, conferring improved drought tolerance (Bhatnagar-Mathur et al., 2014; Banavath et al., 2018; Lokesh et al., 2019; Venkatesh et al., 2019) and the results obtained in our study showed a similar trend suggesting the possible drought tolerant mechanism in groundnut transgenics.

Production of ROS (superoxides, peroxides, hydroxyl ions, etc.) is a common phenomenon in response to drought stress in

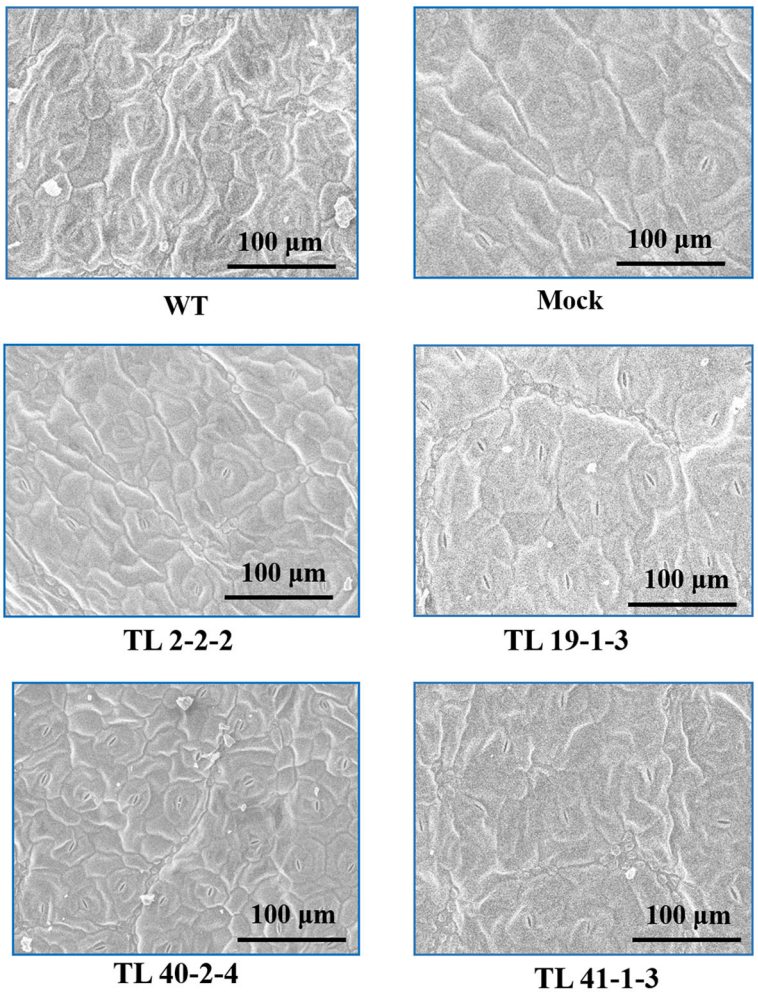

FIGURE 6
Scanning electron microscope (SEM) showing stomata number: The image depicting the variation in the stomata number on the leaf surface (adaxial surface) of wild type (WT), mock and multigene transgenic groundnut lines (TL 2-2-2, TL 19-1-3, TL 40-2-4 and TL 41-1-3) under drought stress. The SEM images were taken at 100µm focal length.

plants, and hyper-accumulation of ROS is lethal (Gill and Tuteja, 2010; Laxa et al., 2019; Soares et al., 2019). Under drought stress, the multigene transgenic groundnut plants exhibited reduced levels of superoxide and hydrogen peroxide content; in contrast, an increased antioxidative enzyme (SOD and APX) activity was observed in transgenic plants over non-transgenic plants (Figure 7). These results were positively correlated with the qRTPCR analysis of *APX3* and *CSD1* genes, which showed 3 to 4-fold higher transcript levels in transgenic plants than in wild type plants (Figure 8). Previous studies in various crop species reported enhanced expression of *MuWRKY3* gene and antioxidative genes (*SOD*, *CAT*, and *POD*) conferred oxidative defense in response to drought stress (Morita et al., 2011; Feng et al., 2014; Guo et al., 2018; Kiranmai et al., 2018) Low levels of malondialdehyde, a biomarker of lipid peroxidation in transgenic plants (Figure 8C), suggest that reduced oxidative damage in the plant cells under drought stress was possibly protected by the improved anti-oxidant machinery (Levine et al., 1994; Ramu et al., 2016; Kiranmai et al., 2018) Following previous studies, the overexpression of the *MuWRKY3* gene under drought stress improves the tolerance of transgenic groundnut (Kiranmai et al., 2018).

Osmoregulation, through the accumulation of osmolytes such as proline, sugars, betaines, polyols, etc., plays a crucial role in maintaining cell turgor under water stress (Verbruggen and Hermans, 2008; Blum, 2017). In the present investigation, we reported a significant accumulation of soluble sugars in multigene transgenic plants in correspondence with wild type plants under drought stress (Figure 8A). Zhang et al. (2017) reported a 17-24% increase in the total soluble sugar content in a

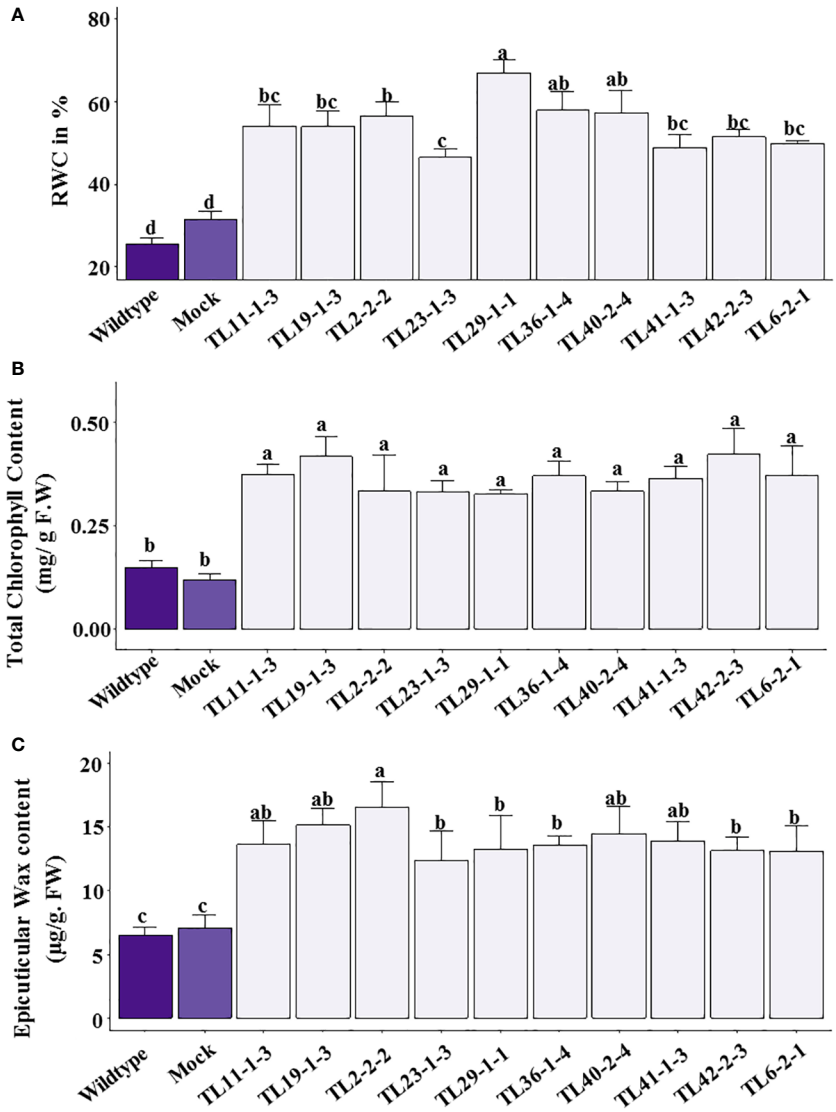

FIGURE 7
Physiological parameters in multigene transgenics lines, wild type and mock plants under drought stress: **(A)** Relative water content (% RWC), **(B)** Total chlorophyll content, **(C)** Epicuticular wax content. The values are mean of 3 biological replicates (n=3) and error bars denotes standard error. The alphabets on the error bars indicate significant variation ($p \leq 0.05$) between transgenic lines, wild type and mock plants.

drought-tolerant groundnut cultivar Shanhua 11 under drought-stress conditions. Overexpression of *PDH45*, *NAC4* and *WRKY3* in groundnut demonstrated hyperaccumulation of soluble sugars under drought stress (Manjulatha et al., 2014; Pandurangaiah et al., 2014; Kiranmai et al., 2018; Kokkanti et al., 2022). In contrast, multigene transgenic groundnut plants showed a lower proline content upon drought stress compared to wild type (Figure 8B). The lower level of proline could possibly be due to the maintenance of better RWC and partial cellular turgor potential in multigene transgenic plants. However, previous studies in groundnut upon co-expression of multiple genes (*Alfin1, PgHSF4*, and *PDH45*) showed increased proline content under moisture stress (Ramu et al., 2016).

A profuse root system has been considered an adaptive strategy to enhance water uptake under water-limited conditions (Basu et al., 2016). In the present study, the multigene transgenic lines showed increased root length (Figure 3A) and growth of lateral root volume than the wild type and mock plants. The current investigation also revealed the expression of root-associated genes such as *LBD16* and *DBP* with increased transcript levels in transgenic plants under drought-stress conditions (Figure 8). Previous reports demonstrated the role of *LBD16* and *DBP* genes

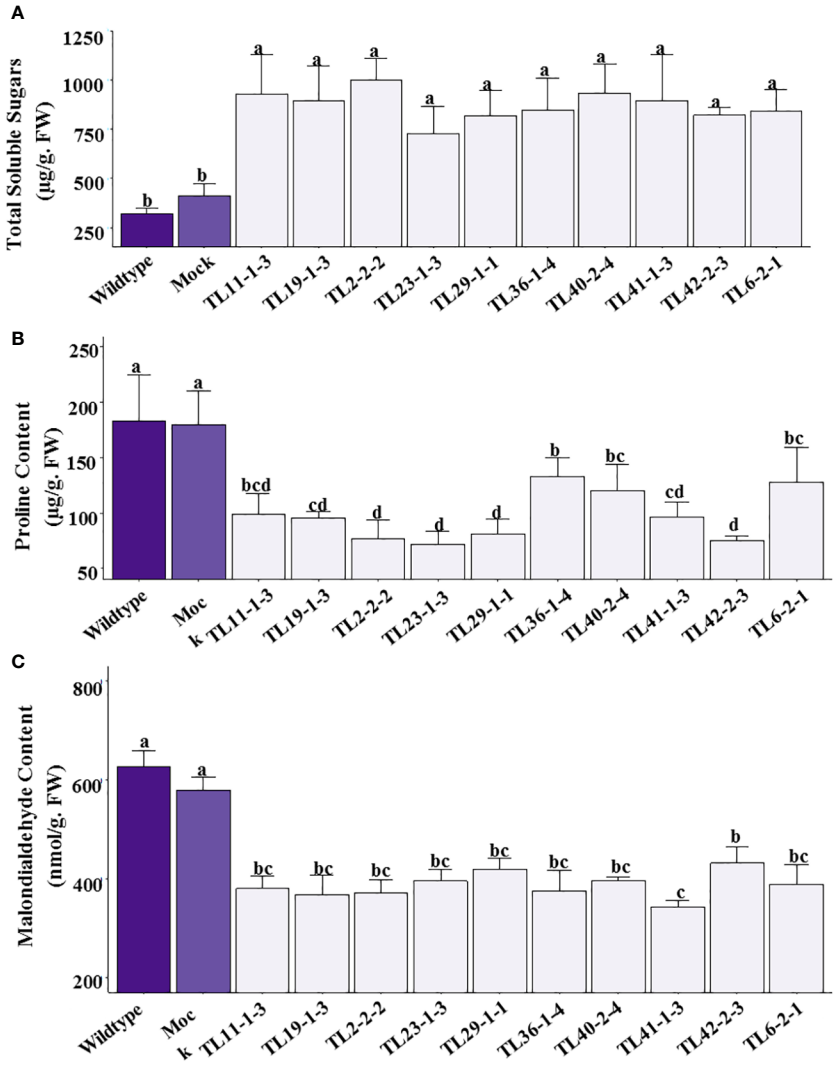

FIGURE 8
Osmolytes and Malondialdehyde content in multigene transgenic lines, wild type and mock plants under drought stress: **(A)**. Total soluble sugars, **(B)**. Free proline content, and **(C)**. Malondialdehyde content. The values are mean of three biological replicates (n=3) and error bars denotes standard error. The alphabets on the error bars indicates significant variation ($p \leq 0.05$) between transgenic lines, wild type and mock plants.

in root initiation and lateral root development in different plant species under various abiotic stresses (Liu et al., 2018; Zhang et al., 2018). Overexpression of the *MuNAC4* transcription factor gene in groundnut resulted in increased root volume and biomass under drought stress (Pandurangaiah et al., 2014). In our study, *MuNAC4* gene expression and other TF genes possibly contribute to improved root architecture in multigene transgenic groundnut plants. In addition, transcript levels of *MuNAC4* were found to be higher in transgenic plants than in wild type plants under drought stress conditions. These results are in concomitant with previous studies by Pandurangaiah et al. (2014). Several studies reported that overexpression of TF genes and regulation of genes involved in root trait development were proved to enhance drought stress tolerance in crop plants (Le et al., 2011; Chen et al., 2018; Figueroa et al., 2021).

Overexpression of TFs, *MuMYB96, MuWRKY3*, and *MuNAC4* contributed to improved physiological and biochemical traits, which resulted in delayed wilting, and stay-green nature of leaves under drought stress, and complete recovery rate after stress withdrawal (Figure 3). Overexpression of single transcription factor genes in groundnut plants conferred stress tolerance against drought stress; however, in this study stacking multiple genes showed enhanced tolerance levels compared to single gene transgenics (Pandurangaiah et al., 2014; Ramu et al., 2016; Kiranmai et al., 2018; Venkatesh et al., 2019). In addition to enhanced drought stress tolerance, better

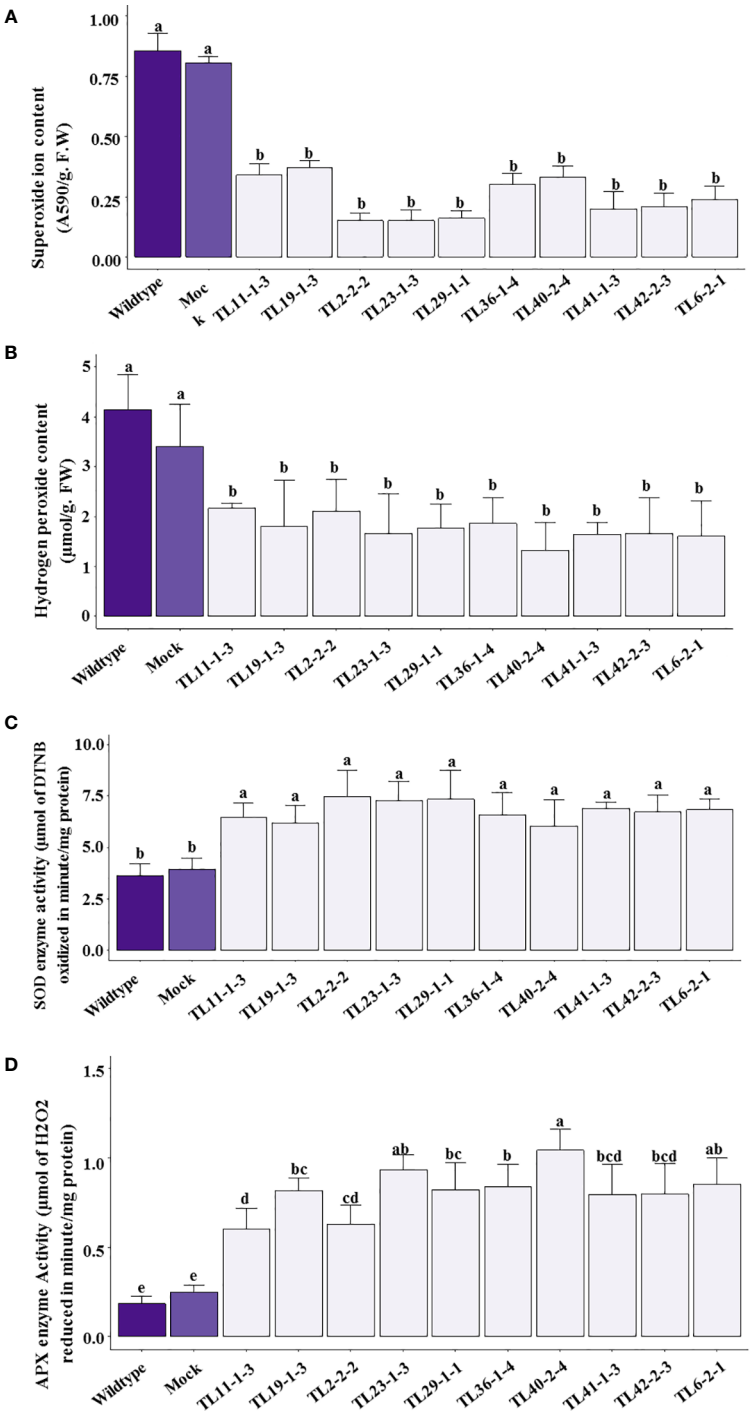

FIGURE 9
Reactive oxygen species (ROS) and anti-oxidative enzyme efficacy in multigene transgenic plants, wild type and mock plants under drought stress: **(A)**. superoxides, and **(B)**. hydrogen peroxide content), **(C)**. superoxide dismutase (SOD) and **(D)**. ascorbate peroxidase (APX) activity in wild type, mock and multigene transgenic groundnut plants under drought stress conditions. The values are mean of three biological replicates (n=3) and error bars denotes standard error. The alphabets on the error bars indicates significant variation ($p<0.05$) between transgenic lines, wild type and mock plants.

growth traits like shoot and root volume, and yield traits like pod number, and pod dry weight in transgenic plants compared to wild type and mock plants also observed (Table 1).

Conclusions

The present study focused on developing transgenic groundnut plants by simultaneously expressing three regulatory genes, *MuMYB96, MuWRKY3*, and *MuNAC4*, to enhance drought tolerance. Expression of the *MuMYB96* gene in multigene transgenic groundnut plants exhibited increased epicuticular wax accumulation, thereby reducing non-stomatal water loss under water-limited conditions. Furthermore, improved water mining traits like root length contributed to maintaining cell turgor and stay-green in transgenic plants under drought stress due to the overexpression of *MuNAC4* gene in multigene transgenics. Furthermore, the transgenic plants displayed increased osmolyte accumulation, anti-oxidant enzyme activity, and detoxification of ROS, resulting in improved cellular level drought tolerance could be due to the expression of the *MuWRKY3* gene along with the other two other TF genes. In summary, improvement of superior water conservation, water mining, and cellular level tolerance traits in groundnut transgenics suggest the pyramiding of multiple TF genes for improving the manifold traits is a viable option to cope with the drought stress impact on crop plants with a limited yield penalty.

Data availability statement

The original contributions presented in the study are included in the article/Supplementary Materials. Further inquiries can be directed to the corresponding author.

Author contributions

CS conceptualized and designed the experiments. BV performed the research. AV, NuJ, and NJ performed data analysis. AA contributed bioinformatics annotation. AV, BR, KM, KK, and MP contributed vector construction. CS, BV, KM, and AV wrote the paper. All authors provided inputs to develop the manuscript. All authors contributed to the article and approved the submitted version.

Funding

CSIR-SRF fellowship (No: 09/383(0051)/2016-EMR-I) and DBT (BT/PR.15503/AGR/02/913/2015).

Acknowledgments

We acknowledge the DBT (BT/PR.15503/AGR/02/913/2015) and CSIR-SRF fellowship (09/383(0051)/2016-EMR-I) Government of India, New Delhi for financial support in the form of a research grant to CS and BV. We greatly acknowledge Late Prof. M. Udayakumar and Dr. Ramu S Vemanna, University of Agricultural Sciences, Bengaluru for providing vectors for multisite gateway technology. We deeply condole the sudden demise of Late Prof. M. Udayakumar and we know that his passing will not only leave a void in our research, but in the hearts of all those who knew him. Prof. Udayakumar will always remain within our hearts and we dedicate this article to Prof. Udayakumar.

Conflict of interest

The authors declare that the research was conducted in the absence of any commercial or financial relationships that could be construed as a potential conflict of interest.

Publisher's note

Supplementary material

The Supplementary Material for this article can be found online at: https://www.frontiersin.org/articles/10.3389/fpls.2022.1055851/full#supplementary-material

References

Ahmad, H. M., Rahman, M. U., Ahmar, S., Fiaz, S., Azeem, F., Shaheen, T., et al. (2021). Comparative genomic analysis of MYB transcription factors for cuticular wax biosynthesis and drought stress tolerance in helianthus annuus l. *Saudi J. Biol. Sci.* 28, 5693–5703. doi: 10.1016/j.sjbs.2021.06.009

Ahmed, H. G. M. D., Zeng, Y., Yang, X., Anwaar, H. A., Mansha, M. Z., Hanif, C. M. S., et al. (2020). Conferring drought-tolerant wheat genotypes through morpho-physiological and chlorophyll indices at seedling stage. *Saudi J. Biol. Sci.* 27, 2116–2123. doi: 10.1016/j.sjbs.2020.06.019

Anjum, S. A., Ashraf, U., Zohaib, A., Tanveer, M., Naeem, M., Ali, I., et al. (2017). Growth and development responses of crop plants under drought stress: a review. *Zemdirbyste.* 104, 267–276. doi: 10.13080/z-a.2017.104.034

Arunyanark, A., Jogloy, S., Akkasaeng, C., Vorasoot, N., Kesmala, T., Nageswara Rao, R. C., et al. (2008). Chlorophyll stability is an indicator of drought tolerance in peanut. *J. Agron. Crop Sci.* 194, 113–125. doi: 10.1111/j.1439-037X.2008.00299.x

Augustine, S. M., Ashwin Narayan, J., Syamaladevi, D. P., Appunu, C., Chakravarthi, M., Ravichandran, V., et al. (2015). Overexpression of *EaDREB2* and pyramiding of *EaDREB2* with the pea DNA helicase gene (*PDH45*) enhance drought and salinity tolerance in sugarcane (*Saccharum* spp. hybrid). *Plant Cell Rep.* 34, 247–263. doi: 10.1007/s00299-014-1704-6

Babitha, K. C., Ramu, S. V., Pruthvi, V., Mahesh, P., Nataraja, K. N., and Udayakumar, M. (2013). Co-Expression of *AtbHLH17* and *AtWRKY28* confers resistance to abiotic stress in arabidopsis. *Transgenic Res.* 22, 327–341. doi: 10.1007/s11248-012-9645-8

Banavath, J. N., Chakradhar, T., Pandit, V., Konduru, S., Guduru, K. K., Akila, C. S., et al. (2018). Stress inducible overexpression of *AtHDG11* leads to improved drought and salt stress tolerance in peanut (*Arachis hypogaea* l.). *Front. Chem.* 6, 34. doi: 10.3389/fchem.2018.00034

Basu, D., Tian, L., Debrosse, T., Poirier, E., Emch, K., Herock, H., et al. (2016). Glycosylation of a fasciclin-like arabinogalactan-protein (*SOS5*) mediates root growth and seed mucilage adherence *via* a cell wall receptor-like kinase (*FEI1/FEI2*) pathway in arabidopsis. *PloS One* 11, 0145092. doi: 10.1371/journal.pone.0145092

Bates, L. S., Waldren, R. P., and Teare, I. D. (1973). Rapid determination of free proline for water-stress studies. *Plant Soil.* 39, 205–207. doi: 10.1007/BF00018060

Bengough, A. G., McKenzie, B. M., Hallett, P. D., and Valentine, T. A. (2011). Root elongation, water stress, and mechanical impedance: a review of limiting stresses and beneficial root tip traits. *J. Exp. Bot.* 62, 59–68. doi: 10.1093/jxb/erq350

Bhatnagar-Mathur, P., Devi, M. J., Reddy, D. S., Lavanya, M., Vadez, V., Serraj, R., et al. (2007). Stress-inducible expression of *At DREB1A* in transgenic peanut (*Arachis hypogaea* l.) increases transpiration efficiency under water-limiting conditions. *Plant Cell Rep.* 26, 2071–2082. doi: 10.1007/s00299-007-0406-8

Bhatnagar-Mathur, P., Rao, J. S., Vadez, V., Dumbala, S. R., Rathore, A., Yamaguchi-Shinozaki, K., et al. (2014). Transgenic peanut overexpressing the *DREB1A* transcription factor has higher yields under drought stress. *Mol. Breed.* 33, 327–340. doi: 10.1007/s11032-013-9952-7

Blum, A. (2017). Osmotic adjustment is a prime drought stress adaptive engine in support of plant production. *Plant Cell Environ.* 40, 4–10. doi: 10.1111/pce.12800

Buscaill, P., and Rivas, S. (2014). Transcriptional control of plant defence responses. *Curr. Opin. Plant Biol.* 20, 35–46. doi: 10.1016/j.pbi.2014.04.004

Chen, D., Chai, S., McIntyre, C. L., and Xue, G. P. (2018). Overexpression of a predominantly root-expressed NAC transcription factor in wheat roots enhances root length, biomass and drought tolerance. *Plant Cell Rep.* 37, 225–237. doi: 10.1007/s00299-017-2224-y

Coudert, Y., Périn, C., Courtois, B., Khong, N. G., and Gantet, P. (2010). Genetic control of root development in rice, the model cereal. *Trends Plant Sci.* 15, 219–226. doi: 10.1016/j.tplants.2010.01.008

de Dorlodot, S., Forster, B., Pagès, L., Price, A., Tuberosa, R., and Draye, X. (2007). Root system architecture: opportunities and constraints for genetic improvement of crops. *Trends Plant Sci.* 12, 474–481. doi: 10.1016/j.tplants.2007.08.012

de Mendiburu, F. (2014). Agricolae: statistical procedures for agricultural research. *R Package version.* 1, 1–4. Available at: http://CRAN-Project.org/package=agricolae.

Erpen, L., Devi, H. S., Grosser, J. W., and Dutt, M. (2018). Potential use of the DREB/ERF, MYB, NAC and WRKY transcription factors to improve abiotic and biotic stress in transgenic plants. *Plant Cell Tissue Organ Cult.* 132, 1–25. doi: 10.1007/s11240-017-1320-6

Fang, Y., and Xiong, L. (2015). General mechanisms of drought response and their application in drought resistance improvement in plants. *Cell. Mol. Life Sci.* 72, 673–689. doi: 10.1007/s00018-014-1767-0

FAOSTAT (2019). Available at: https://www.fao.org/faostat/en/#data/QCL/visualize.

Farooq, M., Hussain, M., Wahid, A., and Siddique, K. H. M. (2012). "Drought stress in plants: An overview," in *Plant responses to drought stress*. Ed. R. Aroca (Berlin, Heidelberg: Springer), 1–33. doi: 10.1007/978-3-642-32653-0_1

Feng, L., Gao, Z., Xiao, G., Huang, R., and Zhang, H. (2014). Leucine-rich repeat receptor-like kinase FON1 regulates drought stress and seed germination by activating the expression of ABA-responsive genes in rice. *Plant Mol. Biol. Rep.* 32, 1158–1168. doi: 10.1007/s11105-014-0718-0

Fich, E. A., Segerson, N. A., and Rose, J. K. (2016). The plant polyester cutin: biosynthesis, structure, and biological roles. *Annu. Rev. Plant Biol.* 67, 207–233. doi: 10.1146/annurev-arplant-043015-111929

Figueroa, N., Lodeyro, A. F., Carrillo, N., and Gómez, R. (2021). Meta-analysis reveals key features of the improved drought tolerance of plants overexpressing NAC transcription factors. *Environ. Exp. Bot.* 186, 104449. doi: 10.1016/j.envexpbot.2021.104449

Franco-Zorrilla, J. M., López-Vidriero, I., Carrasco, J. L., Godoy, M., Vera, P., and Solano, R. (2014). DNA-Binding specificities of plant transcription factors and their potential to define target genes. *Proc. Natl. Acad. Sci.* 111, 2367–2372. doi: 10.1073/pnas.1316278111

Gill, S. S., and Tuteja, N. (2010). Reactive oxygen species and anti-oxidant machinery in abiotic stress tolerance in crop plants. *Plant Physiol. Biochem.* 48, 909–930. doi: 10.1016/j.plaphy.2010.08.016

Goel, P., and Singh, A. K. (2018). "Single-versus multigene transfer approaches for crop abiotic stress tolerance," in *Biochemical, physiological and molecular avenues for combating abiotic stress tolerance in plants*. Ed. S. H. Wani (London, UK: Academic Press), 255–275. doi: 10.1016/B978-0-12-813066-7.00014-0

Gomes, F. P., and Prado, C. H. (2007). Ecophysiology of coconut palm under water stress. *Braz. J. Plant Physiol.* 19, 377–391. doi: 10.1590/S1677-04202007000400.008

Guo, R., Qiao, H., Zhao, J., Wang, X., Tu, M., Guo, C., et al. (2018). The grape *VlWRKY3* gene promotes abiotic and biotic stress tolerance in transgenic *Arabidopsis thaliana*. *Front. Plant Sci.* 9, 545. doi: 10.3389/fpls.2018.00545

Guo, L., Yang, H., Zhang, X., and Yang, S. (2013). *Lipid transfer protein3* as a target of *MYB96* mediates freezing and drought stress in arabidopsis. *J. Exp. Bot.* 64, 1755–1767. doi: 10.1093/jxb/ert040

Hammer, G. L., Dong, Z., McLean, G., Doherty, A., Messina, C., Schussler, J., et al. (2009). Can changes in canopy and/or root system architecture explain historical maize yield trends in the US corn belt? *Crop Sci.* 49, 299–312. doi: 10.2135/cropsci2008.03.0152

Hichri, I., Muhovski, Y., Žižková, E., Dobrev, P. I., Gharbi, E., Franco-Zorrilla, J. M., et al. (2017). The *Solanum lycopersicum* WRKY3 transcription factor *SlWRKY3* is involved in salt stress tolerance in tomato. *Front. Plant Sci.* 8, 1343. doi: 10.3389/fpls.2017.01343

Hiscox, J. D., and Israelstam, G. F. (1979). A method for the extraction of chlorophyll from leaf tissue without maceration. *Canad. J. Bot.* 57, 1332–1334. doi: 10.1139/b79-163

Hodge, A., Berta, G., Doussan, C., Merchan, F., and Crespi, M. (2009). Plant root growth, architecture and function. *Plant Soil.* 321, 153–187. doi: 10.1007/s11104-009-9929-9

Hrmova, M., and Hussain, S. S. (2021). Plant transcription factors involved in drought and associated stresses. *Int. J. Mol. Sci.* 22, 5662. doi: 10.3390/ijms22115662

Huang, H., Ayaz, A., Zheng, M., Yang, X., Zaman, W., Zhao, H., et al. (2022). Arabidopsis *KCS5* and *KCS6* play redundant roles in wax synthesis. *Int. J. Mol. Sci.* 23, 4450. doi: 10.3390/ijms23084450

Iqbal, A., Fahad, S., Iqbal, M., Alamzeb, M., Ahmad, A., Anwar, S., et al. (2020). "Special adaptive features of plant species in response to drought," in *Salt and drought stress tolerance in plants*. Eds. M. Hasanuzzaman and M. Tanveer (Cham: Springer), 77–118. doi: 10.1007/978-3-030-40277-8_4

Janiak, A., Kwaśniewski, M., and Szarejko, I. (2016). Gene expression regulation in roots under drought. *J. Exp. Bot.* 67, 1003–1014. doi: 10.1093/jxb/erv512

Jenks, M. A., Andersen, L., Teusink, R. S., and Williams, M. H. (2001). Leaf cuticular waxes of potted rose cultivars as affected by plant development, drought and paclobutrazol treatments. *Physiol. Plant* 112, 62–70. doi: 10.1034/j.1399-3054.2001.1120109.x

Jongrungklang, N., Toomsan, B., Vorasoot, N., Jogloy, S., Boote, K. J., Hoogenboom, G., et al. (2013). Drought tolerance mechanisms for yield responses to pre-flowering drought stress of peanut genotypes with different drought tolerant levels. *Field Crops Res.* 144, 34–42. doi: 10.1016/j.fcr.2012.12.017

Joshi, R., Wani, S. H., Singh, B., Bohra, A., Dar, Z. A., Lone, A. A., et al. (2016). Transcription factors and plants response to drought stress: current understanding and future directions. *Front. Plant Sci.* 7, 1029. doi: 10.3389/fpls.2016.01029

Jung, H., Chung, P. J., Park, S. H., Redillas, M. C. F. R., Kim, Y. S., Suh, J. W., et al. (2017). Overexpression of *OsERF48* causes regulation of *OsCML16*, a calmodulin-like protein gene that enhances root growth and drought tolerance. *Plant Biotechnol. J.* 15, 1295–1308. doi: 10.1111/pbi.12716

Junglee, S., Urban, L., Sallanon, H., and Lopez-Lauri, F. (2014). Optimized assay for hydrogen peroxide determination in plant tissue using potassium iodide. *Am. J. Anal. Chem.* 5, 730. doi: 10.4236/ajac.2014.511081

Kambiranda, D. M., Vasanthaiah, H. K., Katam, R., Ananga, A., Basha, S. M., and Naik, K. (2011). "Impact of drought stress on peanut (Arachis hypogaea l.) productivity and food safety," in *Plants and environment*. Eds. H. Vasanthaiah and D. Kambiranda, (Croatia: InTech) 249–272.

Kheradmand, M. A., Fahraji, S. S., Fatahi, E., and Raoofi, M. M. (2014). Effect of water stress on oil yield and some characteristics of *Brassica napus*. *Int. Res. J. Basic Appl. Sci.* 8, 1447–1453.

Kiranmai, K., Gunupuru, L. R., Nareshkumar, A., Reddy, V. A., Lokesh, U., Pandurangaiah, M., et al. (2016). Expression analysis of WRKY transcription factor genes in response to abiotic stresses in horsegram (*Macrotyloma uniflorum* (Lam.) verdc.). *Am. J. Mol. Biol.* 6, 125–137. doi: 10.4236/ajmb.2016.64013

Kiranmai, K., Lokanadha Rao, G., Pandurangaiah, M., Nareshkumar, A., Amaranatha Reddy, V., Lokesh, U., et al. (2018). A novel WRKY transcription factor, MuWRKY3 (Macrotyloma uniflorum lam. verdc.) enhances drought stress tolerance in transgenic groundnut (Arachis hypogaea l.) plants. *Front. Plant Sci.* 9, 346. doi: 10.3389/fpls.2018.00346

Kishor, P. B. K., Venkatesh, K., Amareshwari, P., Hima Kumari, P., Punita, D. L., Anil Kumar, S., et al. (2018). Genetic engineering for salt and drought stress tolerance in peanut (*Arachis hypogaea* l.). *Indian J. Plant Physiol.* 23, 647–652. doi: 10.1007/s40502-018-0421-5

Kokkanti, R. R., Vemuri, H., Gaddameedi, A., and Rayalacheruvu, U. (2022). Variability in drought stress-induced physiological, biochemical responses and expression of *DREB2A, NAC4* and *HSP70* genes in groundnut (*Arachis hypogaea* l.). *S. Afr. J. Bot.* 144, 448–457. doi: 10.1016/j.sajb.2021.09.025

Kosar, F., Akram, N. A., and Ashraf, M. (2015). Exogenously-applied 5-aminolevulinic acid modulates some key physiological characteristics and antioxidative defense system in spring wheat (*Triticum aestivum* l.) seedlings under water stress. *S. Afr. J. Bot.* 96, 71–77. doi: 10.1016/j.sajb.2014.10.015

Lai, Z., Vinod, K. M., Zheng, Z., Fan, B., and Chen, Z. (2008). Roles of arabidopsis WRKY3 and WRKY4 transcription factors in plant responses to pathogens. *BMC Plant Biol.* 8, 1–13. doi: 10.1186/1471-2229-8-68

Laxa, M., Liebthal, M., Telman, W., Chibani, K., and Dietz, K. J. (2019). The role of the plant anti-oxidant system in drought tolerance. *Anti-oxidants.* 8, 94. doi: 10.3390/antiox8040094

Lee, S. B., Kim, H., Kim, R. J., and Suh, M. C. (2014). Overexpression of arabidopsis *MYB96* confers drought resistance in *Camelina sativa via* cuticular wax accumulation. *Plant Cell Rep.* 33, 1535–1546. doi: 10.1007/s00299-014-1636-1

Lee, S. B., Kim, H. U., and Suh, M. C. (2016). MYB94 and MYB96 additively activate cuticular wax biosynthesis in arabidopsis. *Plant Cell Physiol.* 57, 2300–2311. doi: 10.1093/pcp/pcw147

Lee, S. B., and Suh, M. C. (2015). Advances in the understanding of cuticular waxes in *Arabidopsis thaliana* and crop species. *Plant Cell Rep.* 34, 557–572. doi: 10.1007/s00299-015-1772-2

Le, D. T., Nishiyama, R., Watanabe, Y., Mochida, K., Yamaguchi-Shinozaki, K., Shinozaki, K., et al. (2011). Genome-wide survey and expression analysis of the plant-specific NAC transcription factor family in soybean during development and dehydration stress. *DNA Res.* 18, 263–276. doi: 10.1093/dnares/dsr015

Levine, A., Tenhaken, R., Dixon, R., and Lamb, C. (1994). H2O2 from the oxidative burst orchestrates the plant hypersensitive disease resistance response. *Cell.* 79, 583–593. doi: 10.1016/0092-8674(94)90544-4

Lewandowska, M., Keyl, A., and Feussner, I. (2020). Wax biosynthesis in response to danger: its regulation upon abiotic and biotic stress. *New Phytol.* 227, 698–713. doi: 10.1111/nph.16571

Li, Z., Hua, X., Zhong, W., Yuan, Y., Wang, Y., Wang, Z., et al. (2020). Genome-wide identification and expression profile analysis of WRKY family genes in the autopolyploid *Saccharum spontaneum*. *Plant Cell Physiol.* 61, 616–630. doi: 10.1093/pcp/pcz227

Liu, W., Yu, J., Ge, Y., Qin, P., and Xu, L. (2018). Pivotal role of *LBD16* in root and root-like organ initiation. *Cell. Mol. Life Sci.* 75, 3329–3338. doi: 10.1007/s00018-018-2861-5

Liu, Q. L., Zhong, M., Li, S., Pan, Y. Z., Jiang, B. B., Jia, Y., et al. (2013). Overexpression of a chrysanthemum transcription factor gene, *DgWRKY3*, in tobacco enhances tolerance to salt stress. *Plant Physiol. Biochem.* 69, 27–33. doi: 10.1016/j.plaphy.2013.04.016

Livak, K. J., and Schmittgen, T. D. (2001). Analysis of relative gene expression data using real-time quantitative PCR and the $2^{-\Delta\Delta CT}$ method. *Methods.* 25, 402–408. doi: 10.1006/meth.2001.1262

Lokesh, U., Venkatesh, B., Kiranmai, K., Nareshkumar, A., Amarnathareddy, V., Rao, G. L., et al. (2019). Overexpression of *ß-ketoacyl Co-a Synthase1* gene improves tolerance of drought susceptible groundnut (*Arachis hypogaea* l.) cultivar K-6 by increased leaf epicuticular wax accumulation. *Front. Plant Sci.* 9, 1869. doi: 10.3389/fpls.2018.01869

Lynch, J. (1995). Root architecture and plant productivity. *Plant Physiol.* 109, 7–13. doi: 10.1104/pp.109.1.7

Mamrutha, H. M., Mogili, T., Lakshmi, K. J., Rama, N., Kosma, D., Kumar, M. U., et al. (2010). Leaf cuticular wax amount and crystal morphology regulate post-harvest water loss in mulberry (*Morus species*). *Plant Physiol. Biochem.* 48, 690–696. doi: 10.1016/j.plaphy.2010.04.007

Manjulatha, M., Sreevathsa, R., Kumar, A. M., Sudhakar, C., Prasad, T. G., Tuteja, N., et al. (2014). Overexpression of a pea DNA helicase (PDH45) in peanut (Arachis hypogaea l.) confers improvement of cellular level tolerance and productivity under drought stress. *Mol. Biotechnol.* 56, 111–125. doi: 10.1007/s12033-013-9687-z

Manna, M., Thakur, T., Chirom, O., Mandlik, R., Deshmukh, R., and Salvi, P. (2021). Transcription factors as key molecular target to strengthen the drought stress tolerance in plants. *Physiol. Plant* 172, 847–868. doi: 10.1111/ppl.13268

Mei, F., Chen, B., Li, F., Zhang, Y., Kang, Z., Wang, X., et al. (2021). Overexpression of the wheat NAC transcription factor *TaSNAC4-3A* gene confers drought tolerance in transgenic arabidopsis. *Plant Physiol. Biochem.* 160, 37–50. doi: 10.1016/j.plaphy.2021.01.004

Mickelbart, M. V., Hasegawa, P. M., and Bailey-Serres, J. (2015). Genetic mechanisms of abiotic stress tolerance that translate to crop yield stability. *Nat. Rev. Genet.* 16, 237–251. doi: 10.1038/nrg3901

Morita, S., Nakatani, S., Koshiba, T., Masumura, T., Ogihara, Y., and Tanaka, K. (2011). Differential expression of two cytosolic ascorbate peroxidases and two superoxide dismutase genes in response to abiotic stress in rice. *Rice Sci.* 18, 157–166. doi: 10.1016/S1672-6308(11)60023-1

Nahar, K., Hasanuzzaman, M., Alam, M., Rahman, A., Mahmud, J. A., Suzuki, T., et al. (2017). Insights into spermine-induced combined high temperature and drought tolerance in mung bean: osmoregulation and roles of anti-oxidant and glyoxalase system. *Protoplasma.* 254, 445–460. doi: 10.1007/s00709-016-0965-z

Nareshkumar, A., Veeranagamallaiah, G., Pandurangaiah, M., Kiranmai, K., Amaranathareddy, V., Lokesh, U., et al. (2015). Pb-Stress induced oxidative stress caused alterations in antioxidant efficacy in two groundnut (*Arachis hypogaea* l.) cultivars. *Agric. Sci.* 6, 1283. doi: 10.4236/as.2015.610123

Nawrath, C. (2006). Unrevealing the complex network of cuticular structure and function. *Curr. Opin. Plant Biol.* 9, 281–287. doi: 10.1016/j.pbi.2006.03.001

Nguyen, T. X., Nguyen, T., Alameldin, H., Goheen, B., Loescher, W., and Sticklen, M. (2013). Transgene pyramiding of the *HVA1* and *mtlD* in T3 maize (*Zea mays* l.) plants confers drought and salt tolerance, along with an increase in crop biomass. *Int. J. Agron.* 2013, 1–13. doi: 10.1155/2013/598163

Nisarga, K. N., Vemanna, R. S., Kodekallu Chandrashekar, B., Rao, H., Vennapusa, A. R., Narasimaha, A., et al. (2017). *Aldo-ketoreductase 1* (*AKR1*) improves seed longevity in tobacco and rice by detoxifying reactive cytotoxic compounds generated during ageing. *Rice.* 10, 1–12. doi: 10.1186/s12284-017-0148-3

Pandian, B. A., Varanasi, A., Vennapusa, A. R., Sathishraj, R., Lin, G., Zhao, M., et al. (2020). Characterization, genetic analyses, and identification of QTLs conferring metabolic resistance to a 4-hydroxyphenylpyruvate dioxygenase inhibitor in sorghum (*Sorghum bicolor*). *Front. Plant Sci.* 11, 596581. doi: 10.3389/fpls.2020.596581

Pandurangaiah, M., Lokanadha Rao, G., Sudhakarbabu, O., Nareshkumar, A., Kiranmai, K., Lokesh, U., et al. (2014). Overexpression of horsegram (*Macrotyloma uniflorum* lam. verdc.) NAC transcriptional factor (*MuNAC4*) in groundnut confers enhanced drought tolerance. *Mol. Biotechnol.* 56, 758–769. doi: 10.1007/s12033-014-9754-0

Parvathi, M. S., Sreevathsa, R., Rama, N., and Nataraja, K. N. (2015). Simultaneous expression of *AhBTF3, AhNF-YA7* and *EcZF* modulates acclimation responses to abiotic stresses in rice (*Oryza sativa* l). *Proc. Environ. Sci.* 29, 236–237. doi: 10.1016/j.proenv.2015.07.290

Pruthvi, V., Narasimhan, R., and Nataraja, K. N. (2014). Simultaneous expression of abiotic stress responsive transcription factors, *AtDREB2A, AtHB7* and *AtABF3* improves salinity and drought tolerance in peanut (*Arachis hypogaea* l.). *PloS One* 9, 111152. doi: 10.1371/journal.pone.0111152

Ramu, V. S., Swetha, T. N., Sheela, S. H., Babitha, C. K., Rohini, S., Reddy, M. K., et al. (2016). Simultaneous expression of regulatory genes associated with specific drought-adaptive traits improves drought adaptation in peanut. *Plant Biotechnol. J.* 14, 1008–1020. doi: 10.1111/pbi.12461

Reddy, P. C. O., Ranganayakulu, G., Thippeswamy, M., Sudhakar Reddy, P., Reddy, M. K., and Sudhakar, C. (2008). Identification of stress-induced genes from the drought tolerant semi-arid legume crop horsegram (*Macrotyloma uniflorum* (Lam.) verdc.) through analysis of subtracted expressed sequence tags. *Plant Science.* 175, 372–384. doi: 10.1016/j.plantsci.2008.05.012

Riederer, M., and Schreiber, L. (2001). Protecting against water loss: analysis of the barrier properties of plant cuticles. *J. Exp. Bot.* 52, 2023–2032. doi: 10.1093/jexbot/52.363.2023

Rohini, V. K., and Rao, K. S. (2001). Transformation of peanut (*Arachis hypogaea* l.) with tobacco chitinase gene: variable response of transformants to leaf spot disease. *Plant Sci.* 160, 889–898. doi: 10.1016/S0168-9452(00)00462-3

Şahin-Çevik, M., Çevik, B., and Karaca, G. (2014). Expression analysis of WRKY genes from *Poncirus trifoliata* in response to pathogen infection. *J. Plant Interact.* 9, 182–193. doi: 10.1080/17429145.2013.796596

Sampaio, M., Neves, J., Cardoso, T., Pissarra, J., Pereira, S., and Pereira, C. (2022). Coping with abiotic stress in plants-an endomembrane trafficking perspective. *Plants* 11, 338. doi: 10.3390/plants11030338

Sarkar, T., Thankappan, R., Kumar, A., Mishra, G. P., and Dobaria, J. R. (2016). Stress inducible expression of *AtDREB1A* transcription factor in transgenic peanut (*Arachis hypogaea* l.) conferred tolerance to soil-moisture deficit stress. *Front. Plant Sci.* 7, 935. doi: 10.3389/fpls.2016.00935

Seo, P. J., Lee, S. B., Suh, M. C., Park, M. J., Go, Y. S., and Park, C. M. (2011). The MYB96 transcription factor regulates cuticular wax biosynthesis under drought conditions in arabidopsis. *Plant Cell.* 23, 1138–1152. doi: 10.1105/tpc.111.083485

Seo, P. J., and Park, C. M. (2011). Cuticular wax biosynthesis as a way of inducing drought resistance. *Plant Signal. Behav.* 6, 1043–1045. doi: 10.4161/psb.6.7.15606

Seo, P. J., Xiang, F., Qiao, M., Park, J. Y., Lee, Y. N., Kim, S. G., et al. (2009). The MYB96 transcription factor mediates abscisic acid signaling during drought stress response in arabidopsis. *Plant Physiol.* 151, 275–289. doi: 10.1104/pp.109.144220

Shao, H., Wang, H., and Tang, X. (2015). NAC transcription factors in plant multiple abiotic stress responses: progress and prospects. *Front. Plant Sci.* 6, 902. doi: 10.3389/fpls.2015.00902

Simms, D., Cizdziel, P. E., and Chomczynski, P. (1993). TRIzol: A new reagent for optimal single-step isolation of RNA. *Focus.* 15, 532–535.

Singla-Pareek, S. L., Reddy, M. K., and Sopory, S. K. (2003). Genetic engineering of the glyoxalase pathway in tobacco leads to enhanced salinity tolerance. *Proc. Natl. Acad. Sci.* 100, 14672–14677. doi: 10.1073/pnas.2034667100

Skibbe, M., Qu, N., Galis, I., and Baldwin, I. T. (2008). Induced plant defenses in the natural environment: *Nicotiana attenuata WRKY3* and *WRKY6* coordinate responses to herbivory. *Plant Cell.* 20, 1984–2000. doi: 10.1105/tpc.108.058594

Soares, C., Carvalho, M. E., Azevedo, R. A., and Fidalgo, F. (2019). Plants facing oxidative challenges-a little help from the anti-oxidant networks. *Environ. Exp. Bot.* 161, 4–25. doi: 10.1016/j.envexpbot.2018.12.009

Tafolla-Arellano, J. C., Báez-Sañudo, R., and Tiznado-Hernández, M. E. (2018). The cuticle as a key factor in the quality of horticultural crops. *Sci. Hortic.* 232, 145–152. doi: 10.1016/j.scienta.2018.01.005

Varshney, R. K., Bansal, K. C., Aggarwal, P. K., Datta, S. K., and Craufurd, P. Q. (2011). Agricultural biotechnology for crop improvement in a variable climate: hope or hype? *Trends Plant Sci.* 16, 363–371. doi: 10.1016/j.tplants.2011.03.004

Vemanna, R. S., Babitha, K. C., Solanki, J. K., Reddy, V. A., Sarangi, S. K., and Udayakumar, M. (2017). Aldo-keto reductase-1 (AKR1) protect cellular enzymes from salt stress by detoxifying reactive cytotoxic compounds. *Plant Physiol. Biochem.* 113, 177–186. doi: 10.1016/j.plaphy.2017.02.012

Vemanna, R. S., Chandrashekar, B. K., Hanumantha Rao, H. M., Sathyanarayanagupta, S. K., Sarangi, K. S., Nataraja, K. N., et al. (2013). A modified multisite gateway cloning strategy for consolidation of genes in plants. *Mol. Biotechnol.* 53, 129–138. doi: 10.1007/s12033-012-9499-6

Venkatesh, B., Amaranatha Reddy, V., Lokesh, U., Kiranmai, K., Anthony Johnson, A. M., Pandurangaiah, M., et al. (2019). Multigenic groundnut transgenics: An advantage over traditional single gene traits in conferring abiotic stress tolerance: A review. *Res. Reviews: J. Agric. Allied Sci.* 7, 113–120.

Vennapusa, A. R., Agarwal, S., Hm, H. R., Aarthy, T., Babitha, K. C., Thulasiram, H. V., et al. (2022). Stacking herbicide detoxification and resistant genes improves glyphosate tolerance and reduces phytotoxicity in tobacco (*Nicotiana tabacum* l.) and rice (*Oryza sativa* l.). *Plant Physiol. Biochem.* 189, 126–138. doi: 10.1016/j.plaphy.2022.08.025

Verbruggen, N., and Hermans, C. (2008). Proline accumulation in plants: a review. *Amino Acids* 35, 753–759. doi: 10.1007/s00726-008-0061-6

Weigel, D., and Glazabrook, J. (2006). Transformation of agrobacterium using the freeze-thaw method. *Cold Spring Harb. Protoc.* 7, 1031–1036. doi: 10.1101/pdb.prot4665

Xiao, Y., Zhou, L., Lei, X., Cao, H., Wang, Y., Dou, Y., et al. (2017). Genome-wide identification of WRKY genes and their expression profiles under different abiotic stresses in *Elaeis guineensis*. *PloS One* 12, e0189224. doi: 10.1371/journal.pone.0189224

Xue, D., Zhang, X., Lu, X., Chen, G., and Chen, Z. H. (2017). Molecular and evolutionary mechanisms of cuticular wax for plant drought tolerance. *Front. Plant Sci.* 8, 621. doi: 10.3389/fpls.2017.00621

Yamaguchi-Shinozaki, K., and Shinozaki, K. (2006). Transcriptional regulatory networks in cellular responses and tolerance to dehydration and cold stresses. *Annu. Rev. Plant Biol.* 57, 781–803. doi: 10.1146/annurev.arplant.57.032905.105444

Yao, G. Q., Nie, Z. F., Turner, N. C., Li, F. M., Gao, T. P., Fang, X. W., et al. (2021). Combined high leaf hydraulic safety and efficiency provides drought tolerance in *Caragana* species adapted to low mean annual precipitation. *New Phytol.* 229, 230–244. doi: 10.1111/nph.16845

Yeats, T. H., and Rose, J. K. (2013). The formation and function of plant cuticles. *Plant Physiol.* 163, 5–20. doi: 10.1104/pp.113.222737

Yoon, J., Cho, L. H., and Jung, K. H. (2022). Hierarchical structures and dissected functions of MADS-box transcription factors in rice development. *J. Plant Biol.* 65, 99–109. doi: 10.1007/s12374-021-09343-0

Yuan, C., Li, C., Lu, X., Zhao, X., Yan, C., Wang, J., et al. (2020). Comprehensive genomic characterization of NAC transcription factor family and their response to salt and drought stress in peanut. *BMC Plant Biol.* 20, 1–21. doi: 10.1186/s12870-020-02678-9

Zhang, M., Wang, L. F., Zhang, K., Liu, F. Z., and Wan, Y. S. (2017). Drought-induced responses of organic osmolytes and proline metabolism during pre-flowering stage in leaves of peanut (*Arachis hypogaea* l.). *J. Integr. Agric.* 16, 2197–2205. doi: 10.1016/S2095-3119(16)61515-0

Zhang, L., Yao, L., Zhang, N., Yang, J., Zhu, X., Tang, X., et al. (2018). Lateral root development in potato is mediated by stu-mi164 regulation of NAC transcription factor. *Front. Plant Sci.* 9, 383. doi: 10.3389/fpls.2018.00383

Zhang, Y. L., Zhang, C. L., Wang, G. L., Wang, Y. X., Qi, C. H., Zhao, Q., et al. (2019). The R2R3 MYB transcription factor MdMYB30 modulates plant resistance against pathogens by regulating cuticular wax biosynthesis. *BMC Plant Biol.* 19, 1–14. doi: 10.1186/s12870-019-1918-4

frontiers | Frontiers in Plant Science

TYPE Review
PUBLISHED 17 January 2023
DOI 10.3389/fpls.2022.1047410

OPEN ACCESS

EDITED BY
Amaranatha Reddy Vennapusa,
Delaware State University,
United States

REVIEWED BY
Balaji Aravindhan Pandian,
Enko Chem Inc., United States
Dominique Clark Galam,
Virginia State University, United States
Abolghassem Emamverdian,
Nanjing Forestry University, China

*CORRESPONDENCE
Praveen Nagella
praveen.n@christuniversity.in
Jameel M. Al-Khayri
jkhayri@kfu.edu.sa

SPECIALTY SECTION
This article was submitted to
Plant Abiotic Stress,
a section of the journal
Frontiers in Plant Science

RECEIVED 18 September 2022
ACCEPTED 05 December 2022
PUBLISHED 17 January 2023

CITATION
Al-Khayri JM, Banadka A, Rashmi R, Nagella P, Alessa FM and Almaghasla MI (2023) Cadmium toxicity in medicinal plants: An overview of the tolerance strategies, biotechnological and omics approaches to alleviate metal stress. *Front. Plant Sci.* 13:1047410. doi: 10.3389/fpls.2022.1047410

Cadmium toxicity in medicinal plants: An overview of the tolerance strategies, biotechnological and omics approaches to alleviate metal stress

Jameel M. Al-Khayri[1]*, Akshatha Banadka[2], R Rashmi[2], Praveen Nagella[2]*, Fatima M. Alessa[3] and Mustafa I. Almaghasla[4,5]

[1]Department of Agricultural Biotechnology, College of Agriculture and Food Sciences, King Faisal University, Al-Ahsa, Saudi Arabia, [2]Department of Life Sciences, CHRIST (Deemed to be University), Bangalore, Karnataka, India, [3]Department of Food Science and Nutrition, College of Agriculture and Food Sciences, King Faisal University, Al-Ahsa, Saudi Arabia, [4]Department of Arid Land Agriculture, College of Agriculture and Food Sciences, King Faisal University, Al-Ahsa, Saudi Arabia, [5]Plant Pests, and Diseases Unit, College of Agriculture and Food Sciences, King Faisal University, Al-Ahsa, Saudi Arabia

Medicinal plants, an important source of herbal medicine, are gaining more demand with the growing human needs in recent times. However, these medicinal plants have been recognized as one of the possible sources of heavy metal toxicity in humans as these medicinal plants are exposed to cadmium-rich soil and water because of extensive industrial and agricultural operations. Cadmium (Cd) is an extremely hazardous metal that has a deleterious impact on plant development and productivity. These plants uptake Cd by symplastic, apoplastic, or *via* specialized transporters such as HMA, MTPs, NRAMP, ZIP, and ZRT-IRT-like proteins. Cd exerts its effect by producing reactive oxygen species (ROS) and interfere with a range of metabolic and physiological pathways. Studies have shown that it has detrimental effects on various plant growth stages like germination, vegetative and reproductive stages by analyzing the anatomical, morphological and biochemical changes (changes in photosynthetic machinery and membrane permeability). Also, plants respond to Cd toxicity by using various enzymatic and non-enzymatic antioxidant systems. Furthermore, the ROS generated due to the heavy metal stress alters the genes that are actively involved in signal transduction. Thus, the biosynthetic pathway of the important secondary metabolite is altered thereby affecting the synthesis of secondary metabolites either by enhancing or suppressing the metabolite production. The present review discusses the abundance of Cd and its incorporation, accumulation and translocation by plants, phytotoxic

implications, and morphological, physiological, biochemical and molecular responses of medicinal plants to Cd toxicity. It explains the Cd detoxification mechanisms exhibited by the medicinal plants and further discusses the omics and biotechnological strategies such as genetic engineering and gene editing CRISPR- Cas 9 approach to ameliorate the Cd stress.

KEYWORDS

cadmium, medicinal plants, transporters, reactive oxygen species, plant secondary metabolites, CRISPR- Cas 9

1 Introduction

Extensive urbanization and expeditious industrialization have primarily contributed to environmental pollution. Environmental pollutants such as inorganic pollutants (including heavy metals), gaseous pollutants, organic and organometallic compounds, radioactive isotopes, and toxicity of some nanoparticles have been polluting the environment (Yadav, 2010). In spite of a worldwide focus on overcoming pollution, it has become a major challenge to be faced due to its dreadful long-term consequences. Environmental pollution has become one of the prominent causes of distress and mortality worldwide. Of all the pollutants, the inorganic heavy metal pollutants have gained special attention due to their omnipresent occurrence and their toxic effects (Benavides et al., 2005).

Heavy metals are high atomic weight elements with a density five times greater than that of water (Tchounwou et al., 2012). There are essential and non-essential heavy metals. The essential heavy metals are required in trace amounts. They are essential for plant growth, animals, and the human body and take part in electron transport, redox reactions, and nucleic acid metabolism (Narender, 2005). However, when these metals accumulate beyond the tolerable limits, they pose a serious threat disturbing the normal functioning of biological organisms. Heavy metals such as Iron (Fe), Molybdenum (Mo), and Manganese (Mn) serve as micronutrients. Heavy metals such as Chromium (Cr), Cobalt (Co), Copper (Cu), Nickel (Ni), Vanadium (Vn), and Zinc (Zn) are needed in trace quantities. However, they can be toxic when they are found in higher concentrations. Some non-essential heavy metals like Antimony (Sb), Arsenic (As), Cadmium (Cd), Lead (Pb), Mercury (Hg), and Silver (Ag) have no biological functions and seem to be toxic to organisms (Benavides et al., 2005). The heavy metal pollutants get into the water and soil through anthropogenic sources like agricultural fungicide and pesticide runoff, domestic garbage dumps, industrial effluents, mining operations, sewage sludges, and urban composts (Srivastava et al., 2017).

The plants grown in such heavy metal contaminated sites or irrigated with heavy metal contaminated water take up the metals. These heavy metal contaminated plants when consumed by animals and humans enter and disturb the food chain (Gall et al., 2015). Thus, heavy metals uptake by plants increases the possibility of these toxic elements entering the food chain. In recent times, heavy metal toxicity studies in medicinal plants have been a topic of considerable interest. Cadmium, one of the heavy metals with extreme toxicity has negatively impacted the plant development and productivity (Patel, 2006a).

Medicinal plant use in traditional medicine and ethnomedicine is a long-standing tradition. Medicinal plants are rich in therapeutic bioactive molecules that can be used to combat a wide variety of diseases. These bioactive molecules are synthesized *via* different metabolic pathways. They possess anticancer, antidiabetic, diuretic, antihypertensive, anti-inflammatory, antimicrobial, hypolipidemic, and many more properties. Medicinal plants and their products have been used in the treatment of lifestyle disorders such as cardiovascular diseases, diabetes, hypertension, inflammatory diseases, mental disorders and skin diseases (Oladeji, 2016; So et al., 2018). Plant-derived herbal medicines are preferred over western medicine and their usage has substantially increased with time. About 60% of the world population with 80% African, 80% Arabians, 48% Australian, 39% Belgium, 30-50% Chinese, 70% Canadian, 76% French, 80% Germans, 70% Indians and 42% USA people rely on herbal medicines (El-Dahiyat et al., 2020; Saggar et al., 2022; Bahl, 2022). It is expected that the global trade of medicinal plants would reach 5 trillion USD by 2050 (Zahra et al., 2020). Although medicinal plant-derived herbal products are gaining more popularity, the safety of use of such products has become a major concern. The herbal products derived from these medicinal plants have shown heavy metal toxicity due to contamination during cultivation, cross-contamination, or deliberate introduction of heavy metals (Street, 2012). When assessed for the heavy metal contamination in *Menthae piperitae* and *Anthodium chamomillae*, nearly 14-16% of cadmium content which exceeded the acceptable limits of World Health

Organization (WHO) standards (10 mg/kg) (Mirosławski and Paukszto, 2018).

Plants grown in heavy metal contaminated sites have adopted different mechanisms to fight stress. They can either be sensitive to heavy metal contamination showing injury or death as a response to stress or they can exhibit coping mechanisms to stress by tolerance or avoidance. Avoiders are those plants that prevent the entry of metal ions into the plant whereas the tolerant plants detoxify the metal ions that have entered the plant system. Based on these strategies they are broadly classified as hyperaccumulators, metal excluders, and indicators (Mehes-Smith et al., 2013). Plants that are sensitive to metals show physiological, biochemical, and genetic changes causing delayed seed germination, stunted growth, chlorosis, limped leaves, less branching, less fruiting, and many more abnormalities (Haque et al., 2021). The tolerant plants release cellular and root exudates as the first line of defense against heavy metal uptake. As a second line of defense, they chelate, sequester, and detoxify the heavy metals. The plants under heavy metal stress produce antioxidants, stress-related hormones, and proteins (Ghori et al., 2019). Heavy metal stress can induce changes in secondary metabolite (SM) production (Nasim and Dhir, 2010; Asgari-Lajayer et al., 2017).

Comprehensive documentation exists on the effects of different heavy metals on plant physiology and their biochemistry in crop plants. But not much attention has been given to the effects of heavy metals on active SMs of medicinal plants. It is, therefore, necessary to evaluate the effect of heavy metals in medicinal plants. Of the various known heavy metals, Cd is one of the most treacherous metals due to its high mobility and toxicity at lower concentrations (Benavides et al., 2005). Taking this into account, the present review discusses the effect of Cd on seed germination, plant growth, physiological characteristics, and biochemical aspects, with an emphasis on the biosynthesis of important SMs in medicinal plants. The review discusses the defense mechanisms and detoxification strategies exhibited by the plants to combat Cd stress. The omics approaches and various biotechnological approaches like genetic engineering approach, and CRISPR Cas 9 gene editing approach for enhancing the ability of plants to survive the Cd stress has been covered.

2 Sources of cadmium

Cadmium is a heavy metal with atomic number 48 designated as Cd. It is a bluish-white, malleable soft metal. It naturally occurs in the environment as a natural cadmium sulfide ore or is found in association with zinc. It is a nonessential heavy metal to biological organisms that are known to cause toxic effects in excretory, gastrointestinal, neurological, reproductive, respiratory, and skeletal systems and negatively affect plant growth. Because of its high toxicity and high solubility in water, Cd has been regarded as a significant pollutant. A soil is considered to be non-polluted, if the Cd levels are between 0.04 to 0.32 mM (Wagner, 1993). However, if the Cd levels cross 0.32 mM and go up to 1 mM the soil is considered to be moderately polluted. Drinking water with Cd level below 1 ppb is considered to be potable (Sanità di Toppi and Gabbrielli, 1999).

The main source of Cd pollution in the environment includes smelting and mining activities both of which can pollute the air with Cd. The Cd compounds can associate with air-borne particles and can be carried across long-distance which then gets deposited into the soil by rain. Incineration of municipal waste, industrial runoffs from metal, pigment-producing, and battery manufacturing industries, contamination with sewage sludges, seepage from waste sites, chemical fertilizers pollutes the soil and water with Cd (Kubier et al., 2019). The underground water is known to be contaminated by mining, the release of industrial effluents, or by seepage from hazardous sites. Once the Cd enters soil and water it can easily get into the food chain through plants which is a major concern (ATSDR, 2013).

3 Cadmium mobilization

The Cd uptake and transfer in plants depend on the ability of the plants to absorb the metals. Some plants resist the uptake of metal, while some facilitate the metal uptake. The Cd uptake is also affected by the metal concentration of soil, the physicochemical properties of soil such as temperature, pH, and redox potential as well as other components including the organic matter of the soil. The uptake and translocation of Cd by plants are represented in Figure 1. The Cd metals gain entry into the plant and are transported within the plant through the different membranes at various levels through non-selective cationic channels or through other metal transporters (Huang et al., 2020). The Cd uptake and translocation in plants take place through apoplastic and symplastic pathways (Song et al., 2017). Roots are the first part of the plant that comes in contact with heavy metals in soil. The Cd in the soil solution gets onto the root surface through root hairs which serve as an active zone of absorption and epidermal cells through ion exchange. Root secretes low molecular compounds such as mugineic acids which chelate Cd^{+} and facilitate its transport. It is then transported into the parenchyma cells across the root cortex through the Casparian strip in the endodermis (Song et al., 2017). Once inside the parenchymal cells, the Cd ion enters the conductive vessels of the xylem through the symplast. Thus, Cd enters into the xylem *via* apoplastic or symplastic pathways. The roots can retain the heavy metals or it can facilitate the metal movement into the shoot. The root cells retain Cd by insolubilization at the root surface and apoplast or avoid the release to the xylem by compartmentation in cells (Page and Feller, 2015). The

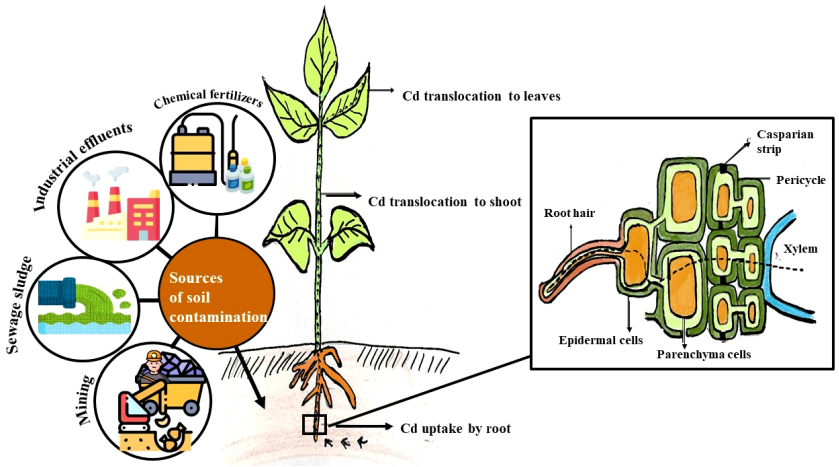

FIGURE 1
Source, uptake and translocation of cadmium from soil to root, shoot and leaves and mechanism underlying the mobilization of cadmium through root hairs to the xylem vessel.

mechanism underlying the mobilization of cadmium through root hairs to the xylem vessel is represented in Figure 1. The heavy metals in the roots are transported to transpiring shoot parts (leaves and stems) through the transpiration stream in the xylem. The chelated or free metal ions move upwards along the xylem sap. The heavy metal concentration in the transpiration stream of the root xylem depends upon the cell wall interaction of xylem vessels during transport. The heavy metals would either accumulate in leaves if there is no further redistribution. The Cd in the leaf cell cytosol is chelated by organic ligands, and it can move to adjacent cells, some of which get accumulated in the vacuole. The heavy metals get redistributed by a symplastic pathway to the other growing plant parts *via* the phloem. The Cd ions also move and accumulate in the reproductive organs, developing fruits and seeds. It might get redistributed to roots where Cd could be expelled (Page and Feller, 2015; Sterckeman and Thomine, 2020).

Diversified groups of metal transporters present in the plasma membrane facilitate the translocation of Cd through the symplastic and apoplastic pathways. The extracellular location and the biological function of these transporters are still unclear. There are four major Cd transporters which include heavy metal transporting ATPase transporter protein (HMA), metal tolerance or transporter proteins (MTPs), the NRAMP (natural resistance-associated macrophage protein), and the ZIP (zinc-regulated transporters, iron-regulated transporter-like proteins/ZRT-IRT-like Proteins) families. Heavy metal ATPase transport protein is a subgroup of the large P-type ATPase family that transports divalent Cd^{2+} ions between cytoplasm, cellular compartments, and xylem. They help in the efflux of heavy metals from the cytoplasm across the plasma membrane or into other organelles. Transporters like NRAMP6 (natural resistance-associated macrophage protein 6), IRT1 (iron-regulated transporter 1) in *Brassica napus* L. take part in Cd accumulation (Chen et al., 2018b). HMA transporters like AtHMA2, and OsHMA2 are HMAs that are located in the plasma membrane, and also take part in the translocation of Cd ions from root to shoots by loading Cd ions into the xylem. Another important HMA, AtHMA1, located in the inner chloroplast membrane, also helps in Cd transport (Fan et al., 2018).

Metal transporter proteins (MTPs) are a group of membrane-bound proteins that belong to the Cation Diffusion Facilitator (CDF) family. The MTPs located in the tonoplast act as antiport and mediate in the transport of divalent cations. Hence, they are also referred to as cation efflux transporters. They help in resisting or tolerating the Cd stress by the sequestration and efflux of Cd^{2+} ions. Nearly eleven MnMTPs are identified as Transporter proteins in *Morus notabilis* which helps in heavy metal transport (Fan et al., 2018). Natural resistance-associated macrophage proteins, abbreviated as NRAMP (Sasaki et al., 2012) are a group of proteins that transport a variety of metals. These proteins help in the translocation of metals from the root to shoot across the cell membrane and vacuolar membrane. *Arabidopsis thaliana* is known to transfer Cd metal and the AtNramp3 gene is known to enhance Cd resistance of root growth translocation of divalent cations across membranes (Thomine et al., 2000). Iron-regulated transporter-like proteins (ZIP) and Zinc-regulated transporters are principal metal transporters. The first identified proteins from their family of transporters were Zinc-regulated transporters and iron-regulated transporter-like proteins,

hence the name ZIP. These proteins are also engaged in the displacement of divalent cations through plasma membranes. ZIP transporters like AtIRT1 in *A. thaliana*, NcZNT1 in *Noccaea caerulescens* (J. & C. Presl) F.K. Meyer, OsIRT1, OsIRT2, OsZIP6 in *Oryza sativa*, MtZIP6, OsNRAMP1, OsNRAMP5 in *Medicago truncatula*, and NRAMP5 in *Hordeum vulgare* all of which are localized on the plasma membrane mediates Cd^{2+} (Komal et al., 2015).

4 Cadmium toxicity

4.1 Impact of Cadmium on various growth stages

The study of heavy metal effects on different growth stages is important to understand the extent to which heavy metals limit plant growth and productivity in general (Patel, 2006a). It also helps to know the possible mechanisms the plants employ to survive the heavy metal stress at different plant growth stages. The ability of plants to uptake, transfer and accumulate heavy metals varies with different stages of plant growth. It is generally known that young seedlings have the ability to uptake metals at a higher rate when compared to mature plants (Souri et al., 2019). Under heavy metal stress, the plants might show delayed germination and exhibit poor vegetative growth at multiple levels with anatomical, morphological and biochemical changes. Plants at reproductive stages are known to be even more sensitive to metal stress (Ma et al., 2020).

4.1.1 Germination

Seed germination is the initial stage and one of the most crucial stages in the plant life cycle. The seed, during its germination, is highly susceptible to the physiological conditions of the rhizosphere (Bewley, 1997). Despite the outermost seed coat covering serving as a protective barrier against the detrimental effects of heavy metals, the metal stress induces slow germination and suppresses response vigor in seeds. Heavy metals suppress seed germination and seedling development by inhibiting food storage and mobilization, morphological changes like reduction in radical and plumule formation, and modification in proteolytic activities. Thus, the consequences of heavy metals on seedling germination and growth must be widely studied (Seneviratne et al., 2019). The effect of different concentrations of Cd ranging from 0- 16 mg L^{-1} has been studied in *Ocimum basilicum* L. The germination percentage was reduced to 4% with the lowest germination at a Cd concentration of 16 mg L^{-1} (Fattahi et al., 2019). In the study conducted by Khatamipour et al. (2011), the effect of different concentrations of cadmium chloride varying from 0-600 mg L^{-1} was studied on the germination in *Silybum marianum*. The increase in Cd concentration showed a noticeable reduction in germination, the shoot and root length of seedlings, and proline content with the lowest. It has been reported to hamper food reserve mobilization due to the disturbance in sugars and amino acids causes mineral leakage leading to nutrient loss, over-accumulation of lipid peroxidation products, inhibition of alpha-amylase and invertases activity all of which resulting in delayed and reduced seed germination (Sethy and Ghosh, 2013). The effect of cadmium on germination in various plants is represented in Table 1.

4.1.2 Vegetative stage

The vegetative stage indicates a period of growth between germination and flowering stages of plant growth during which plants are involved in producing leaves, stems, and branches without flowers (Hangarter, 2000; Gilbert, 2000). Heavy metals like Cd have a wide range of harmful effects on the vegetative stage of plants causing chlorosis, inhibition of photosynthesis, low biomass accumulation, retardation of growth, altered osmoregulation, changes in nutrient assimilation, and senescence, which ultimately results in plant death. Plants of various sorts have diverse development tendencies and respond differently to heavy metal stress (Singh et al., 2015). The metal has been generally known to decrease plant height and biomass. In the heavy metal studies conducted on *Coriandrum sativum* L. it has been observed that the root and shoot length reduced drastically with increasing concentration. The study suggests that the Cd metal accumulated in the root slowed down the mitotic rate in meristematic cells leading to reduced root length. On the other hand, the shoot length is reduced due to a reduction in the meristematic cells. The other possible reason for the reduction in the root and shoot length is due to the action of cotyledonary enzymes that digest carbohydrates and protein in the radical and plumule tips (Faizan et al., 2012). The effect of Cd (5, 10, 50, and 100 μM) on different stages of growth in *Bacopa monnieri* has been studied and it has been observed that the biomass reduced with increasing cadmium (Gupta et al., 2014). The various effects of Cd on plant growth are represented in Table 1.

4.1.3 Reproductive stage

The reproductive stage of plant growth involves the development of flower buds and flowers. The flower, on fertilization, develops into fruit with seeds. The heavy metals induce delayed flowering and fruiting and decrease their yield. This, in turn, decreases flowering and fruiting indices (Shekari et al., 2019). In the study conducted on *Andrographis paniculata*, Cd suppressed the reproductive growth by decreasing the number in the inflorescence branch, flower, and flower buds, and also suppressed the fresh weight of the inflorescence and flower bud (Patel, 2006a). Cadmium affects the production and

TABLE 1 Effect of cadmium on germination, vegetative and reproductive growth in medicinal plants.

Plant name	Metal concentration	Effect on germination	Effect on vegetative growth	Effect on reproductive growth	Reference
Adhatoda vasica L.	0,100, 200, 300, 400, 500, 600 ppm	–	Increasing Cd conc. had inhibitory effect on elongation, fresh and dry weight of root and shoot RRG value, leaf number, fresh weight, and area	Number, dry weight, fresh weight of inflorescence, flower bud, fruit reduced	(Trivedi, 2003)
Alternanthera tanella Colla	0, 50, 100 or 150 µM	–	The shoots and roots reduced with increasing concentration	–	(Rodrigues et al., 2017)
Amaranthus spinosus L.	5-50 ppm for 60 days	–	Significant reduction in root and shoot length and fresh weight in dose dependent manner	–	(Huang Y et al., 2019)
Andrographis paniculata (Burm.f.) Nees	10,50,100,150and 200 ppm	–	Root and stem elongation, RRG values. leaf number, dry and fresh weight of root, stem, and leaf was gradually lowered and percent phytotoxicity values increased with increasing in metal concentration	Inflorescence branch number pollen tube growth and pollen germination, flower, flower bud and fruit number n fresh weight of inflorescence and flower bud decreased	(Patel, 2006a)
Anethum graveolens L.	0, 100 and 200 µM	–	Root length, leaf area, shoot and root dry weight decreased	–	(Aghaz et al., 2013)
Bacopa monnieri L.	5 µM, 10 µM, 50 µM, and 100 µM	–	Browning and stunting of roots with decreased biomass were observed with increasing Cd concentration	–	(Gupta et al., 2014)
Bidens pilosa L.	2.57ppm, 7.94 ppm, 17.33ppm, and 37.17ppm for 40 days	–	Root and shoot biomasses gradually decreased with increasing concentration	–	(Dai et al., 2021)
Brassica juncea L.	200 mg L^{-1} and 300 mg L^{-1}	–	Plant height, root length and biomass reduced	–	(Ahmad et al., 2015)
Cannabis sativa L.	25 mg kg^{-1} Cd for 45 days	–	Shoot and root biomass decreased with increasing concentration	–	(Shi et al., 2012)
Catharanthus roseus var. *rosea* L.	(0, 10, 50, 100, 200, 500 and 1000 µM	0% germination at 1000 µM concentration	The root length was inhibited	–	(Pandey et al., 2007)
Cajanus cajan L.	1,5,10,20,50mg L^{-1}	60% reduction in seed germination with a decrease in the fresh and dry weight reduction in growth, stunting of seedlings	Reduction in fresh and dry weight and stunting of seedlings	–	(Patnaik and Mohanty, 2013)
Centella asiatica L.	50-100 ppm for 30 days	–	The root length remained the same except at 100 ppm while the shoot length increased significantly with metal concentration	–	(Biswas et al., 2020)
Cichorium pumilum Jacq.	50, 100, 200, 400, 800, and 1600 µM	–	Hypocotyl and root length decreased with increasing Cd concentration	–	(Khateeb, 2013)
Coriandrum sativum L.	0, 25, 50, and 100 mg kg^{-1}	Germination % (least at 50mg kg^{-1} Cd)	Root length, shoot length decreased with an elevation of Cd conc. with least at 100mg kg^{-1}Cd	–	(Faizan et al., 2012)
Cuminum cyminum L.	0, 300, 450, 600, 750 and 1050 µM	30% and 23% inhibition in seed germination of Isfahan and Khorasan ecotypes respectively.	43.6% and 48.7% of root growth inhibition of Isfahan and Khorasan ecotypes respectively.	–	(Salarizadeh et al., 2016)

(Continued)

TABLE 1 Continued

Plant name	Metal concentration	Effect on germination	Effect on vegetative growth	Effect on reproductive growth	Reference
Drimia elata Jacq. ex Willd.	2, 5, 10 mg L^{-1}	–	The shoot and bulb dry weight reduced significantly with higher concentrations	–	(Okem et al., 2015)
Melissa officinalis L.	0, 10, 20 and 40 µM	–	Fresh weight increased upto 20 µM	–	(Nourbakhsh Rezaei et al., 2019)
Merwilla plumbea (Lindl.) Speta	1.5 ppm	–	The fresh weight of leaves, bulbs and roots significantly reduced	–	(Lux et al., 2011a)
Moringa oleifera Lam.	1- 5 mM for 30 days	–	The root and shoot length significantly reduced	–	(Srivastava and Yadav, 2017)
Ocimum basilicum L.	5, 10, 15, 20, 25 ppm	–	The fresh and dry weight declined with increasing Cd concentration	–	(Youssef, 2021)
	0-16 mg L^{-1}	4% reduction in germination at 16 mg L −1 Cd	–	–	(Fattahi et al., 2019)
Ocimum canum Sims.	50, 100, 150, 200, 250 mg kg^{-1}	–	The root elongation and stem height inhibited	Flower number and its fresh weight and dry weight, inflorescence, fruit number. dry weight	(Patel, 2006b)
Phyllanthus amarus Schumach. and Thonn.	10-100 mg kg^{-1}	–	The root and shoot growth of plant remained unaffected upto 50 ppm and further decreased with the increasing concentration.	–	(Dwivedi et al., 2013)
Silybum marianum L. Gaertn.	0, 100, 200, 400 and 600 mg L^{-1}	14% seed germination at 600 mg L^{-1}	–	–	(Khatamipour et al., 2011)
Trigonellafoenum-graecum L.	0.1, 0.5, 1 and 10 mM	33% decrease in germination and no radicle growth at 10 mM	–	–	(Zayneb et al., 2015)
Trigonella foenum-graecum L.	0, 5, 15, 30, 50 µg g^{-1}	–	Magnitude of increase of number of leaves, leaf area and number of branches per plant, along with shoot and root length was lowered	–	(Ahmad et al., 2005)
Typha latifolia L.	0.2–0.8 µg g^{-1}	–	Leaf, shoot and root elongation and the dry weight reduced	–	(Ye et al., 1997)
Withania somnifera L. Dunal.	50- 1,000 µM	–	FW and DW was almost same at lower and moderate concentrations and drastically decreased at higher concentration	–	(Mishra et al., 2014)

allocation of amino acids and sugars, absorption, assimilation, and distribution of nutrients in plants (Carvalho et al., 2021). The fruit number and the fruit biomass has reported to be reduced in *Adhatoda vasica* L. grown in Cd treated soil when compared to control. The reduction in fruit number could be attributed to the loss of important nutrients like K, Fe and Zn. Further the reduction in fresh weight of inflorescence resulted in poor seed development (Trivedi, 2003). The effect of Cd on reproduction in medicinal plants is presented in Table 1.

4.2 Anatomical changes

Plant morphology, physiology, and anatomy are likely to reveal information about their ability to adapt to different growth environments. Under Cd toxicity, plants show various anatomical changes, especially in root tissues. Since roots are often the first organs to be exposed to metal ions, they always try to avoid the Cd lodgment in shoots by limiting their entry either by symplastic or by apoplastic pathways. When plant roots are

subjected to high Cd levels, they release phytochelatins to sequester Cd as Cd-chelates in the vacuole of root cells and thus prevent symplastic entry. Meanwhile, they hasten the maturation of endodermis by bearing suberin lamellae, Casparian bands, and lignification near to the root apex to avoid the apoplastic entry of cd (Lux et al., 2011b). The development of hypodermal Suberin-impregnated periderm with impermeable cell walls periderm in the immature sub-apical areas of *Merwilla* roots acts as a defense response of roots that may inhibit radial Cd ion absorption by roots (Lux et al., 2011a). The effect of Cd on plant anatomy is presented in Table 2.

Since leaf is an important site for photosynthesis and leaf morphology and anatomy have vital roles in photosynthetic efficiency. Leaf characteristics like thickness and stomatal density impact metal tolerance and sensitivity directly (Thongchai et al., 2021). Anatomical changes in leaves can reflect biological activity in plants associated with heavy metal tolerance and accumulation processes (Pereira et al., 2016).

4.3 Effect on photosynthesis

Photosynthesis is a well-organized and sequential process involving many components such as photosynthetic pigments, the electron transport system, and CO_2 reduction pathways that are essential to all green plants and microorganisms. Any impairment at any of these steps has a significant impact on total photosynthetic capability (Parmar et al., 2013). Changes in pigment content are connected to visual signs of plant sickness and photosynthetic output, hence plant pigments like Chl a, Chl b, and carotenoid concentration are frequently evaluated in plants to determine the influence of environmental stress (Dresler et al., 2014). The role of Cd in the inhibition of chlorophyll biosynthesis, breakdown of pigments or their precursors, and destruction of the chloroplast membrane by lipid peroxidation due to lack of antioxidants or an increase in peroxidase activity could all contribute to a decrease in total photosynthetic pigment content (Mishra et al., 2014). Cadmium-induced reduction of photosynthetic pigments like Chl a, Chl b, and total chlorophyll has been reported in various medicinal plants like *Drimia elata* (Okem et al., 2015), *Brassica juncea* L. (Ahmad et al., 2015), *Amaranthus spinosus* (Huang J et al., 2019, Huang Y et al., 2019). Decreased performance of photosynthetic enzymes like carbonic anhydrase and RUBISCO under Cd toxicity has also been reported (Mobin and Khan, 2007; Gill et al., 2012; Parmar et al., 2013; Zaid et al., 2020). Exogenous applications of certain organic acids can reduce the phytotoxic effects of heavy metals (Hawrylak-Nowak et al., 2015; Zaheer et al., 2015). Studies revealed the application of citric acid (Mahmud et al., 2018), and salicylic acid (Krantev et al., 2008; Zhang et al., 2015) to restore the pigment content to a significant level. The effect of Cd on photosynthesis has been tabulated in Table 3.

4.4 Effect on membrane structure

The ROS emerges as a response to Cd toxicity plays an important role in the removal of hydrogen from unsaturated

TABLE 2 Anatomical changes in cadmium treated medicinal plants.

Plant	Metal concentration	Anatomical changes	Reference
Alternanthera tenella Colla.	50, 100, 150 ppm	Endodermal and ectodermal wall thickening in roots, damaged inner root cells, reduced epidermal thickness in both adaxial and abaxial surfaces.	(Rodrigues et al., 2017)
Brassica juncea L.	50ppm, 500 ppm,2.5 mM, and 10 mM	Precipitation along cell walls and an increase in the number of vacuoles in root cortical cells, black depositions along the walls of vascular bundles of stems	(Sridhar et al., 2005)
Melissa officinalis L.	10,20,30 ppm	Decreasing number and size of stomata and epidermal cells with increasing Cd concentration	(Kilic, 2017)
Merwilla plumbea (Lindl.) Speta	1,5 ppm	Hypodermal periderm formation near to root apex.	(Lux et al., 2011a)
Salvia sclarea L.	0-100ppm	Reduced epidermal cell size, spongy parenchyma and mesophylls with less intercellular space	(Dobrikova et al., 2021)
Thlaspi caerulescens J. & C. Presl	0.5 to 500 ppm	Damaged cells, irregular intracellular space in root cortex	(Wójcik et al., 2005)
Trigonella foenum-graecum L.	5,15,30,50 ppm	Reduced stomatal density, decreased proportion of pith and vasculature and increased pith and cortex ratio in stem, decreased density and dimensions of xylem vessels in both root and shoot	(Ahmad et al., 2005)

TABLE 3 Changes in photosynthetic pigments and biochemical parameters in cadmium treated medicinal plants.

Plant name	Concentration and duration	Total protein and carbohydrate	Plant pigments	Lipid peroxidation	Proline	Secondary metabolites	Reference
Adhatoda vasica L.	100 - 600 ppm for 180 days	Decreased reducing and non-reducing sugar and total protein content	Decreased Chl a, Chl b, total chlorophyll and carotenoids with increasing concentration	–	Reduction in proline content	Reduced total alkaloids, vasicine and vasicinone	(Trivedi, 2003)
Alternanthera tanella Colla	50 -150 ppm for 30 days	–	Significant reduction in chlorophyll pigments	Increased at highest concentration	–	–	(Rodrigues et al., 2017)
Artemisia annua L.	20, 60 and 100 ppm for 336 days	–	Decreasing chl a, chl b, carotenoids and total chl with increasing concentrations and duration	Insignificant variations in MDA content between control plants and treated plants	–	Increased artemisinin production	(Li et al., 2012)
Bacopa monnieri L.	10- 200 ppm for 144 hours	Decreasing total protein content with increasing concentration	–	Increased lipid peroxidation	–	–	(Mishra et al., 2006; Singh et al., 2006)
Bidens pilosa L.	2.57ppm, 7.94 ppm, 17.33ppmand 37.17ppm for 40 days	–	Chl a, chl b and carotenoid content decreasing with increasing concentration	MDA content increased with increasing concentration	–	–	(Dai et al., 2021)
Brassica juncea L.	0.5 and 1 mM for 3 days	Decreased protein content	–	Increased MDA content	Enhanced production of proline	–	(Bauddh and Singh, 2012; Mahmud et al., 2018)
	200 and 300 ppm	Reduction in protein content	Reduction in chl a, chl b and total chlorophyll content	MDA content decreased	The proline content increased	–	(Ahmad et al., 2015)
Catharanthus roseus var. *rosea* L.	0-1000 µM for 180 days	–	The Chlorophyll content sharply reduced	MDA concentration increased with increasing concentration	–	–	(Pandey et al., 2007)
Centella asiatica (L.) Urb.	5 - 200 ppm for 30 days	–	Reduced amounts of chl a, chl b, and total carotenoids	–	–	Increased total phenolics and flavonoids and increasing centelloside concentrations with increasing concentration	(Biswas et al., 2020)
Drimia elata Jacq. ex Willd	2,5,10 ppm for 6 weeks	–	Significant reduction on chlorophyll a, chl b and total chlorophyll	–	Increased proline content in shoots	Decreased total phenolic and flavonoid content	(Okem et al., 2015)

(Continued)

TABLE 3 Continued

Plant name	Concentration and duration	Total protein and carbohydrate	Plant pigments	Lipid peroxidation	Proline	Secondary metabolites	Reference
Lemna gibba L., *Lemna minor* L.	0.01 - 1.5ppm for 96 hours	Reduced total protein content	Increased chl a, chl b, and total chlorophyll content at lower concentrations, but decreased at high concentration	Decreased MDAcontent indicating low lipid peroxidation	–	–	(Banu Doğanlar, 2013)
Lepidium sativum L.	20, 50 and 100 ppm for 30 days	–	Significant reduction in chl a, chl b, total chl with increasing concentration. Reduced CA activity	Increased TBARS content	–	–	(Gill et al., 2012)
Mentha arvensis L.	50ppm for 100 days	–	Decreased RuBisCO and carbonic anhydrase activity, decreased photosynthetic rate	Increased TBARS content	Increased proline content	–	(Zaid et al., 2020)
Melissa officinalis L.	0, 10, 20, and 40 mM	–	Chlorophyll a and b reduced significantly and total chlorophyll decreased at 40 mM	Malondialdehyde content increased	–	Increasing Cd conc. had a positive effect on phenolic effect with highest of ⅓ folds increase at 40mM	(Nourbakhsh Rezaei et al., 2019)
Moringa oleifera Lam.	1- 5 mM for 30 days	Decreasing protein content with increasing concentrations	–	–	Increasing proline content with increasing concentration	Increasing polyphenols with increasing concentrations	(Srivastava and Yadav, 2017)
Ocimum canum Sims.	50 - 250 mg $kg^{-1}$for 120 days	High non reducing sugar but less amounts of reducing sugar and total protein content	Decreased amounts of Chl a, Chl b, total Chl content and carotenoids with increasing concentration	–	Enhanced proline accumulation	–	(Patel, 2006b)
Phyllanthus amarus Schumach. And Thonn.	10 - 100 ppm for 60 days	–	–	–	Increasing proline content along with increasing concentrations upto 50 ppm, after that a sudden decline in proline content	Decreased alkaloids, tannin and flavonoid content with increasing concentration and duration	(Dwivedi et al., 2013)
Ricinus communis L.	25-150 ppm for 60 days	Decreased protein content	–	Increased MDA content	Increased proline content	–	(Bauddh and Singh, 2012)
Salvia sclarea L.	0- 100 ppm for 8 days	–	Decreased chl a, chl b and chl a/b ratio. Increased anthocyanin content	–	–	Increased phenolics content	(Dobrikova et al., 2021)

(Continued)

TABLE 3 Continued

Plant name	Concentration and duration	Total protein and carbohydrate	Plant pigments	Lipid peroxidation	Proline	Secondary metabolites	Reference
Satureja hortensis L.	2.5-15mg L^{-1} for 2 weeks	Increasing soluble and reducing sugars in both roots and shoots	Reduction of chl a, chl b and total chl but anthocyanin production increased with increasing concentration	–	Enhanced proline production	High anthocyanin content, increased essential oil production	(Azizollahi et al., 2019)
Solanum nigrum L.	50 and 200 ppm for 3 days	Increased protein thiol content	–	Significantly high TBRAS content	–	–	(Deng et al., 2010)
Trigonella foenum-graecum L.	0.5 - 10mM for 30 days	–	–	Increased MDA content	–	Increased total phenolic and flavonoid content	(Zayneb et al., 2015)

fatty acids, and causes severe lipid peroxidation, resulting in the production of lipid radicals and reactive aldehydes. This sets off a cascade reaction that causes lipid bilayer and membrane protein deformation (Logani and Davies, 1980). MDA is the end product of membrane lipid peroxidation, and it might indicate the extent of cell membrane damage induced by oxygen free radicals (Zhang et al., 2007). Enhanced MDA production in Cd treated plants like *B. juncea* (Bauddh and Singh, 2012; Mahmud et al., 2018), *Ricinus communis* (Bauddh and Singh, 2012; Mahmud et al., 2018), *Hibiscus cannabinus* (Li et al., 2013), *Bacopa monnieri* (Mishra et al., 2006; Singh et al., 2006) shows the severity of membrane damage under Cd stress. Decreased MDA content, as reported in *Lemna gibba* (Banu Doğanlar, 2013) can be considered as an indication of low peroxidation of lipids which can be caused by increased activity of antioxidants (Zhang et al., 2007). The antioxidant systems in plants can protect bio membranes from oxidative damage by lipid peroxidation.

4.5 Important biochemical changes

At lower metal concentrations and durations, an increase in protein level may be attributed to the induction of stress proteins. Stress proteins constitute various antioxidant enzymes and other enzymes involved in GSH (Glutathione) and PC (Phytochelatin) biosynthesis, including some heat shock proteins (Mishra et al., 2006). However, at higher metal concentrations, there was a significant decrease in protein content, which may be due to the Cd-induced oxidation of proteins, mediated by H_2O_2 and due to increased proteolytic activity (Pena et al., 2006). Proteolytic activity and protein degradation have been proposed as an index of oxidative stress (Romero-Puertas et al., 2002).

Sugars help to remove free radicals produced during stressful situations; hence their increased synthesis helps to defend against stress. These regulate osmotic potential, participate in

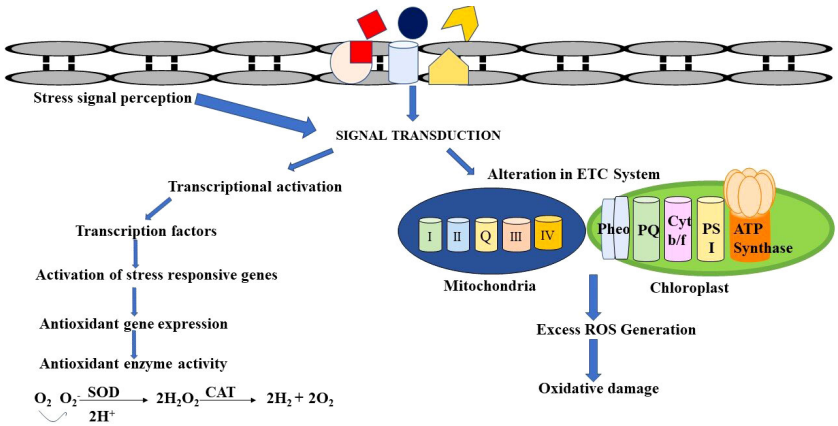

FIGURE 2
Schematic representation of defense mechanisms to counteract heavy metal stress.

redox processes, and aid in the maintenance of macromolecule and membrane structures (Kapoor et al., 2016). Enhanced soluble and reducing sugar has been reported in *Satureja hortensis* (Azizollahi et al., 2019), and *Withania somnifera* (Mishra et al., 2014) as a response to Cd treatment.

Total phenolic content as a surrogate measure can be used to assess antioxidative activity directly or indirectly; this is owing to their redox characteristics (Ali et al., 2007). Phenolics might play a significant role in the H_2O_2 detoxification process by acting as metal chelators. Flavonoids can also act as an antioxidant and have chelating properties due to their structure and substitution pattern of hydroxyl groups (Mishra et al., 2014). Enhanced production of phenolics and flavonoids, and other specific metabolites in response to Cd treatment in previous studies has demonstrated the influence of Cd on SMs (Okem et al., 2015; Srivastava and Yadav, 2017).

Cadmium seems to be the most potent heavy metal for promoting proline synthesis (Alia and Saradhi, 1991). Proline has the ability to preserve photosynthetic equipment, electron transport complexes, membranes, enzymes, and nucleic acids by scavenging ROS (Iqbal et al., 2016; Sharmila et al., 2017). By detoxifying ROS, boosting GSH levels, and preserving antioxidative enzyme activity, proline helped to increase Cd absorption and alleviate toxicity in *Solanum nigrum* (Xu et al., 2009). Proline accumulation is also reported in plants like *Withania somnifera* (Mishra et al., 2014), *Moringa oleifera* (Srivastava and Yadav, 2017), and *Mentha arvensis* (Zaid et al., 2020). The defense mechanism to alleviate metal stress is shown in Figure 2.

The heavy metals that contaminate medicinal plants induce a stress response mechanism that alters the overall growth, biochemistry, and molecular status of the cell. Heavy metals can alter the efficacy of the production of SMs depending on the plant species. The biochemical changes induced by Cd in various plants are tabulated in Table 3. The external metal stress induces oxidative stress, which in turn triggers signal transduction and its transmission into the cell thereby altering the biosynthesis of specific plant metabolites. The ROS produced during the oxidative stress in response to heavy metal stress causes lipid peroxidation, which stimulates the production of active signaling compounds. The signaling molecules initiate or suppress the production of SMs in turn enhancing the medicinal value of the plant (Nasim and Dhir, 2010; Asgari-Lajayer et al., 2017).

In *Satureja hortensis*, low Cd concentrations elevated the levels of α-terpinene, α-thujene, β-phellandrene, and ɣ-terpinene. Meanwhile, the fraction of this component decreased at high concentrations (Azizollahi et al., 2019). Similarly in *Artemisia annua*, an elevated artemisinin content was observed as a response to Cd during the initial exposure as a result of the high conversion rate of dihydroartemisinic acid to artemisinin brought by the oxygen radicals. A decline in artemisinin content was observed at 336 hours due to the enhanced toxic effect of Cd for a long duration (Li et al., 2012). The enhanced production of centelloside in *Centella asiatica* is accompanied by the overexpression of its biosynthetic genes i.e, SQS (Squalene synthase), BAS (β amyrin synthase), and CAS (cycloartenol synthase) in response to Cd treatment at high concentrations is evidence to the toxicity of Cd at the molecular level (Biswas et al., 2020). Similar results were also observed in *Phyllanthus amarus*, in which the accelerated production of phyllanthin and hypophyllanthin in presence of Cd in media, and a reduction in the production of

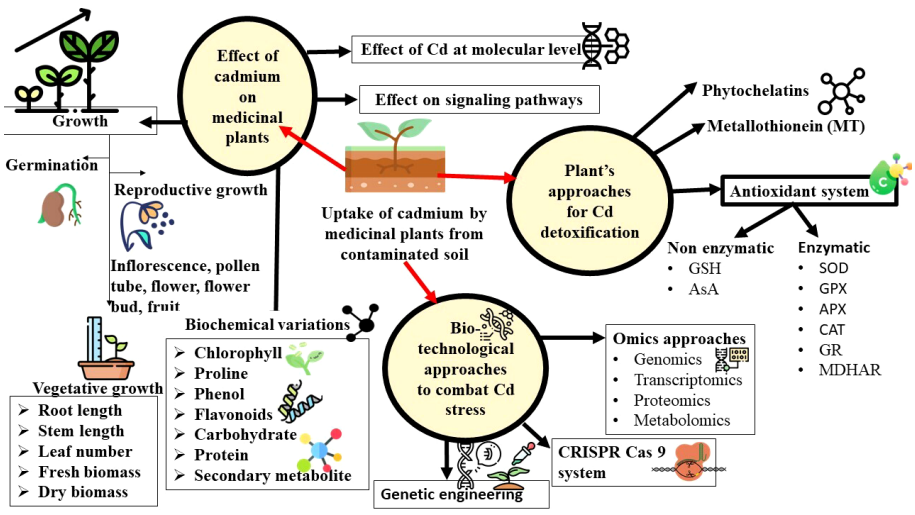

FIGURE 3
Schematic illustration of the effect of cadmium on morphological, physiological, and biochemical characteristics of medicinal plants and biotechnological and omics approaches to alleviate the cadmium stress.

TABLE 4 Bioaccumulation of cadmium in different parts of medicinal plants.

Plant name	Metal Concentration	Accumulation and translocation	Reference
Adhatoda vasica L.	0,100, 200, 300, 400, 500, 600 ppm	Cd accumulation increased with the amount of application	(Trivedi, 2003)
Alternanthera tanella Colla	50- 150 ppm for 30 days	Cd absorption increased with increasing cdamium concentration	(Rodrigues et al., 2017)
Amaranthus spinosus L.	5-50 ppm for 60 days	The metal accumulation increased with increasing Cd concentration	(Huang Y et al., 2019)
Andrographis paniculata (Burm.f.) Nees	10, 50,100,150 and 200 ppm	Accumulation was high at the highest metal concentration supplemented	(Patel, 2006a)
Bacopa monnieri L.	5,10,50,100 μM for 6 weeks	Cd accumulation increased with increasing concentration and duration with highest at 100 μM concentrations	(Gupta et al., 2014)
Cannabis sativa L.	82, 115, 139 µg g^{-1}	The metal accumulated in roots and translocated partially to shoots	(Citterio et al., 2003)
Centella asiatica (L.) Urb.	50-100 ppm for 30 days	Cd accumulation was higher in treated plants than in control	(Biswas et al., 2020)
Duranta erecta	0.1M, 0.5M and 1M s	The plant could not tolerate the Cd stress	(Anarado et al., 2018)
Drimia elata Jacq. ex Willd	2, 5, 10 mg L^{-1}	Accumulation of Cd increased with increasing concentrations. The bulb accumulated higher Cd concentration than shoots	(Okem et al., 2015)
Merwilla plumbea (Lindl.) Speta	1,5 ppm	The root accumulated the highest Cd concentration and increased significantly with concentration	(Lux et al., 2011a)
Moringa oleifera Lam.	1- 5 mM for 30 days	Uptake of Cd was maximum in roots and increased with increasing time interval and Cd concentration	(Srivastava and Yadav, 2017)
Ocimum basilicum L	0, 5 and 10 mg L^{-1} (5 days)	The Cd accumulation was higher in young plants than mature plants in their shoot and increased with increasing concentration	(Souri et al., 2019)
Ocimum canum Sims.	50, 100, 150, 200, 250 mg	The accumulation of Cd was dependent on the concentration of Cd treated	(Patel, 2006b)
Sida acuta Burm. f.	0.1M, 0.5M and 1M	Highest Cd concentration of 6.495 mg kg^{-1} was absorbed and was unable to tolerate further cadmium stress.	(Anarado et al., 2018)

these bioactive components at the high range of Cd exposure (Rai et al., 2005). However, in *Matricaria chamomilla*, the SMs Herniarin and Umbelliferone are unaltered by Cd treatment, while the precursors (Z)-and (E)-2-b-D glucopyranosyl oxy-4-methoxy cinnamic acids (GMCAs) increased in all the Cd concentrations (Kováčik et al., 2006). The morphological, physiological and biochemical changes in plants that are exposed to Cd stress has been represented in Figure 3.

4.6 Accumulation and translocation of heavy metal in medicinal plants

The insoluble heavy metals like Cd remain in the soil for a long time and pose a serious environmental threat. The metals enter the medicinal plants through the root system *via* channel or carrier proteins. The plant roots establish the rhizosphere in the soil by extending their root system. The roots can then accumulate and translocate specific heavy meals to shoot across cellular membranes (DalCorso et al., 2019). It is observed that generally, roots tend to accumulate heavy metals at higher concentrations when compared to stem and leaves (Zhao and Duo, 2015). The bioaccumulation studies conducted in various medicinal plants are represented in Table 4. Roots serve as the first line of defense, protecting other parts of the plant from metal toxicity. However, some studies report the presence of higher metal concentrations in the leaf and stem than in the root.

5 Effects of cadmium on signaling pathways

The sensing and processing of signals in response to stress are key components of the plant Cd defense system and can result in

certain physiologic, metabolic, and gene expression responses. In general, when the plant is exposed to stress, the plant cells activate certain genes through complex signal transduction pathways like the MAPK pathway involving phosphokinase-mediated phosphorylation and dephosphorylation reactions. A similar cascade of phosphorylation was believed to be associated with Cd signaling to the nucleus for the activation of Cd response genes. Additionally, reduced glutathione-oxidized glutathione ratio (GSH/GSSG) and elevated Calcium levels intended for the Ca-calmodulin signaling pathway were also discovered to be implicated in Cd sensing (DalCorso et al., 2010). A recent study on duckweed also supports the calcium mediated signaling of Cd (Yang et al., 2020). Apart from this, phytohormones also play an important role in Cd signaling. ABA is one such phytohormone which is actively involved in sensing Cd and subsequent response mechanisms by activating Cd defense-related genes like HMA2 and HMA4 (metal transporters) (Lu et al., 2020).

6 Effect of Cd at the molecular level

Under heavy metal stress, it has been discovered that transcriptional factors such as the MYB and WRKY family are triggered. OBF5, a transcription factor belonging to the bZIP family, also has been implicated in order to control the production of glutathione S-transferase (GST6) by binding to it during Cd stress thereby protecting the tissues against oxidative stress (Ghosh and Roy, 2019). In *B. juncea*, the orthologue of TGA3 protein, BjCdR15 has been observed as crucial in regulating the expression of phytochelatins and metal transporter genes (Fusco et al., 2005) and thereby taking part in cadmium uptake and long-distance transport from root to shoot. In the study by Yuan et al. (2018), the association of four transcriptional factors MYB, WRKY, ERF and bZIP family for Cd tolerance has been reported in *Agrostis stolonifera*. MYB binds to the promoter region and regulates the expression of the basic helix-loop-helix transcription factors leading to activation of IRT1, which in turn encodes a metal transporter involved in Cd uptake (Zhang et al., 2019). ERF is a transcription factor that binds and regulates MRE containing Cd stress related genes which relieves lipid peroxidation and reduces Cd accumulation (Wang et al., 2023). According to Cai et al. (2020), the TF GmWRKY142 in *Glycine max* directly affects Cd tolerance by binding to W box elements in the promoter region of cadmium stress-responsive genes GmCDT1-1 and GmCDT1-2 which decreases Cd uptake and enhances Cd resistance. The recent study in *Populus* × *canadensis* 'Neva' also reported the upregulated WRKY and NAC family of TF (Li et al., 2021b). Up-regulation of *CaWRKY41* was reported in pepper as a response to Cd stress (Dang et al., 2019).

Epigenetic pathways like DNA methylation and histone modifications have become a significant, intricate aspect in how plants react to heavy metal stressors. However, only a small amount of research has emphasized how epigenetic pathways can enhance plant performance when exposed to Cd stress (Niekerk et al., 2021). When heavy metals burden plants, a key gene regulatory mechanism for plants to respond to stress and minimize toxicity is the change in methylation status in the promoter region (Chakrabarti and Mukherjee, 2021). By raising DNA methylation levels and methylating specific gene loci, plants can inhibit the production of certain genes. Alternatively, it's possible that some genomic DNA loci are demethylated, which causes the production of specific genes and increases the stress resistance of plants (Ding et al., 2019). The hypermethylation was reported in *P. oceanica* (Greco et al., 2012) and *A. thaliana* (Li et al., 2015), while re-methylation was reported in *Raphnus sativus* (Yang et al., 2007) as a response to Cd treatment.

Apart from the epigenetic changes, Cd has been reported as a potential mutagen, which causes DNA damages including single and double-strand breaks which ultimately leads to chromosome aberrations (Ghosh and Roy, 2019). The genotoxicity of different concentrations of Cd on *Pisum sativum* was elucidated by ISSR analysis (Almuwayhi, 2021) and in *Eruca sativa* by RAPD analysis (Al-Qurainy et al., 2010). In *Catharanthus roseus*, the expression of terpenoid indole alkaloid (TIA) genes like STR, DAT, SGD, SLS, PRS, TDC, MTs, TPT, and MDR has been triggered under Cd toxicity (Chen et al., 2018c). In the comparative study of Cd-sensitive and Cd-tolerant *Medicago truncatula*, it was found that the overexpression of GSH and phytochelatin biosynthesis genes such as MtCYS, MtγECS, MtGSHS, MtGR, and MtG6PDH in Cd sensitive plant (García de la Torre et al., 2022). While the enhanced expression of metallothionein genes from the families MT1, MT2 and MT3 in response to Cd stress in *Phytolacca americana* was reported by Chen et al. (2017). In addition, the activation of Potri.010G183900 (ABA gene) was observed in *Populus* × *canadensis* 'Neva' as a response to Cd exposure (Li et al., 2021b).

7 Plant's approaches for cadmium detoxification

On exposure to heavy metals, plants try to avoid or minimize absorption into root cells by binding metal ions to the cell wall or cellular exudates or by limiting them to the apoplast or reducing long-distance transport as the first line of defense. Releasing of some root exudates or other low molecular weight substances to minimize the effect of Cd, like the release` of lubimin and 3-hydroxylubimin in response to Cd toxicity in *Datura stramonium* root cultures, is a kind of such defense (Furze et al., 1991). When metal ions are present at high levels, cells engage an array of detoxification and storage methods, including chelation of metal ions in the cytosol with phytochelatins and

TABLE 5 Defense mechanisms for Cadmium tolerance in medicinal plants.

Plant	Concentration and duration	Chelating agents/detoxification proteins(Phytochelatins and metallothioneins, reduced GSH etc)	Antioxidant enzymes(SOD, CAT etc)	Reference
Alternanthera tanella Colla	50- 150 ppm for 30 days	–	Decreased SOD activity at high concentration and increased APX activity	(Rodrigues et al., 2017)
Bacopa monnieri L.	10- 200 ppm for 144 hours	Enhanced production of phytochelatins along with GSH production.	Enhanced APX and GPX activity but reduced CAT activity with increasing concentration	(Mishra et al., 2006; Singh et al., 2006)
Bidens pilosa L.	2.57ppm, 7.94 ppm, 17.33ppm, and 37.17ppm for 40 days	–	SOD, GPX and GR activity increased with metal concentration	(Dai et al., 2021)
Brassica juncea L.	0.5 and 1mM for 3 days	Enhanced phytochelatin production. GSH content increased at lower concentration, but decreased at high concentration	Increased GPX and SOD activity, reduction in CAT activity at high concentration	(Mahmud et al., 2018)
	200 and 300 ppm	–	SOD, CAT, APX and GR activity increased with increasing concentration	(Ahmad et al., 2015)
Cajanus cajan L.	10-30 ppm	–	CAT and POD increased in leaves, root and stem of seedling	(Patel and Patel, 2012)
Cannabis sativa L.	82, 115, 139 $\mu g\ g^{-1}$	An increase in the PC and GSH was observed	–	(Citterio et al., 2003)
	27 and 82 ppm	Increased GSH and phytochelatin content	–	(Citterio et al., 2003)
Centella asiatica L.	5 - 200 ppm for 30 days	–	Enhanced SOD, GPX and APX activity	(Biswas et al., 2020)
Hibiscus cannabinus L.	20-120 ppm	High GSH content at lower concentrations but decreased at high concentration in both leaves and roots	SOD, CAT and POD activities in roots increased and then dropped at high concentration	(Li et al., 2013)
Lemna gibba L., *Lemna minor* L.	0.01 - 1.5ppm for 96 hours	–	Increased activities of CAT, APX and POD	(Banu Doğanlar, 2013)
Lepidium sativum L.	20, 50 and 100 ppm for 30 days	High GSH content	Increased activities of SOD, APX, CAT and GR	(Gill et al., 2012)
Melissa officinalis L.	0.10, 20, and 40 mM	–	CAT and SOD activities increased	(Nourbakhsh Rezaei et al., 2019)
Mentha arvensis L.	50ppm for 100 days	–	Enhanced activities of SOD, CAT, POX, and GR	(Zaid et al., 2020)
Moringa oleifera Lam.	1- 5 mM for 30 days	Significant increase in metallothionein concentration	Increased CAT, APX and GR activity	(Srivastava and Yadav, 2017)
Phyllanthus amarus Schumach. and Thonn.	10-100 ppm for 60 days	–	Increased CAT and APX activity upto 30 - 60 ppm. Sudden decline at higher concentrations	(Dwivedi et al., 2013)
Satureja hortensis L.	2.5- 15ppm	–	Enhanced CAT and APX activity	(Azizollahi et al., 2019)
Solanum nigrum L.	50 and 200 ppm for 3 days	Increased phytochelatin production and High GSH content	Enhanced activities of SOD, APX, GR, CAT, POD And GSH-PX activity	(Deng et al., 2010)

(Continued)

TABLE 5 Continued

Plant	Concentration and duration	Chelating agents/detoxification proteins(Phytochelatins and metallothioneins, reduced GSH etc)	Antioxidant enzymes(SOD, CAT etc)	Reference
Thlaspi caerulescens J. and C. Presl	500 ppm for 9 weeks	Increased phytochelatin content	–	(Wójcik et al., 2005)
Trigonella foenum-graecum L.	0.5 – 10 mM for 30 days	–	Increasing SOD and APX activity with increasing concentrations in both roots and shoots but, reduced activity of CAT with high concentrations	(Zayneb et al., 2015)
Withania somnifera L. Dunal.	5 - 1000ppm for 30 days	–	Increased activities of CAT, G -POD, POD, GPX, APX, reduced activity of SOD and GR at high concentrations	(Mishra et al., 2014)

metallothioneins, trafficking, and sequestration into the vacuole *via* vacuolar transporters (Zhou et al., 2015). The presence of Cd as electron-dense granules in both cell wall and cytoplasmic compartments of root and vacuoles of spongy and palisade parenchyma cells in leaves of *Thlaspi caerulescens* along with enhanced phytochelatin production might be due to the Cd-phytochelatin complexation followed by compartmentalization (Wójcik et al., 2005).

Cadmium can trigger the generation of phytochelatins, which are tiny metal-binding peptides (PCs) that have the basic structure (-Glu-Cys)n-Gly, with n = 2–11. The PCs bind Cd and form varied complexes with molecular weights of around 2,500–3,600Da. The Cys thiolic groups of PC guard the cytosol from free Cd ions and eventually sequester Cd in the vacuole. The synthesis of PCs from Glutathione is catalyzed by the cytosolic PC synthetase (Cobbett and Goldsbrough, 2002; Ahmad et al., 2019). Various studies on medicinal plants like *Bacopa monnieri* (Mishra et al., 2006; Singh et al., 2006), *Solanum nigrum* (Deng et al., 2010), *Thlaspi caerulescens* (Wójcik et al., 2005), *B. juncea* (Mahmud et al., 2018) reveals the role of phytochelatins in reducing the effects of Cd toxicity.

Reduced glutathione (GSH) is a glutamic acid, cysteine, and glycine amino acid derivative. It can be used as a ligand to chelate heavy metals, and so reduce their toxicity (Yu et al., 2019). GSH is known to alleviate Cd-induced oxidative stress by positively controlling the activities of antioxidant enzymes and the expression of transcription factors involved in the regulation of stress response genes (Hasan et al., 2016). Enhanced GSH production is reported in *Bacopa monnieri* (Mishra et al., 2006; Singh et al., 2006), *Lepidium sativum* (Gill et al., 2012), *Solanum nigrum* (Deng et al., 2010) with increasing Cd concentrations along with the increased antioxidant enzymes.

Metallothionein (MT) is a cysteine-rich, metal-binding protein (Yu et al., 2019) that chelates metal ions and forms MT–metal complexes and tend to be found in the cytosolic compartments. MTs, apart from PCs, are the outcome of mRNA translation associated with heavy metal stress (Cobbett and Goldsbrough, 2002; Ahmad et al., 2019). Increased amounts of metallothionein in response to high concentrations of Cd in plants like *Moringa oleifera* (Srivastava and Yadav, 2017) indicate its importance in Cd detoxification.

The toxic effects of ROS may be alleviated either by non-enzymatic (GSH; ascorbic acid, ASA;-tocopherol and carotenoids) or by enzymatic SOD (superoxide dismutase), CAT (catalase), APX (ascorbate peroxidase), GR (glutathione reductase), MDHAR (monodehydroascorbate reductase dehydroascorbate) antioxidants. Antioxidant enzymes play a crucial role in diminishing the adverse effects of reactive oxygen species formed under Cd stress to improve plant growth and metabolic tolerance (Luo et al., 2011; Biswas et al., 2020).

SOD is an important part of the antioxidative defense machinery, which helps to exclude superoxide radicals, reduce the peroxidation of membrane lipids and retain the stability of the cell membrane (Zhang et al., 2007). The reduction in the SOD activity under a high dose of Cd stress as reported in *Alternanthera tanella* (Rodrigues et al., 2017), *Withania somnifera* (Mishra et al., 2014), and *Hibiscus cannabinus*, might be attributed to enzyme damage due to the excessive production of free radicals and peroxides (Mishra et al., 2006; Li et al., 2013). The SOD converts O_2^- to H_2O_2 and efficiently blocks O_2^- driven cell damage. Since a sheer volume of H_2O_2 limits the plant's capacity to tolerate Cd, the oxidoreductase enzymes CAT, APX, GPX, and POD work together to prevent H_2O_2 buildup (Raza et al., 2020) by reducing them into the water and molecular oxygen by working at different locations in the cell. APX functions in chloroplasts in the ascorbate–glutathione cycle, whereas GPX is basically a cell wall-bound enzyme and is also found in cytoplasm while CAT is present in peroxisomes and mitochondria (Mishra et al., 2006).

According to Li et al. (2013) and Mishra et al. (2006), the reduced CAT activity observed in Cd treated *Bacopa monnieri*

TABLE 6 Omics approaches for understanding response to cadmium stress in medicinal plants.

Omics approach	Plant	Method	Outcome of study	Reference
Genomics	*Brassica napa* L.	TILLING	role of the HMA4 gene has been elucidated	(Navarro-León et al., 2019)
Genomics	*Brassica napa* L.	GWAS	Identified NRAMP6 (natural resistance-associated macrophage protein 6), IRT1 (iron-regulated transporter 1), CAD1 (cadmium-sensitive 1), and PCS2 (phytochelatin synthase 2) genes as candidate genes for Cd accumulation	(Chen et al., 2018b)
Genomics	*Linum usitatissimum* L.	GWAS	Identified 198 ABC transporters and 12 HMA gene	(Khan et al., 2020)
Genomics	*Medicago sativa* L.	GWAS	genes such as oxidative stress response genes, P type transporters genes are associated with Cd tolerance	(Paape et al., 2021)
Genomics	*Oryza sativa* L.	CRISPR Cas 9	Role of OsNramp1, OsNramp5, OsLCT1 gene to reduce Cd uptake	(Wang et al., 2019; Songmei et al., 2019; Chen et al., 2019)
Genomics	*Solanum tuberosum* L.	qRT-PCR analysis	Identification of 11 MTP genes from Mn-MTP, Zn-MTP and Zn/Fe-MTP gene families	(Li et al., 2021a)
Transcriptomics	*Brassica napus* L.	RT-PCR	Identification of 13 conserved miRNAs involved in response mechanism to Cd stress	(Huang et al., 2010)
Transcriptomics	*Brassica napus* L.	high-throughput sequencing	Identification of 44 known miRNAs (belonging to 27 families) and 103 novel miRNAs involved in Cd stress response	(Jian et al., 2018)
Transcriptomics	*Cucumis sativus* L.	RNA sequencing	Identification of transporter genes (CsHMA1, CsNRAMP1, CsNRAMP4, CsZIP1, and CsZIP8)	(Feng et al., 2021)
Metabolomics	*Amaranthus hypochondriacus* L.	LC MS	purine metabolism, Gly, Ser, and Thr metabolism, as well as Pro and Arg metabolism, are all involved in the improved tolerance at the vegetative stage	(Mengdi et al., 2020)
Metabolomics	*Brassica napus* L.	HPLC	Decreased Cd accumulation in roots and shoots	(Ali et al., 2020)
Metabolomics	*Catheranthus roseus* var. *rosea* L.	GC MS	differential accumulation of secondary metabolites was found to be responsible for the cd tolerance	(Rani et al., 2021)
Metabolomics	*Salvia miltiorrhiza* Bunge	GC MS	Cd boosted Rosmarinic Acid production *via* controlling amino acid metabolism but hindered tanshinone synthesis primarily by decreasing the GGPP concentration, with proline, POD, and CAT playing critical roles	(Yuan et al., 2021)
Metallomics	*Arabidopsis halleri*	μ-XRF using high-energy synchrotron radiation	cellular distribution of cadmium	(Fukuda et al., 2020)
miRNAomics	*Boehmeria nivea* L. Gaudich	high-throughput sequencing and *silico* method	Identification of 73 novel miRNAs and 426 potential miRNA targets which has been involved in metal ion absorption, chlorophyll biosynthesis and protein ubiquitination	(Chen et al., 2018b)

plants in both leaves and roots may be attributed to degradation caused by increased peroxisomal proteases, photoinactivation of the enzyme, or inactivation owing to excessive oxygen radicals. A similar reduction of CAT activity was also reported in *Trigonella foenum-graecum* (Zayneb et al., 2015) and *B. juncea* (Mahmud et al., 2018). The enhanced activity of the other two H_2O_2 degrading enzymes, APX and GPX or POD, appears to have compensated for the reduced activity of CAT in all these plants. The cadmium detoxification approaches undertaken by plants are represented in Table 5.

8 Various approaches to ameliorate heavy metal stress in medicinal plants

8.1 Omics approaches

Deciphering the actual mechanisms by which heavy metals induce stress and understanding the physiological, biochemical, and molecular responses to metal toxicity at the cellular level is

an extremely hard and challenging task. Thus, over the last few years, modern biotechnological tools are employed to understand the mechanisms underlying plant-metal interaction. In this section, we will provide a unique perspective of metal-induced toxicity and its reclamation by regulation of proteomics, metabolomics, and epigenomics changes in plants. Omics approaches such as genomics, transcriptomics, miRNAomics, proteomics, metabolomics including metallomics, are pragmatic approaches that provide a complete understanding of physiological, biochemical, and molecular responses to stress in plants (Rai et al., 2021) and can be used to develop stress tolerant and resilience plant systems (Jamla et al., 2021). The various omics approach study conducted in medicinal plants is represented in Table 6.

8.1.1 Genomics

Genomic approach includes the identification of genes involved in metal resistance, transport of heavy metals, and plant stress tolerance. Clustered regularly interspaced short palindromic repeats (CRISPR/Cas9), DNA mismatch repair (MMR), targeted induced local lesions in genomes (TILLING), and Genome-wide association studies (GWAS) are some of the genomic approaches to understand the genes involved in plant -metal interaction (Raza et al., 2020). In *Brassica rapa*, subjected to $CdCl_2$ stress, the role of the HMA_4 gene has been studied using targeted induced local lesions in genomes (TILLING) (Navarro-León et al., 2019). Genome-wide association studies (GWAS) have been conducted in *Brassica rapa* using a 60K Brassica Infinium® SNP array to understand the mechanisms underlying Cd tolerance (Chen et al., 2018b). Another GWAS study in *Medicago sativa* subjected to cadmium stress reveals that the root and leaf response traits are polygenic with multiple quantitative loci (QTL), and genes such as oxidative stress response genes, P-type transporters genes are associated with Cd tolerance (Paape et al., 2021). Studies have been conducted in the OSNramp5 gene to reduce Cd uptake in rice by CRISPR Cas 9 technology (Wang et al., 2019). In the cadmium toxicity studies conducted by Zhao et al. (2020) in *Glycine max* (L.), it has been found that MSH2 and MSH6 of the mismatch repair system (MMR) have played an important role in tolerance to cadmium stress.

8.1.2 Transcriptomics and proteomics

A group of small RNAs, such as miRNA and siRNA, are involved in post-transcriptional regulation. Moreover, a group of miRNAs is reported to be involved in responsive mechanisms to plant stress. A total of 13 conserved miRNAs involved in the response mechanism to Cd stress are identified by transcriptional analysis with RT-PCR (Huang et al., 2010), and a total of 44 known miRNAs (belonging to 27 families) and 103 novel miRNAs have been identified by high-throughput sequencing (Jian et al., 2018) in *Brassica napus* L. A total of 73 novel miRNAs (identified by high throughput sequencing), and 426 potential miRNA targets (identified by *in silico* method) are reported to be involved in metal ion absorption, chlorophyll biosynthesis, and protein ubiquitination in *Boehmeria nivea* L. (Chen et al., 2018a).

In *B. juncea* L. fifty-two genes out of seventy-three Cd responsive transcript derived fragments were identified as gene expression regulators, stress-responding transcriptional factors, and transport facilitation genes by cDNA-amplified fragment length polymorphism (cDNA-AFLP) analysis (Fusco et al., 2005). In the transcriptomics study conducted by Feng et al. (2021) five transporter genes: CsHMA1, CsNRAMP1, CsNRAMP4, CsZIP1, and CsZIP8 have been identified in *Cucumis sativus* L. and it has been observed that the transcript of CsNRAMP4 positively correlated and the expression level of CsHMA1 negatively correlated with Cd accumulation. The transcriptomics study in *Lactuca sativa* L. var. *ramose* using PacBio and Illumina techniques reveal the potential molecular pathway (antioxidant and hormone signal transduction) under Cd stress with and without pre-application of melatonin. The genes involved in Cd detoxification on melatonin application are identified (Yu et al., 2022). The transcriptomic study conducted in two different cultivars of *Brasica rapa* var chinensis (Baiyewuyueman and Kuishan'aijiaoheiye) identified 797 ROS-related proteins and 1167 transcription factors encoding unigenes. These four genes (DEGs, SOD1, POD A2/44/54/62 and GST1) are associated with the differential response to Cd stress between the two cultivars (Yu et al., 2017). Proteomics studies in *Populus yunnanensis* under cadmium stress reveal the protective role of nitrogen in alleviating cadmium stress. It was observed that 42 proteins and 522 proteins were upregulated in groups treated with cadmium along with nitrogen when compared to Cd-treated and control plants, respectively, and 89 proteins and 127 proteins were down-regulated by Cd+ N treatment in comparison to Cd-treated and control plants respectively (Huang J et al., 2019).

8.1.3 Metabolomics

With the aid of metabolomics techniques, scientists may better understand the fundamental metabolite profiles that confer stress resistance in plants and generate these profiles in any crop species to increase their resilience to biotic and abiotic challenges, including climate change (Singh et al., 2021). Primary metabolism, which encompasses sugars, amino acids, and nucleic acids, influences how plants adapt to their environment, while, secondary metabolites are non-essential rather than play pleiotropic functions in modifying plant responses to abiotic and biotic stressors (Zou et al., 2022). An analysis of *Arabidopsis*' proteome and metabolome revealed that the main reaction of the metabolome to Cd stress was to

activate the carbon, nitrogen, and sulfur metabolism, which led to the formation of Cd-chelating compounds (phytochelatins) (Sarry et al., 2006).

According to a study performed on *Amaranthus hypochondriacus*, the nine pathways responsible for antioxidation, osmotic balance regulation, energy supplementation, and the promotion of metabolites that participate in phytochelatin (PC) synthesis were the main sites of involvement for the metabolites under Cd toxicity in various growth stages (Mengdi et al., 2020). Additionally, they discovered that the purine metabolism, Gly, Ser, and Thr metabolism, as well as Pro and Arg metabolism, are all involved in improved tolerance at the vegetative stage. The most significant metabolic indicator of Cd stress in the *Amaranthus hypochondriacus* was discovered to be purine metabolism (Mengdi et al., 2020). Similar to this, a metabolomics investigation in tobacco plants under Cd stress, showed 150 and 76 metabolites, were differently deposited in the roots and leaves respectively. These metabolites were much more abundant in the production of flavone and flavonols, nicotinate and nicotinamide, arginine and proline, and amino acids (Zou et al., 2022).

However, in *Catharanthus roseus*, the differential accumulation of secondary metabolites is thought to be responsible for the Cd tolerance (Rani et al., 2021). The increased levels of metabolites from the monoterpenoid indole alkaloid pathway, including nicotine, coronaridine, vidorosine, vindoline, tabersonine, and indolinine. In addition to isoprenoids and polyamines, other responsive metabolites included terpenes such as caryophyllene, campestrin, phytol, neophytadiene, cedrol, and silicone oil, emphasizing the significance of secondary metabolites in Cd tolerance in *Catharanthus roseus* (Rani et al., 2021). Likewise, the metabolomic findings indicate that Cd boosted RA production *via* controlling amino acid metabolism but hindered tanshinone synthesis primarily by decreasing the GGPP concentration, with proline, POD, and CAT playing critical roles in *Salvia miltiorrhiza*'s capacity to endure Cd stress (Yuan et al., 2021). The reaction to Cd stress in *Calendula officinalis* plant roots appeared to be more influenced by metabolic changes, such as an increase in sterol production simultaneous to a decrease in the triterpenoid content of the plant roots and hairy root culture (Rogowska et al., 2022).

8.1.4 Metallomics

Metallomics involves analytical approaches for characterizing the entirety of metal biomolecules in an organism (metallome) (Gómez Ariza et al. 2013). Metallomics, which includes the identification of metals (qualitative metallomics) and determining their levels (quantitative metallomics), may promote the development of applications for improved techniques in metal-contaminated soils (Singh and Verma 2018). To assure the safety of therapeutic plants and products, harmful metals present in them can be identified using metallomics tools such as HR-ICP-SFMS (Kenny et al. 2022). Identifying metal-binding proteins such as phytochelatins and metallothioneins can be used as biomarkers for the heavy metal stress that medicinal plants experience (Singh and Verma 2018). Fukuda et al. (2020) identified the distribution as well as accumulation of Cd in the leaves and trichomes of *Arabidopsis halleri* ssp. gemmifera using X-ray microfluorescence analysis. Likewise, ICP-MS was used to measure the Cd level in roots, stems, and early leaves. Micro XRF mapping with synchrotron radiation was also used to precisely locate Cd in various plant tissues (Pongrac et al. 2018). In addition, using XAS, the putative S- or O-based Cd ligands in the leaf tissue of several Cd-hyper-accumulating Brassicaceae species have been investigated (Jamla et al. 2021).

8.2 Biotechnological approaches

8.2.1 Genetic engineering approaches

Hyperaccumulator plants survive heavy metal stress and show metal tolerance by active detoxification and sequestration. They gain this ability due to the presence of stress tolerance genes in them. Thus, the metal-sensitive plants can be genetically modified for metal uptake, transport, and sequestration by the transformation of the genes of metal-hyperaccumulating plants that can accumulate, translocate and detoxify metals at a faster rate (Weerakoon, 2019). An attempt to enhance the cadmium accumulation and tolerance in *Solanum nigrum L.* has been made by Ye et al. (2020). The hairy roots of *S. nigrum* were infected with *Agrobacterium rhizogenes* ATCC15834 carrying the iron-regulated transporter gene (IRT1) from *A. thaliana*. The IRT1 gene expressed in transgenic *S. nigrum* reduced the phytotoxic effects of cadmium, enhanced cadmium tolerance, and helped in the normal growth of the plant. Transgenic *Medicago truncatula* expressing Delta(1)-pyrroline-5-carboxylate synthetase (P5CS) has been established by Verdoy et al. (2006) by infecting the host plant with *Agrobacterium rhizogenes* EHA105 carrying *VaP5CS* from *Vigna aconitifolia*. The *VaP5CS gene in* transgenic *Medicago truncatula* has been reported as being involved in conferring cadmium tolerance by enhanced proline accumulation and antioxidant activity by García de la Torre et al., (2022). Very limited attempts at genetic engineering in medicinal plants have been reported till date. Thus, there is a need for extensive studies on genetic improvements to confer metal tolerance mechanisms in medicinal plants. The widely used gene editing approaches such zinc finger nucleases (ZFNs) and transcript activators like effector nucleases (TALENs) is limited due to the frequent mutations at non-targeted sites (Sarma et al., 2021).

8.2.2 CRISPR/Cas system, a gene editing approach for heavy metal tolerance

The CRISPR–Cas9 (clustered regularly interspaced short palindromic repeats (CRISPR)/CRISPR-associated protein 9) system has emerged as an innovative gene editing tool in plant systems (Venegas-Rioseco et al., 2021). It is a quick, cost friendly tool that can be used for improving crop traits against abiotic and biotic stress tolerance (Pandita, 2021). It consists of spacer sequences placed between short palindromic repeats which transcribe to CRISPR RNA (crRNA), which combines with transactivating crRNA (tracrRNA) to form a mature crRNA/tracrRNA complex (guide RNA/gRNA). The gRNA directs the Cas nuclease, which creates a DNA double-strand break (DSB) in the desired DNA sequence, thereby causing gene deletion *via* the repair mechanisms of cells (Rai et al., 2021; Venegas-Rioseco et al., 2021). Thus, gRNA-guided–Cas9 systems can be used for gene knockout, regulation of gene expression, and transcription factors, thereby enhancing heavy metal stress tolerance and phytoremediation in a diverse range of plants (Bao et al., 2019).

The important genes involved in metal stress tolerance in phytoremediator plants such as *Arabidopsis halleri*, *B. juncea, Hirschfeldia incana, Noccaea caerulescens*, and *Pteris vittata* can be identified through transcriptomics to develop ideal hyperaccumulator plants (Kumar and Trivedi, 2018). Further, the incorporation of advanced gene editing technologies such as CRISPR–Cas9 will help enhance phytoextraction technology (Thakur et al., 2020). The Cd accumulation in *Oryza sativa* has been reduced by knocking out the OsNramp5 metal transporter gene using the CRISPR-dCas9 system (Tang et al., 2017). The gene expression can be modulated by fusing the transcription factors with dCas9 to upregulate or downregulate the expression of a gene or a group of genes of interest (Miglani, 2017). The cytoplasmic Cd has been detoxified and enhanced the cadmium tolerance in *A. thaliana* by inducing the gene expression of AtPDF2.6 (Luo et al., 2019). Thus, CRISPR–Cas9 is a promising approach for enhancing the natural capacity of a plant to grow, accumulate, and tolerate heavy metal stress without introducing foreign genes (Figure 3).

9 Conclusion and prospects

In recent years, herbal drugs have been gaining popularity. Thus, the quality of herbal-based drugs has to be guaranteed prior to their marketing. The herbal drugs must be free of heavy metal contaminants, the presence of which would otherwise suppress the growth of the medicinal plant and affect the biosynthesis of important SMs either by upregulating or downregulating the genes involved in the biosynthetic pathway of SMs. In conclusion, it has been observed that the different growth stages including germination, vegetative and reproductive growth, photosynthesis, and biochemical parameters have been affected in different medicinal plants on exposure to cadmium. Most of the medicinal plants exposed to cadmium toxicity exhibit cadmium detoxification mechanisms such as the generation of phytochelatins, and metallothioneins, and triggering non-enzymatic and enzymatic antioxidant responses. The omics technology has been adopted to understand the mechanisms underlying plant-metal interaction. However, it is evident that very few genetic engineering approach studies have been conducted to confer cadmium resistance in medicinal plants and no CRISPR Cas 9 genetic tool approach has been reported in medicinal plants except a few crop plants. As is customary, extensive research has to be conducted to elucidate the defense mechanism involved in cadmium tolerance and its detoxification. Furthermore, CRISPR Cas 9 gene editing technique has to be employed for tailoring medicinal plants against Cd stress. Genetically modified medicinal plants derived through gene editing tools have to be assessed for their reliability. There is a scope for the adoption of synthetic biology approaches to develop improved varieties with heavy metal tolerance.

Discerning the toxic concentration of heavy metals and tolerance indices of medicinal plants would be beneficial in the establishment of a high-quality environment for plant growth. With the findings on the ability of the medicinal plants to uptake, accumulate, and translocate heavy metals, it is possible to have a better management program for growing medicinal plants, its safe consumption and usage in herbal drugs.

Author contributions

PN conceived the review. AB and RR collected the literature and wrote the manuscript. PN, helped in the original draft. PN and JMA-K critically reviewed the initial draft and streamlined the idea. AB and RR prepared and revised the tables and figures. JMA-K helped in funding acquisition and JMA-K, FMA, and MIA helped in revision of the manuscript. All authors carefully read, revised, and approved the manuscript for submission.

Funding

This work was supported by The Deanship of Scientific Research, Vice Presidency for Graduate Studies and Scientific Research, King Faisal University, Saudi Arabia [Project No. GRANT2168].

Acknowledgments

The authors extend their appreciation to the Deanship of Scientific Research, Vice Presidency for Graduate Studies and

Scientific Research, King Faisal University, Saudi Arabia for providing financial support [Project No. GRANT2168].

Conflict of interest

The authors declare that the research was conducted in the absence of any commercial or financial relationships that could be construed as a potential conflict of interest.

Publisher's note

References

Aghaz, M., Bandehagh, A., Aghazade, E., Toorchi, M., and Ghassemi-Gholezani, K. (2013). Effects of cadmium stress on some growth and physiological characteristics in dill (*Anethum graveolens*) ecotypes. *Int. J. Agriculture* 3, 409–413.

Ahmad, J., Ali, A. A., Baig, M. A., Iqbal, M., Haq, I., and Irfan Qureshi, M. (2019). "Role of phytochelatins in cadmium stress tolerance in plants," in *Cadmium toxicity and tolerance in plants*. Eds. M. Hasanuzzaman, M. N. V. Prasad and M. Fujita (London, UK: Academic Press), 185–212.

Ahmad, S. H., Reshi, Z., Ahmad, J., and Iqbal, M. (2005). Morpho-anatomical responses of *Trigonella foenum graecum* linn. to induced cadmium and lead stress. *J. Plant Biol. = Singmul Hakhoe Chi* 48, 64–84. doi: 10.1016/B978-0-12-814864-8.00008-5

Ahmad, P., Sarwat, M., Bhat, N. A., Wani, M. R., Kazi, A. G., and Tran, L.-S. P. (2015). Alleviation of cadmium toxicity in *Brassica juncea* l. (Czern. and coss.) by calcium application involves various physiological and biochemical strategies. *PloS One* 10, e0114571. doi: 10.1007/BF03030566

Alia,, and Saradhi, P. P. (1991). Proline accumulation under heavy metal stress. *J. Plant Physiol.* 138, 554–558. doi: 10.1016/S0176-1617(11)80240-3

Ali, M. B., Hahn, E.-J., and Paek, K.-Y. (2007). Methyl jasmonate and salicylic acid induced oxidative stress and accumulation of phenolics in *Panax ginseng* bioreactor root suspension cultures. *Molecules* 12, 607–621. doi: 10.3390/12030607

Ali, E., Hassan, Z., Irfan, M., Hussain, S., Rehman, H.-U. -., Shah, J. M., et al. (2020). Indigenous tocopherol improves tolerance of oilseed rape to cadmium stress. *Front. Plant Sci.* 11, 547133. doi: 10.3389/fpls.2020.547133

Almuwayhi, M. A. (2021). Effect of cadmium on the molecular and morpho-physiological traits of *Pisum sativum* L. *Biotechnol. Biotechnol. Equip.* 35, 1374–1384. doi: 10.1080/13102818.2021.1978318

Al-Qurainy, F., Alameri, A. A., and Salim, K. (2010). RAPD profile for the assessment of genotoxicity on a medicinal plant; *Eruca sativa*. *J. Med. Plant Res.* 4, 579–586. doi: 10.5897/JMPR10.062

Anarado, C. E., Anarado, C. J. O., Agwuna, C., Okeke, M. O., and Okafor, P. C. (2018). Phytoremediating potentials of *Sida acuta* and *Duranta erecta* for lead, cadmium, cobalt and zinc. *Int. J. Sci. Res.* 7, 969–971. doi: 10.21275/ART20192715

Asgari-Lajayer, B., Ghorbanpour, M., and Nikabadi, S. (2017). Heavy metals in contaminated environment: Destiny of secondary metabolite biosynthesis, oxidative status and phytoextraction in medicinal plants. *Ecotoxicol. Environ. Saf.* 145, 377–390. doi: 10.1016/j.ecoenv.2017.07.035

ATSDR (2013) *Where is cadmium found? cadmium toxicity*. Available at: https://www.atsdr.cdc.gov/csem/cadmium/Where-Cadmium-Found.html.

Azizollahi, Z., Ghaderian, S. M., and Ghotbi-Ravandi, A. A. (2019). Cadmium accumulation and its effects on physiological and biochemical characters of summer savory (*Satureja hortensis* L.). *Int. J. Phytoremediation* 21, 1241–1253. doi: 10.1080/15226514.2019.1619163

Bahl, A. S. (2022) *India's alternative medicine industry grows, boosted by the covid-19 pandemic. times of India*. Available at: https://timesofindia.indiatimes.com/blogs/voices/indias-alternative-medicine-industry-grows-boosted-by-the-covid-19-pandemic/ (Accessed November 25, 2022).

Banu Doğanlar, Z. (2013). Metal accumulation and physiological responses induced by copper and cadmium in *Lemna gibba*, L. minor and *Spirodela polyrhiza*. *Chem. Speciat. Bioavailab.* 25, 79–88. doi: 10.3184/095422913X13706128469701

Bao, A., Burritt, D. J., Chen, H., Zhou, X., Cao, D., and Tran, L.-S. P. (2019). The CRISPR/Cas9 system and its applications in crop genome editing. *Crit. Rev. Biotechnol.* 39, 321–336. doi: 10.1080/07388551.2018.1554621

Bauddh, K., and Singh, R. P. (2012). Cadmium tolerance and its phytoremediation by two oil yielding plants *Ricinus communis* (L.) and *Brassica juncea* (L.) from the contaminated soil. *Int. J. Phytoremediation* 14, 772–785. doi: 10.1080/15226514.2011.619238

Benavides, M. P., Gallego, S. M., and Tomaro, M. L. (2005). Cadmium toxicity in plants. *Braz. J. Plant Physiol.* 17, 21–34. doi: 10.1590/S1677-04202005000100003

Bewley, J. D. (1997). Seed germination and dormancy. *Plant Cell* 9, 1055–1066. doi: 10.1105/tpc.9.7.1055

Biswas, T., Parveen, O., Pandey, V. P., Mathur, A., and Dwivedi, U. N. (2020). Heavy metal accumulation efficiency, growth and centelloside production in the medicinal herb *Centella asiatica* (L.) urban under different soil concentrations of cadmium and lead. *Ind. Crops Prod.* 157, 112948. doi: 10.1016/j.indcrop.2020.112948

Cai, Z., Xian, P., Wang, H., Lin, R., Lian, T., Cheng, Y., et al. (2020). Transcription factor GmWRKY142 confers cadmium resistance by up-regulating the cadmium tolerance 1-like genes. *Front. Plant Sci.* 11, 724. doi: 10.3389/fpls.2020.00724

Carvalho, M. E. A., Gaziola, S. A., Carvalho, L. A., and Azevedo, R. A. (2021). Cadmium effects on plant reproductive organs: Physiological, productive, evolutionary and ecological aspects. *Ann. Appl. Biol.* 178, 227–243. doi: 10.1111/aab.12612

Chakrabarti, M., and Mukherjee, A. (2021). Investigating the underlying mechanism of cadmium-induced plant adaptive response to genotoxic stress. *Ecotoxicol. Environ. Saf.* 209, 111817. doi: 10.1016/j.ecoenv.2020.111817

Chen, Y., Zhi, J., Zhang, H., Li, J., Zhao, Q., Xu, J., et al (2017). Transcriptome analysis of *Phytolacca americana* L. in response to cadmium stress. *PLoS One* 12, e0184681. doi: 10.1371/journal.pone.0184681

Chen, Q., Lu, X., Guo, X., Pan, Y., Yu, B., Tang, Z., et al. (2018c). Differential responses to cd stress induced by exogenous application of Cu, zn or Ca in the medicinal plant *Catharanthus roseus*. *Ecotoxicol. Environ. Saf.* 157, 266–275. doi: 10.1016/j.ecoenv.2018.03.055

Chen, K., Wang, Y., Zhang, R., Zhang, H., and Gao, C. (2019). CRISPR/cas genome editing and precision plant breeding in agriculture. *Annu. Rev. Plant Biol.* 70, 667–697. doi: 10.1146/annurev-arplant-050718-100049

Chen, L., Wan, H., Qian, J., Guo, J., Sun, C., Wen, J., et al. (2018b). Genome-wide association study of cadmium accumulation at the seedling stage in rapeseed (*Brassica napus* L.). *Front. Plant Sci.* 9, 375. doi: 10.3389/fpls.2018.00375

Chen, K., Yu, Y., Sun, K., Xiong, H., Yu, C., Chen, P., et al. (2018a). The miRNAome of ramie (*Boehmeria nivea* L.): identification, expression, and potential roles of novel microRNAs in regulation of cadmium stress response. *BMC Plant Biol.* 18, 369. doi: 10.1186/s12870-018-1561-5

Citterio, S., Santagostino, A., Fumagalli, P., Prato, N., Ranalli, P., and Sgorbati, S. (2003). Heavy metal tolerance and accumulation of cd, cr and Ni by *Cannabis sativa* l. *Plant Soil* 256, 243–252. doi: 10.1023/A:1026113905129

Cobbett, C., and Goldsbrough, P. (2002). Phytochelatins and metallothioneins: roles in heavy metal detoxification and homeostasis. *Annu. Rev. Plant Biol.* 53, 159–182. doi: 10.1146/annurev.arplant.53.100301.135154

Dai, H., Wei, S., Pogrzeba, M., Krzyżak, J., Rusinowski, S., and Zhang, Q. (2021). The cadmium accumulation differences of two *Bidens pilosa* l. ecotypes from clean farmlands and the changes of some physiology and biochemistry indices. *Ecotoxicol. Environ. Saf.* 209, 111847. doi: 10.1016/j.ecoenv.2020.111847

DalCorso, G., Farinati, S., and Furini, A. (2010). Regulatory networks of cadmium stress in plants. *Plant Signal. Behav.* 5, 663–667. doi: 10.4161/psb.5.6.11425

DalCorso, G., Fasani, E., Manara, A., Visioli, G., and Furini, A. (2019). Heavy metal pollutions: State of the art and innovation in phytoremediation. *Int. J. Mol. Sci.* 20 (14), 3412. doi: 10.3390/ijms20143412

Dang, F., Lin, J., Chen, Y., Li, G. X., Guan, D., Zheng, S. J., et al. (2019). A feedback loop between CaWRKY41 and H2O2 coordinates the response to *Ralstonia solanacearum* and excess cadmium in pepper. *J. Exp. Bot.* 70, 1581–1595. doi: 10.1093/jxb/erz006

Deng, X., Xia, Y., Hu, W., Zhang, H., and Shen, Z. (2010). Cadmium-induced oxidative damage and protective effects of n-acetyl-L-cysteine against cadmium toxicity in *Solanum nigrum* l. *J. Hazard. Mater.* 180 (1-3), 722–729. doi: 10.1016/j.jhazmat.2010.04.099

Ding, G.-H., Guo, D.-D., Guan, Y., Chi, C.-Y., and Liu, B.-D. (2019). Changes of DNA methylation of *Isoetes sinensis* under Pb and Cd stress. *Environ. Sci. pollut. Res. Int.* 26, 3428–3435. doi: 10.1007/s11356-018-3864-3

Dobrikova, A. G., Apostolova, E. L., Hanć, A., Yotsova, E., Borisova, P., Sperdouli, I, et al (2021). Cadmium toxicity in *Salvia sclarea* L.: An integrative response of element uptake, oxidative stress markers, leaf structure and photosynthesis. *Ecotoxicol. Environ. Saf.* 209, 111851. doi: 10.1016/j.ecoenv.2020.111851

Dresler, S., Hanaka, A., Bednarek, W., and Maksymiec, W. (2014). Accumulation of low-molecular-weight organic acids in roots and leaf segments of *Zea mays* plants treated with cadmium and copper. *Acta Physiol. Plant* 36, 1565–1575. doi: 10.1007/s11738-014-1532-x

Dwivedi, G. K., Upadhyay, S. K., Mishra, A. K., and Singh, A. K. (2013). Hyper accumulation of cadmium in *Phyllanthus amarus* L. a medicinal plant. *Ind. J. Life Sci.* 3, 21.

El-Dahiyat, F., Rashrash, M., Abuhamdah, S., Abu Farha, R., and Babar, Z.-U.-D. (2020). Herbal medicines: a cross-sectional study to evaluate the prevalence and predictors of use among Jordanian adults. *J. Pharm. Policy Pract.* 13, 2. doi: 10.1186/s40545-019-0200-3

Faizan, S., Haneef, I., Kausar, S., and Perveen, R. (2012). Germination and seedling growth of *Coriandrum sativum* L. under varying levels of mixed cadmium and copper. *J. Funct. Environ. Bot.* 2, 52–58. doi: 10.5958/j.2231-1742.2.1.008

Fan, W., Liu, C., Cao, B., Qin, M., Long, D., Xiang, Z., et al. (2018). Genome-wide identification and characterization of four gene families putatively involved in cadmium uptake, translocation and sequestration in mulberry. *Front. Plant Sci.* 9, 879. doi: 10.3389/fpls.2018.00879

Fattahi, B., Arzani, K., Souri, M. K., and Barzegar, M. (2019). Effects of cadmium and lead on seed germination, morphological traits, and essential oil composition of sweet basil (*Ocimum basilicum* L.). *Ind. Crops Prod.* 138, 111584. doi: 10.1016/j.indcrop.2019.111584

Feng, S., Shen, Y., Xu, H., Dong, J., Chen, K., Xiang, Y., et al (2021). RNA-Seq Identification of Cd Responsive Transporters Provides Insights into the Association of Oxidation Resistance and Cd Accumulation in *Cucumis sativus* L. *Antioxidants (Basel)* 10, 111584. doi: 10.3390/antiox10121973

Fukuda, N., Kitajima, N., Terada, Y., Abe, T., Nakai, I., and Hokura, A. (2020). Visible cellular distribution of cadmium and zinc in the hyperaccumulator *Arabidopsis halleri ssp. gemmifera* determined by 2-d X-ray fluorescence imaging using high-energy synchrotron radiation. *Metallomics* 12, 193–203. doi: 10.1039/c9mt00243j

Furze, J. M., Rhodes, M. J., Parr, A. J., Robins, R. J., Withehead, I. M., and Threlfall, D. R. (1991). Abiotic factors elicit sesquiterpenoid phytoalexin production but not alkaloid production in transformed root cultures of *Datura stramonium*. *Plant Cell Rep.* 10, 111–114. doi: 10.1007/BF00232039

Fusco, N., Micheletto, L., Dal Corso, G., Borgato, L., and Furini, A. (2005). Identification of cadmium-regulated genes by cDNA-AFLP in the heavy metal accumulator *Brassica juncea* l. *J. Exp. Bot.* 56, 3017–3027. doi: 10.1093/jxb/eri299

Gall, J. E., Boyd, R. S., and Rajakaruna, N. (2015). Transfer of heavy metals through terrestrial food webs: a review. *Environ. Monit. Assess.* 187, 201. doi: 10.1007/s10661-015-4436-3

García de la Torre, V. S., Coba de la Peña, T., Lucas, M. M., and Pueyo, J. J. (2022). Transgenic *Medicago truncatula* plants that accumulate proline display enhanced tolerance to cadmium stress. *Front. Plant Sci.* 13, 829069. doi: 10.3389/fpls.2022.829069

Ghori, N.-H., Ghori, T., Hayat, M. Q., Imadi, S. R., Gul, A., Altay, V., et al. (2019). Heavy metal stress and responses in plants. *Int. J. Environ. Sci. Technol.* 16, 1807–1828. doi: 10.1007/s13762-019-02215-8

Ghosh, R., and Roy, S. (2019). "Cadmium toxicity in plants: Unveiling the physicochemical and molecular aspects," in *Cadmium tolerance in plants*. Eds. M. Hasanuzzaman, M. N. Vara Prasad and K. Nahar (London, UK: Academic Press), 223–246.

Gilbert, S. F. (2000). *Vegetative growth in developmental biology* (Sunderland, Massachusetts, USA: Sinauer Associates.,Sunderland).

Gill, S. S., Khan, N. A., and Tuteja, N. (2012). Cadmium at high dose perturbs growth, photosynthesis and nitrogen metabolism while at low dose it up regulates sulfur assimilation and antioxidant machinery in garden cress (*Lepidium sativum* L.). *Plant Sci.* 182, 112–120. doi: 10.1016/j.plantsci.2011.04.018

Gómez Ariza, J. L., García-Barrera, T., García-Sevillano, M. A., González-Fernández, M., and Gómez-Jacinto, V. (2013). "Metallomics and metabolomics of plants under environmental stress caused by metals," *Heavy Metal Stress in Plants* (eds). D. K. Gupta, F. J. Corpas and J. M. Palma (Berlin, Heidelberg: Springer Berlin Heidelberg), 173–201.

Greco, M., Chiappetta, A., Bruno, L., and Bitonti, M. B. (2012). In *Posidonia oceanica* cadmium induces changes in DNA methylation and chromatin patterning. *J. Exp. Bot.* 63, 695–709. doi: 10.1093/jxb/err313

Gupta, P., Khatoon, S., Tandon, P. K., and Rai, V. (2014). Effect of cadmium on growth, bacoside a, and bacopaside I of *Bacopa monnieri* (L.), a memory enhancing herb. *Sci. World J.* 2014, 824586. doi: 10.1155/2014/824586

Hangarter, R. P. (2000) *Vegetative growth. plants in motion*. Available at: https://plantsinmotion.bio.indiana.edu/plantmotion/vegetative/veg.html.

Haque, M., Biswas, K., and Sinha, S. N. (2021). "Phytoremediation strategies of some plants under heavy metal stress," in *Plant stress physiology*. Ed. A. Hossain (London, UK: IntechOpen).

Hasan, M. K., Liu, C., Wang, F., Ahammed, G. J., Zhou, J., Xu, M.-X., et al. (2016). Glutathione-mediated regulation of nitric oxide, s-nitrosothiol and redox homeostasis confers cadmium tolerance by inducing transcription factors and stress response genes in tomato. *Chemosphere* 161, 536–545. doi: 10.1016/j.chemosphere.2016.07.053

Hawrylak-Nowak, B., Dresler, S., and Matraszek, R. (2015). Exogenous malic and acetic acids reduce cadmium phytotoxicity and enhance cadmium accumulation in roots of sunflower plants. *Plant Physiol. Biochem.* 94, 225–234. doi: 10.1016/j.plaphy.2015.06.012

Huang, X., Duan, S., Wu, Q., Yu, M., and Shabala, S. (2020). Reducing cadmium accumulation in plants: Structure-function relations and tissue-specific operation of transporters in the spotlight. *Plants* 9, 223. doi: 10.3390/plants9020223

Huang, J., Wu, X., Tian, F., Chen, Q., Luo, P., Zhang, F., et al. (2019). Changes in proteome and protein phosphorylation reveal the protective roles of exogenous nitrogen in alleviating cadmium toxicity in poplar plants. *Int. J. Mol. Sci.* 21, 278. doi: 10.3390/ijms21010278

Huang, S. Q., Xiang, A. L., Che, L. L., Chen, S., Li, H., Song, J. B., et al. (2010). A set of miRNAs from *Brassica napus* in response to sulphate deficiency and cadmium stress. *Plant Biotechnol. J.* 8, 887–899. doi: 10.1111/j.1467-7652.2010.00517.x

Huang, Y., Xi, Y., Gan, L., Johnson, D., Wu, Y., Ren, D., et al. (2019). Effects of lead and cadmium on photosynthesis in *Amaranthus spinosus* and assessment of phytoremediation potential. *Int. J. Phytoremediation* 21, 1041–1049. doi: 10.1080/15226514.2019.1594686

Iqbal, N., Nazar, R., and Umar, S. (2016). "Evaluating the importance of proline in cadmium tolerance and its interaction with phytohormones," in *Osmolytes and plants acclimation to changing environment: Emerging omics technologies*. Eds. N. Iqbal, R. Nazar and N. A. Khan (New Delhi, India: Springer India), 129–153.

Jamla, M., Khare, T., Joshi, S., Patil, S., Penna, S., and Kumar, V. (2021). Omics approaches for understanding heavy metal responses and tolerance in plants. *Curr. Plant Biol.* 27, 100213. doi: 10.1016/j.cpb.2021.100213

Jian, H., Yang, B., Zhang, A., Ma, J., Ding, Y., Chen, Z., et al. (2018). Genome-wide identification of microRNAs in response to cadmium stress in oilseed rape (*Brassica napus* L.) using high-throughput sequencing. *Int. J. Mol. Sci.* 19, 1431. doi: 10.3390/ijms19051431

Kapoor, D., Rattan, A., Bhardwaj, R., and Kaur, S. (2016). Photosynthetic efficiency, ion analysis and carbohydrate metabolism in *Brassica juncea* plants under cadmium stress. *J. Pharmacog. Phytochem.* 5, 279–286.

Kenny, C.-R., Ring, G., Sheehan, A., Mc Auliffe, M. A.P., Lucey, B., Furey, A., et al (2022). Novel metallomic profiling and non-carcinogenic risk assessment of botanical ingredients for use in herbal, phytopharmaceutical and dietary products using HR-ICP-SFMS. *Sci. Rep.* 12, 17582.

Khan, N., You, F. M., Datla, R., Ravichandran, S., Jia, B., and Cloutier, S. (2020). Genome-wide identification of ATP binding cassette (ABC) transporter and heavy metal associated (HMA) gene families in flax (*Linum usitatissimum* L.). *BMC Genomics* 21, 722. doi: 10.1186/s12864-020-07121-9

Khatamipour, M., Piri, E., Esmaeilian, Y., and Tavassoli, A. (2011). Toxic effect of cadmium on germination, seedling growth and proline content of milk thistle (*Silybum marianum*). *Ann. Biol. Res.* 2, 527–532.

Khateeb, W. (2013). Cadmium-induced changes in germination, seedlings growth, and DNA fingerprinting of *in vitro* grown *Cichorium pumilum* jacq. *Int. J. Biol.* 6, 65. doi: 10.5539/ijb.v6n1p65

Kilic, S. (2017). Effects of cadmium-induced stress on essential oil production, morphology and physiology of lemon balm (*Melissa officinalis* l., lamiaceae). *Appl. Ecol. Environ. Res.* 15, 1653–1669. doi: 10.15666/aeer/1503_16531669

Komal, T., Mustafa, M., Ali, Z., and Kazi, A. G. (2015). "Heavy metal uptake and transport in plants," in *Heavy metal contamination of soils: Monitoring and remediation*. Eds. I. Sherameti and A. Varma (Switzerland: Springer International Publishing), 181–194.

Kováčik, J., Tomko, J., Bačkor, M., and Repčák, M.. (2006). *Matricaria chamomilla* is not a hyperaccumulator, but tolerant to cadmium stress. *Plant Growth Reg.* 50, 239–247. doi: 10.1007/s10725-006-9141-3

Krantev, A., Yordanova, R., Janda, T., Szalai, G., and Popova, L. (2008). Treatment with salicylic acid decreases the effect of cadmium on photosynthesis in maize plants. *J. Plant Physiol.* 165 (9), 920–931. doi: 10.1016/j.jplph.2006.11.014

Kubier, A., Wilkin, R. T., and Pichler, T. (2019). Cadmium in soils and groundwater: A review. *Appl.Geochem.* 108, 1–16. doi: 10.1016/j.apgeochem.2019.104388

Kumar, S., and Trivedi, P. K. (2018). Glutathione s-transferases: Role in combating abiotic stresses including arsenic detoxification in plants. *Front. Plant Sci.* 9, 751. doi: 10.3389/fpls.2018.00751

Li, D., He, G., Tian, W., Huang, Y., Meng, L., He, Y., et al. (2021a) *Genome-wide identification of metal tolerance genes in potato (Solanum tuberosum): response to two heavy metal stress.* Available at: https://www.researchsquare.com/article/rs-166067/latest.pdf.

Li, Z., Liu, Z., Chen, R., Li, X., Tai, P., Gong, Z., et al. (2015). DNA Damage and genetic methylation changes caused by cd in *Arabidopsis thaliana* seedlings. *Environ. Toxicol. Chem.* 34, 2095–2103. doi: 10.1002/etc.3033

Li, X., Mao, X., Xu, Y., Li, Y., Zhao, N., Yao, J., et al. (2021b). Comparative transcriptomic analysis reveals the coordinated mechanisms of *Populus* × *canadensis* "Neva" leaves in response to cadmium stress. *Ecotoxicol. Environ. Saf.* 216, 112179. doi: 10.1016/j.ecoenv.2021.112179

Li, F.-T., Qi, J.-M., Zhang, G.-Y., Lin, L.-H., Fang, P.-P., Tao, A.-F., et al. (2013). Effect of cadmium stress on the growth, antioxidative enzymes and lipid peroxidation in two kenaf (*Hibiscus cannabinus* L.) plant seedlings. *J. Integr. Agric.* 12 (4), 610–620. doi: 10.1016/S2095-3119(13)60279-8

Li, X., Zhao, M., Guo, L., and Huang, L. (2012). Effect of cadmium on photosynthetic pigments, lipid peroxidation, antioxidants, and artemisinin in hydroponically grown *Artemisia annua*. *J. Environ. Sci.* 24, 1511–1518. doi: 10.1016/S1001-0742(11)60920-0

Logani, M. K., and Davies, R. E. (1980). Lipid oxidation: biologic effects and antioxidants–a review. *Lipids* 15, 485–495. doi: 10.1007/BF02534079

Lu, Q., Chen, S., Li, Y., Zheng, F., He, B., and Gu, M. (2020). Exogenous abscisic acid (ABA) promotes cadmium (Cd) accumulation in *Sedum alfredii* hance by regulating the expression of Cd stress response genes. *Environ. Sci. pollut. Res. Int.* 27, 8719–8731. doi: 10.1007/s11356-019-07512-w

Luo, J.-S., Gu, T., Yang, Y., and Zhang, Z. (2019). A non-secreted plant defensin AtPDF2.6 conferred cadmium tolerance *via* its chelation in *Arabidopsis*. *Plant Mol. Biol.* 100, 561–569. doi: 10.1007/s11103-019-00878-y

Luo, H., Li, H., Zhang, X., and Fu, J. (2011). Antioxidant responses and gene expression in perennial ryegrass (*Lolium perenne* L.) under cadmium stress. *Ecotoxicology* 20, 770–778. doi: 10.1007/s10646-011-0628-y

Lux, A., Martinka, M., Vaculík, M., and White, P. J. (2011b). Root responses to cadmium in the rhizosphere: a review. *J. Exp. Bot.* 62 (1), 21–37. doi: 10.1093/jxb/erq281

Lux, A., Vaculík, M., Martinka, M., Lisková, D., Kulkarni, M. G., Stirk, W. A., et al. (2011a). Cadmium induces hypodermal periderm formation in the roots of the monocotyledonous medicinal plant *Merwilla plumbea*. *Ann. Bot.* 107 (2), 285–292. doi: 10.1093/aob/mcq240

Mahmud, J. A., Hasanuzzaman, M., Nahar, K., Bhuyan, M. H. M. B., and Fujita, M. (2018). Insights into citric acid-induced cadmium tolerance and phytoremediation in *Brassica juncea* l.: Coordinated functions of metal chelation, antioxidant defense and glyoxalase systems. *Ecotoxicol. Environ. Saf.* 147, 990–1001. doi: 10.1016/j.ecoenv.2017.09.045

Ma, X., Su, Z., and Ma, H. (2020). Molecular genetic analyses of abiotic stress responses during plant reproductive development. *J. Exp. Bot.* 71 (10), 2870–2885. doi: 10.1093/jxb/eraa089

Mehes-Smith, M., Nkongolo, K., and Cholewa, E. (2013). "Coping mechanisms of plants to metal contaminated soil," in *Environmental change and sustainability*. Eds. S. Silvern and S. Young (London, UK: IntechOpen).

Mengdi, X., Haibo, D., Jiaxin, L., Zhe, X., Yi, C., Xuan, L., et al. (2020). Metabolomics reveals the "Invisible" detoxification mechanisms of *Amaranthus hypochondriacus* at three ages upon exposure to different levels of cadmium. *Ecotoxicol. Environ. Saf.* 195, 110520. doi: 10.1016/j.ecoenv.2020.110520

Miglani, G. S. (2017). Genome editing in crop improvement: Present scenario and future prospects. *J. Crop Improv.* 31, 453–559. doi: 10.1080/15427528.2017.1333192

Mirosławski, J., and Paukszto, A. (2018). Determination of the cadmium, chromium, nickel, and lead ions relays in selected polish medicinal plants and their infusion. *Biol. Trace Elem. Res.* 182, 147–151. doi: 10.1007/s12011-017-1072-5

Mishra, B., Sangwan, R. S., Mishra, S., Jadaun, J. S., Sabir, F., and Sangwan, N. S. (2014). Effect of cadmium stress on inductive enzymatic and nonenzymatic responses of ROS and sugar metabolism in multiple shoot cultures of ashwagandha (*Withania somnifera* dunal). *Protoplasma* 251, 1031–1045. doi: 10.1007/s00709-014-0613-4

Mishra, S., Srivastava, S., Tripathi, R. D., Govindarajan, R., Kuriakose, S. V., and Prasad, M. N. V. (2006). Phytochelatin synthesis and response of antioxidants during cadmium stress in *Bacopa monnieri* L. *Plant Physiol. Biochem.* 44, 25–37. doi: 10.1016/j.plaphy.2006.01.007

Mobin, M., and Khan, N. A. (2007). Photosynthetic activity, pigment composition and antioxidative response of two mustard (*Brassica juncea*) cultivars differing in photosynthetic capacity subjected to cadmium stress. *J. Plant Physiol.* 164, 601–610. doi: 10.1016/j.jplph.2006.03.003

Narender, S. J. (2005) *Heavy metals pollution of soil and plants due to sewage irrigation effect of heavy metals and sewage on seed germination and plant growth. (Doctoral dissertation)*. (Rohtak: Maharshi Dayanand University). Available at: https://shodhganga.inflibnet.ac.in/handle/10603/113472.

Nasim, S. A., and Dhir, B. (2010). Heavy metals alter the potency of medicinal plants. *Rev. Environ. Contam. Toxicol.* 203, 139–149. doi: 10.1007/978-1-4419-1352-4_5

Navarro-León, E., Oviedo-Silva, J., Ruiz, J. M., and Blasco, B. (2019). Possible role of HMA4a TILLING mutants of *Brassica rapa* in cadmium phytoremediation programs. *Ecotoxicol. Environ. Saf.* 180, 88–94. doi: 10.1016/j.ecoenv.2019.04.081

Niekerk, L.-A., Carelse, M. F., Bakare, O. O., Mavumengwana, V., Keyster, M., and Gokul, A. (2021). The relationship between cadmium toxicity and the modulation of epigenetic traits in plants. *Int. J. Mol. Sci.* 22, 7046. doi: 10.3390/ijms22137046

Nourbakhsh Rezaei, S. R., Shabani, L., Rostami, M., and Abdoli, M. (2019). The effect of different concentrations of cadmium chloride on oxidative stress in shoot cultures of lemon balm. *J. Plant Prod.* 42, 509–522. doi: 10.22055/ppd.2019.24806.1567

Okem, A., Southway, C., Stirk, W. A., Street, R. A., Finnie, J. F., and Van Staden, J. (2015). Effect of cadmium and aluminum on growth, metabolite content and biological activity in *Drimia elata* (Jacq.) hyacinthaceae. *S. Afr. J. Bot.* 98, 142–147. doi: 10.1016/j.sajb.2015.02.013

Oladeji, O. (2016). The characteristics and roles of medicinal plants: Some important medicinal plants in Nigeria. *Nat. Prod. Ind. J.* 12, 102.

Paape, T., Heiniger, B., Santo Domingo, M., Clear, M. R., Lucas, M. M., and Pueyo, J. J. (2021). Genome-wide association study reveals complex genetic architecture of cadmium and mercury accumulation and tolerance traits in *Medicago truncatula*. *Front. Plant Sci.* 12, 806949. doi: 10.3389/fpls.2021.806949

Page, V., and Feller, U. (2015). Heavy metals in crop plants: Transport and redistribution processes on the whole plant level. *Agronomy* 5, 447–463. doi: 10.3390/agronomy5030447

Pandey, S., Gupta, K., and Mukherjee, A. K. (2007). Impact of cadmium and lead on *Catharanthus roseus*–a phytoremediation study. *J. Environ. Biol.* 28, 655–662.

Pandita, D. (2021). "CRISPR/Cas-mediated genome editing for improved stress tolerance in plants," in *Frontiers in plant-soil interaction*. Eds. T. Aftab and K. R. Hakeem (London, UK: Academic Press), 259–291.

Parmar, P., Kumari, N., and Sharma, V. (2013). Structural and functional alterations in photosynthetic apparatus of plants under cadmium stress. *Bot. Stud.* 54, 45. doi: 10.1186/1999-3110-54-45

Patel, A. H. (2006a) *Heavy metal impact assessment study on growth and metabolism of medicinal plants. (Doctoral dissertation)* (Ahmedabad: Gujarat University). Available at: https://shodhganga.inflibnet.ac.in/handle/10603/46164.

Patel, J. G. (2006b) *Study on relative toxicity of heavy metals to medicinal plants. (Doctoral dissertation)*. (Ahmedabad: Gujarat University). Available at: https://shodhganga.inflibnet.ac.in/handle/10603/45719.

Patel, K. P., and Patel, K. M. (2012). Cadmium-induced changes in antioxidative enzyme activities and content of leaf pigments in *Cajanus cajan* (L.). *Nat. Environ. pollut. Technol.* 11, 47–50.

Patnaik, A., and Mohanty, B. K. (2013). Toxic effect of mercury and cadmium on germination and seedling growth of *Cajanus cajan* l. (pigeon pea). *Ann. Biol. Res.* 4, 123–126.

Pena, L. B., Pasquini, L. A., Tomaro, M. L., and Gallego, S. M. (2006). Proteolytic system in sunflower (*Helianthus annuus* L.) leaves under cadmium stress. *Plant Sci.* 171, 531–537. doi: 10.1016/j.plantsci.2006.06.003

Pereira, M. P., Rodrigues, L. C., de, A., Corrêa, F. F., de Castro, E. M., Ribeiro, V. E., et al. (2016). Cadmium tolerance in *Schinus molle* trees is modulated by enhanced leaf anatomy and photosynthesis. *Trees* 30, 807–814. doi: 10.1007/s00468-015-1322-0

Pongrac, P., Serra, T. S., Castillo-Michel , H., Vogel-Mikuš , K., Arčon , I., Kelemen , M., et al (2018). Cadmium associates with oxalate in calcium oxalate crystals and competes with calcium for translocation to stems in the cadmium bioindicator *Gomphrena claussenii*. *Metallomics* 10, 1576–1584.

Rai, V., Khatoon, S., Bisht, S. S., and Mehrotra, S. (2005). Effect of cadmium on growth, ultramorphology of leaf and secondary metabolites of *Phyllanthus amarus*

schum. and thonn. *Chemosphere* 61, 1644–1650. doi: 10.1016/j.chemosphere.2005.04.052

Rai, K. K., Pandey, N., Meena, R. P., and Rai, S. P. (2021). Biotechnological strategies for enhancing heavy metal tolerance in neglected and underutilized legume crops: A comprehensive review. *Ecotoxicol. Environ. Saf.* 208, 111750. doi: 10.1016/j.ecoenv.2020.111750

Rani, S., Singh, V., Sharma, M. K., and Sisodia, R. (2021). GC–MS based metabolite profiling of medicinal plant-*Catharanthus roseus* under cadmium stress. *Plant Physiol. Rep.* 26, 491–502. doi: 10.1007/s40502-021-00595-z

Raza, A., Habib, M., Kakavand, S. N., Zahid, Z., Zahra, N., Sharif, R., et al. (2020). Phytoremediation of cadmium: Physiological, biochemical, and molecular mechanisms. *Biology* 9, 177. doi: 10.3390/biology9070177

Rodrigues, L. C. A., Martins, J. P. R., de Almeida Júnior, O., Guilherme, L. R. G., Pasqual, M., and de Castro, E. M. (2017). Tolerance and potential for bioaccumulation of *Alternanthera tenella* colla to cadmium under *in vitro* conditions. *Plant Cell Tiss. Org. Cult.* 130, 507–519. doi: 10.1007/s11240-017-1241-4

Rogowska, A., Pączkowski, C., and Szakiel, A. (2022). Modulation of steroid and triterpenoid metabolism in *Calendula officinalis* plants and hairy root cultures exposed to cadmium stress. *Int. J. Mol. Sci.* 23. doi: 10.3390/ijms23105640

Romero-Puertas, M. C., Palma, J. M., Gómez, M., Del Río, L. A., and Sandalio, L. M. (2002). Cadmium causes the oxidative modification of proteins in pea plants. *Plant Cell Environ.* 25, 677–686. doi: 10.1046/j.1365-3040.2002.00850.x

Saggar, S., Mir, P. A., Kumar, N., Chawla, A., Uppal, J., Shilpa, S., et al. (2022). Traditional and herbal medicines: Opportunities and challenges. *Pharmacognosy Res.* 14, 107–114. doi: 10.5530/pres.14.2.15

Salarizadeh, S., Kavousi, H. R., and Pourseyadi, S. (2016). Effect of cadmium on germination characters and biochemical parameters of two Iranian ecotypes of cumin (*Cuminum cyminum* L.). *J. Medicinal Plants By-Product* 5, 15–22. doi: 10.22092/JMPB.2016.108919

Sanità di Toppi, L., and Gabbrielli, R. (1999). Response to cadmium in higher plants. *Environ. Exp. Bot.* 41, 105–130. doi: 10.1016/S0098-8472(98)00058-6

Sarma, H., Islam, N. F., Prasad, R., Prasad, M. N. V., Ma, L. Q., and Rinklebe, J. (2021). Enhancing phytoremediation of hazardous metal(loid)s using genome engineering CRISPR-Cas9 technology. *J. Hazard. Mater.* 414, 125493. doi: 10.1016/j.jhazmat.2021.125493

Sarry, J.-E., Kuhn, L., Ducruix, C., Lafaye, A., Junot, C., Hugouvieux, V., et al. (2006). The early responses of *Arabidopsis thaliana* cells to cadmium exposure explored by protein and metabolite profiling analyses. *Proteomics* 6, 2180–2198. doi: 10.1002/pmic.200500543

Sasaki, A., Yamaji, N., Yokosho, K., and Ma, J. F. (2012). Nramp5 is a major transporter responsible for manganese and cadmium uptake in rice. *Plant Cell* 24, 2155–2167. doi: 10.1105/tpc.112.096925

Seneviratne, M., Rajakaruna, N., Rizwan, M., Madawala, H. M. S. P., Ok, Y. S., and Vithanage, M. (2019). Heavy metal-induced oxidative stress on seed germination and seedling development: a critical review. *Environ. Geochem. Health* 41, 1813–1831. doi: 10.1007/s10653-017-0005-8

Sethy, S. K., and Ghosh, S. (2013). Effect of heavy metals on germination of seeds. *J. Nat. Sci. Biol. Med.* 4, 272–275. doi: 10.4103/0976-9668.116964

Sharmila, P., Kumari, P. K., Singh, K., Prasad, N. V. S. R. K., and Pardha-Saradhi, P. (2017). Cadmium toxicity-induced proline accumulation is coupled to iron depletion. *Protoplasma* 254, 763–770. doi: 10.1007/s00709-016-0988-5

Shekari, L., Aroiee, H., Mirshekari, A., and Nemati, H. (2019). Protective role of selenium on cucumber (*Cucumis sativus* L.) exposed to cadmium and lead stress during reproductive stage role of selenium on heavy metals stress. *J. Plant Nutr.* 42, 529–542. doi: 10.1080/01904167.2018.1554075

Shi, G., Liu, C., Cui, M., Ma, Y., and Cai, Q. (2012). Cadmium tolerance and bioaccumulation of 18 hemp accession. *Appl. Biochem. Biotechnol.* 168, 163–173. doi: 10.1007/s12010-011-9382-0

Singh, S., Eapen, S., and D'Souza, S. F. (2006). Cadmium accumulation and its influence on lipid peroxidation and antioxidative system in an aquatic plant, *Bacopa monnieri* L. *Chemosphere* 62, 233–246. doi: 10.1016/j.chemosphere.2005.05.017

Singh, N., Mansoori, A., Dey, D., Kumar, R., and Kumar, A. (2021). "Potential of metabolomics in plant abiotic stress management," in *Omics technologies for sustainable agriculture and global food security*, vol. II . Eds. A. Kumar, R. Kumar, P. Shukla and H. K. Patel (Singapore: Springer Singapore), 193–214.

Singh, S., Parihar, P., Singh, R., Singh, V. P., and Prasad, S. M. (2015). Heavy metal tolerance in plants: Role of transcriptomics, proteomics, metabolomics, and ionomics. *Front. Plant Sci.* 6, 1143. doi: 10.3389/fpls.2015.01143

Singh, V., and Verma, K. (2018). Metals from cell to environment: Connecting Metallomics with other omics. *Open Journal of Plant Science* 3, 001–014. doi: 10.1080/15226514.2016.1207598

Song, Y., Jin, L., and Wang, X. (2017). Cadmium absorption and transportation pathways in plants. *Int. J. Phytoremediation* 19, 133–141. doi: 10.1080/15226514.2016.1207598

Songmei, L., Jie, J., Yang, L., Jun, M., Shouling, X., Yuanyuan, T., et al. (2019). Characterization and evaluation of OsLCT1 and OsNramp5 mutants generated through CRISPR/cas9-mediated mutagenesis for breeding low cd rice. *Rice Sci.* 26, 88–97. doi: 10.1016/j.rsci.2019.01.002

So, O., Oyewole, S. O., Akinyemi, O., and Jimoh, K. A. (2018). Medicinal plants and sustainable human health: a review. *Hortic. Int. J.* 2, 194–195. doi: 10.15406/hij.2018.02.00051

Souri, M. K., Hatamian, M., and Tesfamariam, T. (2019). Plant growth stage influences heavy metal accumulation in leafy vegetables of garden cress and sweet basil. *Chem. Biol. Technol. Agric.* 6, 1–7. doi: 10.1186/s40538-019-0170-3

Sridhar, B. B. M., Diehl, S. V., Han, F. X., Monts, D. L., and Su, Y. (2005). Anatomical changes due to uptake and accumulation of zn and cd in Indian mustard (*Brassica juncea*). *Environ. Exp. Bot.* 54, 131–141. doi: 10.1016/j.envexpbot.2004.06.011

Srivastava, V., Sarkar, A., Singh, S., Singh, P., de Araujo, A. S. F., and Singh, R. P. (2017). Agroecological responses of heavy metal pollution with special emphasis on soil health and plant performances. *Front. Environ. Sci.* 5. doi: 10.3389/fenvs.2017.00064

Srivastava, J., and Yadav, S. (2017). Cadmium phytoextraction and induced antioxidant gene response in *Moringa oleifera* lam. *Am. J. Plant Physiol.* 12, 58–70. doi: 10.3923/ajpp.2017.58.70

Sterckeman, T., and Thomine, S. (2020). Mechanisms of cadmium accumulation in plants. Crit. *Rev. Plant Sci.* 39, 322–359. doi: 10.1080/07352689.2020.1792179

Street, R. A. (2012). Heavy metals in medicinal plant products — an African perspective. *S. Afr. J. Bot.* 82, 67–74. doi: 10.1016/j.sajb.2012.07.013

Tang, L., Mao, B., Li, Y., Lv, Q., Zhang, L., Chen, C., et al. (2017). Knockout of OsNramp5 using the CRISPR/Cas9 system produces low cd-accumulating indica rice without compromising yield. *Sci. Rep.* 7, 14438. doi: 10.1038/s41598-017-14832-9

Tchounwou, P. B., Yedjou, C. G., Patlolla, A. K., and Sutton, D. J. (2012). Heavy metal toxicity and the environment. *Exp.* 101, 133–164. doi: 10.1007/978-3-7643-8340-4_6

Thakur, S., Choudhary, S., Majeed, A., Singh, A., and Bhardwaj, P. (2020). Insights into the molecular mechanism of arsenic phytoremediation. *J. Plant Growth Regul.* 39, 532–543. doi: 10.1007/s00344-019-10019-w

Thomine, S., Wang, R., Ward, J. M., Crawford, N. M., and Schroeder, J. I. (2000). Cadmium and iron transport by members of a plant metal transporter family in *Arabidopsis* with homology to nramp genes. *Proc. Natl. Acad. Sci. U.S.A* 97, 4991–4996. doi: 10.1073/pnas.97.9.4991

Thongchai, A., Meeinkuirt, W., Taeprayoon, P., and Chelong, I.-A. (2021). Effects of soil amendments on leaf anatomical characteristics of marigolds cultivated in cadmium-spiked soils. *Sci. Rep.* 11 (1), 15909. doi: 10.1038/s41598-021-95467-9

Trivedi, N. G. (2003) *A study on responses of adhatoda vasica l to heavy metal. (Doctoral dissertation)* (Ahmedabad: Gujarat University). Available at: https://shodhganga.inflibnet.ac.in/handle/10603/46182.

Venegas-Rioseco, J., Ginocchio, R., and Ortiz-Calderón, C. (2021). Increase in phytoextraction potential by genome editing and transformation: A review. *Plants* 11. doi: 10.3390/plants11010086

Verdoy, D., Coba de la Peña, T., Redondo, F. J., Lucas, M. M., and Pueyo, J. J. (2006). Transgenic *Medicago truncatula* plants that accumulate proline display nitrogen-fixing activity with enhanced tolerance to osmotic stress. *Plant Cell Environ.* 29, 1913–1923. doi: 10.1111/j.1365-3040.2006.01567.x

Wagner, G. J. (1993). Accumulation of cadmium in crop plants and its consequences to human health. *Adv. Agron.* 51, 173–212. doi: 10.1016/S0065-2113(08)60593-3

Wang, T., Li, Y., Fu, Y., Xie, H., Song, S., Qiu, M., et al. (2019). Mutation at different sites of metal transporter gene OsNramp5 affects Cd accumulation and related agronomic traits in rice (*Oryza sativa* L.). *Front. Plant Sci.* 10, 1081. doi: 10.3389/fpls.2019.01081

Wang, C., Qiao, F., Wang, M., Wang, Y., Xu, Y., and Qi, X. (2023). PvERF104 confers cadmium tolerance in Arabidopsis: Evidence for metal-responsive element-binding transcription factors. *Environ. Exp. Bot.* 206, 105167. doi: 10.1016/j.envexpbot.2022.105167

Weerakoon, S. R. (2019). "Genetic engineering for metal and metalloid detoxification," in *Transgenic plant technology for remediation of toxic metals and metalloids*. Ed. M. N. V. Prasad (London, UK: Academic Press), 23–41.

Wójcik, M., Vangronsveld, J., D'Haen, J., and Tukiendorf, A. (2005). Cadmium tolerance in *Thlaspi caerulescens*: II. localization of cadmium in *Thlaspi caerulescens*. *Environ. Exp. Bot.* 53, 163–171. doi: 10.1016/S0098-8472(04)00047-4

Xu, J., Yin, H., and Li, X. (2009). Protective effects of proline against cadmium toxicity in micropropagated hyperaccumulator, *Solanum nigrum* L. *Plant Cell Rep.* 28, 325–333. doi: 10.1007/s00299-008-0643-5

Yadav, S. K. (2010). Heavy metals toxicity in plants: An overview on the role of glutathione and phytochelatins in heavy metal stress tolerance of plants. *S. Afr. J. Bot.* 76, 167–179. doi: 10.1016/j.sajb.2009.10.007

Yang, J.-L., Liu, L.-W., Gong, Y.-Q., Huang, D.-Q., Wang, F., and He, L.-L. (2007). Analysis of genomic DNA methylation level in radish under cadmium stress by methylation-sensitive amplified polymorphism technique. *Zhi Wu Sheng Li Yu Fen Zi Sheng Wu Xue Xue Bao* 33, 219–226.

Yang, L., Yao, J., Sun, J., Shi, L., Chen, Y., and Sun, J. (2020). The Ca2+ signaling, glu, and GABA responds to cd stress in duckweed. *Aquat. Toxicol.* 218, 105352. doi: 10.1016/j.aquatox.2019.105352

Ye, Z. H., Baker, A. J. M., Wong, M. H., and Willis, A. J. (1997). Zinc, lead and cadmium tolerance, uptake and accumulation by *Typha latifolia*. *New Phytol.* 136 (3), 469–480. doi: 10.1046/j.1469-8137.1997.00759.x

Ye, P., Wang, M., Zhang, T., Liu, X., Jiang, H., Sun, Y., et al. (2020). Enhanced cadmium accumulation and tolerance in transgenic hairy roots of *Solanum nigrum* L. expressing iron-regulated transporter gene IRT1. *Life* 10. doi: 10.3390/life10120324

Youssef, N. A. (2021). Changes in the morphological traits and the essential oil content of sweet basil (*Ocimum basilicum* L.) as induced by cadmium and lead treatments. *Int. J. Phytoremediation* 23 (3), 291–299. doi: 10.1080/15226514.2020.1812508

Yuan, J., Bai, Y., Chao, Y., Sun, X., He, C., Liang, X., et al. (2018). Genome-wide analysis reveals four key transcription factors associated with cadmium stress in creeping bentgrass (*Agrostis stolonifera* L.). *Peer J.* 6, e5191. doi: 10.7717/peerj.5191

Yuan, J., Fu, H., and Wang, X. (2021). Coupled metabolome with physiology unveiled mechanisms for cadmium affecting active ingredients synthesis in *Salvia miltiorrhiza*, a non-Cd-hyperaccumulator. *Res. Square* 1, 1-22. doi: 10.21203/rs.3.rs-886213/v1

Yu, X., Liang, L., Xie, Y., Tang, Y., Tan, H., Zhang, J., et al. (2022). Comparative analysis of Italian lettuce (*Lactuca sativa* L. var. ramose) transcriptome profiles reveals the molecular mechanism on exogenous melatonin preventing cadmium toxicity. *Genes* 13. doi: 10.3390/genes13060955

Yu, G., Ma, J., Jiang, P., Li, J., Gao, J., Qiao, S., et al. (2019). "The mechanism of plant resistance to heavy metal," in *IOP Conference Series: Earth and Environmental Science* IOP science, Vol. 310. 052004. doi: 10.1088/1755-1315/310/5/052004

Yu, R., Tang, Y., Liu, C., Du, X., Miao, C., and Shi, G. (2017). Comparative transcriptomic analysis reveals the roles of ROS scavenging genes in response to cadmium in two pak choi cultivars. *Sci. Rep.* 7, 9217. doi: 10.1038/s41598-017-09838-2

Zaheer, I. E., Ali, S., Rizwan, M., Farid, M., Shakoor, M. B., Gill, R. A., et al. (2015). Citric acid assisted phytoremediation of copper by *Brassica napus* L. *Ecotoxicol. Environ. Saf.* 120, 310–317. doi: 10.1016/j.ecoenv.2015.06.020

Zahra, W., Rai, S. N., Birla, H., Singh, S. S., Rathore, A. S., Dilnashin, H., et al. (2020). "Economic importance of medicinal plants in Asian countries," in *Bioeconomy for sustainable development*. Ed. C. Keswani (Singapore: Springer), 359–377.

Zaid, A., Mohammad, F., and Fariduddin, Q. (2020). Plant growth regulators improve growth, photosynthesis, mineral nutrient and antioxidant system under cadmium stress in menthol mint (*Mentha arvensis* L.). *Physiol. Mol. Biol. Plants* 26 (1), 25–39. doi: 10.1007/s12298-019-00715-y

Zayneb, C., Bassem, K., Zeineb, K., Grubb, C. D., Noureddine, D., Hafedh, M., et al. (2015). Physiological responses of fenugreek seedlings and plants treated with cadmium. *Environ. Sci. pollut. Res. Int.* 22 (14), 10679–10689. doi: 10.1007/s11356-015-4270-8

Zhang, P., Wang, R., Ju, Q., Li, W., Tran, L.-S. P., and Xu, J. (2019). The R2R3-MYB transcription factor MYB49 regulates cadmium accumulation. *Plant Physiol.* 180, 529–542. doi: 10.1104/pp.18.01380

Zhang, F.-Q., Wang, Y.-S., Lou, Z.-P., and Dong, J.-D. (2007). Effect of heavy metal stress on antioxidative enzymes and lipid peroxidation in leaves and roots of two mangrove plant seedlings (*Kandelia candel* and *Bruguiera gymnorrhiza*). *Chemosphere* 67 (1), 44–50. doi: 10.1016/j.chemosphere.2006.10.007

Zhang, Y., Xu, S., Yang, S., and Chen, Y. (2015). Salicylic acid alleviates cadmium-induced inhibition of growth and photosynthesis through upregulating antioxidant defense system in two melon cultivars (*Cucumis melo* L.). *Protoplasma* 252 (3), 911–924. doi: 10.1007/s00709-014-0732-y

Zhao, S., and Duo, L. (2015). Bioaccumulation of cadmium, copper, zinc, and nickel by weed species from municipal solid waste compost. *Pol. J. Environ. Stud.* 24, 413–417. doi: 10.15244/pjoes/28960

Zhao, Q., Wang, H., Du, Y., Rogers, H. J., Wu, Z., Jia, S., et al. (2020). MSH2 and MSH6 in mismatch repair system account for soybean (*Glycine max* (L.) merr.) tolerance to cadmium toxicity by determining DNA damage response. *J. Agric. Food Chem.* 68, 1974–1985. doi: 10.1021/acs.jafc.9b06599

Zhou, X.-M., Zhao, P., Wang, W., Zou, J., Cheng, T.-H., Peng, X.-B., et al. (2015). A comprehensive, genome-wide analysis of autophagy-related genes identified in tobacco suggests a central role of autophagy in plant response to various environmental cues. *DNA Res.: Int. J. Rapid Publ. Rep. Genes Genomes* 22 (4), 245–257. doi: 10.1093/dnares/dsv012

Zou, C., Lu, T., Wang, R., Xu, P., Jing, Y., Wang, R., et al. (2022). Comparative physiological and metabolomic analyses reveal that Fe_3O_4 and ZnO nanoparticles alleviate cd toxicity in tobacco. *J. Nanobiotechnology* 20, 302. doi: 10.1186/s12951-022-01509-3

Glossary

ABA	Abscisic acid
ATCC15834	*Agrobacterium rhizogenes* ATCC 15834
AtHMA2	*Arabidopsis thaliana* heavy metal transporting ATPase transporter protein 2
AtHMA3	*Arabidopsis thaliana* heavy metal transporting ATPase transporter protein 3
AtHMA4	*Arabidopsis thaliana* heavy metal transporting ATPase transporter protein 4
AtIRT1	*Arabidopsis thaliana* iron-regulated transporter-like proteins 1
BAS	β amyrin synthase
bZIP	Basic leucine zipper family of transcription factors
BjCdR15	*Brassica juncea* Cd resistant gene 1
CaWRKY41	Capsicum WRKY transcription factor family gene 1
Cd	Cadmium
Chl	Chlorophyll
CRISPR- Cas 9	Clustered regularly interspaced short palindromic repeats/ CRISPR associated protein 9
crRNA	CRISPR RNA
CAS	cycloartenol synthase
DEGs	Differentially expressed genes
MMR	DNA mismatch repair
ERF 1 and ERF 2	ethylene response factors 1 & 2
GWAS	Genome-wide association studies
GGPP	Geranylgeranyl diphosphate
GMCAs	glucopyranosyl oxy-4-methoxy cinnamic acids
GSH	Glutathione
GmCDT1-2	*Glycine max* Cd tolerance 1-2
GmWRKY142	*Glycine max* WRKY transcription factor family gene 142
Gly, Ser, and Thr	Glycine, serine and threonine
gRNA	Guide RNA
HMA	heavy metal transporting ATPase transporter protein
HR-ICP-SFMS	High-resolution inductively coupled plasma sector field mass spectrometry
ICP-MS	Inductively coupled plasma mass spectrometry
MDA	Malondialdehyde
MtZIP6	*Medicago truncatula* zinc-regulated transporters 6
MTPs	metal tolerance or transporter proteins
MT1, MT2 and MT3	Metallothionine 1, 2 and 3
miRNA	Micro RNA
Micro XRF	Micro X-ray fluorescence
MAPK	Mitogen-activated protein kinase
MRE	Metal responsive elements
MYB	Myeloblastosis related gene family of transcription factors
NAC, ATAF1/2	(NAM and CUC2) family of proteins
NcZNT1	*Noccaea caerulescens* zink transporter gene 1
NRAMP	Natural resistance-associated macrophage protein
OsHMA2	*Oryza sativa* heavy metal transporting ATPase transporter protein 2
OsHMA3	*Oryza sativa* heavy metal transporting ATPase transporter protein 3
OsIRT1	OsIRT2
Oryza sativa iron-regulated transporter-like proteins 1	*Oryza sativa* iron-regulated transporter-like proteins 2
OsNRAMP1, OsNRAMP5	*Oryza sativa* natural resistance-associated macrophage protein 1 and 5
OsZIP6	*Oryza sativa* zinc-regulated transporters 6
PC	Phytochelatin
Pro and Arg	Proline and Arginine
P5CS	pyrroline-5-carboxylate synthetase
QTL	quantitative loci
RAPD	Random Amplified Polymorphic DNA
GSH/GSSG	reduced glutathione-oxidized glutathione ratio
RT-PCR	Reverse transcription polymerase chain reaction
RUBISCO	Ribulose bisphosphate carboxylase/oxygenase
RA	Rosmarinic acid
DSB	double strand break
SMs	Secondary metabolites
SNP	Single nucleotide polymorphism
siRNA	Small interfering RNA
SQS	Squalene synthase

Continued

SOD1, POD	Super oxide dismutase, peroxidase
TILLING	targeted induced local lesions in genomes
TGA3	TGACG-binding (TGA) transcription factors 3
tracrRNA	transactivating crRNA
TALENs	Transcript activators like effector nucleases
TF	Transcriptional factors
WHO	World Health Organization
WRKY	WRKY transcription factor gene family
XAS	X-ray absorption spectroscopy
ZFNs	Zinc finger nucleases
ZIP	zinc-regulated transporters
ZRT-IRT-like proteins	Zink/iron-regulated transporter-like proteins

frontiers | Frontiers in Plant Science

TYPE Original Research
PUBLISHED 02 February 2023
DOI 10.3389/fpls.2023.1096225

OPEN ACCESS

EDITED BY
Padma Nimmakayala,
West Virginia State University, United States

REVIEWED BY
Pedro M. Barros,
Universidade Nova de Lisboa, Portugal
Bharat Mishra,
University of Alabama at Birmingham, United States

*CORRESPONDENCE
Carlos M. Rodríguez López
cmro267@uky.edu

SPECIALTY SECTION
This article was submitted to Plant Abiotic Stress, a section of the journal Frontiers in Plant Science

RECEIVED 11 November 2022
ACCEPTED 18 January 2023
PUBLISHED 02 February 2023

CITATION
Tan JW, Shinde H, Tesfamicael K, Hu Y, Fruzangohar M, Tricker P, Baumann U, Edwards EJ and Rodríguez López CM (2023) Global transcriptome and gene co-expression network analyses reveal regulatory and non-additive effects of drought and heat stress in grapevine. *Front. Plant Sci.* 14:1096225. doi: 10.3389/fpls.2023.1096225

Global transcriptome and gene co-expression network analyses reveal regulatory and non-additive effects of drought and heat stress in grapevine

Jia W. Tan[1], Harshraj Shinde[1], Kiflu Tesfamicael[1,2], Yikang Hu[2], Mario Fruzangohar[3], Penny Tricker[4,5], Ute Baumann[4], Everard J. Edwards[6] and Carlos M. Rodríguez López[1]*

[1]Environmental Epigenetics and Genetics Group, Department of Horticulture, College of Agriculture, Food and Environment, University of Kentucky, Lexington, KY, United States, [2]School of Biological Science, The University of Adelaide, Adelaide, SA, Australia, [3]The Biometry Hub, School of Agriculture, Food and Wine & Waite Research Institute, University of Adelaide, Glen Osmond, SA, Australia, [4]School of Agriculture, Food and Wine, The University of Adelaide, Hartley Grove, SA, Australia, [5]The New Zealand Institute for Plant and Food Research Limited, Plant & Food Research Canterbury Agriculture & Science Centre, Lincoln, New Zealand, [6]The Commonwealth Scientific and Industrial Research Organisation (CSIRO) Agriculture & Food, Glen Osmond, SA, Australia

Despite frequent co-occurrence of drought and heat stress, the molecular mechanisms governing plant responses to these stresses in combination have not often been studied. This is particularly evident in non-model, perennial plants. We conducted large scale physiological and transcriptome analyses to identify genes and pathways associated with grapevine response to drought and/or heat stress during stress progression and recovery. We identified gene clusters with expression correlated to leaf temperature and water stress and five hub genes for the combined stress co-expression network. Several differentially expressed genes were common to the individual and combined stresses, but the majority were unique to the individual or combined stress treatments. These included heat-shock proteins, mitogen-activated kinases, sugar metabolizing enzymes, and transcription factors, while phenylpropanoid biosynthesis and histone modifying genes were unique to the combined stress treatment. Following physiological recovery, differentially expressed genes were found only in plants under heat stress, both alone and combined with drought. Taken collectively, our results suggest that the effect of the combined stress on physiology and gene expression is more severe than that of individual stresses, but not simply additive, and that epigenetic chromatin modifications may play an important role in grapevine responses to combined drought and heat stress.

KEYWORDS

Vitis vinifera, transcriptome, heat, drought, stress, co-expression network, pathways

1 Introduction

Abiotic stress is a major limiting factor for plant growth and crop production in many regions of the world. Common abiotic factors unfavorable for plant growth and crop yields include drought, saline soils, heat, and cold. Worldwide, extensive agricultural losses result from heat stress, often in combination with drought (Vogel et al., 2019). It is expected that the effects of combined drought and heat stress will become more severe as the climate continues to warm (Zhao et al., 2017; Raza et al., 2019), as it is predicted that an increase in global temperature of 1.5°C will cause more extremely hot days on land, and an increase in the intensity and frequency of drought and precipitation deficits (IPCC, 2018).

Viticulture is highly dependent on climatic conditions during the growing season. Climate determines the ability to successfully grow a particular variety and can greatly affect the value of the fruit produced (Gladstones, 1992; Jones and Davis, 2000; Jones, 2006; Bai et al., 2022). Grape production for winemaking is particularly vulnerable to environmental stress as the environmental conditions occurring during one growing season contribute to the quality of the next vintage (Mullins et al., 1992; Edwards and Clingeleffer, 2013; Martínez-Lüscher and Kurtural, 2021). Viticulture is commonly practiced in regions with a Mediterranean climate, where the growing season is characterized by low rainfall, the majority occurring in winter, and by high air temperature and evaporative demand, temperatures above 40°C are not uncommon. It has been proposed that an increase in ambient temperatures will constitute the primary cause of water shortages for viticulture due to increased evaporative demand (Schultz, 2010), and may eliminate production in many areas (White et al., 2006; Diffenbaugh et al., 2011). It is important to consider the effect of combined stress on grapevines since plants growing in vineyards will be affected by both these interacting factors (Mittler, 2006).

Long-lived perennials, including grapevine, have acquired a myriad of adaptions to cope with stress conditions such as heat and drought (Estravis-Barcala et al., 2020). The importance of identifying protection mechanisms of grapevine against abiotic stresses has motivated research both in the field and in controlled environments (reviewed in Carvalho and Amâncio, 2019). Physiological changes including limiting stomatal opening and a reduction in vegetative growth are common responses to drought, protecting the plant from extensive water loss (Chaves et al., 2002). Similarly, altered leaf structure and increased leaf rolling are also observed in grapevines under stress in relation to water use and status (Patakas et al., 2005; Kulkarni et al., 2007;). In contrast, for example, under heat stress, leaf transpiration may increase because of high stomatal conductance, maintaining a cooler canopy temperature (Moore et al., 2021). The dissection of physiological traits to understand which might be synergistic or antagonistic during combined drought and heat stress may lead to the identification of more tolerant varieties. Common protective mechanisms against damage from various abiotic stresses include increases in concentrations of scavengers of free radicals and hormones involved in systemic stress signaling (Raja et al., 2017; Sachdev et al., 2021). RNA-sequencing analysis has revealed important gene regulation patterns and potential stress tolerance genes under drought (Salman-Haider et al., 2017) and heat (Carvalho et al., 2015).

Plant responses to a combination of stresses can be hard to differentiate from the response to each of the individual stresses (Mittler, 2006) and the timing and persistence of stress and recovery also influence physiology and metabolism in a genotype by environment-dependent manner (Carvalho et al., 2015). Here we focused on the differential responses of *V. vinifera* L. cv. Cabernet Sauvignon (a relatively tolerant genotype) to drought, heat, and combined drought and heat stress to identify key gene co-expression networks and clusters associated with physiological changes, and the differentially expressed genes between different stress treatments to gain insight into the differences between grapevine responses to individual or combined stresses.

2 Materials and methods

2.1 Plant material and experimental design

120 callused dormant cuttings propagated from 6 donor grapevine (*V. vinifera* L. cv. Cabernet Sauvignon) plants were planted in UC potting mix and maintained in a plant propagator under high humidity until root establishment. Each cutting was individually labelled using a unique ID number, to allow the linkage of physiological and gene expression data to conduct downstream analyses. Plants were then transferred to 24 cm pots and randomly allocated into four different groups, each designated to a future treatment (i.e., Control (T0), drought (T1), heat (T2), and combined drought and heat (T3)). These were then randomly allocated into five blocks, such that there were six vines of each treatment per block. The plant positions within a block were also randomized and each block was placed on a separate bench in a glasshouse (CSIRO, Waite Campus, Adelaide, South Australia, Australia) maintained at an air temperature of 27°C Day/20°C Night, until stress treatments were applied. Humidity and light were uncontrolled. Air temperature and humidity were continuously recorded using a TinyTag Plus 2 logger in a small Stephenson shield (Hastings Data Loggers, Port Macquarie, NSW, Australia).

The experimental method was adapted from Edwards et al. (2011) and incorporated drought and high temperature stresses in a factorial design. Utilizing this design had the advantages of providing greater statistical power to the main effects (drought stress, heat stress), whilst allowing a potential interaction between these two stresses to be specifically addressed. Capacity limits referred to only two levels (presence/absence) of each stress could be used. Heat stress was generated by allowing natural insolation to heat the glasshouse (i.e., cooling was not initiated until a higher set temperature was reached than the control). Drought stress was generated by reducing the volume of daily irrigation applied. Once the vines were established, irrigation was removed from the selected plants (T1 and T3) until they were under moderate to severe drought stress. Vine response was monitored by measuring stomatal conductance to water vapor (g_s) using a Delta-T AP4 Porometer (MEA, Magill, SA, Australia). Vines were deemed to be under drought stress when g_s was measured between 75 and 100 mmol/m^2/s. Once plants reached this stage, each pot was weighed and subsequently hand-watered to this weight daily for the duration of the treatment. Once

the drought condition had been maintained for ten days, heat stress was applied to selected plants (T2 and T3) for 48 hours, by setting the thermostatically controlled evaporative air-conditioning system in the greenhouse to 45°C and allowing insolation to heat the chamber. Night-time temperatures were maintained at a minimum of 30°C using a gas heating system. Plants that were not selected for heat stress treatment (i.e., T0 and T1) were moved to an adjacent glasshouse with the same layout but with temperatures maintained at 27/20°C as previously. T0 and T1 plants were transferred back to the initial glasshouse after heat treatment, watering was reinitiated for drought-treated plants and temperature reduced to control conditions for heat-treated plants on the midnight of the 12th day of reduced irrigation. Plants exposed to one of the stress treatments were considered physiologically recovered when their g_s showed no significant difference from that of the control plants (See Supplemental Figure S1 for a schematic representation of the experimental design).

2.2 Physiological measurements

A standardized set of measurements was established and undertaken before drought treatment initiation (ST1), immediately before heat stress initiation (ST2), during heat stress (ST3 and ST4), immediately following initiation of normal irrigation and the removal of heat stress (ST5) and after physiological recovery (ST6) (Supplemental Table S1). These measurements were combined with tissue sampling (see below). To avoid any impact of tissue sampling or leaf removal for stem water potential measurements on subsequent measurements, each plant was only sampled once (i.e., $n_{sampling\ time}$= 20; 5 plants x 4 treatments). At sampling times ST1 and ST2, only plants from the control treatment, and the control and drought treatments, respectively, were sampled for stem water potential and molecular analyses.

Stomatal conductance to water vapor (g_s): First fully expanded leaves were used for measuring g_s using an AP4 Leaf Porometer (as above). Measurements were made at approximately 11 AM to avoid any potential impact of midday depression of g_s, except for ST3 and ST4, which were measured at approximately 4 PM to assess the maximum stress.

Stem water potential (stemΨ): Grapevine water status during the experiment was determined by measuring the stemΨ of the second fully expanded leaf. A Scholander-type pressure chamber (model 3000, Soil Moisture Equipment Corp, Goleta, CA, USA) was employed to measure the second fully expanded leaf of plants selected at each sampling time (Supplemental Figure S1). Leaves were bagged with silvered plastic zip lock bags for a minimum of 20 minutes to ensure equilibration between leaf and stem.

Leaf temperature (LT): The effect of the applied stresses on leaf temperature was studied by measuring the surface LT of the third leaf counting from the plant main stem apex (non-fully expanded leaves), and the first fully expanded leaf of selected plants at each sampling time (Supplemental Figure S1) using a non-contact infrared thermometer (Fluke, USA).

The statistical significance of treatment effects on vine physiology was assessed using univariate ANOVAs fitted with a GLM (IBM SPSS Statistics version 27, New York, USA). The dataset was split into four time periods, pre-treatment, drought-only, combined stress period and recovery. If a time period included more than one measurement date, repeated measures ANOVA was used, with time as the within-subjects effect. For the combined stress and recovery periods a factorial model was used. For the pre-treatment and drought-only periods, a single factor (drought) ANOVA was used. Significance was assumed when an effect probability was below 0.05.

2.3 RNA extraction, library preparation, and sequencing

Sample collection: The second and third leaves counting from the plant's main stem apex were collected for nucleic acid extraction at each sampling time (Supplemental Table S1). Leaves were frozen immediately after collection using liquid nitrogen and stored at -80°C.

RNA was extracted from 100 mg of frozen and ground powder from the collected leaves using the Spectrum™ Plant Total RNA Kit (Sigma, St. Louis, Missouri, USA) according to the manufacturer's Protocol A. RNA quality and quantity were determined by spectrophotometric analysis (NanoDrop™ 1000, Thermo Fisher Scientific, Wilmington, DE, USA) and Experion™ RNA StdSens Chips (BIO-RAD, USA). Extractions presenting 260/280 and 260/230 absorbance ratios between 1.8-2.2 and an RNA quality indicator (RQI) above 7 were used in library preparations (i.e., 94/95 RNA extraction).

4 µg of total RNA per sample was used for ribosomal RNA depletion using Dynabeads mRNA Purification Kit (Thermo Fisher Scientific, USA) following the manufacturer's instructions. 5 µl of ribosomal depleted RNA was used to prepare 94 individually barcoded RNA-seq libraries using the NEBNext® Ultra™ RNA Library Prep Kit for Illumina (New England Biolabs, USA) following the manufacturer's instructions. The Illumina NextSeq 500 HighOutPut platform was used to produce 75 bp single end runs at the Australian Genome Research Facility (AGRF) in Adelaide, Australia. RNA-seq libraries not yielding >18,000,000 reads were re-sequenced, and results merged.

2.4 Bioinformatic analyses

RNA-seq data analysis: Raw sequencing datasets were processed on the University of Adelaide High-Performance Computing Phoenix platform. AdapterRemoval (Lindgreen, 2012) was used to remove adaptors of the raw reads. Sequence quality control was performed with FastQC (http://www.bioinformatics.babraham.ac.uk/projects/fastqc/(2015). Demultiplexed reads were mapped to the 12X grapevine reference genome (NCBI assembly ID: GCF_000003745.3) with the alignment tool (HISAT2) with default setting (Kim et al., 2015; Khalil-Ur-Rehman et al., 2017). The GTF reference of the *Vitis vinifera* genome was downloaded from the *Ensembl Plants* website (http://plants.ensembl.org/Vitis_vinifera/Info/Index). Samtools (Li et al., 2009) was used to generate Binary Alignment Map (BAM) files after mapping the reads to the genome.

2.4.1 Identification of genes expression associated to physiological measurements using weighted co-expression network and co-expressed gene cluster analysis

Transcripts Per Million (TPM) of each plant sample were calculated from the BAM files using the TPMcalculator (Vera

Alvarez et al., 2019). Normalized data (calculated TPMs) was used for the identification of gene expression clusters based on physiological measurements using *clust* v1.8.4 (Abu-Jamous and Kelly, 2018).

Gene co-expression networks and gene modules were identified using R package WGCNA (Langfelder and Horvath, 2008). Hierarchical clustering analysis was used to identify sample outliers using FlashClust (Langfelder and Horvath, 2012). The correlations amongst genes across samples were calculated using the WGCNA algorithm. The standard scale-free network was established after choosing the appropriate soft threshold power. Subsequently, module identification was performed with the dynamic tree cut method by hierarchically clustering the genes using the topological overlap matrix (TOM) as the distance measure with a deep split value of 2 and minimum module size (minClusterSize) of 50 for the resulting dendrogram. Modules showing high similarity were clustered and merged with a height cutoff of 0.25. Co-expression modules and gene information were extracted from each module using the WGCNA algorithm. The correlations between clustered modules and physiological variables (i.e., leaf temperature, stomatal conductance and stem water potential) were estimated by module eigengenes (MEs). The association of the individual module and each physiological variable was determined by Spearman's correlation. Modules were considered significantly associated with a given physiological variable and retained for further analysis when their absolute correlation value was higher than 0.6 and their p-value < 0.05 (Wang et al., 2020).

2.4.2 Differentially expressed genes analysis

Gene expression was estimated using the edgeR package (Robinson et al., 2010) on Rstudio. The raw mapped data of each sample was normalized by edgeR's trimmed mean of M values (TMM). This normalization method estimates scale factors between samples to determine DEGs. Between controls and each treatment, a log2fold change(log2FC) of 2 and a false discovery rate adjusted P-value<0.05 using Benjamini and Hochberg's algorithm was adopted to indicate significant genes. The "pheatmap" package (Kolde, 2012) was used to generate heat maps of gene expression patterns under drought, heat, and combined drought and heat stress treatments.

2.4.3 Gene ontology, KEGG pathway and network analysis

To interpret and classify the DEGs associated with drought, heat, and combined drought and heat stress, GO analysis was performed with agriGO v2.0 (Tian et al., 2017), along with WGCNA modules and clusters assembled by clust. DEGs of each treatment were used to attain the significant GO terms with agriGO v2.0 with the following criteria: Fisher's Exact test method, Yekutieli (FDR under dependency) multi-test adjustment method, significance level <0.05, and selecting complete GO as the gene ontology type. DEGs of each treatment, WCGNA modules, and clusters assembled by clust were used to attain the significant molecular pathways with Kyoto Encyclopedia of Genes and Genomes (KEGG) Automatic Annotation Server (KAAS) (Moriya et al., 2007). Visualization of KEGG functional enrichment pathways of DEGs was generated using the "*clusterProfiler*" package (Yu et al., 2012). A Web tool "REVIGO" was used to summarize the long lists of GO terms (Supek et al., 2011); subsequently, the lists generated by REVIGO were visualized with CirGO (Kuznetsova et al., 2019). The visualization of GO terms identified and enriched for WGCNA modules and clusters were done through Cytoscape, only genes that has gene module membership > 0.5 are considered hub genes (Shannon et al., 2003).

3 Results

3.1 Environmental conditions

Temperature control in the glasshouse consisted of evaporative cooling and gas heating, both thermostatically controlled. The evaporative cooler was unable to fully cool the glasshouse in the extreme heat that can occur during summer in Adelaide, Australia and was of limited effectiveness at night due to the relatively high humidity often seen in greenhouses. Consequently, the efficacy of the temperature control was variable, as can be seen in Supplemental Figure S1. Excluding the heat stress period, the mean daily maximum air temperature was 30.9°C, the mean daily minimum was 22.7°C and the overall mean was 25.9°C throughout the experiment. The mean daily maximum VPD was 1.81 kPa.

The heat stress treatment achieved a maximum air temperature of 38.5°C on the first day and 42.6°C on the second day. VPD increased to 4.2 and 5.3 kPa on days one and two of heat stress respectively. Following the removal of the heat stress, and during the recovery period, glasshouse conditions (mean daily max/min air temperature) were within 0.5°C of the pre-stress conditions.

3.2 Physiological analysis

Stomatal conductance (g_s): No difference in g_s between the plants to be subjected to stress treatments and the controls was observed before the initiation of drought treatment (ST1), consequently, it was assumed that there was no pre-existing bias between the future stress treatments (Figure 1A). The desired level of drought stress was reached after three days of drought treatment initiation and maintained for six days before the initiation of heat stress treatment. At ST2 (immediately before the application of heat stress) g_s was measured at 362 ± 77 mmol/m^{-2}/s^{-1} in the control plants and 55 ± 13 mmol/m^{-2}/s^{-1} in the droughted plants, slightly lower than the aimed for 75-100 mmol/m^{-2}/s^{-1} (Figure 1A). The difference between control and drought treated plants was statistically significant (p=0.016), demonstrating that the intended drought stress was successfully applied to the relevant plants.

Whilst the progress of water deficit treatments are best, and traditionally, monitored using mid-morning g_s, to ensure the peak period of stress (late afternoon) was observed, the primary physiological measurements during the heat stress period were taken later in the day. The space, number of individual plants, and resources available prevented more sets of measurements being taken on a single day, so the direct effects of the stress treatments were compared during the ST3 and ST4. The g_s of control plants at ST3 and ST4 was lower than the mid-morning values observed during the rest of the experiment, reaching only half of the maximal (mid-morning) g_s values recorded during the experiment (See Figure 1A), although

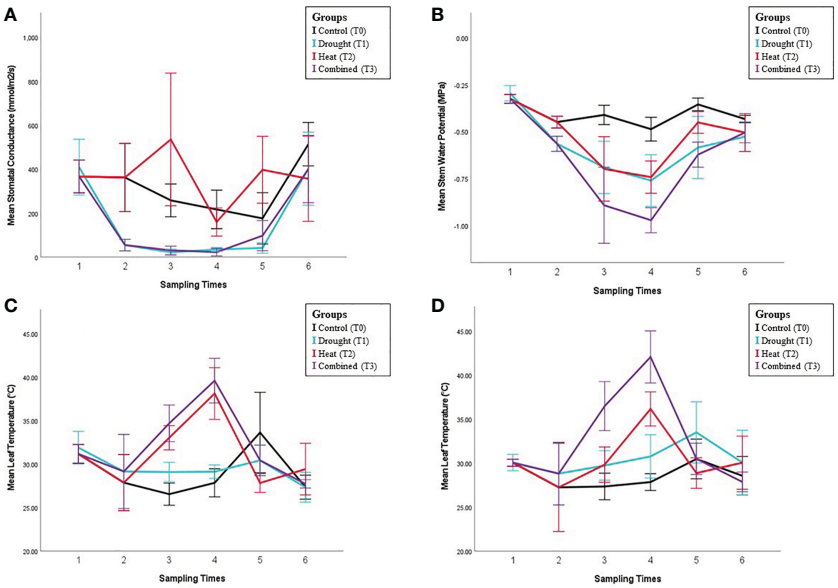

FIGURE 1
Physiological analysis results under different stress conditions. Panels show collected physiological measurements for **(A)** Stomatal conductance (g_s). **(B)** Stem water potential (StemΨ). **(C)** Leaf temperature (LT) of the third young leaf (not fully expanded), and the first fully expanded leaf **(D)**. Error bars indicate the standard error of means (n = 5).

such 'midday depression' of g_s is commonly observed in C_3 plants. Nevertheless, as with the mid-morning measurements prior g_s under drought stress (T1) measured during the afternoon at ST3 and ST4 remained significantly lower than control ($p<0.001$).

There was no significant (main) effect of heat stress (T2 and T3) on g_s. Additionally, the heat and drought interaction term was non-significant over the two days of the applied high-temperature event (ST3-4) (Figure 1A). Consequently, heat stress did not have an effect on g_s regardless of the plant's drought status.

Despite the lack of a heat stress effect on g_s being observed during the high-temperature event itself, there was a difference immediately after the removal of that stress (ST5), with g_s significantly higher in the previously heat-stressed plants (T2 and T3) than those not exposed to heat (T0 and T1) ($p<0.001$). However, there was also a significant interaction between heat and drought treatments ($p=0.023$) due to a much larger absolute increase in g_s with heat treatment in the absence of drought (T2 vs T0) than where drought was present (T3 vs T1). The relative increase was similar in each case, approximately double. It cannot be ruled out that an impact of heat stress would have been observed if mid-morning measurements of g_s were available as the ST3 and ST4 measurements were made in the afternoon. The g_s of drought-treated plants remained significantly lower than controls ($p<0.001$) at this time as the plants had not yet been re-watered.

Sixteen days after all plants were removed from stress treatment (ST6), there were no significant differences in g_s between any of the treatments, indicating physiological recovery (Figure 1A).

Stem water potential (stemΨ): The stemΨ of control plants was consistent at all sampling times (~-0.4 MPa) and did not vary between morning and afternoon measurements (Fig 1B, ST2 vs ST3). StemΨ decreased significantly under drought stress ($p<0.001$) to approximately -0.55 MPa (ST1, ST2 and ST5). Unlike the controls, stemΨ of drought plants was lower in the afternoon than the morning, reaching -0.7 MPa (ST2 vs ST3 and ST4). StemΨ was also significantly lower under heat stress ($p<0.001$). In contrast to g_s, there was an additive effect (no interaction) of the two stresses, with the combined stress treatment having a lower stemΨ than either stress individually (Figure 1B, T3 vs T1 and T2, ST3 and ST4). After stress removal (ST5), the stemΨ of drought-stressed plants remained significantly lower ($p<0.001$) than the control, while no significant difference was observed for heat-stressed plants. Similar to other physiological measurements, there were no significant effects of any former treatment on post-recovery period stemΨ (ST6), indicating a full recovery.

Leaf temperature (LT): No significant differences were observed in temperature between drought-treated and control plants before the initiation of any treatments (ST1) either for non-fully expanded or fully expanded leaves. Leaf temperature was not significantly affected by the initiation of drought treatment (ST2). During ST3 and ST4, the temperature of both non-fully expanded and fully expanded leaves was significantly higher under both heat ($p<0.001$ in each case) and drought ($p=0.025$ and $p<0.001$, respectively) (Figure 1C, D). As with StemΨ, this effect was additive (no interaction), with the highest temperatures occurring in the combined stress treatment (Fig 1 C-D). LTs of both the non-fully expanded leaf and first fully expanded leaf were higher at ST4 than ST3 ($p=0.002$ and $p=0.003$, respectively) in the heat treatment. For the non-fully expanded leaves, there was only a small difference in LT between the heat (T2) and combined (T3) treatments, similar to the difference observed between drought and control leaves. For the fully expanded leaves, the difference was much larger and there was a marginally significant interaction between heat and drought ($p=0.052$), suggesting that the effect of heat on LT was greater in combination with drought (Figures 1C, D).

In measurements made around two hours after stress removal (ST5), LTs for the previously heat-stressed plants were lower than the non-heat stressed plants in all cases except the droughted, still

expanding leaves. This would be expected where g_s was higher as there would be a higher transpiration rate. For the droughted vines not subject to heat stress, LT remained higher than control. Following the period allowed for physiological recovery (ST6), the leaf temperatures of both leaves were fully recovered.

3.3 Gene expression analysis

3.3.1 Next generation sequencing raw data

Transcriptome sequencing yielded a total of 3.3 billion reads, ranging from 2.66 to 9.56 Gbp of sequence per sample after quality filtering. The average number of mappable reads per sample after de-multiplexing was 23,631,104 (85%), ranging from 11,770,042 to 70,017,056 (75-91%) (Supplemental Table S1).

3.3.2 Identification of gene expression associated to physiological measurements using WCGNA and co-expressed gene cluster analysis

TPM counts of 30661 genes for 94 plants were calculated and used for gene expression analysis through WGCNA and clust (Supplemental Table S2).

Clust analysis generated a total of 9, 18 and 15 different co-expression clusters visually representing gene expression patterns for changes in given physiological parameters LT, g_s, and stemΨ of all 94 vine plants, respectively (Supplemental Figures S2-4). 11,250 genes were found in clusters showing either an increase or decrease in gene expression with increasing LT, g_s and stemΨ (Figure 2; Supplemental Table S3). In such clusters, biological regulation, response to stimulus, regulation of biological process and signaling were the most significant GO terms (Supplemental Figure S5). Pathway analysis revealed that genes involved in the seven most significantly enriched pathways, including thermogenesis, plant-pathogen interaction, cytosine and methionine metabolism, plant hormone signal transduction, MAPK signaling pathway in plants, ubiquitin-mediated proteolysis and protein processing in the endoplasmic reticulum (Supplemental Figure S6).

TPM values were clustered by Pearson's correlation and average linkage algorithms with the soft-thresholding power set to β = 8 (Supplemental Figure S7) to generate a scale-free gene co-expression network. 30 module eigengenes were generated by average linkage hierarchical clustering (Figure 3) (See Supplemental Table S4 for all genes, their respective modules and correlation values). Of these, 24 showed the same direction in correlation for g_s and stemΨ (Figure 3). Of these 24, 15 showed the opposite direction of correlation between LT and g_s or stemΨ. The only module deemed significant (i.e., correlation coefficient > 0.6 and p-value < 0.05), darkmagenta, showed a positive correlation with leaf temperature (R=0.66, p<1e-12) and a negative correlation with stem water potential (R=0.61, p<6e-11).

Comparison of the genes forming the darkmagenta module (n = 252) to those contained in the cluster showing increasing gene expression with increasing leaf temperature (n = 3513) (Figure 2A), and the cluster showing decreasing gene expression with increasing stem water potential (n = 4451) (Figure 2F) showed that 79% (n = 200) and 77% (n = 195) of the genes forming the darkmagenta module overlapped with genes in clusters A and F, respectively.

Gene interaction network analysis of the top 50 genes in darkmagenta module revealed five important hub genes (genes with high correlation and connectivity in the module, with gene module membership > 0.5) in this network, namely Inositol Polyphosphate 5-phosphatase 12, Ferric reduction oxidase 2, Histone-lysine N-methyltransferase SUVR3, Pyrrolidone-carboxylate peptidase, and Root primordium defective 1 (Figure 4A). GO analysis of the 252 genes contained in the darkmagenta module identified a total of 41 significantly enriched GO terms. Of these, 27 were Biological Processes, 13 Cellular Components, and 1 Molecular Function terms (i.e., 'protein serine/threonine kinase activity' (Figure 4B)) (Supplemental Table S5). An overrepresentation of genes involved in the processes 'response to stimulus' and 'response to stress' (Supplemental Figure S8) was observed for the darkmagenta module in co-expression network analysis. Similarly, analysis of the top 50 genes in darkmagenta module revealed a total of 11 Cellular Components terms (Supplemental Table S5).

3.3.3 Stress-induced differential gene expression

Differentially expressed genes (DEGs) identified between control and stressed plants (i.e., drought vs. control, heat vs. control,

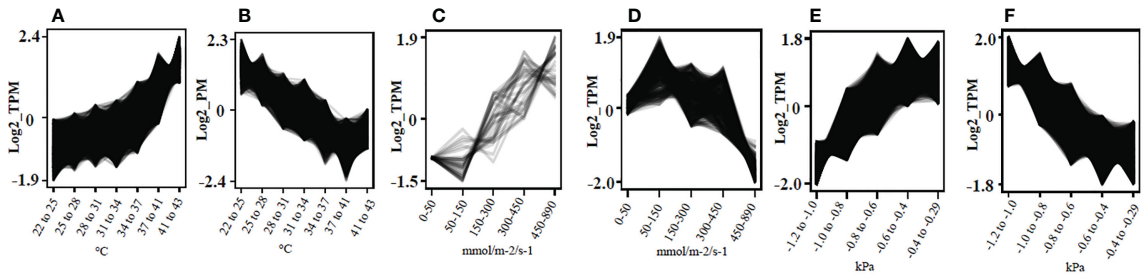

FIGURE 2
Identification of co-expressed genes in response to leaf temperature, stomatal conductance to water vapor, and stem water potential in grapevine. Gene expression clusters were identified based on physiological and transcriptome data generated from 94 plants using *clust* v1.8.4. **(A)** Gene cluster showing positive correlation with temperature (°C) of non-fully expanded leaves, n = 3,513; **(B)** Gene cluster showing negative correlation with temperature (°C) of non-fully expanded leaves, n = 1,918; **(C)** gene cluster showing positive correlation with g_s (mmol/m^{-2}/s^{-1}), n = 36; **(D)** Gene cluster showing negative correlation with g_s (mmol/m^{-2}/s^{-1}), n = 401; **(E)** Gene cluster showing positive correlation with StemΨ (kPa), n = 3,824; **(F)** Gene cluster showing negative correlation with StemΨ (kPa), n = 1,006.

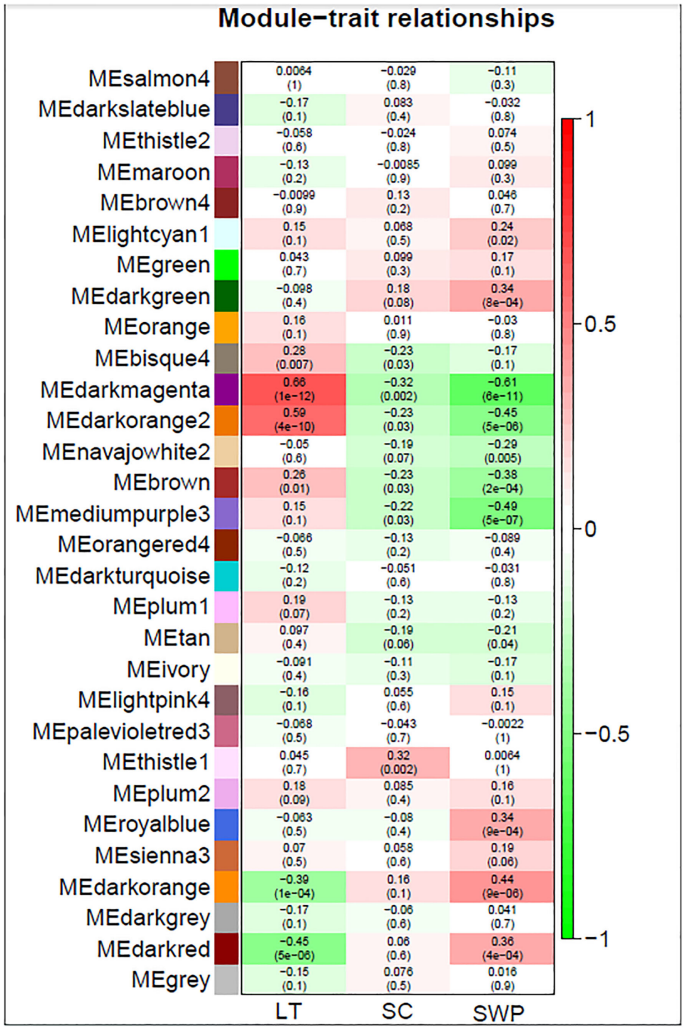

FIGURE 3
WGCNA module identification and correlation analysis of gene expression associated with leaf temperature, stomatal conductance to water vapor, and stem water potential in grapevine. Red and green color denote positive and negative correlations with gene expression, respectively. The top number in each cell indicates the correlation coefficient, and the bottom number indicates the correlation significance (P-value).

combined treatment vs. control) are summarized in Figure 5. In plants under drought stress, the number of identified DEGs peaked on the 11th day of drought treatment (ST3), with 161 up-regulated and 28 down-regulated genes, followed by the 12th day of drought treatment (ST4) with 141 DEGs, 48 up-regulated and 93 down-regulated. On the day of reinitiating normal irrigation and of heat stress removal (ST5), more genes were being down-regulated than up-regulated and no DEGs were detected at physiological recovery (ST6) (Figure 5A). Heat stressed plants produced most DEGs on the second day of stress (ST4, 54 DEGs) and at physiological recovery (ST6, 31 DEGs). The number of DEGs under heat stress was relatively small compared to drought and combined treatments. The majority of DEGs were detected in the combined treatment. The second day of heat stress in the combined treatment (ST4) had the most up-and down-regulated genes (671) and more genes were up-regulated (95) after physiological recovery (ST6) than were down-regulated (1).

The expression pattern of DEGs was visualized using a heat map to display the expression change and tendency (Figure 5). A small number of genes was differentially expressed at all sampling times (13, 0, and 4 genes for drought, heat, and combined treatments, respectively), with most DEGs only found at one sampling time (Figure 5 and Supplemental Table S6). A small number of DEGs (8/564, 2/867, and 4/304 for sampling times 3, 4, and 5, respectively) was observed to be common to all treatments.

A total of 163, 93, and 35 DEGs were common in drought and combined stress, for STs 3, 4, and 5, respectively. No common DEGs were found after physiological recovery (ST6) for drought and combined stress (Figure 6). At this stage, all DEGs in the heat treatment (31) were up-regulated and 95 of 96 DEGs were also up-regulated at physiological recovery in the combined treatment. None of the heat stress DEGs at physiological recovery had been differentially expressed during the treatment, and the small number of DEGs at physiological recovery (25) that overlapped with DEGs during treatment in the combined stress, were now up-regulated when they had previously been down-regulated (Supplemental Table S6).

10.3389/fpls.2023.1096225

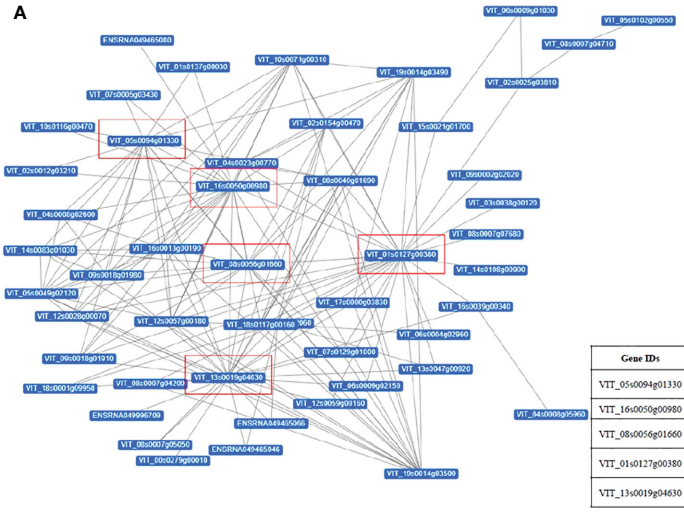

Gene IDs	NCBI gene description	Gene module membership
VIT_05s0094g01330	Inositol polyphosphate 5-phosphatase 12	0.68
VIT_16s0050g00980	Ferric reduction oxidase 2	0.56
VIT_08s0056g01660	Histone-lysine N-methyltransferase SUVR3	0.62
VIT_01s0127g00380	Pyrrolidone-carboxylate peptidase	0.61
VIT_13s0019g04630	ROOT PRIMORDIUM DEFECTIVE 1	0.60

FIGURE 4
Gene interaction network of genes of module 'darkmagenta' associated with leaf temperature and stem water potential. Gene interaction network of top 50 genes of darkmagenta module by Cytoscape. Each node represents a gene, and each line denotes the gene expression interaction between the two nodes. Hub genes are highlighted by red boxes, information about hub genes is given in insert table. **(B)** Gene Ontology molecular function analysis of the module.

3.3.4 GO, network and KEGG pathway analysis of DEGs by treatment

A total of 342, 24, and 594 significant GO terms (P_{adj}-value ≤ 0.05) were identified for DEGs during drought, heat, and combined stress, respectively (Supplemental Figure S9). 107 of the 342 drought-induced GO terms were only identified early during drought stress (ST2). The network visualization of correlated GO terms seemed to follow a trend: while under individual stress, the gene regulation networks were relatively simple (Supplemental Figures S10, 11), under combined stresses, the gene regulatory networks were more complex and acted synergistically (Supplemental Figure S12), indicated by all the interacting GO terms. Seven biological process ontologies made up ~83% of enriched categories in the combined treatment. Highly enriched categories were, histone modification (28.1%), regulation of the cell cycle (19%), response to stimulus (13.6%) and carbohydrate catabolic processes (10.5%) (Figure 7). Both the summary of GO terms and network visualization graph revealed the presence of DEGs associated with epigenetic and post-translational modifications during the latter stage of the combined stress treatment (ST4) and after stress removal (ST5), such as histone methylation, protein methylation, and protein alkylation (Figure 7). This was not observed in either individual drought or heat stress treatment (Supplemental Figure S13).

In the combined treatment, DEGs at ST3 were mostly involved in protein processing in the endoplasmic reticulum, galactose metabolism, plant hormone signal transduction and flavonoid biosynthesis. The same pathways, along with diterpenoid biosynthesis and glycosphingolipid biosynthesis were identified at ST4. The MAPK signaling pathway was significantly enriched at stress removal (ST5), while starch and sucrose metabolism and pentose and glucuronate interconversion were enriched at physiological recovery (ST6) (Figure 8). KEGG pathway analyses of DEGs under individual drought and heat treatments at different sampling times can be found in Supplemental Figures S14 and S15, respectively. Different pathways were significantly enriched for heat and drought DEGs, although protein processing in the endoplasmic

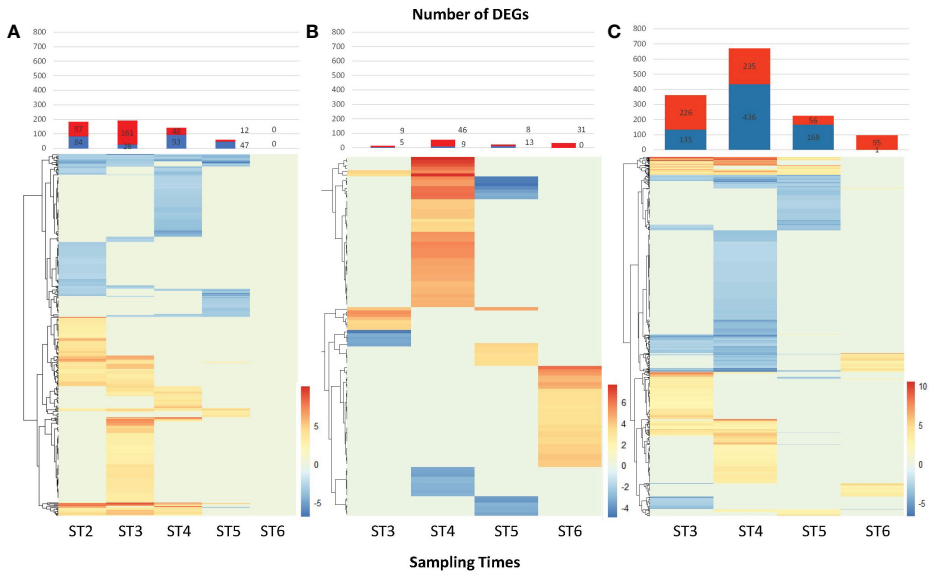

FIGURE 5
Differentially expressed genes (DEGs) identified under drought, heat, and combined treatments. Bar plots indicate the number of DEGs (FDR adjusted P-val. < 0.05) identified per treatment and sampling point. Red and blue bars indicate the number of up-regulated and down-regulated genes, respectively. Heatmaps show the fold change of the identified DEGs. **(A)** DEGs identified under drought treatment, **(B)** Heat, **(C)** Combined (heat plus drought). Heat and combined stress had not been initiated at ST2; therefore, it is not included in here.

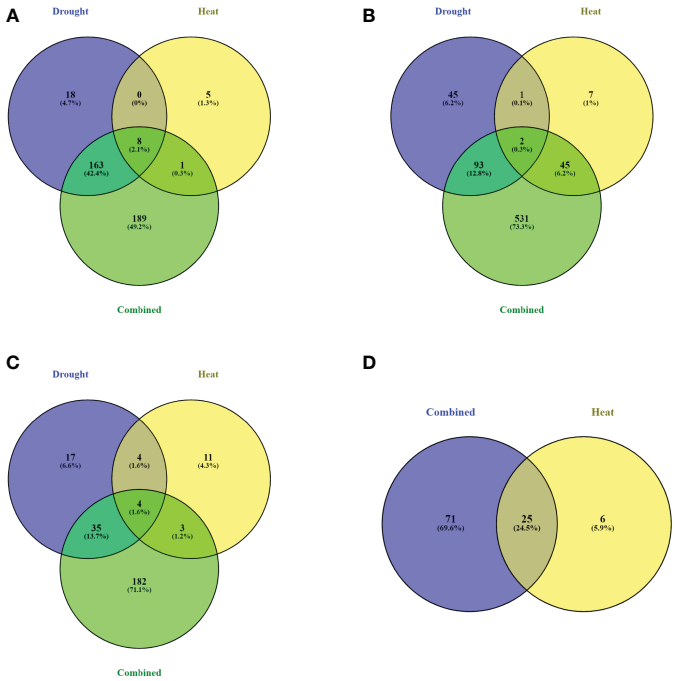

FIGURE 6
Identification of DEGs common for drought, heat, and combined treatment at each sampling time. Number of DEGs identified for each treatment at **(A)** sampling time 3; 11th day of drought treatment and first day of heat treatment. **(B)** sampling time 4; 12th day of drought treatment and second day of heat treatment. **(C)** sampling time 5; day of stress removal. **(D)** sampling time 6; physiological recovery.

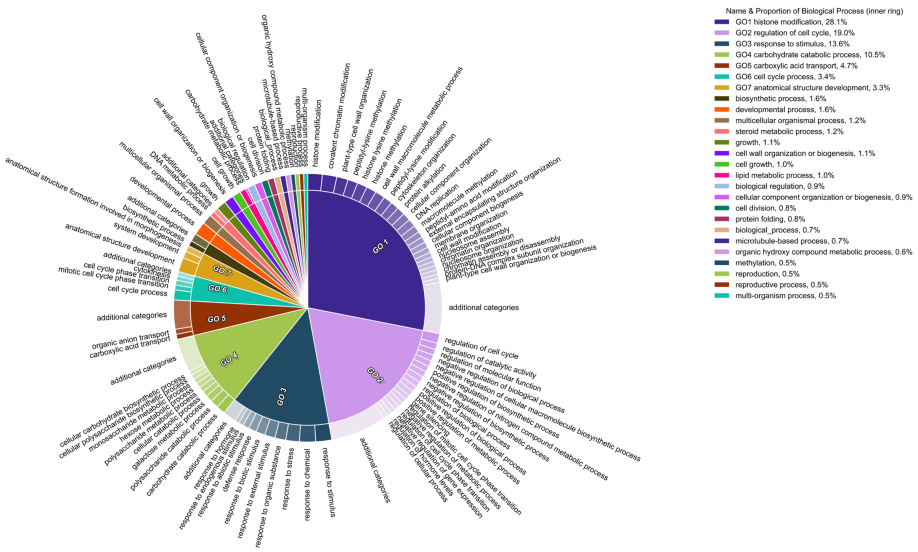

FIGURE 7
Gene ontology terms affected by combined stress. Pie section is a single cluster representative. Different representatives are joined into a summarized section, visualized with different colors. Section size is associated to the P-value of that given GO term.

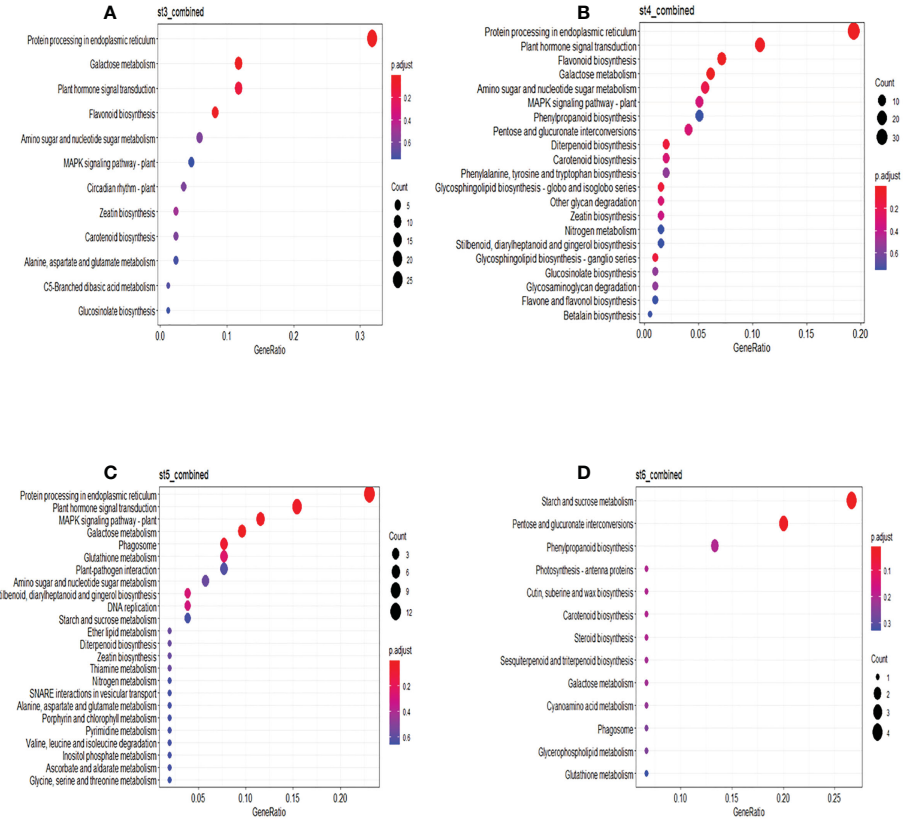

FIGURE 8
KEGG Functional enrichment analysis of DEGs identified. KEGG functional enrich analysis of differentially expressed genes under combined treatment at different sampling time points; **(A)** sampling time 3; **(B)** sampling time 4; **(C)** sampling time 5; **(D)** sampling time 6. Significantly enriched pathways are with adjusted p-value < 0.05.

reticulum was still significantly enriched at specific sampling times (ST3 – ST5) in both treatments.

4 Discussion

4.1 Physiological assessment of stress responses

Plant measurements of water status are usually destructive, so g_s was used as a proxy to monitor the extent of the drought stress imposed. This was then confirmed with measurements of stemΨ and pre-dawn water potential (data not presented) as direct measures of plant water status before imposing heat stress. The data confirmed the successful application of moderate to severe drought stress as intended, with stemΨ at -0.56 MPa, indicative of moderate stress in grapevines (Gambetta et al., 2020). As g_s was used to determine the level of drought stress, it was impacted by the drought treatment by definition. Nevertheless, it was still a useful measure of the relative effect of the treatments on leaf physiology. Leaf temperature is directly influenced by air temperature, but also by transpiration rate through evaporative cooling. As a result, although our physiological measurements were all obtained by independent methods, the results are linked by leaf processes, with stemΨ both influencing g_s and being influenced by g_s, while leaf temperature is also being influenced by g_s. This is supported by the observation in ST4, where stemΨ and g_s were well correlated, albeit with an offset with the heat treatment (r^2 = 0.68 and 0.44 for heat stress and control temperature respectively). The same was observed of g_s and LT of fully expanded leaves (r^2 = 0.80 and 0.51 for heat stress and control temperature respectively), stemΨ and fully expanded LT (r^2 = 0.84 and 0.61 for heat and control temperatures respectively) and the two LT measurements (fully expanded and developing leaves) across all treatments (r^2 = 0.84).

Such relationships are consistent with the literature, including for grapevines. They are linked by transpiration, with g_s determining transpiration rate at a given VPD and transpiration rate as a primary determinant for leaf temperature relative to air, as well as the difference between stemΨ and pre-dawnΨ which, in turn, is proportional to soil water availability (drought stress). It was beyond the capacity of this study to measure transpiration rates under ambient conditions, but differences between treatments can be inferred from g_s and VPD. A similar experimental system was used by Edwards et al. (2011) and reported a three-fold increase in transpiration in well-watered vines under heat stress.

The stemΨ measurements clearly demonstrated the interaction between the two stress treatments and the role of water and transpiration in the plant response. Drought stress alone lowered stemΨ relative to control, as the droughted plants were not able to obtain water from the soil at the rate to maintain the same water status as control plants. Heat stress alone also lowered stemΨ relative to control, as water loss *via* transpiration was increased due to the high VPD. The water uptake from the soil was not enough to compensate. The stemΨ of the combined stress was, however, lower than the drought stress alone; it is reasonable to assume that water loss *via* transpiration was higher in these plants. This is supported by the absence of a difference in g_s on day one of the heat stress treatment. The leaves subjected to the combined treatment would have been under greater stress than those subjected to the two stress treatments individually. Although g_s is typically well correlated with water deficits in grapevine leaves (e.g., Stevens et al., 1995; Cramer, 2010) and was used as an indicator of drought stress in this study (Figure 1A; Supplemental Figure S1), it did not reveal the impact of the heat stress on stemΨ. Furthermore, g_s increased during the first day of heat stress. Such a response has previously been observed both in grapevine (Sommer et al., 2012) and other species (Reynolds-Henne et al., 2010; Marchin et al., 2022). This could be viewed as an adaptation to limit heat stress of the leaf when adequate water is available, as the combined stress treatment did not show a similar increase. Conversely, a study of 20 species found that a significant increase in g_s under combined heat and drought stress was more common than under heat stress alone (Marchin et al., 2022). However, this was influenced by whether a species was classified as isohydric or anisohydric, where the observation is more common in the former group. Grapevine varieties vary significantly in this regard (Schultz, 2003). Anecdotally, the Cabernet Sauvignon cultivar used in this study is considered moderate between these two extremes.

Due to the destructive nature of some of the measurements, it was not possible to undertake all the measurements and sampling for gene transcription on the same leaf. Therefore, a younger leaf was used for the transcriptome samples. LT of the mature and younger leaf were highly correlated (e.g., Figures 1C, D, but the temperature increase of younger leaves under combined stress was less than that of fully expanded ones; this suggests a higher rate of water loss in the still expanding leaves, previously observed in grapevines (Hopper et al., 2014) and other species (Davis et al., 1977; Reich and Borchert, 1988). The observation may be explained by reduced stomatal function in the younger leaves compared with the fully expanded leaves, or possible differences in hydraulics or even the epidermal integrity of younger leaves, which do not appear to have been studied in detail in grapevine.

After the removal of stress, a rapid recovery was observed for all measured parameters in heat stress-treated plants (heat alone or in combination with drought). Leaf temperatures and stem water potential also recovered rapidly in drought-stressed plants, although stomatal conductance was still reduced at the final sampling time in comparison with the controls.

4.2 Gene expression analysis

Analysis of the correlation between physiological parameters and gene expression levels identified clusters and networks of genes that were significantly positively and negatively correlated with measured physiological parameters across treatments. The expression of the largest number of genes was linearly correlated with increasing LT and decreasing stemΨ, and the majority and most significant of co-expression networks also showed this pattern. There were, however, more than 3000 genes strongly induced at water potentials below 1.0 MPa (e.g., Figure 2E, Supplemental Figure S4 clusters C9 and C10) or leaf temperatures above 34 ^{0}C (e.g., Figure 2A, Supplemental Figure S2 cluster C4), suggesting that these thresholds might be indicative of severe stress.

Several pathways where gene expression consistently correlated with physiological parameter measurements were also identified, including thermogenesis, plant-pathogen interaction, cytosine and methionine metabolism, plant hormone signal transduction, MAPK signaling, ubiquitin mediated proteolysis and protein processing in the endoplasmic reticulum. These are indicative of pathways that are important in drought, heat and combined stresses, where changes in gene expression are likely driven by changes in integrated plant physiology, regardless of the specific treatment (Supplemental Figure S6).

Quantitatively, transcriptomic changes were most pronounced in the combined treatment, as indicated by the larger numbers of genes being up- and down-regulated at each sampling time (Figure 5). Gene regulation and interaction networks for the combined drought and heat stress treatment were more complex than for either individual stress indicating that a larger number of genes is influenced (Figure 7, Supplemental Figures S9-13) and that the effect of combined stress on the grapevine transcriptome is more than simply additive, similar to observations in other plants (Rizhsky et al., 2002; Rollins et al., 2013). The five hub genes in the network responding to combined drought and heat stress treatments appeared unique to the combined treatment and, to our knowledge, they have not been reported previously as regulators of gene expression networks in grapevine under either drought or heat stress.

Carvalho et al. (2015) reported differences in recovery of cellular redox status and metabolism following heat stress in two different grapevine varieties depending on whether they had acclimated to the stress and that were strongly dependent on genotype. In our experiment, with a limited number of physiological parameters measured and a short heatwave treatment, Cabernet Sauvignon appeared to recover immediately. There were generally fewer differentially expressed genes after recovery than during the treatments (Figure 5), as has previously been reported for Cabernet Sauvignon (Liu et al., 2012), and the shift to secondary metabolism following stress that has been reported as a general feature of grapevine (Carvalho and Amâncio, 2019) was indicated by the ontology of enriched DEGs.

4.3 Common stress response genes shared among heat, drought, and combined stress

A small number of DEGs was observed to be common to all treatments (Figure 6). More DEGs were shared among drought and combined stress than between heat and combined stress, suggesting that drought stress was the main driver of gene expression regulation for plants under combined stress. Despite the differences in DEGs observed at each sampling time, there were several genes common to all three treatments (Supplemental Table S6). DEGs shared by all three treatments included: (1) heat shock proteins (HSPs) and late embryogenesis abundant (LEA) proteins, where their functions in drought and heat stress have previously been reported (Clément et al., 2011; Liu et al., 2012; Yang et al., 2012; Rocheta et al., 2016; Yu et al., 2018). (2) plant hormone signal transduction and transcription factor activation, as transcription factors are involved in signal transduction networks, regulating the expression of genes that encode proteins and that may act together to respond to multiple stresses (Mahajan and Tuteja, 2005; Bhatnagar-Mathur et al., 2008; Hu et al., 2010; Chen et al., 2012; Licausi et al., 2013; Zhang et al., 2014; Collin et al., 2020;). (3) sucrose and starch metabolism and galactose metabolism pathway genes that has been shown altered expression in response to drought and heat stress (Taji et al., 2002; Greer and Weston, 2010; Pillet et al., 2012; Greer and Weedon, 2013; Thalmann and Santelia, 2017;).

4.4 Differential gene expression exclusive to combined stress

4.4.1 Phenylpropanoids biosynthesis

The phenylpropanoids biosynthetic pathway and biosynthesis of flavonoids (anthocyanin, flavonols, and tannins) are important for wine composition and quality. In this study, DEGs associated with phenylpropanoids and flavonoids biosynthesis were identified in the combined stress treatment (Figure 8). Anthocyanin regulatory C1, which controls the expression of genes involved in anthocyanin biosynthesis (Cone et al., 1993) was exclusively down-regulated under combined stress during the stress period (ST3-ST4). Similarly, down-regulation of chalcone synthase, the first committed enzyme of the flavonoid biosynthetic pathway (Ferrer et al., 1999), was observed under combined stress during ST3-ST4. Previous studies have shown that the concentrations of flavonol and anthocyanin in berries and skins are negatively affected by heat stress (Mori et al., 2007; Movahed et al., 2016; Pastore et al., 2017). Conversely, anthocyanin biosynthesis is strongly up-regulated in grapevines under drought through the up-regulation of flavonoid biosynthetic genes such as chalcone synthase (Castellarin et al., 2007). It has been suggested that anthocyanin accumulation promoted by water-restricted cultivation could potentially alleviate the detrimental effect of excessive heat that causes reduced anthocyanin, although beneficial effects of water restriction may only occur at later growth stages when berries are ripening (reviewed in Scholasch and Rienth, 2019). We observed no differential expression of genes in these pathways under either drought or heat stress in leaves during this earlier developmental phase, but the downregulation of anthocyanin biosynthesis genes during the combined stress at this stage suggests that drought and heat were not able to offset one another, and that the severity of the stress will likely influence transcription of these genes pre-ripening. Overall, it is possible to hypothesize that combined stress will influence the biosynthesis and degradation of phenylpropanoids/flavonoids and stilbene in grapevine differently from individual drought or heat stress through the regulation of important structural genes, such as chalcone synthase and anthocyanin regulatory C1 protein.

4.4.2 Epigenetic changes

The structure of chromatin is important in the regulation of gene expression (Struhl and Segal, 2013; Zentner and Henikoff, 2013), and depends upon several regulatory epigenetic marks, including DNA methylation, and histone modifications (Sahu et al., 2013). Here, the main category of DEGs found under combined stress was genes associated with histone modifications (Figure 7). Terms in this category included histone modification, histone lysine methylation, histone methylation and covalent chromatin modification, while the GO Methylation (*sensu lato*) made up a smaller portion. Upon further

inspection, genes associated with histone-lysine methyltransferase appeared to be exclusively regulated in late-stage combined stress (ST4), while other methylation-associated genes were found at stress removal (ST5). Additionally, histone-lysine N-methyltransferase *SUVR3* was one of the five hub genes in the interaction network for combined stress (Figure 6B). SUVR3 catalyzes the transfer of one, two, or three methyl groups to lysine and arginine residues of histone proteins and plays a role in epigenetic gene regulation (Pontvianne et al., 2010). Studies have found that stress might induce changes in the epigenome and Bond and Finnegan (2007) proposed that modified chromatin is the basis for epigenetic memory. Some stress-induced modifications are reversed once the stress is over, while some may be stable and heritable, thus named the "stress memory" (Kinoshita and Seki, 2014). Although additional data and analyses are required to conclude whether the changes observed in this study are truly an event of epigenetic memory formation, the alteration of the expression of those epigenetic change-related genes is potentially an indication of the establishment of epigenetic memory at the latter stage of combined drought and heat stress.

This study generated valuable transcriptomic datasets for grapevines and provides a useful resource for further targeted studies. However, to fully explore the causalities between gene regulation and physiological changes/stress conditions, future studies will need to carry out targeted studies testing the hypotheses linking the transcriptional regulation of individual genes to specific physiological signals.

5 Conclusions

Differences in rates of stomatal conductance, stem water potentials, leaf temperatures and gene expression patterns were identified between different stress treatments. The combined drought and heat stress had more severe effects on the grapevines' physiology compared with individual stresses. Similarly, networks of genes co-expressing in the combined treatment were more complex than in either individual stress. The expression of a large number of genes was linearly correlated with increasing leaf temperatures or stem water potentials, but the overlap between genes commonly differentially expressed in all treatments and at all sampling times was small, and fewer genes were differentially expressed in the heat treatment than the drought or combined treatments. Of DEGs common to all three stresses, many belonged to gene families previously implicated in abiotic stress responses. In contrast, the suppression of key regulators of the biosynthesis of phenylpropanoids/flavonoids was observed only under the combined stress. Histone modifying DEGs were also unique to the combined drought and heat stress treatment and genes in chromatin-modifying categories were significantly enriched in all analyses for this treatment. Following removal of stress and physiological recovery of the plants, a small number of DEGs remained in the heat and combined stress treatments, but no DEGs remained following drought. These remaining DEGs in the heat stress and combined treatments were almost exclusively up-regulated and only at physiological recovery. They may be particularly important for grapevine acclimation to heat, combined drought and heat stress, or in any effect of encountered stress on the following season in these perennial plants. These results give a collective view of stress response and the similarities and differences in responses between individual and combined stress. They reveal differences in the transcriptomes of grapevine in combined drought and heat stress that are not simply additive of the two individual stresses, but may be largely driven by physiological gradients and result in epigenetic modifications.

Data availability statement

The datasets presented in this study can be found in the sequence read archive (SRA) of the National Center for Biotechnology Information (NCBI) repository, accession number PRJNA662522, https://www.ncbi.nlm.nih.gov/.

Author contributions

CL, PT and EE conceived and designed the study. YH and KT performed the greenhouse and laboratory experiments. JT and HS performed the analysis and analyzed the results. MF, EE and UB contributed analysis methods and tools. All authors contributed to the article and approved the submitted version.

Funding

This study was supported by the Australian Grape and Wine Authority grant ID: UA1503, the National Institute of Food and Agriculture, AFRI Competitive Grant Program Accession number 1018617, and the National Institute of Food and Agriculture, United States Department of Agriculture, Hatch Program accession number 1020852.

Conflict of interest

Author PT is employed by The New Zealand Institute for Plant and Food Research Limited, author EE is employed by CSIRO Agriculture and Food.

The remaining authors declare that the research was conducted in the absence of any commercial or financial relationships that could be construed as a potential conflict of interest.

Publisher's note

Supplementary material

The Supplementary Material for this article can be found online at: https://www.frontiersin.org/articles/10.3389/fpls.2023.1096225/full#supplementary-material

References

Abu-Jamous, B., and Kelly, S. (2018). Clust: automatic extraction of optimal co-expressed gene clusters from gene expression data. *Genome Biol.* 19 (1), 1–11. doi: 10.1186/s13059-018-1536-8

Bai, H., Gambetta, G. A., Wang, Y., Kong, J., Long, Q., Fan, P., et al. (2022). Historical long-term cultivar× climate suitability data to inform viticultural adaptation to climate change. *Sci. Data* 9 (1), 1–10. doi: 10.1038/s41597-022-01367-6

Bhatnagar-Mathur, P., Vadez, V., and Sharma, K. K. (2008). Transgenic approaches for abiotic stress tolerance in plants: retrospect and prospects. *Plant Cell Rep.* 27 (3), 411–424. doi: 10.1007/s00299-007-0474-9

Bond, D. M., and Finnegan, E. J. (2007). Passing the message on: inheritance of epigenetic traits. *Trends Plant Sci.* 12 (5), 211–216. doi: 10.1016/j.tplants.2007.03.010

Carvalho, L. C., and Amâncio, S. (2019). Cutting the Gordian knot of abiotic stress in grapevine: From the test tube to climate change adaptation. *Physiol. plantarum* 165 (2), 330–342. doi: 10.1111/ppl.12857

Carvalho, L. C., Coito, J. L., Colaço, S., Sangiogo, M., and Amâncio, S. (2015). Heat stress in grapevine: the pros and cons of acclimation. *Plant Cell Environ.* 38 (4), 777–789. doi: 10.1111/pce.12445

Castellarin, S. D., Pfeiffer, A., Sivilotti, P., Degan, M., Peterlunger, E., and Di Gaspero, G. (2007). Transcriptional regulation of anthocyanin biosynthesis in ripening fruits of grapevine under seasonal water deficit. *Plant Cell Environ.* 30 (11), 1381–1399. doi: 10.1111/j.1365-3040.2007.01716.x

Chaves, M. M., Pereira, J. S., Maroco, J., Rodrigues, M. L., Ricardo, C. P. P., Osório, M. L., et al. (2002). How plants cope with water stress in the field? photosynthesis and growth. *Ann. Bot.* 89 (7), 907–916. doi: 10.1093/aob/mcf105

Chen, L., Song, Y., Li, S., Zhang, L., Zou, C., and Yu, D. (2012). The role of WRKY transcription factors in plant abiotic stresses. *Biochim. Biophys. Acta (BBA)-Gene Regul. Mech.* 1819 (2), 120–128. doi: 10.1016/j.bbagrm.2011.09.002

Clément, M., Leonhardt, N., Droillard, M. J., Reiter, I., Montillet, J. L., Genty, B., et al. (2011). The cytosolic/nuclear HSC70 and HSP90 molecular chaperones are important for stomatal closure and modulate abscisic acid-dependent physiological responses in arabidopsis. *Plant Physiol.* 156 (3), 1481–1492. doi: 10.1104/pp.111.174425

Collin, A., Daszkowska-Golec, A., Kurowska, M., and Szarejko, I. (2020). Barley ABI5 (Abscisic acid INSENSITIVE 5) is involved in abscisic acid-dependent drought response. *Front. Plant Sci.* 11, 1138. doi: 10.3389/fpls.2020.01138

Cone, K. C., Cocciolone, S. M., Burr, F. A., and Burr, B. (1993). Maize anthocyanin regulatory gene pl is a duplicate of c1 that functions in the plant. *Plant Cell* 5 (12), 1795–1805. doi: 10.1105/tpc.5.12.1795

Cramer, G. R. (2010). Abiotic stress and plant responses from the whole vine to the genes. *Aust. J. Grape Wine Res.* 16, 86–93. doi: 10.1111/j.1755-0238.2009.00058.x

Davis, S. D., Van Bavel, C. H. M., and McCree, K. J. (1977). Effects of leaf aging upon stomatal resistance in bean plants 1. *Crop Sci.* 17 (4), 640–645. doi: 10.2135/cropsci1977.0011183X001700040041x

Diffenbaugh, N. S., White, M. A., Jones, G. V., and Ashfaq, M. (2011). Climate adaptation wedges: a case study of premium wine in the western united states. *Environ. Res. Lett.* 6 (2), 024024. doi: 10.1088/1748-9326/6/2/024024

Edwards, E. J., and Clingeleffer, P. R. (2013). Interseasonal effects of regulated deficit irrigation on growth, yield, water use, berry composition and wine attributes of Cabernet sauvignon grapevines. *Aust. J. Grape Wine Res.* 19 (2), 261–276. doi: 10.1111/ajgw.12027

Edwards, E. J., Smithson, L., Graham, D. C., and Clingeleffer, P. R. (2011). Grapevine canopy response to a high-temperature event during deficit irrigation. *Aust. J. Grape Wine Res.* 17 (2), 153–161. doi: 10.1111/j.1755-0238.2011.00125.x

Estravis-Barcala, M., Mattera, M. G., Soliani, C., Bellora, N., Opgenoorth, L., Heer, K., et al. (2020). Molecular bases of responses to abiotic stress in trees. *J. Exp. Bot.* 71 (13), 3765–3779. doi: 10.1093/jxb/erz532

Ferrer, J. L., Jez, J. M., Bowman, M. E., Dixon, R. A., and Noel, J. P. (1999). Structure of chalcone synthase and the molecular basis of plant polyketide biosynthesis. *Nat. Struct. Biol.* 6 (8), 775–784. doi: 10.1038/11553

Gambetta, G. A., Herrera, J. C., Dayer, S., Feng, Q., Hochberg, U., and Castellarin, S. D. (2020). The physiology of drought stress in grapevine: towards an integrative definition of drought tolerance. *J. Exp. Bot.* 71 (16), 4658–4676. doi: 10.1093/jxb/eraa245

Gladstones, J. (1992). *Viticulture and environment* (Winetitles). Available at: https://www.cabdirect.org/cabdirect/abstract/19930324643.

Greer, D. H., and Weedon, M. M. (2013). The impact of high temperatures on vitis vinifera cv. semillon grapevine performance and berry ripening. *Front. Plant Sci.* 4, 491. doi: 10.3389/fpls.2013.00491

Greer, D. H., and Weston, C. (2010). Heat stress affects flowering, berry growth, sugar accumulation and photosynthesis of vitis vinifera cv. semillon grapevines grown in a controlled environment. *Funct. Plant Biol.* 37 (3), 206–214.

Haider, M. S., Zhang, C., Kurjogi, M. M., Pervaiz, T., Zheng, T., Zhang, C., et al. (2017). Insights into grapevine defense response against drought as revealed by biochemical, physiological and RNA-seq analysis. *Sci. Rep.* 7 (1), 1–15. doi: 10.1038/s41598-017-13464-3

Hopper, D. W., Ghan, R., and Cramer, G. R. (2014). A rapid dehydration leaf assay reveals stomatal response differences in grapevine genotypes. *Horticul. Res.* 1. doi: 10.1038/hortres.2014.2

Hu, R., Qi, G., Kong, Y., Kong, D., Gao, Q., and Zhou, G. (2010). Comprehensive analysis of NAC domain transcription factor gene family in populus trichocarpa. *BMC Plant Biol.* 10 (1), 1–23. doi: 10.1186/1471-2229-10-145

IPCC (2018). *Global warming of 1.5°C. an IPCC special report on the impacts of global warming of 1.5°C above pre-industrial levels and related global greenhouse gas emission pathways, in the context of strengthening the global response to the threat of climate change, sustainable development, and efforts to eradicate poverty*. V. Masson-Delmotte, P. Zhai, H. O. Pörtner, D. Roberts, J. Skea, P. R. Shukla, et al eds. Available at: https://www.ipcc.ch/sr15/.

Jones, G. V. (2006). "Climate and terroir: impacts of climate variability and change on wine," in *Geoscience Canada*. Eds. R. W. Macqueen and L. D. Meinert (St John's, Newfoundland: Geological Association of Canada), 1–14.

Jones, G. V., and Davis, R. E. (2000). Climate influences on grapevine phenology, grape composition, and wine production and quality for Bordeaux, France. *Am. J. enol. viticul.* 51 (3), 249–261. doi: 10.5344/ajev.2000.51.3.249

Khalil-Ur-Rehman, M., Sun, L., Li, C. X., Faheem, M., Wang, W., and Tao, J. M. (2017). Comparative RNA-seq based transcriptomic analysis of bud dormancy in grape. *BMC Plant Biol.* 17 (1), 1–11. doi: 10.1186/s12870-016-0960-8

Kim, D., Langmead, B., and Salzberg, S. L. (2015). HISAT: a fast spliced aligner with low memory requirements. *Nat. Methods* 12 (4), 357–360. doi: 10.1038/nmeth.3317

Kinoshita, T., and Seki, M. (2014). Epigenetic memory for stress response and adaptation in plants. *Plant Cell Physiol.* 55 (11), 1859–1863. doi: 10.1093/pcp/pcu125

Kolde, R. (2012). *Pheatmap: pretty heatmaps. r package version*, Vol. 1. https://cran.r-project.org/web/packages/pheatmap/index.html.

Kulkarni, M., Borse, T., and Chaphalkar, S. (2007). Anatomical variability in grape (Vitis venifera) genotypes in relation to water use efficiency (WUE). *Am. J. Plant Physiol.* 2, 36–43. doi: 10.3923/ajpp.2007.36.43

Kuznetsova, I., Lugmayr, A., Siira, S. J., Rackham, O., and Filipovska, A. (2019). CirGO: an alternative circular way of visualising gene ontology terms. *BMC Bioinf.* 20 (1), 1–7. doi: 10.1186/s12859-019-2671-2

Langfelder, P., and Horvath, S. (2008). WGCNA: an r package for weighted correlation network analysis. *BMC Bioinf.* 9 (1), 1–13. doi: 10.1186/1471-2105-9-559

Langfelder, P., and Horvath, S. (2012). Fast r functions for robust correlations and hierarchical clustering. *J. Stat. software* 46 (11), i11.

Licausi, F., Ohme-Takagi, M., and Perata, P. (2013). APETALA 2/Ethylene responsive factor (AP 2/ERF) transcription factors: Mediators of stress responses and developmental programs. *New Phytol.* 199 (3), 639–649. doi: 10.1111/nph.12291

Li, H., Handsaker, B., Wysoker, A., Fennell, T., Ruan, J., Homer, N., et al. (2009). The sequence alignment/map (SAM) format and SAMtools. *Bioinformatics* 25 (16), 2078–2079. doi: 10.1093/bioinformatics/btp352

Lindgreen, S. (2012). AdapterRemoval: easy cleaning of next-generation sequencing reads. *BMC Res. Notes* 5 (1), 1–7. doi: 10.1186/1756-0500-5-337

Liu, G. T., Wang, J. F., Cramer, G., Dai, Z. W., Duan, W., Xu, H. G., et al. (2012). Transcriptomic analysis of grape (Vitis viniferaL.) leaves during and after recovery from heat stress. *BMC Plant Biol.* 12 (1), 1–10. doi: 10.1186/1471-2229-12-174

Mahajan, S., and Tuteja, N. (2005). Cold, salinity and drought stresses: an overview. *Arch. Biochem. biophys.* 444 (2), 139–158. doi: 10.1016/j.abb.2005.10.018

Marchin, R. M., Backes, D., Ossola, A., Leishman, M. R., Tjoelker, M. G., and Ellsworth, D. S. (2022). Extreme heat increases stomatal conductance and drought-induced mortality risk in vulnerable plant species. *Global Change Biol.* 28 (3), 1133–1146. doi: 10.1111/gcb.15976

Martínez-Lüscher, J., and Kurtural, S. K. (2021). Same season and carry-over effects of source-sink adjustments on grapevine yields and non-structural carbohydrates. *Front. Plant Sci.* 12, 695319. doi: 10.3389/fpls.2021.695319

Mittler, R. (2006). Abiotic stress, the field environment and stress combination. *Trends Plant Sci.* 11 (1), 15–19. doi: 10.1016/j.tplants.2005.11.002

Moore, C. E., Meacham-Hensold, K., Lemonnier, P., Slattery, R. A., Benjamin, C., Bernacchi, C. J., et al. (2021). The effect of increasing temperature on crop photosynthesis: from enzymes to ecosystems. *J. Exp. Bot.* 72 (8), 2822–2844. doi: 10.1093/jxb/erab090

Mori, K., Goto-Yamamoto, N., Kitayama, M., and Hashizume, K. (2007). Loss of anthocyanins in red-wine grape under high temperature. *J. Exp. Bot.* 58 (8), 1935–1945. doi: 10.1093/jxb/erm055

Moriya, Y., Itoh, M., Okuda, S., Yoshizawa, A. C., and Kanehisa, M. (2007). KAAS: an automatic genome annotation and pathway reconstruction server. *Nucleic Acids Res.* 35 (suppl_2), W182–W185. doi: 10.1093/nar/gkm321

Movahed, N., Pastore, C., Cellini, A., Allegro, G., Valentini, G., Zenoni, S., et al. (2016). The grapevine VviPrx31 peroxidase as a candidate gene involved in anthocyanin degradation in ripening berries under high temperature. *J. Plant Res.* 129 (3), 513–526. doi: 10.1007/s10265-016-0786-3

Mullins, M. G., Bouquet, A., and Williams, L. E. (1992). *Biology of the grapevine* (Cambridge University Press). Available at: https://books.google.com/books?hl=en&lr=&id=wnNvmRjfxgQC&oi=fnd&pg=PP11&dq=Biology+of+the+grapevine+(Cambridge+University+Press).

Pastore, C., Dal Santo, S., Zenoni, S., Movahed, N., Allegro, G., Valentini, G., et al. (2017). Whole plant temperature manipulation affects flavonoid metabolism and the transcriptome of grapevine berries. *Front. Plant Sci.* 8, 929. doi: 10.3389/fpls.2017.00929

Patakas, A., Noitsakis, B., and Chouzouri, A. (2005). Optimization of irrigation water use in grapevines using the relationship between transpiration and plant water status. *Agriculture Ecosyst. Environ.* 106 (2-3), 253–259. doi: 10.1016/j.agee.2004.10.013

Pillet, J., Egert, A., Pieri, P., Lecourieux, F., Kappel, C., Charon, J., et al. (2012). VvGOLS1 and VvHsfA2 are involved in the heat stress responses in grapevine berries. *Plant Cell Physiol.* 53 (10), 1776–1792. doi: 10.1093/pcp/pcs121

Pontvianne, F., Blevins, T., and Pikaard, C. S. (2010). "Arabidopsis histone lysine methyltransferases," in *Advances in botanical research*, vol. 53. (Academic Press), 1–22. Available at: https://www.sciencedirect.com/science/article/abs/pii/S0065229610530015.

Raja, V., Majeed, U., Kang, H., Andrabi, K. I., and John, R. (2017). Abiotic stress: Interplay between ROS, hormones and MAPKs. *Environ. Exp. Bot.* 137, 142–157. doi: 10.1016/j.envexpbot.2017.02.010

Raza, A., Razzaq, A., Mehmood, S. S., Zou, X., Zhang, X., Lv, Y., et al. (2019). Impact of climate change on crops adaptation and strategies to tackle its outcome: A review. *Plants* 8 (2), 34. doi: 10.3390/plants8020034

Reich, P. B., and Borchert, R. (1988). Changes with leaf age in stomatal function and water status of several tropical tree species. *Biotropica* 20 (1), 60–69. doi: 10.2307/2388427

Reynolds-Henne, C. E., Langenegger, A., Mani, J., Schenk, N., Zumsteg, A., and Feller, U. (2010). Interactions between temperature, drought and stomatal opening in legumes. *Environ. Exp. Bot.* 68 (1), 37–43. doi: 10.1016/j.envexpbot.2009.11.002

Rizhsky, L., Liang, H., and Mittler, R. (2002). The combined effect of drought stress and heat shock on gene expression in tobacco. *Plant Physiol.* 130 (3), 1143–1151. doi: 10.1104/pp.006858

Robinson, M. D., McCarthy, D. J., and Smyth, G. K. (2010). edgeR: a bioconductor package for differential expression analysis of digital gene expression data. *bioinformatics* 26 (1), 139–140. doi: 10.1093/bioinformatics/btp616

Rocheta, M., Coito, J. L., Ramos, M. J., Carvalho, L., Becker, J. D., Carbonell-Bejerano, P., et al. (2016). Transcriptomic comparison between two vitis vinifera l. varieties (Trincadeira and touriga nacional) in abiotic stress conditions. *BMC Plant Biol.* 16 (1), 1–19. doi: 10.1186/s12870-016-0911-4

Rollins, J. A., Habte, E., Templer, S. E., Colby, T., Schmidt, J., and Von Korff, M. (2013). Leaf proteome alterations in the context of physiological and morphological responses to drought and heat stress in barley (Hordeum vulgare l.). *J. Exp. Bot.* 64 (11), 3201–3212. doi: 10.1093/jxb/ert158

Sachdev, S., Ansari, S. A., Ansari, M. I., Fujita, M., and Hasanuzzaman, M. (2021). Abiotic stress and reactive oxygen species: Generation, signaling, and defense mechanisms. *Antioxidants* 10 (2), 277. doi: 10.3390/antiox10020277

Sahu, P. P., Pandey, G., Sharma, N., Puranik, S., Muthamilarasan, M., and Prasad, M. (2013). Epigenetic mechanisms of plant stress responses and adaptation. *Plant Cell Rep.* 32 (8), 1151–1159. doi: 10.1007/s00299-013-1462-x

Scholasch, T., and Rienth, M. (2019). Review of water deficit mediated changes in vine and berry physiology; consequences for the optimization of irrigation strategies. *Oeno One* 53 (3). doi: 10.20870/oeno-one.2019.53.3.2407

Schultz, H. R. (2003). Differences in hydraulic architecture account for near-isohydric and anisohydric behaviour of two field-grown vitis vinifera l. cultivars during drought. *Plant Cell Environ.* 26 (8), 1393–1405. doi: 10.1046/j.1365-3040.2003.01064.x

Schultz, H. R. (2010). Climate change and viticulture: research needs for facing the future. *J. Wine Res.* 21 (2-3), 113–116. doi: 10.1080/09571264.2010.530093

Shannon, P., Markiel, A., Ozier, O., Baliga, N. S., Wang, J. T., Ramage, D., et al. (2003). Cytoscape: a software environment for integrated models of biomolecular interaction networks. *Genome Res.* 13 (11), 2498–2504. doi: 10.1101/gr.1239303

Sommer, K., Edwards, E., Unwin, D., Mazza, M., and Downey, M. (2012). "Strategies to maintain productivity and quality in a changing environment-impacts of global warming on grape and wine production," in *Future farming systems research*, (Victoria, Australia).

Stevens, R. M., Harvey, G., and Aspinall, D. (1995). Grapevine growth of shoots and fruit linearly correlate with water stress indices based on root-weighted soil matric potential. *Aust. J. Grape Wine Res.* 1 (2), 58–66. doi: 10.1111/j.1755-0238.1995.tb00079.x

Struhl, K., and Segal, E. (2013). Determinants of nucleosome positioning. *Nat. Struct. Mol. Biol.* 20 (3), 267. doi: 10.1038/nsmb.2506

Supek, F., Bošnjak, M., Škunca, N., and Šmuc, T. (2011). REVIGO summarizes and visualizes long lists of gene ontology terms. *PloS One* 6 (7), e21800. doi: 10.1371/journal.pone.0021800

Taji, T., Ohsumi, C., Iuchi, S., Seki, M., Kasuga, M., Kobayashi, M., et al. (2002). Important roles of drought-and cold-inducible genes for galactinol synthase in stress tolerance in arabidopsis thaliana. *Plant J.* 29 (4), 417–426. doi: 10.1046/j.0960-7412.2001.01227.x

Thalmann, M., and Santelia, D. (2017). Starch as a determinant of plant fitness under abiotic stress. *New Phytol.* 214 (3), 943–951. doi: 10.1111/nph.14491

Tian, T., Liu, Y., Yan, H., You, Q., Yi, X., Du, Z., et al. (2017). agriGO v2. 0: a GO analysis toolkit for the agricultural community 2017 update. *Nucleic Acids Res.* 45 (W1), W122–W129. doi: 10.1093/nar/gkx382

Vera Alvarez, R., Pongor, L. S., Mariño-Ramírez, L., and Landsman, D. (2019). TPMCalculator: one-step software to quantify mRNA abundance of genomic features. *Bioinformatics* 35 (11), 1960–1962. doi: 10.1093/bioinformatics/bty896

Vogel, E., Donat, M. G., Alexander, L. V., Meinshausen, M., Ray, D. K., Karoly, D., et al. (2019). The effects of climate extremes on global agricultural yields. *Environ. Res. Lett.* 14 (5), 054010. doi: 10.1088/1748-9326/ab154b

Wang, Q., Zeng, X., Song, Q., Sun, Y., Feng, Y., and Lai, Y. (2020). Identification of key genes and modules in response to cadmium stress in different rice varieties and stem nodes by weighted gene co-expression network analysis. *Sci. Rep.* 10 (1), 1–13. doi: 10.1038/s41598-020-66132-4

White, M. A., Diffenbaugh, N. S., Jones, G. V., Pal, J. S., and Giorgi, F. (2006). Extreme heat reduces and shifts united states premium wine production in the 21st century. *Proc. Natl. Acad. Sci.* 103 (30), 11217–11222. doi: 10.1073/pnas.0603230103

Yang, Y., He, M., Zhu, Z., Li, S., Xu, Y., Zhang, C., et al. (2012). Identification of the dehydrin gene family from grapevine species and analysis of their responsiveness to various forms of abiotic and biotic stress. *BMC Plant Biol.* 12 (1), 140. doi: 10.1186/1471-2229-12-140

Yu, G., Wang, L. G., Han, Y., and He, Q. Y. (2012). clusterProfiler: an r package for comparing biological themes among gene clusters. *Omics: J. Integr. Biol.* 16 (5), 284–287. doi: 10.1089/omi.2011.0118

Yu, Z., Wang, X., and Zhang, L. (2018). Structural and functional dynamics of dehydrins: a plant protector protein under abiotic stress. *Int. J. Mol. Sci.* 19 (11), 3420. doi: 10.3390/ijms19113420

Zentner, G. E., and Henikoff, S. (2013). Regulation of nucleosome dynamics by histone modifications. *Nat. Struct. Mol. Biol.* 20 (3), 259. doi: 10.1038/nsmb.2470

Zhang, Y. P., Zhou, J. H., and Wang, L. (2014). Mini review roles of the bZIP gene family in rice. *Genet. Mol. res.: GMR* 13 (2), 3025–3036. doi: 10.4238/2014.April.16.11

Zhao, C., Liu, B., Piao, S., Wang, X., Lobell, D. B., Huang, Y., et al. (2017). Temperature increase reduces global yields of major crops in four independent estimates. *Proc. Natl. Acad. Sci.* 114 (35), 9326–9331. doi: 10.1073/pnas.1701762114

frontiers | Frontiers in Plant Science

TYPE Original Research
PUBLISHED 02 March 2023
DOI 10.3389/fpls.2023.1121805

OPEN ACCESS

EDITED BY
Pasala Ratnakumar,
Indian Institute of Oilseeds Research (ICAR), India

REVIEWED BY
Anita Rani Sehrawat,
Maharshi Dayanand University, India
Surendra Pratap Singh,
Indian Institute of Sugarcane Research (ICAR), India
Ashok Singamsetti,
Department of Genetics and Plant Breeding, Banaras Hindu University, India

*CORRESPONDENCE
Parvender Sheoran
parvender.sheoran@icar.gov.in
Arvind Kumar
arvind.kumar2@icar.gov.in

†PRESENT ADDRESS
Parvender Sheoran,
ICAR-Agricultural Technology Application Research Institute, Ludhiana, India

‡These authors contributed equally to this work and share first authorship

SPECIALTY SECTION
This article was submitted to Plant Abiotic Stress, a section of the journal Frontiers in Plant Science

RECEIVED 12 December 2022
ACCEPTED 07 February 2023
PUBLISHED 02 March 2023

CITATION
Kumar A, Sheoran P, Mann A, Yadav D, Kumar A, Devi S, Kumar N, Dhansu P and Sharma DK (2023) Deciphering trait associated morpho-physiological responses in pearlmillet hybrids and inbred lines under salt stress.
Front. Plant Sci. 14:1121805.
doi: 10.3389/fpls.2023.1121805

Deciphering trait associated morpho-physiological responses in pearlmillet hybrids and inbred lines under salt stress

Ashwani Kumar[1‡], Parvender Sheoran[2*†], Anita Mann[1‡], Devvart Yadav[3], Arvind Kumar[1*], Sunita Devi[1], Naresh Kumar[1,4], Pooja Dhansu[5] and Dinesh K. Sharma[1]

[1]Division of Crop Improvement, ICAR-Central Soil Salinity Research Institute, Karnal, India, [2]Division of Social Sciences Research, ICAR-Central Soil Salinity Research Institute, Karnal, India, [3]Chaudhary Charan Singh Haryana Agricultural University, Hisar, India, [4]Department of Chemistry and Biochemistry Eternal University, Baru, Sahib, India, [5]ICAR–Sugarcane Breeding Institute, Regional Center, Karnal, India

Pearl millet is a staple food for more than 90 million people residing in highly vulnerable hot arid and semi–arid regions of Africa and Asia. These regions are more prone to detrimental effects of soil salinity on crop performance in terms of reduced biomass and crop yields. We investigated the physiological mechanisms of salt tolerance to irrigation induced salinity stress (EC_{iw} ~3, 6 & 9 dSm^{-1}) and their confounding effects on plant growth and yield in pearl millet inbred lines and hybrids. On average, nearly 30% reduction in above ground plant biomass was observed at EC_{iw} ~6 dSm^{-1} which stretched to 56% at EC_{iw} ~9 dSm^{-1} in comparison to best available water. With increasing salinity stress, the crop performance of test hybrids was better in comparison to inbred lines; exhibiting relatively higher stomatal conductance (gS; 16%), accumulated lower proline (Pro; −12%) and shoot Na^+/K^+(−31%), synthesized more protein (SP; 2%) and sugars (TSS; 32%) compensating in lower biomass (AGB; −22%) and grain yield (GY: −14%) reductions at highest salinity stress of EC_{iw} ~9 dSm^{-1}. Physiological traits modeling underpinning plant salt tolerance and adaptation mechanism illustrated the key role of 7 traits (AGB, Pro, SS, gS, SPAD, Pn, and SP) in hybrids and 8 traits (AGB, Pro, PH, Na^+, K^+, Na^+/K^+, SPAD, and gS) in inbred lines towards anticipated grain yield variations in salinity stressed pearl millet. Most importantly, the AGB alone, explained >91% of yield variation among evaluated hybrids and inbreed lines at EC_{iw} ~9 dSm^{-1}. Cumulatively, the better morpho–physiological adaptation and lesser yield reduction with increasing salinity stress in pearl millet hybrids (HHB 146, HHB 272, and HHB 234) and inbred lines (H77/833–2–202, ICMA 94555 and ICMA 843–22) substantially complemented in increased plant salt tolerance and yield stability over a broad range of salinity stress. The information generated herein will help address in deciphering the trait associated physiological alterations to irrigation induced salt stress, and developing potential hybrids in pearl millet using these parents with special characteristics.

KEYWORDS

saline irrigation, salt tolerance, morpho–physiological traits, regression analysis, trait modeling, pearl millet yield

1 Introduction

Pearl millet [*Pennisetum glaucum* (L.) R. Br.] is a C4 type, small–grained cereal crop occupying ~26 million ha (m ha) area worldwide, provides food and nutritional security to millions of people inhabiting arid and semi–arid regions (Yadav et al., 2012; Shivhare and Lata, 2017). In India, pearl millet is the fourth most extensively cultivated food crop after rice, wheat and maize with 6.93 m ha area and 1.2 t ha^{-1} average productivity (Directorate of Millets Development, 2020). Being hardy and robust in nature, pearl millet could survive under multiple abiotic stresses particularly drought, heat and alkalinity/salinity (Yadav et al., 2012a; Toderich et al., 2018). Given its high nutritional (Zn and Fe) value, well balanced amino acid profile and rich source of insoluble dietary fiber, pearl millet is better suited for drier areas fulfilling both food and feed requirements. These adaptive and nutritional features make pearl millet an important crop that can effectively address the emerging and intersecting challenges of global warming, water crisis, land degradation and food-related health issues. Despite these innate benefits and exceptional buffering capacity against harsh climatic conditions, the resilience and sustainability issues in pearl millet production still demand for development of new plant types with multiple stress tolerance, efficient resource use and yield stability amidst unprecedented effects of climate change and associated environmental hazards.

Dryland salinity is one of the major abiotic constraints negatively affecting the plant growth and crop productivity. Moreover, the natural and anthropological factors and increased dependency on marginal quality underground water for irrigation further accelerates the process of soil salinization. In consequence, nearly 10 million hectares of land gets salinized every year at global scale, and if the current trend continues unabated, ~16.2 million hectares area in India only will be degraded by different degrees of soil salinization by 2050 (Sharma et al., 2015). Salinity induced changes in morpho–physiological processes cause several inhibitory effects on plant growth and development by dint of restricted nutrient uptake, partial stomata closure, unbalanced ion homeostasis and cell membrane injury, and ultimately reduced crop yields (Wang et al., 2014; Dhansu et al., 2021; Kumar et al., 2021). Identifying specific variability in these morpho-physiological characteristics associated with plant salt tolerance is highly complex; being polygenic in nature and influenced by genetic and environmental factors. Therefore, interlinking physiological basis of salt tolerance might help improve our understanding in underpinning the plant tolerance mechanisms and stabilizing crop productivity in degraded environments.

Under these circumstances, the management options including improved irrigation techniques offer tremendous potential to prevent and mitigate the adverse effects of soil salinization, but often remain prohibitively expensive. Contrarily, varietal adaptation strategy seems to be less expensive and more viable in bridging the yield gaps and harnessing the agricultural potential in stress–prone areas (Sheoran et al., 2021; Soni et al., 2021). Several studies on genotypic variability for salinity tolerance have been documented in cereal crops including pearl millet (Maiti and Satya, 2014; Shivhare and Lata, 2017). However, a better understanding of the plant physiological mechanisms governing the plant salt tolerance, prioritization of important traits of interest, and identification of superior parent lines/hybrids are of great interest in breeding programs related to marginal environments. With this hypothesis, the present investigation was carried out to define the relevance of physiological trait associated variability and their contribution in plant salt tolerance, and identify the best performing inbred lines/hybrids to stabilize pearl millet production over a broad range of irrigation induced salinity stress.

2 Material and methods

2.1 Experimental setup and treatment details

Pearl millet genotypes consisting of 10 inbred lines and 7 hybrids (Supplementary Table 1) were collected from CCS Haryana Agricultural University, Hisar, Haryana. These genotypes were evaluated under controlled conditions in factorial randomized complete block design with five replications at ICAR–Central Soil Salinity Research Institute, Karnal (29°43' N latitude, 76°58' E longitude) during kharif season of 2018-19. The seeds were sown in 20 kg capacity porcelain pots, filled with 16 kg saline soil (EC_e ~ 5.98 dSm^{-1}, bulk density: 1.45 g cc^{-1} porosity: ~40%). Nine seeds per pot were sown at 3–4 cm depth and these pots were immediately saturated with deionized water upto the field capacity (28% v/v). After 15 days of seedlings emergence, thinning was done to retain three seedlings per pot for imposing the salt stress treatments and recording biometric observations. Thereafter, the osmotic and ionic stress was imposed by applying three levels of saline irrigations as mild salinity of EC_{iw} ~3 dSm^{-1}, moderate salinity of EC 6 dSm^{-1} and high salinity of EC 9 dSm^{-1} with one additional set of plants as control irrigated with best available water (BAW) having EC_{iw} ~0.6 dSm^{-1}. Treatment–wise need based saline irrigations were applied as per crop requirement up to physiological maturity. The soil salinity was maintained through saline irrigations of EC_{iw} 3, 6, and 9 dSm^{-1} during the plant growing season. The salinity build-up during the experiment was monitored by analysis of soil EC at initial (before sowing and saline irrigation) and final (at harvesting of the crop) stages (Supplementary Figure 1). The pot house was covered with high density transparent polythene sheet to prevent the entry of rain water, and also to maintain the desired levels of salinity stress.

Abbreviations: AGB, Above ground biomass; BAW, Best available water; CC, Chlorophyll content; DMSO, Dimethyl sulphoxide; dSm^{-1}, Deci siemens per meter; E, transpiration rate; EC_e, Electrical conductivity of saturated paste extract; EC_{iw}, Electrical conductivity of irrigation water; gS, Stomatal conductance; GY, Grain yield; kg ha^{-1}, Kilogram per hectare; m ha, million hectare; MI, Membrane injury; Na^+/K^+, Sodium (Na^+) to potassium (K^+) ratio; PAR, Photosynthetically active radiations; PH, Plant height; Pn, Photosynthetic rate; Pro, Proline; ROS, Reactive oxygen species; RWC, Relative water content; SPAD, Soil plant analysis development; TSP, Total soluble protein; TSS, Total soluble sugars.

2.2 Physiological and biochemical observations and estimations

Salinity–induced changes in physiological parameters of crop growth were recorded at anthesis stage. The changes in quantitative variables; plant height (PH, cm), above ground biomass (AGB, g plant^{-1}), photosynthetic rate (Pn, µmol m^{-2} s^{-1}), stomatal conductance (gS, mol m^{-2} s^{-1}), transpiration rate (E, mmol m^{-2} s^{-1}), membrane injury (MI, %), total chlorophyll content (CC, mg g^{-1}), soil plant analysis development (SPAD) chlorophyll meter reading measuring the greenness of the leaves, relative water content (RWC, %), proline (Pro, mg g^{-1}), total soluble sugars (TSS, mg g^{-1}), total soluble protein (TSP, g g^{-1}), sodium content (Na^+, %), potassium content (K^+, %), sodium to potassium (Na^+/K^+) ratio were recorded accordingly to understand their influences on grain yield (GY, g plant^{-1}) under variable salinity stress.

2.2.1 Gas exchange parameters

The observations on gas exchange parameters; photosynthetic rate (Pn), stomatal conductance (gS) and transpiration rate (E) were recorded on five randomly tagged, fully expanded flag leaves through portable gas exchange system Infra-red gas analyzer (LICOR–6400XT, LICOR Inc., Lincoln, NE). Measurements were performed at 25°C cuvette temperature, 1100 µmol m^{-2} s^{-1} PAR, and ambient CO_2 of 400 ppm growth environments, respectively.

2.2.2 Total chlorophyll content

Total chlorophyll content was determined by incubating 100 mg flag leaf tissue in 10 ml DSMO solvent for 1 hr at 60–65°C in a water bath. After tissue decolorization, the solvent was cooled down at room temperature (for 30 min), and absorbance was measured at 665 nm and 648 nm with a UV–VIS spectrophotometer (Electronics, India). Total chlorophyll concentration was expressed as mg g^{-1} fresh weight and was estimated according to Barnes et al. (1992).

$$\text{Total chlorophyll content}\left(\text{mg g}^{-1}\right) = (7.49 * A_{665} + 20.34 * A_{648}) \times [V/(1000 * \text{W})]$$

Where, A_{665} is the absorbance measured at 665 nm wavelength, and A_{648} is the absorbance measured at 648 nm wavelength; V is the final volume of the solvent (ml); and W is the weight of leaf tissue (mg).

2.2.3 SPAD index

SPAD 502 PLUS (KONICA MINOLTA) was used to measure the SPAD readings in both control and salt treated plants. It was measured on the same leaf which was taken for chlorophyll estimation.

2.2.4 Relative water content

The representative leaf samples were collected and immediately weighed to record the fresh weight (FW). These leaves were then immersed in distilled water for 4 hrs in closed petri dishes for estimating the turgid weight (TW), and kept thereafter for drying in pre–heated hot air oven at 60°C for 72 hrs or till attainment of constant dry weight (DW). The RWC was calculated according to the formula given by Weatherley (1950).

$$\text{RWC}\ (\%) = [(\text{FW} - \text{DW})/(\text{TW} - \text{DW})] * 100$$

2.2.5 Membrane injury

Membrane injury was determined by following the method of Dionisio-Sese and Tobita (1998). The sample leaves were washed properly in distilled water and individually cut into small pieces of 1 cm size, and then immersed in 10 ml deionised water at 25°C. After 5 hrs, the electrical conductivity (EC) of the solution was measured using the EC meter (CON 700, Eutech, India) and designated as EC_a. Total rupturing of plant tissue was attained by keeping the sampled leaves in boiling water bath (100°C) for 60 min. After cooling, the EC of the solution was again measured and designated as EC_b. The MI was calculated using the following formula and expressed in per cent:

$$\text{MI}(\%) = [EC_a/(EC_a + EC_b)] * 100$$

2.2.6 Osmolytes accumulation

Fresh leaves were collected between 9–10 AM and immediately sealed in humified polythene bags, weighed and analyzed for osmolytes accumulation following the standard analytical procedures for estimation of proline (Bates et al., 1973), total soluble protein (Bradford, 1976) and total soluble sugars (Yemm and Willis, 1954).

2.2.6.1 Proline

Fresh leaves (200 mg) were homogenized in 5 ml solution of 3% sulphosalicylic acid. After centrifugation at 10,000 rpm for 10 min at 4°C, 2 ml of supernatant was added to a test tube containing 2 ml of acid ninhydrin reagent (1.25 g ninhydrin dissolved in 20 ml of 6*N* O–phosphoric acid and 30 ml of glacial acetic acid) and 2 ml of glacial acetic acid and incubated at 100°C for 1 hr. After cooling, 4 ml of toluene was added and vortexed. Absorbance was measured at 520 nm wavelength using upper phase on UV spectrophotometer (SPECORD 210 PLUS) with toluene as blank. Proline content was calculated by using the standard curve of different concentrations of L–proline.

2.2.6.2 Total soluble protein

Fresh leaves (1 g) were crushed in 2.5 ml of chilled tris buffer (pH 8.0, 0.1 M) having 0.1% PVP (polyvinyl pyrrolidone) to prepare a sample extract. A reaction mixture was prepared by adding 2.5 ml Bradford reagent (ready to use) and 50 µl of protein sample. Absorbance of the protein mixture was measured at 595 nm wavelength after 10 min and the protein content was determined using a standard curve of Bovine Serum Albumin (BSA).

2.2.6.3 Total soluble sugars

Fresh leaves (100 mg) were crushed in 2.5 ml of 80% ethanol, and centrifuged at 10,000 rpm for 10 min at 4°C. Supernatant (100

μl) was pipetted in a test tube containing 5 ml of anthrone reagent (0.4% anthrone prepared in chilled concentrated sulphuric acid) and incubated at 100°C for 10 min. Thereafter, the absorbance was measured at 620 nm wavelength on UV spectrophotometer using anthrone reagent as blank. Standard curve of D–glucose was used for calculation of total soluble sugars as mg g^{-1} FW.

2.2.7 Ionic analysis

For estimating Na^+ and K^+, fresh leaf samples were collected, washed with distilled water and then dried in oven at 70°C. Finely-grounded 100 mg sample was digested in 10 ml of HNO_3:$HClO_4$ (3:1 ratio) di–acid mixture, and the concentrations of Na^+ and K^+ were determined using NaCl and KCl as standards on flame photometer (Systronics 128, India).

2.3 Yield measurements and salinity buildup

The crop was harvested at physiological maturity when the leaves turned yellow and dried up, and the grains became hard and firm with a black spot in the hilar region. Treatment–wise earheads were harvested first, and the stalks were cut from the ground level, stacked and dried accordingly. The earheads were threshed manually to calculate the grain yields after adjusting it to 14% moisture content by measuring on the Seed moisture meter. To observe the changes in salinity buildup, the soil samples were collected and analyzed before sowing and just after crop harvest and measured in terms of EC_e (dSm^{-1}).

2.4 Data analysis

Prior to analysis, the observed and estimated values of five plants (68 data points) under each replication of the variables were tested for their normality (Q–Q plot of residuals) through Spahiro–Wilk (W) test (Shapiro and Wilk, 1965) at the 95% confidence of interval (p>0.05) (Supplementary Table 2). It is used for testing the pre-requisite hypothesis (whether the random sample drawn from a normal Gaussian probability distribution ($X \sim N(\mu,\sigma^2)$) for ANOVA or other parametric statistical analysis. The observations of nine variables (Plant height-PH, Relative water content-RWC, Photosynthetic rate-Pn, Membrane injury-MI, Proline content-Pro, sodium content-Na, potassium content-K, Na/K Ratio, above ground biomass-BM) were not following normal probability; therefore, log transformation was applied accordingly. Two–way analysis of variance (ANOVA) technique was employed to dissect the variability within genotype (G), salinity (S) and G × S effects for each test variable in Split Plot Design with three replications using the Generalized Linear Model with mixed effect through STAR statistical software (IRRI, 2013).

$$y_{i\ \ jk} = \mu + \alpha_i + \beta_j + e_{i\ \ j} + \ \beta_k + (\alpha\beta)_{jk} + \epsilon_{ijk}$$

Where, i = 3, number of blocks (replication); j = 4, Levels of salinity stress (0, 3, 6, and 9); k = 17, number of genotypes; μ = overall mean for particular variable; ρ_i = effect of block; α_j = main effect of salinity stress (fixed effect); e_{ij} = block by salinity interaction (the whole plot error, random random); β_k = main effect of genotypes (fixed); $(\alpha\beta)_{jk}$ = interaction between salinity and genotypes (fixed); ϵ_{ijk} = residual effect (subplot error) (random). (Table 1). Multiple comparisons were performed for 84 data points in hybrids and 120 data points in inbreds using Tukey's HSD test (Tukey, 1977) to determine the significant differences between treatments at 5% level of significance. Key morpho–physiological traits were prioritized separately among evaluated pearl millet hybrids and inbred through traits modeling using stepwise regression (backward elimination) approach in STAR statistical software. Pearson correlation coefficients (Pearson, 1948) were estimated to determine the association cumulatively across the irrigation induced salinity stress for evaluated parameters. Biplot analysis was performed manually through Microsoft excel 2016.

3 Results

Exposure to irrigation induced salinity stress was evaluated in terms of morphological (growth and yield) and physiological (plant water status, gas exchange, osmolytes accumulation and ionic balance) parameters of crop growth in pearl millet. Our results indicated that the effects of saline irrigation water, tested genotypes (hybrids and inbred lines) and their interactions were highly significant (p<0.01 & 0.05) for all the evaluated parameters (Table 1).

The group comparison (hybrids *vs* inbred lines) analysis (Table 2) revealed test hybrids performed better while maintaining higher stomatal conductance (gS; 16% and transpiration rate (E; 5%), lower proline accumulation (Pro; –10%) and ionic balance (Na^+/K^+ ratio; –20%) in shoot portion under prevalent salinity stress culminating in better crop performance (ABG; 368% and GY; 82%). With increasing salinity stress, significant reduction in expression of all the morphological traits was noticed where we can see more than 40% decrease in grain yield (48%) biomass (40%) in inbreds and less than 30% change in physiological traits like chlorophyll content, SPAD index, photosynthetic rate etc. Similarly, most of the physiological parameters decreased significantly, except for MI, Pro, TSP, Na^+ and Na^+/K^+, which significantly (p<0.05) increased in response to increasing salinity stress levels (Table 3).

3.1 Plant height, leaf water status and chlorophyll content

Progressive decline in plant height (PH) was noticed with each gradual increase in salinity stress; albeit to a greater extent in inbred lines compared to the hybrids. On an average, the PH reduced by 6%, 18% and 34% with irrigation water salinity (EC_{iw}) of 3, 6 and 9 dSm^{-1}, respectively (Table 3). Across salinity levels, hybrid HHB 146 attained maximum PH (137 cm) (Supplementary Figure 2) while minimum was observed in HHB 226 (124 cm). Within inbred

TABLE 1 Analysis of variance (ANOVA) for morpho–physiological traits in pearl millet under salinity stress.

Source of Variation	DF	Mean Squares							
		PH	RWC	MI	CC	SPAD	Pn	gS	E
Block	2	673.21***	109.66***	15.97^{ns}	0.19^{ns}	126.24***	0.80^{ns}	0.000^{ns}	0.10*
Salinity	3	19547.29***	3272.55***	7101.06***	2.55*	1759.32***	2512.01***	0.457***	132.84***
Error(a)	6	13.75	0.14	5.11	0.27	0.20	0.54	0.000	0.02
Genotypes	16	6076.29***	100.20***	45.18***	0.18^{ns}	134.75***	70.52***	0.023***	4.62***
Hybrids *vs* Inbreds	1	42712.86***	126.29***	79.16***	0.03^{ns}	37.13***	6.20**	0.171***	3.69***
Genotypes × Salinity	48	412.01***	21.24***	33.59***	0.05^{ns}	26.63***	27.09**	0.003***	0.47***
(Hybrids *vs* Inbreds) × Salinity	3	1598.48***	33.79***	22.80***	0.01^{ns}	96.51***	97.83***	0.003***	0.12***
Error(b)	128	5.95	0.15	0.22	0.12	0.16	0.35	0.000	0.02
		Pro	TSS	TSP	Na^+	K^+	Na^+/K^+	AGB	GY
Block	2	0.04 ^{ns}	6.59 ^{ns}	0.26 ^{ns}	0.00 ^{ns}	0.01 ^{ns}	0.00 ^{ns}	11.68***	0.14^{ns}
Salinity	3	271.79***	1278.39***	264.25***	2.64***	5.82***	0.17***	4931.78***	605.03***
Error(a)	6	0.06	15.88	0.47	0.00	0.01	0.00	0.48	0.10
Genotypes	16	2.40***	85.24***	30.27***	0.60***	7.22***	0.04***	523.79***	95.07***
Hybrids *vs* Inbreds	1	14.28***	0.01^{ns}	39.02***	0.56***	21.39***	0.03***	3439.36***	1009.08***
Genotypes × Salinity	48	0.14***	20.36***	9.73***	0.64***	4.33***	0.04***	71.66***	5.04***
(Hybrids *vs* Inbreds) × Salinity	3	0.32***	40.05***	11.90***	0.06***	7.62***	0.01***	147.68***	16.39***
Error(b)	128	0.02	0.38	0.19	0.00	0.02	0.00	0.10	0.05

***significant at p<0.001; **significant at p<0.01; *significant at p<0.05; ns, non–significant; DF, degree of freedom; PH, plant height (cm); RWC, relative water content (%); MI, membrane injury (%); CC: chlorophyll content (mg g^{-1}), SPAD, soil plant analysis development (SPAD) chlorophyll meter reading; Pn, photosynthetic rate (μmol m^{-2} s^{-1}); gS, stomatal conductance (mol m^{-2} s^{-1}); E, transpiration rate (mmol m^{-2} s^{-1}); Pro, proline content (mg g^{-1}); TSP: total soluble protein (mg g^{-1}); SS, total soluble sugars (mg g^{-1}); Na^+, sodium content (%); K^+, potassium content (%); Na^+/K^+, sodium to potassium ratio; AGB, above ground biomass (g $plant^{-1}$); GY, grain yield (g $plant^{-1}$).

lines, the PH ranged from 64 cm (HMS 7A) to 124 cm (ICMA 97111) (Table 4).

Increasing salt concentration reduced the leaf relative water content (RWC); being 91.5% in control treatment which gets decreased to 73.0% at EC_{iw} ~9 dSm^{-1} (Table 3). Genotypic variations and their differential response to irrigation induced salinity stress also revealed significant differences in leaf RWC; remained highest in inbred lines HMS 7A (90%) and HBL–11 (87%) compared to hybrids HHB 272, HHB 226 and HHB 146 (85%) (Table 4).

In the present study, salinity stress caused membrane injury (MI) to the extent of 11%, 21% and 35% with saline irrigation of EC_{iw} ~3, 6 and 9 dSm^{-1}, respectively in comparison to control (Table 3). In general, the pearl millet inbred lines were less prone to oxidative damage (MI) with increasing salt stress than hybrids. Wide variations in MI was noticed due to irrigation induced salinity stress (Table 4); where, only 6 inbred lines (ICMA 97111, ICMA 94555, HMS 7A, ICMA 95222, HBL11, HTP 94154) and 3 hybrids (HHB 146, HHB 197, HHB 223) had MI <19% (the mean value of MI across salinity stresses). Lowest MI was observed in HTP 94/54 (15%) while the highest in HMS 47A (22%).

Chlorophyll content (CC), an important trait affecting the photosynthetic capacity of plant tissues, showed significant reductions of 16%, 24% and 39% when irrigated with saline water (EC_{iw}) of 3, 6 and 9 dSm^{-1}, respectively in comparison to control (Table 3). The highest CC was observed in HHB 226 (1.32 mg g^{-1}) followed by HHB 272 (1.15 mg g^{-1}) and HBL 11, H77/833–2–2 (1.14 mg g^{-1}), while the total chlorophyll content ranging between 0.85–0.95 mg g^{-1} was observed in others, HHB 223, HHB 234, HHB 146, HMS 7A and ICMA 843–2 (Table 4). Highest SPAD value was observed in inbred line ICMA 97111 followed by hybrid line HHB 272 (Table 4). Similar to chlorophyll content, SPAD values also decreased with increasing levels of salinity with significant changes in range of 8.5 -12.5% (Table 3). In hybrids, the SPAD values decreased by 30% whereas in inbred lines 35% reduction was observed (Table 2).

3.2 Gas exchange parameters

Plants exposure to salinity stress exhibited significant changes in gas exchange parameters elucidating 54% reduction in photosynthetic rate (Pn), 44% reduction in stomatal conductance (gS) and 48% reduction in transpiration rate (E) at EC_{iw} ~9 dSm^{-1} (Table 3). Differential genotypic responses to gas exchange parameters were noticed among evaluated pearl millet genotypes. Notably, only four hybrids (HHB 226, HHB 197, HHB 146, HHB 67 Improved) and two inbred lines (AC 04–13 and ICMA 94555) had cumulative response more than their average values of Pn >21.4 μmol m^{-2} s^{-1}, gS >0.40 mol m^{-2} s^{-1} and E >6.01 mmol m^{-2} s^{-1}. The

TABLE 2 Effects of salinity stress on various traits in pearl millet hybrids and inbreds through group comparison analysis (averaged across 7 hybrids and 10 inbred lines).

Traits	Units	Hybrids		Inbreds		F_{cal}	$p>$ (F)
		Mean	% change over control	Mean	% change over control		
Plant height (PH)	cm	128.8 ± 12.9	-11.04	96.7 ± 30.8	-25.82	7178.4	0.0000
Relative water content (RWC)	%	82.9 ± 8.4	-12.44	84.1 ± 7.5	-10.84	838.9	0.0000
Membrane injury (MI)	%	19.5 ± 11.2	-27.26	18.40 ± 10.6	-25.88	355.6	0.0000
Chlorophyll content (CC)	mg g^{-1} FW	1.09± 0.39	-20.49	1.08± 0.38	-14.05	0.30	0.5874
SPAD	–	46.5 ± 7.5	-30.11	45.5 ± 5.9	-35.38	236.4	0.0000
Photosynthetic rate (Pn)	µmol CO_2 m^{-2} s^{-1}	20.8 ± 5.9	-23.48	21.7 ± 7.7	-31.66	17.7	0.0000
Stomatal conductance (gS)	mol H_2O m^{-2} s^{-1}	0.43± 0.08	-28.85	0.37± 0.10	-31.08	1835.6	0.0000
Transpiration rate (E)	mmol H_2O m^{-2} s^{-1}	6.18± 1.50	196.59	5.90± 1.61	150.77	152.4	0.0034
Proline content (Pro)	mg g^{-1} FW	5.19	3.86± 2.08	177.96	681.0	0.0000	
Total soluble sugars (TSS)	mg g^{-1} FW	17.8 ± 4.2	111.75	17.4 ± 6.4	124.76	0.03	0.8695
Total soluble protein (TSP)	mg g^{-1} FW	10.3 ± 2.8	9.94	10.9 ± 3.0	-15.07	203.8	0.0000
Sodium content (Na^+)	%	0.36± 0.51	96.12	0.50± 0.47	201.37	1307.2	0.0000
Potassium content (K^+)	%	4.76± 0.74	56.18	5.52± 1.51	36.85	893.8	0.0000
Sodium to potassium ratio (Na^+/K^+)	–	0.08± 0.11	-28.19	0.10± 0.13	-34.41	1442.4	0.0000
Above ground biomass (AGB)	g $plant^{-1}$	36.8 ± 8.4	-24.36	27.1 ± 11.7	-40.5	33610.9	0.0000
Grain yield (GY)	g $plant^{-1}$	10.9 ± 3.8	-35.7	6.0± 3.1	-48.75	18444.5	0.0000

Soil Plant Analysis Development (SPAD) chlorophyll meter reading; Data represents mean value of 30 pooled measurements (4 levells of salinity × 3 plants per pot × 5 replications); ± indciate standard deviation from the mean value.Negative sign in percent cahnge values shows decrease w.r.t control.

TABLE 3 Effect of salinity stress on morpho–physiological attributes of crop growth and yield in pearl millet (averaged across 7 hybrids and 10 inbred lines).

Irrigation water salinity	Traits							
	PH	RWC	MI	CC	SPAD	Pn	gS	E
BAW	128.35^a	91.48^a	8.32^d	1.35^a	52.54^a	28.46^a	0.50^a	7.77^a
EC_{iw} ~3 dSm^{-1}	121.31^a	87.68^b	11.35^c	1.09^b	48.41^b	25.67^b	0.44^b	6.72^b
EC_{iw} ~6 dSm^{-1}	105.74^b	82.16^c	21.18^b	1.09^b	43.78^c	18.17^c	0.36^c	5.55^c
EC_{iw} ~9 dSm^{-1}	84.18^c	73.03^d	34.51^a	0.8^c	38.93^d	13.08^d	0.28^d	4.01^d
	Pro	TSS	TSP	Na^+	K^+	Na^+/K^+	AGB	GY
BAW	1.49^d	8.03^d	23.07^a	0.23^c	5.48^a	0.04^b	41.39^a	11.67^a
EC_{iw} ~3 dSm^{-1}	2.55^c	9.88^c	18.71^b	0.30^{bc}	5.17^{ab}	0.06^b	35.49^b	9.54^b
EC_{iw} ~6 dSm^{-1}	3.94^b	13.39^a	17.45^b	0.49^b	5.42^a	0.10^b	29.00^c	7.16^c
EC_{iw} ~9 dSm^{-1}	6.82^a	11.43^b	10.96^c	0.74^a	4.74^b	0.17^a	18.43^d	3.63^d

Means followed by similar lowercase letter within a column for a partiuclar trait are not statistically significant ($p<0.05$) using Tukey's HSD test; Data represents mean value of 255 pooled measurements (17 genotypes × 3 plants per pot × 5 replications); BAW, best available water; EC_{iw}, electrical conductivity of irrigation water; dSm^{-1}, deci siemens per meter; PH, plant height (cm); RWC, relative water content (%); MI, membrane injury (%); CC, chlorophyll content (mg g^{-1}), SPAD, soil plant analysis development (SPAD) chlorophyll meter reading; Pn, photosynthetic rate (µmol m^{-2} s^{-1}); gS, stomatal conductance (mol m^{-2} s^{-1}); E, transpiration rate (mmol m^{-2} s^{-1}); Pro, proline content (mg g^{-1}); TSP, total soluble protein (mg g^{-1}); TSS, total soluble sugars (mg g^{-1}); Na^+, sodium content (%); K^+, potassium content (%); Na^+/K^+, sodium to potassium ratio; AGB, above ground biomass (g $plant^{-1}$); GY, grain yield (g $plant^{-1}$).

highest Pn of >24 μmol m^{-2} s^{-1} was observed in inbred lines ICMA 97111 and ICMA 94555 (Table 4). Due apparently, the evaluated hybrids had lower photosynthetic rate than the inbred lines.

3.3 Osmolyte accumulation

Increasing salinity stress triggered the accumulation of proline (Pro), total soluble protein (TSP) and total soluble sugars (TSS). On an average, 1.7, 2.6 and 4.6–fold increase in Pro accumulation was observed at EC_{iw} ~3, 6 and 9 dSm^{-1}, respectively as against the mean value of 1.5 mg g^{-1} in control treatment (Table 3). By comparison, pearl millet inbred lines showed higher Pro accumulation (3.2–4.2 mg g^{-1}) than the hybrids (2.9–3.9 mg g^{-1}). All the inbred lines except ICMA 95222 and 3 hybrids (HHB 223, HHB 234 and HHB 146) had Pro content >3.7 mg g^{-1} (mean value across salinity stress). The maximum Pro of 4.32 mg g^{-1} was observed in inbred line HMS 47A. Similarly, maximum TSP was observed in HMS 7A (14.2 mg g^{-1}) followed by H77/833–2–202, HMS 47A and ICMA 95222 (>12 mg g^{-1}). Plants accumulated higher TSP with increasing salinity stress; being 23% higher at EC_{iw} ~3 dSm^{-1} and 67% higher at EC_{iw} ~6 dSm^{-1}. However, further increase in salinity stress (EC_{iw} ~9 dSm^{-1}) caused reduction in TSP compared to preceeding level but it was relatively higher (42%) than the control. Under stress conditions, the TSS decreased by 59%, 71% and 159% at EC_{iw} of 3, 6 and 9 dSm^{-1}, respectively (Table 4).

3.4 Ionic balance

Salinity stress increased shoot Na^+ concentration to the extent of 0.30%, 0.49% and 0.73% with saline water irrigations of EC_{iw} ~3, 6 and 9 dSm^{-1}. No significant changes were observed for K^+ content upto EC_{iw} ~6 dSm^{-1}; however, further increase in salinity stress

TABLE 4 Mean response of evaluated hybrids and inbred lines for plant water relations, gas exchange, osmolyte accumulation, ionic balance and yield parametes in pearl millet (averaged across salinity levels).

Traits	PH	RWC	MI	CC	SPAD	Pn	gS	E	Pro	TSP	TSS	Na^+	K^+	Na^+/K^+	AGB	GY
Hybrids																
HHB 67 Improved	128.0^{cd}	78.9^{c}	20.4^{b}	1.06^{c}	44.3^{d}	23.6^{a}	0.46^{a}	6.51^{a}	2.85^{e}	8.31^{d}	17.19^{d}	0.54^{b}	5.01^{a}	0.106	32.8^{e}	10.0^{e}
HHB 146	137.3^{a}	85.7^{a}	17.3^{d}	0.93^{a}	43.9^{d}	22.2^{b}	0.45^{a}	6.59^{a}	3.93^{a}	9.81^{c}	19.25^{ab}	0.16^{e}	5.02^{a}	0.032^{f}	40.3^{b}	12.4^{b}
HHB 197	129.5^{bc}	79.5^{c}	17.7^{cd}	1.05^{a}	48.2^{b}	21.2^{c}	0.46^{a}	6.23^{b}	3.52^{c}	11.20^{a}	18.39^{bc}	0.86^{a}	4.44^{c}	0.190^{a}	32.4^{e}	9.1^{f}
HHB 226	124.1^{d}	85.9^{a}	20.5^{b}	1.32^{a}	46.9^{c}	22.4^{b}	0.44^{b}	6.51^{a}	3.38^{d}	10.31^{bc}	19.99^{a}	0.23^{d}	4.27^{d}	0.056^{d}	34.1^{d}	9.4^{f}
HHB 223	124.4^{d}	82.3^{b}	18.3^{c}	0.85^{a}	43.3^{e}	18.1^{d}	0.38^{d}	5.92^{c}	3.76^{b}	10.81^{ab}	18.24^{c}	0.23^{d}	5.08^{a}	0.040^{e}	37.4^{c}	10.7^{d}
HHB 234	133.0^{ab}	82.2^{b}	21.5^{a}	0.93^{a}	47.4^{c}	16.9^{e}	0.41^{c}	5.86^{c}	3.93^{a}	10.69^{ab}	15.75^{e}	0.36^{c}	4.78^{b}	0.074^{c}	43.2^{a}	12.9^{a}
HHB 272	125.1^{cd}	85.7^{a}	20.5^{b}	1.15^{a}	50.7^{a}	21.0^{c}	0.41^{c}	5.64^{d}	2.88^{e}	11.05^{a}	15.50^{e}	0.18^{e}	4.74^{b}	0.038^{ef}	37.3^{c}	11.9^{c}
Inbred lines																
ICMA 97111	123.9^{a}	82.9^{e}	15.6^{e}	1.07^{a}	51.9^{a}	24.1^{ab}	0.42^{a}	5.99^{c}	4.02^{bcd}	8.84^{d}	15.24^{e}	0.64^{c}	4.72^{f}	0.134^{c}	29.1^{c}	6.5^{c}
ICMA 843-22	84.0^{f}	81.2^{g}	19.6^{c}	0.96^{a}	46.2^{e}	22.5^{cd}	0.38^{cd}	6.78^{a}	4.05^{abc}	10.83^{c}	15.87^{de}	0.43^{f}	5.01^{ef}	0.081^{f}	32.0^{b}	6.0^{d}
ICMA 94555	76.4^{g}	81.9^{f}	17.6^{d}	1.00^{a}	43.8^{g}	25.1^{a}	0.40^{b}	6.95^{a}	3.85^{d}	8.43^{d}	16.70^{d}	0.32^{h}	6.02^{b}	0.048^{h}	28.5^{d}	6.1^{d}
HMS 7A	64.3^{h}	80.8^{g}	18.0^{d}	0.95^{a}	46.8^{d}	22.3^{cd}	0.36^{ef}	5.79^{c}	4.16^{ab}	14.16^{a}	18.18^{c}	0.39^{g}	5.30^{de}	0.087^{ef}	26.6^{f}	6.0^{d}
HMS 47A	90.8^{e}	90.0^{a}	22.2^{a}	1.06^{a}	41.4^{h}	18.3^{f}	0.34^{f}	4.90^{e}	4.23^{a}	12.19^{b}	24.02^{a}	0.79^{a}	5.36^{cd}	0.216^{a}	18.3^{i}	4.1^{f}
ICMA 95222	119.8^{b}	82.9^{e}	18.0^{d}	1.01^{a}	41.3^{h}	22.7^{cd}	0.39^{bc}	6.04^{c}	3.18^{e}	12.16^{b}	15.47^{e}	0.76^{b}	5.66^{c}	0.169^{b}	34.8^{a}	7.9^{a}
HBL 11	80.1^{g}	87.3^{b}	18.0^{d}	1.14^{a}	49.5^{b}	17.4^{f}	0.30^{g}	5.27^{d}	4.1^{abc}	11.07^{c}	21.46^{b}	0.20^{i}	5.03^{ef}	0.039^{i}	21.6^{h}	4.7^{e}
H77/833-2-202	106.7^{d}	83.7^{d}	19.4^{c}	1.14^{a}	45.1^{f}	22.0^{d}	0.37^{de}	6.02^{c}	3.94^{cd}	12.46^{b}	18.36^{c}	0.46^{e}	5.52^{cd}	0.089^{e}	29.0^{c}	7.3^{b}
AC 04-13	106.3^{d}	85.2^{c}	20.3^{b}	1.03^{a}	48.4^{c}	23.2^{bc}	0.40^{b}	6.49^{b}	3.92^{cd}	10.83^{c}	12.89^{f}	0.56^{d}	7.70^{a}	0.071^{g}	27.8^{e}	6.5^{c}
HTP 94/54	114.4^{c}	84.9	15.3^{e}	1.03^{a}	40.4^{i}	19.9^{e}	0.35^{f}	4.76^{e}	3.16^{e}	8.43^{d}	15.84^{de}	0.42^{f}	4.83^{f}	0.116^{d}	23.3^{g}	4.7^{e}

Means followed by at least one letter common (for hybrids and inbred lines) are not statistically significant ($p<0.05$) using Tukey's HSD test; PH, plant height (cm); RWC, relative water content (%); MI, membrane injury (%); CC, chlorophyll content (mg g^{-1}), Pn, photosynthetic rate (μmol m^{-2} s^{-1}); gS, stomatal conductance (mol m^{-2} s^{-1}); E, transpiration rate (mmol m^{-2} s^{-1}); Pro, proline content (mg g^{-1}); TSP, total soluble protein (mg g^{-1}); TSS, total soluble sugars (mg g^{-1}); Na^+, sodium content (%); K^+, potassium content (%); Na^+/K^+, sodium to potassium ratio; AGB, above ground biomass (g $plant^{-1}$); GY, grain yield (g $plant^{-1}$).

(EC_{iw} ~9 dSm^{-1}) reduced K^+ content by 13.5% (Table 3). Wide variations in shoot Na^+ was observed in evaluated genotypes; notably only one inbred line (HBL 11) and 4 hybrids (HHB 146, HHB 223, HHB 226 and HHB 272) had Na^+ accumulation <0.23%. It is interesting to note that inbred lines showed more K^+ affinity than the hybrids. Within inbred lines, highest K^+ accumulation was observed in AC 04–13 (7.7%) and lowest in ICMA 97111 (4.7%). All inbred lines except HTP 94/54 and ICMA 843–22 had shoot K^+ >5.2%, the average value across variable salinity stress. Among hybrids, HHB 223 had the highest K^+ accumulation (5.1%) while lowest was recorded in HHB 226 (4.3%). Evidently, none of the hybrid showed K^+ accumulation more than 5.2% (Table 4). Out of 17 genotypes, two hybrids (HHB 67 Improved and HHB 234) and three inbred lines (HMS 7A, HMS 47A and ICMA 95222) showed increasing Na^+/K^+ trend with increasing stress intensity, while rest exhibited a gradual increase only upto EC_{iw} 6 ~dSm^{-1} and a declining trend was observed thereafter.

3.5 Yield assessment

Plants exposure to salinity stress negatively affected the above ground biomass (AGB) accumulation. Compared to the control, the crop biomass production reduced by 17%, 40% and 65% across inbred lines, and 12%, 18% and 43% across hybrids with saline water irrigations of EC_{iw} ~3, 6 and 9 dSm^{-1}, respectively (Figure 1). Five inbred lines (ICMA 94555, ICMA 95222, H7/822–2–202, HMS 7A and ICMA 97111) had biomass reduction upto 30% at EC_{iw} ~6 dSm^{-1}, while this reduction stretched between 39–90% at higher salinity stress of EC_{iw} ~9 dSm^{-1}. Within inbred lines, lowest biomass reduction was noticed for H77/833–2–202 (39%), followed by ICMA 94555 (40%), ICMA 97111 (42%) and ICMA 843–22 (48%). Most of the evaluated hybrids performed equally well upto EC_{iw} 6 dSm^{-1} attaining 31–43 g $plant^{-1}$ dry biomass. Further increase in salinity stress had more pronounced effect on biomass reduction, except HHB 223, HHB 234 and HHB 272 for which <30% biomass reduction was noticed even when irrigated with EC_{iw} of 9 dSm^{-1} (Figure 1).

Experimental results indicated that the test genotypes displayed significant variability ($p<0.0001$) for grain yield in response to irrigation induced salinity stress (Figure 1). On an average, substantial yield reductions to the tune of 18%, 41% and 70% with saline water irrigations of EC_{iw} ~3, 6 and 9 dSm^{-1}, respectively were observed; albeit to a greater extent in inbred lines compared to hybrids. On an average, hybrids produced 10.8–16.2 g $plant^{-1}$ grain yield at EC_{iw} ~3 dSm^{-1}, 7.7–12.9 g $plant^{-1}$ at EC_{iw} ~6 dSm^{-1} and 3.4–7.4 g $plant^{-1}$ at EC_{iw} ~9 dSm^{-1} (Figure 1). At higher salinity stress (EC_{iw} ~9 dSm^{-1}), HHB 146 produced the highest grain yield (7.4 g $plant^{-1}$) followed by HHB 223 (7.2 g $plant^{-1}$), HHB 272 and HHB 234 (6.8 g $plant^{-1}$) More importantly, the proportionate yield reductions remained <40% in the sequence of HHB 223 (39%) <HHB 234 (33%) <HHB 272 (29%) <HHB 146 (28%) when

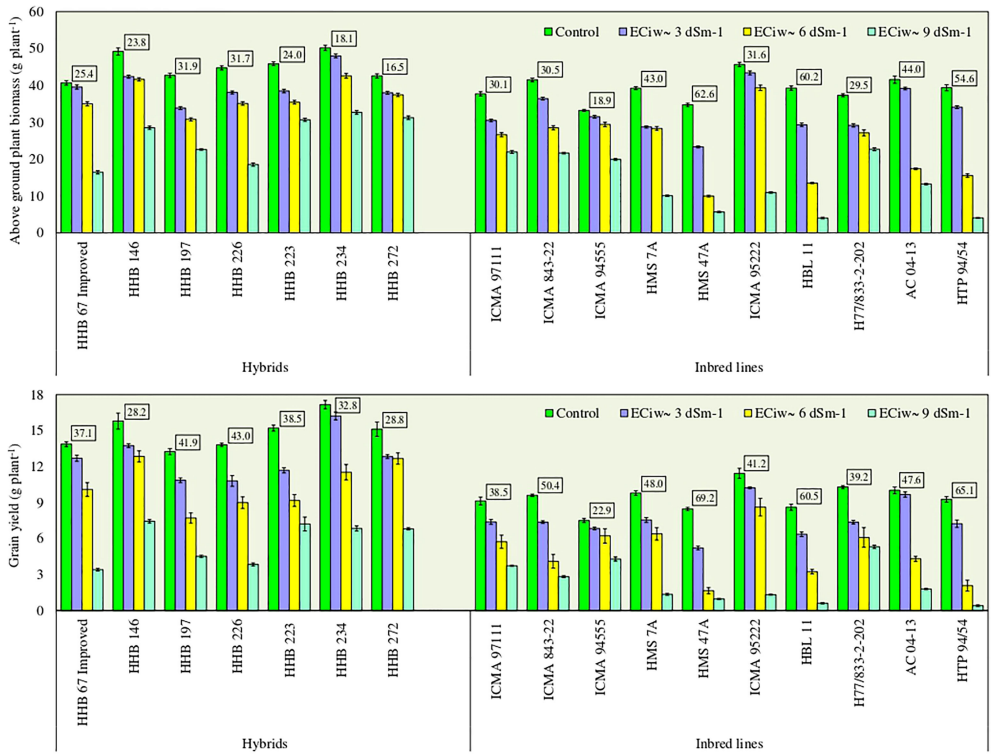

FIGURE 1
Effect of irrigation induced salinity stress on above ground plant biomass (AGB; g $plant^{-1}$) and grain yield (GY; g $plant^{-1}$) in pearl millet hybrids and inbred lines. Data represents mean value of 15 pooled measurements (3 plants per pot x 5 replications). Vertical bars labelled with boxes represent mean per cent reduction in AGB and GY due to salinity stress (averaged acrossed EC_{iw} of 3, 6 and 9 dS m^{-1}) in comparison to control treatment receiving best available water (EC_{iw}-0.6 dS m^{-1}). Capped lines represent ± standard error of the mean values.

compared with their yields obtained at control. Conversely, inbred lines displayed higher yield reductions of 20% at EC_{iw} ~3 dSm^{-1}, 49% at EC_{iw} ~6 dSm^{-1} and 76% at EC_{iw} ~9 dSm^{-1} (Figure 1). Across inbred lines, grain yield ranging between 1.7–8.6 g $plant^{-1}$ with mean yield of 4.8 g $plant^{-1}$ at EC_{iw} ~6 dSm^{-1} and 0.4–5.3 g $plant^{-1}$ with mean yield of 2.3 g $plant^{-1}$ at EC_{iw} ~9 dSm^{-1} was recorded. Similar to biomass trend, lowest yield reduction was noticed in ICMA 94555, followed by ICMA 97111, H77/833–2–202 and ICMA 95222.

3.6 Biplot analysis

A biplot between estimated grain yields and Na^+/K^+ ratio at EC_{iw} 9 dSm^{-1} illustrated that 4 pearl millet hybrids HHB 234, HHB 272, HHB 223 and HHB 146 exhibited better crop performance with low Na^+/K^+ accumulation in comparison to others (Figure 2); indicating their better adapatability and ion homeostasis in response to salinity stress. Similarly, only 2 inbred lines H77/833–2–202 and ICMA 94555 performed equally well at EC_{iw} 9 dSm^{-1} with yield ranging from 4–6 g $plant^{-1}$ and lower Na^+/K^+ ratio (Figure 2). Osmolyte accumulation measured in terms of proline content showed that pearl millet hybrids HHB 234, HHB 272, HHB 223, HHB 197 and HHB 146, and inbred lines H77/833–2–202 and ICMA 94555 had higher osmolyte accumulation under higher salinity stress (Figure 2). Seven genotypes; including 2 inbred lines (H77/833–2–202 and ICMA 94555) and 5 hybrids (HHB 146, HHB 226, HHB 272, HHB 197 and HHB 67 Improved) confirmed their better adaptation to saline conditions showing relatively better stomatal conductance and yield performance at higher salinity stress (Figure 2). For biomass accumulation, a key fodder trait; 5 hybrids (HHB 146, HHB 197, HHB 223, HHB 234, HHB 272) and 2 inbred lines (ICMA 94555 and H77/833–2–202) showed their superiority producing higher biomass yield even at higher salinity stress of EC_{iw} ~9 dSm^{-1} (Figure 2).

3.7 Physiological traits association and trait modeling for higher grain yield under salinity stress

Correlation matrix showing the association between different morpho-physiological traits of interest and the final output revealed a positive association of pearl millet yield with most of the evaluated parameters except for Na^+, Na^+/K^+, Pro, MI and TSP (Figure 3). A strong and significant correlation was noticed between grain yield with AGB (0.93**), gS and E (>0.70**) and Pro (–0.74**) reflecting the influence of trait associated adaptation strategies to induced salinity stress, and their confounding effect on crop harvest. It was interesting to note a strong association between Na^+ and Na^+/K^+ (0.95**), Pn, gS and E (>0.80**), RWC and MI (–0.80**) indicating a strong inter–dependence among physiological parameters of crop growth. Furthermore, a negative association of all the physiological traits was observed with shoot Na^+ except MI and Pro which further increased with increasing levels of salinity. Inclusively, the trait association analysis revealed that most of the physiological traits were directly related to yield, and any deviation/disturbance in these traits led to decline in corresponding yield. The similar pattern of inter-trait associations were observed in inbreeds as well in hybrids except potassium content (K), which is significantly associated with the studied traits in inbreeds lines, but not in case of hybrids (Supplementary Table 3). Furthermore, all the studied traits (RWC,

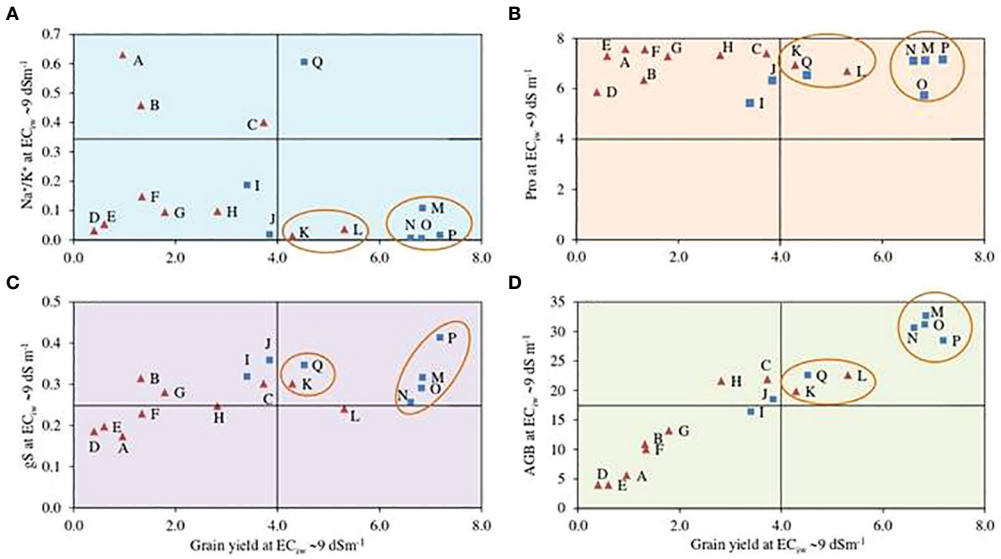

FIGURE 2
Biplots representing the interaction of important physiological traits; **(A)** sodium to potassium (Na^+/K^+) ratio, **(B)** proline content (Pro; mg g^{-1}), **(D)** above ground biomass (AGB; g $plant^{-1}$) and **(C)** stomatal condcutance (gS; mol m^{-2} s^{-1}) with grain yield (GY; g $plant^{-1}$) of pearl millet hybrids (blue □) and inbred lines (red Δ) at EC_{iw} -99 dSm^{-1}. Data represents mean value of 15 pooled measurements (3 plants per pot x 5 replications); A: HMS 47A; B: ICMA 95222; C: ICMA 971ll; D: HTP 94/54; E: HBL 11; F: HMS 7A; G: AC04-13; H: ICMA 843-22; I: ICMA 94555; J: H77/833-2-202; K: HHB 67 Improved; L: HHB 226; M: HHB 234; N: HHB 223; O: HHB 272; P: HHB 146; Q: HHB 197.

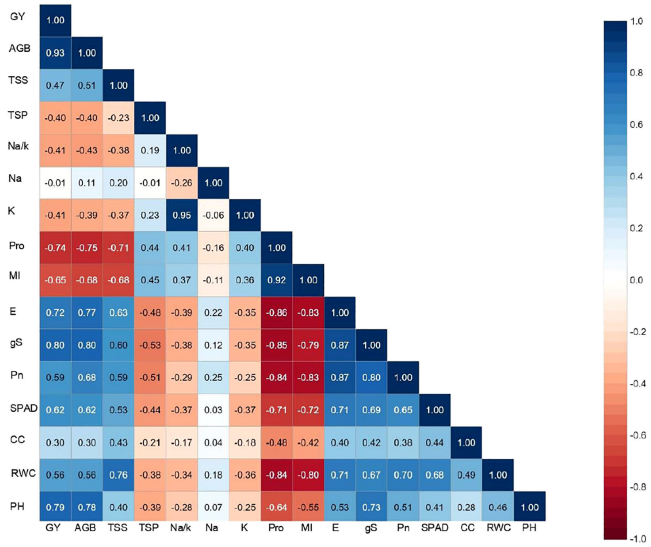

FIGURE 3
Traits association among morpho-physiological and yield parameters under irrigation induced salinity stress in pearl millet (averaged across evaluated hybrids and inbred lines). PH, plat height; RWC, relative water content; MI, membrane injury; CC; chlorophyll content; SPAD, soil plant analysis development (SPAD) chlorophyll meter reading; Pn, photosynthetic rate; gS, stomatal conductance; E, transpiration rate; Pro, proline; SP, soluble proteins; SS, soluble sugars; Na, sodium content; K, potassium content; Na/K, sodium to potassium ratio; AGB, above ground biomass.

CC, SPAD, Pn, gS, E, MI, Pro, Na, K, Na/K, PRT, TS, BM) showed significant association with grain yield (Y) in control condition in both hybrids and inbreed lines, however, in salinity stress only seven physiological traits i.e. RWC, gS, E, Pro, Na, Na/K and BM were significantly associated (Supplementary Table 4).

To select the model physiological traits contributing maximum towards grain yield variations at higher salinity stress (EC_{iw} ~9 dSm^{-1}), a stepwise regression approach (backward selection) was performed (Supplementary Table 5). The regression analysis indicated that a total of 7 traits (AGB, Pro, TSS, gS, SPAD, Pn, and TSP) in hybrids and 8 traits (AGB, Pro, PH, Na^+, K^+, Na^+/K^+, SPAD, and gS) in inbred lines significantly contributed towards grain yield variations in pearl millet (Table 5; Supplementary Table 6). It was interesting to note that above ground biomass (AGB) alone could justify >91% of grain yield variation in hybrids and inbreed lines at EC_{iw} ~9 dSm^{-1}. Explicator traits such as Na^+, K^+ and Na^+/K^+ could only be utilized for the screening of inbred lines while AGB, Pro, gS and SPAD have higher weightage for pearl millet genotypes (inbred/hybrid) screening.

3.8 Genotypic ranking for salinity tolerance

With the help of estimated regression coefficients of resp nbred lines and hybrids.

Grain yield for inbred lines

$$= -6.56 + 0.014 \times PH + 0.031 \times SPAD + 3.418 \times gS + 0.156 \times Pro + (-3.598) \times Na^+ + 0.288 \times K^+ + 12.065 \times Na^+/K^+ + 0.222 \times AGB$$

Grain yield for hybrids

$$= -1.520 + (-0.050) \times SPAD + 0.050 \times Pn + 8.750 \times gS + (-0.440) \times Pro + 0.050 \times TSP + (-0.180) \times TSS + 0.380 \times AGB$$

Based on predicted yields and resultant ranking, 3 pearl millet hybrids; HHB 146, HHB 272, and HHB 234 and 3 inbred lines; H77/833–2–202, ICMA 94555 and ICMA 843–22 had relatively higher ranking; suggesting that they would be more tolerant to irrigation induced salinity stress (Supplementary Table 7A–D). Conversely, HHB 226, HHB 67 Improved, and HHB 197 among evaluated hybrids, and HBL 11, HTP 94/54 and HMS 47A among inbred lines ranked lower and were found to be more sensitive to salt stress.

4 Discussion

The adverse effects of salinity and associated plant traits for tolerance have always been a researchable issue for plant scientists for development of better performing plant types. Herein, we evaluated the pearl millet hybrids and inbred lines for their response to saline irrigations, and identify key contributing traits for enhanced plant salt tolerance. In the present study, the genotypic differences within evaluated genotypes, and their consequent response to irrigation induced salinity stress led to alterations in plant morpho–physiological parameters of crop growth and their confounding effect on final harvest. Herein, the salinity induced reductions in plant height may be attributed to reduced osmotic pressure resulting in restricted water and nutrient

TABLE 5 Traits modeling for salinity tolerance in pearl millet through multiple linear regressions approach.

Dependent Variable	Steps and Variables	C(p)	R^2-value	Adjusted R^2-value
	Hybrids			
GY	AGB	140.412	91.46	91.35
	Pro + AGB	51.497	94.98	94.86
	Pro + TSS + AGB	30.916	95.86	95.70
	gS + Pro + TSS + AGB	14.941	96.55	96.38
	SPAD + gS + Pro + TSS + AGB	9.538	96.84	96.64
	SPAD + Pn + gS + Pro + TSS + AGB	7.772	96.99	96.75
	SPAD + Pn + gS + Pro + TSP + TSS + AGB	8.000	97.05	96.78
	Inbred lines			
GY	AGB	68.358	94.10	94.05
	Pro + AGB	49.566	94.77	94.68
	PH + Na^+ + AGB	33.343	95.35	95.23
	Na^+ + K^+ + Na^+/K^+ + AGB	26.000	95.65	95.50
	PH + Na^+ + K^+ + Na^+/K^+ + AGB	11.693	96.17	96.00
	PH + SPAD + Na^+ + K^+ + Na^+/K^+ + AGB	8.396	96.34	96.15
	PH + SPAD + gS + Na^+ + K^+ + Na^+/K^+ + AGB	8.997	96.39	96.16
	PH + SPAD + gS + Pro + Na^+ + K^+ + Na^+/K^+ + AGB	9.000	96.45	96.19

Mallows' Cp Criterionis a way to assess the fit of a multiple regression model; Smaller Cp values are better as they indicate smaller amounts of unexplained error; GY, grain yield; AGB, above ground biomass; Pro, proline content; TSP, total soluble protein; TSS, total soluble sugars; PH, plant height; Na^+, sodium content; K^+, potassium content; Na^+/K^+, sodium to potassium ratio; SPAD, soil plant analysis development (SPAD)chlorophyll meter reading; gS, Stomatal conductance.

uptake by the growing plants. Leaf RWC that generally represent the plant water status, declined substantially with stress mediated stomatal closure and restricted water loss from transpirational pathways compromising the leaf turgor (Polash et al., 2018). These variations in evaluated pearl millet genotypes could presumably be due to repressive effects of higher ion accumulation and hyper–osmotic stress on root hydraulic conductance and accelerated water loss from the leaf tissues (Dhansu et al., 2021; Sheoran et al., 2021). Earlier studies have also reported efficient water conservation system in pearl millet by means of lowering the leaf transpiration rate and reducing leaf area; hence, improved transpiration efficiency, plant water relations (RWC) and membrane stability under stress conditions (Vijayalakshmi et al., 2012; Reddy et al., 2022; Sheoran et al., 2022).

Salinity stress negatively affects both of the photosystems (PS I and PS II) and chlorophyll content (CC), owing to excessive accumulation of Na^+ and Cl^- in the leaf tissues. This PS II mainly binds chlorophyll pigment for photosynthesis which tends to photo–damaged under stress conditions and hence, disturbs the metabolic pathways and enzyme activities responsible for synthesis/degradation of chlorophyll pigment (Kumar et al., 2018), thereby, decreasing chlorophyll content (Sneha et al., 2014). Chlorophyll meters are being used for monitoring leaf N status in agricultural crops in yield prediction, but the effects of environmental factors and leaf characteristics on leaf N estimations are still unclear. Xiong et al. (2015) observed a positive correlation between SPAD and chlorophyll content in different plant species including monocot and dicot species but the correlation of SPAD with total leaf nitrogen was different in two plant species of monocot and dicot. Our experimental findings also indicated that irrigation induced salinity stress significantly reduced the leaf gaseous exchange (Pn, gS and E), CC and SPAD values wherein the hybrids have higher photosynthetic efficiency than inbred lines. This could possibly be due to partial stomatal closure leading to reduction in intercellular CO_2 concentration or chlorophyll degradation or reduced enzymatic activities or down regulation of proteins required to maintain structural integrity of photosystems (Kumar et al., 2016). Dudhate et al. (2018) also reported reduced photosynthesis due to decreased CC and SPAD values in pearl millet when exposed to drought stress. The genotypic differences and disturbed enzymes activities of ROS and photosynthetic pigments has also been reported earlier depicting their correlation with the presence or absence of a major terminal drought tolerance QTL (Kholova et al., 2011). The gene for chlorophyll a/b binding associated with both stay-green and grain yield traits under drought stress has been reported as a functional marker for selection of high yielding pearl millet genotypes with 'stay green' character under drought stress (Sehgal et al., 2015).

Exposure of plants to salinity stress triggers overproduction of ROS, which disrupts cell organelles and membrane components, inactivate enzyme, and also degrade protein complexes as well as nucleic acid (Tufail et al., 2018). Earlier reports have also shown the

pronounced effects of salt stress on enhanced lipid peroxidation and protein oxidative damage, which in turn induces permeability impairment (Füzy et al., 2019). For osmotic adjustments, plants tend to accumulate compatible organic solutes (proline), soluble proteins and sugars for maintaining cellular homeostasis and osmoticum under saline conditions (Gharsallah et al., 2016). This could possibly be due to accumulation of low molecular weight proteins that might be utilized in the form of nitrogen during recovery process. Recently, putative WRKY protein factors have been identified in pearl millet in response to both dehydration and salinity stress involved in tolerance mechanisms (Chanwala et al., 2020). Upregulation of salt-induced proteins impart salt tolerance in tolerant pearl millet accessions with reduced expression in the sensitive accessions (Jha et al., 2022). Further, the sugars get accumulated under abiotic stress conditions due to decreased rate of respiration as well as down regulation of glycolysis (Nguyen et al., 2010).With increasing salinity stress, protective soluble proteins are synthesized *de novo* or may be present inheritably (Soni et al., 2020). Kusaka et al. (2005) and Ibrahimova et al. (2021) reported higher accumulation of osmolytes such as organic solutes (sucrose, glucose) and amino acids (proline) towards enhanced tolerance in pearl millet and wheat under stress conditions. Herein also, the osmolytes (Pro, TSP and TSS) were higher in inbred lines than pearl millet hybrids showing protective role of these osmolytes in better plant performance under salinity. This variability could have contributed towards their differential response in relative osmo–protectant and detoxification functions, and their role in buffering the cellular redox potential and protecting cellular structure under stress conditions (Sharma et al., 2021). Proteomic and physiological signatures also revealed the role of stress–related proteins in the root, mitochondrial electron transport, TCA cycle, C1–metabolism in leaf imparting stress tolerance in pearl millet (Ghatak et al., 2021). These genetic variations for proline accumulation in inbred lines could be ascribed to *de novo* synthesis or decrease in degradation of P5CS activity that allows favorable osmotic adjustments to regulate the adverse effects of salt stress (Sharma et al., 2014). Similar reports on positive interaction of osmotic stress, drought, and cold stress on proline synthesizing enzyme, P5CS1 was identified through network analysis in wheat through proline accumulation highlighting its protective role under abiotic stress conditions (Maghsoudi et al., 2019).

Ion homeostasis in a plant cell ensures its growth and development in normal environments as well as under unfavorable conditions through the absorption and compartmentalization of ions. Low levels of Na^+/K^+ ratio along with reduced Na^+ and Cl^- loadings into the xylem is one of the major factor for normal functioning of the plant cell under stress conditions (Sharma et al., 2021).Similarly, K^+ plays a key role in a myriad of physiological functions; protein synthesis, stomata opening and closing, phloem sugar loading and also acts as an organic osmolyte. Under salt stress, equilibrium status of Na/K plays an important role in balancing the ion toxicity in the cell. Previous studies have also documented the repressive effects of salinity stress on ionic imbalances in different crops including pearl millet (Venkata et al., 2012; Makarana et al., 2019a). This could be ascribed to restricted entry of Na^+ into the leaf tissues and/or compartmentalization of Na^+ either into the vacuoles or in stem portion. Since plants tend to accumulate toxic Na^+ at the expense of essential K^+ under salt stress; hence, favorable Na^+/K^+ ratio is a key indicator to visualize the stress associated plants behavior in maintaining ion balance. Our experimental evidences also highlighted the relevance of genotypic differences for salt tolerance in pearl millet by modulating favorable ionic balance through improved Na^+ discrimination and preferential K^+ uptake. We also observed that pearlmillet inbred lines maintained lower Na/K ratio than the hybrids by accumulating more K over Na ions (Table 4). Further, inbred lines AC 04-13 and ICMA 94555 and hybrids, HHB 223 and HHB 67 had higher K uptake than other plant types contributing towards better ion homeostasis and hence, salt tolerance. Chakraborty et al. (2022) also identified stress responsive genes in pearl millet inbred lines corresponding to ion and osmotic homeostasis, signal transduction, physiological adaptation and detoxification.

In our study, higher level of salinity stress (EC_{iw} ~9 dSm^{-1}) induced an immediate and substantial adverse effect on plant growth and biomass accumulation, whereas moderate stress (EC_{iw} ~3 and 6 dSm^{-1}) compensated in cumulative response compared to the control plants. Higher biomass production under these conditions might be due to accumulation of inorganic ions and compatible organic solutes for osmotic adjustments. A significant positive correlation of yield with leaf water potential, relative water content, stomatal conductance, photosynthetic rate, proline, total soluble sugars, free amino acids, membrane stability index, leaf area index and total biomass under water-deficit stress (Vijayalakshmi et al., 2012) and salt stress (Makarana et al., 2019b) has been reported earlier in pearl millet A positive correlation of MDA content and proline has been reported with accumulation of green and dry biomass in best-performing pearl millet lines under ionic stress (Toderich et al., 2018).Association analysis of a total of 392,493 SNPs identified QTLs for biomass production in early drought stress conditions and for stay-green trait in pearlmillet using Genotyping-by-Sequencing (GBS) (Debieu et al., 2018). In our studies, the comparative analysis of association of physiological traits between pearl millet hybrids and inbred lines indicated a parallel trait association among the two although the K^+ ion uptake discriminated the two (Supplementary Table 3). As the SPAD reading (indicative of leaf greenness) increases total chlorophyll content also increased in both hybrids and inbreeds with higher magnitude in hybrids. Because, abiotic stress tend to reduce leaf area and hence, concentrate of leaf pigments. Consequently, higher photosynthetic rate in inbred lines than the hybrids was observed in our experiments. Further, at higher salinity level, accumulation of higher proline and total proteins have a negative association with the total soluble sugars in hybrids than the inbred lines.

In finger millet (*Eleusine coracana*), the sensitivity of the growth stage towards drought stress was indicated through biplot analysis along with significant genotypic variation (Mude et al., 2020). Contrarily, the reduction in biomass may be linked to restricted hydrolysis of reserved foods with limited nutrient uptake and their translocation to the growing plant parts (Yamazaki et al., 2020).

Grain yield formation in plants depends entirely on the ability of the crop plants to assimilate and utilize the available growth

resources, and thus, is an interplay of several cellular and functional components contributing towards final harvest. Ghatak et al. (2021) explored physiological and proteomic signatures for drought resilience and observed maintenance of pearl millet and wheat grain yield under drought stress. Identification of an important SNP in putative acetyl CoA carboxylase gene has showed significant association with grain yield, grain harvest index and panicle yield under drought stress in pearl millet (Sehgal et al. (2015). Generally, all the glycophytes show yield reductions under saline conditions owing to disturbed water and nutritional balance, decreased source to sink ratio and poor plant photosynthetic efficiency (Yadav et al., 2020). Further, reduction in the grain yield might possibly be due to decreased pollen viability, stigma receptivity, poor seed setting and reduced seed weight under saline environments that ultimately culminate in lower crop yields (Sharma et al., 2021). In this study, increasing salinity stress might have restricted the availability of growth resources for plant survival and hindered photosynthetic activity exposing them to deficient minerals nutrition and water uptake and ultimately reduced the crop (Toderich et al., 2018; Yadav et al., 2020). Recently, genome–wide association (GWAS) and genomic prediction for improving drought stress tolerance in pearl millet revealed high prediction accuracy and heritability between yield–associated traits and hybrid performance across different drought prone growing environments (Varshney et al., 2017). More importantly, the prediction of hybrid performance through genomic selection strategy with additive and dominance effects identified 159 combinations which have never been used in breeding programme and therefore, these were proposed as good candidates for development of high–yielding pearl millet hybrids.

5 Conclusions

The performance of pearl millet hybrids and inbred lines assessed through traits modeling approach helped to identify key morpho–physiological traits governing the anticipated salt tolerance, plant adaptation and grain yield variations in response to irrigation induced salinity stress. The plant functioning traits like higher photosynthetic rate, lower Na^+/K^+ ratio and higher biomass accumulation could be effectively utilized for screening and identification of potential salt tolerant pearl millet germplasm. The experimental findings revealed that the pearl millet hybrids; HHB 146, HHB 272, HHB 234 and the inbred lines; H77/833–2–202, ICMA 94555 and ICMA 843–22, showed trait-associated better adaptation mechanisms and perceived lesser yield reduction with increasing salinity stress. These pearl millet hybrids could be recommended for enhancing the crop resilience, stabilize production and generate higher income in saline agro –ecosystems. More importantly, the identified inbred lines with special characteristics (salt tolerance) may be utilized as potential genetic source in pearl millet developmental program for salt –affected ecologies. Recent advancements of biotechnological and genomic tools like genome-wide SNPs mining through genome sequencing and resequencing in pearl millet breeding are being applied as in other important crops, which will further facilitate the efforts for mapping of complex, polygenic controlled important traits, such as abiotic stress tolerance (salinity, drought and heat), yield contributing traits and will speed up the pearl millet improvement program.

Data availability statement

The original contributions presented in the study are included in the article/Supplementary Material. Further inquiries can be directed to the corresponding authors.

Author contributions

AsK and PS: investigation, data visualization, original draft preparation; AM, DY and DKS: conceptualization and final editing; ArK: statistical analysis, SD: original draft preparation, NK and PD: data visualization. All authors contributed to the article and approved the submitted version.

Acknowledgments

We would like to sincerely thank the Director, ICAR-CSSRI, Karnal for providing the logistic support and CCSHAU, Hisar for providing the pearl millet germplasm for completion of this study.

Conflict of interest

The authors declare that the research was conducted in the absence of any commercial or financial relationships that could be construed as a potential conflict of interest.

Publisher's note

Supplementary material

The Supplementary Material for this article can be found online at: https://www.frontiersin.org/articles/10.3389/fpls.2023.1121805/full#supplementary-material

References

Barnes, J. D., Balaguer, L., Manrique, E., Elvira, S., and Davison, A. W. (1992). A reappraisal of the use of dmso for the extraction and determination of chlorophylls a and b in lichens and higher plants. *Environ. Exp. Bot.* 32, 85–100. doi: 10.1016/0098-8472(92)90034-Y

Bates, L., Waldren, R., and Teare, I. (1973). Rapid determination of free proline for water-stress studies. *Plant Soil* 39, 205–207. doi: 10.1007/BF00018060

Bradford, M. M. (1976). A rapid and sensitive method for the quantitation of microgram quantities of protein utilizing the principle of protein-dye binding. *Anal. Biochem.* 72, 248–254. doi: 10.1016/0003-2697(76)90527-3

Chakraborty, A., Viswanath, A., Malipatil, R., Semalaiyappan, J., Shah, P., Ronanki, S., et al. (2022). Identification of candidate genes regulating drought tolerance in pearl millet. *Int. J. Mol. Sci.* 23, 6907. doi: 10.3390/ijms23136907

Chanwala, J., Satpati, S., Dixit, A., Parida, A., Giri, M. K., and Dey, N. (2020). Genome-wide identification and expression analysis of WRKY transcription factors in pearl millet (*Pennisetum glaucum*) under dehydration and salinity stress. *BMC Genomics* 21, 231. doi: 10.1186/s12864-020-6622-0

Debieu, M., Sine, B., Passot, S., Grondin, A., Akata, E., Gangashetty, P., et al. (2018). Response to early drought stress and identification of QTLs controlling biomass production under drought in pearl millet. *PloS One* 13 (10), e0201635. doi: 10.1371/journal.pone.0201635

Dhansu, P., Kulshreshtha, N., Kumar, R., Raja, A. K., Pandey, S. K., Goel, V., et al. (2021). Identification of drought-tolerant co-canes based on physiological traits, yield attributes and drought tolerance indices. *Sugar Tech.* 23, 747–761. doi: 10.1007/s12355-021-00967-7

Dionisio-Sese, M. L., and Tobita, S. (1998). Antioxidant responses of rice seedlings to salinity stress. *Plant Sci.* 135, 1–9. doi: 10.1016/S0168-9452(98)00025-9

Directorate of Millets Development. (2020) (Department of Agriculture, Co-operation & Farmers Welfare, Ministry of Agriculture & Farmers Welfare, Government of India).

Dudhate, A., Shinde, H., Tsugama, D., Liu, S., and Takano, T. (2018). Transcriptomic analysis reveals the differentially expressed genes and pathways involved in drought tolerance in pearl millet [*Pennisetum glaucum* (L.) r. br]. *PloS One* 13 (4), e0195908. doi: 10.1371/journal.pone.0195908

Füzy, A., Kovács, R., Cseresnyés, I., Parádi, I., Szili-Kovács, T., Kelemen, B., et al. (2019). Selection of plant physiological parameters to detect stress effects in pot experiments using principal component analysis. *Acta Physiol. Plantarum* 41, 1–10. doi: 10.1007/s11738-019-2842-9

Gharsallah, C., Fakhfakh, H., Grubb, D., and Gorsane, F. (2016). Effect of salt stress on ion concentration, proline content, antioxidant enzyme activities and gene expression in tomato cultivars. *AoB Plants* 8, plw055. doi: 10.1093/aobpla/plw055

Ghatak, A., Chaturvedi, P., Bachmann, G., Valledor, L., Ramšak, Ž, Bazargani, M. M., et al. (2021). Physiological and proteomic signatures reveal mechanisms of superior drought resilience in pearl millet compared to wheat. *Front. Plant Sci.* 11. doi: 10.3389/fpls.2020.600278

Ibrahimova, U., Zivcak, M., Gasparovic, K., Rastogi, A., Allakhverdiev, S. I., Yang, X., et al. (2021). Electron and proton transport in wheat exposed to salt stress: is the increase of the thylakoid membrane proton conductivity responsible for decreasing the photosynthetic activity in sensitive genotypes? *Photosynth Res.* 150, 195–211. doi: 10.1007/s11120-021-00853-z

IRRI. (2013). *International rice research institute (IRRI)* (Philippines). Available at: http://bbi.irri.org/products.

Jha, S., Maity, S., Singh, J., Chouhan, C., Tak, N., and Ambatipudi, K. (2022). Integrated physiological and comparative proteomics analysis of contrasting genotypes of pearl millet reveals underlying salt-responsive mechanisms. *Physiol. Plant* 174, e13605. doi: 10.1111/ppl.13605

Kholova, J., Hash, C. T., Kočová, M., and Vadez, V. (2011). Does a terminal drought tolerance QTL contribute to differences in ROS scavenging enzymes and photosynthetic pigments in pearl millet exposed to drought? *Environ. Exp. Bot.* 71 (1), 99–106. doi: 10.1016/j.envexpbot.2010.11.001

Kumar, A., Lata, C., Kumar, P., Devi, R., Singh, K., Krishnamurthy, S. L., et al. (2016). Salinity and drought induced changes in gas exchange attributes and chlorophyll fluorescence characteristics of rice (Oryza sativa) varieties. *Indian J. Agric. Sci.* 86(6), 19–27. Available at: https://epubs.icar.org.in/index.php/IJAgS/article/view/58833

Kumar, A., Kumar, A., Kumar, P., Lata, C., and Kumar, S. (2018). Effect of individual and interactive alkalinity and salinity on physiological, biochemical and nutritional traits of Marvel grass. *Indian J. Exp. Biol.* 56(8), 573–81.

Kumar, A., Mann, A., Kumar, A., Kumar, N., and Meena, B. L. (2021). Physiological response of diverse halophytes to high salinity through ionic accumulation and ROS scavenging. *Int. J. Phytoremed* 23 (10), 1041–1051. doi: 10.1080/15226514.2021.1874289

Kusaka, M., Ohta, M., and Fujimura, T. (2005). Contribution of inorganic components to osmotic adjustment and leaf folding for drought tolerance in pearl millet. *Physiol. Plant* 125, 474–489. doi: 10.1111/j.1399-3054.2005.00578.x

Maghsoudi, K., Emam, Y., Ashraf, M., Pessarakli, M., and Arvin, M. J. (2019). Silicon application positively alters pollen grain area, osmoregulation and antioxidant enzyme activities in wheat plants under water deficit conditions. *J. Plant Nutr.* 42, 2121–2132. doi: 10.1080/01904167.2019.1648677

Maiti, R. K., and Satya, P. (2014). Research advances in major cereal crops for adaptation to abiotic stresses. *GM Crops Food* 5, 259–279. doi: 10.4161/21645698.2014.947861

Makarana, G., Kumar, A., Yadav, R. K., Kumar, R., Soni, P. G., Lata, C., et al. (2019a). Effect of saline water irrigations on physiological, biochemical and yield attributes of dual purpose pearl millet (*Pennisetum glaucum*) varieties. *Indian Agric. Sci.* 89, 624–633. doi: 10.56093/ijas.v89i4.88847

Makarana, G., Yadav, R. K., Kumar, A., Kumar, R., Sheoran, P., and Kushwaha M and Yadav, T. (2019b). Physiological, biochemical and yield traits of pearl-millet (Pennisetum glaucum l.) accessions under saline irrigation. *J. Soil Salinity Water Qual.* 11 (1), 1–10.

Mude, L. N., Mondam, M., Gujjula, V., Jinka, S., Pinjari, O. B., Yellodu Adi Reddy, N., et al. (2020). Morpho-physiological and biochemical changes in finger millet [*Eleusine coracana* (L.) gaertn.] under drought stress. *Physiol. Mol. Biol. Plants* 26 (11), 2151–2171. doi: 10.1007/s12298-020-00909-9

Nguyen, G., Hailstones, D., Wilkes, M., and Sutton, B. (2010). Drought stress: role of carbohydrate metabolism in drought induced male sterility in rice anthers. *J. Agron. Crop Sci.* 196, 346–357. doi: 10.1111/j.1439-037X.2010.00423.x

Pearson, K. (1948). *Early statistical papers*. (Cambridge, England: University Press).

Polash, M. A. S., Saki, M. A., Tahjib-Ul-Arif, M., and Hossain, M. A. (2018). Effect of salinity on osmolytes and relative water content of selected rice genotypes. *Trop. Plant Res.* 5, 227–232. doi: 10.22271/tpr.2018.v5.i2.029

Reddy, P. S., Dhaware, M. G., Sivasakthi, K., Divya, K., Nagaraju, M., Sri Cindhuri, K., et al. (2022). Pearl millet aquaporin gene PgPIP2;6 improves abiotic stress tolerance in transgenic tobacco. *Front. Plant Sci.* 13. doi: 10.3389/fpls.2022.820996

Sehgal, D., Skot, L., Singh, R., Srivastava, R. K., Das, S. P., Taunk, J., et al. (2015). Exploring potential of pearl millet germplasm association panel for association mapping of drought tolerance traits. *PloS One* 10 (5), e0122165. doi: 10.1371/journal.pone.0122165

Shapiro, S. S., and Wilk, M. B. (1965). An analysis of variance test for normality (Complete samples). *Biometrika* 52, 591–611. doi: 10.1093/biomet/52.3-4.591

Sharma, P. C., Kumar, A., and Mann, A. (2021). "Physiology of salt tolerance in crops," in *Managing salt affected soils for sustainable agriculture*. Eds. P. S. Minhas, R. K. Yadav and P. C. Sharma (New Delhi: ICAR), 199–226.

Sharma, D. K., Thimmappa, K., Chinchmalatpure, A. R., Mandal, A. K., Yadav, R. K., and Chaudhari, S. K. (2015). *Assessment of production and monetary losses from salt-affected soils in India*. (Karnal, India: ICAR-Central Soil Salinity Research Institute), 99.

Sharma, P. C., Singh, D., Sehgal, D., Singh, G., Hash, C. T., and Yadav, R. S. (2014). Further evidence that a terminal drought tolerance qtl of pearl millet is associated with reduced salt uptake. *Environ. Exp. Bot.* 102, 48–57. doi: 10.1016/j.envexpbot.2014.01.013

Sheoran, P., Basak, N., Kumar, A., Yadav, R. K., Singh, R., Sharma, R., et al. (2021). Ameliorants and salt tolerant varieties improve rice-wheat production in soils undergoing sodification with alkali water irrigation in indo–gangetic plains of India. *Agric. Water Manage* 243, 106492. doi: 10.1016/j.agwat.2020.106492

Sheoran, P., Sharma, R., Kumar, A., Singh, R. K., Barman, A., Prajapat, K., et al. (2022). Climate resilient integrated soil–crop management (CRISCM) for salt affected wheat agri–food production systems. *Sci. Total Environ.* 837, 155843. doi: 10.1016/j.scitotenv.2022.155843

Shivhare, R., and Lata, C. (2017). Exploration of genetic and genomic resources for abiotic and biotic stress tolerance in pearl millet. *Front. Plant Sci.* 7, 2069. doi: 10.3389/fpls.2016.02069

Sneha, S., Rishi, A., and Chandra, S. (2014). Effect of short term salt stress on chlorophyll content, protein and activities of catalase and ascorbate peroxidase enzymes in pearl millet. *Am. J. Plant Physiol.* 9, 32–37. doi: 10.3923/ajpp.2014.32.37

Soni, S., Kumar, A., Sehrawat, N., Kumar, N., Kaur, G., Kumar, A., et al. (2020). Variability of durum wheat genotypes in terms of physio-biochemical traits against salinity stress. *Cereal Res. Commun.* 49 (1), 45–54. doi: 10.1007/s42976-020-00087-0

Soni, S., Kumar, A., Sehrawat, N., Kumar, A., Kumar, N., Lata, C., et al. (2021). Effect of saline irrigation on plant water traits, photosynthesis and ionic balance in durum wheat genotypes. *Saudi J. Biol. Sci.* 24 (4), 2510–2517. doi: 10.1016/j.sjbs.2021.01.052

Toderich, K., Shuyskaya, E., Rakhmankulova, Z., Bukarev, R., Khujanazarov, T., Zhapaev, R., et al. (2018). Threshold tolerance of new genotypes of *Pennisetum glaucum* (L.) r. br. to salinity and drought. *Agron.* 8, 230. doi: 10.3390/agronomy8100230

Tufail, A., Li, H., Naeem, A., and Li, T. X. (2018). Leaf cell membrane stability-based mechanisms of zinc nutrition in mitigating salinity stress in rice. *Plant Biol.* 20, 338–345. doi: 10.1111/plb.12665

Tukey, J. W. (1977). *Exploratory data analysis.* (Reading: Addison-Wesley) 2, 131–160.

Varshney, R. K., Shi, C., Thudi, M., Mariac, C., Wallace, J., Qi, P., et al. (2017). Pearl millet genome sequence provides a resource to improve agronomic traits in arid environments. *Nat. Biotechnol.* 35 (10), 969–976. doi: 10.1038/nbt.3943

Venkata, A. R. P., Kumari, P. K., Dev, T. S. S. M., Rao, M. V. S., and Manga, V. (2012). Genetic analysis of sodium content and na/k ratio in relation to salinity tolerance in pearl millet *Pennisetum glaucum* (L.) r. br. *J. Crop Sci. Biotech.* 15, 195–203. doi: 10.1007/s12892-011-0078-3

Vijayalakshmi, T., Varalaxmi, Y., Jainender, S., Yadav, S., Vanaja, M., Jyothilakshmi, N., et al. (2012). Physiological and biochemical basis of water-deficit stress tolerance in pearl millet hybrid and parents. *Am. Plant Sci.* 3 (12), 1730–1740. doi: 10.4236/ajps.2012.312211

Wang, L., Czedik-Eysenberg, A., Mertz, R. A., Si, Y. Q., Tohge, T., Nunes-Nesi, A., et al. (2014). Comparative analyses of c–4 and c–3 photosynthesis in developing leaves of maize and rice. *Nat. Biotechnol.* 32, 1158–1165. doi: 10.1038/nbt.3019

Weatherley, P. (1950). Studies in the water relations of the cotton plant: I. the field measurement of water deficits in leaves. *New Phytol.* 49, 81–97. doi: 10.1111/j.1469-8137.1950.tb05146.x

Xiong, D., Che, J., Yu, T., Gao, W., Ling, X., Li, Y., et al. (2015). SPAD-based leaf nitrogen estimation is impacted by environmental factors and crop leaf characteristics. *Sci. Rep.* 5, 13389. doi: 10.1038/srep13389

Yadav, T., Kumar, A., Yadav, R. K., Yadav, G., Kumar, R., and Kushwaha, M. (2020). Salicylic acid and thiourea mitigate the salinity and drought stress on physiological traits governing yield in pearl millet-wheat. *Saudi J. Biol. Sci.* 27, 2010–2017. doi: 10.1016/j.sjbs.2020.06.030

Yadav, O. P., Rai, K. N., Rajpurohit, B. S., Hash, C. T., Mahala, R. S., Gupta, S. K., et al. (2012). *Twenty-five years of pearl millet improvement in India*, Jodhpur, Rajasthan, India: All India Coordinated Pearl Millet Improvement Project, .

Yadav, O. P., Rajpurohit, B. S., Kherwa, G. R., and Kumar, A. (2012a). Prospects of enhancing pearl millet (Pennisetum glaucum) productivity under drought environments of north-western India through hybrids. *Indian J. Gen. Plant Breed* 72, 25–30.

Yamazaki, K., Ishimori, M., Kajiya-Kanegae, H., Takanashi, H., Fujimoto, M., Yoneda, J., et al. (2020). Effect of salt tolerance on biomass production in a large population of sorghum accessions. *Breed. Sci.* 70, 167–175. doi: 10.1270/jsbbs.19009

Yemm, E., and Willis, A. (1954). The estimation of carbohydrates in plant extracts by anthrone. *Biochem. J.* 57, 508. doi: 10.1042/bj0570508

frontiers | Frontiers in Plant Science

TYPE Original Research
PUBLISHED 03 March 2023
DOI 10.3389/fpls.2023.1147424

OPEN ACCESS

EDITED BY
Pasala Ratnakumar,
Indian Institute of Oilseeds Research (ICAR), India

REVIEWED BY
Purushothaman Ramamoorthy,
Mississippi State University, United States
Rajkumar U. Zunjare,
Indian Agricultural Research Institute (ICAR), India

*CORRESPONDENCE
Ashok Singamsetti
ashok.singamsetti@gmail.com
Pervez H. Zaidi
phzaidi@cgiar.org

SPECIALTY SECTION
This article was submitted to Plant Abiotic Stress, a section of the journal Frontiers in Plant Science

RECEIVED 18 January 2023
ACCEPTED 15 February 2023
PUBLISHED 03 March 2023

CITATION
Singamsetti A, Zaidi PH, Seetharam K, Vinayan MT, Olivoto T, Mahato A, Madankar K, Kumar M and Shikha K (2023) Genetic gains in tropical maize hybrids across moisture regimes with multi-trait-based index selection.
Front. Plant Sci. 14:1147424.
doi: 10.3389/fpls.2023.1147424

Genetic gains in tropical maize hybrids across moisture regimes with multi-trait-based index selection

Ashok Singamsetti[1]*, Pervez H. Zaidi[2]*, Kaliyamoorthy Seetharam[2], Madhumal Thayil Vinayan[2], Tiago Olivoto[3], Anima Mahato[4], Kartik Madankar[1], Munnesh Kumar[1] and Kumari Shikha[1]

[1]Department of Genetics and Plant Breeding, Institute of Agricultural Sciences, Banaras Hindu University, Varanasi, India, [2]Asia Regional Maize Programme, The International Maize and Wheat Improvement Center (CIMMYT)-Hyderabad, Patancheru, India, [3]Department of Plant Science, Federal University of Santa Cataria, Florianópolis, Brazil, [4]Indian Council of Agricultural Research (ICAR) - Indian Agricultural Research Institute (IARI), Barhi, Jharkhand, India

Unpredictable weather vagaries in the Asian tropics often increase the risk of a series of abiotic stresses in maize-growing areas, hindering the efforts to reach the projected demands. Breeding climate-resilient maize hybrids with a cross-tolerance to drought and waterlogging is necessary yet challenging because of the presence of genotype-by-environment interaction (GEI) and the lack of an efficient multi-trait-based selection technique. The present study aimed at estimating the variance components, genetic parameters, inter-trait relations, and expected selection gains (SGs) across the soil moisture regimes through genotype selection obtained based on the novel multi-trait genotype–ideotype distance index (MGIDI) for a set of 75 tropical pre-released maize hybrids. Twelve traits including grain yield and other secondary characteristics for experimental maize hybrids were studied at two locations. Positive and negative SGs were estimated across moisture regimes, including drought, waterlogging, and optimal moisture conditions. Hybrid, moisture condition, and hybrid-by-moisture condition interaction effects were significant ($p \leq 0.001$) for most of the traits studied. Eleven genotypes were selected in each moisture condition through MGIDI by assuming 15% selection intensity where two hybrids, viz., ZH161289 and ZH161303, were found to be common across all the moisture regimes, indicating their moisture stress resilience, a unique potential for broader adaptation in rainfed stress-vulnerable ecologies. The selected hybrids showed desired genetic gains such as positive gains for grain yield (almost 11% in optimal and drought; 22% in waterlogging) and negative gains in flowering traits. The view on strengths and weaknesses as depicted by the MGIDI assists the breeders to develop maize hybrids with desired traits, such as grain yield and other yield contributors under specific stress conditions. The MGIDI would be a robust and easy-to-handle multi-trait selection process under various test environments with minimal multicollinearity issues. It was found to be a powerful tool in developing better selection strategies and optimizing the breeding scheme, thus contributing to the development of climate-resilient maize hybrids.

KEYWORDS

genotype-by-environment interaction (GEI), moisture regimes, multi-trait index, drought, waterlogging, climate-resilient maize, selection gains

1 Introduction

Maize yields in the Asian tropical rainfed environments are now becoming increasingly vulnerable to various climate-induced stresses, especially drought and waterlogging, which often come in combination to severely impact maize crops (Prasanna et al., 2021). The potential climate changes and abnormalities associated with a number of abiotic stresses severely affect the growth and development of crops (Brown and Funk, 2008; Lobell et al., 2008). Among many unpredictable changes, moisture stresses including low soil moisture stress (drought) and excess soil moisture stress (waterlogging/flooding) are the major constraints worldwide that result in almost 90% yield loss. A large portion of maize in the Asian tropics is cultivated in low-land tropics (<1,000 masl), representing a major mega-environment, followed by sub-tropical and tropical highlands (Zaidi et al., 2020). Approximately 80% of maize is being grown as a rainfed crop, prone to the vagaries of monsoon rains associated with a series of abiotic and biotic constraints. The erratic/uneven distribution of monsoon pattern leads to untimely rains, often causing intermittent dry spells/drought or excess soil moisture/waterlogging at different crop growth stages within the crop growing period (Zaidi et al., 2016a), and is a major factor responsible for the relatively low productivity in maize. The regular occurrence of temporary excessive soil moisture or waterlogging stress resulted in an almost 18% reduction in total maize in Southeast Asia (Zaidi et al., 2010). A few recent reports anticipated that the Asian tropics will experience a sharper increase in surface temperatures due to adverse weather conditions, resulting in shifting seasons and frequent drought and waterlogging at critical crop stages that could severely impact the maize production in the tropical regions (ADB, 2009; Lobell et al., 2011; Cairns et al., 2012; Zaidi et al., 2020).

In contrast, recent studies reported that the average global demand for maize has increased by 45% in 2020 when compared to 1997, with East Asia (85%) showing the highest increase in demand, followed by Sub-Saharan Africa (79%), Southeast Asia (70%), and South Asia (36%) (FAOSTAT, 2022; Ulfat et al., 2022). The development of improved germplasm with combined tolerance against extreme climate vagaries such as excess moisture and drought will be necessary in many areas of Asia, Africa, and Latin America (Zaidi et al., 2010). The international wheat and maize improvement center (CIMMYT)–Asia maize program largely focused on the development of breeding strategies to reach attainable yields across a range of environments by incorporating reasonable levels of cross-tolerance against a combination of major abiotic stresses without compromising grain yields under favorable/optimal growing conditions. It implies the maximum yield potential under optimal conditions along with a guarantee of average yields under stress-prone areas by improving the stress-resilient breeding pipelines through precision phenotyping, index-based selection for secondary traits, and stage-wise gateway screening (Zaidi et al., 2020). Under the various environmental conditions in India, developing climate-resilient and location-specific high-yielding hybrids became a primary goal of maize technologists. To achieve this, researchers must perform multi-environment trials (METs) prior to national trials. MET evaluates a set of genotypes under different test environments, which may be spatially varied (geographic locations), time-separated (seasons/years), different managed stresses (drought, waterlogging, low nitrogen, etc.), or a combination of any of these. METs can efficiently identify genotypes with a constant trait performance among different test environments (Yan and Kang, 2003). Comprehensive assessment of promising genotypes with higher yield potential and desirable agronomic characteristics is the key to breed hybrids with wide adaptability and stability. The undeniable existence of genotype-by-environment interaction (GEI) causes confusion in screening out promising genotypes, and it misleads the ranking pattern of test genotypes across environments. Thus, a deep understating of the degree and pattern of GEI across environments is crucial for successful crop improvement programs (Vaezi et al., 2019). Various analysis models and techniques such as analysis of variance (ANOVA), principal component analysis (PCA), cluster analysis, additive main effects and multiplicative interaction (AMMI), and genotype and genotype plus environment (GGE) biplots were developed to unravel the unpredictable effects of genotype, environment, and their interaction (Kendal, 2016).

Although grain yield is the most important characteristic of genotypes, other secondary traits are also common, such as days to flowering, plant height, ear height, ear length, and number of kernel rows (Gauch, 2013). The yield gains could be the result of the direct selection of grain yield that is accompanied by the desirable expression of other secondary traits. Previous reports on yield–trait relations provided a breakthrough for plant breeders in terms of defining a set of target traits to bring together new, high-performance hybrids (Nardino et al., 2016; Olivoto et al., 2017). It could be more efficient if the selection of genotypes is based on grain yield combined with other agronomic traits. However, an effective incorporation of multiple trait data without multicollinearity in the selection method has been a challenge for breeders. A widely used multi-trait selection index, the Smith–Hazel (SH) index (Smith, 1936; Hazel, 1943), is not being recommended for METs, where the presence of biased index coefficients and multicollinearity issues erodes the real genetic gains (Rocha et al., 2018; Olivoto et al., 2019a; Olivoto et al., 2019b; Jarquin et al., 2020; Woyann et al., 2020; Zuffo et al., 2020). Similarly, the recently proposed genotype × yield × trait (GYT) biplots (Yan and Frégeau-Reid, 2018) offer an effective and comprehensive analysis method for the evaluation of genotypes based on the combined grain yield and various evaluated agronomic traits. However, the method determines the influencing factors from yield–trait combinations by a classical linear multivariate model under diversified environments, but it does not involve any subjective weights and cutting points that provide a better picture of the strengths and weaknesses of test genotypes (Yan and Frégeau-Reid, 2018; Kendal, 2019; Nikolay et al., 2020; Singamsetti et al., 2022).

In that perspective, a novel multi-trait genotype–ideotype distance index (MGIDI) was proposed to select genotypes with desirable mean performances of multiple traits that overcome the fragility of classical linear indices (Olivoto and Nardino, 2021). A few previous attempts at multiple traits in the selection of maize hybrids with multi-environment data have been reported (Langner

et al., 2019; Olivoto et al., 2021; Oliveira et al., 2020; Singamsetti et al., 2021; Peixoto et al., 2021; Shojaei et al., 2022; Yue et al., 2022c). The purpose of this research was mainly to select the promising maize hybrids based on multiple traits suitable for different moisture regimes including drought, waterlogging, and optimal conditions and across all moisture conditions. The study was carried out to reveal genetic parameters such as variance components, accuracy and heritability, inter-trait associations, and the patterns of GEI effects under individual and across moisture conditions.

2 Materials and methods

2.1 Plant material

The experimental material consists of 75 medium-duration maize hybrids including five commercial checks (Supplementary Table 1) leveraged from the Asian Regional Office, CIMMYT, Hyderabad, India. The 70 hybrids were developed from the biparental crosses obtained from a pool of 600 elite maize lines of the CIMMYT gene bank crossed with two abiotic stress-susceptible (mostly drought and waterlogging) testers, viz., CML451 and CL02450. These were globally released leading testers with high combining ability belonging to different heterotic groups, A and B, that resulted in test cross progeny with substantial stress tolerance. The materials were evaluated under different soil moisture stresses including drought, waterlogging, and optimal conditions by a stage-wise gateway process under the "Climate Resilient Maize for Asia" (CRMA) project supported by BMZ/GIZ, Germany. The studied hybrids were at the Stage III screening process that aimed to identify stress/location-specific hybrids and also those across different locations/stresses.

2.2 Testing environment

The trials across the different soil moisture conditions (described later in this article) were conducted at two locations, viz., Banaras Hindu University (BHU), Varanasi, India (Location 1) and CIMMYT, Hyderabad, ICRISAT Campus, India (Location 2), during winter 2017 and its subsequent summer–rainy season 2018. Location 1 is situated in the middle of the Indo-Gangetic plains of northern India, which experiences alternating floods and high temperatures in a year, while Location 2 is represented by the arid region of the Deccan Plateau with evident frequent occurrence of water scarcity followed by scattered rainfalls. The soil type of the experiment site at Location 1 was sandy loam, whereas it was shallow black soils at Location 2. The detailed information of seven test environments (E1 to E7) including three moisture conditions with season and location combinations is shown in Table 1. The meteorological data based on standard weeks including temperature and rainfall during the crop growing period at both locations are shown in Supplementary Figure 1.

2.3 Experimental design and stress management

Test hybrids at each environment were sown in alpha lattice (0, 1) design (Patterson and Williams, 1976) with two replications. Manual sowing was done in two rows of 4 m length with a standard spacing of 75 cm between the rows and 20 cm within a row. A final plant population of 66,666 plants ha^{-1} was maintained by thinning in over-sown plots. All the recommended agronomic and cultural operations including irrigation were taken care of for optimal soil moisture (well-watered) trials. Drought and waterlogging phenotyping protocols by CIMMYT were strictly followed in both locations during managed stress trials (Zaman-Allah et al., 2016; Zaidi et al., 2016b). Field selection and protection measures were taken with utmost care to avoid other potential interruptions of plant growth and development during the moisture-stress period.

2.3.1 Managed drought trials

Planting dates were adjusted to the dry period, i.e., winter or delayed *Rabi* season, and irrigation schedule was modified to impose drought stress at the reproductive stage of the crop. Cumulative growing degree days (GDD) were calculated from the day of life irrigation to ensure accurate stress intensity at the target stage of the crop at all the test environments. Withdrawal of irrigation at 550 cumulative GDD and release of stress by providing "rescue irrigation" at 1,000 cumulative GDD were

TABLE 1 Details of test environments adopted for evaluation of 75 maize hybrids during the cropping seasons winter 2017–2018 and summer–rainy 2018.

Environment	Moisture regime	Crop season	Test location	Planting date
E1	Optimal	Winter	BHU, Varanasi	25 December 2017
E2	Managed drought	Winter	BHU, Varanasi	25 December 2017
E3	Managed drought	Winter	CIMMYT, Hyderabad	15 December 2017
E4	Optimal	Summer–rainy	BHU, Varanasi	6 July 2018
E5	Managed waterlogging	Summer–rainy	BHU, Varanasi	6 July 2018
E6	Optimal	Summer–rainy	CIMMYT, Hyderabad	8 July 2018
E7	Managed waterlogging	Summer–rainy	CIMMYT, Hyderabad	10 July 2018

BHU, Banaras Hindu University; CIMMYT, The International Maize and Wheat Improvement Center.

followed to expose flowering to severe moisture stress (Zaman-Allah et al., 2016).

$$\text{Growing Degree Days (GDD)} = \sum \left(\frac{T_{max} + T_{min}}{2}\right) - T_{base}$$

where T_{max} = maximum temperature, T_{min} = minimum temperature, and T_{base} = base temperature (10°C).

Progress in imposing stress was tracked by measuring moisture depletion at different soil depths up to 100 cm at 10-cm intervals with the "Delta-T PR2 soil moisture profile probe". The probe was pre-installed in the fields where drought trials were conducted and weekly data were recorded from the first week after withdrawal of irrigation (a few days before anthesis), until the stress is relieved. Rescue irrigation was confirmed by the soil moisture content reaching the "permanent wilting point" (PWP), i.e., 16.8% v/v at the soil depth of 30–40 cm. Cumulative vapor–pressure deficit or ∑VPD values were also recorded as complementary to GDDs to endorse pausing and to resume the irrigation at 120 VPD and at 220 kPa VPD values, respectively.

2.3.2 Managed waterlogging trials

Fields with proper irrigation and drainage facilities were selected for waterlogging phenotyping. These are well-leveled with no inclination, thus ensuring a depth of 10 ± 0.5 cm stagnation of water continuously for 7 days to impose waterlogging stress at the target crop stage, i.e., V_5–V_6 leaf stage or "knee-high" stage. Considering evaporation and seepage losses, additional need-based irrigation was provided to maintain the depth of water during the stress period. The crop was relieved from the stress by draining out the excess water in the experimental plots from the seventh day and a normal irrigation schedule was recommenced (Zaidi et al., 2016b).

2.4 Traits evaluated

During the flowering, maturity, and post-harvest stages of the crop, a total of 12 agronomic traits were recorded as per guidelines of standard abiotic stress phenotyping protocols by CIMMYT (Zaman-Allah et al., 2016; Zaidi et al., 2016b). The mean values at the plot level for the traits, viz., days to 50% anthesis (D50A), days to 50% silking (D50S), and anthesis–silking interval (ASI), were determined, whereas plant height (PH, in cm), ear height (EH, in cm), chlorophyll content (SPAD readings), ear length (EL, in cm), ear girth (EG, in cm), kernel number per row (KNR), kernel rows per ear (KRE), and test weight (TW, in g) were recorded as the mean of five randomly selected plants in each plot. SPAD readings were taken before and after imposing stress by the SPAD-502 plant chlorophyll meter. Moisture and shelling percent were measured by converting fresh weight of ears without husk per each plot to grain yield per hectare (GY, in t/ha) at 12.5% moisture (ASTM 2001).

$$\text{Grain Yield (t/ha)} = \frac{\text{Fresh ear weight (kg/plot)} \times 10 \times (100 - \text{MC}) \times \text{SH}}{(100 - \text{Adjusted MC}) \times \text{Plot area (m}^2\text{)}}$$

where MC is moisture content, SH is shelling percentage, and adjusted MC is the required standardized moisture percentage (12.5%)

2.5 Data analysis and software

The combined data from all the test environments were checked using the Shapiro–Wilk test (Shapiro and Wilk, 1965) for ANOVA residuals and confirmed normal distribution. Homogeneity of the data of an individual environment as well as of similar moisture conditions was confirmed through Bartlett's test (Bartlett, 1937).

2.5.1 Variance component analysis

For each soil moisture condition, the traits were initially fitted into a linear mixed-effect model by considering genotype, genotype-by-environment, and incomplete blocks within complete replicates as random effect and locations and complete replicates as fixed effect (Olivoto et al., 2019a). The following standard linear mixed model (Yang, 2007) was computed with the function *gamem_met()* from the metan package (Olivoto and Lúcio, 2020).

$$\mathbf{y} = \mathbf{X\beta} + \mathbf{Zu} + \boldsymbol{\epsilon}$$

where $\mathbf{y}$ is a vector of response variable (such as grain yield), $\boldsymbol{\beta}$ is a vector of fixed effects, $\mathbf{u}$ is a vector of random effects; $\mathbf{X}$ is a design matrix of 0s and 1s relating $\mathbf{y}$ to $\boldsymbol{\beta}$, $\mathbf{Z}$ is a design matrix of 0s and 1s relating $\mathbf{y}$ to $\mathbf{u}$, and $\boldsymbol{\epsilon}$ is a vector of random errors.

The estimates of variance components were obtained by REstricted Maximum Likelihood (REML) using the expectation-maximum algorithm (Dempster et al., 1977). A likelihood ratio test (LRT) with a two-tailed chi-square test with one degree of freedom was performed to test the significance of the random effects. Broad-sense heritability based on genotypic mean performance (h^2_{mg}) was estimated as follows:

$$h^2_{mg} = \frac{\hat{\sigma}^2_g}{\left[\hat{\sigma}^2_g + \frac{\hat{\sigma}^2_i}{e} + \frac{\hat{\sigma}^2_e}{eb}\right]}$$

Where $\hat{\sigma}^2_g$, $\hat{\sigma}^2_i$, and $\hat{\sigma}^2_e$ are the variances related to genotypes, genotype–environment interaction, and error terms, respectively; e and b are the number of environments and blocks per environments, respectively.

2.5.2 Genetic correlations

To better understand the inheritable relationships among traits and to see if these relationships are changed across moisture regimes, a genetic correlation was performed in each moisture condition. The correlation matrix was represented as network plots.

2.5.3 The multi-trait genotype–ideotype distance index

The estimation of MGIDI values for test hybrids in each moisture condition was based on two-way Best Linear Unbiased Predictions (BLUPs) for each genotype (row) and trait (column) and was carried out in four steps, i.e., rescaling of the studied traits,

exploratory factor analysis (EFA) to reduce the dimensionality, planning for ideotype with maximum rescaled value, and calculation of Euclidean distance between the genotypes and ideotype planned as the MGIDI index (Olivoto and Nardio, 2021). Rescaling the traits was performed so that all have a similar range, i.e., 0–100. The rescaled value (rX_{ij}) of the jth trait (column) of the ith genotype (row) was calculated using the following formula:

$$rX_{ij} = \frac{\eta_{nj} - \varphi_{nj}}{\eta_{0j} - \varphi_{0j}} \times (\theta_{ij} - \eta_{oj}) + \eta_{nj}$$

where η_{0j} and φ_{0j} are the original maximum and minimum values for the trait j, respectively; θ_{ij} is the original value for the jth trait of the ith genotype/hybrid; and η_{nj} and φ_{nj} are the new maximum and minimum values for the trait j after rescaling, respectively. The values for η_{nj} and φ_{nj} are chosen according to the desirability as follows. For the traits PH, EH, SPAD, EL, EB, TW, KRE, KNR, and GY in which positive gains are desired, we used η_{nj} = 100 and φ_{nj} = 0. For D50A, A50S, and ASI in which negative gains are desired, we considered η_{nj} = 0 and φ_{nj} = 100. The correlation matrix of the original set of trait values (X_{ij}) was maintained by the rescaled trait values (rX_{ij}) in a two-way table in which each column with a range of 0–100 made a selection, i.e., increase or decrease.

In the second step, the factorial scores of each test hybrid/genotype was estimated by performing EFA with rescaled values (rX_{ij}) to group correlated traits into "*factors*". By assuming p and f are the number of traits included and common factors retained through EFA, respectively, the scores were calculated as follows:

$$\mathbf{X}=\boldsymbol{\mu}+\mathbf{L}\mathbf{f}+\boldsymbol{\epsilon}$$

where $\boldsymbol{X}$ is a $p \times 1$ vector of rescaled observations; $\boldsymbol{\mu}$ is a $p \times 1$ vector of standardized means; $\boldsymbol{L}$ is a $p \times f$ matrix of factorial loadings; $\boldsymbol{f}$ is a $p \times 1$ vector of common factors; and ϵ is a $p \times 1$ vector of residuals. Furthermore, the initial loadings were obtained by the traits having more than one eigenvalue that are acquired from the correlation matrix of *rXij*. Then, final loadings were estimated by using *varimax* rotation criterion (Kaiser, 1958; Olivoto et al., 2019a) as given by:

$$\mathbf{F}=\mathbf{Z}(\mathbf{A}^{\mathbf{T}}\mathbf{R}^{-\mathbf{1}})^{\mathbf{T}}$$

where $\boldsymbol{F}$ is a $g \times f$ matrix with the factorial scores; $\boldsymbol{Z}$ is a $g \times p$ matrix with the standardized means (rescaled); $\boldsymbol{A}$ is a $p \times f$ matrix of canonical loadings; and $\boldsymbol{R}$ is a $p \times p$ correlation matrix between the traits. g, f, and p denote the number of test hybrids/genotypes (rows), factors retained (FA), and traits analyzed, respectively.

The ideotype (ID) was designed by assuming that it has the highest rescaled value, i.e., 100 for all the traits analyzed. Thus, the ID can be defined by $1 \times p$ vector ID such that ID = [100, 100, …., 100]. The final scores for ID were also obtained according to the above formula. Finally, the MGIDI values were computed with the function *mgidi()* from the metan package. If g and f are the number of genotypes/rows and factors retained, respectively, the MGIDI for the ith genotype ($MGIDI_i$) is calculated as follows:

$$MGIDI_i = [\sum_{j=1}^{f}(\gamma_{ij} - \gamma_j)^2]^{0.5}$$

where γ_{ij} is the score of the ith genotype (row) in the jth factor (i = 1, 2, …, g; j = 1, 2, …, f) and γ_j is the jth score of the ideotype. The genotypes with the lowest MGIDI values, i.e., genotypes closer to the ID, exhibited the desired values for all the traits studied. The strengths and weaknesses of a genotype were represented by the proportion of the MGIDI index of the ith row/genotype explained by the jth factor (ij) estimated as follows:

$$\omega_{ij} = \frac{\sqrt{D_{ij}^2}}{\sum_{j=1}^{f}\sqrt{D_{ij}^2}}$$

where D_{ij} is the distance between the ith genotype (row) and the ID for the jth factor. Low contributions of a factor specify that the traits within that factor are similar to the ideotype designed.

2.5.4 Selection differential

The hybrids were selected under different soil moisture regimes through MGIDI values by assuming a selection intensity of ~15% and the selection differential in the percentage of population mean ($\Delta S\%$) was then computed for each trait as follows:

$$\Delta S\,\% = \frac{(X_S - X_0)}{X_0} \times 100$$

where X_s and X_0 are the mean performance value of the selected hybrids and population (original population) mean, respectively.

2.6 Statistical software

All the statistical analyses were carried out on the RStudio, R version 4.1.2 (R Core Team, 2021) software with "metan" version v1.15.0 (Olivoto and Lúcio, 2020) and "ggplot2" version 3.3.4 (Wickham, 2016) packages. Functions such as *gamem_met()* for genotype analysis in multi-environments using mixed-effect or random-effect models, *gmd()* for extracting variance components, and *mgidi()* for the computation of MGIDI values were supplied. The network plots of the pairwise correlation data frame were constructed by using "corrr" package version 0.4.4 (Kuhn et al., 2022).

3 Results

3.1 Mean performances

Mean performances of 75 genotypes for 12 agronomic traits over seven test environments including three moisture regimes are presented in Figure 1. Hybrids 22 (ZH161289; 10.48 t/ha) followed by 30 (ZH161047, 10.35 t/ha), 6 (ZH161361; 9.87 t/ha), 14 (ZH161303; 9.85 t/ha), and 19 (ZH161458; 9.77 t/ha) were identified as top yielders under optimal soil moisture; hybrids 36

(ZH161053; 6.07 t/ha) followed by 22 (ZH161289; 5.96 t/ha), 9 (ZH161384; 5.89 t/ha), 44 (ZH161063; 5.89 t/ha), and 41 (ZH161051; 5.81 t/ha) were the top yielders under drought; and hybrids 30 (ZH161047; 6.21 t/ha) followed by 49 (ZH161398; 6.06 t/ha), 22 (ZH161289; 5.94 t/ha), 14 (ZH161303; 5.90 t/ha), and 44 (ZH161063; 5.57 t/ha) were the top yielders under waterlogging (Supplementary Tables 2A–C). The hybrids ZH161053, ZH161289, ZH161063, ZH161398, and ZH161047 were found to be common under all three moisture conditions in terms of grain yield.

3.2 Variance components across moisture regimes

The genotype had a highly significant effect ($p \leq 0.001$, $p \leq 0.01$, and $p \leq 0.05$) for most of the studied traits except for ASI, SPAD, and KNR under optimal moisture conditions, D50S and EG under drought, and D50 and ASI under waterlogging according to LRT (Table 2). The test showed that the GEI revealed a highly significant effect ($p \leq 0.001$ and $p \leq 0.01$) on all the studied traits except PH across three moisture conditions, D50S under drought, and EH under waterlogging. Similarly, the environment effect was highly significant ($p \leq 0.001$ and $p \leq 0.01$) for all the evaluated traits except for KRE under optimal and drought environment and D50S, ASI, and EL under waterlogging stress conditions. The proportions of total variation explained by genotype, environment, and their interactions (GEI) under individual moisture regimes are shown in Figure 2 (Supplementary Table 3). The accuracy of hybrid selection for the studied traits ranged from 0.40 (PH) to 0.96 (D50A and D50S) under optimal conditions, 0.31 (SPAD) to 0.88 (PH) under drought, and 0.65 (ASI) to 0.93 (SPAD) under waterlogging conditions. The coefficients of determination for GEI effects (R^2_{ge}) were high for GY, KNR, KRE, TW, EG, and EL under all the moisture conditions, indicating that GEI holds an important part of the phenotypic variance component. Most of the traits showed high heritability on genetic mean basis ($h^2_{mg} > 0.60$) under optimal (except ASI and SPAD) and waterlogging conditions (except D50S and ASI), whereas only a few traits such as PH, EH, KRE, and GY showed high heritability.

3.3 Loadings and factor description for MGIDI

According to final loadings obtained from PCA followed by EFA, three factors (FAs with more than 1 eigenvalue) contributing 68.7% of total variability were retained under optimal conditions whereas four factors with 69.6% and four factors with 76.4% towards total variability were retained under drought and waterlogging conditions, respectively (Table 3). Under optimal conditions, PH, EH, SPAD, EL, KNR, and GY belonged to FA1; D50A, D50S, ASI, and TW were included in FA2; and EG and KRE were included in FA3. Among four factors retained in drought, FA1 included TW, EL, KNR, and GY; FA2 included D50A, D50S, and ASI; FA3 included EG and KRE; and FA4 included PH, EH, and SPAD. Similarly, under waterlogging, FA1 included SPAD, TW, EL, KNR, and GY; FA2 included D50A, PH, and EH; FA3 included EG and KRE; and F4 included D50S and ASI.

3.4 Genetic correlations

The pairwise correlation coefficients (r-values) for studied traits were estimated under each moisture regime. The network plots

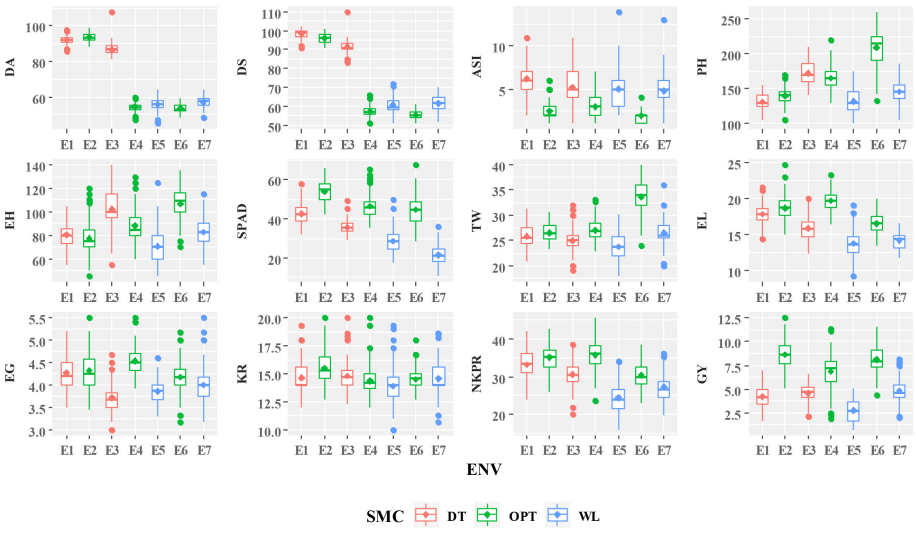

FIGURE 1
Mean performances of studied traits of 75 maize genotypes under different soil moisture conditions including drought (DT), optimal (OPT), and waterlogging (WL). DA, days to 50% anthesis (#); DS, days to 50% silking (#); ASI, anthesis–silking interval (#); PH, plant height (cm); EH, ear height (cm); SPAD, chlorophyll content (SPAD readings); TW, test weight (g); EL, ear length (cm); EG, ear girth (cm); KR, number of kernel rows per ear (#); NKPR, number of kernels per row (#); GY, grain yield (t/ha); SMC, soil moisture condition; DT, drought; WL, waterlogging; OPT, optimal; ENV, environments.

10.3389/fpls.2023.1147424

TABLE 2 Likelihood ratio test and genetic parameters for 12 agronomic traits of 75 maize hybrids under three moisture regimes, namely, optimal, drought, and waterlogging.

Trait	Genetic Parameters									
	LRT_g	LRT_{ge}	σ_p^2	R_{ge}^2	h_{mg}^2	As	E/F	CV_g	CV_r	CV_g/CV_r
Optimal										
D50A	95.49***	12.33***	4.60	0.12	0.93	0.96	11,807.00***	2.32	1.72	1.34
D50S	83.10***	19.17***	5.80	0.16	0.92	0.96	7,061.00***	2.40	1.77	1.36
ASI	0.15^{ns}	29.43***	1.09	0.39	0.16	0.40	14.55***	5.79	32.47	0.17
PH	6.60*	112.39^{ns}	297.50	0.59	0.61	0.78	221.3***	3.91	4.87	0.81
EH	45.10***	14.14***	169.0	0.18	0.86	0.93	81.64***	8.68	9.21	0.94
SPAD	0.87ns	167.65**	33.57	0.72	0.33	0.57	58.29***	2.86	5.63	0.50
EL	7.06***	144.21***	2.03	0.62	0.62	0.78	90.38***	3.15	3.56	0.89
EG	8.14**	145.25***	0.12	0.60	0.63	0.79	27.43***	3.33	3.67	0.91
KRE	14.94***	175.24***	1.39	0.58	0.73	0.85	20.66^{ns}	4.00	3.23	1.24
KNR	1.57^{ns}	239.05***	12.67	0.79	0.40	0.63	48.17***	2.95	3.71	0.79
TW	7.09**	258.82***	5.89	0.70	0.61	0.78	235.2***	3.49	2.92	1.19
GY	18.19***	274.26***	2.08	0.62	0.75	0.86	31.48***	9.76	5.27	184
Managed Drought Stress										
D50A	10.31**	8.71**	7.10	0.21	0.54	0.73	201.9***	1.54	2.11	0.72
D50S	1.89 ^{ns}	2.52 ^{ns}	5.12	0.15	0.29	0.53	245.8***	0.73	1.92	0.38
ASI	4.18*	23.14***	3.87	0.35	0.38	0.62	14.99***	14.56	23.31	0.62
PH	34.01***	1.12 ^{ns}	195.3	0.06	0.78	0.88	288.3***	6.09	5.71	1.06
EH	21.91***	10.65**	186.2	0.19	0.68	0.83	124.2***	9.41	9.11	1.03
SPAD	9.10***	9.47***	19.16	0.23	0.51	0.31	99.31***	5.59	7.81	0.71
EL	4.39*	30.36***	2.04	0.39	0.38	0.62	75.96***	3.71	5.48	0.68
EG	2.11 ^{ns}	67.28***	0.11	0.58	0.30	0.53	96.11***	3.17	4.29	0.74
KRE	16.02***	45.13***	1.68	0.35	0.61	0.78	0.83^{ns}	5.45	4.53	1.20
KNR	5.61*	44.53***	11.42	0.44	0.42	0.65	37.04***	5.04	6.11	0.83
TW	8.26**	57.25***	5.05	0.46	0.49	0.70	18.11***	4.96	4.33	1.09
GY	13.85***	138.34***	0.96	0.50	0.59	0.76	12.19***	13.96	7.17	1.95
Managed Waterlogging Stress										
D50A	7.80**	20.1***	9.15	0.33	0.77	0.88	4.07*	2.66	3.36	0.79
D50S	1.61 ^{ns}	47.31***	13.33	0.54	0.55	0.74	1.27^{ns}	2.06	3.37	0.61
ASI	0.68^{ns}	89.31***	4.77	0.66	0.43	0.65	0.73^{ns}	12.93	22.46	0.57
PH	9.08**	0.76^{ns}	233.0	0.08	0.81	0.89	4.04*	4.86	8.01	0.61
EH	4.33*	1.00^{ns}	148.7	0.09	0.71	0.84	9.70***	5.92	12.56	0.47
SPAD	17.76***	57.76***	26.73	0.37	0.86	0.93	139.4***	13.24	9.67	1.37
EL	12.55***	144.24***	2.38	0.52	0.82	0.91	1.51^{ns}	6.78	3.61	1.88
EG	11.58***	72.56***	0.11	0.45	0.81	0.90	6.34**	4.87	3.77	1.29
KRE	6.57*	161.57***	2.20	0.62	0.74	0.86	10.01**	5.48	3.44	1.60
KNR	10.42**	161.26***	13.06	0.56	0.78	0.89	33.33***	8.21	4.38	1.88

(Continued)

TABLE 2 Continued

Trait	Genetic Parameters									
	LRT_g	LRT_{ge}	σ_p^2	R_{ge}^2	h_{mg}^2	As	E/F	CV_g	CV_r	CV_g/CV_r
TW	5.05*	105.18***	6.34	0.59	0.71	0.84	49.63***	4.81	3.95	1.22
GY	12.99***	196.68***	1.45	0.55	0.83	0.91	157.3***	19.74	7.88	2.51

***significant at 0.1% (p< 0.001); **significant at 1% (p< 0.01); *significant at 5% (p< 0.05); ns, nonsignificant. LRT_g and LRT_{ge}, Likelihood ratio tests for genotype and genotype-by-environment interaction (GEI), respectively; σ_p^2, phenotypic variance; R_{ge}^2, the coefficient of determination for GEI effects; h_{mg}^2 mg, heritability of the genotypic mean; As, the accuracy of genotype selection; E/F, the F value for environment effects; CV_g and CV_r, the genotypic and variation coefficients of variation, respectively. D50A, days to 50% anthesis; D50S, days to 50% silking; ASI, anthesis–silking interval; PH, plant height; EH, ear height; SPAD, chlorophyll content; EL, ear length; EG, ear girth; KRE, number of kernel rows per ear; KNR, number of kernels per a row; TW, test weight and GY, grain yield.

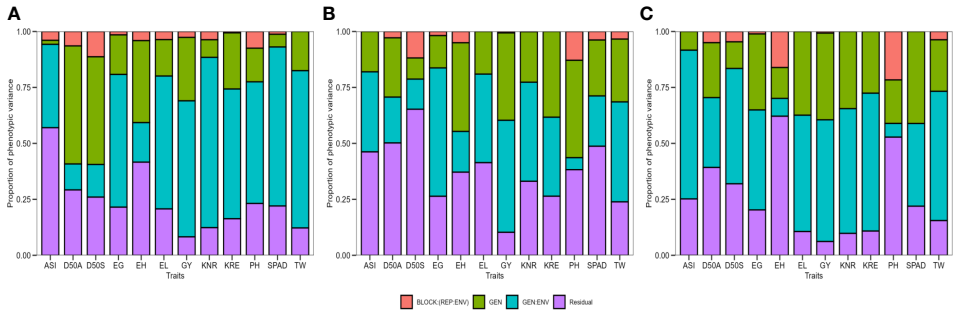

FIGURE 2
The proportion of phenotypic variance for 12 agronomic traits of 75 maize hybrids evaluated under **(A)** optimal, **(B)** drought, and **(C)** waterlogging during winter 2017 and summer–rainy 2018. D50A, days to 50% anthesis; D50S, days to 50% silking; ASI, anthesis–silking interval; PH, plant height; EH, ear height; SPAD, chlorophyll content; EL, ear length; EG, ear girth; KRE, number of kernel rows per ear; KNR, number of kernels per a row; TW, test weight and GY, grain yield.

TABLE 3 Eigenvalues, explained variance, cumulative variance, and final loadings of factors retained after superposition by exploratory factor analysis.

Traits	Optimal			Managed Drought				Managed Waterlogging			
	FA1	FA2	FA3	FA1	FA2	FA3	FA4	FA1	FA2	FA3	FA4
D50A	0.14	−0.88	0.11	0.11	0.98	−0.04	0.15	−0.30	0.67	−0.19	0.38
D50S	0.07	−0.95	−0.03	−0.34	0.78	−0.10	−0.17	−0.32	0.38	−0.13	0.83
ASI	−0.23	−0.52	−0.44	−0.48	−0.59	−0.06	−0.38	−0.10	−0.33	0.07	0.82
PH	−0.82	0.16	0.20	−0.23	−0.19	0.12	−0.81	−0.12	−0.83	−0.14	0.05
EH	−0.76	0.35	0.10	−0.07	0.02	−0.02	−0.92	−0.17	−0.77	−0.18	0.14
SPAD	−0.59	−0.20	0.45	−0.34	0.07	−0.17	−0.36	−0.65	−0.19	−0.48	0.21
TW	−0.23	−0.52	0.33	−0.44	0.25	0.44	0.31	−0.77	0.25	−0.04	0.19
EL	−0.71	−0.22	0.05	−0.79	−0.03	0.12	−0.06	−0.86	−0.14	0.15	−0.03
EG	−0.22	−0.06	0.78	−0.18	0.09	−0.73	0.10	0.01	−0.22	−0.83	0.15
KRE	−0.31	−0.01	0.82	−0.08	0.03	−0.81	−0.04	−0.16	0.03	−0.87	−0.13
KNR	−0.83	−0.04	0.24	−0.74	0.01	−0.31	−0.28	−0.67	−0.46	−0.17	0.12
GY	−0.70	−0.29	0.53	−0.81	0.03	−0.31	−0.20	−0.75	−0.02	−0.37	0.35
Eigenvalues	4.54	2.51	1.21	3.47	2.21	1.43	1.25	4.16	2.40	1.47	1.14
Variance (%)	37.83	20.93	10.10	28.90	18.38	11.94	10.39	34.64	20.02	12.26	9.52
Accumulated (%)	37.83	58.77	68.86	28.90	47.28	59.22	69.61	34.64	54.66	66.92	76.43

D50A, days to 50% anthesis; D50S, days to 50% silking; ASI, anthesis–silking interval; PH, plant height; EH, ear height; SPAD, chlorophyll content; EL, ear length; EG, ear girth; KRE, number of kernel rows per ear; KNR, number of kernels per a row; TW, test weight and GY, grain yield.

(Figure 3) of the correlation data frames of each moisture regime representing more highly associated traits appear to cluster together and connected by stronger paths where blue colored paths indicated positive correlations while red indicated negative correlations. The proximity of traits in the plots was determined by using multidimensional clustering. Inter-trait relationships are mostly positive and stronger under optimal moisture but did not follow the same trend under stress conditions. Grain yield showed a positively strong association with most of the traits under optimal moisture but not under stress. For example, GY had a strong positive correlation with PH (r = 0.63) under optimal conditions and had a weak correlation under drought (r = 0.27) and waterlogging (r = 0.17) conditions (Supplementary Table 4). Flowering traits such as D50A, D50S, and ASI showed negative correlation with GY across the moisture conditions.

3.5 Multi-trait genotype–ideotype distance index and selection gains

The 11 hybrids were selected in each soil moisture condition according to the MGIDI by assuming the selection index 15% (Table 4). Genotypes 14 (ZH161303, MGIDI = 2.91), 26 (ZH161042, 2.97), 30 (ZH161047, 3.04), 22 (ZH161289, 3.25), 60 (ZH161129, 3.34), 58 (ZH161064, 3.45), 44 (ZH161063, 3.57), 49 (ZH161398, 3.64), 64 (ZH161078, 3.67), 59 (ZH161068, 3.76), and 36 (ZH161053, 3.79) were screened under optimal environment (Figure 4A), while genotypes 22 (ZH161289, 2.49), 44 (ZH161063, 2.98), 19 (ZH161458, 3.06), 41 (ZH161051, 3.13), 74 (P3502, 3.33), 50 (ZH161410, 3.63), 14 (ZH161303, 3.68), 37 (ZH161083, 3.72), 9 (ZH161384, 3.82), 53 (ZH161484, 3.87), and 46 (ZH161071, 4.01) were screened under drought (Figure 4B), and genotypes 49 (ZH161398), 14 (ZH161303), 30 (ZH161047), 13 (ZH161358), 19 (ZH161458), 22 (ZH161289), 8 (ZH161330), 60 (ZH161129), 75 (Hytech 5106), 58 (ZH161064), and 64 (ZH161078) were screened under waterlogging stress (Figure 4C). The selected hybrids under each individual moisture condition and the two hybrids, viz., 22 (ZH161289) and 14 (ZH161303), that shared in common the three moisture regimes are given in a Venn diagram (Figure 5, Supplementary Table 5).

The selected genotypes under each moisture regime resulted in desired selection gains (SGs) for the mean performance of all the studied traits, i.e., positive SGs for GY, PH, EH, EG, EL, KNR, KRE, and SPAD, and negative gains for the flowering traits such as D50A, D50S, and ASI (Table 5). The mean performance of selected genotypes for GY increased more than 11% SG under optimal and drought conditions, whereas it was 22.6% under waterlogging. The contribution of each factor retained towards the distance from MGIDI to the ideotype (ID) under the three moisture regimes is shown in Supplementary Table 6.

3.6 The strengths and weaknesses view of selected hybrids

The radar plot (Figures 6A–C) depicts the strengths and weaknesses of the selected hybrids over three moisture conditions. For each selected hybrid, the contribution of each factor towards the MGIDI is ranked from the most contributing factor (close to plot center) to the least contributing factor (away from the plot center). Smaller proportions explained by a factor that is placed closer to the external edge indicate that the trait within that factor is more similar to the ideotype. A view on strengths and weaknesses under optimal moisture revealed that the performance of the selected genotypes, viz., 22 (ZH161289) and 14 (ZH161303), showed strengths related to factor FA1 that holds PH, EH, SPAD, EL, KNR, and GY with positive SGs, whereas genotypes 59 (ZH161068), 26 (ZH161042), 44 (ZH161063), 58 (ZH161064), and 60 (ZH161129) showed strengths related to FA2 with flowering characteristics (D50A, D50S, and ASI) showing negative gains (Figure 6A). Concerning FA3, genotypes 30 (ZH161047) and 49 (ZH161398) performed well. Under managed drought (Figure 6B), most of the selected hybrids contributed more towards MGIDI through FA1 except 19 (ZH161458) and 41 (ZH161051). Hybrids 50 (ZH161410), 44 (ZH161063), 37 (ZH161083), and 46 (ZH161071) showed strength related to FA2 with desirable negative gain in flowering traits such as D50A, D50S, and ASI. Genotypes 9 (ZH161384) and 46 (ZH161071) had strength for FA3 whereas 53 (ZH161484) followed by 74 (P3502), 44 (ZH161063), 50 (ZH161410), and 9 (ZH161384) showed strengths pertaining to FA4. Similarly

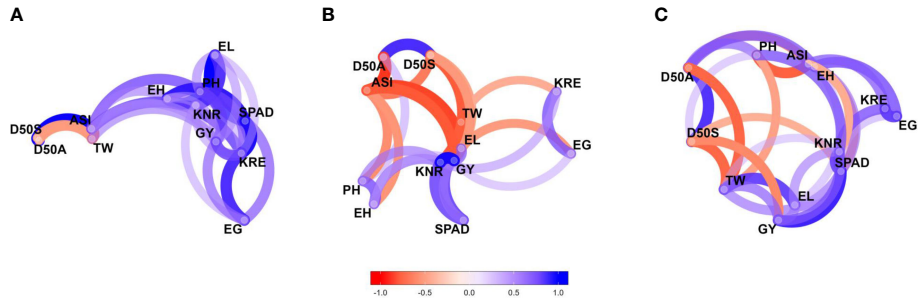

FIGURE 3
Genetic correlation network plots of 12 agronomic traits of 75 maize hybrids evaluated under **(A)** optimal, **(B)** drought, and **(C)** waterlogging during winter 2017 and summer–rainy 2018. Blue paths indicate positive correlations, and red paths indicate negative correlations. D50A, days to 50% anthesis; D50S, days to 50% silking; ASI, anthesis–silking interval; PH, plant height; EH, ear height; SPAD, chlorophyll content; EL, ear length; EG, ear girth; KRE, number of kernel rows per ear; KNR, number of kernels per a row; TW, test weight and GY, grain yield.

TABLE 4 Multi-trait genotype–ideotype distance index (MGIDI) values of the 75 maize hybrids tested across seven environments during winter 2017–2018 and summer–rainy 2018.

Hybrids	MGIDI value			Hybrids	MGIDI value			Hybrid	MGIDI value		
	OPT	MDT	MWL		OPT	MDT	MWL		OPT	MDT	MWL
1	4.83	5.58	5.33	26	**2.97**	4.54	4.66	51	4.95	5.95	5.61
2	4.12	5.92	7.23	27	5.78	5.59	5.33	52	6.26	6.28	6.69
3	5.21	4.66	5.71	28	5.88	6.08	4.50	53	4.33	**3.87**	5.56
4	5.62	5.51	4.53	29	5.45	4.94	5.46	54	5.91	5.27	5.76
5	5.00	7.01	6.64	30	**3.04**	4.10	**3.22**	55	5.20	4.51	4.23
6	3.81	5.10	5.13	31	5.10	4.39	4.65	56	5.94	5.15	5.09
7	5.54	6.08	5.66	32	7.15	6.50	5.46	57	6.54	7.03	6.59
8	4.06	4.59	**3.48**	33	5.42	6.38	6.52	58	**3.45**	5.45	**4.14**
9	6.09	**3.82**	4.58	34	5.23	5.01	5.96	59	**3.76**	4.92	4.26
10	5.31	5.53	5.53	35	5.22	5.20	5.92	60	**3.34**	5.16	**4.05**
11	6.43	5.96	5.50	36	**3.79**	7.04	4.45	61	5.73	4.40	4.32
12	5.07	5.21	6.42	37	5.17	**3.72**	4.46	62	6.38	5.01	5.59
13	5.44	5.28	**3.33**	38	5.73	4.91	5.92	63	5.21	5.78	6.19
14	**2.91**†	**3.68**	**3.13**	39	4.68	5.21	4.90	64	**3.67**	4.44	**4.16**
15	6.24	4.53	6.24	40	4.98	4.95	5.62	65	5.92	6.89	5.63
16	5.11	5.22	5.49	41	3.88	**3.13**	4.59	66	4.93	5.54	5.32
17	5.46	4.40	5.26	42	4.65	4.09	4.94	67	5.20	5.65	5.41
18	4.98	4.60	5.97	43	4.64	6.45	5.52	68	5.63	6.79	5.74
19	3.85	**3.06**	**3.39**	44	**3.57**	**2.98**	4.37	69	4.67	6.44	5.40
20	5.27	5.66	5.51	45	4.99	5.65	5.11	70	5.67	5.46	5.89
21	5.58	5.07	4.86	46	4.94	**4.01**	5.56	71	3.98	5.72	4.56
22	**3.25**	**2.49**	**3.43**	47	4.79	5.56	4.87	72	4.96	4.31	4.41
23	5.77	6.14	5.54	48	4.07	5.23	5.98	73	4.16	4.12	4.75
24	6.89	4.65	5.79	49	**3.64**	4.92	**2.95**	74	4.60	**3.33**	4.66
25	5.16	4.82	4.87	50	5.02	**3.63**	4.46	75	4.24	5.07	**4.10**

MGIDI, multi-trait genotype–ideotype distance index; OPT, optimal; MDT, managed drought; MWL, managed waterlogging.
†Bold values indicate selected hybrids by assuming 15% selection intensity.

under waterlogging conditions (Figure 6C), most of the selected genotypes showed strengths related to all the factors except FA3. According to FA1, genotype 30 (ZH161047) performed very well while genotype 14 (ZH161303) performed poorly with a maximum contribution towards the MGIDI. All the 11 selected hybrids showed strengths related to FA2 and FA3 and weaknesses related to FA3.

4 Discussion

The study focused on the performance evaluation of 75 pre-released medium-duration maize hybrids for 12 agronomic characteristics in two consecutive years (2017–2018) under three soil moisture regimes including optimal, drought, and waterlogging at two locations. In general, the grain yield potential and the performance of other yield-contributing characteristics of the available germplasm are a very crucial step in identifying genotypes with ideal trait combinations suitable across target environments, which can be used in future breeding programs (Bocianowski et al., 2019). The maize crop in the farmer's field is exposed to a combination of stresses in a single life cycle. Banziger et al. (2000) screened a set of tropical maize hybrids independently under drought and low N environments and identified several physiological traits associated with tolerance under a single stress and conferred tolerance for the other stress. Our results showed that the environment and GEI effects for most of the traits recorded were statistically significant ($p \leq 0.001$ or $p \leq 0.01$). This shows that hybrid mean performances varied across the soil moisture conditions, which can be attributed more towards the diversification of genotypes and provides ample amount of variation for easy selection (Oliveira et al., 2014). The results from the present investigation suggested that

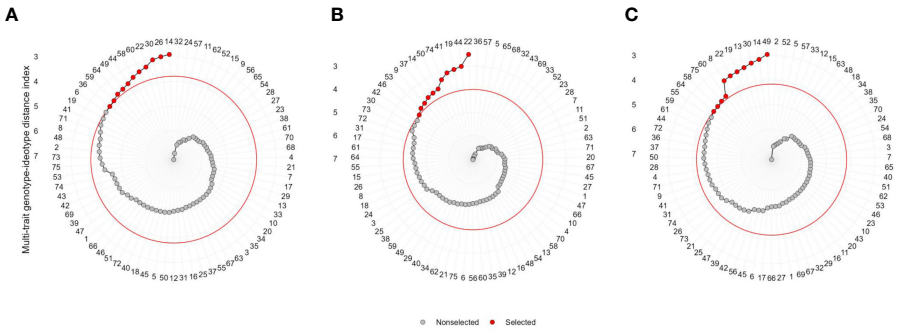

FIGURE 4
Genotype ranking in ascending order for the MGIDI index tested under **(A)** optimal, **(B)** drought, and **(C)** waterlogging. The selected hybrids are shown in red color and the red colored circle represents the cut-point according to the selection pressure (~15%).

selection of maize hybrids based on multi-factorial analysis is effective and that most of the potential and wide adoptive maize hybrids were influenced by soil moisture status and genetic factors, as well as their interactions (GEI). Understanding the complexity of GEI through suitable statistical techniques is the best way to screen out the wide adoptable stress-resilient maize hybrids in the target environment. Statistically significant variation of G, E, and GEI among evaluated hybrids across the moisture regimes would make it possible to identify genotypes for both stress and non-stress environments. Previous works also reported the existence of significant variations among maize hybrids tested across managed stresses for grain yield (Wegary et al., 2014; Abakemal et al., 2016; Njeri et al., 2017; Adeseye et al., 2018; Mebratu et al., 2019; Singamsetti et al., 2021).

Since the physiological and molecular responses of crop plants exposed to a combination of stresses are fairly known, understanding the effects of different individual stresses on crop plants as well as their combinations is vital (Voesenek and Pierik, 2008). Early flowering (D50A and D50S), high ASI values, and lower mean performances for PH, EH, TW, EL, EG, NKE, and NKR under moisture stress conditions compared to optimal environments resulted in poor grain yields (Supplementary Tables 2A–C). The impact of moisture level on traits' expression can be observed by their mean performances under different environments (Figure 1). A few outliers in the box plots of recorded traits were probably due to inconsistent expressions that indicated the severity of stress and interaction of genotype with soil moisture level (Figure 1). Delayed flowering and maturity due to cool temperature at early stages followed by prolonged day length and drought periods at later stages resulted in the drastic decline (up to 30%–90%) in the crop yield in late *Rabi*/winter maize crop (Sah et al., 2020). Our study also witnessed early senescence probably due to the reduction in lamellar content of light harvest chlorophyll proteins under water-limited situations (Anjum et al., 2011; Verma et al., 2004). The observed significant reduction in mean GY under waterlogging conditions with a poor performance of other secondary traits is probably due to the reduced leaf growth, and a worse effect on the cell turgor could be attributed to the decline in the carotenoid content (El-Shihaby et al., 2002; Tripathi et al., 2003).

Understanding the magnitude and direction of correlations among studied traits and how they change across the moisture regimes along with variability parameters would assist the breeders in improving a characteristic that brings simultaneous improvement in other characteristics. The results explained the importance of flowering traits, especially ASI, in the development of drought-tolerant maize cultivars. The larger ASI values lead to the failure of a proper seed set due to poor availability of viable pollen for late emerged female flowers owing to the delay in silk extrusion, premature lodging, and reduced rates of net photosynthesis arising from oxidative damage to chloroplasts (Nelimor et al., 2020). The relationship between GY and ASI in our findings was in agreement with previous reports on maize under water deficit (Edmeades and Daynard, 1979) and under waterlogging conditions (Zaidi and Singh, 2001; Zaidi et al., 2004; Zaidi et al., 2007). The stronger associations between grain yield and phenological traits under drought conditions than under optimal moisture were reported by Sah et al. (2020). In contrast, our results suggested that the direct selection of most of the traits would be more

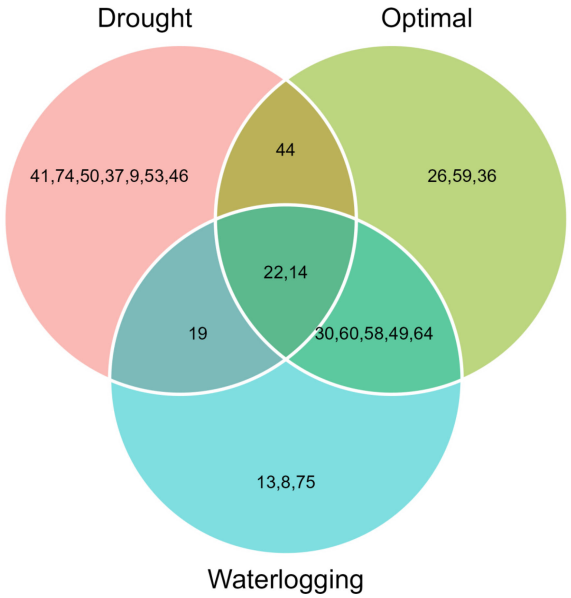

FIGURE 5
Common maize hybrid shared across the soil moisture regimes including optimal, drought, and waterlogging shown in the Venn chart.

TABLE 5 Selection gains for mean performance of 75 maize hybrids within the soil moisture regime based on MGIDI values.

Trait†	Factor	Sense	Goal	Mean performance			
				Xo	Xs	SD	SD%
Optimal							
PH	FA1	Increase	Yes	170.96	174.14	3.18	1.86
EH	FA1	Increase	Yes	90.66	92.67	2.01	2.22
SPAD	FA1	Increase	Yes	48.30	49.05	0.75	1.55
EL	FA1	Increase	Yes	18.26	18.63	0.37	2.02
KNR	FA1	Increase	Yes	33.73	34.22	0.49	1.46
GY	FA1	Increase	Yes	7.87	8.74	0.87	11.09
D50A	FA2	Decrease	Yes	67.18	66.18	−1.00	−1.48
D50S	FA2	Decrease	Yes	69.60	68.59	−1.02	−1.46
ASI	FA2	Decrease	Yes	2.42	2.42	−0.01	−0.23
TW	FA2	Increase	Yes	29.05	29.82	0.77	2.65
EG	FA3	Increase	Yes	4.34	4.41	0.07	1.58
KRE	FA3	Increase	Yes	14.80	15.20	0.40	2.70
Managed Drought							
TW	FA1	Increase	Yes	25.36	25.28	0.08	0.32
EL	FA1	Increase	Yes	16.79	17.13	0.34	2.05
KNR	FA1	Increase	Yes	31.82	33.13	1.31	4.11
GY	FA1	Increase	Yes	4.39	4.90	0.51	11.67
D50A	FA2	Decrease	Yes	89.30	88.47	−0.83	−0.93
D50S	FA2	Decrease	Yes	95.00	94.48	−0.52	−0.54
ASI	FA2	Decrease	Yes	5.71	5.58	−0.13	−2.28
EG	FA3	Increase	Yes	3.99	4.04	0.05	1.17
KRE	FA3	Increase	Yes	14.72	14.98	0.26	1.76
PH	FA4	Increase	Yes	151.36	153.83	2.47	1.63
EH	FA4	Increase	Yes	91.25	96.72	5.47	6.00
SPAD	FA4	Increase	Yes	39.14	40.22	1.09	2.77
Managed Waterlogging							
SPAD	FA1	Increase	Yes	25.04	28.52	3.48	13.90
TW	FA1	Increase	Yes	25.10	25.62	0.52	2.07
EL	FA1	Increase	Yes	13.92	14.25	0.33	2.40
KNR	FA1	Increase	Yes	25.84	27.31	1.47	5.68
GY	FA1	Increase	Yes	3.80	4.65	0.86	22.59
D50A	FA2	Decrease	Yes	56.33	55.97	−0.36	−0.64
PH	FA2	Increase	Yes	138.49	141.44	2.95	2.13
EH	FA2	Increase	Yes	76.56	78.60	2.03	2.66

(Continued)

TABLE 5 Continued

Trait†	Factor	Sense	Goal	Mean performance			
				Xo	Xs	SD	SD%
EG	FA3	Increase	Yes	3.93	4.04	0.11	2.79
KRE	FA3	Increase	Yes	14.23	14.60	0.37	2.61
D50S	FA4	Decrease	Yes	61.23	60.74	−0.48	−0.79
ASI	FA4	Decrease	Yes	4.89	4.69	−0.20	−4.06

FA1, factor 1; FA2, factor 2; FA3, factor 3; FA4, factor 4; †D50A, days to 50% anthesis; D50S, days to 50% silking; ASI, anthesis–silking interval; PH, plant height; EH, ear height; SPAD, chlorophyll content; EL, ear length; EG, ear girth; KRE, number of kernel rows per ear; KNR, number of kernels per a row; TW, test weight and GY, grain yield; SD, selection differential; SD%, percent selection differential; Xo, mean of the original population; Xs, mean of the selected hybrids.

effective under optimal conditions due to the resulting strong correlation, while there is only moderate correlation under moisture stress conditions (Figure 3). Several previous correlation studies on maize genotypes under a single environment have been reported, but there is limited literature available with regard to changing a trait's expression and the association of a trait with other traits across various environments. A few researchers reported genetic correlations among maize lines evaluated across two moisture regimes, namely, moisture-deficit and well-water conditions, across two seasons/years (Oyekunle and Badu-Apraku, 2018; Nelimor et al., 2019; Al-Naggar et al., 2020; Nelimor et al., 2020; Singamsetti et al., 2021).

Plant breeding programs aiming at initial selection under a single environment with no stress or only a single stress condition may lead to the loss of desirable alleles or genetic variability for additional stresses other than target stress (Cairns et al., 2013). Thus, the use of the MGIDI becomes especially important for screening hybrids based on multiple traits such as many secondary traits along with grain yield under various stress environments. Apart from many classical linear multi-trait phenotypic selection techniques available (Smith, 1936; Hazel, 1943; Bhering et al., 2012; Jahufer and Casler, 2015; Bizari et al., 2017; Cerón-Rojas and Crossa, 2018; Burdon and Li, 2019), MGIDI is a unique selection technique that is free from weighing (economic) coefficients (Bizari et al., 2017) and multicollinearity issues (Smith, 1936), and it uses the distance between genotypes and a defined ideotype based on the breeder's requirement (Olivoto and Nardino, 2021). The method emerged as a powerful tool to identify the genotypes with better mean performance and desired SGs and also to estimate the strengths and weaknesses of hybrids (selected/unselected). The multi-trait selection index (MTSI) and MGIDI evaluation systems are novel and unique techniques that have many practical applications in plant breeding practices (Nelimor et al., 2020; Benakanahalli et al., 2021; Koundinya et al., 2021; Pour-Aboughadareh et al., 2021; Hadou el hadj et al., 2022; Yue et al., 2022a; Yue et al.,2022b; Nardino et al., 2022; Dhand and Garg, 2023; Memon et al., 2023). The multi-trait frameworks and MGIDI and MTSI indices follow a similar rescaling process to retain the unchanged correlation structure of original data and to identify the superior genotypes with respect to multiple traits simultaneously (Olivoto et al., 2019b). The rescaling technique requires a selection direction, and it places all the agronomic traits in a range of 0–100 and the ideotype defined by traits' rescaled value is assumed to be 100. The dimensional reduction was carried out by performing exponential factorial analysis in which 12 traits represented a few (three in optimal and four each in drought and waterlogging) final latent variables (FAs, factors) with maximum trait loadings.

According to the MGIDI index, the selected genotypes in optimal moisture were ZH161303, ZH161042, ZH161047, ZH161289, ZH161129, ZH161064, ZH161063, ZH161398, ZH161078, ZH161068, and ZH161053; the selected genotypes under drought conditions were ZH161289, ZH161063,

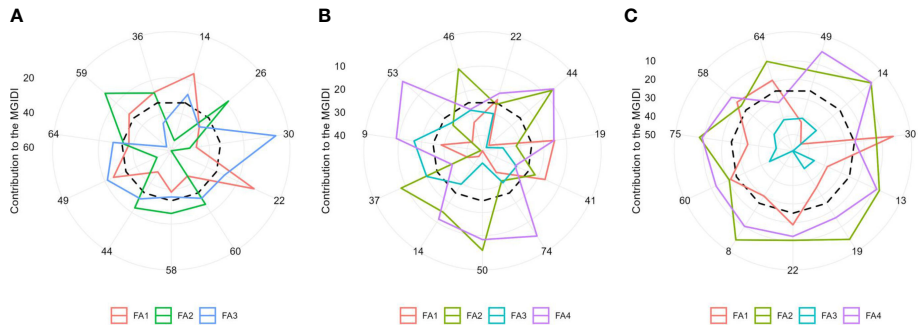

FIGURE 6
The strengths and weaknesses view of the selected hybrids is shown as the proportion of each factor on the computed MGIDI values over three soil moisture regimes, namely, **(A)** optimal, **(B)** drought, and **(C)** waterlogging. The smallest the proportion explained by a factor (closer to the external edge), the closer the traits within that factor are to the ideotype. The dashed line shows the theoretical value if all the factors had contributed equally.

ZH161458, ZH161051, P3502, ZH161410, ZH161303, ZH161083, ZH161384, ZH161484, and ZH161071; and the selected genotypes under waterlogging stress were ZH161398, ZH161303, ZH161047, ZH161358, ZH161458, ZH161289, ZH161330, ZH161129, Hytech 5106, ZH161064, and ZH161078. Apart from the genotypes selected above, genotypes 6 (ZH161361), 42 (ZH161054), and 55 (ZH15449) were placed at the cutting points under optimal, drought, and waterlogging conditions, respectively (Figure 4). These hybrids had interesting features that could be exploited in future breeding programs. The MGIDI index is a unique and easy-to-interpret selection procedure that has many practical applications to obtain long-term genetic gain in primary traits (such as grain yield) without jeopardizing gains of secondary traits (such as plant height). The proportion explained by each factor towards the MGIDI index, i.e., "strengths and weaknesses view" (Figures 6A–C), is an important graphical tool to identify the strengths and weaknesses of test hybrids in terms of "trait (group of traits) need to be improved" and is an added advantage over existing indices. For example, under optimal moisture, the lower contribution of FA1 in genotype 14 (ZH161303) revealed that the genotype was highly productive in terms of PH, EH, SPAD, EL, KNR, and GY, but the same genotype had a poor performance in terms of flowering traits, which can be inferred due to the higher contribution of FA2 towards MGIDI (Figure 6A). Similarly, FA3 was placed almost near the dashed lines of the radar plot, which represented the theoretical value if all the factors had contributed equally. The high contribution of FA1 (Figure 6B) and FA3 (Figure 6C) towards genotype–ideotype index distance indicated that there is a possibility of improvement in TW, EL, KNR, and GY in selected genotypes (except 19 and 41) under drought and in EG and KRE under waterlogging conditions. A similar study was reported by Gabriel et al. (2019) and Olivoto and Nardino (2021), who evaluated a set of 13 strawberry cultivars, wherein the strengths were described by employing MGIDI. Benakanahalli et al. (2021) proposed a framework for identifying promising guar genotypes with productive traits such as gum and seed yield across three seasons by using MGIDI.

5 Conclusion

Our experimental findings recommended that MGIDI can be used for the effective selection of superior hybrids/genotypes by considering multiple traits and helping plant breeders make better strategic decisions. The results showed that the hybrids ZH161053, ZH161289, ZH161063, ZH161398, and ZH161047 were found to be common across all the three moisture regimes solely on the basis of grain yield, while two genotypes, ZH161289 and ZH161303, were found to be common in terms of all the studied traits. Also, the study helps improve a certain trait or a group of traits (either yield contributors or stress-responsive ones) in particular moisture stress environments.

Data availability statement

The original contributions presented in the study are included in the article/Supplementary Material. Further inquiries can be directed to the corresponding authors.

Author contributions

AS, PZ, and KSe contributed to the conceptualization and design of the study, field experimentation, and preparation of the manuscript. KSe, MV, and AM revised and edited the original manuscript. AS and TV contributed to formal analysis of data and visualization. AS, KM, MK and KSh contributed to field experiments and data recording. All authors have read and approved the final manuscript.

Acknowledgments

Banaras Hindu University, Varanasi and CIMMYT-Asia, Hyderabad were acknowledged for providing necessary facilities, material, and financial grants. The first author was highly grateful to the Project Coordinator, CRMA, CIMMYT, Hyderabad for constant support and guidance on which this manuscript was developed. On a personal note, the work has been dedicated to the Chairman of this Ph.D. program, Prof. J. P. Shahi, who made a significant contribution towards the maize community of the Indo-Gangetic plains of India until his last breath.

Conflict of interest

The authors declare that the research was conducted in the absence of any commercial or financial relationships that could be construed as a potential conflict of interest.

Publisher's note

Supplementary material

The Supplementary Material for this article can be found online at: https://www.frontiersin.org/articles/10.3389/fpls.2023.1147424/full#supplementary-material

References

Abakemal, D., Shimelis, H., and John, D. (2016). Genotype-by-environment interaction and yield stability of quality protein maize hybrids developed from tropical-highland adapted inbred lines. *Euphytica* 209, 757–769. doi: 10.1007/s10681-016-1673-7

ADB (2009) *Climate change threatens water, food security of 1.6 billion south asians*. Available at: https://reliefweb.int/report//.

Adeseye, A. O., Amusa, N. A., Ijagbone, I. F., Aladele, S. E., and Ogunkanri, L. A. (2018). Genotype-by-environment interactions of twenty accessions of cowpea (*Vigna unguiculata* (L) walp) across two locations in Nigeria. *Ann. Agrar. Sci.* 16, 481–489. doi: 10.1016/j.aasci.2018.03.001

Al-Naggar, A. M. M., Shafik, M. M., Musa, R. Y. M., Younis, A. S. M., and Anany, A. H. (2020). Genetic variability of maize hybrids and populations and interrelationships among grain yield and its related traits under drought and low n using multivariate analysis. *Asian J. Biochemistry Genet. Mol. Biol.* 4 (2), 26–44. doi: 10.9734/ajbgmb/2020/v4i230102

Anjum, S. A., Farooq, M., Wang, L. C., Xue, L. L., Wang, S. G., Wang, L., et al. (2011). Gas exchange and chlorophyll synthesis of maize cultivars are enhanced by exogenously-applied glycinebetaine under drought conditions. *Plant Soil Environ.* 57 (7), 326–331. doi: 10.17221/41/2011-PSE

Banziger, M., Edmeades, G. O., Beck, D., and Bellon, M. (2000). *Breeding for drought and low nitrogen tolerance: From theory to practice* (Mexico: CIMMYT). D.F.

Bartlett, M. S. (1937). Properties of sufficiency and statistical tests. *Proc. R. Soc. London. Ser. A Math. Phys. Sci.* 160 (901), 268–282. doi: 10.1098/rspa.1937.0109

Benakanahalli, N. K., Sridhara, S., Ramesh, N., Olivoto, T., Sreekantappa, G., Tamam, N., et al. (2021). Framework for identification of stable genotypes basedon MTSI and MGDII indexes: An example in guar (*Cymopsis tetragonoloba* l.). *Agronomy* 11, 1221. doi: 10.3390/agronomy11061221

Bhering, L. L., Laviola, B. G., Salgado, C. C., Sanchez, C. F. B., Rosado, T. B., and Alves, A. A. (2012). Genetic gains in physic nut using selection indexes. *Pesquisa Agropecuaria Bras.* 47, 402–408. doi: 10.1590/S0100-204X2012000300012

Bizari, E. H., Val, B. H. P., Pereira, E. D. M., Mauro, A. O. D., Unêda-Trevisoli, S. H., and Bizari, E. H. (2017). Selection indices for agronomic traits in segregating populations of soybean. *Rev. Ciencia Agronomica* 48, 110–117. doi: 10.5935/1806-6690.20170012

Bocianowski, J., Niemann, J., and Nowosad, K. (2019). Genotype-by-environment interaction for seed quality traits in interspecific cross-derived brassica lines using additive main effects and multiplicative interaction model. *Euphytica* 215 (1), 7. doi: 10.1007/s10681-018-2328-7

Brown, M. E., and Funk, C. C. (2008). Food security under climate change. *Sci. (New York N.Y.)* 319, 580–581. doi: 10.1126/science.1154102

Burdon, R. D., and Li, Y. (2019). Genotype–environment interaction involving site differences in expression of genetic variation along with genotypic rank changes: simulations of economic significance. *Tree Genet. Genomes* 15, 1–10. doi: 10.1007/s11295-018-1308-3

Cairns, J. E., Crossa, J., Zaidi, P. H., Grudloyma, P., Sanchez, C., Araus, J. L., et al. (2013). Identification of drought, heat and combined drought and heat tolerant donors in maize. *Crop Sci.* 53 (4), 1335–1346. doi: 10.2135/cropsci2012.09.0545

Cairns, J. E., Sonder, K., Zaidi, P. H., Verhulst, N., Mahuku, G., Babu, R., et al. (2012). Maize production in a changing climate: impacts, adaptation, and mitigation strategies. *Adv. Agron.* 114, 1–58. doi: 10.1016/B978-0-12-394275-3.00006-7

Cerón-Rojas, J. J., and Crossa, J. (2018). *Linear selection indices in modern plant breeding* (Cham, Switzerland: Springer).

Dempster, A. P., Laird, N. M., and Rubin., D. B. (1977). Maximum likelihood from incomplete data *via* the EM algorithm. *J. R. Stat. Soc B* 39, 1–38.

Dhand, A., and Garg, N. (2023). Genotype × environment interaction using AMMI and MTSI analysis for growth and yield attributes of radish (*Raphanus sativus* l.) under high temperature stress conditions of north Indian plains. *Scientia Hortic.* 313, 111880. doi: 10.1016/j.scienta.2023.111880

Edmeades, G. O., and Daynard, T. B. (1979). The development of plant-to-plant variability in maize at different planting densities. *Can. J. Plant Sci.* 59, 561–576. doi: 10.4141/cjps79-095

El-Shihaby, O. A., Alla, M. M. N., Younis, M. E., and El-Bastawisy, Z. M. (2002). Effect of kinetin on photosynthetic activity and carbohydrate content in waterlogged or sea-water treated *Vigna sinensis* and *Zea mays* plants. *Plant Biosyst.* 136, 277–290. doi: 10.1080/11263500212331351189

FAOSTAT (2022) Statistical Database. (Rome: Food and Agriculture Organization of the United Nations). Available at: http://faostat.fao.org.

Gabriel, A., De Resende, J. T., Zeist, A. R., Resende, L. V., Resende, N., and Zeist, R. A. (2019). Phenotypic stability of strawberry cultivars based on physicochemical traits of fruits. *Hortic. Bras.* 37, 75–81. doi: 10.1590/s0102-053620190112

Gauch, H. G. (2013). A simple protocol for AMMI analysis of yield trials. *Crop Sci.* 53 (5), 1860–1869. doi: 10.2135/cropsci2013.04.0241

Hadou el hadj, D., Tellah, S., Goumeida, K., Aitouakli, S., Tifest, C., Ammi, N., et al. (2022). Evaluation of adaptability of different faba bean landraces under Mediterranean field conditions of central-northern Algeria. *Agronomy.* 12 (7), 1660. doi: 10.3390/agronomy12071660

Hazel, L. N. (1943). The genetic basis for constructing selection indexes. *Genetics* 28, 476–490. doi: 10.1093/genetics/28.6.476

Jahufer, M. Z. Z., and Casler, M. D. (2015). Application of the smith-hazel selection index for improving biomass yield and quality of switch grass. *Crop Sci.* 55, 1212–1222. doi: 10.2135/cropsci2014.08.0575

Jarquin, D., Howard, R., Crossa, J., Beyene, Y., Gowda, M., Martini, J. W., et al. (2020). Genomic prediction enhanced sparse testing for multi-environment trials. *G3 Genes Genomes Genet.* 10, 2725–2739. doi: 10.1534/g3.120.401349

Kaiser, H. F. (1958). The varimax criterion for analytic rotation in factor analysis. *Psychometrika* 23, 187–200. doi: 10.1007/BF02289233

Kendal, E. (2016). GGE biplot analysis of multi-environment yield trials in barley (Hordeum vulgare L.) cultivars. *Ekin J. Crop Breed. Gen.* 2 (1), 90–99.

Kendal, E. (2019). Comparing durum wheat cultivars by genotype × yield × trait and genotype × trait biplot method. *Chil. J. Agric. Res.* 79 (4), 512–522. doi: 10.4067/S0718-58392019000400512

Koundinya, A. V. V., Ajeesh, B. R., Hegde, V., Sheela, M. N., Mohan, C., and Asha, K. I. (2021). Genetic parameters, stability and selection of cassava genotypes between rainy and water stress conditions using AMMI, WAAS, BLUP and MTSI. *Sci. Hortic.* 281, 109949. doi: 10.1016/j.scienta.2021.109949

Kuhn, M., Jackson, S., and Cimentada, J. (2022). *"Corrr: Correlations in r"*. Available at: https://github.com/tidymodels/corrr.

Langner, J. A., Zanon, A. J., Streck, N. A., Reiniger, L. R., Kaufmann, M. P., and Alves, A. F. (2019). Maize: Key agricultural crop in food security and sovereignty in a future with water scarcity. *Rev. Bras. Eng. Agric. e Ambient.* 23 (9), 648–654. doi: 10.1590/1807-1929/agriambi.v23n9p648-654

Lobell, D. B., Burke, M. B., Tebaldi, C., Mastrandrea, M. D., Falcon, W. P., and Naylor, R. L. (2008). Prioritizing climate change adaptation and needs for food security in 2030. *Science* 319, 607–610. doi: 10.1126/science.1152339

Lobell, D. B., Schlenker, W., and Costa-Roberts, J. (2011). Climate trends and global crop production since 1980. *Science* 333, 616–620. doi: 10.1126/science.1204531

Mebratu, A., Wegary, D., Mohammed, W., Teklewold, A., and Tarekegne, A. (2019). Genotype × environment interaction of quality protein maize hybrids under contrasting management conditions in Eastern and southern Africa. *Crop Sci.* 59, 1576–1589. doi: 10.2135/cropsci2018.12.0722

Memon, J., Patel, R., Parmar, D. J., Kumar, S., Patel, N. A., Patel, B. N., et al. (2023). Deployment of AMMI, GGE-biplot and MTSI to select elite genotypes of castor (*Ricinus communis* l.). *Heliyon*. 9. doi: 10.1016/j.heliyon.2023.e13515

Nardino, M., Perin, E. C., Aranha, B. C., Carpes, S. T., Fontoura, B. H., Sousa, D. J. P., et al. (2022). Understanding drought response mechanisms in wheat and multi-trait selection. *PloS One* 17, e0266368. doi: 10.1371/journal.pone.0266368

Nardino, M., Souza, V. Q. D., Baretta, D., Konflanz, V. A., Carvalho, I. R., Follmann, D. N., et al. (2016). Association of secondary traits with yield in maize F_1's. *Ciec. Rural* 46, 776–782. doi: 10.1590/0103-8478cr20150253

Nelimor, C., Badu-Apraku, B., Tetteh, A. Y., Garcia-Oliveira, A. L., and N'guetta, A. S.-P. (2020). Assessing the potential of extra-early maturing landraces for improving tolerance to drought, heat, and both combined stresses in maize. *Agronomy.* 10 (3), 318. doi: 10.3390/agronomy10030318

Nelimor, C., Badu-Apraku, B., Tetteh, A. Y., and N'guetta, A. S. P. (2019). Assessment of genetic diversity for drought, heat and combined drought and heat stress tolerance in early maturing maize landraces. *Plants.* 8, 518. doi: 10.3390/plants8110518

Nikolay, T., Todor, G., and Ivan, Y. (2020). Genotype selection for grain yield and quality based on multiple traits of common wheat (*Triticum aestivum* l.). *Cereal Res. Commun.* 49 (3), 1–6. doi: 10.1007/s42976-020-00080-7

Njeri, S. G., Makumbi, D., Warburton, M. L., Diallo, A., Jumbo, M. B., and Cheminingwa, G. (2017). Genetic analysis of tropical quality protein maize (*Zea mays* l.) germplasm. *Euphytica* 213, 261. doi: 10.1007/s10681-017-2048-4

Oliveira, T. R. A., Carvalho, H. W. L., Nascimento, M., Costa, E. F. N., Oliveira, G. H. F., Gravina, G. A., et al. (2020). Adaptability and stability evaluation of maize hybrids using Bayesian segmented regression models. *PloS One* 15 (7), e0236571. doi: 10.1371/journal.pone.0236571

Oliveira, E. J. D., Freitas, J. P. X. D., and Jesus, O. N. D. (2014). AMMI analysis of the adaptability and yield stability of yellow passion fruit varieties. *Scientia Agricola* 71 (2), 139–145. doi: 10.1590/S0103-90162014000200008

Olivoto, T., de Souza, V. Q., Nardino, M., Carvalho, I. R., Ferrari, M., de Pelegrin, A. J., et al. (2017). Multicollinearity in path analysis: a simple method to reduce its effects. *Agron. J.* 109 (1), 131–142. doi: 10.2134/agronj2016.04.0196

Olivoto, T., and Lúcio, A. D. C. (2020). Metan: An r package for multi-environment trial analysis. *Methods Ecol. Evol.* 11 (6), 783–789. doi: 10.1111/2041-210X.13384

Olivoto, T., Lúcio, A. D. C., da Silva, J. A. G., and Marchioro, V. S. (2019a). Mean performance and stability in multi-environment trials I: Combining features of AMMI and BLUP techniques. *Agron. J.* 111 (6), 2949–2960. doi: 10.2134/agronj2019.03.0220

Olivoto, T., Lúcio, A. D. C., da Silva, J. A. G., Sari, B. G., and Diel, M. I. (2019b). Mean performance and stability in multi-environment trials II: selection based on multiple traits. *Agron. J.* 111, 2961–2969. doi: 10.2134/agronj2019.03.0221

Olivoto, T., Nardino, M., Meira, D., Meier, C., Follmann, D. N., Souza, V. Q., et al. (2021). Multi-trait selection for mean performance and stability in maize. *Agron. J.* 1–16.

Oyekunle, M., and Badu-Apraku, B. (2018). Assessment of interrelationships among grain yield and secondary traits of early-maturing maize inbred lines under drought and well-watered conditions. *Maydica.* 2018, 63.

Patterson, H. D., and Williams, E. R. (1976). A new class of resolvable incomplete block designs. *Biometrika* 63, 83–92. doi: 10.1093/biomet/63.1.83

Peixoto, M. A., Coelho, I. F., Evangelista, J. S. P. C., Santos, S. S. D. O., Alves, R. S., Pinto, J. F. N., and Bhering, L. L. (2021). Selection of maize hybrids: an approach with multi-trait, multi-environment, and ideotype design. *Crop Breed. Appl. Biotechnol.* 21 (2), e34582122. doi: 10.1590/1984-70332021v21n2a31

Pour-Aboughadareh, A., Sanjani, S., Chaman-Abad, H. N., Mehrvar, M. R., Asadi, A., and Amini, A. (2021). MGIDI and WAASB indices: The useful approaches for selection of salt-tolerant barley genotype at the early growth and maturity stages. *Res. Square.* doi: 10.21203/rs.3.rs-304576/v1

Prasanna, B. M., Cairns, J. E., Zaidi, P. H., Beyene, Y., Makumbi, D., Gowda, M., et al. (2021). Beat the stress: breeding for climate resilience in maize for the tropical rainfed environments. *Theor. Appl. Gen.* 134, 1729–1752. doi: 10.1007/s00122-021-03773-7

R Core Team. (2021). *R: A Language and Environment for Statistical Computing*. (Vienna, Austria: R Foundation for Statistical Computing) Available at: https://www.r-project.org/.

Rocha, J. R. D. A. S. D. C., Machado, J. C., and Carneiro, P. C. S. (2018). Multitrait index based on factor analysis and ideotype-design: Proposal and application on elephant grass breeding for bioenergy. *GCB Bioenergy* 10 (1), 52–60. doi: 10.1111/gcbb.12443

Rstudio (2020). *RStudio: Integrated development for r. RStudio* (Boston, MA).

Sah, R. P., Chakraborty, M., Prasad, K., Pandit, M., Tudu, V. K., Chakravarty, M. K., et al. (2020). Impact of water deficit stress in maize: phenology and yield components. *Sci. Rep.* 10 (1), 1–15. doi: 10.1038/s41598-020-59689-7

Shapiro, S. S., and Wilk, M. B. (1965). An analysis of variance test for normality (Complete samples). *Biometrika* 52, 591–611. doi: 10.1093/biomet/52.3-4.591

Shojaei, S. H., Mostafavi, K., Bihamta, M. R., Omrani, A., Mousavi, S. M. N., Illeés, Á, et al. (2022). Stability on maize hybrids based on GGE biplot graphical technique. *Agronomy* 12, 394. doi: 10.3390/agronomy12020394

Singamsetti, A., Shahi, J. P., Zaidi, P. H., and Seetharam, K. (2022). Study on applicability of genotype × yield × trait (GYT) biplots over genotype × trait (GT) biplots in selection of maize hybrids across soil moisture regimes. *Indian J. Agric. Res*. A-5850. doi: 10.18805/IJARe.A-5850

Singamsetti, A., Shahi, J. P., Zaidi, P. H., Seetharam, K., Vinayan, M. T., Kumar, M., et al. (2021). Genotype × environment interaction and selection of maize (*Zea mays* l.) hybrids across moisture regimes. *Field Crops Res.* 270, 108224. doi: 10.1016/J.FCR.2021.108224

Smith, H. (1936). A discriminant function for plant selection. *Ann. Eugenics* 7, 240–250. doi: 10.1111/j.1469-1809.1936.tb02143.x

Tripathi, S., Warsi, M. Z. K., and Verma, S. S. (2003). Waterlogging tolerance in inbred lines of maize (*Zea mays* l.). *Cereal Res. Commun.* 31, 221–226. doi: 10.1007/BF03543271

Ulfat, A., Abasi, F., Munir, A., Rafaqat, A., Majid, S. A., Raja, N. I., et al. (2022). "How to deal with climate change in maize production," in *Sustainable crop productivity and quality under climate change* (Academic Press), 157–169.

Vaezi, B., Pour-Aboughadareh, A., Mohammadi, R., Mehraban, A., Hossein-Pour, T., Koohkan, E., et al. (2019). Integrating different stability models to investigate genotype x environment interactions and identify stable and high-yielding barley genotypes. *Euphytica* 215, 63. doi: 10.1007/s10681-019-2386-5

Verma, V., Foullces, M. J., Worland, A. J., Sylvester-Bradley, R., Caligari, P. D. S., and Snape, J. W. (2004). Mapping quantitative trait loci for flag leaf senescence as a yield determinant in winter wheat under optimal and drought-stressed environments. *Euphytica* 135, 255–263. doi: 10.1023/B:EUPH.0000013255.31618.14

Voesenek, L. A., and Pierik, R. (2008). Plant stress profiles. *Science* 320 (5878), 880–881. doi: 10.1126/science.1158720

Wegary, D., Vivek, B. S., and Labuschagne, M. T. (2014). Combining ability of certain agronomic traits in quality protein maize under stress and non-stress environments in eastern and southern Africa. *Crop Sci.* 54, 1004–1014. doi: 10.2135/cropsci2013.09.0585

Wickham, H. (2016). *ggplot2: Elegant graphics for data analysis* (New York: Springer-Verlag). Available at: https://ggplot2.tidyverse.org.

Woyann, L. G., Meira, D., Matei, G., Zdziarski, A. D., Dallacorte, L. V., and Madella, L. A. (2020). Selection indexes based on linear-bilinear models applied to soybean breeding. *Agron. J.* 112, 175–182. doi: 10.1002/agj2.20044

Yan, W., and Frégeau-Reid, J. (2018). Genotype by yield × trait (GYT) biplot: a novel approach for genotype selection based on multiple traits. *Sci. Rep.* 8, 8242. doi: 10.1038/s41598-018-26688-8

Yan, W., and Kang, M. S. (2003). *GGE biplot analysis a graphical tool for breeders, geneticists, and agronomists* (Boca Raton, FL: CRC Press).

Yang, R. C. (2007). Mixed-model analysis of crossover genotype–environment interactions. *Crop Sci.* 47, 1051–1062. doi: 10.2135/cropsci2006.09.0611

Yue, H., Olivoto, T., Bu, J., Li, J., Wei, J., Xie, J., et al. (2022a). Multi-trait selection for mean performance and stability of maize hybrids in mega-environments delineated using envirotyping techniques. *Front. Plant Sci.* 13. doi: 10.3389/fpls.2022.1030521

Yue, H., Wei, J., Xie, J., Chen, S., Peng, H., Cao, H., et al. (2022b). A study on genotype-by-Environment interaction analysis for agronomic traits of maize genotypes across Huang-Huai-Hai region in China. *Phyton* 91 (1), 57. doi: 10.32604/phyton.2022.017308

Yue, H., Gauch, H. G., Wei, J., Xie, J., Chen, S., Peng, H., and Jiang, X. (2022c). Genotype by environment interaction analysis for grain yield and yield components of summer maize hybrids across the huanghuaihai region in China. *Agriculture* 12 (5), 602.

Zaidi, P. H., Maniselvan, P., Srivastava, A., Yadav, P., and Singh, R. P. (2010). Genetic analysis of water-logging tolerance in tropical maize (*Zea mays* l.). *Maydica* 55 (1), 17–26.

Zaidi, P. H., Maniselvan, P., Sultana, R., Yadav, M., Singh, R. P., Singh, S. B., et al. (2007). Importance of secondary traits in improvement of maize (*Zea mays* l.) for enhancing tolerance to excessive soil moisture stress. *Cereal Res. Commun.* 35 (3), 1427–1435. doi: 10.1556/CRC.35.2007.3.7

Zaidi, P. H., Nguyen, T., Ha, D. N., Thaitad, S., Ahmed, S., Arshad, M., et al. (2020). Stress-resilient maize for climate-vulnerable ecologies in the Asian tropics. *Aust. J. Crop Sci.* 14 (8), 1264–1274. doi: 10.21475/ajcs.20.14.08.p2405

Zaidi, P. H., Rafique, S., Rai, P. K., Singh, N. N., and Srinivasan, G. (2004). Tolerance to excess moisture in maize (*Zea mays* l.): Susceptible crop stages and identification of tolerant genotypes. *Field Crop Res.* 90, 189–202. doi: 10.1016/j.fcr.2004.03.002

Zaidi, P. H., Seetharam, K., Vinayan, M. T., and Prasanna, B. M. (2016a). "Stress-resilient maize for adaptation to climate-change effects in Asia," in *7th International Crop Science Congress*, Beijing, China, 14-19 Aug.

Zaidi, P. H., and Singh, N. N. (2001). Effect of water logging on growth, biochemical compositions and reproduction in maize. *J. Plant Biotechnol.* 28, 61–69.

Zaidi, P. H., Vinayan, M. T., and Seetharam, K. (2016b). *Phenotyping for abiotic stress tolerance in maize: Waterlogging stress. a field manual* (Hyderabad, India: CIMMYT).

Zaman-Allah, M., Zaidi, P. H., Trachsel, S., Cairns, J. E., Vinayan, M. T., and Seetharam, K. (2016). *Phenotyping for abiotic stress tolerance in maize: Drought stress. a field manual* (Mexico: CIMMYT).

Zuffo, A. M., Steiner, F., Aguilera, J. G., Teodoro, P. E., Teodoro, L. P. R., Busch, A., et al. (2020). Multi-trait stability index: a tool for simultaneous selection of soya bean genotypes in drought and saline stress. *J. Agron. Crop Sci.* 206 (6), 815–822. 00. doi: 10.1111/jac.12409

frontiers | Frontiers in Plant Science

TYPE Original Research
PUBLISHED 27 March 2023
DOI 10.3389/fpls.2023.1113838

OPEN ACCESS

EDITED BY
Pasala Ratnakumar,
Indian Institute of Oilseeds Research (ICAR), India

REVIEWED BY
Sarla Neelamraju,
Indian Institute of Rice Research (ICAR), India
Chandra Obul Reddy Puli,
Yogi Vemana University, India

*CORRESPONDENCE
R. Beena
beena.r@kau.in

SPECIALTY SECTION
This article was submitted to Plant Abiotic Stress, a section of the journal Frontiers in Plant Science

RECEIVED 01 December 2022
ACCEPTED 06 March 2023
PUBLISHED 27 March 2023

CITATION
Stephen K, Aparna K, Beena R, Sah RP, Jha UC and Behera S (2023) Identification of simple sequence repeat markers linked to heat tolerance in rice using bulked segregant analysis in F_2 population of NERICA-L 44 × Uma.
Front. Plant Sci. 14:1113838.
doi: 10.3389/fpls.2023.1113838

Identification of simple sequence repeat markers linked to heat tolerance in rice using bulked segregant analysis in F_2 population of NERICA-L 44 × Uma

K. Stephen[1], K. Aparna[1], R. Beena[1]*, R. P. Sah[2], Uday Chand Jha[3] and Sasmita Behera[2]

[1]Department of Plant Physiology, College of Agriculture, Vellayani, Kerala Agricultural University, Thiruvananthapuram, India, [2]Crop Improvement Division, Indian Council of Agricultural Research (ICAR)-National Rice Research Institute, Cuttack, India, [3]Crop Improvement Division, Indian Institute of Pulses Research, Kanpur, India

The damage caused by high temperature is one of the most important abiotic stress affecting rice production. Reproductive stage of rice is highly susceptible to high temperature. The present investigation was undertaken to identify polymorphic microsatellite markers (SSR) associated with heat tolerance. The rice cultivars NERICA– L 44 (heat tolerant) and Uma (heat susceptible) were crossed to generate F^1 and F^2 populations. The F^2 population was subjected to heat stress at >38°C and the 144 F^2 plants were evaluated for their tolerance. The results note that the mean of the F^2 population was influenced by the tolerant parent with regards to the traits of plant height, membrane stability index, photosynthetic rate, stomatal conductance, evapotranspiration rate, pollen viability, spikelet fertility and 1000 grain weight. Ten each of the extremely susceptible and tolerant plants were selected based on the spikelet fertility percentage. Their DNA was pooled into tolerant and susceptible bulks and Bulked Segregant Analysis (BSA) was carried out using 100 SSR markers to check for polymorphism. The survey revealed a polymorphism of 18% between the parents. RM337, RM10793, RM242, RM5749, RM6100, RM490, RM470, RM473, RM222 and RM556 are some of the prominent markers that were found to be polymorphic between the parents and the bulks. We performed gene annotation and enrichment analysis of identified polymorphic markers. Result revealed that the sequence specific site of that chromosome mostly enriched with biological processes like metabolic pathway, molecular mechanism, and subcellular function. Among that RM337 was newly reported marker for heat tolerance. Expression analysis of two genes corresponds to RM337 revealed that *LOP1* (LOC_Os08g01330) was linked to high temperature tolerance in rice. The results demonstrate that BSA using SSR markers is useful in identifying genomic regions that contribute to thermotolerance.

KEYWORDS

Bulked Segregant Analysis (BSA), heat tolerance, SSR markers, NERICA-L 44, rice physiology, gene annotation

Introduction

Research into the genetic mechanism of heat tolerance is becoming increasingly important for the utilization of heat-tolerant genes in the development of new rice varieties. Advances in rice genomics research and the completion of the rice genome sequence have made it possible to identify and precisely map several genes through linkage to DNA markers. By determining the allele of a DNA marker, plants that possess favorable genes or quantitative trait loci (QTLs) may be identified based on their genotype (Foolad and Sharma, 2004). Many stress resistance genes that are tightly linked to SNP, SSR, and STS markers are available (Das et al., 2017). Radha et al. (2023) reviewed the impact of high temperatures on rice yield and grain quality parameters and QTLs linked to high temperature tolerance in rice. Marker-assisted selection (MAS) can integrate these genes into breeding populations in combination with conventional breeding approaches.

Bulked segregant analysis (BSA) is a technique that is used to rapidly identify markers that are tightly linked to genes for a given phenotype (Zou et al., 2016). With the release of sequenced genomes, the combined application of bulked segregant analysis (BSA) and next-generation sequencing technology represents a new way to accelerate the identification of candidate genes controlling important agronomic traits in various crops (Tiwari et al., 2016). As heat-stress responses are governed by polygenes or QTL/thermotolerance genes, concerted efforts should be made to understand tolerance mechanisms at molecular and physiological levels.

Due to the low cost, wide availability, and easy technique, in addition to their high polymorphism rate, simple sequence repeats (SSR) are the most widely employed markers in MAS in the present times (Gao et al., 2016; Beena et al., 2018b; Rejeth et al., 2020). Due to parental genetic diversity, each offspring group of a cross is distinct at morphological and molecular levels. Even though many markers linked to different traits for resistance to heat stress are reported, the markers verified in a particular cross of parental genotypes may not be applicable to other populations. Therefore, using bulked segregant analysis, the current work sought to identify the molecular markers linked to high temperature tolerance in rice from the F_2 population of NERICA-L 44 and Uma, and the identified markers were subjected to gene annotation and enrichment analysis.

Materials and methods

Location

The experiment was carried out at the College of Agriculture in Vellayani, Kerala. The institute is in southern India (8.44° N, 76.99° E), where the climate is typically humid and tropical, with average summer temperatures reaching around 35°C and average winter temperatures of about 20°C.

Crop growth conditions

The experiment was conducted as a pot culture study in a control facility. The size of each pot was 25 × 15 cm, with soil and farmyard manure filled in a 2:1 ratio. The average weight of the pot after filling was about 6 kg. The seedlings were raised in a nursery and transplanted into the pots after 18 days. Fertilizer was applied as recommended (100:60:40 kg ha^{-1} of $N:P_2O_5:K_2O$) for this region. The first dose was applied as a basal dressing in each pot before transplanting, and the remaining amount was applied as a top dressing 15 days after transplanting, at the maximum tillering and booting stage.

The F_2 seeds produced from the F_1 progeny were germinated and raised following standard crop management according to the package of practices (KAU [Kerala Agricultural University], 2016). The plants were grown in lowland conditions, i.e., with standing water for most of the crop duration except for mid-season drainage at 40 and 60 days. Until the maximum tillering stage, the plants were kept in normal environmental conditions with the average daytime temperature ranging around 30–32°C and night temperature around 24–26°C. The plants were thereafter moved to a high-temperature polyhouse, where the average temperature was around 38–42°C during the day. The plants were kept under high temperature conditions until their harvest. The physiological parameters were recorded at the flowering phase and yield parameters were recorded at the grain-filling phase.

Materials used

The rice varieties Uma and NERICA L-44 (New Rice for Africa-Lowland 44) were selected for the present study. Uma (MO-16) is a popular and high-yielding rice variety developed by the Kerala Agricultural University, but it is susceptible to high temperature stress (Waghmare et al., 2018), while the rice NERICA L-44 (NL-44), derived from the crossing of the African rice (*O. glaberimma* Steud.) and the Asian rice (*O. sativa* L.), was reported as a heat-tolerant line (Bahuguna et al., 2015; Ravikiran et al., 2020). The two rice varieties, Uma and NL-44 were sown in a staggered planting pattern to coincide with the date of flowering between the two parents. Standard crop management was followed according to the package of practices recommend for this region (KAU [Kerala Agricultural University], 2016), at ambient temperature of 26–34°C without any stress during the crop growth period. The variety NL-44 (donor) was crossed with Uma to produce a good number of F_1 seeds. The F_1 seeds were raise in the field to produce 150 F_2 seeds.

Morphological parameters recorded

The F_2 lines were evaluated along with their two parents, NL-44 and Uma, by calculating the mean and the deviation of each plant from the mean. The range of data was estimated by dividing the

data into quartiles, and the shape of the normal curve for each parameter was determined. The physiological parameters were recorded at the flowering phase, and yield parameters were recorded at the grain filling phase.

Morphological parameters were recorded on plant height (cm), tiller number, number of productive tillers, days to 50% flowering, time of anthesis, panicle length (cm), 1,000 grain weight (TGW) (g), spikelet fertility (SF) (%) was calculated using the formula: SF (%) = (Number of fertile spikelets/Total number of spikelets) × 100.

The physiological parameters pollen stainability (%), cell membrane stability, photosynthetic rate, transpiration rate, stomatal conductance, and leaf temperature were measured. Pollen stainability (%) (which indicates pollen viability) was calculated by the iodine-potassium iodide method. The pollen viability percentage was calculated by the formula: (number of stained pollen grains/total number of pollen grains) × 100. Cell membrane stability was measured according to the procedure given by Sairam et al. (1997). The membrane stability index (MSI) was calculated using the formula: MSI = [1 − (C1/C2)] × 100, where C1 and C2 are the initial and final electrical conductance measured when leaf discs (100 mg) were heated in a water bath at 40°C (30 min) and 100°C (10 min), respectively. The photosynthetic rate, transpiration rate, stomatal conductance, and leaf temperature were measured using an Infra-Red Gas Analyzer (LI-COR 6400XT, USA).

Genomic DNA isolation and marker assay

The DNA was isolated using the method suggested by Dellaporta et al. (1983), and the quality and quantity were estimated using the ratio of absorbance at 260 nm and 280 nm. A ratio (A_{260}/A_{280}) of 1.8–2.0 was obtained for the samples, which is good quality DNA. The PCR reaction to check for DNA polymorphism was carried out by preparing a standard mixture having the following components: 10× Taq buffer (2 µl), forward primer (0.75 µl), reverse primer (0.75 µl), dNTP mix (1.5 µl), Taq polymerase (1 µl/5 reactions), and sterile water (12.7 µl), and DNA template (1 µl/reaction). The thermal profile of the PCR cycling conditions was standard except for the annealing temperature, which was specific to the individual markers. The cycling conditions for the PCR reaction were: 1) initial denaturation (95°C—5 min), 2) denaturation (94°C—1 min), 3) annealing (57°C—1 min), 4) extension (72°C—2 min), and 5) final extension (72°C—5 min). Steps 2 to 4 were repeated for 30 cycles. The quality of the PCR products was checked by separating them on a 3% agarose gel using the electrophoresis technique.

Identification of genetic loci linked with heat tolerance traits through BSA

Bulked segregant analysis (BSA) was utilized to identify polymorphic markers between the tolerant and the susceptible bulks. The markers that differentiated between the tolerant and susceptible bulks through the difference in the amplicon size of the marker, separated through gel electrophoresis, were considered polymorphic. Through BSA, the polymorphic markers between the tolerant and susceptible bulks were used to study the segregation of the alleles in the individual lines constituting the tolerant and susceptible bulks.

In this method, based upon the phenotypic evaluation of the F_2 lines using spikelet fertility percentage as a phenotypic marker for heat tolerance, 10 extremely tolerant and 10 extremely susceptible lines were selected. DNA was extracted from the selected 10 heat-tolerant and 10 susceptible segregant lines, and an equal quantity of DNA was pooled. The bulked DNA samples were screened using 100 simple sequence repeat (SSR) primers. The putative polymorphic markers between the bulks were checked among the parents as well as the individual lines constituting the tolerant and susceptible bulks. Polymorphic markers were subjected to gene annotation and enrichment analysis using all the genes separately (http://bis.zju.edu.cn/ricenetdb/).

Gene expression

The leaf samples were taken at the vegetative stage. The total RNA was isolated using TRI reagent from HiMedia. The isolated samples were quantified using a Qubit reagent. The cDNA was prepared using RT superscript enzyme as well as without RT superscript enzyme. The genes *LOP1* (LOC_Os08g01330) and *LOP2* (LOC_Os08g0112) were amplified using primers of concentration 10 picomoles per microliter using a cDNA quantity corresponding to 10ng of total RNA used for cDNA preparation. The qPCR was carried out using a 2× master mix containing SYBR Green reagent. For each sample, three replicates were used. In the analysis software, samples and controls were marked. After the completion of qPCR, the data was auto analyzed using CFX Analysis Manager. The primer sequence is given in Table 1.

TABLE 1 List of primers used for qRT-PCR.

Gene name	Forward primer	Reverse primer
LOC_Os08g01330 (*LOP1*)	CGACTGGAACCTGCTCAC	CGATGAAGCCTGACGAAGAA
LOC_Os08g01120 (*LOP2*)	TACGCTACGAGCAGGACTT	CGTTGACGAGCACGATGA

Results

Phenotypic evaluation of F_2 population of NL-44 × Uma for high temperature tolerance

Growth parameters

The mean plant height (Figure 1) of the population was 99.09 cm, with the minimum height being 64 cm and the maximum recorded at 121 cm. The plant height of the Uma variety was recorded at 96.73 cm, while NL-44 recorded 105.62 cm. The average number of tillers was 10.17, with the highest number recorded as 17 and the least being 5 (Table 2). The number of tillers recorded in Uma was 11, while NL-44 produced eight. The average number of productive tillers was 5.58, with the lowest number being 2, while the maximum productive tiller number was 11. The Uma variety recorded eight productive tillers under heat stress, whereas NL-44 recorded six tillers. The mean MSI of the population was calculated at 75.84%, with a minimum MSI of 56% and a maximum MSI of 90%. The MSI of the Uma variety was 68% while that of NL-44 was 79%.

Characteristics of flowering

The population's mean flowering time was calculated to be 87.5 days, with a range of 30 days, with the least being 71 days and the most being 101 days. The variety Uma was recorded to flower in around 83 days, while NL-44 took 71 days to flower. The mean time of anthesis (Figure 2) for the F_2 population was 9:47 am, with a range of 3 h and 45 min, with the earliest anthesis occurring at 8:00 am and the most delayed anthesis occurring at 11:45 am. The time of anthesis of the Uma variety was recorded at 10:15 am, while that of NL-44 was 10:45 am. The population's mean pollen viability percentage was calculated to be 77.76%. This was within a range of 32%, with the lowest pollen viability percentage being 59% and the highest pollen viability percentage being 91%. The pollen viability of the Uma variety was 74%, while NL-44 was 86.67%.

Gas exchange related parameters

The population's mean photosynthetic rate (Pn) was calculated to be 24.35 mol $cm^{-2}s^{-1}$, with a minimum Pn of 15.6 mol $cm^{-2}s^{-1}$ and a maximum Pn of 29.7 mol $cm^{-2}s^{-1}$. The Pn of the Uma variety was 20.68 µmol $cm^{-2}s^{-1,}$ while that of NL-44 was 27.21 µmol $cm^{-2}s^{-1}$. The mean stomatal conductance of the F_2 population was 0.234 mol $m^{-2}s^{-1}$, where the maximum Gs was recorded at 0.345 mol $m^{-2}s^{-1}$ and the minimum Gs was 0.181 mol $m^{-2}s^{-1}$. The Gs of the Uma variety was recorded to be 0.213 mol $m^{-2}s^{-1}$, while that of NL-44 was 0.236 mol $m^{-2}s^{-1}$. The mean transpiration rate of the F_2 population was 5.91 mmol $m^{-2}s^{-1}$ with a range of 2.52 mmol $m^{-2}s^{-1}$, where the maximum transpiration rate was recorded as 7.15 mmol $m^{-2}s^{-1}$ and the minimum was 4.63 mmol $m^{-2}s^{-1}$. The transpiration rate of the Uma variety was recorded at 5.45 mmol $m^{-2}s^{-1}$, while that of NL-44 was 6.24 mmol $m^{-2}s^{-1}$. The average leaf temperature was calculated to be 34.4°C, with a maximum of 35.8°C and a minimum of 33.1°C. The leaf temperature of the Uma variety was 34.87°C, and that of the NL-44 variety was 34.16°C (Figure 3).

Yield parameters

The mean panicle length of the population (Figure 4) was calculated as 22.94 cm, having a range of 10.2 cm, with the least panicle length of 17.6 cm and the highest panicle length of 27.8 cm. The panicle length of the Uma variety was recorded at 23.4 cm, and that of NL-44 was 27.62 cm. The mean spikelet fertility percentage of the population was 41.54% with the minimum spikelet fertility of 15.17% and the maximum recorded as 75.27%. The spikelet fertility

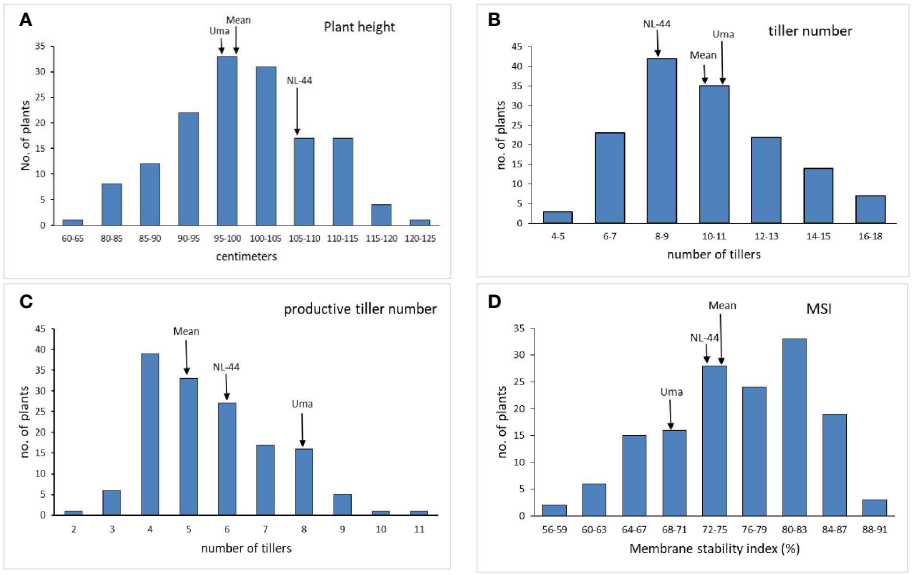

FIGURE 1
Frequency distribution of plant height **(A)**, tiller number **(B)**, productive tiller number **(C)**, and membrane stability index (MSI) **(D)** under the effect of high temperature stress among the F_2 population.

TABLE 2 Descriptive statistics of various parameters of the F_2 population of NL-44 × Uma under the effect of heat stress.

Descriptive statistical parameter	Plant height (cm)	tiller number	Productive tiller number	Days to flowering	Time of anthesis (a.m.)	MSI (%)	Photosynthetic rate (μmol $cm^{-2}s^{-1)}$	Stomatal conductance (mol $m^{-2}s^{-1)}$	Transpiration rate (mmol $m^{-2}s^{-1)}$	Leaf temperature (˚C)	Pollen viability (%)	Panicle length (cm)	Spikelet fertility (%)	1,000 grain weight (g)
Mean	99.09	10.17	5.58	87.5	9:47	75.84	24.35	0.23	5.91	34.41	77.76	22.94	41.54	22.11
Standard Error	0.74	0.23	0.13	0.53	0.06	0.60	0.28	0.0029	0.051	0.05	0.56	0.17	1.05	0.14
Median	99	10	5	87	9:47	76.5	25.3	0.23	5.82	34.43	79	23.1	40.90	22.5
Mode	104	9	4	91	10:00	81	23.4	0.234	5.14	34.91	81	24.2	46.53	22.5
Standard Deviation	9.01	2.83	1.66	6.41	0.75	7.30	3.47	0.035	0.62	0.60	6.82	2.07	12.69	1.74
Sample Variance	81.20	8.03	2.76	41.20	0.56	53.38	12.08	0.0012	0.39	0.36	46.53	4.31	161.07	3.053
Kurtosis	0.66	−0.34	−0.05	−0.64	−0.52	−0.58	−0.51	0.37	−0.86	−0.74	0.035	−0.32	−0.05	−0.76
Skewness	−0.31	0.44	0.61	0.01	0.08	−0.40	−0.64	0.79	0.16	−0.15	−0.62	−0.18	0.33	−0.58
Range	57	12	9	30	3:45	34	14.1	0.164	2.52	2.67	32	10.2	60.1	6.6
Minimum	64	5	2	71	8:00	56	15.6	0.181	4.63	33.14	59	17.6	15.17	18.2
Maximum	121	17	11	101	11:45	90	29.7	0.345	7.15	35.81	91	27.8	75.27	24.8
Count	146	146	146	146	146	146	146	146	146	146	146	146	146	146
Confidence Level (95.0%)	1.47	0.46	0.27	1.04	0.12	1.19	0.56	0.0058	0.10	0.098	1.11	0.33	2.075	0.28

10.3389/fpls.2023.1113838

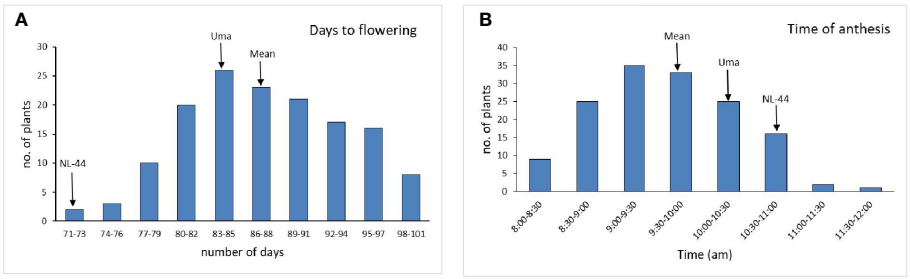

FIGURE 2
Frequency distribution of days to flowering **(A)** and time of anthesis **(B)** under the effect of high temperature stress among the F_2 population.

of the Uma variety was calculated as 35.16% while that of NL-44 was 56.15%. The mean thousand grain weight (TGW) of the population was 22.11 g, with the least TGW of 18.2 g and the maximum recorded at 24.8 g. The TGW of the Uma variety was recorded at 20.14 g, while that of NL-44 was 23.27 g.

Correlation analysis

The correlation matrix of the parameters assessed in the F_2 population under high temperature stress is presented in Table 3. The tiller number was positively correlated with the productive tiller number, days to flower, and pollen viability. Similarly, the productive tiller number was positively correlated with the membrane stability index. The membrane stability index was significantly correlated with pollen viability, spikelet fertility, and 1,000 grain weights in a positive manner. Pollen viability was also found to have a significant positive correlation with spikelet fertility and 1,000 seed weights. The correlation between spikelet fertility and 1,000 grain weights was positive at the $p \leq 0.001$ level. The parameters of photosynthetic rate, evapotranspiration rate, stomatal conductance, and leaf temperature were positively and strongly correlated with each other. The time of anthesis was negatively correlated with spikelet fertility and 1,000 grain weight, while pollen viability was negatively correlated with leaf temperature.

Identification of polymorphic molecular markers linked to high temperature tolerance

Based on the results of the phenotypic evaluation of the 144 F_2 generation plants, 10 plants from extremely heat tolerant and extremely heat susceptible were selected. The F_2 generation plant numbers P3, P6, P7, P56, P79, P82, P49, P98, P121, and P143 were in the extremely tolerant group, and plant numbers P25, P54, P72, P73, P92, P93, P103, P104, P126, and P141 were in the extremely

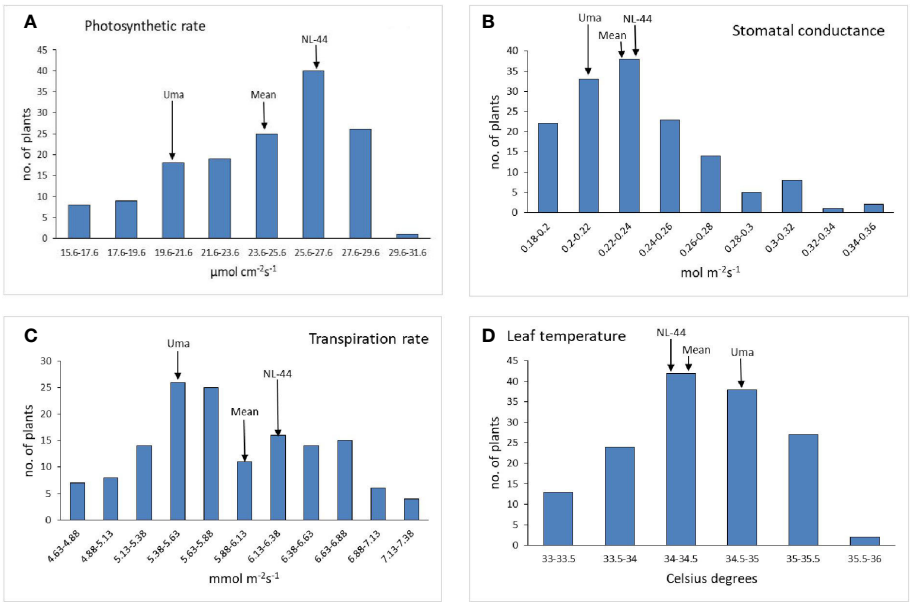

FIGURE 3
Frequency distribution of photosynthetic rate **(A)**, stomatal conductance **(B)**, transpiration rate **(C)**, and leaf temperature **(D)** under the effect of high temperature stress among the F_2 population.

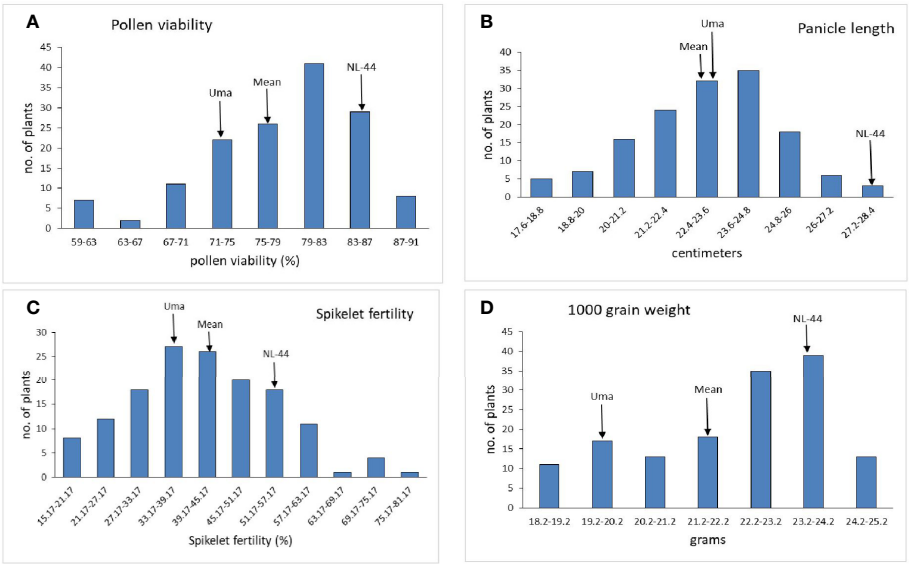

FIGURE 4
Frequency distribution of pollen viability **(A)**, panicle length **(B)**, spikelet fertility **(C)**, and 1,000 grain weight **(D)** under the effect of high temperature stress among the F_2 population.

susceptible group. Based on the amplification pattern obtained, 18 markers were determined to exhibit polymorphism between the parents (Table 4). The amplification pattern and polymorphism level between the parents, bulks, and debulks of 10 markers (RM337, RM10793, RM242, RM5749, RM6100, RM490, RM3475, RM470, RM473, and RM556) clearly indicate their ability to separate the heat tolerance or susceptible plants (Figure 5).

Gene annotation and enrichment analysis

To get a deeper insight into how these genes participate in heat tolerance, we performed GO (gene annotation) and enrichment analysis (http://bis.zju.edu.cn/ricenetdb/) on all the genes separately (Figure 5). Result revealed that the sequence-specific site of that chromosome was mostly enriched with biological processes like metabolic pathways, molecular mechanisms, and subcellular function. Out of the 10 markers identified in the BSA (RM337, RM10793, RM242, RM5749, RM6100, RM490, RM3475, RM470, RM473, and RM556), nine of the markers have been previously reported for heat tolerance traits, while one marker, RM337, is newly identified in the present study.

The genes in the 200 kb vicinity of the RM markers were retrieved from the Rice Annotation Project database (https://rapdb.dna.affrc.go.jp/viewer/gbrowse/irgsp1/, accessed on 18 August 2022) based on their putative function related to heat tolerance. Upon screening of the loci in the proposed region, known heat tolerance genes and characterized genes were identified (Supplementary Table 1: Gene annotation and enrichment analysis).

Annotation, GO enrichment analysis, and trait ontology (TO) were performed for all the significant markers. The marker information was searched through the RiceNetDB and Oryzabase databases. RM 490, which is located at chromosome number 01, had 426 genes that were significantly enriched and involved in different pathways, among them 10 that were involved in heat tolerance. Four of them were characterized genes (*OsHSP16.9C* (Jung et al., 2014), *OsHsp18.0* (Kuang et al., 2017), *WRKY10* (Chen et al., 2022), and *OsDREB2A* (TO:0000259)) and have an active role in abiotic stress tolerance and heat shock, and are involved in seed maturation, anther traits, leaf senescence, seed germination, plant growth and development, signal transduction, and metabolic processes. RM 10793, located on chromosome number 01, showed 788 genes significantly enriched and involved in different pathways (SF1). A total of 19 genes were known for heat tolerance, including 10 characterized genes (*OsHSP16.9C*) (Jung et al., 2014), *WRKY10* (Chen et al., 2022), *OsHsp18.0* (Kuang et al., 2017), *OsNTL3* (Liu et al., 2020), *OsDREB2AOsNLP3*, *OsSUN2*, *OsGAS2*, *OsTGA5*, and *OsGI with* TO:0000259), which have active roles in abiotic stress tolerance, osmotic stress, heat tolerance, seed maturation, chlorophyll content, and flowering time regulator. The RM 470, located on chromosome number 4, showed 880 genes significantly enriched and involved in different pathways. Approximately, 17 of them were known for heat tolerance-related activities, including eight characterized genes for different traits (*BAD1*, *OsABA1*, *OsZEP*, *OsFPFL4*, *OsNLP2*, *OsWRKY36* with TO:0000259), *OsFKBP65* (Magiri et al., 2006), and *RPL6* (Moin et al., 2016), which have an active role in temperature tolerance, abiotic stress tolerance, and modulating root and flower development. The marker RM 5749, located on chromosome number 04, showed 298 genes significantly enriched and involved in different pathways (SF2). Five were known for heat tolerance, including two characterized genes (*OsFKBP65* (Suzuki et al., 2015) and *OsFPFL4* (TO:0000259)) which have an active role in tissue-specific heat tolerance, abiotic stress tolerance, pollen, root, and anther development. Marker RM 473, located on chromosome

TABLE 3 Correlation matrix of F_2 population under high temperature stress.

	Plant Height	No. of tillers	Productive tiller no.	Days to flowering	Time of anthesis	MSI	Pollen Viability	Panicle length (cm)	Spikelet fertility	1000 seed weight	Pn	E	Gs	T
Plant Height	1	0.073	0.157	−0.014	0.023	−0.002	−0.074	0.095	0.022	−0.069	0.006	−0.039	0.054	0.041
No. of tillers	0.073	1	0.789***	0.195*	0.151	0.136	0.171*	0.035	0.079	0.071	−0.197*	−0.15	−0.151	−0.246**
Productive tiller no.	0.157	0.789***	1	0.017	0.102	0.177*	0.161	0.002	0.115	0.112	−0.209*	−0.178*	−0.139	−0.261**
Days to flowering	−0.014	0.195*	0.017	1	0.023	0.133	−0.007	−0.001	−0.004	0.041	0.096	0.061	0.133	0.035
Time of anthesis	0.023	0.151	0.102	0.023	1	−0.111	−0.151	−0.009	−0.165*	−0.184*	0.022	0.047	0.051	0.007
MSI	−0.002	0.136	0.177*	0.133	−0.111	1	0.458***	0.06	0.324***	0.274***	0.039	−0.008	0.035	−0.073
Pollen Viability	−0.074	0.171*	0.161	−0.007	−0.151	0.458***	1	0.074	0.315***	0.298***	−0.116	−0.161	−0.158	−0.253**
Panicle length (cm)	0.095	0.035	0.002	−0.001	-0.009	0.06	0.074	1	0.001	−0.052	−0.144	−0.165*	−0.037	−0.226**
Spikelet fertility	0.022	0.079	0.115	−0.004	−0.165*	0.324***	0.315***	0.001	1	0.861***	0.036	−0.015	−0.055	−0.107
1,000 seed weight	−0.069	0.071	0.112	0.041	−0.184*	0.274***	0.298***	−0.052	0.861***	1	−0.026	−0.064	−0.115	−0.151
Pn	0.006	−0.197*	−0.209*	0.096	0.022	0.039	−0.116	−0.144	0.036	−0.026	1	0.896***	0.679***	0.764***
E	−0.039	-0.15	−0.178*	0.061	0.047	−0.008	−0.161	−0.165*	−0.015	−0.064	0.896***	1	0.706***	0.835***
Gs	0.054	−0.151	−0.139	0.133	0.051	0.035	−0.158	−0.037	−0.055	−0.115	0.679***	0.706***	1	0.66***
T	0.041	−0.246**	−0.261**	0.035	0.007	−0.073	−0.253**	−0.226**	−0.107	−0.151	0.764***	0.835***	0.66***	1

***indicates significance at 0.001 level (two tailed), ** indicates significance at 0.01 level (two tailed) and * indicates significance at 0.05 level (two tailed).

10.3389/fpls.2023.1113838

TABLE 4 List of SSR markers exhibiting polymorphism between parents.

Marker	Chromosome
RM237	1
RM490	1
RM3475	1
RM10793	1
RM3586	3
RM554	3
RM471	4
RM470	4
RM5749	4
RM413	5
RM320	7
RM473	7
RM337	8
RM556	8
RM310	8
RM242	9
RM6100	10
RM222	10

number 07, showed 922 genes significantly enriched and involved in a different pathway (SF3). Five were known for heat tolerance, including one characterized gene (*ZFP177*), which actively contributes to temperature stress tolerance (Huang et al., 2008). The annotation of the marker RM 337 region on chromosome number 8 showed 23 genes significantly enriched and involved in different pathways, out of which seven were known characterized genes controlling traits like chlorophyll content, plant growth hormone sensitivity, inflorescence development trait, bacterial blight disease resistance, UV light sensitivity, seed development trait, and drought tolerance. Among these genes *NAC31* (*OsSWN3*; *LOC_Os08g01330*) a NAC involved in regulation of cellulose synthesis, regulation of secondary wall biosynthesis (*Os08t0103900-01*) said to be involved in heat tolerance. NAC transcription factors are also responsive to thermomemory in Arabidopsis (Alshareef et al., 2022). This marker is position centric between these two genes. LOC_*Os08g01120* (86,388–87,854) RM 337 (152,299–152,485) LOC_*Os08g01330* (210,422–212,411).

The RM 242, located on chromosome number 09, had 489 genes significantly enriched and involved in different pathways, among them eight were known for heat tolerance and included six characterized genes (*ACO1* (TO:0000259), *OsFBN1* (Li et al., 2019), *OsHTAS* (Jan et al., 2021), *OsNSUN2* (Tang et al., 2020), and *Amy3C* and *PDIL2;3* (TO:0000259)) that have an active role in heat tolerance at the seedling stage grain-filling percent and RNA methyltransferase of *OsNSUN2* for heat tolerance. Similarly, RM 6100, located on chromosome number 10, showed 246 genes significantly enriched and involved in different pathways (Figure 6). Seven were known for heat tolerance, including one characterized gene (*CYP75B3/F3'H;* Trait ontology—0000259) in cereal grasses that belongs to the cytochrome P450 family and catalyzes the 3′-hydroxylation of the B-ring of flavonoids (Jia et al., 2019). The RM 222, on chromosome number 10, was annotated and showed 170 genes significantly enriched and involved in different pathways, out of which 14 were known characterized genes controlling traits like growth and development trait, bacterial leaf streak disease resistance, grain size, grain weight, leaf development trait, plant height, cold tolerance, salt tolerance, days to head, drought tolerance, brown planthopper resistance, anther color, pollen fertility, anther shape, anther length, etc. Among these genes *OsADF* (*LOC_Os10g03660*, anther development F-box), involved in anther color, pollen fertility, anther shape, and anther length traits and was selected for heat tolerance gene. *OsADF* gene family participate in plant abiotic stress response or tolerance (https://thericejournal.springeropen.com/articles/10.1186/1939-8433-5-33).

Gene expression analysis

The genes *LOP1* (LOC_Os08g01330) and *LOP2* (LOC_Os08g0112) were found to be associated with the marker RM337, and therefore their expression was analyzed in the two rice varieties under both control and high temperature conditions (Figure 7). *LOP1* was found to be significantly upregulated in the NL-44 variety under high temperature condition compared to the normal temperature conditions and susceptible variety, Uma. *LOP1* is a NAC transcription factor that is reported to be involved in the regulation of cellulose synthesis, secondary wall biosynthesis (*Os08t0103900-01*), and inflorescence development, all of which contribute to better physical tolerance characteristics during vegetative growth as well as the maintenance of an improved pollination rate, which can be observed in the tolerant NL-44. On the other hand, the gene *LOP2* was found to be upregulated in both varieties under the higher temperature condition compared to their respective controls. However, the relative expression in Uma was higher than in NL-44. *LOP2*, also known as *OsMOT1* (Cobb et al., 2021), is a molybdate transporter that is involved in the uptake and translocation of molybdate (*Os08t0101500-01*). This gene is reported to be involved in drought, cold, and salt tolerance, as well as seed development. Its higher relative expression in the heat-susceptible variety Uma might indicate that it might possess tolerance traits for other traits other than high temperature as abiotic stresses are found to be affecting the crops in conjunction. Comparatively, the upregulation in NL-44 might be attributed to its improved tolerance under heat stress conditions.

Discussion

The effects of climate change, which include rising temperatures, longer droughts, and desertification, are anticipated to make several places unfit for agricultural use. Rice has been

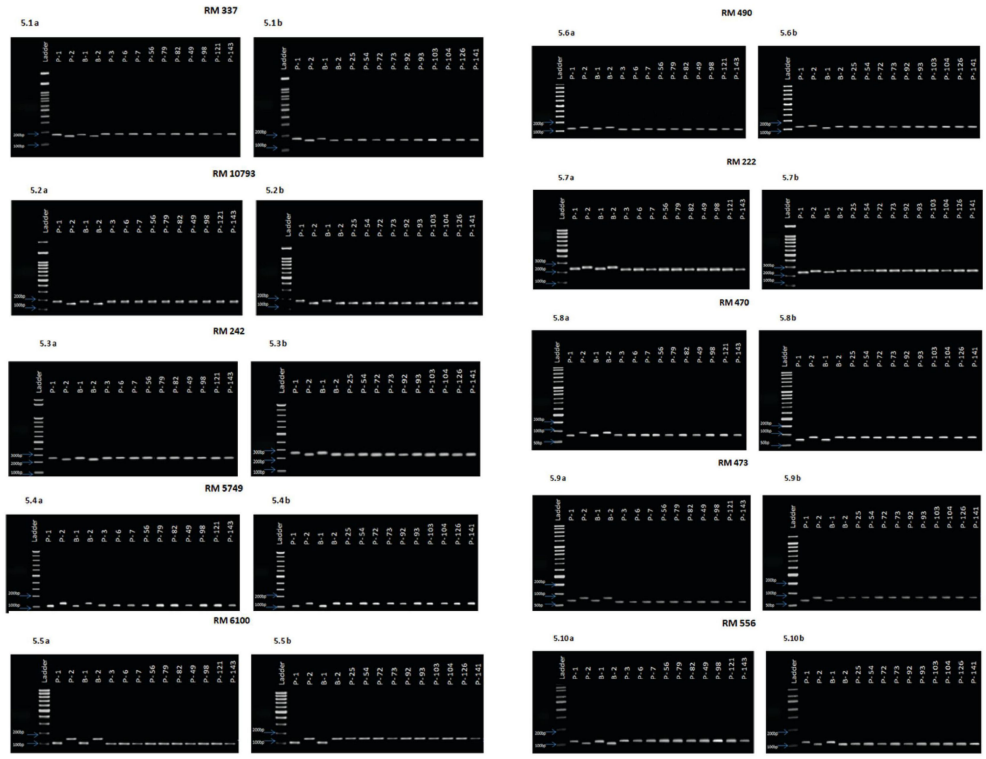

FIGURE 5
(5.1A). Amplification pattern of SSR markers 100 bp Ladder, P1—NL 44, P2—Uma, B1—Tolerant bulk, B2—Susceptible bulk, P 3, P 6, P 7, P 56, P 79, P 82, P 49, P 98, P 121, P 143—Tolerant lines. **(5.1B)**. Amplification pattern of SSR markers100 bp Ladder, P1—NL 44, P2—Uma, B1—Tolerant bulk, B2—Susceptible bulk, P 25, P 54, P 72, P 73, P 92, P 93, P 103, P 104, P 126, P 141—Susceptible lines,.

produced under a variety of climatic conditions throughout history; high temperatures are particularly detrimental, causing spikelet sterility which lowers rice production even when other yield components develop normally. Long-term rice yield in tropical, subtropical, and temperate regions is imperiled by heat stress during flowering (Beena, 2013). Therefore, it is imperative that heat-tolerant rice cultivars be created for future rice production (Costa and Farrant, 2019). According to short-term forecasts, the rice output in South Asia might fall by 10% of the yield by 2030. (Lobell et al., 2008). According to the medium- to long-term

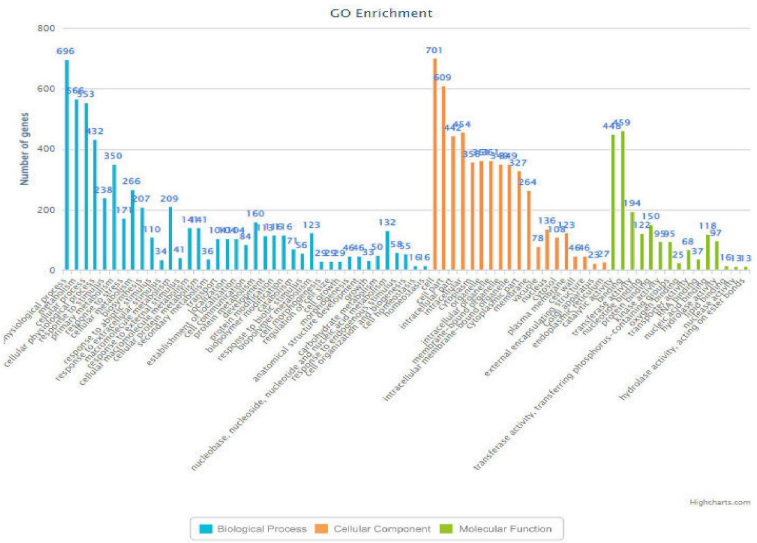

FIGURE 6
Bar-chart (RM6100) indicating the functions of the genes associated with various biological processes along with their frequency.

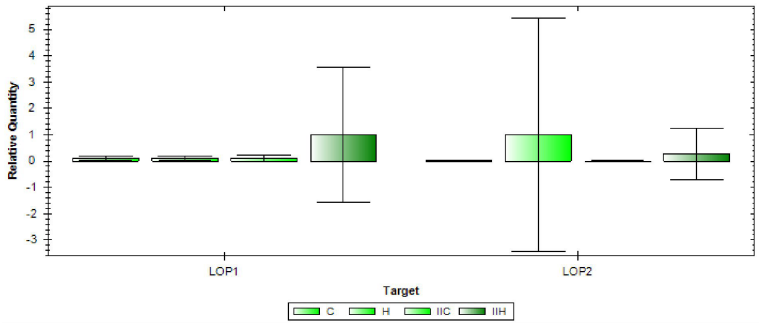

FIGURE 7
Gene expression of LOP1 and LOP2 [(C—Uma (control), H—Uma (high temperature), IIC-NL-44 (control), IIH-NL-44 (high temperature)].

projections of Cline (2008), rice yields in developing countries might decline by 10%–25% by 2080, and in India, by 30%–40%. Since heat tolerance is quantitative in nature, the underlying genetic process is complicated. Rarely are these prospective genes used to develop high-yielding, heat-resistant rice cultivars. Therefore, it is essential to conduct more studies to uncover probable genes and linked markers for heat tolerance.

Evaluation of F_2 population

Influence of high temperature stress on growth

The Uma variety recorded a lower height compared to NL-44, with the mean of the population lying between the two genotypes. Kilasi et al. (2018) identified several QTLs that were associated with shoot length and root length under high temperature conditions. NL-44 recorded lower tiller number compared to Uma, with the mean lying in between with 10 tillers. The mean tiller number was found to be greater than in NL-44 variety and closer to the Uma variety. The mean of the population was lower than both the genotypes with NL-44 producing lower number compared to that of Uma.

Comparing the productive tiller number, the lower value of the mean shows that the trait in the F_2 population was influenced to a greater extent by NL-44 and was depressed compared to both parents. Regarding membrane stability index, the mean of the population was greater than both parental genotypes, clearly indicating that most of the population has the potential for producing MSI greater than that of the parents. A similar trend was observed in the study by Prince et al. (2015) in the F_8 population of IR20 and Nootripathu under drought conditions.

Influence of high temperature stress on characteristics of flowering

The genotype NL-44 took the least number of days to attain flowering compared to that of Uma. The mean value being greater than Uma shows that the trait in most plants has been influenced by Uma. The variety NL-44 had a greater pollen viability percentage compared to Uma with the population mean value greater than the susceptible variety Uma. This indicates that the majority of the F_2 population has a pollen viability percentage that has been influenced by the tolerant parent, NL-44.

The time of anthesis for the F_2 population had a range spanning 3 h and 45 min, where the mean of the population was lower than that of both parents. This shows that most of the population had an earlier time of onset. Among the parents, Uma had earlier anthesis compared to NL-44. The earlier time of anthesis is a trait that is useful for escaping the high temperature stress. Bheemanahalli et al. (2017) reported a near-isogenic line (IR64 + qEMF3) possessing the early morning flowering (EMF) trait to have minimized spikelet sterility by 71%. The beneficial effects of the novel QTL, qEMF3, on mitigating heat stress damage in rice at flowering were also observed by Hirabayashi et al. (2015). Therefore, incorporating such traits could be a useful strategy to combat heat stress.

Influence of high temperature stress on gas exchange related parameters

The Uma variety recorded a lower photosynthetic rate compared to NL-44, with the mean of the population lying between the two genotypes. The mean of the population being greater than the susceptible Uma shows that most of the population had a higher photosynthetic rate, which was influenced by the tolerant NL-44. The Uma variety recorded a lower stomatal conductance compared to NL-44, with the mean lying between the parents. Similar results have also been noted under high temperature conditions, wherein the lower photosynthetic rate and stomatal conductance were observed in the susceptible rice varieties investigated (Beena et al., 2018a).

The Uma variety recorded a lower transpiration rate compared to NL-44, with the mean of the population lying between the two. The mean value being greater than that of the susceptible Uma variety indicates that most of the population had a higher transpiration rate. The variety NL-44 recorded a lower leaf temperature compared to Uma, with the mean lying between them. The mean being closer to NL-44 and lower than Uma shows that most of the population has a lower leaf temperature. The study by Stephen et al. (2022) also reported the decrease in canopy temperature of NL-44 under high temperature conditions.

Influence of high temperature on yield

The panicle length of the tolerant NL-44 was extremely high, while that of Uma was lower. The mean of the F_2 population was lower than both the parental genotypes and relatively close to Uma. This clearly indicates that the panicle length of most of the population was influenced by the Uma variety. Zhu et al. (2017) explored the genetic basis of heat tolerance in rice and identified the QTL *qHTB3-3* on the third chromosome that was associated with heat stress at the booting stage. The tolerant parent NL-44 recorded a higher 1,000 grain weight compared to the susceptible parent, while the mean was greater than the Uma variety and in between the two parental genotypes. The mean being closer to NL-44 clearly indicates that the trait has been greatly influenced by the tolerant parent. Chen et al. (2021) indicated that the gene *OsSAP5* (stress-associated proteins) might be induced by spermidine, which prevents the damage to rice seed resulting from high temperature stress during the grain-filling stage. This would be beneficial for maintaining crop yield under stressful conditions.

The tolerant variety NL-44 had much higher spikelet fertility compared to its susceptible parent. The mean of the population lies between the two parental genotypes. The greater value of the mean compared to Uma indicates that this important trait for heat tolerance has been beneficially transferred from the parent NL-44 to most of the population. Takai et al. (2020), while studying QTLs associated with spikelet fertility noted that the expression of QTLs may be dependent on their genetic background. Therefore, the varieties selected and the alleles present in them must be carefully considered while undertaking breeding programs. The reduction in spikelet fertility in rice at higher temperatures was also corroborated by Beena et al. (2021) and Pravallika et al. (2020). Ye et al. (2022) used the strategy of marker-assisted pyramiding of "early morning flowering" and heat tolerance QTLs (qEMF3 and qHTSF 4.1) in rice, to ensure a higher spikelet fertility rate and enhance resilience to heat stress.

Analysis of correlation between the parameters

The 1,000-grain weight was significantly correlated with the tolerance contributing traits such as membrane stability index, pollen viability, and spikelet fertility which explains their positive impact on the yield characteristics. The positive correlation of the membrane stability index with pollen viability and spikelet fertility is a major contribution to the heat tolerance of the plants. The negative correlation of the time of anthesis with spikelet fertility and 1,000 grain weight indicate that an earlier time of anthesis is a trait that is beneficial in avoiding the effects of high temperature stress, leading to a higher grain yield. This observation of rice was also confirmed by Raghunath and Beena (2021).

The positive correlation of the stomatal conductance with the photosynthetic rate is important as a higher rate of gaseous exchange significantly improves the photosynthetic rate due to a greater influx of carbon dioxide, whereas the positive correlation between the photosynthetic rate and the evapo-transpiration points to the beneficial effect of transpirational cooling under high temperature stress (Vijayakumar and Beena, 2020). The negative correlation between leaf temperature and pollen viability shows that lower temperatures contribute to a higher pollen viability percentage. As the correlation matrix is a result of mathematical inference, all parameters cannot be assumed to be correctly correlated, as the physiological functions of the parameters also need to be considered. In this regard, the negative correlation obtained between certain parameters cannot be explained, as the physiological basis of their relationship is not possible.

Inference of the evaluation of the F_2 population

Based on the results of the phenotypic evaluation of the F_2 population and their parents, we can characterize the NL-44 variety as a tolerant parent as it has performed better with regards to traits such as 1,000 grain weight, spikelet fertility, pollen viability, transpiration rate, photosynthetic rate, membrane stability index, and days to flower compared to the variety Uma under high temperature stress conditions. The poor performance of the Uma variety under stress conditions makes it a suitable candidate for characterization as a susceptible variety to heat stress. The mean of the population was close to NL-44 with regards to the traits of plant height, membrane stability index, photosynthetic rate, stomatal conductance, transpiration rate, pollen viability, spikelet fertility, and 1,000 grain weight. However, for traits such as tiller number, days to flower, time of anthesis, leaf temperature, and panicle length, the mean of the population was influenced by the susceptible parent, Uma. The yield-contributing characteristics, such as productive tiller number, have been depressed in the F_2 population.

Polymorphic markers related to high temperature tolerance

Simple sequence repeats (SSR) are molecular markers that are relatively more efficient, cheaper, and easier to use in marker assisted selection for crop improvement, as there is a probability of a higher polymorphism rate (Beena et al., 2012; Gao et al., 2016). Identifying SSR markers that are associated with QTLs contributing to heat tolerance has huge potential in breeding programs through gene pyramiding (Ye et al., 2015; Ali et al., 2022). In this regard, bulked segregant analysis is a technique that can rapidly identify markers that are tightly linked to genes for a given phenotype (Zou et al., 2016).

In the current study, out of the 100 SSR markers tested on the parental genotypes and the bulks, 18 were found to be polymorphic indicating a polymorphism of 18%. BSA was used to link the markers to heat tolerance based on spikelet fertility percentage recorded under stress conditions. Waghmare et al. (2018) had demonstrated the efficiency of BSA, through which they had identified 41 SSR markers that were found to be polymorphic between parents and associated with QTLs for heat tolerance. Varying levels of polymorphism between the tolerant and susceptible parents were obtained, ranging from 8.07% to 27.99%, in studies that had utilised SSR markers to link them with heat

tolerance (Kanagaraj et al., 2010; Salunkhe et al., 2011; Vikram et al., 2011; Wei et al., 2013).

Although a good number of markers linked to different traits for tolerance to heat stress have been reported, each segregated population is unique due to genetic differences between the parents, and therefore, the markers validated in a particular cross of parental genotypes may not be applicable to other populations. In the present study, a significant proportion of previously reported validated markers for heat tolerance were used, but only a few of them could be confirmed with the results we have obtained. Out of the 18 polymorphic markers identified, only one (RM337) is expected to be unique to the current investigation, and it has not been reported in the literature surveyed. Among the 18 polymorphic markers, the markers RM222, RM237, RM556, and RM3475 have also been linked to drought tolerance traits (Yue et al., 2006; Freeg et al., 2016).

The rest of the identified polymorphic markers have been reported to be linked to various aspects of heat tolerance. RM554 was reported to be associated with QTLs that controlled the unfilled grain percentage (Buu et al., 2014). RM3586 was validated to be associated with QTLs responsible for phenotypic variation in heat tolerance at the flowering stage (Zhang et al., 2009; Buu et al., 2014). Xiao et al. (2011) associated RM471 with QTLs influencing seed set percentage. The marker RM242 was reported to influence the erect panicle trait (Kong et al., 2007) and was also associated with plant height, panicle length, and spikelet fertility under heat stress by Wei et al. (2013); Pradhan et al. (2016), and Mohapatra et al., 2021. Sunoharaa et al., (2016) reported that RM3475 and RM237 were associated with controlling panicle characters. Identified RM473 as a polymorphic marker that was strongly associated with heat tolerance. RM473 was also found to be associated with the QTL *qEHD10*, that regulates the thermosensitive-linked heading date in rice (Kovi et al., 2015). Pradhan et al. (2016) had associated RM3586 with days to 50% flowering and spikelet fertility percentage under high temperature stress. Bharathkumar et al. (2014), in their study, found association between RM6100 and a major quantitative trait locus affecting tolerance to heat stress at the flowering stage. The association of RM6100 with high temperature tolerance in rice was also reported by Stephen et al. (2022a). Revathi et al. (2013) reported that RM6100 linked to the fertility restoration gene, Rf4, had 85% efficiency in identifying restoration lines in rice. Waghmare et al. (2021) identified RM5749 as a polymorphic marker that could differentiate between the tolerant and susceptible bulks under heat stress in a cross of the parental genotypes, N22 and Uma. RM222 was noted to be 11.8 cM from the AFLP marker Rev1 that was linked to the recessive thermogenic male sterility (tgms) associated gene, i.e., *rtms1* (Jia et al., 2001). However, the direct association of RM222 with the quantitative character of heat tolerance has not been widely studied. Aliyu et al. (2011) validated the association of RM10793 with the QTL *SALTOL*, which indicates its association with multiple abiotic stress factors.

Through QTL analysis, the identified polymorphic markers can be linked to traits known to contribute to heat tolerance. The polymorphic markers are useful in identifying marker loci associated with various phenotypic traits. In the studied F_2 population, the plants were segregated into tolerant or susceptible genotypes based on the spikelet fertility percentage alone. Therefore, the markers may or may not be linked to other phenotypic traits that were used for evaluation. However, an inference can be made from the correlation analysis between the traits, wherein the spikelet fertility percentage was significantly and positively associated with tolerance and yield contributing traits such as pollen viability, MSI, and 1,000 grain weight. The markers can be utilized for marker-assisted selection to incorporate tolerance traits. As some of the markers have been reported to be associated with drought, further studies are needed to identify markers that are specific to heat tolerance. These studies will be used to identify traits that may be useful for such characterization.

The identified polymorphic markers have been further investigated using bioinformatics tools to annotate genes associated with them. The genomic regions in which the markers are present have been found to encode several important genes that are involved in varied metabolic, structural, and stress-related functions. The annotation of such genes provides a clue to the mechanisms or pathways that might involve their plant functions. For instance, the gene Snf-7 (Sucrose non-fermenting 7) family protein, which is involved in regulating sucrose metabolism under stress conditions, has been found to be associated with the marker RM10793. Apart from this, genes for nitrate transporter and nitrogen-use efficiency, as well as the NAC transcription factor protein, which regulates the synthesis of starch and storage proteins, have been annotated, among several other critical genes. The marker RM473 was found to be associated with the gene GPI (Glycophosphatidylinositol)-anchored membrane protein, which regulates leaf rolling and maintains epidermal integrity, cell wall formation, and homeostasis, as well as the gene SLG-7-like protein, which regulates the slender grain shape formation. Expression analysis of the genes *LOP1* (LOC_Os08g01330) and *LOP2* (LOC_Os08g0112) associated with the marker RM337 revealed that *LOP1* was linked with high temperature tolerance in rice as per the phenotypic evaluation. The diverse functions of the genes indicate their involvement in the regulation of stress responses.

Conclusion

The phenotyping of the F_2 generation indicated that the tolerance traits in the population were majorly contributed by the tolerant parent, i.e., NL-44. The identified polymorphic markers were able to segregate the individual lines of the F_2 population into tolerant and susceptible genotypes. The association of molecular markers linked to the heat tolerance traits in the segregating second-generation filial populations is validated to be beneficial in undertaking crop improvement studies to introgress the tolerance traits into high-yielding regional varieties. Most of the genes annotated are yet to be exploited for their beneficial effects. Further studies are required to link them specifically to the tolerance traits. The genomic areas associated with heat tolerance traits should be further investigated or fine-mapped to discover potential genes or putative QTLs controlling the pathways

underpinning heat tolerance traits for marker-assisted selection programs.

Data availability statement

The original contributions presented in the study are included in the article/Supplementary Material. Further inquiries can be directed to the corresponding author.

Author contributions

RB conceptualized the study. KS, KA and RB performed the work. Data analysis was done by KS, KA RPS, BS and UCJ. All authors reviewed and approved the manuscript.

Acknowledgments

Authors are thankful to Kerala Agricultural University for providing the M.Sc. and Ph.D. fellowship and all other research facilities

Conflict of interest

The authors declare that the research was conducted in the absence of any commercial or financial relationships that could be construed as a potential conflict of interest.

Publisher's note

Supplementary material

The Supplementary Material for this article can be found online at: https://www.frontiersin.org/articles/10.3389/fpls.2023.1113838/full#supplementary-material

References

Ali, A., Beena, R., Manikanta, C., Swapna, A., Soni, K. B., and Viji, M. M. (2022). Molecular characterization and varietal identification for multiple abiotic stress tolerance in rice (*Oryza sativa* l.). *Oryza –An Int. J. Rice* 59 (1), 140–15). doi: 10.35709/ory.2022.59.1.7

Aliyu, R., Adamu, A. K., Muazu, S., Alonge, S. O., and Gregorio, G. B. (2011). "Tagging and validation of SSR markers to salinity tolerance QTLs in rice (Oryza spp)," in *International conference on biology, environment and chemistry IPCBEE*, Vol. 1 (Singapore: IACSIT Press).

Alshareef, N. O., Otterbach, S. L., Allu, A. D., Woo, Y. H., deWerk, T., Kamranfar, I., et al. (2022). NAC transcription factors ATAF1 and ANAC055 affect the heat stress response in *Arabidopsis*. *Sci. Rep.* 12, 11264. doi: 10.1038/s41598-022-14429-x

Bahuguna, R. N., Jha, J., Pal, M., Shah, D., Lawas, L. M., Khetarpal, S., et al. (2015). Physiological and biochemical characterization of NERICA-L-44: a novel source of heat tolerance at the vegetative and reproductive stages in rice. *Physiologia plantarum* 154 (4), 543–559. doi: 10.1111/ppl.12299

Beena, R. (2013). "Research paradigm and inference of studies on high temperature stress in rice (Oryza sativa l.)," in *Advances in plant physiology, an international treatise series*. Ed. A. Hemantaranjan (India: Scientific Publishers), 14:497–511.

Beena, R., Praveenkumar, V. P., Vighneswaran, V., and Narayankutty, M. C. (2018b). Bulked line analysis: A useful tool to identify microsatellite markers linked to drought tolerance in rice. *Indian J. Plant Physiol.* 23 (1), 7–15. doi: 10.1007/s40502-017-0321-0

Beena, R., Sheshshayee, M. S., Madhura, J. N., Prasad, T. G., and Udayakumar, M. (2012). "Development of SSR markers and genetic variability in physiological traits in bambara groundnut (Vigna subterranea l. verdc)," in *Prospects in bioscience: Addressing the issues*. Eds. A. Sabu and A. Anu (India: Springer Nature Publishing), 229–242.

Beena, R., Veena, V., Jaslam, M. P. K., Nithya, N., and Adarsh, V. S. (2021). Germplasm innovation for high temperature tolerance from traditional rice accessions of kerala using genetic variability, genetic advance, path coefficient analysis and principal component analysis. *J. Crop Sci. Biotechnol.* 24 (5), 555–566. doi: 10.1007/s12892-021-00103-7

Beena, R., Vighneswaran, V., Sindumole, P., Narayankutty, M. C., and Voleti, S. R. (2018a). Impact of high temperature stress during reproductive and grain filling stage in rice. *Oryza Int. J. Rice* 55 (1), 126–133. doi: 10.5958/2249-5266.2018.00015.2

Bharathkumar, S., Pragnya, P. J., Jitendra, K., Archana, B., Singh, O. N., and Reddy, J. N. (2014). Identification of rice germplasms associated with microsatelite (SSR) markers for heat tolerance at reproductive stage and expression of heat stress related gene. *Indian Res. J. Genet. Biotech.* 6, 424–427.

Bheemanahalli, R., Sathishraj, R., Manoharan, M., Sumanth, H. N., Muthurajan, R., Ishimaru, T., et al. (2017). Is early morning flowering an effective trait to minimize heat stress damage during flowering in rice? *Field Crops Res.* 203, 238–242. doi: 10.1016/j.fcr.2016.11.011

Buu, B. C., Ha, P. T. T., Tam, B. P., Nhien, T. T., Van Hieu, N., Phuoc, N. T., et al. (2014). Quantitative trait loci associated with heat tolerance in rice (Oryza sativa l.). *Plant Breed. Biotechnol.* 2 (1), 14–24. doi: 10.9787/PBB.2014.2.1.014

Chen, S., Cao, H., Huang, B., Zheng, X., Liang, K., Wang, G. L., et al. (2022). The WRKY10-VQ8 module safely and effectively regulates rice thermotolerance. *Plant Cell Environ.* 45 (7), 2126–2144. doi: 10.1111/pce.14329

Chen, L., Wang, Q., Tang, M., Zhang, X., Pan, Y., Yang, X., et al. (2021). QTL mapping and identification of candidate genes for heat tolerance at the flowering stage in rice. *Front. Genet.* 11, 621871. doi: 10.3389/fgene.2020.621871

Cobb, J. N., Chen, C., Shi, Y., Maron, L. G., Liu, D., Rutzke, M., et al. (2021). Genetic architecture of root and shoot ionomes in rice (Oryza sativa l.). *Theor. Appl. Genet.* 134 (8), 2613–2637. doi: 10.1007/s00122-021-03848-5

Costa, M. C. D., and Farrant, J. M. (2019). Plant resistance to abiotic stresses. *Plants* 8, 553. doi: 10.3390/plants8120553

Das, G., Patra, J. K., and Baek, K. H. (2017). Insight into MAS: a molecular tool for development of stress resistant and quality of rice through gene stacking. *Front. Plant Sci.* 8, 985. doi: 10.3389/fpls.2017.00985

Dellaporta, S. L., Wood, J., and Hicks, J. B. (1983). A plant DNA minipreparation: version II. *Plant Mol. Biol. Rep.* 1 (4), 19–21. doi: 10.1007/BF02712670

Foolad, M. R., and Sharma, A. (2004). Molecular markers as selection tools in tomato breeding. *I Int. Symposium Tomato Dis.* 695, 225–240. doi: 10.17660/ActaHortic.2005.695.25

Freeg, H. A., Anis, G. B., Abo-Shousha, A. A., El-Banna, A. N., and El-Sabagh, A. (2016). Genetic diversity among some rice genotypes with different drought tolerance based on SSR markers. *Cercetari Agronomice Moldova* 49 (3), 39–50. doi: 10.1515/cerce-2016-0024

Gao, L., Jia, J., and Kong, X. (2016). A SNP-based molecular barcode for characterization of common wheat. *PloS One* 11 (3), e0150947. doi: 10.1371/journal.pone.0150947

Hirabayashi, H., Sasaki, K., Kambe, T., Gannaban, R. B., Miras, M. A., Mendioro, M. S., et al. (2015). qEMF3, a novel QTL for the early-morning flowering trait from wild rice, oryza officinalis, to mitigate heat stress damage at flowering in rice, o. sativa. *J. Exp. Bot.* 66 (5), 1227–1236. doi: 10.1093/jxb/eru474

Huang, J., Wang, M. M., Jiang, Y., Bao, Y. M., Huang, X., Sun, H., et al. (2008). Expression analysis of rice A20/AN1-type zinc finger genes and characterization of ZFP177 that contributes to temperature stress tolerance. *Gene* 420 (2), 135–144. doi: 10.1016/j.gene.2008.05.019

Jan, M., Shah, G., Yuqing, H., Xuejiao, L., Peng, Z., Hao, D., et al. (2021). Development of heat tolerant two-line hybrid rice restorer line carrying dominant locus of OsHTAS. *Rice Sci.* 28 (1), 99–108. doi: 10.1016/j.rsci.2020.11.011

Jia, Y., Li, B., Zhang, Y., Zhang, X., Xu, Y., and Li, C. (2019). Evolutionary dynamic analyses on monocot flavonoid 3′-hydroxylase gene family reveal evidence of plant-environment interaction. *BMC Plant Biol.* 19 (1), 1–16. doi: 10.1186/s12870-019-1947-z

Jia, J. H., Zhang, D. S., Li, C. Y., Qu, X. P., Wang, S. W., Chamarerk, V., et al. (2001). Molecular mapping of the reverse thermo-sensitive genic male-sterile gene (rtms1) in rice. *Theor. Appl. Genet.* 103 (4), 607–612. doi: 10.1007/PL00002916

Jung, Y. J., Nou, I. S., and Kang, K. K. (2014). Overexpression of Oshsp16. 9 gene encoding small heat shock protein enhances tolerance to abiotic stresses in rice. *Plant Breed. Biotechnol.* 2 (4), 370–379. doi: 10.9787/PBB.2014.2.4.370

Kanagaraj, P., Prince, K. S. J., Sheeba, J. A., Biji, K. R., Paul, S. B., Senthil, A., et al. (2010). Microsatellite markers linked to drought resistance in rice (Oryza sativa l.). *Curr. Sci.* 836–839.

KAU [Kerala Agricultural University] (2016). *Package of practices recommendations: Crops. 15th Ed* (Thrissur, India: Kerala Agricultural University), 392.

Kilasi, N. L., Singh, J., Vallejos, C. E., Ye, C., Jagadish, S. K., Kusolwa, P., et al. (2018). Heat stress tolerance in rice (Oryza sativa l.): Identification of quantitative trait loci and candidate genes for seedling growth under heat stress. *Front. Plant Sci.* 9, 1578. doi: 10.3389/fpls.2018.01578

Kong, F. N., Wang, J. Y., Zou, J. C., Shi, L. X., De Jin, M., Xu, Z. J., et al. (2007). Molecular tagging and mapping of the erect panicle gene in rice. *Mol. Breed.* 19 (4), 297–304. doi: 10.1007/s11032-006-9062-x

Kovi, M. R., Hu, Y., Bai, X., and Xing, Y. (2015). QTL mapping for thermo-sensitive heading date in rice. *Euphytica* 205 (1), 51–62. doi: 10.1007/s10681-015-1383-6

Kuang, J., Liu, J., Mei, J., Wang, C., Hu, H., Zhang, Y., et al. (2017). A class II small heat shock protein OsHsp18. 0 plays positive roles in both biotic and abiotic defense responses in rice. *Sci. Rep.* 7 (1), 1–14. doi: 10.1038/s41598-017-11882-x

Li, J., Yang, J., Zhu, B., and Xie, G. (2019). Overexpressing OsFBN1 enhances plastoglobule formation, reduces grain-filling percent and jasmonate levels under heat stress in rice. *Plant Sci.* 285, 230–238. doi: 10.1016/j.plantsci.2019.05.007

Liu, X. H., Lyu, Y. S., Yang, W., Yang, Z. T., Lu, S. J., and Liu, J. X. (2020). A membrane-associated NAC transcription factor OsNTL3 is involved in thermotolerance in rice. *Plant Biotechnol. J.* 18 (5), 1317–1329. doi: 10.1111/pbi.13297

Lobell, D. B., Burke, M. B., Tibaldi, C., Mastrandrea, M. D., Falcon, W., and Naylor, R. L. (2008). Prioritizing climate change adaptation needs for food security in 2030. *Science* 319 (5863), 607–610. doi: 10.1126/science.1152339

Magiri, E. N., Farchi-Pisanty, O., Avni, A., and Breiman, A. (2006). The expression of the large rice FK506 binding proteins (FKBPs) demonstrate tissue specificity and heat stress responsiveness. *Plant Sci.* 170 (4), 695–704. doi: 10.1016/j.plantsci.2005.09.013

Mohapatra, S., Barik, S. R., Panigrahi, D., and Pradhan, S. K. (2021). Donors identification and molecular markers validation for high temperature stress tolerance in rice. *Ann. Agri-Bio Res.* 26 (1), 11–19.

Pradhan, S. K., Barik, S. R., Sahoo, A., Mohapatra, S., Nayak, D. K., Mahender, A., et al. (2016). Population structure, genetic diversity and molecular marker-trait association analysis for high temperature stress tolerance in rice. *PloS One* 11 (8), e0160027. doi: 10.1371/journal.pone.0160027

Pravallika, K., Arunkumar, C., Vijayakumar, A., Beena, R., and Jayalekshmi, V. G. (2020). Effect of high temperature stress on seed filling and nutritional quality of rice (Oryza sativa l.). *J. Crop Weed* 16 (2), 18–23. doi: 10.22271/09746315.2020.v16.i2.1310

Prince, S. J., Beena, R., Michael Gomez, S., Senthivel, S., and Chandra Babu, R. (2015). Mapping consistent yield QTLs under drought stress in target rainfed environments. *Rice* 8 (1), 53. doi: 10.1186/s12284-015-0053-6

Radha, B., Sunitha, N. C., Sah, R. P., T. P., M. A., Krishna, G. K., Umesh, D. K., et al. (2023). Physiological and molecular implications of multiple abiotic stresses on yield and quality of rice. *Front. Plant Sci.* 13. doi: 10.3389/fpls.2022.996514

Raghunath, M. P., and Beena, R. (2021). Manipulation of flowering time to mitigate high temperature stress in rice (*Oryza sativa* l.). *Indian J. Agric. Res.* 1-4. doi: 10.18805/IJARe.A-5707

Ravikiran, K. T., Gopala Krishnan, S., Vinod, K. K., Dhawan, G., Dwivedi, P., Kumar, P., et al. (2020). A trait specific QTL survey identifies NL44, a NERICA cultivar as a novel source for reproductive stage heat stress tolerance in rice. *Plant Physiol. Rep.* 25 (4), 664–676. doi: 10.1007/s40502-020-00547-z

Rejeth, R., Manikanta, C., Beena, R., Roy, S., Manju, R. V., and Viji, M. M. (2020). Water stress mediated root trait dynamics and identification of microsatellite markers associated with root traits in rice (*Oryza sativa* l.). *Physiol. Mol. Biol. Plants* 26 (6), 1225–1236. doi: 10.1007/s12298-020-00809

Revathi, P., Medoju, P., Singh, A. K., Sundaram, R. M., Raju, S., Senguttuve, P., et al. (2013). Efficiency of molecular markers in identifying fertility restoration trait of WA-CMS system in rice. *Indian J. Genet. Plant Breed.* 73 (01), 89–93. doi: 10.5958/j.0019-5200.73.1.012

Sairam, R. K., Deshmukh, P. S., and Shukla, D. S. (1997). Tolerance of drought and temperature stress in relation to increased antioxidant enzyme activity in wheat. *J. Agron. Crop Sci.* 178 (3), 171–178. doi: 10.1111/j.1439-037X.1997.tb00486.x

Salunkhe, A. S., Poornima, R., Prince, K., Kanagaraj, P., Sheeba, J. A., Amudha, K., et al. (2011). Fine mapping QTL for drought resistance traits in rice (Oryza sativa l.) using bulk segregant analysis. *Mol. Biotechnol.* 49 (1), 90–95. doi: 10.1007/s12033-011-9382-x

Stephen, K., Beena, R., Kiran, A. G., Shanija, S., and Saravanan, R. (2022b). Changes in physiological traits and expression of key genes involved in sugar signaling pathway in rice under high temperature stress. *3 Biotech.* 12 (2), 183. doi: 10.1007/s13205-022-03242-y

Stephen, K., Beena, R., Neethu, M., and Shanija, S. (2022a). Identification of heat-tolerant rice genotypes and their molecular characterisation using SSR markers. *Plant Sci. Today*, 1–12. doi: 10.14719/pst.1639. ISSN 2348-1900 Vol x(x): xx–xx.

Suzuki, K., Aoki, N., Matsumura, H., Okamura, M., Ohsugi, R., and Shimono, H. (2015). Cooling water before panicle initiation increases chilling-induced male sterility and disables chilling-induced expression of genes encoding OsFKBP 65 and heat shock proteins in rice spikelets. *Plant Cell Environ.* 38 (7), 1255–1274. doi: 10.1111/pce.12498

Sunoharaa, M. D., Gottschall, N., Craiovana, E., Wilkes, G., Toppb, E., Freya, S. K., et al. (2016). Controlling tile drainage during the growing season in Eastern Canada to reduce nitrogen, phosphorus, and bacteria loading to surface water. *Agric. Water Manage.* 178 (2016), 159–170.

Takai, T., Lumanglas, P., and Simon, E. V. (2020). Genetic mechanism of heat stress tolerance at anthesis among three different rice varieties with different fertilities under heat stress. *Plant Production Sci.* 23 (4), 529–538. doi: 10.1080/1343943X.2020.1766363

Tang, Y., Gao, C. C., Gao, Y., Yang, Y., Shi, B., Yu, J. L., et al. (2020). OsNSUN2-mediated 5-methylcytosine mRNA modification enhances rice adaptation to high temperature. *Dev. Cell* 53 (3), 272–286. doi: 10.1016/j.devcel.2020.03.009

Tiwari, S., Sl, K., Kumar, V., Singh, B., Rao, A. R., Mithra SV, A., et al. (2016). Mapping QTLs for salt tolerance in rice (Oryza sativa l.) by bulked segregant analysis of recombinant inbred lines using 50K SNP chip. *PloS One* 11 (4), e0153610. doi: 10.1371/journal.pone.0153610

Vijayakumar, A., and Beena, R. (2020). Impact of temperature difference on the physicochemical properties and yield of tomato: A review. *Chem. Sci. Rev. Lett.* 9 (35), 665–681.

Vikram, P., Swamy, B. P., Dixit, S., Ahmed, H. U., Teresa Sta Cruz, M., Singh, A. K., et al. (2011). qDTY 1.1, a major QTL for rice grain yield under reproductive-stage drought stress with a consistent effect in multiple elite genetic backgrounds. *BMC Genet.* 12 (1), 1–15. doi: 10.1186/1471-2156-12-89

Waghmare, S. G., Sindhumole, P., Mathew, D., Shylaja, M. R., Francies, R. M., Abida, P. S., et al. (2021). Identification of QTL linked to heat tolerance in rice (Oryza sativa l.) using SSR markers through bulked segregant analysis. *Electronic J. Plant Breed.* 12 (1), 46–53. doi: 10.37992/2021.1201.007

Waghmare, S. G., Sindhumole, P., Shylaja, M. R., Mathew, D., Francies, R. M., Abida, P. S., et al. (2018). Analysis of simple sequence repeat (SSR) polymorphism between N22 and uma rice varieties for marker assisted selection. *Electronic J. Plant Breed.* 9 (2), 511–517. doi: 10.5958/0975-928X.2018.00062.5

Wei, H., Liu, J., Wang, Y., Huang, N., Zhang, X., Wang, L., et al. (2013). A dominant major locus in chromosome 9 of rice (Oryza sativa l.) confers tolerance to 48 c high temperature at seedling stage. *J. Heredity* 104 (2), 287–294. doi: 10.1093/jhered/ess103

Xiao, Y., Pan, Y., Luo, L., Zhang, G., Deng, H., Dai, L., et al. (2011). Quantitative trait loci associated with seed set under high temperature stress at the flowering stage in rice (Oryza sativa l.). *Euphytica* 178 (3), 331–338. doi: 10.1007/s10681-010-0300-2

Ye, C., Ishimaru, T., Lambio, L., Li, L., Long, Y., He, Z., et al. (2022). Marker-assisted pyramiding of QTLs for heat tolerance and escape upgrades heat resilience in rice (Oryza sativa l.). *Theor. Appl. Genet.* 135 (4), 1345–1354. doi: 10.1007/s00122-022-04035-w

Ye, C., Tenorio, F. A., Argayoso, M. A., Laza, M. A., Koh, H. J., Redoña, E. D., et al. (2015). Identifying and confirming quantitative trait loci associated with heat tolerance at flowering stage in different rice populations. *BMC Genet.* 16 (1), 1–10. doi: 10.1186/s12863-015-0199-7

Yue, B., Xue, W., Xiong, L., Yu, X., Luo, L., Cui, K., et al. (2006). Genetic basis of drought resistance at reproductive stage in rice: separation of drought tolerance from drought avoidance. *Genetics* 172 (2), 1213–1228. doi: 10.1534/genetics.105.045062

Zhang, G. L., Chen, L. Y., Xiao, G. Y., Xiao, Y. H., Chen, X. B., and Zhang, S. T. (2009). Bulked segregant analysis to detect QTL related to heat tolerance in rice (Oryza sativa l.) using SSR markers. *Agric. Sci. China* 8 (4), 482–487. doi: 10.1016/S1671-2927(08)60235-7

Zhu, S., Huang, R., Wai, H. P., Xiong, H., Shen, X., He, H., et al. (2017). Mapping quantitative trait loci for heat tolerance at the booting stage using chromosomal segment substitution lines in rice. *Physiol. Mol. Biol. Plants* 23 (4), 817–825. doi: 10.1007/s12298-017-0465-4

Zou, C., Wang, P., and Xu, Y. (2016). Bulked sample analysis in genetics, genomics and crop improvement. *Plant Biotechnol. J.* 14 (10), 1941–1955. doi: 10.1111/pbi.12559

Frontiers in Plant Science

Cultivates the science of plant biology and its applications

The most cited plant science journal, which advances our understanding of plant biology for sustainable food security, functional ecosystems and human health.

Discover the latest Research Topics

See more →

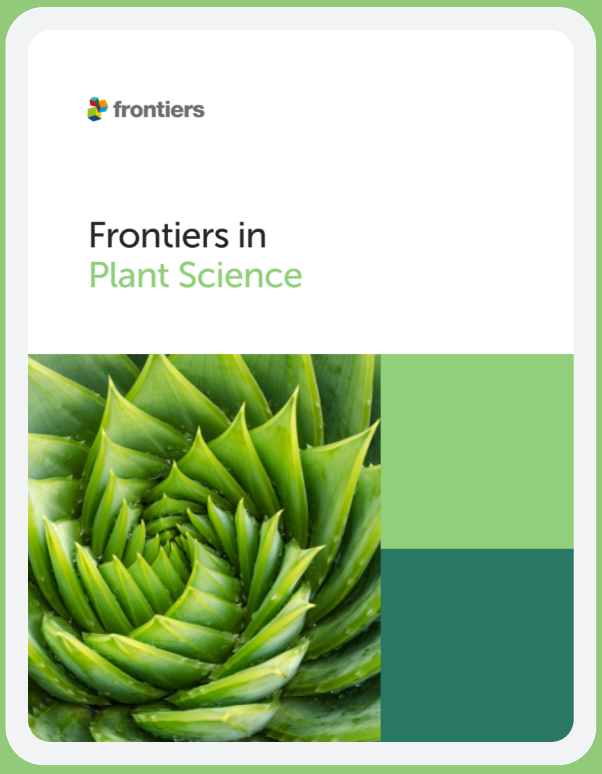

Frontiers

Avenue du Tribunal-Fédéral 34
1005 Lausanne, Switzerland
frontiersin.org

Contact us

+41 (0)21 510 17 00
frontiersin.org/about/contact